La Variabilité Régionale du Niveau de la Mer

Benoit Meyssignac

Université de Toulouse

THÈSE

En vue de l'obtention du

DOCTORAT DE L'UNIVERSITÉ DE TOULOUSE

Délivré par *l'Université Toulouse III - Paul Sabatier*
Discipline ou spécialité : *Océanographie Spatiale*

Présentée et soutenue par *Benoit Meyssignac*
Le *19 Octobre 2012*

Titre : *La Variabilité Régionale du Niveau de la Mer*

JURY

Isabelle Dadou	*(Présidente du Jury)*
Gilles Reverdin	*(Rapporteur)*
Jacques Verron	*(Rapporteur)*
Don P. Chambers	*(Examinateur)*
David Salas y Mélia	*(Examinateur)*
Detlef Stammer	*(Examinateur)*
Laurent Terray	*(Examinateur)*
Anny Cazenave	*(Directrice de Thèse)*

Ecole doctorale : SDU2E
Unité de recherche : *LEGOS UMR 5566*
Directeurs de Thèse : *Anny Cazenave et Rosemary Morrow*
Rapporteurs : *voir le Jury*

Remerciements

Je voudrais tout d'abord remercier Anny pour tout ce qu'elle a fait pour moi durant ces 3 années de thèse. A son contact j'ai découvert le vaste monde de la Géophysique et appris énormément sur tout ces aspects de la planète Terre qui m'étaient inconnus. Ça a été passionnant de travailler au quotidien à ses côtés, de partager sa curiosité pour les Sciences et son enthousiasme pour les découvertes. Je suis très reconnaissant de tout ce qu'elle m'a transmi, et honoré d'avoir réalisé ma thèse sous sa direction.

Je voudrais aussi remercier Rosemary Morrow et Philippe Maisongrande sans qui cette thèse n'aurait pas pu se faire. J'ai beaucoup profité de leurs conseils et j'ai particulièrement apprécié leur soutien permanent.

Merci à Catherine Lambert, Michel Avignon et Christophe Valorge du CNES, de m'avoir proposé le poste que j'occupe au LEGOS et de m'avoir permis de réaliser cette thèse dans le cadre de mon travail.

Merci aussi à tous les collègues et amis avec qui j'ai eu plaisir à travailler pendant ces 3 années : William, Mélanie, Samuel, Sarah, Kurt, Hindumathi, Nicolas, Jean-François, Flavien, Luciana, Marta, Francesc, David, Olivier, Joël, Nadine, Martine...

Enfin, au moment de terminer ce manuscrit, mes pensées vont à ma famille et en particulier à Rocío. Merci beaucoup de ta patience, de ton aide et de ton soutien... Merci aussi à Carmen qui m'a supporté les mercredis après-midi.

La Variabilité Régionale du Niveau de la Mer

Auteur : Benoit Meyssignac.
Directrices de thèse : Anny Cazenave et Rosemary Morrow.
Discipline : Océanographie Spatiale.
Lieu et date de soutenance : Observatoire Midi-Pyrénées, le 19 Octobre 2012.
Laboratoire : LEGOS, UMR 5566 CNRS/CNES/IRD/UPS, OMP, 14 avenue Edouard Belin, 31400 Toulouse, France.

Résumé : Au cours du XX^{ème} siècle, les mesures marégraphiques ont permis d'estimer la hausse du niveau de la mer global à 1.7 mm.a^{-1}. Depuis deux décennies, les observations faites par les satellites altimétriques indiquent une hausse du niveau de la mer plus rapide, de 3.2 mm.a^{-1} sur la période 1993-2011. Grâce à leur couverture quasi-globale, les observations spatiales ont aussi révélé une forte variabilité régionale dans la hausse du niveau de la mer qui dépasse de beaucoup la hausse moyenne globale dans de nombreuses régions du globe. Cette composante régionale qui s'ajoute à la hausse globale pour donner le niveau de la mer total local, est essentielle dans l'étude des impacts de la hausse du niveau de la mer sur les régions côtières et les îles basses. Dans cette thèse, nous analysons les observations de la variabilité régionale de la hausse du niveau de la mer, nous proposons une reconstrution de cette variabilité régionale depuis 1950 (i.e. avant l'avènement de l'altimétrie spatiale) et nous étudions ses causes et ses origines.

Dans une première partie, nous analysons les différentes contributions à la variabilité régionale de la hausse du niveau de la mer observée depuis 1993 par les satellites altimétriques. Nous estimons la hausse régionale issue de l'expansion thermo-haline de l'océan et montrons que la variabilité régionale des vitesses de variation du niveau de la mer s'explique essentiellement par celle de l'expansion thermique de l'océan. Les variations de masse de l'océan jouent aussi un rôle mais qui est difficile à estimer régionalement du fait du faible signal. Nous reconstruisons ensuite la variabilité régionale du niveau de la mer dans le passé (avant la période altimétrique) en combinant des données marégraphiques avec les structures spatiales propres de l'océan déduites des modèles d'océan. Cette méthode permet de reconstruire le niveau de la mer en 2 dimensions depuis 1950, sur la majeure partie du globe, avec une résolution proche de celle de l'altimétrie spatiale.

Dans une seconde partie, nous appliquons la méthode de reconstruction pour estimer la variabilité régionale de la hausse du niveau de la mer passée dans trois régions sensibles au réchauffement climatique : le Pacifique tropical, la mer Méditerranée et l'océan Arctique. Nous en déduisons pour ces régions la hausse totale (régionale plus moyenne globale) du niveau de la mer local au cours des dernières décennies. Pour les sites où l'on dispose de mesures du mouvement de la croûte terrestre, nous évaluons la hausse local du niveau de la mer relatif (i.e. hausse du niveau de la mer totale plus mouvement de la croûte local) depuis 1950. Le but est de permettre les études de l'impact local de la hausse du niveau de la mer aux échelles climatiques.

Dans la dernière partie de cette thèse, nous analysons l'origine de la variabilité régionale de la hausse du niveau de la mer pour déterminer si elle est dûe à l'activité anthropique ou si elle résulte de la variabilité naturelle du système climatique. Nous nous focalisons sur le Pacifique tropical qui est marqué par une très forte variabilité régionale de la hausse du niveau de la mer depuis 1993. Grâce à la reconstruction du niveau de la mer depuis 1950, nous montrons que cette variabilité régionale récente (17 dernières années) n'est pas stationnaire dans le temps mais qu'elle fluctue en lien avec une basse fréquence du mode de variabilité ENSO. Avec les modèles de climat du projet CMIP3, nous montrons de plus que cette variabilité régionale est essentiellement d'origine naturelle (variabilité interne du système climatique) et que l'impact anthropique y est trop faible pour l'instant pour y être détecté.

Mots clés : Hausse du niveau de la mer, changement climatique global, impacts, altimétrie spatiale, Argo, GRACE, variabilité régionale, fluctuations décennales, reconstruction du niveau de la mer, variabilité climatique naturelle, impacts anthropiques.

Regional Variability in Sea Level Rise

Author : Benoit Meyssignac.
PhD Advisors : Anny Cazenave and Rosemary Morrow.
Scientific Field : Space Oceanography.
Place and date of defense : Observatoire Midi-Pyrénées, the 19th of October, 2012.
Laboratory : LEGOS, UMR 5566 CNRS/CNES/IRD/UPS, OMP, 14 avenue Edouard Belin, 31400 Toulouse, France.

Summary : Over the XXth century, tide gauge records indicate a rise in global sea level of 1.7 mm.a^{-1}. For the past two decades, satellite altimetry data indicate a faster sea level rise of 3.2 mm.a^{-1} (period 1993-2011). Thanks to its global coverage, they also reveal a strong regional variability in sea level rise that is several times bigger than the global rise in many regions of the world. This regional signal, which must be added to the global sea level rise to compute the total sea level signal, is essential when assessing the potential impacts of sea level rise in coastal areas and low lying islands. In this thesis, we analyse the observed regional variability in sea level rise from satellite altimetry (since 1993), we propose a reconstruction of the past regional variability since 1950 (i.e. prior to altimetry) and we discuss its causes (thermal expansion of the ocean plus land ice loss) and origins (from natural or anthropogenic origin).

First, we analyse the contributions to the regional variability observed by satellite altimetry since 1993. The thermo-haline expansion of the ocean is estimated over this period. It shows that the regional variability in thermal expansion of the ocean explain most of the regional variability in sea level rise. The regional variability in ocean mass also plays a role locally but this role is difficult to estimate because its contribution to the regional variability in sea level rise is weak compared to the thermal expansion one. For the past decades, before the altimetry era, we reconstruct the sea level variations by combining tide gauge records with the principal spatial structures of the ocean deduced from ocean general circulation models. This method enables to reconstruct the 2 dimensional sea level variations since 1950 with a spatial coverage and resolution similar to the satellite altimetry ones.

In the second part of this thesis, the reconstruction method is applied to estimate the past regional variability in three regions which are particularly vulnerable to sea level rise : the tropical Pacific, the Mediterranean sea and the Arctic ocean. For each region, the reconstruction gives an estimation of the total (regional component plus global mean) 2-dimensional sea level rise over the past decades. For the sites where vertical crustal motion monitoring is available, we compute as well the total relative sea level (i.e. total sea level rise plus the local vertical crustal motion) since 1950. The objective is to provide estimates of the relative local sea level rise at climatic time scales to allow further studies on the coastal impacts of sea level rise.

In the last part of this thesis, the question of the origins of the regional variability in sea level rise is addressed. We examine whether the regional variability in observed sea level rise since 1993 is a consequence of the anthropogenic activity or if it results essentially from the natural variability of the climate system. We focus on the Tropical Pacific where the regional variability in sea level rise is particularly strong since 1993. On the basis of the reconstruction of the sea level variations since 1950, we show that the recent regional variability in sea level rise observed by satellite (over the last 17 years) in this region is not stationnary. It fluctuates with time, following some low frequency of the ENSO climate mode of variability. With the CMIP3 climate models, we show that this regional variability is dominated by the natural variability of the climate system (essentially by the internal variability of the climate system) and that the signature of the anthropogenic activity is still too weak in this region to be detected.

Keywords : Sea level rise, global climate change, impacts, satellite altimetry, Argo, GRACE, regional variability, decadal fluctuations, sea level reconstruction, natural climate variability, anthropogenic signature.

Table des matières

Introduction

Plusieurs dizaines de millions de personnes vivent aujourd'hui sur la fine bande littorale qui entoure les continents car elles sont attirées par le climat, les terres fertiles (en particulier dans les deltas), les infrastructures socio-économiques (transport, developpements touristiques, accés portuaires, pêcheries etc) ou encore le cadre de vie. A ces populations s'ajoutent celles qui vivent sur les îles océaniques qui ne dépassent pas le niveau de la mer de plus de quelques mètres. L'ensemble fait une quarantaine de millions de personnes environ, qui habitent aujourd'hui la proximité des océans (0.6% de la population mondiale, *Nicholls et al.* [2008]). Ce développement démographique des côtes s'est accompagné d'un développement économique considérable et les deux se sont accélérés au cours des 50 dernières années (*Nicholls et al.* [2008]). Cependant ceci s'est fait sans prendre en compte la montée rapide du niveau de la mer que l'on observe depuis plusieurs décennies.

Au cours des 4 derniers millénaires le niveau de la mer ne s'est pas élevé à plus de ± 0.5 mm.a^{-1}. En revanche, les observations des marégraphes historiques, installés le long des côtes, montrent une accélération du niveau de la mer depuis la fin du XIX$^{\text{ème}}$ siècle. Elles convergent vers une augmentation du niveau marin de 1.7 mm.a^{-1} au cours du XX$^{\text{ème}}$ siècle, soit une valeur 3 à 4 fois supérieure à celle des derniers millénaires. Sur les 20 dernières années, les observations par satellites altimétriques, Topex/Poseidon, Jason 1 et 2, indiquent une hausse globale du niveau de la mer encore plus forte : de 3.2 mm.a^{-1}.Elles ont aussi mis en évidence une forte variabilité régionale dans la hausse du niveau de la mer avec des régions comme l'Ouest du Pacifique tropical où le niveau de la mer augmente très vite (3 à 4 fois plus vite que la hausse du niveau global) et des régions où il stagne, voire même diminue légèrement depuis 1993, comme sur la côte Nord-Ouest des Etats-Unis. La forte accélération du niveau marin au cours du XX$^{\text{ème}}$ siècle est attribuée, pour sa majorité, au réchauffement global d'origine anthropique que l'on observe depuis plusieurs décennies (*Solomon et al.* [2007]). Elle a déjà engendré des impacts environn ementaux, économiques et sociétaux visibles sur certaines zones côtières en particulier du fait du développement intense de ces régions depuis les années 1950.

L'augmentation du niveau de la mer ne devrait pas ralentir dans un proche avenir. La plupart des scénarii de développement économique futur, utilisés pour estimer les projections climatiques du XXI$^{\text{ème}}$ siècle dans le 4$^{\text{ème}}$ rapport du GIEC, prévoient une augmentation des émissions anthropiques de gaz à effet de serre jusqu'aux années 2050, au moins. Dans ce contexte, les mêmes causes provoquant les mêmes effets, les modèles de climat indiquent que le niveau de la mer va continuer à augmenter de manière régulière jusqu'en 2100 et au delà. Le 4$^{\text{ème}}$ rapport du GIEC estime que les impacts associés seront

très importants (*Parry et al.* [2007]) et identifie la montée du niveau de la mer dûe au changement climatique comme l'un des défis majeurs auxquels sera confrontée l'humanité au cours du XXI$^{\text{ème}}$ siècle.

L'augmentation du niveau de la mer global depuis les années 1950, ses origines anthropiques et ses impacts significatifs ont été confirmés par de nombreuses études depuis le dernier rapport du GIEC (*Jevrejeva et al.* [2008]; *Cazenave and Llovel* [2010]; *Church and White* [2011]; *Church et al.* [2011] ; etc) et sont sans équivoques aujourd'hui. De même, la communauté scientifique s'accorde sur le fait que le niveau de la mer global va continuer à augmenter dans les décennies à venir. Cependant, de nombreuses incertitudes subistent en ce qui concerne la variabilité spatio-temporelle du niveau de la mer passée et future. Pourtant, c'est l'estimation et la compréhension détaillée de son amplitude et des échelles caractéristiques auxquelles elle évolue (dans le temps et dans l'espace) qui permettra de déterminer, à l'échelle régionale, les variations locales du niveau de la mer relatif et d'estimer précisement les impacts associés. Ma thèse s'intéresse à ce point précis : elle contribue à une meilleure estimation et compréhension de la variabilité régionale du niveau de la mer passé (qui se superpose à la hausse moyenne globale) et de son évolution dans le temps et l'espace. Elle traite aussi des causes qui génèrent la variabilité dans le niveau de la mer et cherche à déterminer si elles sont d'origine anthropique ou naturelle.

Ce manuscrit s'articule en 4 chapitres.

Le chapitre 1 consiste en une introduction générale sur les variations du niveau marin à toutes les échelles spatio-temporelles. Ce chapitre ne présente pas de travaux de thèse. Il résume les principaux résultats concernant les variations du niveau de la mer que l'on trouve dans la litterature. Après un rappel rapide sur les interactions fortes qui lient le niveau de la mer aux changements climatiques au cours des temps géologiques, nous nous focalisons sur les 150 dernières années. Nous passons en revue les différents moyens d'observation du niveau de la mer que sont les marégraphes et les satellites altimétriques. Nous exposons les variations du niveau de la mer global telles qu'elles sont observées par les marégraphes depuis 1850 et celles de sa variabilité régionale telle qu'elles sont observées par les satellites altimétriques depuis 1993. Nous en analysons les causes et nous présentons les projections attendues pour la fin du XXI$^{\text{ème}}$ siècle. Nous résumons à la fin de ce chapitre les enjeux scientifiques majeurs actuels qui sont liés à l'étude du niveau de la mer.

Les chapitres 2, 3 et 4 présentent les travaux de thèse. Le chapitre 2 présente les travaux que nous avons réalisés sur l'estimation de la variabilité régionale du niveau de la mer dans le passé et sur ses causes. Il est divisé en deux parties. La première partie se focalise sur la période altimétrique, de 1993 à aujourd'hui, pour laquelle nous disposons d'une mesure de la variabilité régionale du niveau de la mer grâce aux satellites altimétriques. Dans cette partie, nous montrons que la variabilité régionale du niveau de la mer s'explique essentiellement par la variabilité régionale du réchauffement océanique. Les variations de masse de l'océan jouent aussi un rôle mais qui est difficile à estimer de manière régionale du fait du faible signal. Cependant nous montrons que pour des régions assez grandes de l'ordre du demi-bassin océanique, ou pour des évènements intenses comme El Niño 1997/1998, ce signal peut être estimé précisement et sa contribution aux variations locales du niveau de la mer est non-négligeable. La deuxième partie du chapitre s'intéresse aux dernières décennies, pour lesquelles nous ne disposons que des mesures marégraphiques dont

l'échantillonnage spatial est très épars et inhomogène. Nous montrons qu'il est possible sur cette période, d'estimer la variabilité régionale du niveau de la mer en combinant les données marégraphiques avec les structures spatiales propres de l'océan déduites des modèles océaniques. Cette méthode permet de reconstruire le niveau de la mer en 2D depuis 1950 sur la majeure partie du globe. Elle donne une estimation convaincante de la variabilité régionale sur les dernières décennies quand on la compare à des données indépendantes, aux réanalyses océaniques ou à des méthodes plus anciennes de reconstruction. Ceci donne un outil efficace pour analyser les variations régionales du niveau de la mer aux échelles climatiques (30 ans et plus) et en déterminer les origines.

Dans le chapitre 3, nous appliquons la méthode de reconstruction pour estimer les variations passées du niveau de la mer 2D dans trois régions sensibles au réchauffement climatique : le Pacifique tropical, la mer Méditerranée et l'océan Arctique. Dans le Pacifique tropical où la variabilité régionale du niveau de la mer est extrêmement forte sur la période altimétrique, nous montrons que sur les dernières décennies (depuis 1950) la variabilité régionale est moins forte et présente des structures spatiales très différentes de celles observées sur la période altimétrique (20 dernières années). Ce résultat, confirmé par des marégraphes indépendants, nous permet d'estimer pour 9 îles de l'ouest du Pacifique, la montée relative du niveau de la mer depuis 1950. De cette manière, nous mettons en évidence que les variations climatiques du niveau de la mer ne sont, en général, pas le seul facteur qui joue dans l'augmentation locale du niveau de la mer : il y a aussi le mouvement de la croûte local d'origine naturelle ou anthropique. En mer Méditérranée, la reconstruction en 2D depuis 1970 révèle que les variations du niveau de la mer sont dominées par les variations du niveau moyen du bassin et que la variabilité régionale est faible en comparaison. Nous nous focalisons alors sur le niveau moyen et nous en estimons les composantes stérique et massique. Nous montrons que la composante massique est pilotée par l'évaporation au dessus du bassin et les entrées/sorties au détroit de Gibraltar. Nous montrons que l'augmentation du niveau de la mer en Méditerranée depuis 1970 est essentiellement d'origine massique et qu'elle est comparable en amplitude à celle du niveau global. Dans l'océan Arctique, nous analysons les variations du niveau de la mer depuis 1950 à partir des données des marégraphes Norvégiens et Russes. La moyenne des marégraphes indique une augmentation du niveau de la mer Arctique comparable à celle du niveau global depuis 1950. En revanche, le niveau de la mer Arctique semble avoir connu deux phases distinctes : une première phase jusqu'en 1990 durant laquelle le niveau est resté stable et une seconde phase, après 1990, marquée par une hausse très rapide. Ce résultat, visible à la fois dans les marégraphes Russes et Norvégiens, semble général à l'océan Arctique. Il est confirmé par l'altimétrie sur la période récente (depuis 1993) et par les données stériques dans le Nord de l'Atlantique. Les résultats préliminaires de la reconstruction 2D du niveau de la mer en Arctique confirment aussi cette accélération rapide à partir des années 1990 qui est générale au bassin Arctique.

Dans le dernier chapitre (chapitre 4), nous analysons l'origine de l'augmentation du niveau de la mer sur les dernières décennies pour déterminer si elle est anthropique ou naturelle. Ce chapitre se décompose en deux parties. Dans la première partie nous analysons les origines de l'augmentation du niveau de la mer global. Plusieurs études de la littérature ont quantifié l'impact des émissions anthropiques de gaz à effet de serre et des forçages naturels du système climatique (tel que la variabilité solaire ou volcanique) sur la variabilité des différents contributeurs à la hausse du niveau de la mer. Nous résumons ces études

et par une étude de bilan sur les dernières décennies, nous montrons que les émissions anthropiques de gaz à effet de serre sont impliquées dans au moins 65% de l'augmentation du niveau de la mer global. Dans la deuxième partie du chapitre, nous nous appuyons sur les reconstructions 2D du niveau de la mer pour développer la première étude de détection et attribution du signal anthropique sur la variabilité régionale du niveau de la mer. Nous nous focalisons sur le Pacifique tropical qui est marqué par une très forte variabilité régionale du niveau de la mer depuis 1993 et qui est particulièrement sensible au changement climatique du fait de la présence de nombreuses îles basses. Nous montrons que cette variabilité régionale récente (17 dernières années) n'est pas stable dans le temps mais qu'elle est en fait la phase haute d'une fluctuation basse fréquence (de période 25 à 30 ans) liée au mode de variabilité ENSO. Avec les modèles de climat du projet CMIP3, nous montrons que ces fluctuations relèvent essentiellement de la variabilité interne du système climatique : elles apparaissent de manière significative dans les simulations du climat qui n'intègrent pas les forçages extérieurs. De plus, leur variabilité est si forte dans la région du Pacifique tropical que l'introduction des forçages extérieurs d'origine naturelle ou anthropique ne fait pas apparaitre de modification significative jusqu'à aujourd'hui. Nous en concluons que la forte variabilité régionale observée par l'altimétrie aujourd'hui dans le Pacifique tropical est essentiellement d'origine naturelle (variabilité interne du système climatique) et que l'impact anthropique y est trop faible pour l'instant pour y être détecté. Ce résultat vient d'être confirmé très récemment dans la litterature.

Chapitre 1

Les variations du niveau de la mer des temps géologiques à nos jours

Dans ce chapitre, nous présentons une synthèse des connaissances actuelles sur les variations du niveau de la mer des temps géologiques à nos jours. Cette synthèse résume les principaux résultats sur le sujet que l'on trouve dans la littérature. Nous insistons plus particulièrement sur les résultats liés à la variabilité inter-annuelle à multi-décennale du niveau de la mer car c'est le thème central de cette thèse. Ce chapitre ne présente pas de travaux de thèse, il fait office d'introduction et pose les questions scientifiques actuellement ouvertes sur le sujet du niveau de la mer. Dans les chapitres suivants (2, 3 et 4), nous développons nos travaux de thèse et nous montrons les éléments de réponse qu'ils apportent à ces questions.

1.1 Les variations du niveau de la mer dans le passé

1.1.1 Aux échelles de temps géologiques

Les variations du niveau de la mer résultent des variations du volume d'eau des océans et/ou des variations de la forme des bassins océaniques (qui s'accompagnent aussi de variations de l'équipotentielle de gravité). Ces deux composantes font varier le niveau de la mer à des échelles de temps caractéristiques différentes et avec des amplitudes différentes (voir Fig.1.1, et par exemple *Pitman and Golovchenko* [1983]; *Miller et al.* [2005]). Aux échelles de temps géologiques longues, de 10^7 à 10^8 ans, ce sont les changements de forme des bassins océaniques, sous l'effet des processus tectoniques (production de plancher océanique et collision des continents) ou de la sédimentation, qui dominent les variations du niveau de la mer. A ces échelles de temps, les variations du niveau de la mer sont lentes (<0.01 $mm.an^{-1}$), de forte amplitude (>100 m) et sont principalement causées par les variations dans la production de plancher océanique (*Rowley* [2002]; *Cogné and Humler* [2004]; *Müller et al.* [2008]).

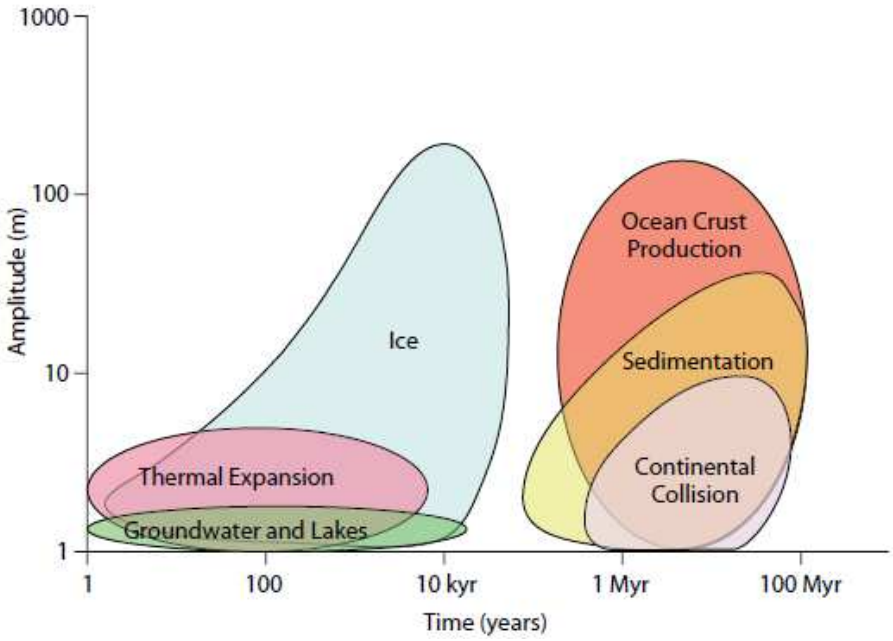

Figure 1.1 – Les causes des variations du niveau de la mer aux différentes échelles de temps et l'amplitude de leur impact sur les variations du niveau de la mer. Figure tirée de *Miller et al.* [2011].

En dessous de 10^6 ans, ce sont, au contraire, les variations du volume d'eau des océans qui dominent la variabilité du niveau de la mer (voir Fig. 1.1). En particulier pour des temps caractéristiques compris entre 10^3 et 10^6 ans, le principal mécanisme responsable des variations du niveau de la mer est la formation/disparition de calottes de glace continentales. A ces échelles de temps, elles sont responsables de variations rapides du niveau de la mer (jusqu'à 40 mm.an^{-1}, *Bard et al.* [2010]; *Deschamps et al.* [2012]) avec de fortes amplitudes ($>$ 100 m) (e.g. *Miller et al.* [2005, 2011]; *Rohling et al.* [2009]).

Il existe 3 types de données qui permettent de reconstruire les variations passées du niveau de la mer sur la dernière centaine de millions d'années : la datation des récifs coraliens, les mesures de l'isotope O^{18} de l'oxygène contenu dans les sédiments marins, la stratigraphie séquentielle. La datation précise (à l'uranium-thorium) des récifs coraliens permet d'obtenir des enregistrements du niveau de la mer qui remontent sur plusieurs centaines de milliers d'années avec une précision de ± 5 m (e.g. *Bard et al.* [1991]; *Bard et al.* [2010]). La mesure de l' isotope O^{18} de l'oxygène dans les sédiments marins donne une estimation du volume des glaces continentales et donc des variations de masse des océans (*Rohling et al.* [2004, 2007]; *Siddall et al.* [2003, 2006]). En effet la glace emmagasine preférentiellement l'isotope O^{16} de l'oxygène qui est plus léger, ainsi les formations/disparitions de calottes continentales se traduisent par des augmentations/diminutions de la proportion en isotope O^{18} dans les sédiments marins. Par cette technique, sont obtenues des mesures de variation du volume d'eau des océans qui remontent à -80 millions d'années sous réserve que les données soient corrigées des variations de température de l'océan (voir la courbe rouge sur la Fig. 1.2 et *Cramer et al.* [2009]). La stratigraphie séquentielle quand à elle, se fait essentiellement par analyse de la réflexion des ondes sismiques dans la croûte terrestre ou par carottage et permet de

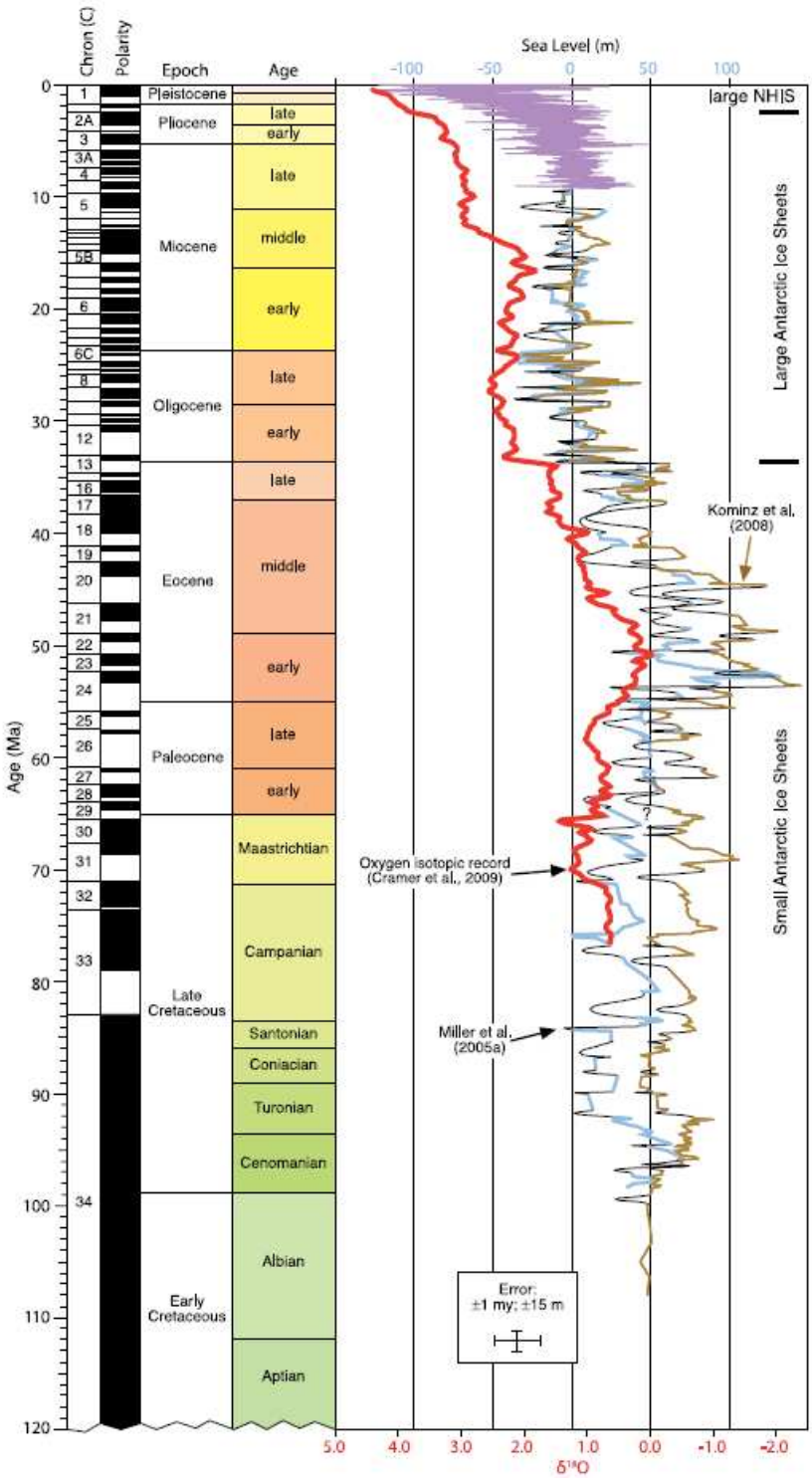

Figure 1.2 – Variations du niveau de la mer au New Jersey (USA) depuis 110 millions d'années estimées par *Miller et al.* [2005] et *Kominz et al.* [2008]. Ces courbes donnent une estimation du niveau de la mer global depuis 110 millions d'années. En rouge est superposée la synthèse de l'oxygène isotopique de *Cramer et al.* [2009]. (NHIS : Northern Hemisphere ice sheets. Ma : Millions of years ago). Figure tirée de *Miller et al.* [2011].

déterminer les dépôts sédimentaires qui se produisent sur les marges continentales lors des régressions/transgressions successives du niveau de la mer. Elle donne ainsi des informations sur les variations relatives du niveau de la mer qui remontent à plusieurs centaines de millions d'années (e.g. *Vail et al.* [1977]; *Haq and Al-Qahtani* [2005]; *Haq and Schutter* [2008]).

En combinant ces 3 types de données, corrigées des effets de charge et de compaction des sédiments ainsi que de la thermo-isostasie de la croûte terrestre, la courbe des variations du niveau de la mer global peut être reconstruite jusqu'à -110 millions d'années dans le passé (voir Fig. 1.2 et *Miller et al.* [2005]; *Kominz et al.* [2008]; *Cramer et al.* [2009]). Sur la Fig. 1.2 sont reproduites les courbes du niveau de la mer de *Miller et al.* [2005], de *Kominz et al.* [2008] et la courbe des variations en isotope O^{18} de *Cramer et al.* [2009]. Les 2 courbes de niveau de la mer de *Miller et al.* [2005] et de *Kominz et al.* [2008] sont globalement en accord. Elles montrent une amplitude de $\pm$100 m sur la période totale des 110 millions d'années et sont bien expliquées par les variations de masse de l'océan (voir la courbe de *Cramer et al.* [2009] sur la Fig. 1.2). Au cours des 2.6 derniers millions d'années, on peut observer de fortes variations du niveau de la mer qui suivent les âges de glace du Pliocène et du Pleistocène. Elles sont dûes à la formation/disparition de larges calottes polaires dans l'hémisphère Nord. Au cours des 780 000 dernières années, ces formations/disparitions se sont succédées environ tous les 100 000 ans à la fréquence d'oscillation de l'excentricité de la Terre et ont provoqué des fluctuations du niveau de la mer de $\pm$100 m (*Raymo and Mitrovica* [2012]). Auparavant (entre -780 000 ans et -2.6 millions d'années) elles se succédaient avec une période de $\sim$41 000 ans, correspondant à la période de précession de la Terre, et provoquaient des variations du niveau de la mer plus faibles de $\pm$60 m (*Lambeck et al.* [2002]; *Rohling et al.* [2009]; *Dutton et al.* [2009]).

1.1.2 Du dernier maximum glaciaire aux premières mesures marégraphiques

Lors du dernier maximum glaciaire, il y a environ 20 000 ans, le niveau de la mer global se situait $\sim$130 m plus bas que le niveau actuel (*Lambeck et al.* [2002]). Puis la fonte des calottes polaires de l'hémisphère Nord a provoqué une augmentation du niveau de la mer qui a duré plus de 10 000 ans, de -19 000 ans environ à -6 000 ans, comme le montre la Fig. 1.3. L'histoire de cette déglaciation est complexe (e.g. *Peltier* [2004]), et les indicateurs du niveau de la mer de type géologiques (érosion des falaises, géomorphologie des littoraux, etc) ou biologiques (corail, micro-atols, etc) montrent des périodes pendant lesquelles le niveau global a accéléré et d'autres périodes durant lesquelles il a décéléré. Par exemple, il y a $\sim$14 000 ans, le niveau de la mer a augmenté rapidement à un rythme prés de 40 $mm.a^{-1}$ (*Bard et al.* [2010]; *Deschamps et al.* [2012]). Au début de l'Holocène (il y a 11 000 ans), il a continué à augmenter mais significativement plus lentement puis il s'est stabilisé entre $\sim$-6 000 ans et $\sim$-2 000 ans (voir Fig.1.4 et *Lambeck et al.* [2010]).

Au cours des 2 000 dernières années, le niveau de la mer global n'a pas connu de larges fluctuations. La datation des micro-fossiles dans les marais maritimes (*Gehrels et al.* [2006a,b]; *Lambeck et al.* [2010]; *Leorri et al.* [2010]; *Kemp et al.* [2011]), et l'analyse des sites archéologiques (tels que les piscicultures romaines, *Lambeck et al.* [2004]) montrent

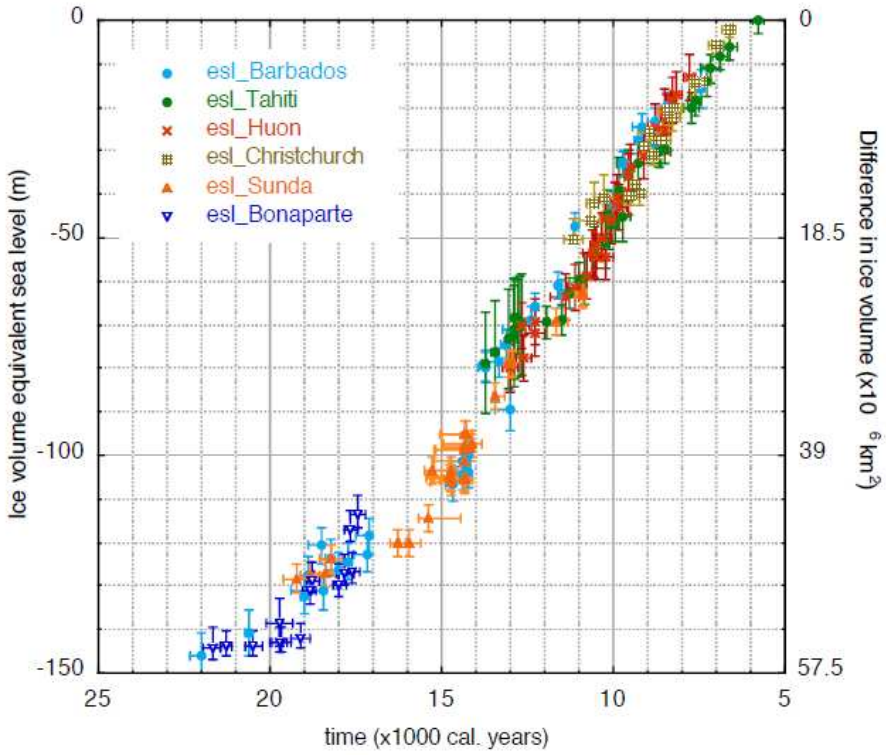

Figure 1.3 – Variations du volume de glace global et du niveau de la mer équivalent, du dernier maximum glaciaire à aujourd'hui. La figure est basée sur des données de niveau de la mer en différents endroits du globe, corrigées de la réponse isostatique locale de la croûte terrestre à la déglaciation. Figure mise à jour sur la base de *Lambeck et al.* [2002] avec de nouvelles données concernant le plateau continental de Sunda (*Hanebuth et al.* [2009]).

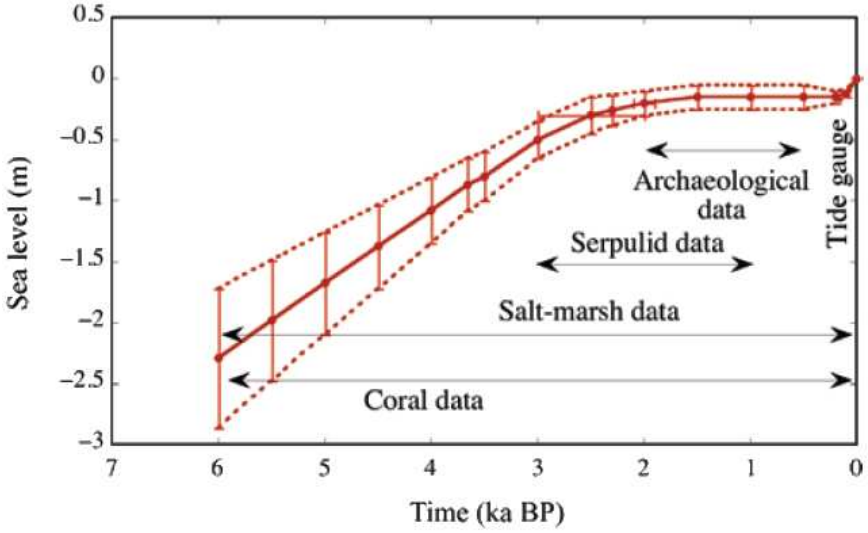

Figure 1.4 – Estimation des variations du niveau de la mer global entre -6000 ans et aujourd'hui à partir des données géologiques, archéologiques et marégraphiques (pour le XX^{ème} siècle). Figure tirée de *Lambeck et al.* [2010].

que le niveau de la mer n'a pas augmenté de plus de 0.5-0.7 mm.a^{-1} au cours des 2 derniers millénaires (voir aussi *Miller et al.* [2009]). La Fig. 1.5 (de *Kemp et al.* [2011]) qui montre le niveau de la mer des 2 000 dernières années sur la côte Est des Etats Unis, estimé à partir des micro-fossiles de marais maritimes, illustre bien ce fait. Selon cette étude, le niveau de la mer était plus haut de quelques décimètres durant l'optimum médiéval (du XII^{ème} au XIV^{ème} siècle) et plus bas d'un décimètre durant le petit âge glaciaire (du XVI^{ème} au XVIII^{ème} siècle). Mais les tendances du niveau global sont restées faibles jusqu'au début de l'ère industrielle (au milieu du XIX^{ème}siècle). A partir de cette époque, jusqu'à aujourd'hui, le niveau de la mer est marqué par une forte tendance positive (*Gehrels et al.* [2005, 2006a]; *Jevrejeva et al.* [2008]; *Kemp et al.* [2011]; *Woodworth et al.* [2011]). C'est à cette époque que commencent les mesures du niveau de la mer à l'aide d'instruments tels que les marégraphes puis plus tard, à partir des années 1990, avec les satellites altimétriques.

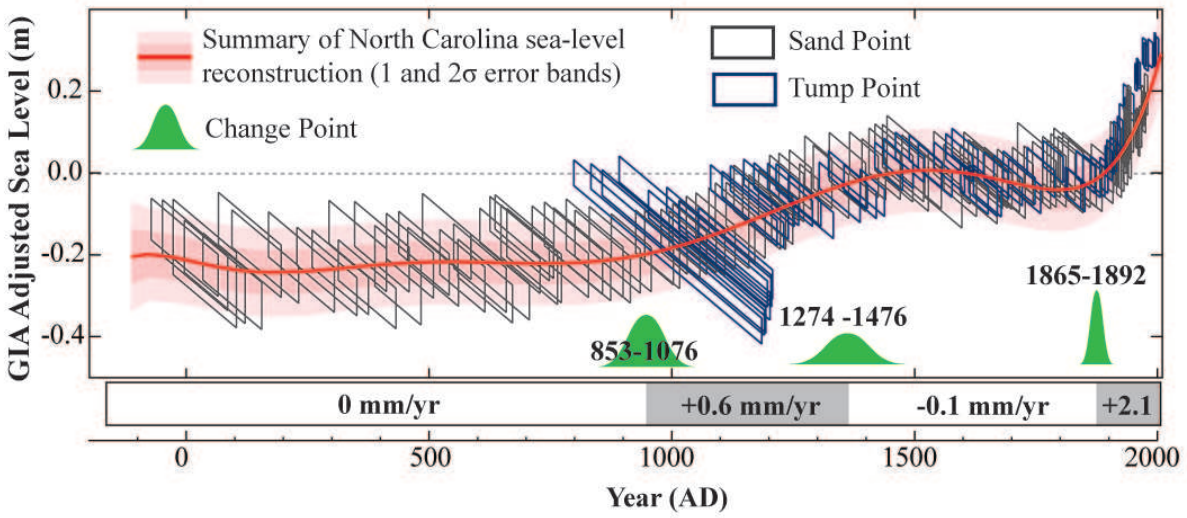

Figure 1.5 – Variations du niveau de la mer en Caroline du Nord au cours des 2 000 dernières années estimées à partir de l'analyse des micro-fossiles des marais maritimes. Figure tirée de *Kemp et al.* [2011].

1.2 Les variations du niveau de la mer depuis qu'il est mesuré

1.2.1 Les marégraphes

Les premiers marégraphes furent installés dans les ports Européens au XVIII$^{\text{ème}}$ siècle pour mesurer le marnage à leur entrée et faciliter l'accès des navires (*Mitchum et al.* [2010]). Jusque vers 1850, c'est essentiellement dans le Nord-Ouest de l'Europe que l'on trouve des enregistrements marégraphiques. Le marégraphe de Stockholm (Suède) délivre un enregistrement continu depuis 1774 (*Ekman* [1999]), celui de Liverpool (Angleterre) depuis 1768, celui de Brest (France) depuis 1807 (*Woppelmann et al.* [2006, 2008]) et celui de Swinoujscie (Pologne) depuis 1811. D'autres enregistrements remontant au XVIII$^{\text{ème}}$ siècle se sont arrêtés depuis. Le marégraphe d'Amsterdam donne un enregistrement de 1700 à 1925 et celui de Kronstadt de 1773 à 1993.

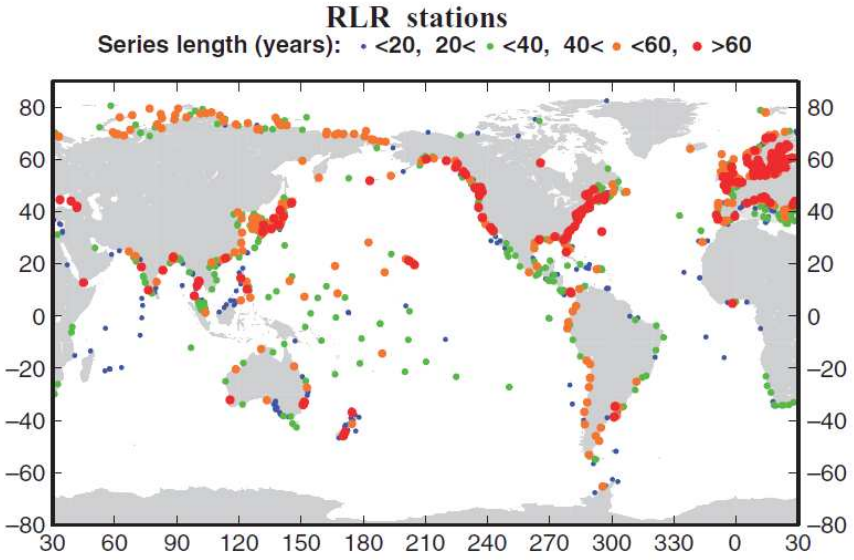

Figure 1.6 – Répartition géographique et longueur des enregistrements marégraphiques collectés par le Permanent Service for Mean Sea Level (*Woodworth and Player* [2003]). Figure adaptée de *Mitchum et al.* [2010].

Au cours du XIX$^{\text{ème}}$ siècle, le réseau marégraphique s'est progressivement densifié et en particulier, le niveau de la mer commence à être mesuré dans l'hémisphère Sud (voir Fig. 1.6). Il existe à Port Arthur en Tasmanie (Australie) un enregistrement qui remonte à 1841 (*Hunter et al.* [2003]). A Fremantle (Australie) un enregistrement continu remonte à 1897 tandis que celui de Sydney (Australie), continu lui aussi, remonte à 1886. Malgré cette densification, le nombre d'enregistrements présentant plus de 60 ans de données reste petit et leur répartition géographique est fortement biaisée vers l'hémisphère Nord (voir Fig. 1.6). De plus, la majorité des enregistrements marégraphiques présente des trous de mesures de plusieurs années voire dizaines d'années et ils sont souvent pollués par des discontinuités liées à la maintenance du matériel. Combinés, ces deux facteurs font

que très peu de marégraphes sont utilisables pour des études du niveau de la mer aux échelles climatiques et ils sont inégalement répartis sur le globe. Déduire de ces données des estimations des variations historiques du niveau de la mer n'est donc pas simple. C'est un problème scientifique qui a fait l'objet de nombreuses publications au cours des dernières décennies (e.g. *Douglas et al.* [2001]) et qui est encore très activement étudié aujourd'hui (*Mitchum et al.* [2010]).

Les marégraphes fournissent une mesure du niveau de la mer relative au sol sur lequel ils sont fixés. Dans leurs mesures ils n'enregistrent donc pas seulement les variations du niveau de la mer mais aussi celles du sol. Or, en général, le niveau du sol varie. Sur l'ensemble du globe par exemple, le rebond post-glaciaire qui est la réponse visco-élastique de la croûte terrestre à la dernière déglaciation (appelé Glacial Isostatique Adjustment -GIA- en anglais) génère des mouvements verticaux de la croûte terrestre de 0.1-10 $mm.a^{-1}$ (*Peltier* [2004]; *Lambeck et al.* [2010]; *Tamisiea and Mitrovica* [2011]). Localement, dans de nombreuses régions du monde, le sol s'affaisse pour des raisons naturelles (e.g. dans les deltas des grands fleuves, le sol s'affaisse sous la charge des sédiments fluviaux) ou du fait des activités humaines telles que le pompage de l'eau et des hydrocarbures (suite au pompage, les sédiments se compactent et le sol s'affaisse, voir *Syvitski et al.* [2009]). Dans les régions d'activité tectonique ou volcanique le niveau du sol varie aussi : il suit les mouvements locaux de la croûte terrestre soumise aux forces internes de la Terre (*Kontogianni et al.* [2002]; *Meltzner et al.* [2006]; *Shaw et al.* [2008]). Ces mouvements sont importants à prendre en compte lorsqu'on cherche à estimer localement les variations du niveau de la mer relatif total. Il faut savoir aussi les estimer et les séparer lorsque l'on cherche à calculer les variations historiques du niveau de la mer en relation avec le climat. Ceci ajoute à la complexité des mesures marégraphiques.

Pour contourner cette complexité, plusieurs stratégies ont été développées afin de déduire des mesures marégraphiques une courbe historique du niveau de la mer global "absolu". Une première stratégie a consisté à selectionner un très petit nombre de marégraphes (quelques dizaines) situés dans des régions tectoniquement stables et pour lesquels on disposait de plus de 60 ans d'enregistrement de bonne qualité (i.e. sans discontinuités, ni trous). Les auteurs qui ont suivi cette stratégie ont ensuite corrigé les marégraphes du GIA seulement, et ont déduit le niveau global de la mer par moyennation des enregistrements marégraphiques (*Douglas* [1991]; *Douglas et al.* [2001]; *Gornitz and Lebedeff* [1987]; *Peltier et al.* [2001]; *Holgate* [2007]). D'autres auteurs, au contraire, ont cherché à utiliser un jeu de marégraphes plus grand avec des enregistrements provenant de nombreuses régions et couvrant des périodes différentes. Pour compenser l'hétérogénéité de leur jeu de données, ils ont proposé des méthodes de moyennation plus complexes pour en déduire le niveau global. Par exemple *Jevrejeva et al.* [2006, 2008] utilise un critère de cohérence régionale entre les enregistrements marégraphiques d'une même zone afin d'éliminer, avant moyennation, les enregistrements suspects (enregistrements affectés par exemple par des mouvements verticaux de la croûte importants ou encore affectés par des sauts inexpliqués et absents dans les marégraphes voisins). *Church et al.* [2004]; *Church and White* [2006, 2011] ont développé quand à eux une méthode de reconstruction du niveau global dans laquelle la moyennation des marégraphes est pondérée par les modes principaux de variabilité de l'océan déduits de l'altimétrie spatiale (voir section 2.2.2). Les deux stratégies donnent des résultats différents (voir Fig. 1.7). Néanmoins, malgré leurs différences, elles convergent vers des estimations

similaires de la tendance du niveau de la mer à 1.7 ± 0.3 mm.a^{-1} sur la période 1950-2000 et sur le XX^{ème} siècle.

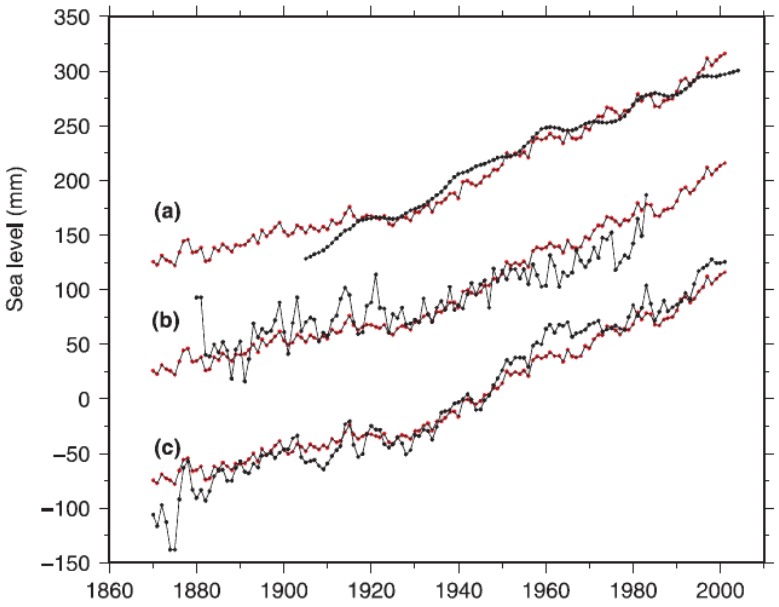

Figure 1.7 – Courbes du niveau de la mer global à partir des données marégraphiques depuis 1870, adaptées de *Woodworth et al.* [2009]. La courbe rouge est la courbe reconstruite de *Church and White* [2006]. Les autres courbes (en noir) sont de a) *Holgate* [2007], b) *Gornitz and Lebedeff* [1987] et c) *Jevrejeva et al.* [2006].

Les études des enregistrements marégraphiques ont aussi montré qu'il y avait eu une accélération de la hausse du niveau de la mer entre le XIX^{ème} et le XX^{ème} siècle. Cette accelération était déjà visible dans les données issues de l'analyse des marais maritimes (voir section 1.1.2). Elle a été mise en évidence dans l'analyse, un à un, des enregistrements marégraphiques les plus longs d'Europe (*Douglas* [1992]; *Gornitz and Solow* [1991]; *Woodworth* [1999]). Dans l'analyse du niveau global de la mer, *Church and White* [2006] trouvent aussi une accélération significative de la hausse du niveau de la mer à 0.013 ± 0.006 mm.a^{-2} sur la période 1870-2001. De même, *Jevrejeva et al.* [2006] avec une méthode alternative qui sépare les fluctuations à 2-30 ans des tendances long-terme dans le niveau de la mer, trouve une accélération du niveau de la mer, mais qui pourrait avoir commencé plus tôt, vers 1800 (*Jevrejeva et al.* [2008]) . Outre cette accélération, ces différentes études ont toutes mis en évidence des variations décennales des tendances du niveau de la mer globale avec des périodes durant lesquelles la montée du niveau de la mer s'accélère (e.g. après 1930) et des périodes durant lesquelles elle décélère (e.g. dans les années 1960). Néanmoins certaines de ces variations pourraient être dûes à la faible couverture spatiale des marégraphes (*Merrifield et al.* [2009]).

Une limitation importante de toutes les études citées précédemment, est que, faute de données, elles ne corrigent pas les enregistrements marégraphiques de tous les mouvements verticaux du sol qui les affectent. En effet, elles ne prennent en compte que le GIA (dont on a une estimation globale grâce aux modèles). Cependant, depuis quelques années, l'instal-

lation de balises GPS (Global Positionning System) sur des sites marégraphiques a permis d'obtenir une mesure directe des mouvements du sol à la base de ces marégraphes. Cette approche a été utilisée par *Woppelmann et al.* [2007, 2009]. Même si les enregistrements GPS sont encore courts (de 10 à 15 ans environ), il est généralement admis qu'ils permettent déjà de déterminer les tendances long-terme affectant le mouvement des sols localement (*Woppelmann et al.* [2007]). En appliquant les corrections du mouvement des sols observé, *Woppelmann et al.* [2009] obtient une tendance du niveau de la mer de 1.61 ± 0.19 mm.a^{-1} sur le XX$^{\text{ème}}$ siècle. Ceci confirme les résultats obtenus par les études précédentes.

1.2.2 L'altimétrie spatiale

Depuis le milieu des années 1970, le niveau de la mer est mesuré par des satellites altimétriques. Les premiers altimètres satellites (GEOS3, SEASAT et GEOSAT) ne disposaient pas d'une précision suffisante pour étudier les variations du niveau de la mer. Ils ont servi principalement à l'étude du géoïde marin et des fonds océaniques (*Cazenave and Royer* [2001]). A partir d'octobre 1992 en revanche, une amélioration considérable de l'estimation des orbites et des techniques de mesure embarquée a permis la création d'une nouvelle génération de satellites altimétriques qualifiés de "haute précision" qui ont permis l'étude des variations du niveau marin aux échelles mensuelles à multi-décennales (dont l'amplitude est de l'ordre de 10 cm, voir Fig. 1.8). C'est la série de Topex-Poséidon, Jason-1/2, ERS-1/2 et Envisat (*Chelton* [2001]; *Fu and Cazenave* [2001]).

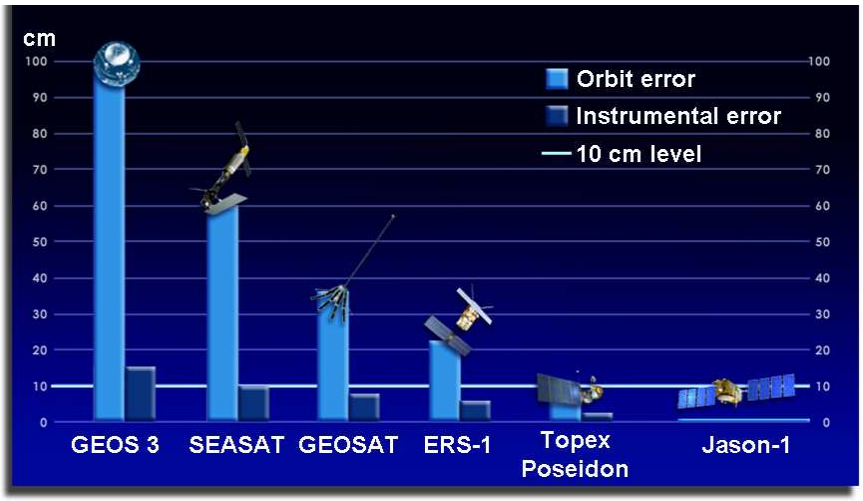

Figure 1.8 – L'évolution de la précision des satellites altimétriques de 1975 à 2000. Source : CNES/AVISO.

La mesure altimétrique par satellite se déroule de la manière suivante (voir Fig. 1.9) : le radar altimètre, à bord du satellite, émet un signal micro-onde radar en direction de la surface de la mer qui reflète une partie de cette onde vers le satellite. La mesure du trajet aller-retour de l'onde permet le calcul de la distance du satellite à la surface instantanée de la mer. La hauteur locale de la mer est déduite ensuite de la différence entre la distance du satellite au centre de masse de la Terre (calculée par orbitographie précise) avec la distance

du satellite à la surface instantanée de la mer (calculée avec la mesure du radar altimètre). Dans le cas des satellites altimétriques de haute précision, l'orbitographie précise donne une mesure très fine de la distance du satellite au centre de masse de la Terre grâce aux instruments GPS et DORIS (Doppler Orbitography and Radiopositioning Integrated by Satellite) embarqués à bord.

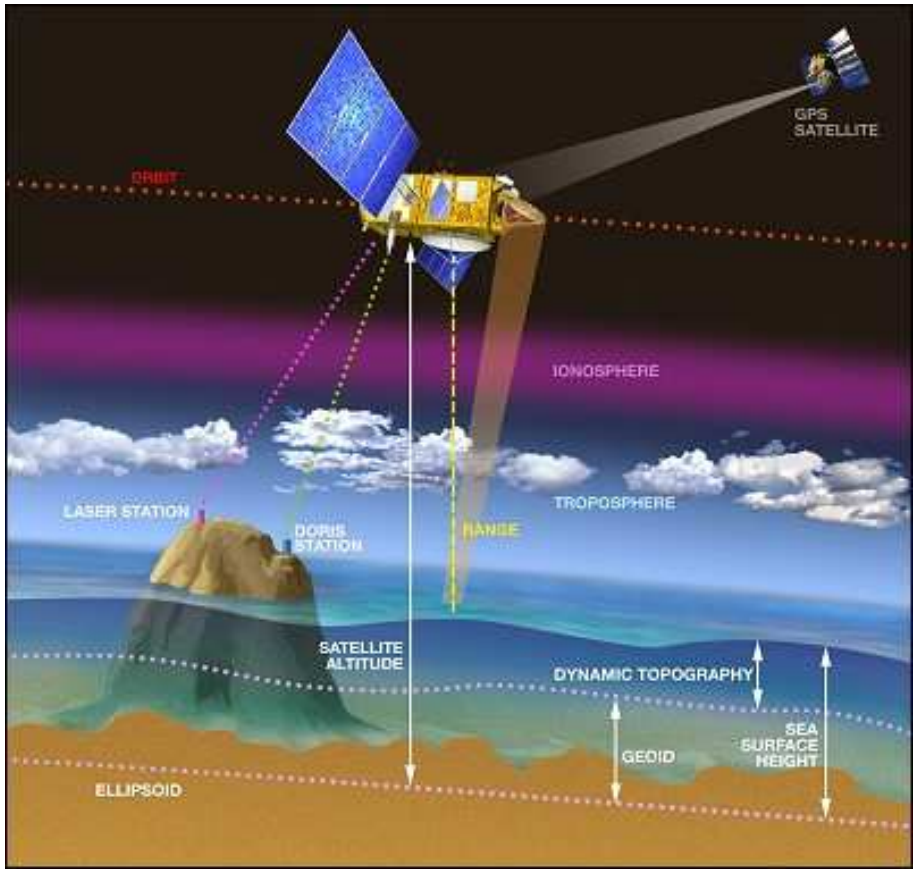

Figure 1.9 – Principe de la mesure par satellite altimétrique. Source : CNES/AVISO.

La mesure de hauteur de mer doit être corrigée de différents retards dans le trajet de l'onde radar, dûs à la traversée de la troposphère et de l'ionosphère. Elle doit aussi être corrigée de biais entre la surface moyenne apparente de la mer observée par reflection électromagnétique de l'onde radar et la surface moyenne de la mer réelle, à l'interface air-mer (en effet la présence de vagues à la surface de la mer introduit un biais dans la surface moyenne de la mer observée car les creux des vagues participent plus à la reflection nadir de l'onde radar que leurs crêtes ; l'écho radar retour est alors, en proportion, composé de plus de signal venant des creux des vagues que de leur crêtes ce qui fait apparaitre, après moyennation, une surface de mer anormalement basse). D'autres corrections dûes à des effets géophysiques tels que les marées de la Terre solide, les marées polaires ou océaniques sont aussi appliquées.

Les satellites altimétriques couvrent l'ensemble du globe en quelques jours appelés cycle orbital (le cycle orbital est de 10 jours pour la série Topex-Poséidon, Jason-1 et Jason-2, voir Fig. 1.10, et il est de 35 jours pour ERS-1/2 et Envisat). La moyennation spatiale de toutes les mesures locales de hauteur de mer au cours d'un cycle orbital donne une

mesure du niveau de la mer global. En compilant les mesures des cycles orbitaux successifs on obtient une courbe du niveau global de la mer au cours du temps. Comme le satellite survole les même points géographiques d'un cycle orbital à l'autre, il est aussi possible de construire pour chaque point géographique survolé, une courbe temporelle du niveau de la mer local et donc de déduire globalement la variabilité régionale du niveau de la mer.

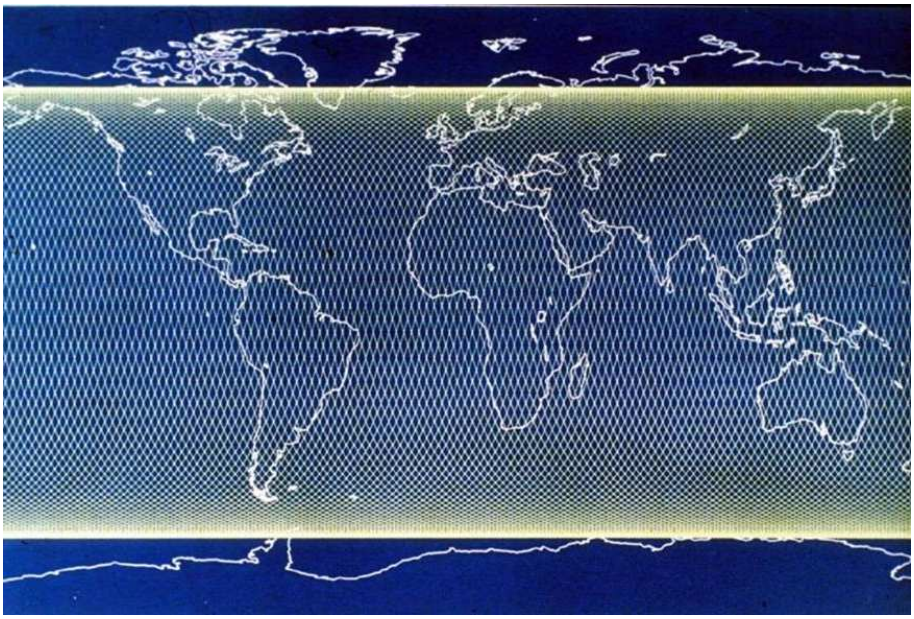

Figure 1.10 – Couverture géographique des satellites Topex-Poséidon, Jason-1 et Jason-2 au cours d'un cycle orbital de 10 jours. Source : CNES/AVISO.

La précision de la mesure de hauteur de mer par la série de satellites Topex-Poséidon, Jason-1 et Jason-2 atteint aujourd'hui les 1-2 cm (e.g. *Ablain et al.* [2009]; *Nerem et al.* [2010]; *Beckley et al.* [2010]; *Mitchum et al.* [2010]). Moyennées spatialement, ces mesures donnent une tendance du niveau global de la mer précise à environ 0.5-0.6 mm.a^{-1}. Cette barre d'erreur est estimée par analyse du bilan d'erreur total de la chaîne de mesure altimétrique et elle est confirmée par comparaison avec les mesures marégraphiques (*Ablain et al.* [2009]). Elle est le fruit d'une analyse et d'un contrôle rigoureux menés depuis 18 ans pour corriger les dérives instrumentales des satellites car celles-ci se traduisent dans la mesure altimétrique par des dérives sur les corrections appliquées qui biaisent la tendance du niveau de la mer global.

La Fig. 1.11 présente le niveau de la mer global mesuré par les satellites altimétriques superposé sur la courbe du niveau de la mer global au cours du XX$^{\text{ème}}$ siècle reconstruite par *Church and White* [2011] à partir des enregistrements marégraphiques. La courbe altimétrique présente une augmentation du niveau de la mer quasiment linéaire sur toute la période 1993-2011 sauf autour de l'évènement El Niño de 1997/1998 et des évènements La Niña de 2007/2008 et 2010/2011. Sur cette période de 18 ans (1993-2011), la tendance du niveau de la mer global mesuré par altimétrie s'élève à 3.2 $\pm$ 0.5 mm.a^{-1} (e.g. *Cazenave and Llovel* [2010]; *Nerem et al.* [2010]; *Mitchum et al.* [2010]). Cette valeur de la tendance est corrigée de l'impact du GIA sur le niveau global de la mer qui s'élève à -0.3 mm.a^{-1} (voir section 1.3.3). Les deux courbes de niveau global de la mer déduites des marégraphes et de l'altimétrie diffèrent en variabilité inter-annuelle (voir Fig. 1.11). Cependant en tendance,

sur ces échelles de temps de 10 ans et plus, elles sont en accord (*Prandi et al.* [2009]; *Ablain et al.* [2009]). Les différences observées dans la variabilité inter-annuelle pourraient s'expliquer par l'échantillonnage spatial hétérogène des marégraphes (*Prandi et al.* [2009]). Enfin, il est intéressant de noter que sur les 18 dernières années, la tendance du niveau de la mer global est significativement supérieure à la tendance de 1.7 mm.a^{-1} donnée par les marégraphes sur les périodes 1950-2000 et 1900-2000. Ceci suggère une accélération du niveau de la mer global (*Merrifield et al.* [2009]) à considérer cependant avec précaution étant donné la variabilité décennale que l'on peut trouver dans les tendances du niveau de la mer (voir section 1.2.1).

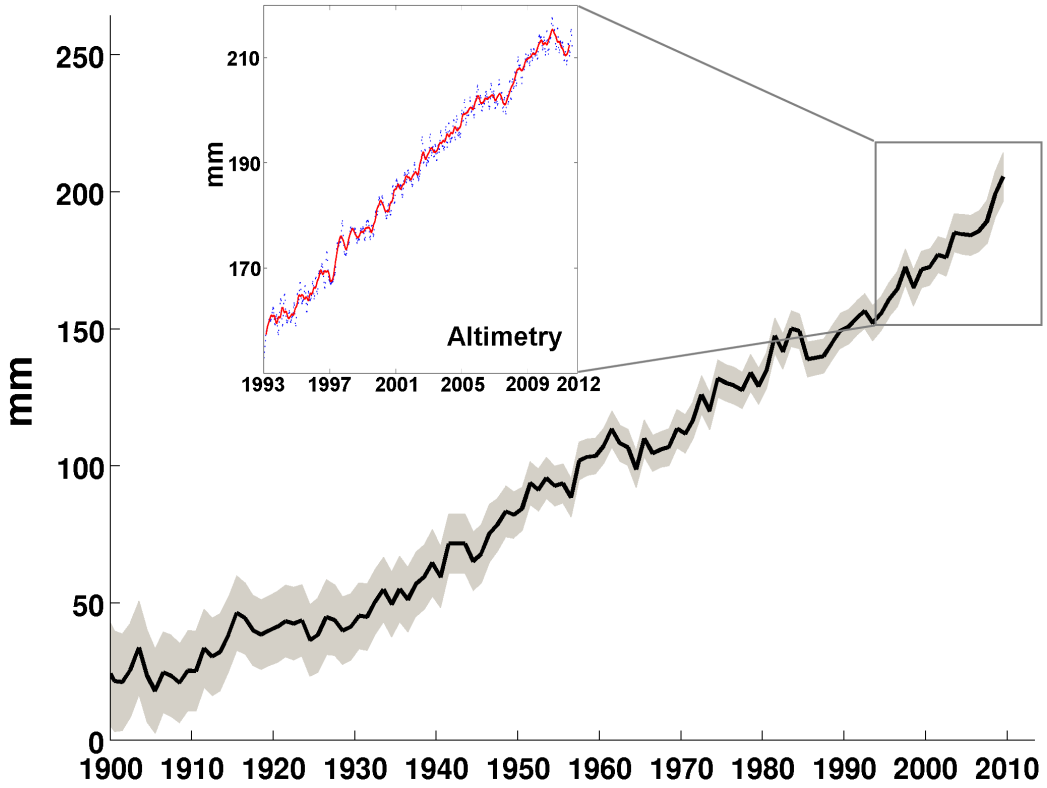

Figure 1.11 – Courbes du niveau de la mer global. En noire est reproduite la courbe reconstruite par *Church and White* [2011] à partir des marégraphes (voir section 1.2.1). La région grisée indique la barre d'erreur à 1σ de la courbe noire. Dans l'encart, la courbe rouge donne le niveau de la mer global calculé à partir des données altimétriques de 1993 à 2011. Les points bleus indiquent les données de chaque cycle orbital. La courbe rouge est une moyennation à 3 mois de ces données. (Les données ont été obtenues du site AVISO : http ://www.aviso.oceanobs.com/en/data/products/sea-surface-height-products/global/msla/index.html). Figure adaptée de *Meyssignac et al.* [2012].

La couverture quasi-globale des satellites altimétriques permet de calculer des cartes de la variabilité régionale du niveau de la mer et de ses tendances. Ceci a révélé que l'augmentation du niveau de la mer était loin d'être uniforme. Dans certaines régions (comme à l'Ouest de l'océan Pacifique) le niveau de la mer augmente 3 à 4 fois plus vite

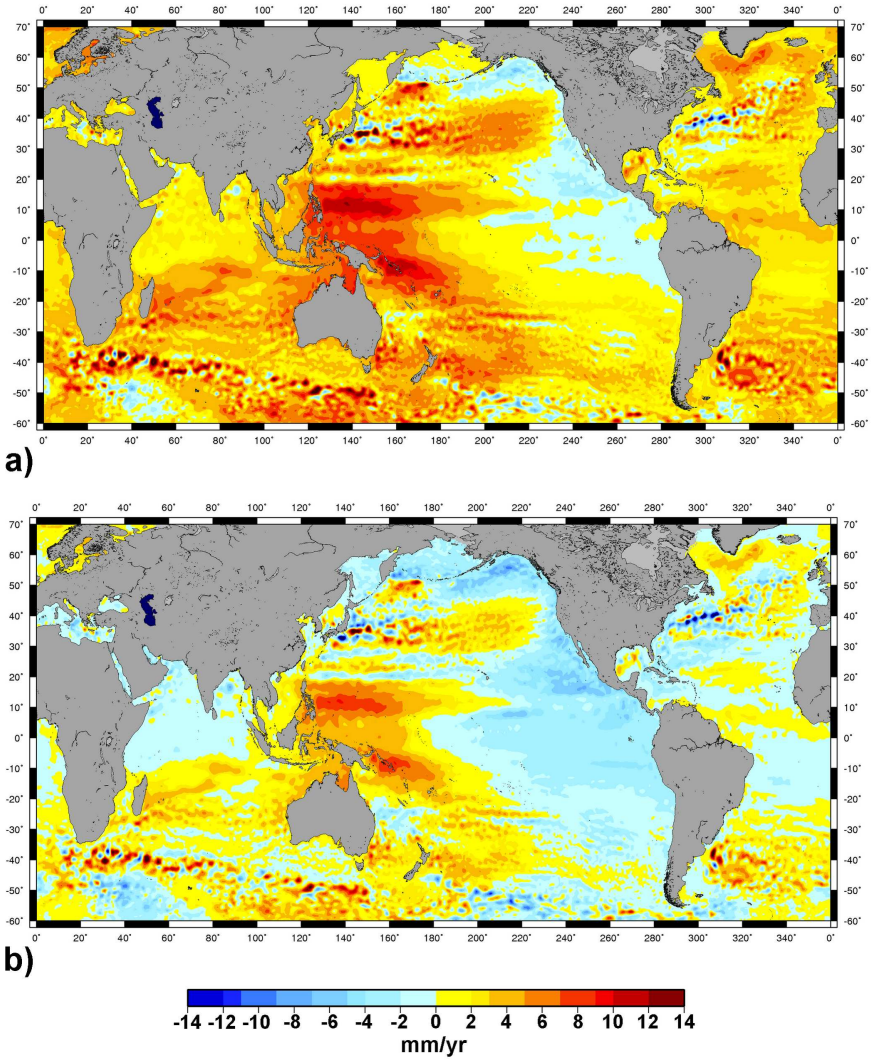

Figure 1.12 – a) Tendances du niveau de la mer calculées à partir des données altimétriques sur la période 1993-2011. b) Même figure que a) sauf que la tendance du niveau global de la mer de 3.2 mm.a^{-1} a été retirée. Figure adaptée de *Meyssignac and Cazenave* [2012].

que la moyenne globale depuis deux décennies. Dans d'autres régions, au contraire, les tendances du niveau de la mer sont plus faibles que celle de la moyenne globale. Elles peuvent même être légèrement négatives à certains endroits (e.g. dans l'est de l'océan Pacifique). La Fig. 1.12a montre les tendances du niveau de la mer calculées à partir des données altimétriques sur la période 1993-2011. Lorsqu'on soustrait aux tendances régionales, la tendance du niveau global de la mer (3.2 mm.a^{-1}), la forte variabilité régionale du niveau de la mer devient encore plus évidente : voir la Fig. 1.12b. Dans des régions telles qu'à l'Ouest et au Nord du Pacifique, le Sud de l'océan Indien ou encore l'océan Atlantique juste au Sud du Groenland, la variabilité régionale est si forte qu'elle y domine, en fait, le signal total de niveau de la mer sur la courte période 1993-2011. Il apparaît ainsi clair, depuis l'altimétrie spatiale, que dans l'estimation du niveau de la mer local, la contribution de la variabilité régionale est essentielle. Ceci est en particulier vrai pour toutes les études sur les impacts de la hausse du niveau de la mer.

1.3 Les causes des variations du niveau de la mer (échelle inter-annuelle à multi-décennale ; global et régional).

Les deux principales causes des variations du niveau de la mer aux échelles inter-annuelles à multi-décennales sont l'expansion thermique de l'océan et l'apport d'eau douce des continents aux bassins océaniques. L'expansion thermique moyenne globale est une conséquence du réchauffement de l'océan tandis que l'apport d'eau douce est le résultat de la fonte des glaces continentales (i.e. fonte des glaciers de montagne et perte de masse des calottes polaires) et des échanges d'eau avec les bassins fluviaux. D'autres facteurs, liés par exemple aux déformations des bassins océaniques suite à la fonte des glaces actuelles et passées (dernier maximum glaciaire), jouent aussi un rôle, mais il est secondaire. Les tendances récentes des contributions de l'expansion thermique et de la fonte des glaces ont pour cause, essentiellement, le changement climatique global induit par les émissions anthropiques de gaz à effet de serre. Cependant, la variabilité inter-annuelle à multi-décennale reste très influencée par la variabilité interne du système climatique et les forçages naturels (variabilité solaire et volcanique).

1.3.1 L'expansion thermique des océans et les variations de salinité

a - L'expansion thermique des océans

Les anomalies de température et de salinité dans l'océan changent la densité des colonnes d'eau et donc leur hauteur. Ceci donne lieu à des variations du niveau de la mer que l'on qualifie de "stériques" ("thermostérique" quand il s'agit de variations dûes aux anomalies de température uniquement et "halostérique" si elles sont dûes aux anomalies de salinité uniquement).

Les mesures hydrographiques de température et de salinité, collectées par les navires marchands et les campagnes océanographiques depuis le milieu du XX$^{\text{ème}}$ siècle, ont montré que, globalement, l'océan se réchauffe ($+0.0017^{\circ}$C.a^{-1} entre 0 et 700m de profondeur et $>+0.01^{\circ}$C.a^{-1} entre 0 et 75m de profondeur en moyenne sur la période 1967-2010 d'après les données de *Levitus et al.* [2009]). Depuis la fin des années 1960, la température de l'océan a été essentiellement mesurée par des bathythermographes jetables (expendable bathythermographs -XBT- en anglais) le long des routes des navires marchands. A ces mesures s'ajoutent les mesures par bathythermographes mécaniques (MBT) et les systèmes Conductivité-Température-Profondeur (Conductivity-Temperature-Depth -CTD- en anglais) (*Levitus* [1994]; *Boyer et al.* [2009]; *Levitus et al.* [2009]). Depuis le début des années 2000, un programme international de bouées profilantes, Argo (voir http ://www.argo.ucsd.edu, *Roemmich et al.* [2009]), a été mis en place progressivement. Depuis la fin du déploiement en 2005, il fournit des mesures de température et de salinité jusqu'à 2000 m de profondeur avec une répétitivité de l'ordre de 10 jours et une couverture globale de 3°x3°.

L'ensemble des données in-situ, historiques et actuelles, est maintenu et mis à jour dans plusieurs bases de données : le World Ocean Database (WOD, *Boyer et al.* [2009]), Coriolis (http ://www.coriolis.eu.org/), USGODAE (http ://www.usgodae.org/argo/argo.html)...

Les données historiques présentent deux problèmes majeurs. D'une part, les données XBT ont un biais systématique qui vient de l'incertitude sur la profondeur à laquelle ont été prises les mesures de température. Cette incertitude vient du fait que les instruments XBT ne mesurent pas la profondeur lors de leur trajet vers le fond. Elle est en fait déduite de l'équation de la trajectoire du XBT et du temps écoulé depuis son entrée dans l'eau. Même avec des équations de trajectoire calibrées (*Hanawa et al.* [1995]), il reste des biais systématiques dans l'estimation de la profondeur (*Gouretski and Koltermann* [2007]). D'autre part les données historiques de température ont une faible couverture géographique et descendent en général peu profond (∼700 m). De plus cette couverture spatiale se dégrade quand on remonte dans le temps. Il est difficile de remédier à ce problème. Une solution consiste à utiliser des Modèles de Circulation Générale Océanique -OGCM- qui assimilent les données aux dates et lieux où elles sont disponibles et comblent l'absence de mesure dans les autres régions sur la base des équations de Navier - Stokes (voir section 2.2.1). Les estimations de l'expansion thermique sont donc biaisées par le manque de données dans certaines régions telles que l'hémisphère Sud par exemple (*Levitus et al.* [2005]; *Antonov et al.* [2005]).

Malgré ces limitations, plusieurs équipes ont proposé une estimation des températures de l'océan à l'échelle du globe ces dernières années : *Domingues et al.* [2008]; *Guinehut et al.* [2004]; *Ishii et al.* [2006]; *Ishii and Kimoto* [2009]; *Levitus et al.* [2005, 2009, 2012]; *Willis et al.* [2004]. Les études récentes prennent en comptent les corrections de biais systematique des XBT et MBT. Ce sont celles que nous résumons ici : *Domingues et al.* [2008]; *Ishii and Kimoto* [2009]; *Levitus et al.* [2009]. Comparées aux études antérieures, les nouvelles analyses montrent une variabilité inter-annuelle et multi-décennale de l'expansion thermique significativement différente (voir la Fig. 1.13), en particulier dans les années 1970. Sur la période 1955-2000, on observe une tendance positive dans l'expansion thermique de 0.4 ± 0.01 mm.a^{-1} pour *Levitus et al.* [2009, 2012] et 0.3 ± 0.01 mm.a^{-1} pour *Ishii and Kimoto* [2009]. *Domingues et al.* [2008] estiment quand à eux, une tendance de 0.5 ± 0.08 mm.a^{-1} sur la période 1961-2003.

Sur la période 1955-2000, l'expansion thermique des 700 premiers mètres de l'océan explique donc ∼25% de la tendance à 1.7 mm.a^{-1} du niveau de la mer. Pour l'océan profond, les estimations entre 1955 et 2000 sont moins fiables du fait du manque de données en particulier dans les années 1950 et 1960. Entre 700 et 3000 m, la moyenne globale de l'expansion thermique de l'océan est estimée par corrélation avec l'expansion thermique des couches supérieures (0-700m). La corrélation est calibrée sur la période récente pour laquelle les données en profondeur sont plus nombreuses, puis elle est étendue au passé pour couvrir la période durant laquelle les données profondes sont moins nombreuses. A partir des données de *Levitus et al.* [2009] et *Ishii and Kimoto* [2009] sur la période 1955-2000, ceci donne une contribution respective de 0.07 ± 0.1 mm.a^{-1} et 0.05 ± 0.1 mm.a^{-1} au niveau de la mer. En dessous de 3000 m, les données sont encore plus rares si bien que *Levitus et al.* [2009] et *Ishii and Kimoto* [2009] ne donnent pas d'estimation du réchauffement à ces profondeurs. Les seules mesures dont on dispose viennent soit des campagnes océanographiques régulières le long de transects de référence, réalisées depuis 2 à

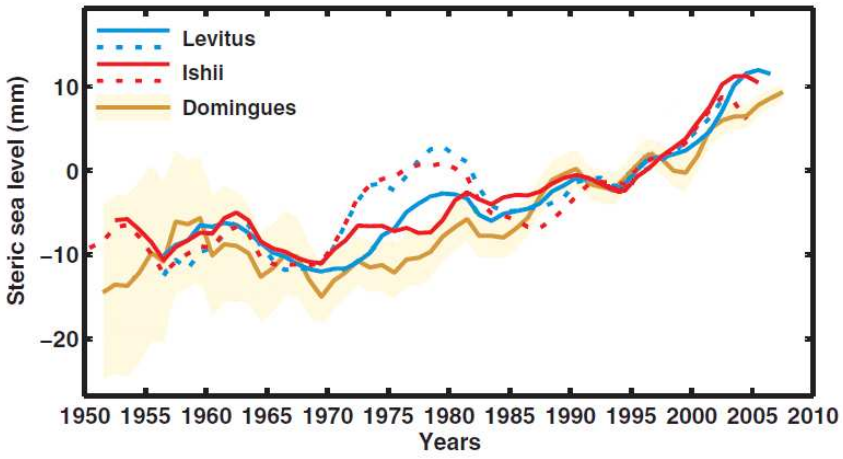

Figure 1.13 – Estimations du niveau de la mer thermostérique global pour la couche supérieure de l'océan (0-700m). Les courbes en pointillé donnent des estimations qui ne tiennent pas compte de la correction des biais systématiques des XBT et MBT : la courbe rouge est tirée de *Levitus et al.* [2005] et la courbe bleue de *Ishii et al.* [2006]. En trait plein sont les courbes équivalentes tenant compte de cette correction : la courbe rouge est tirée de *Levitus et al.* [2009], la courbe bleue de *Ishii and Kimoto* [2009] et la courbe marron de *Domingues et al.* [2008]. La région ombrée donne la barre d'erreur à 1σ de la courbe de *Domingues et al.* [2008]. Figure adaptée de *Church et al.* [2010]

3 décennies (*Johnson* [2008]), soit de quelques stations hydrographiques fixes (e.g. stations BATS dans les Bermudes ou HOT dans le Pacifique, *Aucan and Llovel* [in revision]). *Purkey and Johnson* [2010] ont montré à partir de ces mesures que l'océan abyssal (en dessous de 3000m) s'est réchauffé au cours des dernières décennies avec un signal plus fort à mesure que l'on se rapproche de l'Antarctique. Ils estiment que depuis les années 1980 ceci a contribué à une augmentation du niveau de la mer de 0.09 ± 0.06 mm.a^{-1}. Très peu de mesures remontent au delà de 1980, Il est donc difficile de dire si cette tendance est valable sur une période plus longue comme 1955-2000. Etant donné ces incertitudes, si l'on ajoute maintenant à l'expansion thermique des 700 premiers mètres de l'océan, la contribution de l'océan profond sur les dernières décennies, le réchauffement de l'océan explique ∼0.6 ± 0.1 mm.a^{-1} soit 30% à 40% de l'augmentation du niveau de la mer (voir aussi *Church et al.* [2011]).

Sur la période 1993-2010, l'expansion thermique globale des couches supérieures de l'océan (0-700m) a connu deux phases. De 1993 à 2003, elle a été en forte augmentation (voir Fig. 1.14 et *Lyman et al.* [2010]; *Levitus et al.* [2009]; *Ishii and Kimoto* [2009]) tandis qu'à partir de 2003 l'augmentation s'est affaiblie (voir Fig. 1.14 et *Lyman et al.* [2010]; *Llovel et al.* [2010b]; *von Schuckmann and Le Traon* [2011]). Au total, entre 1993 et 2010, l'expansion thermique de l'océan dûe au réchauffement est estimée à 0.8 ± 0.3 mm.a^{-1} d'après les données de *Ishii and Kimoto* [2009] et 0.9 ± 0.3 mm.a^{-1} d'après les données de *Levitus et al.* [2009]. Ceci est confirmé par *Church et al.* [2011] qui estiment l'expansion thermique des couches supérieures de l'océan entre 1993 et 2008, à 0.71 ± 0.31 mm.a^{-1} pour les 700 premiers mètres de l'océan et à 0.17 ± 0.16 mm.a^{-1} pour les couches profondes. Ces valeurs de l'expansion thermique des couches supérieures de l'océan (0-700m) sont plus petites que les 1.6 mm.a^{-1} donnés par le 4$^{\text{ème}}$ rapport du Groupement International

des Experts sur l'évolution du Climat -GIEC- sur la période 1993-2003. Ceci est dû au ralentissement de l'expansion thermique observé depuis 2003. Au total, le réchauffement des couches supérieures de l'océan (0-700m) représente ∼25% de l'augmentation du niveau de la mer depuis 1993 (*Cazenave and Llovel* [2010]; *Cazenave and Remy* [2011]; *Church et al.* [2011]).

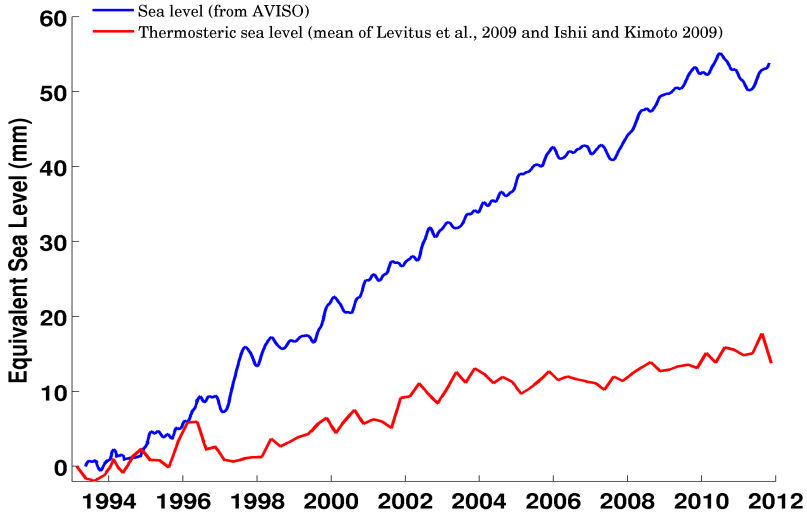

Figure 1.14 – Niveau de la mer global observé par altimétrie de 1993 à 2010 (courbe bleue). Expansion thermique de l'océan (courbe rouge) déduite de la moyenne des courbes de *Levitus et al.* [2009] et *Ishii and Kimoto* [2009]. Figure adaptée de *Meyssignac and Cazenave* [2012].

Ce ralentissement de l'expansion thermique global depuis 2003 a été détecté et estimé par plusieurs équipes à partir des données Argo dont la couverture est devenue quasi-globale en 2004. *Willis et al.* [2008] ont calculé que sur la période mi-2003 à mi-2007 l'expansion thermique avait diminué, contribuant pour -0.5 ± 0.5 mm.a^{-1} tandis que *Cazenave et al.* [2009]; *Leuliette and Miller* [2009] ont trouvé que sur la période 2004-2007 elle avait augmenté (moins vite que par le passé) au rythme de 0.4 ± 0.1 mm.a^{-1} et 0.8 ± 0.8 mm.a^{-1} respectivement. *von Schuckmann and Le Traon* [2011] trouvent aussi que l'expansion thermique globale augmente entre 2005 et 2010 à la vitesse de 0.75 ± 0.15 mm.a^{-1}. Ces valeurs diffèrent beaucoup entre elles. Même si l'on écarte la valeur de *Willis et al.* [2008] qui présente probablement un biais froid du fait d'une couverture spatiale encore trop éparse des bouées Argo en 2003, la dispersion entre les différentes estimations reste grande (*Llovel et al.* [2010b]; *Lyman et al.* [2010]). Cependant, malgré ces écarts, toutes ces études s'accordent pour montrer que le ralentissement de l'expansion thermique globale est significatif depuis 2003. *Llovel et al.* [2011b] ont pu localiser l'origine du ralentissement : ils ont montré que ce ralentissement était dû à un refroidissement de l'océan Atlantique depuis 2003 tandis que les autres régions du globe continuaient à se réchauffer (voir une description détaillée de cette étude à laquelle j'ai participé, dans la section 2.1.1). De tels ralentissement de l'expansion thermique globale ont déjà été observés par le passé sur des périodes de quelques années voire d'une dizaine années (voir Fig. 1.13). De même, l'océan Atlantique a connu des refroidissements sur plusieurs années aussi dans le passé comme entre 1959 et 1967 par exemple (voir la figure S11 des annexes de *Levitus et al.* [2009]). Il est donc probable

que ce ralentissement reflète un effet de la variabilité court-terme du climat plutôt qu'une tendance à long terme (*Cazenave and Llovel* [2010]).

L'expansion thermique des océans n'a pas seulement un impact sur la hausse globale du niveau de la mer, elle a aussi un impact sur sa variabilité régionale. En effet l'expansion thermique n'est pas uniforme (voir Fig. 1.15b) et les changements locaux de température conduisent à des changements locaux de niveau de la mer (*Lombard et al.* [2005b]; *Bindoff et al.* [2007]; *Wunsch et al.* [2007]; *Levitus et al.* [2009]). Ces variations régionales sont liées aux interactions océan-atmosphère (principalement le vent dans la région Indo-Pacifique en particulier, mais aussi les échanges de chaleur et d'eau douce) et à la circulation océanique qui en découle (*Köhl and Stammer* [2008]; *Timmermann et al.* [2010]).

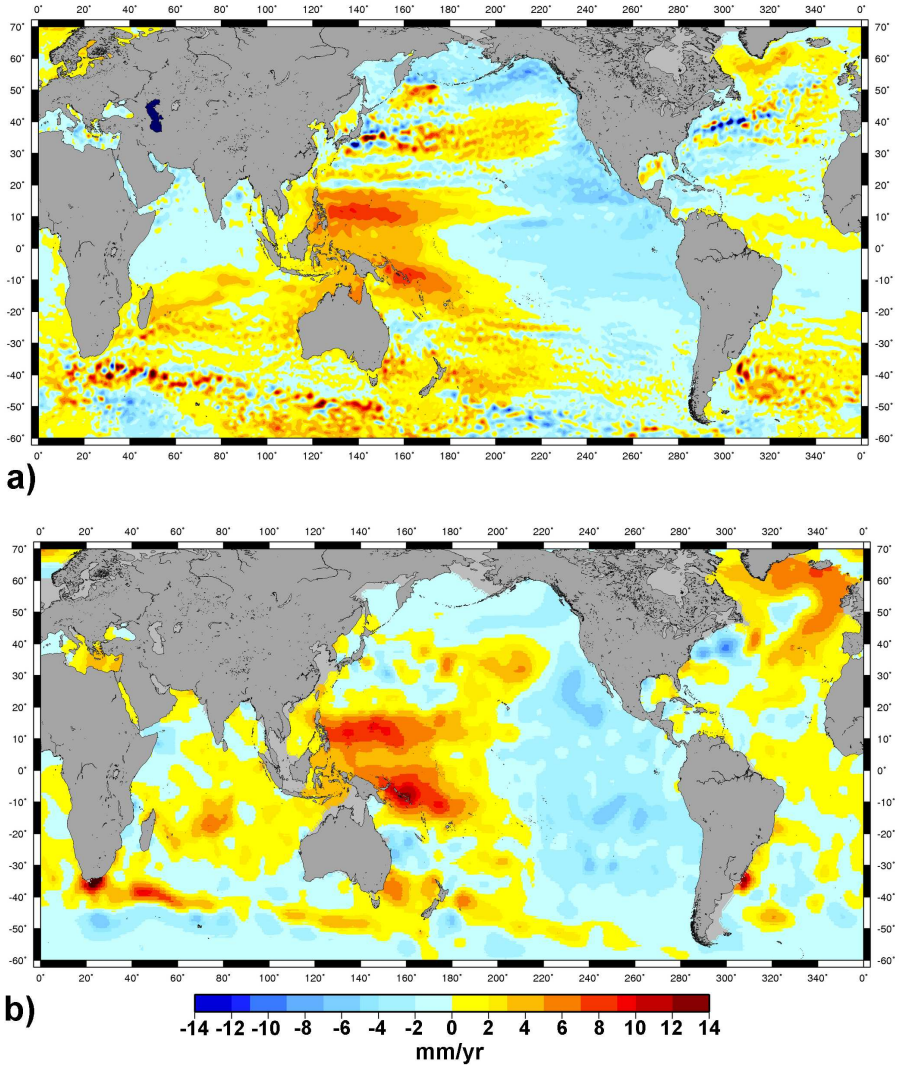

Figure 1.15 – a) Tendances du niveau de la mer calculées à partir des données altimétriques sur la période 1993-2011. La tendance du niveau global de la mer a été soustraite (même figure que la Fig. 1.12b). b) Tendances du niveau de la mer thermostérique calculées à partir des données (de 0 à 700 m) de *Levitus et al.* [2009]. La tendance du niveau global a été soustraite. Figure adaptée de *Meyssignac and Cazenave* [2012].

Durant la période altimétrique (depuis 1993), la principale contribution à la variabilité régionale du niveau de la mer est l'expansion thermique (*Bindoff et al.* [2007]). Ceci est montré par la comparaison des tendances du niveau de la mer calculées à partir de l'altimétrie (Fig. 1.15a) avec les tendances du niveau de la mer thermostérique (couches de 0 à 700 m de profondeur) calculées à partir des données hydrographiques (Fig. 1.15b, *Ishii and Kimoto* [2009]; *Levitus et al.* [2009]; *Lombard et al.* [2005a,b]). Ce résultat est confirmé par les modèles de circulation océaniques qui assimillent des données (*Wunsch et al.* [2007]; *Köhl and Stammer* [2008]; *Carton and Giese* [2008]) ou non (*Lombard et al.* [2009]). Dans les tropiques en particulier, les tendances thermostériques sont principalement dûes à la redistribution de chaleur provoquée par l'effet du vent sur la circulation océanique (*Lee and McPhaden* [2008]; *Timmermann et al.* [2010]; *Merrifield and Maltrud* [2011]). Dans les régions subtropicales et aux plus hautes latitudes, les variations du vent génèrent une expansion et un approfondissement des gyres subtropicaux (*Roemmich et al.* [2007]; *Lee and McPhaden* [2008]) et un déplacement vers le Sud des fronts polaires (*Morrow et al.* [2010]).

Le réchauffement de l'océan sur les dernières décennies est lié au réchauffement global observé à l'échelle de la planète (*Bindoff et al.* [2007]). Selon *Levitus et al.* [2001, 2009], la chaleur emmagasinée dans l'océan au cours des 40 dernières années ($\sim$16x10^{22}J) est environ 15 fois plus grande que celle qui a été stockée par les continents et 20 fois plus grande que celle qui a été stockée dans l'atmosphère. Au total, *Levitus et al.* [2009] estime que $\sim$85% du réchauffement global, observé depuis 40 ans, se trouve dans l'océan. En estimant le déséquilibre énergétique de la Terre (la Terre reémet vers l'Espace moins d'énergie qu'elle n'en absorbe du Soleil) à partir de mesures et d'un modèle de climat incluant les forçages naturels (variabilité solaire, éruptions volcaniques, albedo) et anthropiques (émissions de gaz à effet de serre, émissions d'aérosols et occupation des sols), *Hansen et al.* [2011] estiment que, sur la période 1993-2008, la Terre a absorbé un excés d'énergie de 0.80 $\pm$ 0.20 W.m^{-2} dont 90% (i.e. 0.72 $\pm$ 0.12 W.m^{-2}) se retrouvent stockés dans les différentes couches de l'océan sous forme de chaleur. Ceci est en accord avec l'estimation de *Church et al.* [2011] qui trouvent aussi que l'océan a emmagasiné 90% de l'énergie excédente de la Terre sur les deux périodes 1972-2008 et 1993-2008 en réponse aux émissions de gaz à effet de serre.

b - Les variations de salinité

Les variations de salinité, bien qu'elles puissent être régionalement importantes, n'ont pas d'impact significatif sur le niveau de la mer global (*Antonov et al.* [2002] et J. Gregory, communication personnelle). En revanche à l'échelle globale, elles sont un indicateur des apports d'eau douce à l'océan et donc des variations de sa masse (*Antonov et al.* [2002]; *Munk* [2003]). Ceci permet des estimations des variations de masse de l'océan complémentaires de celles qui sont faites à partir des variations du stock d'eau continentale total (glaces comprises, voir section 1.3.2). *Antonov et al.* [2002] a estimé la tendance du niveau de la mer global halostérique sur la période 1957-1994 à 0.05 $\pm$ 0.02 mm.a^{-1} et *Ishii et al.* [2006] l'a estimé à 0.04 $\pm$ 0.01 mm.a^{-1} sur la période 1955-2003. *Antonov et al.* [2002] ont montré que la diminution de la salinité de l'océan de 1957 à 1994 correspondait à une augmentation de la masse de l'océan de 1.3 $\pm$ 0.5 mm.a^{-1} en équivalent niveau de la mer si l'on supposait

que toute l'eau douce supplémentaire provenait des continents. Cependant, *Wadhams and Munk* [2004] ont estimé que plus de la moitié de la diminution de la salinité observée sur 1957-1994 provenait de la fonte des glaces de mer réduisant ainsi l'augmentation de masse de l'océan à 0.6 mm.a^{-1} (équivalent niveau de la mer). Ce dernier résultat est à peu près en accord avec les estimations des contributions des glaciers et des calottes polaires sur la même période. Cependant, si l'on ajoute aux erreurs de mesures de salinité, les erreurs sur l'estimation de la quantité de glace de mer dans le passé et la répartition géographique particulièrement mauvaise des données de salinité lorsque l'on remonte dans le passé, cela donne une très grande incertitude sur ces estimations de la variation de masse de l'océan au cours des dernières décennies. Les résultats des études de *Antonov et al.* [2002] et *Wadhams and Munk* [2004] sont donc à prendre avec précaution et les barres d'erreur qu'ils donnent sont probablement sous-estimées.

A l'inverse de la situation en global, la contribution de la salinité à la variabilité régionale du niveau de la mer est non-négligeable (*Wunsch et al.* [2007]; *Köhl and Stammer* [2008]; *Lombard et al.* [2009]). Dans certaines régions comme au Nord de l'océan Atlantique, elle peut compenser en partie l'effet de l'expansion thermique (*Lombard et al.* [2009]). Cette compensation s'élève à ∼25% de la contribution thermique à la variabilité régionale du niveau de la mer (*Wunsch et al.* [2007]).

1.3.2 Les variations de masse de l'océan dues aux échanges d'eau avec les réservoirs continentaux

a - La fonte des glaciers et les calottes polaires

La fonte des glaciers :

Les glaciers de montagne et les petites calottes de glace sont extrêmement sensibles au réchauffement climatique. Pour cette raison, tout autour du globe, ils rétrécissent depuis plusieurs décennies. Ce rétrécissement s'est accéléré de manière significative depuis le début des années 1990 (*Bindoff et al.* [2007]). Sur la centaine de milliers de glaciers que compte la Terre (∼120000, *Radic and Hock* [2010]; *Cogley* [2010]), quelques centaines (∼300) font l'objet d'observations (au moins 1 an d'observations). Pour une cinquantaine d'entre eux les observations sont régulières. Les observations proviennent soit de mesures in-situ (accumulation annuelle de neige, masse annuelle fondue) soit de mesures par avion ou satellite (mesure de la hauteur de surface des glaciers par altimétrie aéroportée ou imagerie spatiale, e.g. *Berthier et al.* [2011]). Les données sont collectées et mises à disposition par le World Glacier Monitoring Service (http ://www.geo.unizh.ch/wgms/). C'est sur les études de bilan de masse de ces ∼300 glaciers qu'est estimée la contribution globale de la fonte des glaciers au niveau de la mer (*Meier et al.* [2007]; *Kaser et al.* [2006]; *Cogley* [2009]; *Dyurgerov* [2010]; *Church et al.* [2011]). Pour la période 1993-2010 , la contribution de cette fonte à la hausse du niveau de la mer est estimée à $+1.1 \pm 0.25$ mm.a^{-1} (équivalent niveau de la mer), soit environ 30% de la hausse totale sur cette période (voir Fig. 1.17). Sur la période 2002-2006 elle est estimée à 0.95 mm.a^{-1} (*Dyurgerov* [2010]). Une autre méthode, développée plus récemment, s'appuie sur les mesures de gravimétrie spatiale, disponibles

depuis 2002 avec la mission GRACE, pour estimer région par région, la perte de masse des glaciers de montagnes (*Chen et al.* [2006, 2007]; *Luthcke et al.* [2008]; *Arendt et al.* [2008]; *Jacob et al.* [2012]). Dans une étude très récente, *Jacob et al.* [2012] ont évalué sur l'ensemble du globe, à partir de GRACE, la perte de masse des glaciers de montagne. Ils estiment que sur la même période 2002-2006, la contribution des glaciers de montagne au niveau de la mer s'élève à 0.61 mm.a^{-1}, soit 30% de moins que ce qui a été estimé par la méthode du bilan de masse (*Dyurgerov* [2010]). Cette différence vient en grande partie d'une différence dans l'estimation de la fonte des glaciers Himalayens. Elle pourrait s'expliquer par un comportement hétérogène des glaciers himalayens, mal mesuré par la faible couverture spatiale des données in-situ (*Gardelle et al.* [2012]), mais ceci reste à confirmer. Sur la période 2003-2010, *Jacob et al.* [2012] évaluent la contribution des glaciers de montagne au niveau de la mer à 0.41 $\pm$ 0.08 mm.a^{-1}.

La perte de masse des calottes polaires :

En ce qui concerne les calottes polaires (Groenland et Antarctique), on trouve peu de résultats concernant leur bilan de masse dans la littérature avant 1990 car il y avait très peu d'observations. Depuis, les techniques de mesure embarquée (à bord d'avions ou de satellites), telles que l'altimétrie Laser et Radar, l'interférométrie Radar (Synthetic Aperture Radar Interferometry en anglais) ou encore la gravimétrie spatiale depuis 2002 (mission GRACE), ont fourni de nombreux résultats sur les variations de masse du Groenland et de l'Antarctique (e.g. *Allison et al.* [2009]). Cependant, chacune de ces techniques présente des biais et des limitations qui lui sont propres. Les estimations faites avec GRACE par exemple, sont très sensibles à la correction du GIA : sur l'Antarctique, la correction GIA de GRACE est du même ordre de grandeur que la perte de masse estimée. Les estimations de perte de masse à partir de l'altimétrie Laser, utilisent une distribution de densité de la glace avec la profondeur qui est, en fait, très mal connue. L'altimétrie radar, quand à elle, ne permet pas un bon échantillonnage des zones côtières où se produisent les pertes de masses les plus importantes. Lorsqu'on compare les estimations faites avec les différentes techniques, les résultats sont assez dispersés (voir Fig.1.16). Néanmoins, toutes les techniques de mesure montrent que les deux calottes polaires perdent de la masse au profit de l'océan et que cette perte s'accélère avec le temps (voir Fig.1.16 et par exemple *Chen et al.* [2009]; *Velicogna* [2009]; *Rignot et al.* [2008a,b, 2011]; *Steffen et al.* [2010]; *Sasgen et al.* [2012]).

Sur la période 1993-2003, la communauté scientifique s'accorde sur le fait que seulement 0.42 $\pm$ 0.36 mm.a^{-1} (i.e. 13.5%) de la hausse du niveau de la mer s'expliquait par la perte de masse des calottes polaires (*Bindoff et al.* [2007]). Cette contribution a augmenté à $\sim$1.0 mm.a^{-1} (soit $\sim$40%) depuis 2003-2004 (valeur moyenne entre les différentes techniques de mesure). Si bien que, en moyenne sur la période 1993-2010, la perte de masse des calottes explique 0.7 $\pm$0.4 mm.a^{-1} (soit $\sim$25%) de la tendance du niveau de la mer. Cette perte se divise en 0.4$\pm$ 0.2 mm.a^{-1} (équivalent niveau de la mer) pour le Groenland et 0.3 $\pm$ 0.2 mm.a^{-1} (équivalent niveau de la mer) pour l'Antarctique (voir Fig. 1.17 et *Cazenave and Remy* [2011]; *Church et al.* [2011]).

La principale raison de la perte de masse des calottes polaires n'est pas la fonte de la glace mais une accélération de l'écoulement dynamique de la glace vers l'océan (bien que dans le cas du Groenland la fonte estivale de surface explique 50% de la perte de

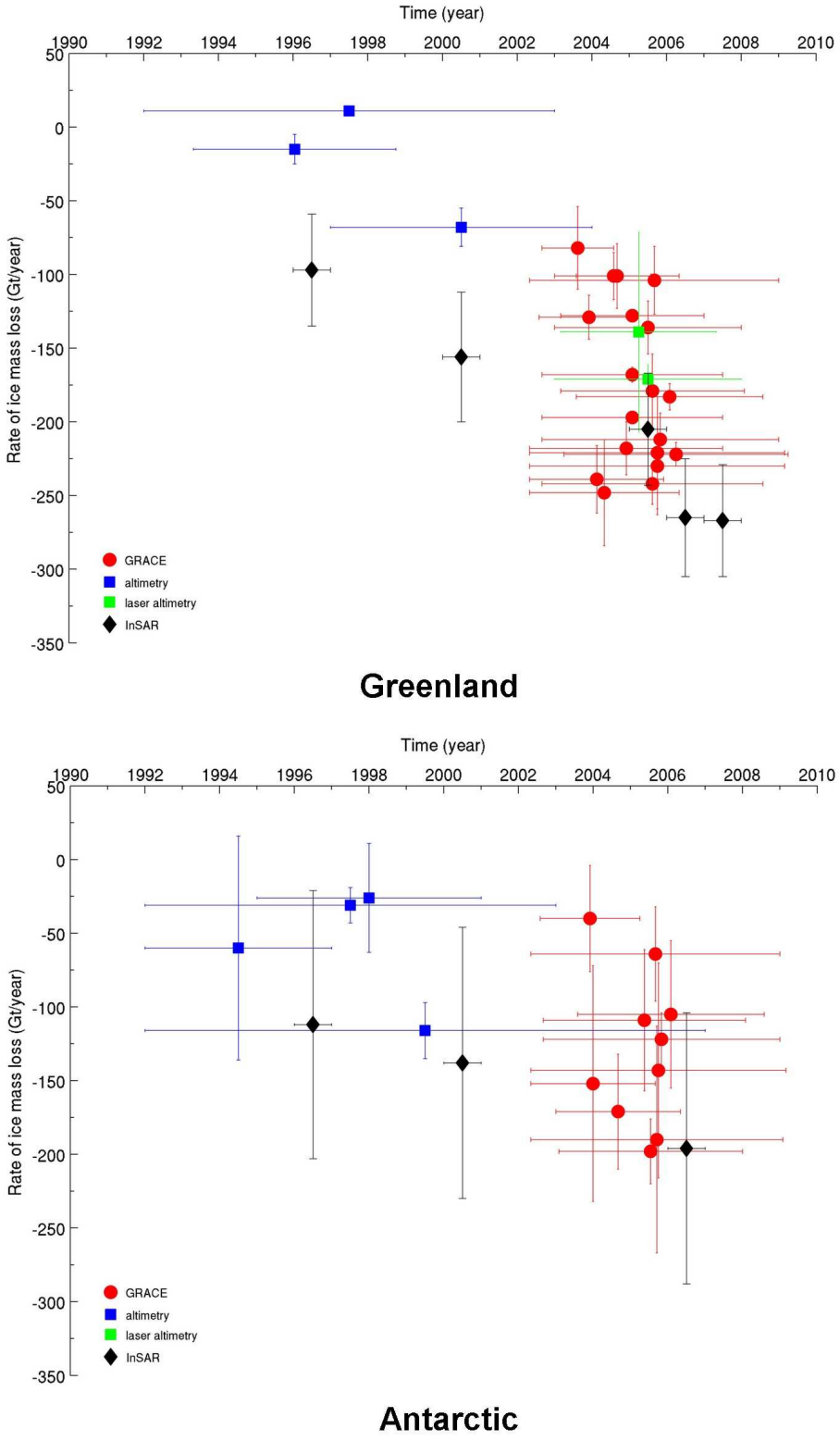

Figure 1.16 – Compilation des vitesses de perte de masse des calottes polaires publiées au cours des deux dernières décennies. Les barres verticales indiquent l'erreur de l'estimation de perte de masse tandis que les barres horizontales indiquent la période sur laquelle a été estimée la vitesse de perte de masse. Figure adaptée de *Cazenave and Remy* [2011].

masse, *Rignot et al.* [2008b]; *van den Broeke et al.* [2009]). La majorité de la masse perdue vient de glaciers situés sur les côtes du Groenland (au Sud et à l'Ouest) et de l'Ouest de l'Antarctique (*Alley et al.* [2007, 2008]; *Steffen et al.* [2010]). Deux processus ont été proposés pour expliquer cette accélération de perte de masse des calottes : 1) la lubrification de l'interface entre le glacier et son socle rocheux suite à l'infiltration par les crevasses de quantités anormales d'eau fondue en surface au cours des étés, et 2) l'amincissement et la rupture des glaciers émissaires qui ralentissent l'écoulement de la glace vers l'océan. Même si le premier mécanisme peut jouer un rôle non-négligeable dans le cas du Groenland pour lequel la fonte estivale de surface est significative, les glaciologues estiment aujourd'hui que c'est le second mécanisme qui explique principalement l'accélération de l'écoulement de la glace (*Alley et al.* [2007, 2008]; *Holland et al.* [2008]; *Steffen et al.* [2010]; *Pritchard et al.* [2012]). L'amincissement dynamique des glaciers des calottes est principalement observé le long des côtes où l'on trouve des glaciers qui reposent sur un socle rocheux en dessous du niveau de la mer (e.g. au Nord-Est et Sud-Ouest du Groenland ou à l'Ouest de l'Antarctique). De récentes observations ont montré que pour ces glaciers, le réchauffement des eaux océaniques de subsurface et des changements dans la circulation océanique pouvaient faire fondre leur base provoquant ainsi leur rupture et déclencher des instabilités dynamiques dans l'écoulement amont de la glace (*Gille* [2008]; *Holland et al.* [2008]; *Pritchard et al.* [2012]) .

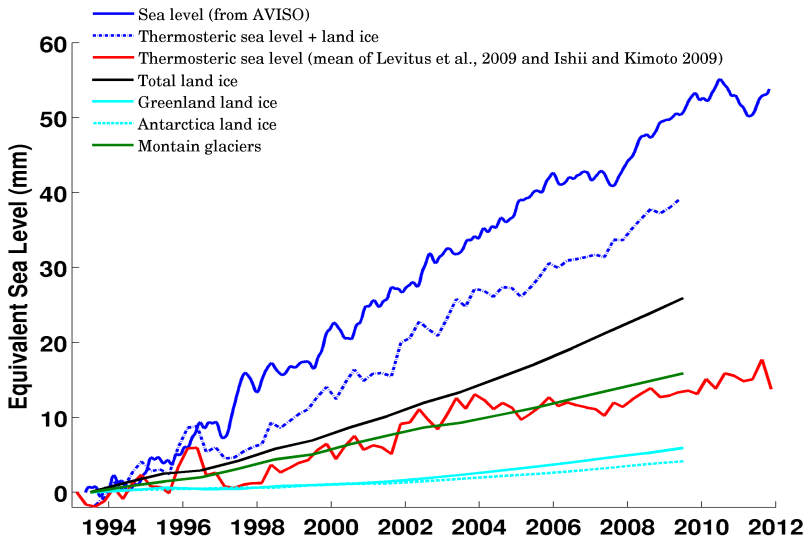

Figure 1.17 – Niveau de la mer global observé par altimétrie de 1993 à 2010 (courbe bleue). Expansion thermique de l'océan (courbe rouge) déduite de la moyenne des courbes de *Levitus et al.* [2009] et *Ishii and Kimoto* [2009]. Contribution des calottes polaires (Groenland et Antarctique, courbe turquoise) et des glaciers (courbe verte). La courbe noire représente la contribution totale des glaces continentales. La courbe bleue en pointillé donne la somme totale des contibutions climatiques au niveau de la mer. Figure tirée de *Meyssignac and Cazenave* [2012].

Bilan du niveau de la mer :

Si l'on ajoute la contribution des glaciers de montagne, des petites calottes et des calottes polaires, on obtient une contribution totale des glaces continentales à la tendance du niveau de la mer de 1.8 $\pm$ 0.35 mm.a^{-1} sur la période 1993-2010, soit $\sim$55% de la ten-

dance totale (voir Fig. 1.17). En ajoutant encore la contribution de l'expansion thermique qui s'élève à 1.0 ± 0.3 mm.a^{-1} sur la même période (voir section 1.3.1), on obtient une contribution totale des facteurs climatiques à la tendance du niveau de la mer de 2.8 ± 0.4 mm.a^{-1} (voir Fig. 1.17). Ceci montre que sur la période 1993-2010 la tendance du niveau de la mer s'explique bien (en considérant les barres d'erreur) par la somme des tendances de l'expansion thermique et de la fonte des glaces continentales (voir Fig. 1.17).

Variabilité régionale du niveau de la mer induite par la fonte des glaces continentales

La fonte actuelle des glaces (glaciers de montagne et calottes polaires) ne participe pas seulement à la hausse globale du niveau de la mer, elle a aussi un impact sur sa variabilité régionale pour deux raisons. D'une part, l'apport d'eau douce venant des continents modifie localement (à l'entrée dans l'océan), la structure en densité des colonnes d'eau et donc modifie la circulation océanique (*Stammer* [2008]; *Stammer et al.* [2011]). En réponse, le niveau de la mer s'ajuste dynamiquement sur la région, aux échelles inter-annuelles à multi-décennales (voir Fig. 1.18 et *Okumura et al.* [2009]; *Stammer* [2008]; *Stammer et al.* [2011]) et génère de la variabilité régionale. D'autre part, la redistribution de masse d'eau des continents vers l'océan provoque une réponse élastique de la croûte terrestre qui déforme les bassins océaniques et modifie le géoïde. Cette composante génère aussi de la variabilité régionale dans le niveau de la mer (voir section 1.3.3). Aujourd'hui, ces contributions à la variabilité régionale du niveau de la mer sont prédites par des modèles (*Okumura et al.* [2009]; *Stammer* [2008]; *Stammer et al.* [2011]; *Tamisiea and Mitrovica* [2011]). Cependant elles sont encore très petites et n'ont pas été détectés dans les mesures (voir section 1.3.3).

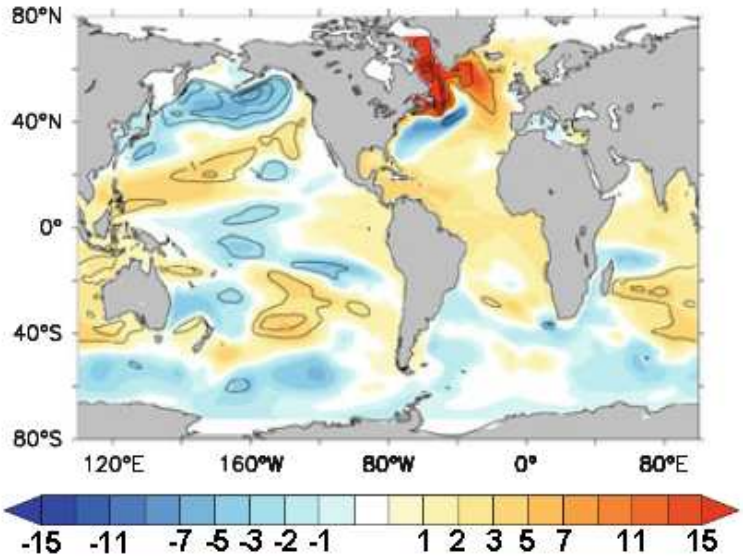

Figure 1.18 – Réponse du niveau de la mer aux apports d'eau douce induits par une perte de masse du Groenland équivalente à 2 mm.a^{-1} (pour mémoire, la perte actuelle est estimée à 0.4 mm.a^{-1} depuis 1993). La carte représente les anomalies de niveau de la mer, moyennées sur 4 ans, induites après 28 ans de simulations d' un modèle couplé. La barre de couleur est en cm. Figure adaptée de *Stammer et al.* [2011].

b - Les échanges d'eau avec les bassins fluviaux

En dehors des calottes polaires et des glaciers, de l'eau douce est stockée dans de nombreux autres réservoirs continentaux tels que la couverture neigeuse, les fleuves, les lacs, les réservoirs artificiels, les marais, les zones inondées et les aquifères. Ces eaux continentales sont en échange permanent avec l'atmosphère et l'océan à travers les flux verticaux (évapo-transpiration, précipitation) et horizontaux (écoulements de surface et souterrains) de masse. Elles font partie intégrante du système climatique dans lequel elles jouent un rôle important de connections et de rétroactions entre régions éloignées par leur influence sur le bilan d'énergie de surface et sur les flux d'eau entre océans, continents et atmosphère. En particulier, les variations climatiques influent sur ces stocks d'eau. Certaines activités humaines aussi, telles que le pompage des eaux souterraines (particulièrement dans les régions arides et semi-arides), la construction de barrages ou le drainage des marais. D'autres activités anthropiques, qui modifient les propriétés physiques de l'environnement, telles que l'urbanisation, l'agriculture ou la déforestation ont aussi un impact. Tous ces effets se traduisent, après intégration par les bassins fluviaux, par une augmentation ou une diminution du débit des fleuves (flux horizontaux) et une modification du bilan "Précipitation moins Evaporation" local (flux verticaux). In fine, ceci contribue à la variation du niveau de la mer.

Les fluctuations des stocks d'eau en réponse aux variations climatiques des dernières décennies et leur contribution au niveau de la mer ne peuvent pas être évaluées car il n'existe quasiment pas de mesures à l'échelle globale. En revanche on peut calculer des estimations à l'aide des modèles hydrologiques globaux développés à l'origine pour les études de l'atmosphère et du climat. Ces modèles calculent les transferts d'eau, le bilan d'énergie et donc les stocks d'eau à la surface de la Terre à partir des données de la basse atmosphère (précipitation, température, humidité, vent) et des données du bilan radiatif à la surface. Avec les réanalyses atmosphériques sur 1950-2000 et le modèle hydrologique Orchidee, *Ngo-Duc et al.* [2005] ont montré qu'ils ne trouvaient pas de tendances à long terme dans la contribution des stocks d'eau continentaux au niveau de la mer. Ils ont mis en évidence cependant une forte variabilité inter-annuelle à multi-décennale (amplitude de plusieurs millimètres). Ce résultat a été confirmé par *Milly et al.* [2003], à l'aide du modèle hydrologique LAD, sur la période 1980-2000.

Les interventions directes de l'Homme sur les stocks d'eau continentaux et leurs contributions au niveau de la mer ont été estimées dans plusieurs études résumées par *Huntington* [2006]; *Milly et al.* [2010]. La plus grande contribution vient du pompage des eaux souterraines (pour l'agriculture, l'industrie et les usages domestiques) et du remplissage des réservoirs artificiels. Malgré les différentes estimations des auteurs et le manque de données dans le passé, il semble que la diminution des eaux souterraines au cours des dernières décennies a eu pour conséquence une augmentation du niveau de la mer entre 0.3 et 0.8 $mm.a^{-1}$ (*Huntington* [2006]; *Milly et al.* [2010]; *Wada et al.* [2010, 2012]; *Konikow* [2011]). Par ailleurs, au cours des 50 dernières années, des dizaines de milliers de barrages ont été construits pour créer des réservoirs artificiels. Ceci a eu une contribution négative au niveau de la mer. *Chao et al.* [2008] estiment cette contribution à -0.55 $mm.a^{-1}$. Au total, les effets opposés du pompage des eaux souterraines et de la construction des barrages semblent s'être compensés au cours des dernières décennies. En effet *Church et al.* [2011]

estiment que la somme de ces 2 facteurs a contribué pour -0.1 ± 0.2 mm.a^{-1} au niveau de la mer entre 1970 et 2008. Dans le futur, Il est probable que ceci change du fait d'une forte diminution des constructions de barrages (la plupart des sites propices étant déjà équipés) et d'une augmentation du pompage dans les régions arides fortement peuplées (*Lettenmaier et Milly 2009*).

Dans une étude très récente, basée sur un modèle, *Pokhrel et al.* [2012] aboutissent à une contribution totale des stocks d'eau continentaux au niveau de la mer de +0.77 mm.a^{-1} entre 1961 et 2003. Cette valeur est bien supérieure à celle obtenue par *Church et al.* [2011]. Le résultat de *Pokhrel et al.* [2012] vient d'une estimation très élevée, par leur modèle, du pompage des eaux souterraines entre 1950 et 2000 : ∼359 km^3.a^{-1}. Cette estimation est bien supérieure à ce qu'indiquent les données collectées depuis 1961 : ∼82 ±22 km^3.a^{-1} entre 1961 et 2008 d'après *Konikow* [2011] par exemple. Pour cette raison, ce résultat est considéré peu fiable par la communauté scientifique qui s'intéresse au niveau de la mer.

Depuis 2002, Il existe une mesure globale des stocks d'eau continentaux avec le satellite GRACE. GRACE mesure les variations spatio-temporelles du champ de gravité terrestre. Sur les continents, ces variations peuvent être converties en variations temporelles du contenu en eau, intégré sur la verticale (i.e. eaux de surface + humidité des sols + eaux souterraines). Les mesures GRACE ne permettent pas de séparer les contributions individuelles de chaque réservoirs ni de discriminer les variations de stock d'eau dûes au climat de celles qui sont dûes à l'activité anthropique. *Ramillien et al.* [2008] ont estimé la tendance du stock d'eau contenu dans les 27 plus grands bassins fluviaux du monde à partir des données GRACE de 2003 à 2006. Ils ont trouvé des tendances soit positives soit négatives selon les bassins. Mais en global, la tendance du stock total donnait une contribution au niveau de la mer <0.2 mm.a^{-1}. *Llovel et al.* [2010a], dans une étude similaire prenant en compte les 32 plus grands bassins du monde et basée sur les données GRACE de 2003 à 2008, trouvent une contribution de ∼-0.2 mm.a^{-1}. Ces résultats confirment la faible participation des stocks d'eau continentaux à la tendance du niveau de la mer sur la dernière décennie. En résumé que ce soit sur les dernières décennies ou depuis 2002, les variations des stocks d'eau continentaux n'ont qu'un impact faible sur la tendance du niveau de la mer.

En dehors d'une tendance faible depuis 2002, *Ramillien et al.* [2008]; *Llovel et al.* [2010a] ont mis en évidence avec GRACE une forte variabilité inter-annuelle dans les variations des stocks d'eau continentaux. *Llovel et al.* [2011a] ont confirmé ce résultat avec le modèle hydrologique ISBA-TRIP développé par Météo-France, sur toute la période 1993-2010 et ont montré que c'est le bassin Amazonien qui dominait le signal en particulier durant les évènements El Niño. Sur la Fig. 1.19 (mise à jour de *Llovel et al.* [2011a]) sont superposées les deux courbes du stock d'eau total sur les continents (équivalent niveau de la mer) et du niveau de la mer global (une fois la tendance retirée). La courbe des stocks d'eau continentaux (calculée avec le modèle ISBA-TRIP) est inversement corrélée (corrélation de 0.7) avec la courbe du niveau de la mer global (*Llovel et al.* [2011a]) révélant que les fluctuations inter-annuelles du niveau de la mer global s'expliquent, en fait, par la variation des stocks d'eau sur les continents. De plus, les deux courbes sont fortement corrélées à l'oscillation du Pacifique tropical (El Niño-Southern Oscillation -ENSO- en anglais) avec des anomalies positives du niveau de la mer au cours des évènements El Niño (e.g. 1997-1998) et des anomalies négatives au cours des évènements La Niña (e.g. 2007-2008) (voir *Nerem et al.* [2010]; *Llovel et al.* [2011a]). Cette corrélation s'explique par le fait que

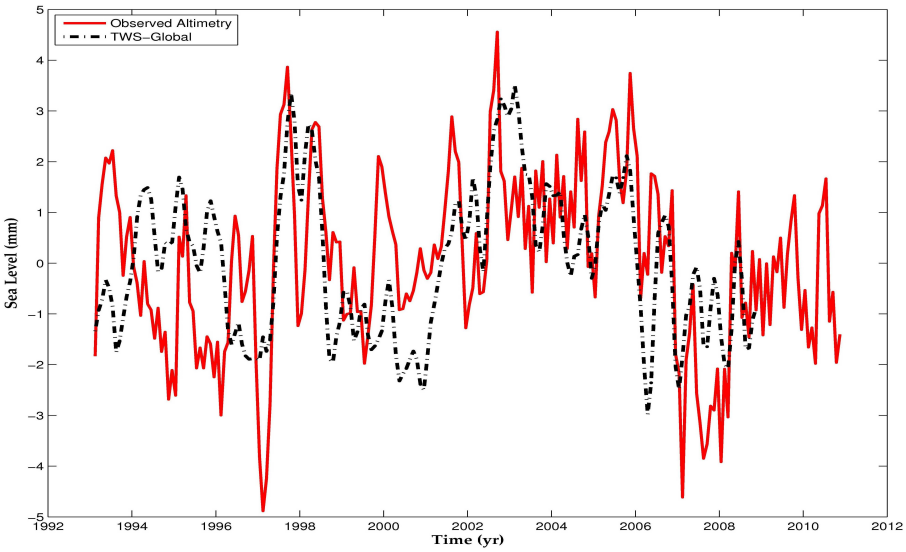

Figure 1.19 – Courbe du niveau de la mer mesuré par altimetrie une fois la tendance globale de 3.2 mm.a^{-1} retirée (courbe rouge). Stock d'eau continental total exprimé en équivalent niveau de la mer (courbe noire, le signe de la courbe a été inversé pour faciliter la comparaison). Figure mises à jour à partir de *Llovel et al.* [2011a].

les évènements ENSO provoquent des changements à grande échelle dans les régimes de précipitation des tropiques : ils génèrent plus de précipitations sur les océans et moins sur les continents durant les évènements El Niño et l'inverse durant les évènements La Niña (e.g. *Gu and Adler* [2011]). De plus il semble que durant les épisodes El Niño, les anomalies positives de niveau de la mer global viennent d'anomalies positives de masse d'eau localisées sur le Pacifique tropical. Ces anomalies de masses coïncident avec une réduction du transport des eaux de l'océan Pacifique vers l'océan Indien par les détroits Indonésiens (*Tillinger and Gordon* [2010]) révélant que la circulation océanique joue un rôle important dans les transferts de masse durant les évènements ENSO (voir une description détaillée de cette étude à laquelle nous avons participé, dans la section 2.1.2).

1.3.3 Les autres facteurs qui font varier le niveau de la mer à l'échelle régionale

D'autres facteurs font encore varier le niveau de la mer, mais leur impact sur le niveau de la mer global est faible ou nul. En revanche, leur impact peut être non-négligeable sur la variabilité régionale du niveau de la mer.

La réponse de la croûte terrestre aux transferts de masse d'eau à la surface de la Terre :

L'un de ces facteurs est la réponse visco-élastique de la croûte terrestre aux transferts de masse dans l'enveloppe fluide de la Terre. Cette réponse a un impact très lent sur le niveau de la mer si bien que pour les études climatiques cet effet est souvent qualifié d'"effet quasi-statique". Par exemple, le GIA qui est la réponse visco-élastique de la croûte terrestre à la dernière déglaciation, qui a commencé il y a ∼20 000 ans, génère des changements très lents du champ de gravité ainsi que des déformations des bassins océaniques qui produisent de

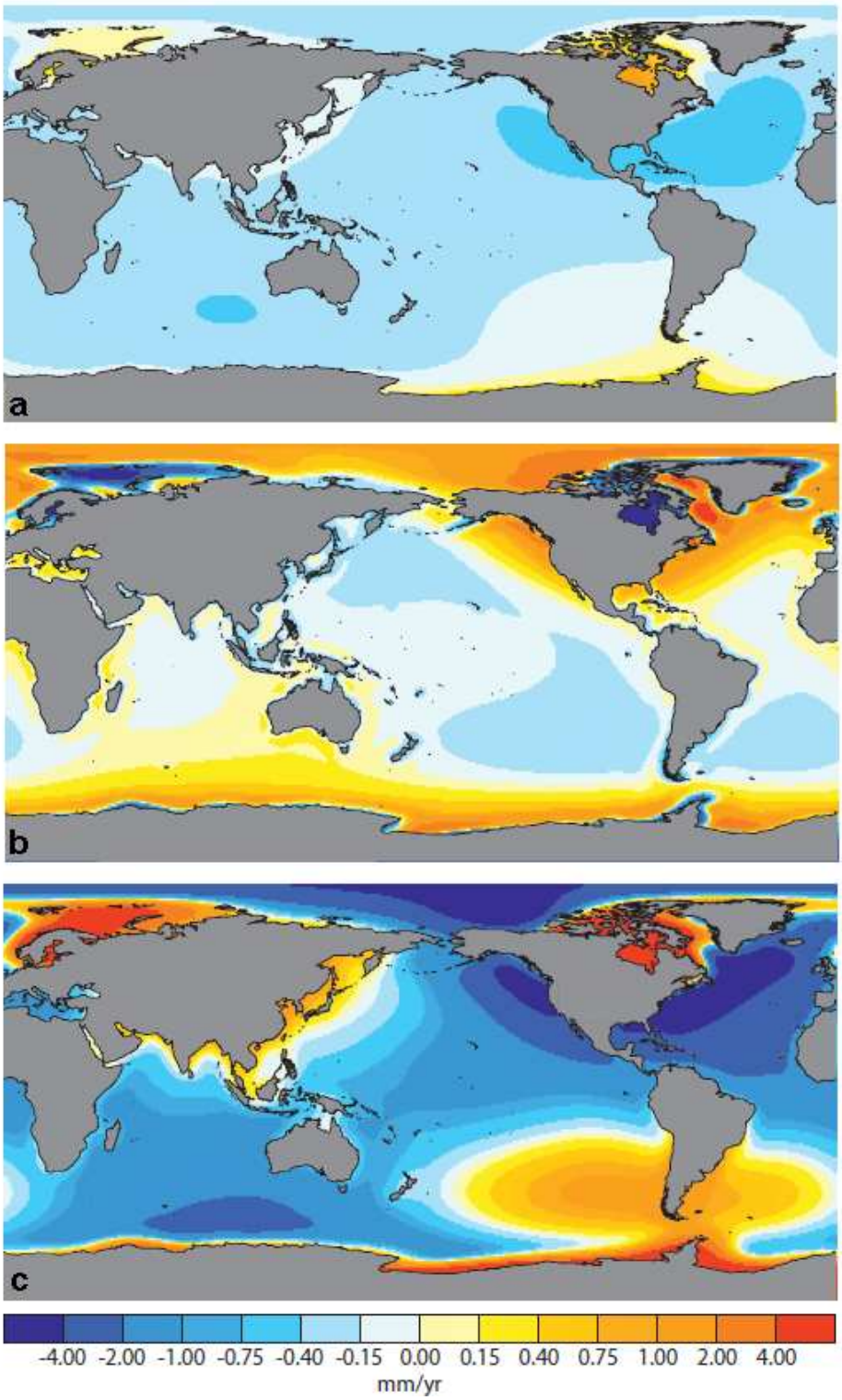

Figure 1.20 – Contribution à la variabilité régionale des tendances du niveau de la mer de la réponse visco-élastique de la Terre à la dernière déglaciation. Elle est représentée telle qu'elle serait mesurée par l'altimetrie a), par les marégraphes b) et par GRACE c). Figure adaptée de *Tamisiea and Mitrovica* [2011].

la variabilité régionale dans les tendances du niveau de la mer (voir Fig. 1.20a et *Milne and Mitrovica* [2008]; *Mitrovica et al.* [2001]; *Tamisiea and Mitrovica* [2011]). Cette variabilité est particulièrement forte au voisinage des régions qui étaient recouvertes par des calottes glaciaires lors du dernier maximum glaciaire (en Fennoscandie, autour de la baie d'Hudson, en Patagonie et en Antarctique ; voir Fig. 1.20). Mais on trouve aussi du signal dans les régions éloignées comme l'océan Pacifique. En moyenne sur tout l'océan, l'impact du GIA sur le niveau de la mer n'est pas tout à fait nul. En effet quand on moyenne le signal de la Fig.1.20a entre 66°S et 66°N, on trouve une contribution légèrement négative du GIA au niveau de la mer de -0.3 mm.a^{-1}. C'est cette composante qu'il faut soustraire au niveau de la mer global calculé avec les données altimétriques quand on veut estimer la composante climatique du niveau de la mer (i.e. celle qui est liée aux variations de masse et de température de l'océan).

La croûte terrestre ne répond pas seulement à la fonte des glaces du dernier maximum glaciaire. Elle répond aussi à la fonte actuelle des glaces du Groenland, de l'Antarctic et des glaciers de montagne (*Gomez et al.* [2010]; *Milne et al.* [2009]; *Mitrovica et al.* [2001, 2009]; *Tamisiea and Mitrovica* [2011]). Cependant, la fonte étant récente, la réponse de la croûte est dans ce cas élastique. De plus les régions touchées par la fonte actuelle ne sont pas les mêmes que celles qui furent touchées par la fonte du dernier maximum glaciaire. En conséquence, les déformations des bassins océaniques ainsi que les changements du géoïde et de la rotation de la Terre induits par cette fonte actuelle des glaces sont différents de ceux qui sont induits par le GIA (voir Fig. 1.21 à comparer avec la Fig.1.20b). Ces effets quasi-statiques engendrent aussi de la variabilité régionale dans le niveau de la mer qui s'ajoute à celle qui est induite par le GIA.

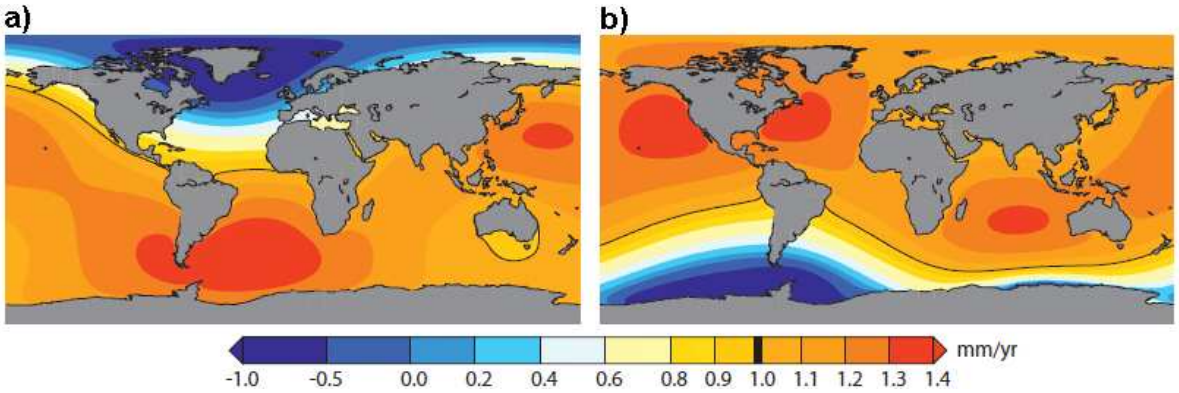

Figure 1.21 – Tendances du niveau de la mer induites par la réponse de la Terre solide (i.e. déformation élastique de la croûte + variations du géoïde + variations de la rotation de la Terre) à a) une perte de masse du Groenland équivalente à 1 mm.a^{-1} et b) une perte de masse de l'Antarctique équivalente à 1 mm.a^{-1}, telles qu'elles seraient mesurées par des marégraphes. Figure adaptée de *Tamisiea and Mitrovica* [2011].

Il faut noter que, ces contributions à la variabilité régionale du niveau de la mer de la réponse de la croûte terrestre aux transferts de masse à la surface, sont encore petits comparés à la variabilité régionale du niveau de la mer stérique (voir section 1.3.1). Jusqu'à aujourd'hui, ils n'ont pas été observés dans les données altimétriques ou marégraphiques et leur détection semble encore difficile étant donné les performances des sytèmes de mesure actuels (*Kopp et al.* [2010]). Cette détection est d'autant plus difficile que la signature de ces

phénomènes n'est pas la même selon qu'on la mesure avec l'altimétrie, les marégraphes ou GRACE (voir Fig. 1.20a,b et c). Néanmoins, si les pertes de glace continentale continuent au rythme actuel ou s'accélèrent, elles pourraient produire dans le futur une forte variabilité régionale dans le niveau de la mer devenant un de ses contributeurs majeurs (voir section 1.4.2 et *Mitrovica et al.* [2009]; *Slangen et al.* [2011]). Elle seront alors plus faciles à détecter et mesurer. Aujourd'hui, ce domaine de recherche est encore largement ouvert : par exemple, actuellement, il n'existe pas d'estimation publiée de la signature altimétrique attendue de la réponse élastique de la croûte terrestre à la fonte actuelle des glace (i.e. il n'existe pas de figure équivalente à la Fig.1.21 pour l'altimétrie).

Les processus géologiques qui déforment la croûte terrestre :

D'autres phénomènes tels que l'érosion, la déposition ou la compaction des sédiments, peuvent jouer un rôle dans la variabilité locale du niveau de la mer à travers la réponse de la croûte océanique qu'ils génèrent (*Blum and Roberts* [2009]). C'est aussi le cas de la déformation de la Terre sous l'effet de la convection mantellique et des processus tectoniques qui peuvent produire des variations du niveau de la mer faible en moyenne (<1 mm.a^{-1}, voir *Moucha et al.* [2008]), excepté pour les tremblements de Terre.

1.4 Les projections du niveau de la mer dans le futur.

1.4.1 Les projections du niveau de la mer global

Il faut s'attendre à ce que le réchauffement global continue et même s'accroisse dans les prochaines décennies car les émissions de gaz à effet de serre, qui en est la cause principale, continueront très probablement d'augmenter dans le futur. Une estimation récente des émissions de CO_2 dûes à la combustion des énergies fossiles, par *Friedlingstein et al.* [2010], révèle une augmentation forte durant les années 2000 malgré de légers ralentissements provoqués par les crises économiques. Parmi les émissions totales de CO_2 provenant des énergies fossiles et de l'industrie du ciment, 45% s'accumulent actuellement dans l'atmosphère et participent à l'effet de serre, tandis que l'océan et la végétation en stockent respectivement 25% et 30% (*Durant et al.* [2011]).

Différents scenarii d'émissions de gaz à effet de serre (exprimés en terme de forçage radiatif) et de réponse du système climatique (exprimés en terme d'augmentation de la température globale de la Terre) sont possibles pour les décennies à venir (*Solomon et al.* [2007]). Par exemple dans le 4ème rapport du GIEC, le scénario SRES-A1B prévoit un réchauffement global en 2100 de +2.8°C en moyenne (entre 1.4°C et 6.4°C) par rapport à aujourd'hui tandis que les scenarii SRES-B1 et SRES-A2 prévoient un réchauffement moyen de +1.8°C (entre 1.1°C et 2.9°C) et +3.4°C (entre 2°C et 5.4°C) respectivement. Pour le 5ème rapport du GIEC, dont la publication est prévue en septembre 2013, ces scenarii ont été modifiés et renommés "Representative Concentration Pathways" -RCP- (*Moss et al.* [2010]; *van Vuuren et al.* [2012]) . Ils ne donnent plus d'estimations des emissions de gaz à effet de serre. Ils donnent désormais directement une estimation de leur concentration dans l'atmosphère à partir de 2006. Malgré quelques différences, les nouveaux scenarii RCP restent proches des anciens scenarii SRES en terme de forçage radiatif d'ici 2100. Seul le scénario SRES-A2 qui est le plus extrême en terme de forçage radiatif et de réchauffement en 2100, a été revu significativement à la hausse dans sa nouvelle version RCP8.5. Les scenarii SRES-B1 et SRES-A1B restent en revanche très proches de leur nouvelles versions respectives RCP4.5 et RCP6.0. Chacun de ces scenarii prévoit une augmentation du niveau de la mer au cours du XXIème siècle et au delà, car ils indiquent tous une augmentation du réchauffement de l'océan et de la fonte des glaces continentales (voir Fig 1.22 et e.g. *Solomon et al.* [2007]).

Les projections du 4ème rapport du GIEC, publié en 2007 (*Bindoff et al.* [2007]), indiquaient que le niveau de la mer global devrait être supérieur à sa valeur actuelle de 40 cm en 2100 (avec une incertitude de ± 15 cm dûe à la dispersion des modèles utilisés et à l'incertitude sur les émissions futures de gaz à effet de serre, voir Fig. 1.22). Après la publication de ce rapport, il a été suggéré que ces valeurs étaient faibles car elles prenaient en compte seulement le réchauffement de l'océan, la fonte des glaciers et le bilan de surface des calottes polaires. Elles ne prenaient pas en compte l'accélération de l'écoulement dynamique des glaces vers l'océan qui est la raison majeure des pertes de masse actuellement observées au Groenland et en Antarctique de l'Ouest (voir section 1.3.2). Des études récentes suggèrent que la perte de masse des calottes polaires serait bien plus grande qu'attendue. *Pfeffer et al.* [2008] estime qu'en 2100 cette contribution pourrait valoir entre 16

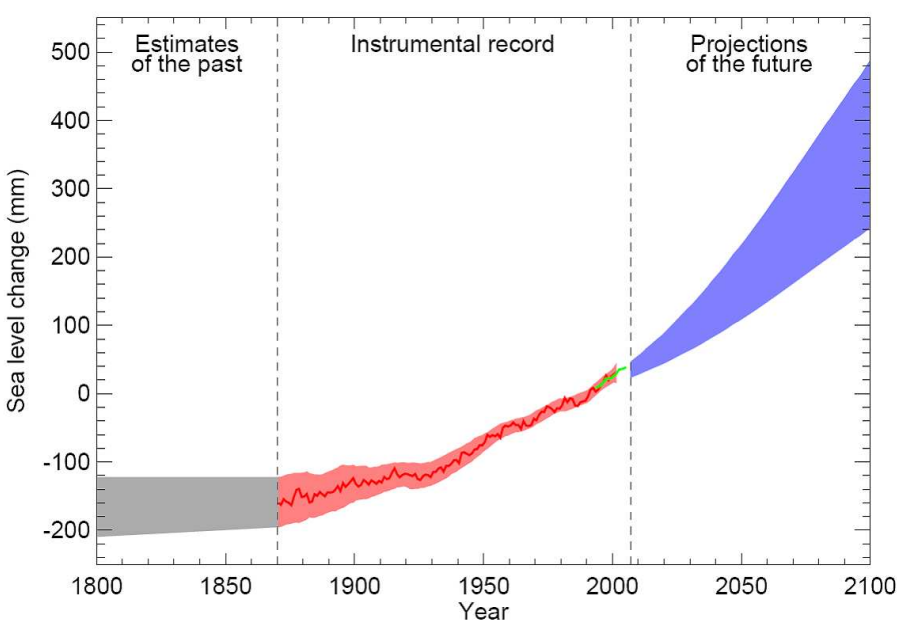

Figure 1.22 – Evolution du niveau global de la mer entre 1800 et 2100 (*Bindoff et al.* [2007]). La courbe grise représente les estimations obtenues à partir des données géologiques. La courbe rouge représente le niveau de la mer observé par les marégraphes (*Church and White* [2011]). La courbe verte représente le niveau de la mer observé par altimétrie. L'enveloppe bleue donne les estimations du niveau de la mer futur du 4ème rapport du GIEC.

cm et 54 cm pour le Groenland et entre 13 cm et 62 cm pour l'Antarctique (avec comme valeurs probables 16 cm et 15 cm respectivement). En extrapolant l'accélération observée actuellement dans la perte de masse du Groenland et de l'Antarctique, *Rignot et al.* [2011] estiment une contribution des calottes polaires au niveau de la mer en 2100 de ∼56 cm. En résumé, la contribution totale des glaces continentales au niveau de la mer du XXIème siècle reste très incertaine et des valeurs autour de 40-50 cm en 2100 sont envisageables. Si l'on ajoute le réchauffement de l'océan (avec une contribution de l'ordre de 10-40 cm, *Bindoff et al.* [2007]), le niveau de la mer pourrait s'élever de 50 à 80 cm au dessus de sa valeur actuelle en 2100.

Une autre approche, basée sur des modèles semi-empiriques, a été proposée pour estimer le niveau de la mer du XXIème siècle (*Horton et al.* [2008]; *Vermeer and Rahmstorf* [2009]; *Grinsted et al.* [2010]; *Rahmstorf et al.* [2011]; *Jevrejeva et al.* [2010, 2012]). Les modèles semi-empiriques sont basés sur des relations simples entre les variations du niveau de la mer global et les variations de la température moyenne (ou du forçage radiatif moyen) de la Terre. Ces relations sont calibrées sur le XXème siècle (ou des périodes plus longues). Elles permettent ensuite d'estimer des projections du niveau de la mer global à partir des projections de température moyenne (ou de forçage radiatif moyen) obtenues par les modèles climatiques couplés du GIEC (la température moyenne et le forçage radiatif moyen sont les paramètres les plus précis des paramètres modélisés par les modèles de climat couplés). Cette approche donne des projections du niveau de la mer global plus élevées en 2100 que l'approche traditionnelle. Mais les raisons de cette différence restent incomprises (voir Fig. 1.23).

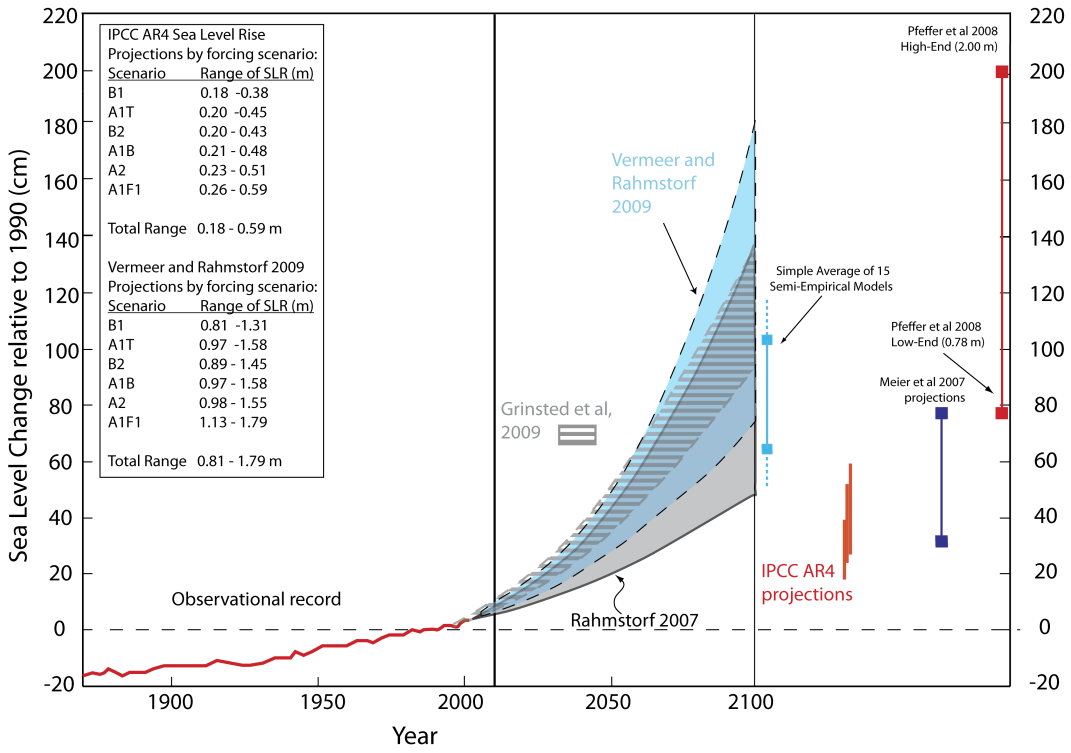

Figure 1.23 – Evolution du niveau global de la mer entre 1860 et 2100 (*Bindoff et al.* [2007]). La courbe rouge représente le niveau de la mer observé par les marégraphes puis l'altimetrie. Les enveloppes bleues, grises et hachurées donnent les estimations du niveau de la mer futur à partir des modèles semi empiriques. Les barres rouges donnent celles du 4ème rapport du GIEC.

1.4.2 Les projections de la variabilité régionale du niveau de la mer

Les variations du niveau de la mer actuel ne sont pas uniformes (voir section 1.2.2). On s'attend de la même manière à ce que les variations du niveau de la mer futur ne soient pas uniformes. En effet, la variabilité régionale du niveau de la mer future sera dominée par les effets stériques non-uniformes (*Pardaens et al.* [2011]; *Yin et al.* [2010]; *Suzuki and Ishii* [2011]).

Bien qu'il y ait des différences parmi les projections, globalement les différents modèles de climat s'accordent sur les grandes structures régionales du niveau de la mer futur (voir Fig. 1.24b). Ces grandes structures sont les suivantes. La moyenne des projections (Fig. 1.24a) montre une augmentation du niveau de la mer plus grande que celle du niveau global dans l'océan Arctique. Ceci est dû à l'augmentation du flux d'eau douce dans cette région suite à la fonte des glaces de mer et de la glace venant du Groenland ainsi qu'à l'augmentation du débit des fleuves affluents. Une compensation est prédite entre les fortes contributions thermostériques et halostériques dans l'océan Atlantique qui se solde par une légère domination de l'expansion thermique. Dans l'océan Antarctique autour de 60°S, on observe une baisse du niveau de la mer par rapport à la moyenne alors qu'un peu

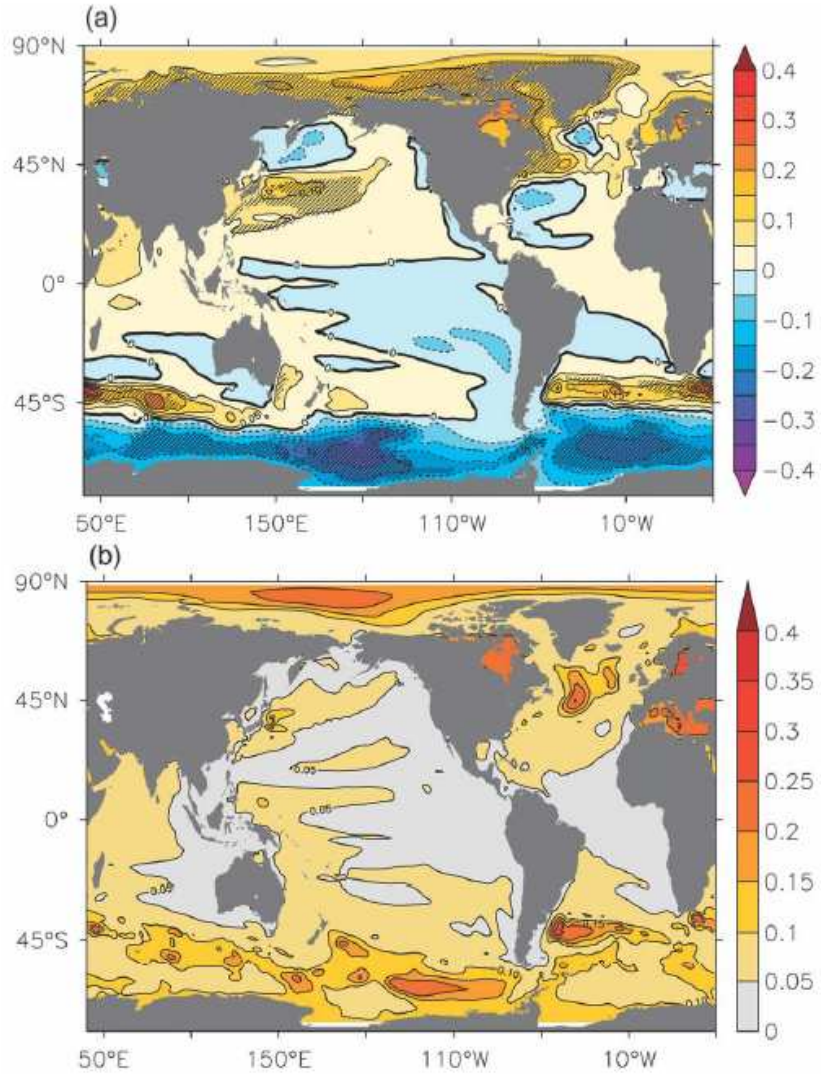

Figure 1.24 – Moyenne des projections (scénario A1B) de la variabilité régionale du niveau de la mer en 2091-2100 par rapport au niveau de la mer en 1991-2000, sur la base de 12 modèles utilisés pour le 4ème rapport du GIEC. a) Moyenne des projections du niveau de la mer dynamique en m. b) Ecart type des projections en m. Les régions hachurées sur la Fig. 1.24a indiquent les zones pour lesquelles le rapport de la moyenne sur l'écart-type est >1.5. Figure tirée de *Yin et al.* [2010].

plus au Nord (autour de 45°S) on observe une bande zonale pour laquelle le niveau de la mer augmente. Ce comportement dipolaire est associé aux changements du courants Antarctique circumpolaire en réponse à l'augmentation du vent autour de 50°S. En effet cette augmentation du vent intensifie la convergence et la subduction des eaux modales et intermédiaires (donc augmente le niveau de la mer) au Nord vers 40°S tandis qu'il génère plus de divergence et d'"upwelling" (donc diminue le niveau de la mer) au Sud vers 60°S (*Sen Gupta et al.* [2009]). Dans l'océan Indien les projections prévoient en général une augmentation du niveau de la mer légèrement plus grande que la moyenne.

D'autres facteurs, en dehors des effets stériques, génèrent de la variabilité régionale dans le niveau de la mer comme par exemple les effets gravitationnels et la déformation

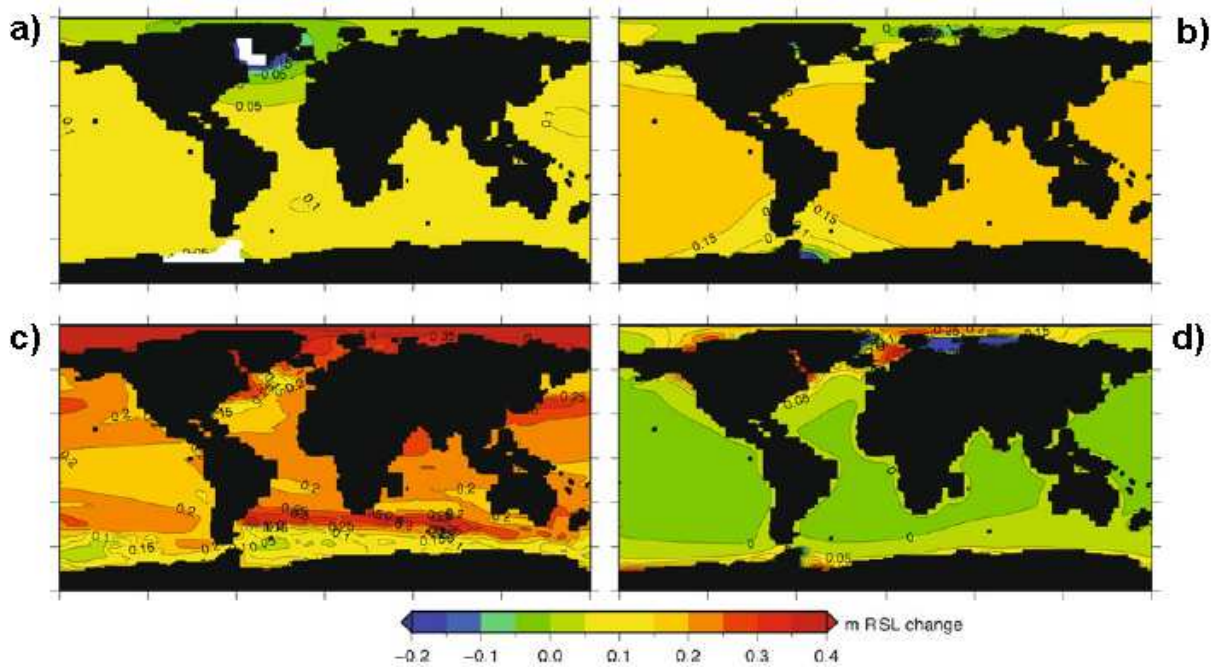

Figure 1.25 – Contributions de chaque facteur à la variabilité régionale du niveau de la mer en 2090-2099 par rapport à 1990-1999. Les figures sont la moyenne des projections du scénario A1B obtenues pour 12 modèles de climats. a) Contribution des calottes polaires. b) Contribution des glaciers. c) Contribution des effets stériques. d) Contribution de la réponse de la Terre solide à la dernière déglaciation (GIA). Figure tirée de *Slangen et al.* [2011].

des bassins océaniques induits par la réponse visqueuse et élastique de la Terre aux redistributions (présente et passée) de masses d'eau (voir sections 1.3.2 et 1.3.3). Jusqu'à maintenant ces facteurs n'étaient pas pris en compte dans la projection de la variabilité régionale. Pour la première fois *Slangen et al.* [2011] les ont évalués dans leurs projections des différents scenarii de réchauffement climatique. Ces auteurs ont modélisé le niveau de la mer régional en prenant en compte les effets stériques et les effets induits par la réponse de la Terre solide à la dernière déglaciation (voir section 1.3.3) et à la fonte des glaces actuelles (voir section 1.3.2). La Fig. 1.25 (tirée de *Slangen et al.* [2011]) montre la contribution de chacun de ces facteurs à la variabilité régionale du niveau de la mer pour la décennie 2090-2099 par rapport à 1990-1999 et pour le scénario A1B (réchauffement global de 2.8°C et hausse du niveau de la mer global ∼50 cm en 2090-2099). Ces cartes sont basées sur la moyenne de 12 modèles de climat utilisés pour les projections du 4ème rapport du GIEC. Elles montrent un niveau de la mer régional entre ∼-4 m (au voisinage des calottes polaires) et +80 cm.

La Fig. 1.26 (tirée aussi de *Slangen et al.* [2011]) donne la projection de la variabilité régionale dûe à la somme des facteurs présentés Fig. 1.25 pour trois scenarii différents : A1B, B1 et A2. Comme pour la Fig. 1.25, la hausse du niveau global est incluse dans les cartes présentées Fig. 1.26. Dans ces projections, la variabilité stérique domine toujours le niveau de la mer régional comme dans les projections antérieures réalisées pour le 4ème rapport du GIEC. Mais localement, au voisinage des régions qui ont perdu ou qui perdent aujourd'hui de la glace, les effets de la Terre solide produisent une forte contribution négative aux variations du niveau de la mer. Dans certaines régions de l'Arctique par

exemple, ils compensent l'augmentation du niveau de la mer dûe à la baisse de la salinité. Cette figure montre que la variabilité régionale attendue en 2090-2099 est très forte comparée au niveau global pour les trois scenarii A1B, B1 et A2. Il est primordial de la prendre en compte.

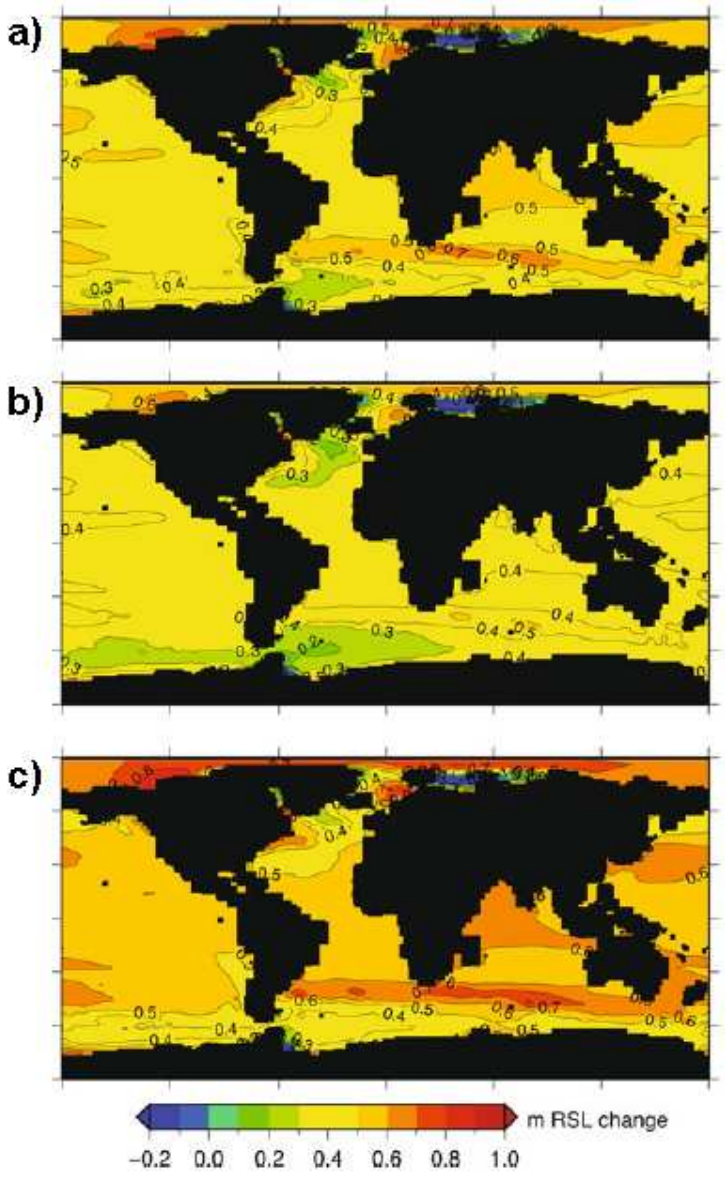

Figure 1.26 – Variabilité régionale du niveau de la mer en 2090-2099 par rapport à 1990-1999 (moyenne de 12 modèles de climat) dûe à la somme de tous les facteurs montrés sur la Fig. 1.25. Le résultat est donné pour 3 scenarii différents : a) scénario A1B (+2.8˚ en 2100), b) scénario B1 (+1.8˚ en 2100), c) scénario A2 (+3.4˚ en 2100). Le niveau de la mer global (de ∼50 cm pour A1B, ∼40 cm pour B1 et ∼55 cm pour A2) n'a pas été enlevé. Figure tirée de *Slangen et al.* [2011].

1.5 Les enjeux scientifiques actuels liés au niveau de la mer.

Ce chapitre montre que depuis une vingtaine d'années de nombreux progrès ont été réalisés dans l'estimaton des variations du niveau de la mer. Elles sont mesurées à la précision de 1-2 cm depuis octobre 1992 avec une couverture quasi-globale grâce aux satellites altimétriques. les estimations des tendances du niveau global convergent sur le XX$^{\text{ème}}$ siècle, les dernières décennies et la période altimétrique. Depuis 1993, on a une vision claire de la forte variabilité régionale qui caractérise le niveau de la mer avec une précision sur les tendances locales de 1 à 2 mm.a^{-1}. Mais il reste encore des incertitudes. La variabilité inter-annuelle du niveau global est mal connue avant la période altimétrique et de nombreuses différences apparaissent entre les différentes estimations. Ceci est encore plus vrai pour la variabilité régionale.

L'étude du bilan du niveau de la mer et de ses contributions montre aussi des limites. Sur la période 1993-2010, l'expansion thermique de l'océan observé par les données hydrographiques d'une part, et la fonte des glaciers de montagne et des calottes polaires observée par les mesures in-situ et aéroportées d'autre part expliquent bien la tendance du niveau de la mer. De même les variations inter-annuelles des stocks d'eau des grands bassins fluviaux du monde sont en accord avec la variabilité inter-annuelle du niveau marin. Mais sur la période 2002-2010 les mesures GRACE des variations de masse de l'océan ne s'accordent pas avec les mesures in-situ et aéroportées de la fonte des glaciers de montagne et des calottes polaires. On trouve aussi sur cette periode des différences surprenantes entre les différentes estimations de la tendance du niveau de la mer à partir des données satellites (*Masters et al.* [in press]) si bien que le bilan du niveau de la mer reste controversé entre 2002 et 2010. Sur la période 1950-2010 le bilan apparait fermé (*Church et al.* [2011]) mais avec de grandes barres d'erreur concernant l'expansion thermique et surtout la contribution des glaces.

Concernant les projections, Il est bien établi aujourd'hui que le niveau de la mer va continuer à monter dans le futur. En revanche, nous ne savons pas à combien de dizaines de cm de niveau de la mer supplémentaires nous devons nous préparer pour 2100. Doit-on s'attendre à 20 cm de plus, comme le prédisent les projections les plus optimistes du 4$^{\text{ème}}$ rapport du GIEC (*Bindoff et al.* [2007]) ou devrait-on déjà se preparer à une augmentation de 1,8 m comme le suggèrent les simulations semi-empiriques les plus pessimistes (*Vermeer and Rahmstorf* [2009]) ? Le niveau de la mer répond de façon complexe aux changements des différentes composantes du système climatique et à leurs interactions. Sa modélisation n'est pas simple. L'incertitude principale provient de notre méconnaissance de l'évolution future des calottes polaires. Les observations spatiales (par altimétrie Radar et Laser, interférométrie Radar InSAR et gravimétrie spatiale GRACE) ont clairement mis en évidence une accélération récente de la perte de masse de glace des régions côtières du Groenland et de l'Antarctique de l'Ouest. Des mécanismes ont été proposés (instabilités dynamiques des glaciers côtiers dues au réchauffement de l'océan et -au moins au Groenland- à la lubrification basale de la calotte par les eaux provenant de la fonte en surface). Mais ils ne sont pas encore complètement compris et leur modélisation reste un défi. Par ailleurs les modèles climatiques couplés n'expliquent que 60% de la hausse observée du niveau de la mer pour le XX$^{\text{ème}}$ siècle (alors que la contribution des calottes était probablement faible,

Bindoff et al. [2007]) et ils reproduisent mal la variabilité régionale passée. Certains processus physiques clés dans la circulation océanique ne sont pas pris en compte comme le rôle joué par les tourbillons (*Hogg et al.* [2009]) aux échelles climatiques ou la stabilité des masses d'eau profondes.

D'importants progrès sont donc à réaliser pour estimer précisement les variations passées du niveau de la mer et produire des projections réalistes (en global et régional). Nous listons ici les grandes questions et principaux défis scientifiques auxquels la communauté climatologique est confrontée actuellement sur cette thématique :

(a) Concernant les observations du niveau de la mer :

1. L'augmentation du niveau de la mer observée au cours du XX$^{\text{ème}}$ siècle est-elle anormale comparée aux variations observées durant les siècles et millénaires précédents ? La réponse est probablement oui, si on la compare aux variations du niveau de la mer durant les 2000 dernières années (*Miller et al.* [2009]; *Kemp et al.* [2011]). Mais si on la compare à des augmentations abruptes mesurées au cours de la dernière déglaciation elle semble modeste : *Deschamps et al.* [2012] rapporte une augmentation du niveau de la mer de $\sim$40 mm.a^{-1} durant 350 ans qui serait survenue il y a $\sim$14500 ans.

2. Est ce que la hausse du niveau de la mer actuel est en train d'accélérer ? Ceci a été suggéré par *Merrifield et al.* [2009]. Mais *Nerem et al.* [2010] a montré que la vitesse du niveau de la mer n'a pas augmenté dans les années 2000 comparé aux décennies précédentes du fait en particulier de l'occurence d'évènements La Niña exceptionellement forts. Néanmoins au cours de la période altimétrique, la tendance du niveau de la mer global est 2 fois plus grande qu'au cours des 50 dernières années. S'agit il d'une accélération ou a-t-on à faire à de la variabilité décennale ? La réponse à cette question reste controversée.

3. Peut-on réduire l'incertitude qu'il subsiste sur la tendance du niveau de la mer observée par altimétrie ? Cette incertitude s'élève aujourd'hui à 0.5-0.6 mm.a^{-1} (*Ablain et al.* [2009]). Plusieurs signaux physiques qui ont un impact sur le niveau de la mer sont de cet ordre de grandeur voire un peu plus petit : la tendance des stocks d'eau continentaux, les effets quasi-statiques (GIA et réponse de la croûte terrestre à la fonte actuelle des glaces), etc. Il est nécessaire d'améliorer la performance des mesures altimétriques sur ce point.

4. Peut'on réduire les différences en variabilité inter-annuelle qui existent entre les courbes du niveau de la mer calculées avec les données altimétriques par les différentes équipes de recherche (e.g. *Masters et al.* [in press]). Ceci est primordial dans l'étude des causes des variations du niveau de la mer.

5. Quel est la variabilité du niveau de la mer dans l'océan Arctique ? Monte-t-il plus vite en Arctique que dans le reste du monde comme le suggèrent les modèles ? Et si oui, quelle est sa contribution à la hausse du niveau de la mer global ? les données de Topex/Poseidon et Jason1-2 ne montent pas au dessus de 66°N. En revanche les données de ERS et Envisat qui couvrent en partie l'océan Arctique ainsi que les données des marégraphes Norvégiens et Russes récemment rendues publiques devraient donner des éléments de réponse à ces questions.

6. Peut-on estimer de manière fiable la variabilité régionale du niveau de la mer sur les dernières décennies ? La variabilité régionale peut être étudiée avant la periode altimétrique à l'aide des OGCM, des réanalyses océaniques et des reconstructions en 2 dimensions du niveau de la mer (voir section 2.2). Cependant ces différentes techniques présentent des resultats différents. Peut'on les améliorer ?

7. Qu'est ce qui explique la variabilité régionale du niveau de la mer aux échelles inter-annuelles à multi-décennales ? Quel rôle jouent le stress du vent et les échanges de masse et de chaleur entre l'océan et l'atmosphère ?

8. Est ce que la variabilité régionale du niveau de la mer que l'on observe par altimétrie depuis 1993 (Fig. 1.12) est stable dans le temps ? Si non, quels sont les temps caractéristiques de son évolution ?

9. Des études récentes suggèrent que la variabilité régionale de l'expansion thermique (qui est en grande partie à l'origine de la variabilité régionale du niveau de la mer) évolue dans le temps et l'espace avec les modes de variabilité du système climatique comme ENSO, PDO, SAM et NAO. Peut-on déterminer précisement ces fluctuations à l'aide des mesures et des modèles ? Peut'on établir le lien avec les modes de variabilité naturelle du climat ?

10. Sur la base des deux questions précédentes, peut t'on déterminer la cause première dans le système climatique qui détermine la variabilité régionale du niveau de la mer observée par altimétrie ? Est elle largement dominée par la variabilité interne du système climatique ou peut t'on y détecter l'impact des forçages naturels (tels que la variabilité solaire et volcanique) ou anthropiques (tels que les gaz à effet de serre ou les aérosols) ?

(b) Concernant les contributions au niveau de la mer :

11. Comment expliquer les différences importantes à l'échelle inter-annuelle entre les niveaux de la mer stériques (thermostérique et halostérique) des différentes bases de données ?

12. Quelle est la contribution de l'océan profond au niveau de la mer stérique ? Peut-on en calculer une limite supérieure à défaut d'une estimation précise ? (Les bouées Argo ne descendent pas plus bas que 2000 m, et avant 2003 on ne dispose pas de données spatialement bien réparties en dessous de 700m.)

13. Avec quelle précision peut t'on estimer la contribution stérique de chaque bassin océanique ? Peut'on suivre en temps et profondeur le réchauffement des bassins ?

14. Peut t'on expliquer le ralentissement observé depuis 2003 dans l'expansion thermique globale (en particulier avec le réseau Argo) ?

15. Peut t'on améliorer les observations GRACE des variations de masse globale de l'océan ? GRACE permet une estimation directe des variations de la masse de l'océan depuis 2002. Quand on compare les mesures GRACE moyennées sur l'océan avec les apports d'eau venant de la fonte des glaciers de montagne et des calottes polaires,

estimés par ailleurs avec les mesures in-situ et satellitaires, on obtient des différences importantes. Les mesures GRACE sont très sensibles au GIA et à la fonte actuelle des glaces dont les corrections gravimétriques sont encore mal connues. Est ce que cela explique les différences ? N'y a t'il pas aussi des erreurs dans les mesures in-situ ?

16. Les glaciers de montagne contribuent-ils à la variabilité inter-annuelle du niveau de la mer ?

17. Peut t'on réconcilier les différentes observations de la perte de masse au Groenland et en Antarctique (Altimetrie Radar et Laser, inSAR, GRACE) ?

18. La perte de masse des calottes polaires est-elle en train d'accélérer ? S'agit-il d'un phénomène temporaire ou de la signature d'une tendance à long terme ?

19. Le cycle global de l'eau s'intensifie t'il ? Quel en est la conséquence sur les stocks d'eau continentaux et donc sur le niveau de la mer ?

20. Comprend-on les processus qui expliquent la covariance aux échelles inter-annuelles entre les stocks d'eau continentaux et le niveau de la mer ?

21. Peut t'on détecter dans les observations des variations du niveau de la mer les contributions non-stériques à la variabilité régionale ?

22. La variabilité régionale non stérique de l'océan est dûe aux variations régionales de masse de l'océan. Ces variations régionales de masses sont provoquées soit par des variations du geoïde suite aux redistribution de masse à la surface de la Terre (GIA, fonte actuelle des glaces) soit par des variations de la dynamique océanique en réponse au forçage extérieur (vent, échanges de masse et de chaleur avec l'atmosphère ou les continents). Peut t'on estimer la signature spatiale et l'amplitude de chacun de ces 2 termes ?

23. Les variations régionales de masse de l'océan peuvent être estimées de 2 manières : de manière indirecte en corrigeant le niveau de la mer du niveau de la mer stérique (e.g. en calculant "Altimetrie moins Argo" sur la période récente 2004-2009) ou de manière directe avec les mesures GRACE depuis 2002 . Ces deux méthodes donnent des résultats différents (e.g. Llovel et al. 2010). D'où viennent ces différences ? Peut on les expliquer ?

(c) Concernant les projections du niveau de la mer et de sa variabilité régionale

24. Quelle sera la contribution des calottes polaires à l'augmentation du niveau de la mer dans le futur ?

25. Pourquoi les projections des modèles de climat couplés donnent une augmentation du niveau de la mer plus faible dans le futur que celles des modèles semi-empiriques ?

26. Quelle sera la variabilité régionale du niveau de la mer dans le futur ? Une première estimation a été donnée par *Slangen et al.* [2011] sur la base des simulations CMIP3. Les résultats seront ils identiques avec les simulations CMIP5 ?

27. Les projections du niveau de la mer pour les 20 à 30 ans à venir vont elles être très différentes des projections pour 2100 ? Quel degrès de confiance peut-on accorder à ces projections décennales ?

(d) Concernant les impacts dans les zones côtières

28. Est on capable d'estimer précisemment le niveau de la mer relatif (i.e. somme du niveau de la mer global de la variabilité régionale locale et du mouvement vertical de la croûte terrestre à la côte) dans les régions vulnérables pour les dernières décennies ?

29. Quelle est la contribution de l'augmentation du niveau de la mer à l'érosion des côtes ? Est elle significative comparée aux autres facteurs naturels ou anthropiques d'érosion ?

30. Y a t-il un seuil dans la vitesse d'augmentation du niveau de la mer à partir duquel les facteurs d'érosion locaux deviennent secondaires ?

31. Est on capable de fournir aux décideurs et aux élus des projections fiables du niveau de la mer relatif pour les prochaines décennies ?

1.6 Résumé des variations du niveau de la mer : les observations, les causes et les projections

Dans les chapitres suivants nous présentons nos travaux de thèse et les éléments de réponse qu'ils apportent aux questions scientifiques n°6, 7, 8, 9, 10, 11, 13, 14, 20, 21, 22, 23, 28, 29 et 30 de la liste ci-dessus. Ce sont les questions scientifiques qui portent sur la variabilité régionale du niveau de la mer, ses causes, ses origines et les impacts associés. Auparavant nous proposons un article de synthèse sur les variations passées et actuelles du niveau de la mer et ses causes, que nous avons publié dans le journal "Journal of Geodynamics" en Mars 2012. Cet article s'intitule "Sea level : a review of present-day and recent-past changes and variability". Il résume le chapitre 1.

Journal of Geodynamics 58 (2012) 96–109

Contents lists available at SciVerse ScienceDirect

Journal of Geodynamics

journal homepage: http://www.elsevier.com/locate/jog

Review

Sea level: A review of present-day and recent-past changes and variability

Benoit Meyssignac*, Anny Cazenave

LEGOS-CNES, Toulouse, France

ARTICLE INFO

Article history:
Received 12 December 2011
Received in revised form 9 March 2012
Accepted 10 March 2012
Available online 19 March 2012

Keywords:
Sea level
Altimetry
Global mean sea level
Regional sea level
Sea level reconstruction
Climate change

ABSTRACT

In this review article, we summarize observations of sea level variations, globally and regionally, during the 20th century and the last 2 decades. Over these periods, the global mean sea level rose at rates of 1.7 mm/yr and 3.2 mm/yr respectively, as a result of both increase of ocean thermal expansion and land ice loss. The regional sea level variations, however, have been dominated by the thermal expansion factor over the last decades even though other factors like ocean salinity or the solid Earth's response to the last deglaciation can have played a role. We also present examples of total local sea level variations that include the global mean rise, the regional variability and vertical crustal motions, focusing on the tropical Pacific islands. Finally we address the future evolution of the global mean sea level under ongoing warming climate and the associated regional variability. Expected impacts of future sea level rise are briefly presented.

Contents

1. Introduction

Sea level variations spread over a very broad spectrum. The largest global-scale sea level changes (100-200 m in amplitude) occurred on geological time scales (on the order of ~100 million years) and depended primarily on tectonic processes (e.g. large-scale change in the shape of ocean basins associated with seafloor spreading and mid-ocean ridges expansion) (e.g. Haq and Schutter, 2008; Mueller et al., 2008; Miller et al., 2011). With the formation of the Antarctica ice sheet about 34 million years ago, global mean sea level dropped by about 50 m. More recently, cooling of the Earth starting about 3 million years ago, led to glacial/interglacial cycles driven by incoming insolation changes in response to variations of the Earth's orbit and obliquity (Berger, 1988). Corresponding growth and decay of northern hemisphere ice caps on time scales of tens of thousand years produced large

* Corresponding author.
E-mail address: benoit.meyssignac@legos.obs-mip.fr (B. Meyssignac).

0264-3707/$ – see front matter © 2012 Elsevier Ltd. All rights reserved.
doi:10.1016/j.jog.2012.03.005

oscillations of the global mean sea level, on the order of >100 m (e.g. Lambeck et al., 2002; Rohling et al., 2009; Yokoyama and Esat, 2011). On shorter (decadal to multi centennial) time scales sea level fluctuations are mainly driven by climate change in response to natural forcing factors (e.g. solar radiation variations, volcanic eruptions) and to internal variability of the climate system (related for example to atmosphere–ocean perturbations such as El Niño-Southern Oscillation – ENSO, North Atlantic Oscillation – NAO, Pacific Decadal Oscillation – PDO). Since the beginning of the industrial era, about two centuries ago, mean sea level is also responding to anthropogenic global warming. In effect, sea level is a very sensitive index of climate change and variability. For example, as the ocean warms in response to global warming, sea waters expand, and thus sea level rises. As mountain glaciers melt in response to increasing air temperature, sea level rises because of fresh water mass input to the oceans. Similarly, ice mass loss from the ice sheets causes sea level rise. Corresponding increase of fresh water into the oceans changes water salinity, hence sea water density as well as ocean circulation that in turn affects sea level at a regional scale. Modification of the land hydrological cycle due to climate variability and direct anthropogenic forcing leads to changes in precipitation/evaporation regimes and river runoff, hence ultimately to sea level changes. Thus global, regional and local climate changes affect sea level (e.g. Bindoff et al., 2007).

In this article, we review observations of sea level variations, globally and regionally, focusing on the 20th century and the last 2 decades (Sections 2–4). We also examine the causes of sea level variations, and discuss successively components of the global mean sea level rise over the past two decades, and the contributions to the interannual global mean sea level (Section 5). Regional variability in sea level is addressed in Sections 6 and 7. In Section 8, we show examples of total sea level changes measured over the past 5–6 decades. In the last section (Section 9) we briefly address the future evolution of the global mean sea level under warming climate and associated regional variability. Concluding remarks are proposed in Section 10.

2. Paleo sea level (since the last glacial maximum and last 2000 years)

Quaternary ice ages caused large-scale fluctuations of the global mean sea level, of >±100 m amplitude, as a result of the growing and decay of northern hemisphere ice caps (Rohling et al., 2009). Since about 800,000 years, the characteristic periodicity of these fluctuations is ~100,000 years. At the last glacial maximum, ~20,000 years ago, global mean sea level was −130 m below present level (Lambeck et al., 2002). Subsequent melting of the northern hemisphere ice caps caused by insolation changes led to sustained sea level rise during more than 10,000 years, as illustrated in Fig. 1 (from Lambeck et al., 2002). Due to the complex history of ice cap melting (e.g. Peltier, 2004), the rate of sea level rise was not constant, as evidenced by several paleo sea level indicators of geological and biological origin (e.g. coral data, micro-atolls, beach rocks, notches, etc.). For example, episodes of rapid rise (>1 m per century) have been reported at about −14,000 years (Bard et al., 2010). At the beginning of the Holocene (11,000 years ago), the rate of rise decreased significantly and sea level stabilized between −6000 years and −2000 years ago (Lambeck et al., 2010).

There is no evidence of large fluctuations of the global mean sea level during the past two millennia. Dating of microfossils in salt-marsh environments (Lambeck et al., 2010; Kemp et al., 2011) and archaeological evidence (e.g. from Roman fish tanks, Lambeck et al., 2004) indicate that sea level rise did not exceed 0.05–0.07 m per century over the past 2000 years (see also Miller et al., 2009). Fig. 2 (from Kemp et al., 2011) illustrates this fact. It shows the

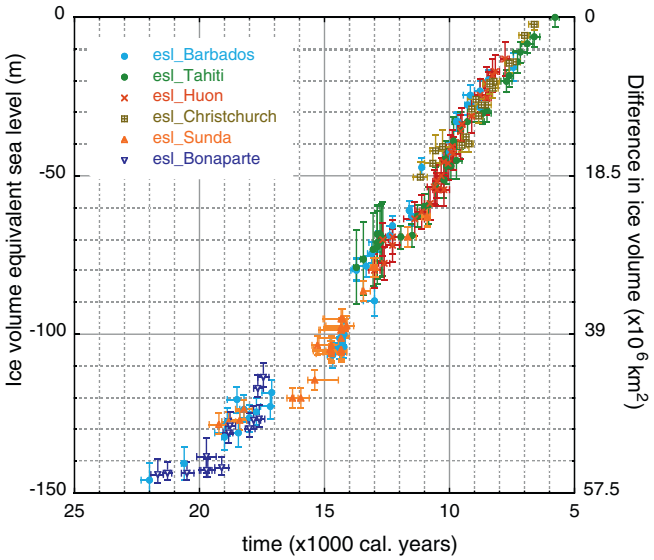

Fig. 1. Changes in global ice volume and sea level equivalent from the last glacial maximum to the present. The figure shows ice-volume equivalent sea level for the past 20 kyr based on isostatically adjusted sea-level data from different localities (updated from Lambeck et al., 2002 with a revised dataset for the Sunda shelf from Hanebuth et al., 2009).

sea level evolution of the last two millennia based on salt-marsh microfossils analyses along the eastern coast of North America. According to this study, sea level was a few decimeters higher/lower during the Middle Age (12th–14th century)/Little Ice Age (16th–18th century), but rates of rise remained very low until the beginning of the industrial era (late 18th to early 19th century) when a large upward trend of the mean sea level becomes well apparent (Kemp et al., 2011; also Gehrels et al., 2005, 2006; Woodworth et al., 2011a). This epoch corresponds to the beginning of the instrumental era that allowed direct sea level measurements with tide gauges (Woodworth et al., 2008, 2011b) and now satellites (e.g. Fu and Cazenave, 2001; Church et al., 2010), unlike during the previous centuries/millennia for which sea level variations are deduced indirectly from proxy records.

3. The tide gauge-based instrumental record (20th century)

The very first tide gauges were installed in ports of northwestern Europe to provide information on ocean tides (e.g. Mitchum et al., 2010). Tide gauges records from Amsterdam (the Netherlands), Stockholm (Sweden) and Liverpool (UK) extend back to the early to mid-18th century, while those from Brest (France) and Swinoujscie (Poland) started in the early 19th century. In the southern hemisphere, tide gauge records at Sydney and Freemantle (Australia) are among the longest (starting in the late 19th century). Progressively, the tide gauge network extended (see for example Fig. 5.2 from Mitchum et al., 2010) but for long term sea level studies, the number of records remains nevertheless very small and the geographical spread is quite inhomogeneous. Besides, tide gauge records often suffer from multi-year- or even multi-decade-long gaps. The sparse and heterogeneous coverage of tide gauge records, both temporally and geographically, is clearly a problem for estimating reliable historical mean sea level variations.

Tide gauges measure sea level relatively to the ground, hence monitor also ground motions. In active tectonic and volcanic regions, or in areas subject to strong ground subsidence due to natural causes (e.g. sediment loading in river deltas) or human activities (ground water pumping and oil/gas extraction), tide gauge data are directly affected by the corresponding ground motions. Post

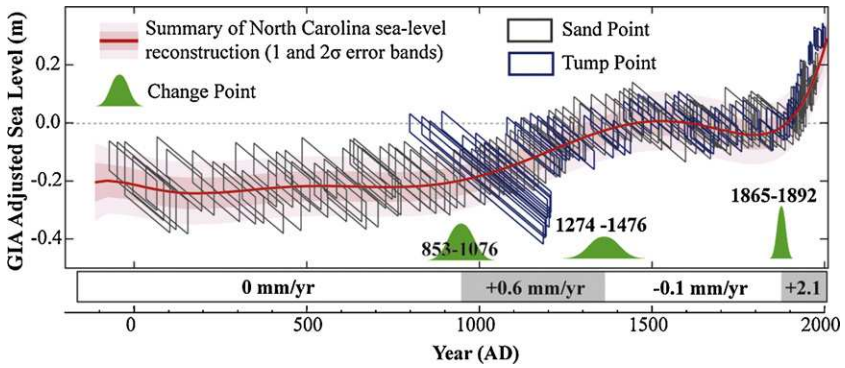

Fig. 2. Relative sea level reconstruction for the last 2000 years from salt-marsh data analyses. (From Kemp et al., 2011.)

glacial rebound, the visco-elastic response of the Earth crust to last deglaciation (also called Glacial Isostatic Adjustment – GIA) is another process that gives rise to vertical land movement. While vertical ground motions need to be considered when estimating total local (relative) sea level change (see Section 8), to compare observed sea level variations with climate-related components, the ground motions need to be subtracted.

To provide a reliable historical sea level time series based on tide gauge records, various strategies have been developed. Some authors only considered a few tens of long (>60 years) good quality tide gauges records from tectonically stable continental and island coasts, and corrected the data for GIA only (e.g. Douglas, 1991, 2001; Peltier, 2001; Holgate, 2007). Other authors used a larger set of records from a variety of regions, covering different time periods, and developed different approaches to derive the mean sea level curve. For example, Jevrejeva et al. (2006, 2008) used a regional coherency criterium among tide gauge records in order to exclude outliers (e.g. tide gauge affected by large local vertical ground motions). Church et al. (2004) and Church and White (2006, 2011) developed a 'reconstruction' method (see Section 6) to determine a 'global mean' sea level curve from sparse tide gauge records since 1870. In these studies, the only vertical motion corrected for is GIA. Since a few years, the availability of GPS-based precise positioning at some tide gauge sites has allowed direct measurements of vertical ground motion. This is the approach used by Woppelmann et al. (2007, 2009). GPS-based vertical ground motions are still based on short records (10–15 year-long only) but it is generally assumed that these are representative of long-term trends. In spite of a variety of approaches, the results based from these studies are rather homogeneous and give a mean rate 20th century rise in the range of 1.6–1.8 mm/yr. The Church and White (2011)'s tide gauge-based mean sea level curve since 1870 is shown in Fig. 3. According to this figure, 20th century sea level rise was not linear. In fact, interannual to decadal variability (in addition to shorter-term fluctuations not considered here) are superimposed on the mean trend. These will be discussed in Section 5.2.

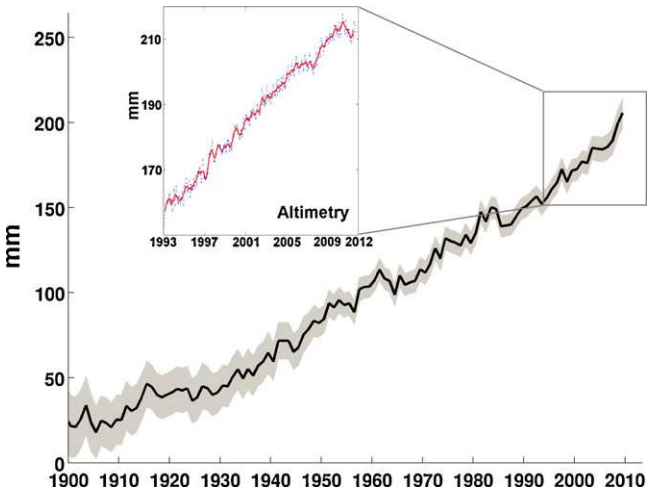

Fig. 3. 20th century sea level curve (in black and associated uncertainty in light gray) based on past sea level reconstruction using tide gauge data and additional information (from Church and White, 2011). In the box: altimetry-based sea level curve between 1993 and 2011 (data from AVISO; http://www.aviso.oceanobs.com/en/data/products/sea-surface-height-products/global/msla/index.html) (blue points: data at 10-day interval; the red curve is based on a 3-month smoothing of the blue data).

4. The altimetry era

Since the early 1990s, sea level variations are measured by altimeter satellites (Chelton et al., 2001; Fu and Cazenave, 2001). The satellite altimetry measurement is derived as follows (see Fig. 4): the onboard radar altimeter transmits microwave radiation towards the sea surface which partly reflects back to the satellite. Measurement of the round-trip travel time provides the height of the satellite above the instantaneous sea surface. The sea surface height measurement is deduced from the difference between the satellite distance to the Earth's centre of mass (deduced from precise orbitography) and the satellite altitude above the sea surface

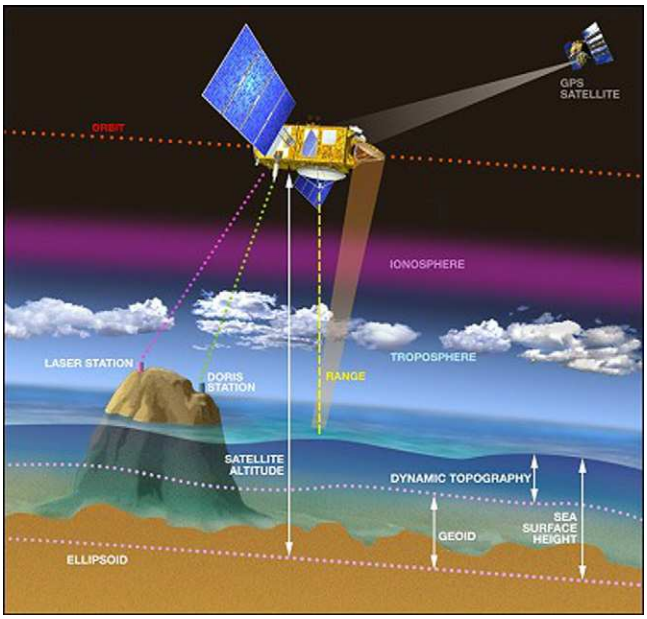

Fig. 4. Principle of the satellite altimetry measurement.

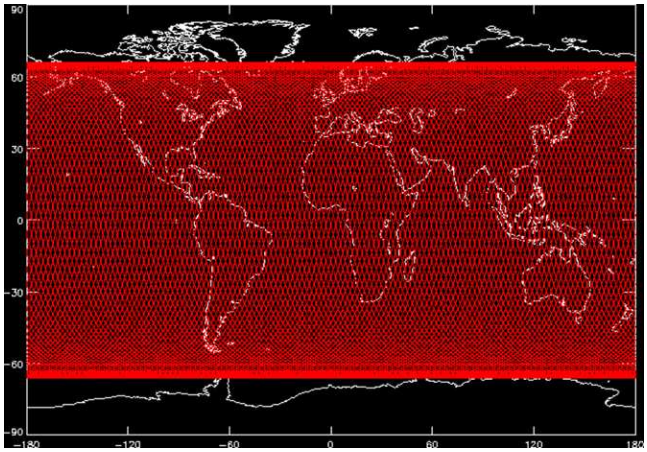

Fig. 5. Earth's coverage by the Topex/Poseidon, Jason-1 and Jason-2 altimeter satellites during an orbital cycle of 10 days.

(deduced from the radar altimeter measurement). The sea surface height measurement needs to be corrected for various factors due to ionospheric and tropospheric delay, and for biases between the mean electromagnetic scattering surface and the sea surface at the air-sea interface. Other corrections due geophysical effects, such as solid Earth, pole and ocean tides are also applied. Altimeter satellites cover the whole Earth surface within a few days – called orbital cycle (see Fig. 5). Geographical averaging of all individual sea surface heights measurements during an orbital cycle allows determining a global mean sea level value, and further constructing a global mean sea level time series. As the satellite flies over the same areas from one orbital cycle to another, it is also possible to construct a 'local' sea level time series, hence deduce regional variability in sea level.

High-precision satellite altimetry began with the launch of the Topex/Poseidon satellite in 1992 and its successors, Jason-1 (2001) and Jason-2 (2008). The precision of an individual sea surface height measurement based on these missions has now reached the 1–2 cm level (e.g. Nerem et al., 2010; Beckley et al., 2010; Mitchum et al., 2010). Precision on the global mean rate of rise is currently of ~0.4–0.5 mm/yr. This value is based on error budget analyses of all sources of error affecting the altimetry system or on comparisons with tide gauge-based sea level measurements (e.g. Ablain et al., 2009). In Fig. 3, the altimetry-based global mean sea level curve since early 1993 is superimposed on the tide-gauge-based 20th century sea level curve. We note an almost linear increase (except for temporary anomalies associated with the 1997/1998 El Niño and the 2007/2008 and 2010/2011 La Niña events). Over this 18 year-long period, the rate of global mean sea level rise amounts to 3.2 ± 0.5 mm/yr (e.g. Cazenave and Llovel, 2010; Nerem et al., 2010; Mitchum et al., 2010). This rate is significantly higher than the mean rate recorded by tide gauges over the past decades, eventually suggesting sea level rise acceleration (Merrifield et al., 2009).

5. Causes of present-day GMSL changes

5.1. Global mean rise

The main factors causing current global mean sea level rise are thermal expansion of sea waters, land ice loss and fresh water mass exchange between oceans and land water reservoirs. The recent trends of these contributions most likely result from global climate change induced by anthropogenic greenhouse gases emissions.

5.1.1. Ocean warming

Analyses of in situ ocean temperature data collected over the past 50 years by ships and recently by Argo profiling floats (Argo Data Management Team, 2008; Roemmich et al., 2009) indicate that ocean heat content, and hence ocean thermal expansion, has significantly increased since 1950 (e.g. Levitus et al., 2009; Ishii and Kimoto, 2009; Domingues et al., 2008; Church et al., 2011a). Ocean warming explains about 30%–40% of the observed sea level rise of the last few decades (e.g. Church et al., 2011b). A steep increase was observed in thermal expansion over the decade 1993–2003 (e.g. Lyman et al., 2010; Levitus et al., 2009; Ishii and Kimoto, 2009), but since about 2003, thermal expansion has increased less rapidly (Lyman et al., 2010; Llovel et al., 2010; von Schuckmann and Le Traon, 2011). The recent slower rate of steric rise likely reflects short-term variability rather than a new long-term trend. On average, over the satellite altimetry era (1993–2010), the contribution of ocean warming to sea rise accounts for ~30% (Cazenave and Llovel, 2010; Cazenave and Remy, 2011; Church et al., 2011b).

5.1.2. Glaciers melting

Being very sensitive to global warming, mountain glaciers and small ice caps have retreated worldwide during the recent decades, with significant acceleration since the early 1990s. From mass balance studies of a large number of glaciers, estimates have been made of the contribution of glacier ice melt to sea level rise (Meier et al., 2007; Kaser et al., 2006). For the period 1993–2010, glaciers and ice caps have accounted for ~30% of sea level rise (e.g. Cogley, 2009; Steffen et al., 2010; Church et al., 2011b).

5.1.3. Ice sheets

While little was known before the 1990s on the mass balance of the ice sheets because of inadequate and incomplete observations, different remote sensing techniques available since then (e.g. airborne and satellite radar and laser altimetry, Synthetic Aperture Radar Interferometry – InSAR, and since 2002, space gravimetry from the GRACE mission) have provided important results on the changing mass of Greenland and (west) Antarctica (e.g. Allison et al., 2009). These data indicate that both ice sheets are currently losing mass at an accelerated rate (e.g. Steffen et al., 2010). Most recent mass balance estimates from space-based observations unambiguously show ice mass loss acceleration in the recent years (e.g. Chen et al., 2009; Velicogna, 2009; Rignot et al., 2008a, b, 2011). For the period 1993–2003, <15% of the rate of global sea level rise was due to the ice sheets (IPCC AR4). But their contribution has increased up to ~40% since 2003–2004. Although not constant through time, on average over 2003–2010 ice sheets mass loss explains ~25% of the rate of sea level rise (Cazenave and Remy, 2011; Church et al., 2011a).

There is more and more evidence that recent negative ice sheet mass balance mainly results from rapid outlet glacier flow along some margins of Greenland and West Antarctica, and further iceberg discharge into the surrounding ocean (Alley et al., 2007, 2008; Steffen et al., 2010). This dynamical thinning process is generally observed in coastal regions where glaciers are grounded below sea level (e.g. in northeast and southwest Greenland, and Amundsen Sea sector, West Antarctica). Thinning and subsequent break-up of floating ice tongues or ice shelves that buttressed the glaciers result in rapid grounding line retreat and accelerated glacier flow. Several recent observations have shown that warming of subsurface ocean waters could trigger these short-term dynamical instabilities (e.g. Holland et al., 2008).

Fig. 6 (updated from Cazenave and Llovel, 2010) compares the observed global mean sea level rise to the different components and their sum over the altimetry era.

5.2. Interannual variability of the global mean sea level

If the (linear) global mean trend is removed from the altimetry-based sea level curve shown in Fig. 3, significant interannual

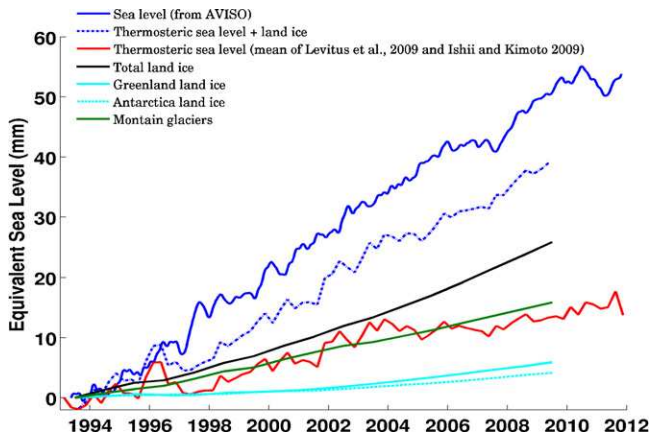

Fig. 6. Observed sea level from satellite altimetry over 1993–2010 (blue solid curve). Thermal expansion (red curve; mean value based on temperature data from Levitus et al., 2009; Ishii and Kimoto, 2009). Contribution from Greenland and Antarctica (cyan curves) and glaciers (green curve). The black curve represents the total land ice contribution while the blue dotted curve represents the total climatic contribution (sum of thermal expansion and land ice) (updated from Cazenave and Llovel, 2010).

variability is visible in the (detrended) global mean sea level (Fig. 7). Nerem et al. (2010) noticed that this detrended global mean sea level is highly correlated with ENSO, with positive/negative sea level anomalies observed during El Niño/La Niña. For example, in Fig. 7 a large positive anomaly in the global mean sea level, of several mm amplitude, is observed during the 1997–1998 El Niño (the warm phase of ENSO) and negative anomalies during the 2007–2008 La Niña (ENSO cold phase). The ENSO influence on the global mean sea level might result from changes in either global ocean heat content or global ocean mass. Llovel et al. (2011) reported that interannual global mean sea level variations are inversely correlated with ENSO-driven variations of global land water storage (with the Amazon basin as a dominant contributor to the latter), thus favouring the second option. In Fig. 7, the total land water storage – expressed in equivalent sea level (updated from Llovel et al., 2011) – is superimposed to the detrended global mean sea level. A high correlation (0.7) is noticed between the two curves. This correlation can be understood as follows: ENSO events produce large scale changes in precipitation regimes in the tropics, with more rainfall over oceans and less rainfall over land during El Niño, and opposite variations during La Niña (e.g. Gu and Adler, 2011). Recent investigations suggest in addition that positive/negative global mean sea level anomalies during El Niño/La Niña essentially result from positive/negative mass anomalies in the north tropical Pacific Ocean, possibly associated with reduced/increased transport of Pacific waters into the Indian Ocean through the Indonesian straits (Cazenave et al., under revision).

6. Causes of present-day and past-decade regional variability

The global coverage of satellite altimetry allows mapping the regional variability of the sea level rates. This has led to the discovery that sea level rise is far from being uniform. In some regions (e.g. western Pacific), the rates of sea level rise have been faster by a factor up to 3–4 the global mean rate over the past two decades. In other regions rates are slower than the global mean or even slightly negative (e.g. eastern Pacific). Fig. 8a shows the altimetry-based spatial trend patterns in sea level over 1993–2010. This variability is emphasized when we remove the global mean sea level trend of 3.2 mm/yr (Fig. 8b). In some regions such as the western and northern Pacific, the southern Indian Ocean or south of Greenland, the local departures from the global mean trend are so large that they actually dominate the sea level rate signal over the short period 1993–2010. Besides the global mean sea level rise and its causes, it is essential to understand the regional variability in sea level rates (i.e. its evolution with time and space and its drivers) if we want to assess for example the potential impacts of the sea level rise in coastal areas.

All processes that influence the global mean sea level (see Section 5.1) actually exhibit a time and space varying signature. For example, local changes in the ocean temperature and salinity fields lead to local sea level changes through associated variations of the

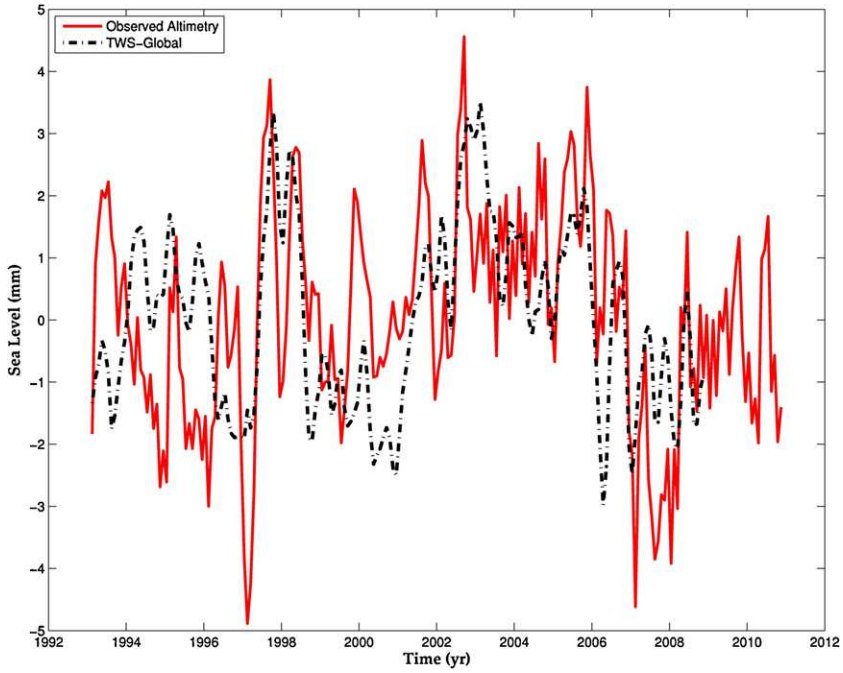

Fig. 7. Detrended global mean sea level curve (from satellite altimetry) over 1993–2010 (in red); total land water storage (noted TWS) expressed in equivalent sea level (black dashed curve) (updated from Llovel et al., 2011).

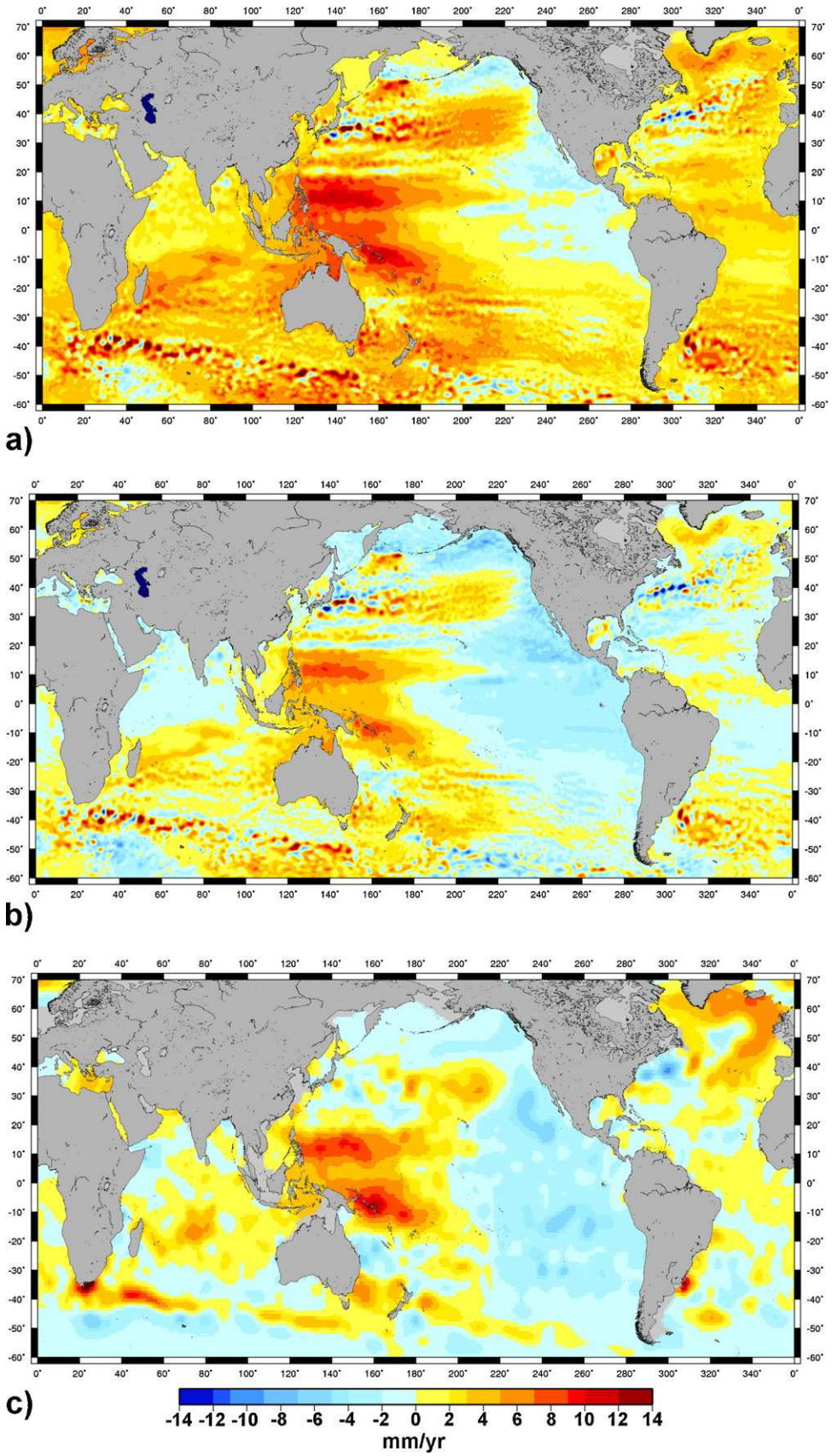

Fig. 8. (a) spatial trend patterns in sea level from satellite altimetry data over 1993–2010. (b) Spatial trend patterns in sea level from satellite altimetry data over 1993–2010 but with the global mean trend of 3.2 mm/yr removed. (c) Spatial trend patterns in thermosteric sea level over 1992–2010. (data from Levitus et al., 2009) (global mean trend removed).

water columns density and volume (thermosteric and halosteric effects respectively) (Bindoff et al., 2007; Wunsch et al., 2007; Lombard et al., 2009; Levitus et al., 2009). These variations are tightly linked to atmosphere–ocean interactions (mostly through wind stress, especially in the tropical Indo-Pacific region, but also through exchanges of heat and fresh water) and associated changes in the ocean flow field (Kohl and Stammer, 2008; Timmermann et al., 2010). Hence they produce regional variability in the rates of sea level change.

Ongoing land ice melting also gives rise to regional variability in sea level change. This comes from two processes. First the influx of freshwater in the ocean from land changes the density structure of the ocean and hence the ocean circulation (Stammer, 2008; Stammer et al., 2011). This results in regional dynamical adjustments of the sea level on inter-annual to multi-decadal time scales (Okumura et al., 2009; Stammer, 2008; Stammer et al., 2011). Second, the transfer of water mass from land into the ocean induced by land ice loss causes an elastic response of the solid Earth that deforms ocean basins. In addition, this mass redistribution produces changes of the geoid (an equipotential of the Earth's gravity field that coincides with the mean sea level) and of the Earth's rotation with a gravitational feedback. These processes (large-scale deformations of the ocean basins and gravitational changes) give rise to regional variability in sea level (Gomez et al., 2010; Milne et al., 2009; Mitrovica et al., 2001, 2009; Tamisiea and Mitrovica, 2011). Such effects associated with present-day land ice loss are still small and hard to detect in the altimetry-based observations of regional variability (Kopp et al., 2010). However, future land ice loss may produce large changes in regional sea level (Mitrovica et al., 2009; Slangen et al., 2011).

The gravitational and deformational (i.e. change in shape of ocean basins) effects associated with the visco-elastic Earth response to the last deglaciation (GIA) also produce non uniform sea level rise, in particular in the vicinity of regions occupied by the continental ice caps that covered the northern hemisphere during the Last Glacial Maximum (~20,000 years ago). But far-field sea level changes also occur (Milne and Mitrovica, 2008; Mitrovica et al., 2001; Tamisiea and Mitrovica, 2011).

Other phenomena such as erosion, deposition and compaction of sediments play some role locally, through the response of ocean floor to loading (Blum and Roberts, 2009). Finally the deformation of the Earth due to convective flow of the mantle and tectonic processes (with the exception of earthquakes) can add an extra contribution to sea level rates at regional scale but it is very low on average (<0.1 mm/yr in sea level equivalent, Moucha et al., 2008).

During the altimetry era (since 1993), the main contribution to the regional variability in sea level rise comes from the ocean temperature and salinity changes (Bindoff et al., 2007). This is evidenced by the comparison between altimetry-based and steric (i.e. the sum of thermosteric and halosteric effects) trend patterns deduced from in situ hydrographic measurements (Ishii and Kimoto, 2009; Levitus et al., 2009; Lombard et al., 2005a, b) and ocean circulation models (OGCMs) outputs (Wunsch et al., 2007; Kohl and Stammer, 2008; Carton and Giese, 2008; Lombard et al., 2009). This is illustrated in Fig. 8c showing the thermosteric trend patterns over 1993–2010 (sea level trends due to temperature variations only) computed from hydrographic measurements collected by ships and Argo profiling floats (data from Levitus et al., 2009). This figure shows that the thermosteric component is the most important contribution to the observed sea level regional variability. OGCM runs with or without data assimilation confirm that point. However salinity changes also play some role at regional scale, e.g. in the Atlantic ocean, partly compensating temperature effects (e.g. Wunsch et al., 2007; Kohl and Stammer, 2008; Lombard et al., 2009). It is worth noticing however that steric effects estimated in open oceans may be significantly different from those estimated in adjacent coastal zones because of the presence of boundary currents (Bingham and Hughes, 2012).

In the tropics, thermosteric trends are principally caused by changes in the surface wind stress and associated changes in the ocean circulation, hence heat redistribution (Timmermann et al., 2010; Merrifield and Maltrud, 2011). Merrifield (2011) noticed that in the most western part of the tropical Pacific, trade winds increased in the early 1990s, leading to a large upward trend in sea level in that region.

Prior to the altimetry era, very sparse measurements of sea level are available because it was only monitored by tide gauges on coastal areas. Moreover, for historical reasons, the tide gauge dataset is largely biased towards the northern hemisphere, leaving large gaps in the southern hemisphere. Hence it is not possible to get a satisfactory global picture of the regional variability in sea level over the past decades from the tide gauge records alone.

One approach to get information on the regional variability in sea level over the last 5 decades consists of analysing sea level time series produced by ocean circulation models and ocean reanalyses (i.e. OGCMs with data assimilation) (e.g. Carton and Giese, 2008; Kohl and Stammer, 2008). OGCMs and ocean reanalyses deduce sea level from the sum of the thermosteric and halosteric components, to which is added a small barotropic component. This allows mapping the spatio-temporal behaviour of both temperature and salinity contributions to the sea level under a prescribed external meteorological forcing. Over the altimetry era, OGCMs and ocean reanalyses reproduce fairly well the regional variability in sea level trends observed by altimetry. They confirm the thermosteric origin of the patterns (Wunsch et al., 2007; Lombard et al., 2009) and the predominant role of the wind stress in their formation (Kohl and Stammer, 2008; Timmermann et al., 2010).

Over the past 5–6 decades, however, the sea level trend patterns are quite different from those observed over the altimetry era with much lower amplitude (on the order of 3–4 times smaller). On such time scales, the predominant contribution of wind-driven thermosteric effects still holds (Kohl and Stammer, 2008) in particular in the tropical Pacific (Timmermann et al., 2010) and Indian Ocean (Han et al., 2010).

Another approach that partly relies on tide gauge data was developed in the recent years to derive spatial sea level trend patterns before the altimetry era (i.e. last 5–6 decades). It combines information from the tide gauges with spatial patterns from altimetry or OGCMs (e.g. Church et al., 2004; Berge-Nguyen et al., 2008; Llovel et al., 2009; Church and White, 2011; Hamlington et al., 2011; Ray and Douglas, 2011; Meyssignac et al., in press-a). Unlike OGCMs and ocean reanalyses, this approach (called past sea level reconstruction) does not allow separating the various contributions (e.g. from temperature and salinity) to the sea level. But, since it uses tide gauge observations, it is expected to carry more information on the regional variability than OGCMs, and thus is complementary to the latter.

This method interpolates (in an optimal way) the long tide gauge records with Empirical Orthogonal Functions (EOFs here after; Preisendorfer, 1988) representative of the principal modes of variability of the ocean deduced from the altimetry record or OGCMs (see Kaplan et al., 1998, 2000 for more details on the method). It gives 2-dimensional past sea level reconstructions back to around the early 1950s. Reconstructions are then evaluated by comparison with independent tide gauge records that were not used in the reconstruction process. Fig. 9 shows the reconstructed sea level trend patterns over 1960–2009 from Meyssignac et al. (in press-a) with and without the global mean sea level trend (Fig. 9a and 9b respectively).

Reconstruction methods rely strongly on the assumption that the principal modes of variability of the ocean deduced from the

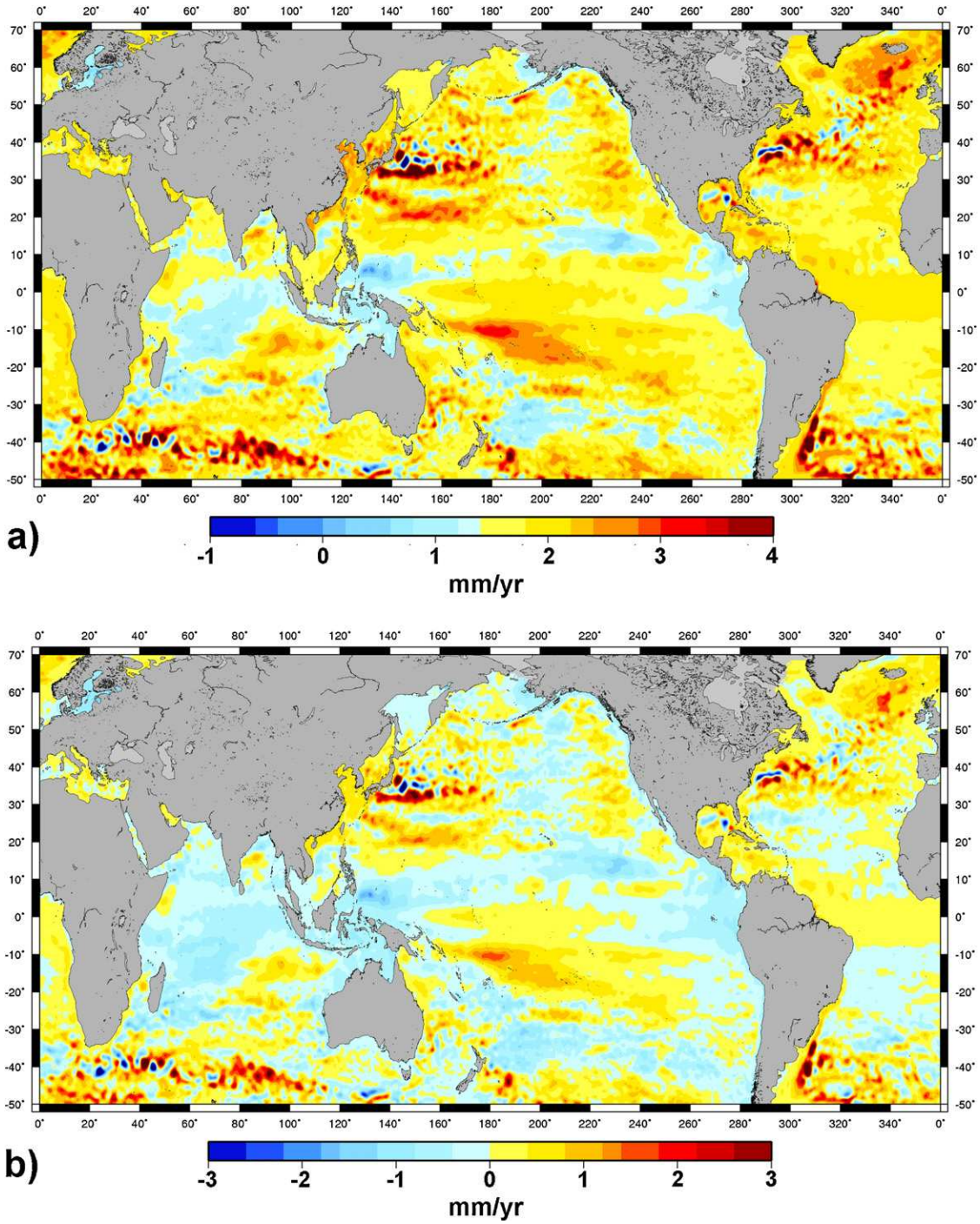

Fig. 9. (a) Spatial trend patterns in sea level over 1950–2009 from Meyssignac et al. (in press-a) reconstruction. (b) Spatial trend patterns in reconstructed sea level over 1950–2009 but with the global mean trend of 1.8 mm/yr removed.

relatively short altimetry record or from imperfect OGCMs (little information on the meteorological forcing is available before 1980) are stationary with time and representative of the modes of variability of the ocean over the long reconstructed period 1950–2010. In this respect, each type of reconstruction shows advantages and drawbacks. Reconstructions based on long EOFs (1958–2007) computed from OGCMs better capture the low-frequency oceanic signal. In that sense, they better stick to the assumption of stationarity. But reconstructions based on the EOFs from altimetry seem to give more realistic modes of variability of the ocean. Finally the various reconstructions give more or less similar results and no case appears to perform better over the globe (Meyssignac et al., in press-a). Over a given region, the best reconstruction available will be the reconstruction that compares well with local independent tide gauge records (see for example Becker et al., 2012).

Despite these differences, all past sea level reconstructions show, like OGCMs and ocean reanalyses, significantly different trend patterns over the last 60 years than those observed over the altimetry era (compare Figs. 8 and 9), with smaller amplitudes (between 3 and 4 times). Comparison with thermal expansion

trends (not shown) indicates that on multidecadal time scale, the regional variability in sea level rates has also a dominant thermal origin.

7. Non stationarity of spatial trend patterns and internal variability of the ocean–atmosphere system

We have seen in the previous section that past sea level either from OGCMs and ocean reanalyses or reconstructions, exhibit regional long-term trend patterns (over the last 5–6 decades) that differ significantly from the short-term ones observed over the altimetry era. This suggests that contemporary sea level trend patterns (from altimetry) are not long-lived features. This point is also supported by the thermosteric origin of the sea level regional variability. Indeed, observations have shown that thermosteric spatial patterns are not stationary but fluctuate in time and space in response to driving mechanisms such as ENSO, NAO, and PDO. (Lombard et al., 2005a; Di Lorenzo et al., 2010; Lozier et al., 2010). Thus thermosteric trend patterns and hence regional sea level trend patterns are expected to be different prior to the altimetry era compared to those observed over the altimetry period, as confirmed by OGCMs, reanalyses and reconstructions.

Past sea level reconstructions by Meyssignac et al. (in press-b) have shown that in the Pacific ocean, altimetry era patterns can be observed in the past at various periods with a changing amplitude. The amplitude appears to fluctuate with time following a low-frequency modulation of ENSO. This suggests that the local regional variability in sea level rates observed by altimetry is actually tightly linked to natural modes of the climate system. This link is further confirmed by coupled Atmosphere–Ocean Climate Model runs (AOCM) without and with external forcing (i.e. anthropogenic greenhouse gas emissions plus aerosols, volcanic eruptions and solar radiation changes). Comparisons of model-based sea level regional variability without and with external forcing enabled Meyssignac et al. (in press-b) to analyze the role of the internal variability of the climate system with respect to the forcing factors, in particular the anthropogenic forcing. The impact of the latter on the observed regional variability of the tropical Pacific is still not visible suggesting that only the intrinsic variability of the climate system is still the main driver of the spatial patterns in sea level observed by satellite altimetry. But further analyses are required to confirm this.

8. Local sea level changes in a few selected regions

Satellite altimetry provides an absolute sea level measurement with respect to the Earth's center of mass while tide gauges, attached to the Earth's surface, give relative sea level measurements that include vertical crustal motions. The latter have a large variety of causes, e.g. GIA, tectonic and volcanic activity causing either uplift or subsidence, ground subsidence due to sediment loading (in particular in large river deltas) or due to ground water and hydrocarbon extraction, etc. (Milne et al., 2009; Woppelmann et al., 2009). If one is interested in estimating sea level change at a given site, it is the 'total' relative sea level that needs to be considered. The word 'total' here means the sum of two components: (1) the climatic component expressed by the sum of the global mean rise plus the regional variability discussed above, and (2) the vertical crustal motion component. Recent studies have shown that each of these components (and their sum) can give rise to very large deviation of local sea level change with respect to the global mean (see for example Braitenberg et al., 2011 or Fenoglio-Marc et al., 2012; Ballu et al., 2011; Becker et al., 2012).

Using GPS precise positioning, Ballu et al. (2011) showed that the Torres islands (north Vanuatu, southwest Pacific) experienced very large subsidence (of about −10 mm/yr) of seismic origin during the past ∼2 decades. Because of earthquake-related vertical land motion, the local rate of sea level rise is about three times the absolute, climate-related sea level rise (of 3.3 mm/yr of that period).

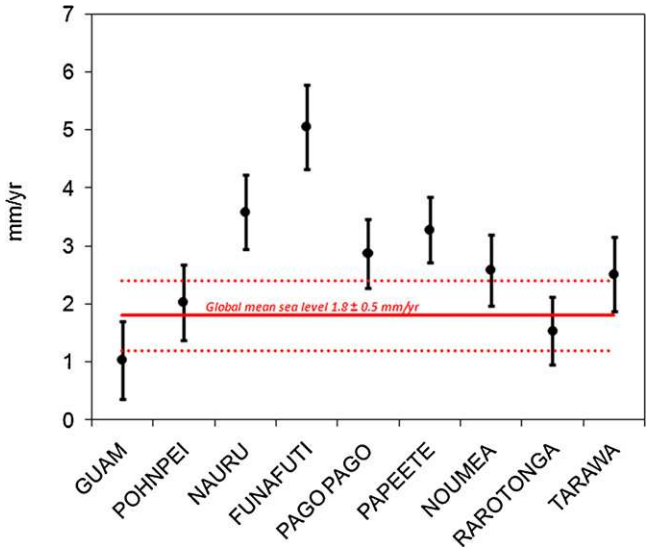

Fig. 10. Total rate of sea level rise at Guam, Pohnpei, Nauru, Funafuti, Pago Pago, Papeete, Noumea, Rarotonga and Tarawa estimated over 1950–2009 due to climate components and vertical crustal motion. The horizontal lines represent the global mean sea level trend over this period (1.8 mm/yr) and its uncertainty range (from Becker et al., 2012).

Becker et al. (2012) estimated the total relative rate of sea level change since 1950 at selected islands of the western tropical Pacific, as a result of the climate-related sea level change (uniform-global mean-sea level rise plus regional variability) and vertical crustal motion estimated from GPS. This allowed them to determine the amount of "total" sea level change effectively felt by the populations over the last ∼60 years. They found that at Guam, Pohnpei and Rarotonga Islands the 'total' sea level trend is about equal to global mean sea level rise (of ∼1.8 mm/yr between 1950 and 2010). At Nauru, Funafuti (Tuvalu), Papeete (French Polynesia), Noumea (New Caledonia), the 'total' sea level trend was found to be significantly higher than the global mean. This is illustrated in Fig. 10 (from Becker et al., 2012). At Funafuti, the capital atoll of the Tuvalu Archipelago, the total rate of sea level rise was found to be >5 mm/yr over the last 60 years. This corresponds to a sea level elevation of ∼30 cm during this time span. These results corroborate that at this particular location, sea level rise is not insignificant – as felt by the population, even if such a rate does not necessarily produce shoreline erosion as shown by Webb and Kench (2010). In effect, other local factors such as changes in sediment deposition, coastal waves and currents are yet the main drivers of shoreline morphological changes; in the future, higher rates of sea level rise may however have larger impacts.

9. Global warming and future large-scale sea level changes

There is little doubt that global warming will continue and even increase during the future decades as green house gas emissions, the main contributor to anthropogenic global warming, will likely continue to grow in the future. A recent update by Friedlingstein et al. (2010) in carbon dioxide (CO_2) emissions due to fossil fuel burning shows a steep increase during the 2000s, even though global economic crises can produce slight temporary decline. From the total CO_2 emissions due to fossil fuels and cement industry, plus deforestation and land use changes (about 9.1 Gt/yr presently), about 45% accumulate into the atmosphere (ocean and vegetation

uptake accounting for 25% and 30% of CO_2 sinks respectively) (Durand et al., 2011). There are different scenarios of emissions and responses of the climate system (expressed in terms of radiative forcing and global Earth's temperature increase) for the coming decades (IPCC, 2007). All correspond to an increase in global mean sea level during the 21th century and beyond because of expected continuing ocean warming and land ice loss (e.g. Meehl et al., 2007). IPCC AR4 projections indicated that sea level should be higher than today's value by ~40 cm by 2100 (within a range of ±15 cm due to model results dispersion and uncertainty on emissions) (Meehl et al., 2007). After the publication of the IPCC 4th Assessment Report, it has been suggested that this value could be a lower bound because the climate models used at that time essentially accounted for ocean warming, glaciers melting and ice sheet surface mass balance only. As discussed above, a large proportion of current Greenland and West Antarctica ice mass loss results from coastal glacier flow into the ocean through complex dynamical instabilities. Such processes became quite active during the last decade and were not taken into account in IPCC AR4 sea level projections. Recent studies have thus suggested that ice sheet mass loss could represent a much larger contribution than expected to future sea level rise. For example, Pfeffer et al. (2008) infer possible contributions to 2100 sea level of 16 cm–54 cm for Greenland and 13 cm–62 cm for Antarctica (although preferred values by these authors are 16 cm and 15 cm for Greenland and Antarctica respectively). Extrapolating the presently observed acceleration of Greenland and Antarctica ice mass loss, Rignot et al. (2011) suggest a total (Greenland plus Antarctica) contribution to sea level rise of ~56 cm by 2100.

Clearly, the total land ice contribution to 21st century sea level rise remains highly uncertain. But values around 40–50 cm by 2100 may not be ruled out for the sum of glaciers and ice sheets contributions. If we add the ocean warming contribution (in the range 10–40 cm; IPCC, 2007), global mean sea level could eventually exceed present-day elevation by 50–80 cm.

Alternative approaches based on semi-empirical modeling have been proposed to estimate sea level rise in the 21st century (e.g. Rahmstorf et al., in press; Jevrejeva et al., 2010, 2011). These are based on simple relationships established for the 20th century (or longer time spans) between observed global mean sea level rate of rise and observed global mean Earth's temperature (or radiative forcing). Using global mean temperature projections (the most precisely modeled climate parameter by coupled climate models) or radiative forcing, future global mean sea level can be extrapolated using the simple relationship valid for the past. This method leads to higher ranges of sea level rise by 2100 than climate model projections. Such a discrepancy remains so far poorly understood.

Present-day sea level rise is not uniform. This is also expected for the future. Geographical patterns of future sea level changes are dominated by non uniform steric effects (i.e. ocean thermal expansion and salinity changes) (e.g. Pardaens et al., 2010; Yin et al., 2010; Suzuki and Ishii, 2011). Although some differences in projected regional variability exist among the different coupled climate models, the patterns agree rather well. Ensemble means indicate higher sea level rise (with respect to the global mean) in the Arctic ocean due less salty waters caused by fresh water input in that region (from sea ice melting and Greenland ice loss increased precipitation ad Arctic river runoff). Strong compensation between thermosteric and halosteric effects is predicted in the Atlantic Ocean, with a slight dominating effect from thermal expansion. In the Southern Ocean, at latitudes centered near 60°S, there is a tendency for sea level fall compared to the global mean, just south of a band of sea level rise; such a dipole-like behaviour is associated with changes of the Antarctic Circumpolar Current. In the Indian Ocean, projections generally indicate sea level to rise slightly higher than the global mean.

Other factors give rise to regional variability, in particular gravitational effects and solid Earth's viscoelastic or elastic response to large-scale water mass redistribution associated with past and on-going land ice melt (see Section 6). For the first time, these factors have been taken into account in regional sea level projections for different scenarios of future climate warming (Slangen et al., 2011). These authors indeed model local relative sea level rise accounting for steric effects plus last deglaciation-induced GIA and additional deformational and gravitational effects due to future land ice melt. While steric effects dominate the regional variability as in the IPCC AR 4 projections, past and on-going land ice melt can lead to strong deviation around the global mean rise in the vicinity of the melting bodies where negative sea level changes are noticed. In some regions of the Arctic Ocean, this

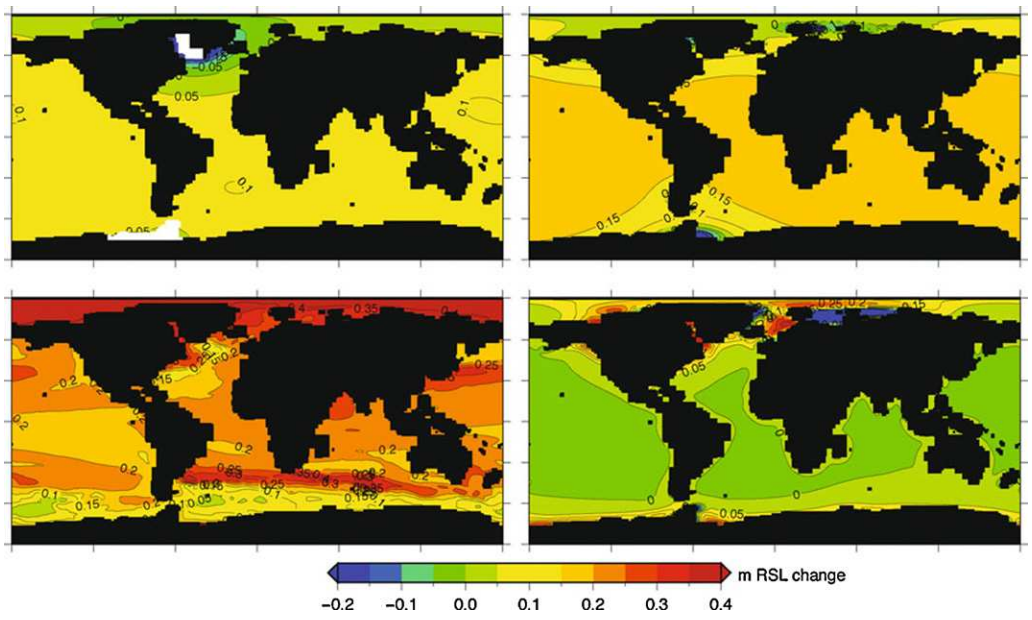

Fig. 11. Individual contributions (from an ensemble mean of 12 climate models) to regional (relative) sea level changes for the decade 2090–2099 relative to 1980–1999 and A1B warming scenario (i.e. global mean Earth's temperature increase of +2.8 °C over this period range; IPCC, 2007. Upper left panel: future ice sheet melting; upper right panel: glacier melting; lower left panel: steric effects; lower right panel: GIA effect. (from Slangen et al., 2011).

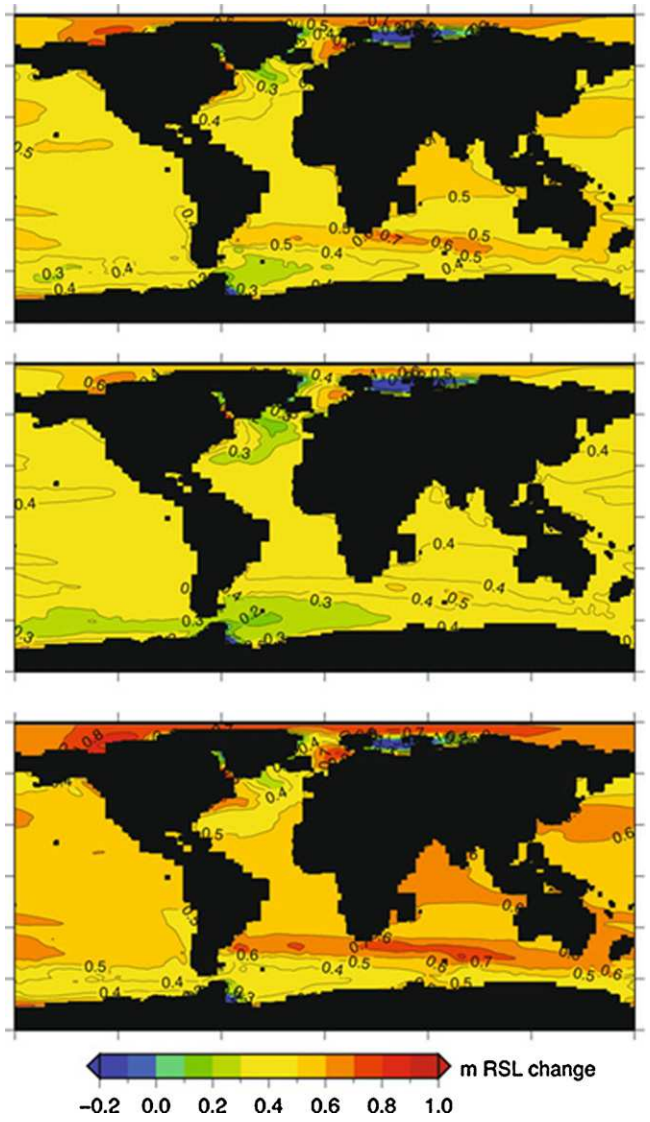

Fig. 12. Maps of the regional sea level variability (in m) between 1980–1999 and 2090–2099 (ensemble mean of ~12 climate models) due the sum of all factors shown in Fig. 11, for three different warming scenarios: A1B (top panel), B1 (1.8 °C mean temperature increase) – middle panel, and A2 (+3.4 °C mean temperature increase) – lower panel. Global mean rise included (amounting ~50 cm for A1B, ~40 cm for B1 and 55 cm for A2) (from Slangen et al., 2011).

factor compensates sea level rise due to freshening. Fig. 11 from Slangen et al. (2011) shows individual contributions (i.e. future ice sheet and glacier melting, last deglaciation – induced GIA and steric effects) to regional (relative) sea level changes for the decade 2090–2099 relative to 1980–1999 and A1B warming scenario (i.e. global mean Earth's temperature increase of +2.8 °C over this period range; IPCC, 2007). These maps are based on an ensemble mean of 12 climate models. The corresponding global mean rise in this case is ~50 cm. But local relative sea level rise ranges from ~–4 m (nearby the ice sheets) to +80 cm. Fig. 12, also from Slangen et al. (2011), presents maps of the regional variability (ensemble mean of ~12 climate models) due the sum of all factors and three different warming scenarios: A1B as for Fig. 11, B1(+1.8 °C mean temperature increase), and A2 (+3.4 °C mean temperature increase). As in Fig. 11, the global mean rise is included in Fig. 12 (amounting ~40 cm for B1 and 55 cm for A2). These figures clearly demonstrate the utmost importance of regional variability of the rates of sea level change.

10. Outlook

Particular attention has been paid to the sea level rise problem during the recent years because it clearly represents a major threat of global warming. The physical impacts of sea level rise on coastal zones are well identified (Nicholls et al., 2007; Nicholls and Cazenave, 2010; Nicholls, 2010). The immediate effect is submergence and increased flooding of coastal land, as well as saltwater intrusion of surface waters. Longer-term effects also occur as the coast adjusts to the new conditions, including increased erosion and saltwater intrusion into groundwater. The coastal impacts are primarily produced by relative sea level rise as the sum of climate-related and non climate-related processes (as discussed above). For example, relative sea level is rising more rapidly than climate-induced trends on subsiding coasts. In many regions, human activities are exacerbating subsidence on susceptible coasts including most river deltas (e.g. the Ganges–Brahmaputra and Mekong deltas, Ericson et al., 2006). During the 20th century, several near coastal megacities have suffered ground subsidence of several meters because of groundwater withdrawal (e.g. Phienwej et al., 2006). The non-climate components of sea level change have in general received much less attention than climate components, because they are considered as a local issue. However, they are so common that they need to be studied more systematically. Besides the very local issues, regional variability of sea level change due to ocean thermosteric and halosteric factors may considerably amplify the global mean rise. This was the case over the past few decades in the low islands such as the Tuvalu or in the future in the Maldives island region in the Indian Ocean. As we have discussed above, additional factors such as changes in shape of ocean basins because of land ice loss and water mass redistribution are additional causes of regional variability. The combination of all these factors produces complex regional sea level patterns with important deviation with respect to the global mean rise in some areas.

Until recently, the consequences of anthropogenic global warming on sea level were essentially addressed in terms of the global mean trend. However, more and more consideration is given to the large-scale regional variability and to more local factors (of non climatic origin). While the latter are difficult – if not impossible – to predict, significant progress has been made recently to provide realistic regional sea level projections that account for the climate-related contributions and associated large-scale water mass redistribution. Such new projections should help to develop realistic climate mitigation policies for coastal management and adaptation to future climate change. In parallel, sustained and systematic monitoring of sea level and other climate parameters causing sea level rise (ocean heat content, land ice loss, etc.) from space-based and in situ observing systems is crucial (e.g. Wilson et al., 2010). This will help in improving our understanding of present-day sea level rise and variability, and ultimately will contribute to improve model projections of future sea levels.

Acknowledgements

We are very grateful to Carla Braitenberg and Roland Gehrels for their helpful comments that led us to improve our manuscript. We also thank K. Lambeck, A. Kemp and A. Slangen for allowing us to use figures from their published papers.

References

Ablain, M., Cazenave, A., Guinehut, S., Valladeau, G., 2009. A new assessment of global mean sea level from altimeters highlights a reduction of global slope from 2005 to 2008 in agreement with in situ measurements. Ocean Sci. 5, 193–201.
Alley, R., Spencer, M., Anandakrishnan, S., 2007. Ice sheet mass balance, assessment, attribution and prognosis. Ann. Glaciol. 46, 1–7.

Alley, R., Fahnestock, M., Joughin, I., 2008. Understanding glacier flow in changing time. Science 322, 1061–1062.
Allison, I., Alley, R.B., Fricker, H.A., Thomas, R.H., Warner, R.C., 2009. Ice sheet mass balance and sea level. Antarct. Sci. 21, 413–426.
Argo Data Management Team, 2008. 9th Argo data management meeting report. 29–31 October 2008. Honolulu, Hawaii, USA. <http://www.argo.ucsd.edu>.
Ballu, V., Bouin, M.N., Simeoni, P., Crawford, W.C., Calmant, S., Bore, J.M., Kana, T., Pelletier, B., 2011. Comparing the role of absolute sea level rise and vertical tectonic motions in coastal flooding, Torres Islands (Vanuatu). PNAS 108, 13019–13022, doi:10.1073/pnas.1102842108.
Bard, E., Hamelin, B., Delanghe-Sabatier, D., 2010. Deglacial meltwater pulse 1B and Youndger dryas sea level revisited with boreholes at Tahiti. Science 327, 1235–1237, doi:10.1126/science.1180557.
Becker, M., Meyssignac, B., Llovel, W., Cazenave, A., Delcroix, T., 2012. Sea level variations at Tropical Pacific Islands during 1950–2009. Glob. Planet. Change 80/81, 85–98.
Beckley, B.D., Zelensky, N.P., Holmes, S.A., Lemoine, F.G., Ray, D.R., Mitchum, G.T., Desai, S.D., Brown, S.T., 2010. Assessment of the Jason-2 extension to the TOPEX/Poseidon, Jason-1 sea surface height time series for global mean sea level monitoring. Mar. Geodesy 33, 447–471.
Berge-Nguyen, M., Cazenave, A., Lombard, A., Llovel, W., Viarre, J., Cretaux, J.F., 2008. Reconstruction of past decades sea level using thermosteric sea level, tide gauge, satellite altimetry and ocean reanalysis data. Glob. Planet. Change 62, 1–13.
Berger, A., 1988. Milankovitch theory and climate. Rev. Geophys. 26, 624–657.
Bindoff, N., Willebrand, J., Artale, V., Cazenave, A., Gregory, J., Gulev, S., Hanawa, K., Le Quéré, C., Levitus, S., Nojiri, Y., Shum, C.K., Talley, L., Unnikrishnan, A., 2007. Observations: oceanic climate and sea level. In: Solomon, S., Qin, D., Manning, M., Chen, Z., Marquis, M., Averyt, K.B., Tignor, M., Miller, H.L. (Eds.), Climate Change 2007: The Physical Science Basis Contribution of Working Group I to the Fourth Assessment Report of the Intergovernmental Panel on Climate Change. Cambridge University Press, Cambridge, UK/New York, USA.
Bingham, R.J., Hughes, C.W., 2012. Local diagnostics to estimate density-induced sea level variations over topography and along coastlines. J. Geophys. Res. 117, C01013, doi:10.1029/2011JC007276.
Blum, M.D., Roberts, H.H., 2009. Drowning of the Mississippi Delta due to insufficient sediment supply and global sea-level rise. Nat. Geosci. 2, 488–491.
Braitenberg, C., Mariani, P., Tunini, L., Grillo, B., Nagy, I., 2011. Vertical crustal motions from differential tide gauge observations and satellite altimetry in southern Italy. J. Geodynamics 51, 233–244, doi:10.1016/j.jog.2010.09.003.
Carton, J., Giese, B., 2008. A reanalysis of ocean climate using Simple Ocean Data Assimilation (SODA). Monthly Weather Rev. 136, 2999–3017.
Cazenave, A., Llovel, W., 2010. Contemporary sea level rise. Ann. Rev. Mar. Sci. 2, 145–173.
Cazenave, A., Remy, F., 2011. Sea level and climate: measurements and causes of changes. Interdisciplinary Rev.: Clim. Change 2 (5), 647–662, doi:10.1002/wcc.139.
Cazenave, A., Henry, O., Munier, S., Meyssignac, B., Delcroix, T., Llovel, W., Palanisamy, H., Gordon, A. Estimating ENSO influence on the global mean sea level. Mar. Geodesy, under revision.
Chelton, D.B., Ries, J.C., Haines, B.J., Fu, L.L., Callahan, P.S., 2001. Satellite altimetry. In: Fu, L.L., Cazenave, A. (Eds.), Satellite Altimetry and Earth Sciences, A Handbook of Techniques and Applications. Academic Press, pp. 1–131, vol. 69 of Int. Geophys. Series.
Chen, J.L., Wilson, C.R., Blankenship, D., Tapley, B.D., 2009. Accelerated Antarctic ice loss from satellite gravity measurements. Nat. Geosci. 2 (12), 859–862.
Church, J.A., White, N.J., Coleman, R., Lambeck, K., Mitrovica, J.X., 2004. Estimates of the regional distribution of sea-level rise over the 1950 to 2000 period. J. Clim. 17 (13), 2609–2625.
Church, J.A., White, N.J., 2006. A 20th century acceleration in global sea-level rise. Geophys. Res. Lett. 33, L01602, doi:10.1029/2005GL024826.
Church, J.A., Woodworth, P.L., Aarup, T., Wilson, W.S., 2010. Understanding Sea Level Rise and Variability. Wiley-Blackwell Publishing, London, UK.
Church, J.A., White, N.J., 2011. Sea-level rise from the late 19th to the early 21st century. Surveys Geophys. 4/5, 585–602, doi:10.1007/s10712-011-9119-1.
Church, J.A., Gregory, J.M., White, N.J., Platten, S.M., Mitrovica, J.X., 2011a. Understanding and projecting sea level change. Oceanography 24 (2), 130–143, doi:10.5670/oceanog.2011.33.
Church, J.A., White, N.J., Konikow, L.F., Domingues, C.M., Cogley, J.G., Rignot, E., Gregory, J.M., van den Broeke, M.R., Monaghan, A.J., Velicogna, I., 2011b. Revisiting the Earth's sea level and energy budgets from 1961 to 2008. Geophys. Res. Lett. 38, L18601, doi:10.1029/2011GL048794, 2011.
Cogley, J.C., 2009. Geodetic and direct mass balance measurements: comparison and joint analysis. Ann. Glaciol. 50, 96–100.
Di Lorenzo, E., Cobb, K.M., Furtado, J.C., Schneider, N., Anderson, B.T., Bracco, A., Alexander, M.A., Vimont, D.J., 2010. Central Pacific El Niño and decadal climate change in the North Pacific Ocean. Nat. Geosci. 3, 762–765.
Domingues, C., Church, J., White, N., Glekler, P.J., Wijffels, S.E., Barker, P.M., Dunn, J.R., 2008. Improved estimates of upper ocean warming and multidecadal sea level rise. Nature 453, 1090-U6, doi:10.1038/nature07080.
Douglas, B.C., 1991. Global sea-level rise. J. Geophys. Res. Oceans 96, 6981–6992.
Douglas, B.C., 2001. Sea level change in the era of the recording tide gauge. In: Douglas, B.C., Kearney, M.S., Leatherman, S.P. (Eds.), Sea Level Rise, History and Consequences. Academic Press, San Diego, pp. 37–64.
Durand, A.J., Le Quere, C., Hope, C., Friend, A.D., 2011. Economic value of improved quantification in global sources and sinks of carbon dioxide. Philos. Trans. R. Soc. A: Math. Phys. Eng. Sci. 1943, 1967–1979.
Ericson, J.P., Vorosmarty, C.J., Dingman, S.L., Ward, L.G., Meybeck, L., 2006. Effective sea level rise and deltas. Causes of change and human dimension implications. Glob. Planet. Change 50, 63–82.
Fu, L.L., Cazenave, A., 2001. Satellite Altimetry and Earth Sciences. A Handbook of Techniques and Application. Academic Press, San Diego, USA, International Geophysics Series, vol. 69, 463 p.
Fenoglio-Marc, L., Braitenberg, C., Tunini, L., 2012. Sea level variability and trends in the Adriatic Sea in 1993–2008 from tide gauges and satellite altimetry. Phys. Chem. Earth 40/41, 47–58.
Friedlingstein, P., Houghton, R.A., Marland, G., Hackler, J., Boden, T.A., Conway, T.J., Canadell, J.G., Raupach, M.R., Ciais, P., Le Quere, C., 2010. Update on CO_2 emissions. Nat. Geosci. 3, 811–812.
Gehrels, W.R., Kirby, J.R., Prokoph, A., Newnham, R.M., Achterberg, E.P., Eavans, H., Black, S., Scott, D., 2005. Onset of recent rapid sea level rise in the western Atlantic Ocean. Quat. Sci. Rev. 24, 2083–2100.
Gehrels, W.R., Marshall, W.A., Gehrels, M.J., Larsen, G., Kirby, J.R., Eiriksson, J., Heinemeier, J., Shimmield, T., 2006. Rapid sea-level rise in the North Atlantic Ocean since the first half of the nineteenth century. Holocene 16, 949–965.
Gomez, N., Mitrovica, J., Tamisiea, M., Clark, P., 2010. A new projection of sea level change in response to collapse of marine sectors of the Antarctic Ice Sheet. Geophys. J. Int. 180, 623–634.
Gu, G., Adler, R.F., 2011. Precipitation and temperature variations on the interannual time scale: assessing the impact of ENSO and volcanic eruptions. J. Clim. 24, 2258–2270.
Hamlington, B.D., Leben, R., Nerem, S., Han, W., Kim, K.Y., 2011. Reconstructing sea level using cyclostationary empirical orthogonal functions. J. Geophys. Res. 116, C12015, doi:10.1029/2011JC007529.
Han, W.Q., Meehl, G.A., Rajagopalan, B., Fasullo, J.T., Hu, A.X., Lin, J.L., Large, W.G., Wang, J.W., Quan, X.W., Trenary, L.L., Wallcraft, A., Shinoda, T., Yeager, S., 2010. Patterns of Indian Ocean sea-level change in a warming climate. Nat. Geosci. 3, 546–550.
Hanebuth, T.J.J., Stattegger, K., Bojanowski, A., 2009. Termination of the Last Glacial Maximum sea-level lowstand: the Sunda-Shelf data revisited. Glob. Planet. Change 66, 76–84.
Haq, B.U., Schutter, S.R., 2008. A chronology of Paleozoic sea level changes. Science 322, 64–68.
Holgate, S., 2007. On the decadal rates of sea level change during the twentieth century. Geophys. Res. Lett. 34, L01602, doi:10.1029/2006GL028492.
Holland, D., Thomas, R.H., De Young, B., Ribergaard, M.H., Lyberth, B., 2008. Acceleration of Jakobshawn Isbrae triggered by warm subsurface ocean waters. Nat. Geosci. 1, 659–664, doi:10.1038/ngeo316.
IPCC, 2007. In: Solomon, S., Qin, D., Manning, M., Chen, Z., Marquis, M., Averyt, K.B., Tignor, M., Miller, H.L. (Eds.), IPCC 4th Assessment Report. Climate Change 2007: The Physical Science Basis. Contribution of Working Group I to the Fourth Assessment Report of the Intergovernmental Panel on Climate Change. Cambridge University Press, Cambridge, UK/New York, USA.
Ishii, M., Kimoto, M., 2009. Reevaluation of historical ocean heat content variations with varying XBT and MBT depth bias corrections. J. Oceanogr. 65, 287–299.
Jevrejeva, S., Grinsted, A., Moore, J.C., Holgate, S., 2006. Nonlinear trends and multiyear cycles in sea level records. J. Geophys. Res. 111, doi:10.1029/2005JC003229 C09012.
Jevrejeva, S., Moore, J.C., Grinsted, A., Woodworth, P.L., 2008. Recent global sea level acceleration started over 200 years ago? Geophys. Res. Lett. 35, L08715, doi:10.1029/2008GL033611.
Jevrejeva, S., Moore, J., Grinsted, A., 2010. How will sea level respond to changes in natural and anthropogenic forcings by 2100? Geophys. Res. Lett. 37, L07703.
Jevrejeva, S., Moore, J.C., Grinsted, A., 2011. Sea level projections to AD 2500 with a new generation of climate change scenarios. Glob. Planet. Change 80/81, 14–20.
Kaplan, A., Cane, M.A., Kushnir, Y., Clement, A.C., Blumenthal, M.B., Rajagopalan, B., 1998. Analyses of global sea surface temperature 1856–1991. J. Geophys. Res., 18567–18589.
Kaplan, A., Kushnir, Y., Cane, M.A., 2000. Reduced space optimal interpolation of historical marine sea level pressure: 1854–1992. J. Clim. 13, 2987–3002.
Kaser, G., Cogley, J.G., Dyurgerov, M.B., Meier, M.F., Ohmura, A., 2006. Mass balance of glaciers and ice caps: consensus estimates for 1961–2004. Geophys. Res. Lett. 33, L19501, doi:10.1029/2006GL027511.
Kemp, A.C., Horton, B., Donnelly, J.P., Mann, M.E., Vermeer, M., Rahmstorf, S., 2011. Climate related sea level variations over the past two millennia. PNAS 108, 11017–11022, doi:10.1073/pnas.1015619108.
Kohl, A., Stammer, D., 2008. Decadal sea level changes in the 50-year GECCO ocean synthesis. J. Clim. 21, 1876–1890.
Kopp, R.E., Mitrovica, J.X., Griffies, S.M., Yin, J., Hay, C.C., Stouffer, R.J., 2010. The impact of Greenland melt on local sea levels: a partially coupled analysis of dynamic and static equilibrium effects in idealized water-hosing experiments. Clim. Change 103, 619–625.
Lambeck, K., Esat, T.M., Potter, E.K., 2002. Links between climate and sea levels for the past three million years. Nature 419, 199–206.
Lambeck, K., Anzidei, M., Antonioli, F., Benini, A., Esposito, A., 2004. Sea level in Roman time in the Central Mediterranean and implications for recent change. Earth Planet. Sci. Lett. 224, 563–575.
Lambeck, K., Woodroffe, C.D., Antonioli, F., Anzidei, M., Gehrels, W.D., Laborel, J., Wright, A., 2010. Paleoenvironmental records, geophysical modelling and reconstruction of sea level trends and variability on centennial and longer time scales. In: Church, J.A., Woodworth, P.L., Aarup, T., Wilson, W.S. (Eds.), Understanding Sea Level Rise and Variability. Wiley-Blackwell Publishing, London, UK.

Levitus, S., Antonov, J.L., Boyer, T.P., Locarnini, R.A., Garcia, H.E., Mishonov, A.V., 2009. Global Ocean heat content 1955–2008 in light of recently revealed instrumentation. Geophys. Res. Lett. 36, L07608, doi:10.1029/2008GL037155.

Llovel, W., Cazenave, A., Rogel, P., Lombard, A., Nguyen, M.B., 2009. Two-dimensional reconstruction of past sea level (1950–2003) from tide gauge data and an Ocean General Circulation Model. Clim. Past 5, 217–227, doi:10.5194/cp-5-217-2009.

Llovel, W., Guinehut, S., Cazenave, A., 2010. Regional and interannual variability in sea level over 2002–2009 based on satellite altimetry. Argo float data and GRACE ocean mass. Ocean Dyn. 60, 1193–1204, doi:10.1007/s10236-010-0324-0.

Llovel, W., Becker, M., Cazenave, A., Jevrejeva, S., Alkama, R., Decharme, B., Douville, H., Ablain, M., Beckley, B., 2011. Terrestrial waters and sea level variations on interannual time scale. Glob. Planet. Change 75, 76–82, doi:10.1016/j.gloplacha.2010.10.008.

Lombard, A., Cazenave, A., DoMinh, K., Cabanes, C., Nerem, R., 2005a. Thermosteric sea level rise for the past 50 years; comparison with tide gauges and inference on water mass contribution. Glob. Planet. Change 48, 303–312.

Lombard, A., Cazenave, A., Le Traon, P.Y., Ishii, M., 2005b. Contribution of thermal expansion to present-day sea level rise revisited. Glob. Planet. Change 47, 1–16.

Lombard, A., Garric, G., Penduff, T., Molines, J.M., 2009. Regional variability of sea level change using a global ocean model at ¼° resolution. Ocean Dyn. 3, 433–449, doi:10.1007/s10236-009-0161-6.

Lozier, M., Roussenov, V., Reed, M., Williams, R., 2010. Opposing decadal changes for the North Atlantic meridional overturning circulation. Nat. Geosci. 3, 805.

Lyman, J.M., Godd, S.A., Gouretski, V.V., Ishii, M., Johnson, G.C., Palmer, M.D., Smith, D.M., Willis, J.K., 2010. Robust warming of the global upper ocean. Nature 465, 334–337, doi:10.1038/nature09043.

Meehl, G.A., Stocker, T.F., Collins, W.D., Friedlingstein, P., Gaye, A.T., Gregory, J.M., Kitoh, A., Knutti, R., Murphy, J.M., Noda, A., Raper, S.C.B., Watterson, I.G., Weaver, A.J., Zhao, Z.C., 2007. Global climate projections. In: Solomon, S., Qin, D., Manning, M., Chen, Z., Marquis, M., Averyt, K.B., Tignor, M., Miller, H.L. (Eds.), Climate Change 2007: The Physical Science Basis. Contribution of Working Group I to the Fourth Assessment Report of the Intergovernmental Panel on Climate Change. Cambridge University Press, Cambridge, UK/New York, USA, p. 2007.

Meier, M.F., Dyurgerov, M.B., Rick, U.K., O'Neel, S., Pfeffer, W.T., Anderson, R.S., Anderson, S.P., Glazovsky, A.F., 2007. Glaciers dominate Eustatic sea-level rise in the 21st century. Science 317 (5841), 1064–1067.

Merrifield, M.A., Merrifield, S.T., Mitchum, G.T., 2009. An anomalous recent acceleration of global sea level rise. J. Clim. 22, 5772–5781.

Merrifield, M.A., Maltrud, M.E., 2011. Regional sea level trends due to a Pacific trade wind intensification. Geophys. Res. Lett. 38, L21605.

Merrifield, M.A., 2011. A shift in western tropical Pacific sea level trends during the 1990. J. Clim. 24, 4126–4138, doi:10.1175/2011JCLI3932.1.

Meyssignac, B., Becker, M., Llovel, W., Cazenave, A. An assessment of two-dimensional past sea level reconstructions over 1950–2009 based on tide gauge data and different input sea level grids. Surv. Geophys., doi:10.1007/s10712-011-9171-x, in press-a.

Meyssignac, B., Salas Melia, D., Llovel, W., Cazenave, A. Tropical Pacific spatial trend patterns in observed sea level: internal variability and/or anthropogenic signature. Clim. Past, in press-b.

Miller, K.G., Sugarman, P.J., Browning, J.V., Horton, B.P., Stanley, A., Kahn, A., Uptegrove, J., d Aucott, M., 2009. Sea level rise in New Jersey over the past 5000 years: implications to anthropogenic changes. Glob. Planet. Change. 66, 10–18.

Miller, K., Mountain, G.S., Wright, J.D., Browning, J.V., 2011. A 180 million year record of sea level and ice volume variations from continental margin deep sea isotopic records. Oceanography 24 (2), 40–53, doi:10.5670/oceanog.2011.26.

Milne, G., Mitrovica, J., 2008. Searching for eustasy in deglacial sea-level histories. Quat. Sci. Rev. 27, 2292–2302.

Milne, G., Gehrels, W.R., Hughes, C., Tamisiea, M., 2009. Identifying the causes of sea level changes. Nat. Geosci. 2, 471–478.

Mitchum, G.T., Nerem, R.S., Merrifield, M.A., Gehrels, W.R., 2010. Modern sea level changes estimates. In: Church, J.A., Woodworth, P.L., Aarup, T., Wilson, W.S. (Eds.), Understanding Sea Level Rise and Variability. Wiley-Blackwell Publishing, London, UK.

Mitrovica, J.X., Tamisiea, M.E., Davis, J.L., Milne, G.A., 2001. Recent mass balance of polar ice sheets inferred from patterns of global sea-level change. Nature 409, 1026–1029.

Mitrovica, J.X., Gomez, N., Clark, P.U., 2009. The sea-level fingerprint of West Antarctic collapse. Science 323, 753.

Mueller, R.D., Sdrolias, M., Gaina, C., Steinberger, B., Heine, C., 2008. Long-term sea level fluctuations driven by ocean basin dynamics. Science 319, 1357–1362.

Moucha, R., Forte, A., Mitrovica, J.X., Rowley, D., Quere, S., Simmons, N., Grand, S., 2008. Dynamic topography and long-term sea-level variations: there is no such thing as a stable continental platform. Earth Planet. Sci. Lett. 271, 101–108.

Nerem, R.S., Chambers, D.P., Choe, C., Mitchum, G.T., 2010. Estimating mean sea level change from the TOPEX and Jason altimeter missions. Mar. Geodesy. 33 (1), 435–446.

Nicholls, R.J., Wong, P.P., Burkett, V.R., Codignotto, J.O., Hay, J.E., McLean, R.F., Ragoonaden, S., Woodroffe, C.D., 2007. Coastal systems and low-lying areas. Climate change 2007: impacts, adaptation and vulnerability. Fourth Assessment Report of the Intergovernmental Panel on Climate Change, pp. 315–356.

Nicholls, R.J., Cazenave, A., 2010. Sea level change and the impacts in coastal zones. Science 328, 1517–1520.

Nicholls, R.J., 2010. Impacts of and responses to sea level rise. In: Church, J.A., Woodworth, P.L., Aarup, T., Wilson, W.S. (Eds.), Understanding Sea Level Rise and Variability. Wiley-Blackwell Publishing, London, UK.

Okumura, Y.M., Deser, C., Hu, A., Timmermann, A., Xie, S.P., 2009. North Pacific climate response to freshwater forcing in the Subarctic North Atlantic: oceanic and atmospheric pathways. J. Clim. 22, 1424–1445.

Pardaens, A.K., Gregory, J.M., Lowe, J.A., 2010. Model study of factors influencing projected changes in regional sea level over the twenty-first century. Clim. Dyn. 36, 2015–2033, doi:10.1007/s00382-009-0738-x.

Peltier, W.R., 2001. Global glacial isostatic adjustment and modern instrumental records of relative sea level history. In: Douglas, B.C., Kearney, M.S., Leatherman, S.P. (Eds.), Sea Level Rise, History and Consequences. Academic Press, San Diego, pp. 65–95.

Peltier, W.R., 2004. Global glacial isostasy and the surface of the ice-age Earth: the ICE-5G (VM2) model and GRACE. Annu. Rev. Earth Planet Sci. 32, 111–149.

Pfeffer, W.T., Harper, J.T., O'Neel, S., 2008. Kinematic constraints on glacier contributions to 21st-century sea level rise. Science 321, 1340–1343.

Phien-wej, N., Giao, P.H., Nutalaya, P., 2006. Land subsidence in Bangkok. Thailand Eng. Geol. 82, 187–201.

Preisendorfer, R.W., 1988. Principal component analysis in meteorology and oceanography. Dev. Atmos. Sci. 17, 425 (Elsevier).

Rahmstorf, S., Perrette, M., Vermeer M. Testing the robustness of semi-empirical sea level projections. Clim. Dyn, doi:10.1007/s00382-011-1226-7, in press.

Ray, R., Douglas, B., 2011. Experiments in reconstructing twentieth-century sea level. Prog. Oceanogr. 91, 496–515.

Rignot, E., Bamber, J.L., Van den Broecke, M.R., Davis, C., Li, Y., Van de Berg, W.J., Van Meijgaard, E., 2008a. Recent Antarctic ice mass loss from radar interferometry and regional climate modelling. Nat. Geosci. 1, 106–110.

Rignot, E., Box, J.E., Burgess, E., Hanna, E., 2008b. Mass balance of the Greenland ice sheet from 1958 to 2007. Geophys. Res. Lett. 35, L20502, doi:10.1029/2008GL035417.

Rignot, E., Velicogna, I., van den Broeke, M.R., Monaghan, A., Lenaerts, J., 2011. Acceleration of the contribution of the Greenland and Antarctic ice sheets to sea level rise. Geophys. Res. Lett. 38, L05503.

Roemmich, D., Johnson, G.C., Riser, S., Davis, R., Gilson, J., Owens, W.B., Garzoli, S.L., Schmid, C., Ignaszewski, M., 2009. The Argo Program observing the global ocean with profiling floats. Oceanography 22, 34–43.

Rohling, E.J., Grant, K., Bolshaw, M., Sidall, M., Hemlebben, Ch., Kucera, M., 2009. Antarctic temperature and global sea level closely coupled over the past five glacial cycles. Nat. Geosci. 2, 500–504.

Slangen, A.B.A., Katsman, C.A., van de Val, R.S.W., Vermeersen, L.L.A., Riva, R.E.M., 2011. Towards regional projections of twenty-first century sea level change based on IPCC SRES scenarios. Clim. Dyn. 38, 1191–1209, doi:10.1007/s00382-011-1057-6.

Stammer, D., 2008. Response of the global ocean to Greenland and Antarctica melting. J. Geophys. Res. 113, C06022, doi:10.1029/2006JC001079.

Stammer, D., Agarwal, N., Herrmann, P., Köhl, A., Mechoso, C.R., 2011. Response of a coupled ocean–atmosphere model to Greenland ice melting. Surv. Geophys. 32, 621–642.

Steffen, K., Thomas, R.H., Rignot, E., Cogley, J.G., Dyurgerov, M.B., Raper, S.C.B., Huybrechts, P., Hanna, E., 2010. Cryospheric contributions to sea level rise and variability. In: Church, J.A., Woodworth, P.L., Aarup, T., Wilson, W.S. (Eds.), Understanding Sea Level Rise and Variability. Wiley-Blackwell Publishing, London, UK.

Suzuki, T., Ishii, M., 2011. Regional distribution of sea level changes resulting from enhanced greenhouse warming in the Model for Interdisciplinary Research on Climate version 3.2. Geophys. Res. Lett. 38, L02601, doi:10.1029/2010GL045693.

Tamisiea, M.E., Mitrovica, J.X., 2011. The moving boundaries of sea level change: understanding the origins of geographic variability. Oceanography 24 (2), 24–39, doi:10.5670/oceanog.2011.25.

Timmermann, A., McGregor, S., Jin, F., 2010. Wind effects on past and future regional sea level trends in the Southern Indo-Pacific. J. Clim. 23, 4429–4437.

Velicogna, I., 2009. Increasing rates of ice mass loss from the Greenland and Antarctic ice sheets revealed by GRACE. Geophys. Res. Lett. 36, 2009.

von Schuckmann, K., Le Traon, P.Y., 2011. How well can we derive global ocean indicators from Argo data? Ocean Sci. 7, 783–791.

Webb, A.P., Kench, P.S., 2010. The dynamic response of reef islands to sea-level rise: evidence from multi-decadal analysis of island change in the Central Pacific. Glob. Planet. Change 72, 234–246.

Wilson, W.S., Abdalati, W., Alsdorf, D., Benveniste, J., Bonekamp, H., Cogley, J.G., Drinkwater, M.R., Fu, L.L., Gross, R., Haines, B.J., Harrison, D.E., Johnson, G.C., Johnson, M., Labrecque, J.L., Lindstrom, E.J., Merrifield, M.A., Miller, L., Pavlis, E.C., Piotrowicz, S., Roemmich, D., Stammer, D., Thomas, R.H., Thouvenot, E., Woodworth, P.L., 2010. Observing systems needed to address sea-level rise and variability. In: Church, J.A., Woodworth, P.L., Aarup, T., Wilson, W.S. (Eds.), Understanding Sea Level Rise and Variability. Wiley-Blackwell Publishing, London, UK.

Woodworth, P.L., White, N.J., Jevrejeva, S., Holgate, S.J., Chuch, J.A., Gehrels, W.R., 2008. Evidence for the accelerations of sea level on multi-decade and century time scales. Int. J. Clim. 29, 777–789, doi:10.1002/joc.1771.

Woodworth, P.L., Menendez, M., Gehrels, W.R., 2011a. Evidence for century-time scale acceleration in mean sea levels and for recent changes in extrem sea levels. Surv. Geophys. 4/5, 603–618, doi:10.1007/s10712-011-91112-8.

Woodworth, P.L., Gehrels, W.R., Nerem, R.S., 2011b. Nineteenth and twentieth century changes in sea level. Oceanography 24 (2), 80–93.

Woppelmann, G., Martin Miguez, B., Bouin, M.-N., Altamimi, Z., 2007. Geocentric sea-level trend estimates from GPS analyses at relevant tide gauges world-wide. Glob. Planet Change 57 (3–4), 396–406.
Woppelmann, G., Letetrel, C., Santamaria, A., Bouin, M.N., Collilieux, X., Altamimi, Z., Williams, S.D.P., Miguez, B.M., 2009. Rates of sea-level change over the past century in a geocentric reference frame. Geophys. Res. Lett. 36, L12607, doi:10.1029/2009gl038720.
Wunsch, C., Ponte, R.M., Heimbach, P., 2007. Decadal trends in sea level patterns: 1993–2004. J. Clim. 20 (24), 5889–5911, doi:10.1175/2007JCLI1840.1.
Yin, J., Griffies, S.M., Stouffer, R.J., 2010. Spatial variability of sea level rise in the twenty-first century projections. J. Clim. 23, 4585–4607.
Yokoyama, Y., Esat, T.M., 2011. Global climate and sea level: enduring variability and fluctuations over the past 150,000 years. Oceanography 24 (2), 54–69.

Chapitre 2

La variabilité régionale du niveau de la mer

Au cours de cette thèse, nous nous sommes intéressés, dans un premier temps, aux questions scientifiques du groupe (a) et (b) (voir section 1.5) qui portent sur les observations du niveau de la mer et ses contributions. Nous nous sommes focalisés sur la variabilité régionale, c'est à dire le signal du niveau de la mer auquel on retire la tendance moyenne globale de 3.2 mm.a^{-1}. Nous avons étudié en particulier deux périodes : la période altimétrique (1993-2011) et les dernières décennies (depuis 1950).

Sur la période altimétrique, nous avons une mesure précise de la variabilité régionale du niveau de la mer grâce à la couverture globale des satellites altimétriques (voir section 1.2.2) et nous disposons aussi de mesures globales de la contribution stérique (température et salinité) avec les mesures XBT et CTD. De plus, depuis ∼2004, les mesures de la contribution stérique ont une couverture spatiale et temporelle quasi-homogène grâce aux données Argo, ce qui donne une bonne estimation de la variabilité régionale du niveau de la mer stérique. Depuis 2002 la mission gravimétrique GRACE donne aussi une estimation de la variabilité régionale de la masse de l'océan. En comparant et combinant ces différentes informations nous avons cherché à répondre aux questions scientifiques n° 7, 11, 13, 14, 20, 21, 22 et 23 (questions de la section 1.5 qui traitent des contributions à la variabilité régionale du niveau de la mer). C'est ce que nous présentons dans la section 2.1.

Sur les dernières décennies (1950-2011), nous disposons seulement des marégraphes comme mesures des variations du niveau de la mer. Cela donne très peu d'informations sur la variabilité régionale du niveau de la mer aux échelles inter-annuelles à multi-décennales du fait de leur mauvais échantillonnage spatial. Les seules sources d'informations sur la variabilité régionale à ces échelles sont les OGCMs ou les reconstructions 2D du niveau de la mer. Cependant chacune de ces deux techniques a des défauts et leurs résultats présentent des différences. Cela soulève des interrogations sur les estimations de la variabilité régionale produites et empêche de donner une réponse claire à des questions comme les questions scientifiques n° 6, 7, 8, 9, 21, 22, 28, 29 (questions de la section 1.5 qui traitent de la variabilité régionale du niveau de la mer). Nous présentons dans la section 2.2 une nouvelle technique de reconstruction à 2 dimensions du niveau de la mer qui s'appuie à la fois sur

les marégraphes et sur les OGCMs pour améliorer les estimations de la variabilité régionale aux échelles décennales et apporter de nouveaux éléments de réponse à ces questions.

2.1 Durant la période altimétrique : de 1993 à 2011

2.1.1 L'expansion thermique

Comme nous l'avons vu dans la section 1.3.1, la variabilité régionale des tendances du niveau de la mer sur la période altimétrique peut être très forte, voire dépasser de beaucoup la tendance moyenne globale dans certaines régions. Elle présente des structures complexes (voir Fig. 1.15a), déterminées par les processus dynamiques océaniques et les effets quasi-statiques liés aux redistributions de masse passées et actuelles dans les enveloppes fluides de la Terre (voir section 1.3.3). Ces effets quasi-statiques ont un impact très faible sur la variabilité régionale du niveau de la mer aux échelles de temps inter-annuelles à décennales (voir section 1.3.3 et *Tamisiea and Mitrovica* [2011] par exemple). Pour cette raison ils n'ont pas été détectés jusqu'à maintenant dans les données altimétriques qui couvrent seulement 18 ans, de 1993 à 2011 (*Kopp et al.* [2010]). En revanche sur cette période, les processus dynamiques océaniques, qui comprennent les redistributions dynamiques de masses d'eau et les variations de leurs caractéristiques thermo-halines, dominent la variabilité régionale des tendances du niveau de la mer. En effet, nous avons vu que, sur la periode altimétrique, la variabilité régionale des tendances du niveau de la mer était essentiellement d'origine stérique (voir section 1.3.1 et *Levitus et al.* [2005, 2009]; *Ishii and Kimoto* [2009]; *Lombard et al.* [2005a,b]). Plus précisement, la variabilité régionale est dominée par les variations thermostériques des couches supérieures de l'océan (0-700 m). Ceci est confirmé par les 3 jeux de données stériques globaux de *Levitus et al.* [2009]; *Ishii and Kimoto* [2009]; *Domingues et al.* [2008] qui prennent en compte les dernières corrections des biais XBT et MBT. En effet, en terme de variabilité régionale, les trois jeux de données donnent des tendances similaires entre elles et similaires à l'altimétrie sur la periode altimétrique (voir Fig. 1.15b et Fig. 2.1). Quasiment dans toutes les régions du globe, les tendances altimétriques s'expliquent par les variations thermostériques des couches supérieures de l'océan (Fig. 2.1) excepté dans quelques régions comme l'océan Atlantique et le Sud de l'océan Pacifique pour lesquelles on observe une légère compensation par les variations halostériques des couches supérieures (voir Fig. 2.1c), et dans le Nord-Est de l'océan Atlantique où le signal halostérique est intense. Ces résultats sont confirmés par les réanalyses océaniques (modèles d'océan qui assimilent des données, voir *Carton et al.* [2005]; *Wunsch et al.* [2007]; *Köhl and Stammer* [2008]) ainsi que par des modèles d'océan sans assimilation mais forcés par des données atmosphériques (*Lombard et al.* [2009]).

Les variations thermostériques des couches supérieures de l'océan n'expliquent pas seulement les tendances régionales du niveau de la mer sur la période 1993-2011. Elles expliquent aussi les variations inter-annuelles à multi-décennales de la variabilité régionale du niveau de la mer. La Fig. 2.2 présente le mode dominant de variabilité du niveau de la mer (Fig. 2.2a) et du niveau de la mer thermostérique des 700 premiers mètres de l'océan (Fig. 2.2b, basée sur les données de *Levitus et al.* [2009]) extrait par une analyse en Fonctions Em-

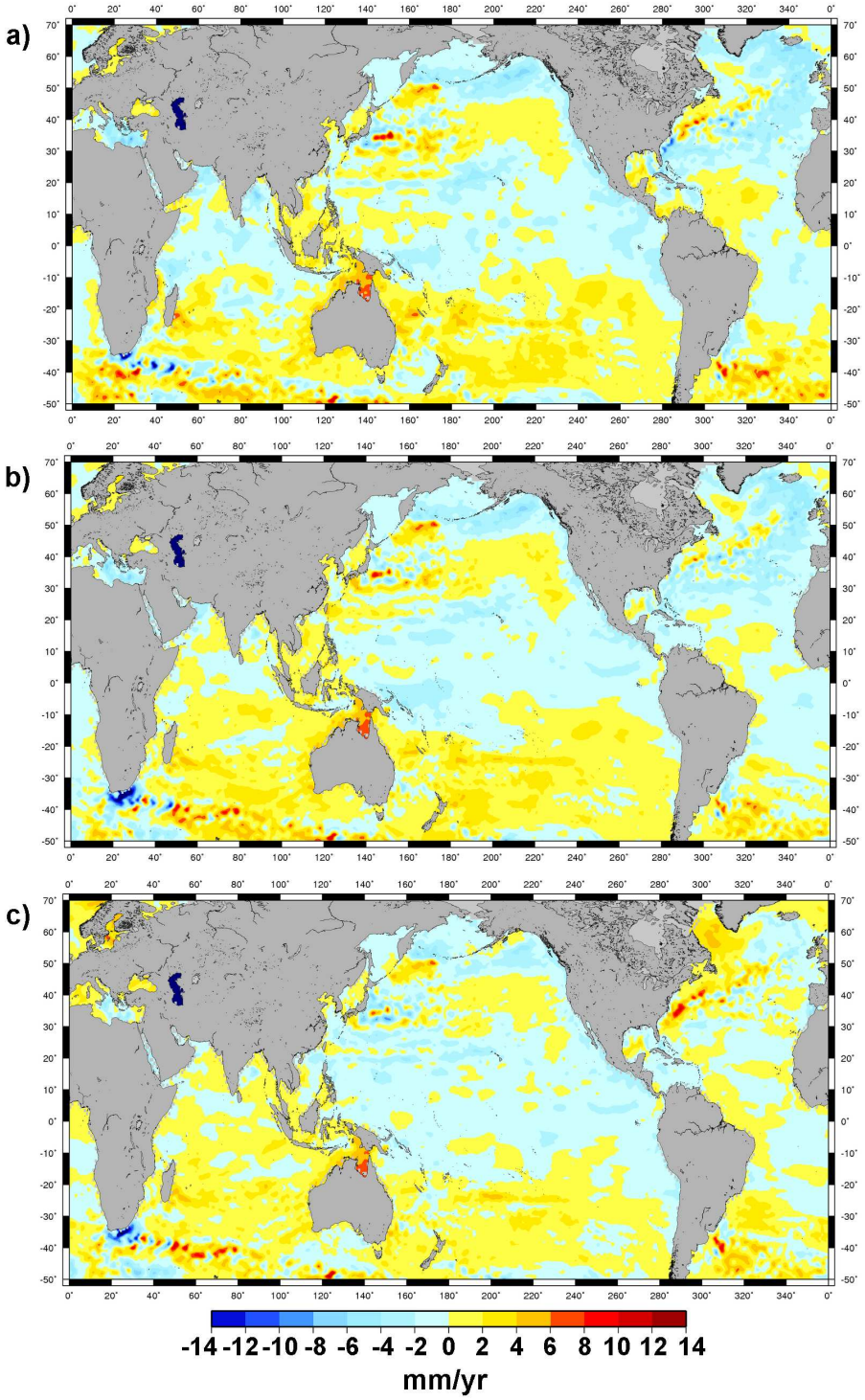

Figure 2.1 – Différences entre les tendances du niveau de la mer calculées à partir des données altimétriques (voir Fig.1.15a) et (a) les tendances du niveau thermostérique calculées avec les données de *Levitus et al.* [2009], (b) les tendances thermostériques et (c) stériques calculées avec les données de *Ishii and Kimoto* [2009]. Pour le calcul des hauteurs stériques et thermostériques on a utilisé les couches de 0 à 700m. Les tendances moyennes globales ont été rétirées de chaque carte. L'échelle de couleur est la même que celle qui a été utilisée pour la Fig. 1.15

piriques Orthogonales -EOF- sur la période 1993-2011. Les 2 modes dominants sont très similaires dans toutes les régions du globe excepté dans le Nord de l'océan Atlantique et dans l'océan Austral. De même, les composantes principales associées à ces modes (courbes noire et bleue sur la Fig. 2.2c) sont fortement corrélées (coefficient de correlation de 0.97 avec un niveau de significativité -SL- >99%) révélant que les variations thermostériques des 700 premiers mètres de l'océan expliquent les variations du niveau de la mer aux échelles inter-annuelles.

Ces variations sont aussi fortement corrélées à l'indice Southern Oscillation Index -SOI- qui est un indicateur du mode de climat ENSO. La correlation est de 0.87 (SL>99%) entre la composante principale du mode 1 du niveau de la mer mesuré par altimétrie et l'indice SOI. Elle est de 0.89 (SL>99%) entre la composante principale du mode 1 des données thermostériques et l'indice SOI. Ceci montre qu'aux échelles inter-annuelles, la variabilité régionale du niveau de la mer est largement d'origine thermostérique et qu'elle fluctue dans le temps en suivant des modes de variabilité du système climatique tel que ENSO (voir *Lombard et al.* [2005a,b]; *Levitus et al.* [2005]).

Ces résultats sont confirmés sur une periode plus courte, de 2002 à 2009, pour laquelle on dispose de données thermostériques et halostériques à l'échantillonnage plus dense et plus homogène sur l'ensemble de l'océan grâce au programme Argo. En effet, en analysant 4 jeux de données Argo (données Argo venant de CLS, SCRIPPS, IPRC et NOAA), *Llovel et al.* [2010b] trouvent aussi que les tendances et l'évolution temporelle de la variabilité régionale du niveau de la mer s'expliquent par les variations thermostériques des 700 premiers mètres de l'océan. Ils montrent aussi que ces variations thermostériques suivent principalement les modes de variabilité de ENSO et du dipôle Indien qui est un autre mode de variabilité du système climatique centré sur l'océan Indien (Indian Ocean Dipole -IOD- en anglais, voir *Behera et al.* [2008]; *Schott et al.* [2009]).

Il est étonnant de constater que la variabilité régionale du niveau de la mer s'explique par l'expansion thermique de l'océan sur cette période récente de 2002 à 2009, car sur cette même période le réchauffement de l'océan n'a pas présenté d'accroissement significatif. C'est d'ailleurs le sujet de la question scientifique n°14 (voir section 1.5). Nous avons vu plus haut (voir section 1.3.1) qu'entre 2003 et 2009, l'expansion thermique globale de l'océan avait ralenti, n'expliquant plus que 20% à 30% de l'augmentation globale du niveau de la mer (*Lyman et al.* [2010]; *Llovel et al.* [2010b]; *Cazenave and Llovel* [2010]) alors qu'elle en expliquait 50% sur la periode 1993-2003 (voir section 1.3.1 et *Bindoff et al.* [2007]). Ceci soulève un double problème. Comment expliquer d'une part que l'expansion thermique ait ralentie au cours de la dernière décennie alors que le niveau de la mer, en moyenne globale, a continué son augmentation au même rythme qu'auparavant ? Comment expliquer d'autre part que, malgré ce ralentissement thermostérique global, l'expansion thermique explique toujours la variabilité régionale du niveau de la mer ?

C'est ce double problème que nous avons analysé dans notre étude "Steric sea level variations over 2004-2010 as a function of region and depth : Inference on the mass component variability in the North Atlantic Ocean". Nous avons choisi pour cela une approche régionale en analysant, bassin par bassin, les niveaux de la mer stériques et thermostériques.

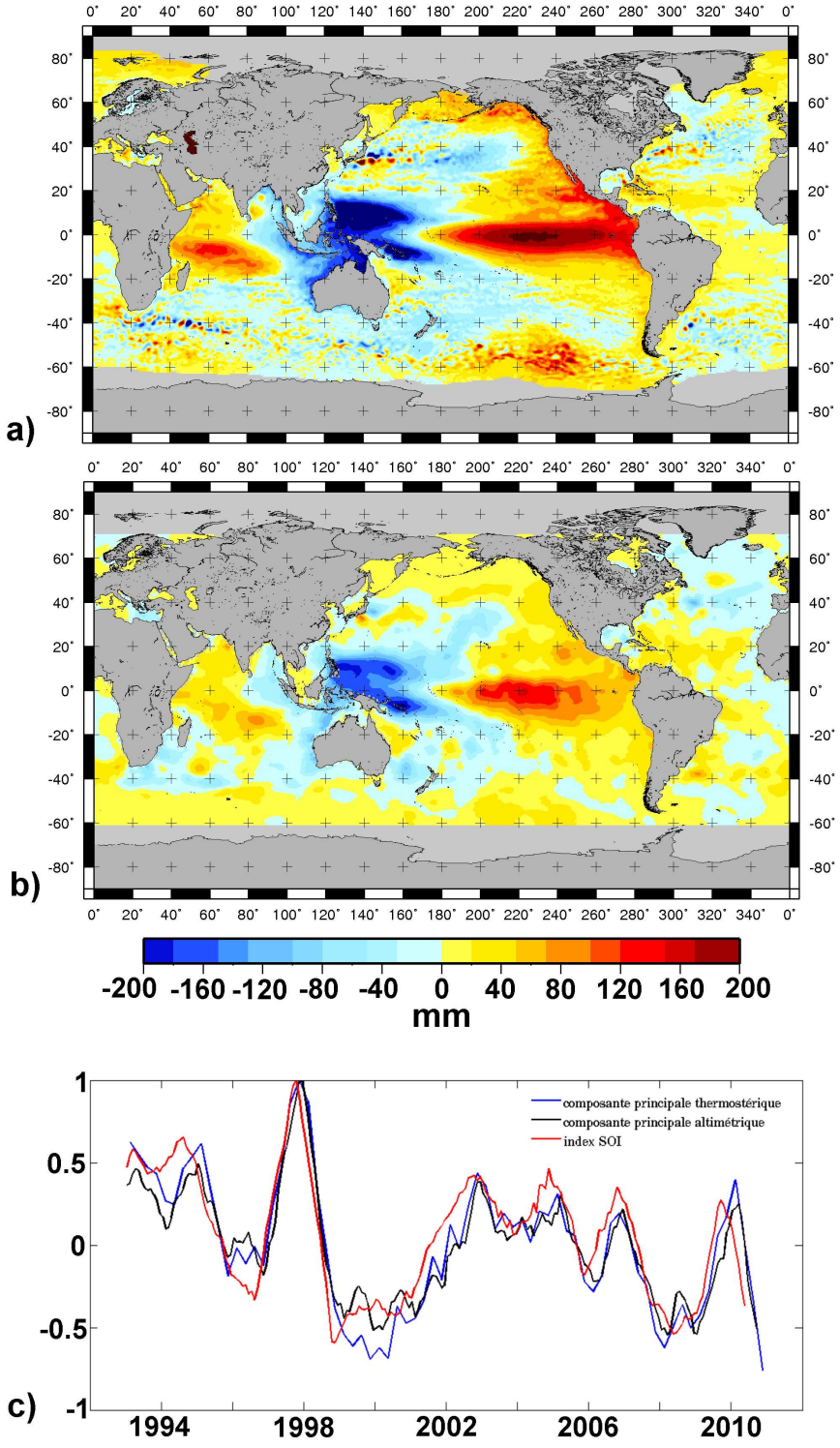

Figure 2.2 – Mode n°1 de l'analyse en EOF des champs altimétriques et thermostériques (*Levitus et al.* [2009]) sur la période 1993-2010. a) Amplitude spatiale du mode 1 de l'altimérie (16% de la variance totale expliquée). b) Amplitude spatiale du mode 1 des données thermostériques (9% de la variance totale expliquée). c) composantes principales des modes 1 de l'altimétrie (courbe noire) et des données thermostériques (courbe bleue) ainsi que l'indice SOI (courbe rouge).

Résumé de l'article : "Steric sea level variations over 2004-2010 as a function of region and depth : Inference on the mass component variability in the North Atlantic Ocean" (l'article original est inséré à la fin de cette section 2.1.1) :
Dans cette étude, nous avons estimé les variations du niveau de la mer stérique et thermostérique des océans Indien, Pacifique et Atlantique entre 2004 et 2010 sur 3 couches de profondeurs différentes : les couches 0-300 m, 300-700 m et 700-2000 m. Notre objectif était de déterminer quelles régions et quelles couches de l'océan étaient responsables du ralentissemment du niveau stérique global sur la période 2003-2010 pour amener des éléments de réponse à la question scientifique n°14. Nous avons montré, sur cette période, que l'océan Indien s'est réchauffé de manière significative de 0 à 2000 m contribuant ainsi à une hausse du niveau de la mer thermostérique global de 1.2 $\pm$ 0.4 mm.a^{-1}. En revanche l'océan Atlantique s'est refroidi de 0 à 2000 m de profondeur, et a contribué à une baisse du niveau de la mer thermostérique global de -1.0 $\pm$ 0.35 mm.a^{-1}. L'océan Pacifique quand à lui s'est légèrement réchauffé ce qui a donné une contribution de 0.35 $\pm$ 0.25 mm.a^{-1} au niveau thermostérique global. C'est donc le refroidissement de l'océan Atlantique sur la dernière décennie qui est responsable du ralentissement global dans le niveau de la mer thermostérique. En se focalisant sur l'océan Atlantique, nous avons montré de plus que ce refroidissement s'est accompagné d'une augmentation significative de la masse de l'Atlantique Nord. C'est ce qui explique que la hausse niveau de la mer global sur la dernière décennie ne s'est pas ralentie alors que dans le même temps, le niveau thermostérique global diminuait. Enfin on a pu observer dans les océans Indien et Pacifique, que c'est bien la variabilité thermostérique inter-annuelle de la couche de surface (0-300 m) qui explique la majorité de la variabilité inter-annuelle du niveau de la mer. Même si dans l'océan Atlantique, les couches profondes (300-2000 m) ainsi que les variations de salinité jouent un rôle non-négligeable, c'est toujours la variabilité régionale de l'expansion thermique qui explique celle du niveau de la mer.

En résumé, les observations montrent que sur la période altimétrique, la variabilité régionale du niveau de la mer (en terme de tendances et de variations inter-annuelles) s'explique par celle du niveau thermostérique des 700 premiers mètres de l'océan. De plus cette variabilité thermostérique n'est pas stationnaire. Elle fluctue dans le temps et l'espace avec les grands modes naturels de variabilité du système couplé océan-atmosphère tel que ENSO mais aussi l'oscillation Nord Atlantique -NAO- et l'Oscillation Décennale Pacifique-PDO- (*Di Lorenzo et al.* [2010]; *Lozier et al.* [2010]; *Levitus et al.* [2005]; *Lombard et al.* [2005a,b]).

Les fluctuations de la variabilité thermostérique du niveau de la mer sont essentiellement dûes aux redistributions de chaleur et de sel provoquées par les fluctuations des vents en lien avec les modes de variabilité climatiques. Localement les échanges d'eau douce et de chaleur entre océan et atmosphère peuvent aussi jouer un rôle (*Köhl and Stammer* [2008]; *Piecuch and Ponte* [2012]). Par exemple, les fortes tendances positives du niveau de la mer que l'on observe à l'Ouest du Pacifique et les tendances négatives à l'Est du Pacifique sur la période 1993-2010 (voir Fig. 1.15) s'expliquent par un renforcement des vents d'Est dans le Pacifique tropical sur la même période (*Lee and McPhaden* [2008]; *Timmermann et al.* [2010]; *Merrifield* [2011]). Dans l'océan Indien, *Han et al.* [2010] ont suggéré aussi que les tendances du niveau de la mer depuis 1960 s'expliquaient par des changements de vent à la surface de l'océan eux même liés à des renforcements des cellules de Walker et Hadley locales.

Steric sea level variations over 2004–2010 as a function of region and depth: Inference on the mass component variability in the North Atlantic Ocean

W. Llovel,[1,2] B. Meyssignac,[1] and A. Cazenave[1]

Received 22 March 2011; revised 1 May 2011; accepted 2 May 2011; published 2 August 2011.

[1] We investigate the regional-ocean depth layer (down to 2000 m) contributions to global mean steric sea level from January 2004 to March 2010, using Argo-based ocean temperature and salinity data from the SCRIPPS Oceanographic Institution database. We find that Indian ocean warming is almost compensated by Atlantic ocean cooling, so that the total global mean steric sea level increases only slightly over the considered period (0.35 ± 0.30 mm/yr). Salinity variations also contribute, at lower rate, to the observed steric compensation. Meanwhile, the Pacific steric sea level increases only slightly (0.35 ± 0.25 mm/yr). In the North Atlantic region, the mass component (estimated by the difference between satellite altimetry-based minus steric sea level over the same area) is negatively correlated over 2004–2010 with the steric component. During that period, North Atlantic sea level variability seems mostly driven by the North Atlantic Oscillation (NAO). This is unlike during the previous years (1997 to 2004), a period during which we observe significant correlation between North Atlantic sea level and El Nino-Southern Oscillation (ENSO), with positive sea level corresponding to ENSO cold phases (La Nina). **Citation:** Llovel, W., B. Meyssignac, and A. Cazenave (2011), Steric sea level variations over 2004–2010 as a function of region and depth: Inference on the mass component variability in the North Atlantic Ocean, *Geophys. Res. Lett.*, *38*, L15608, doi:10.1029/2011GL047411.

1. Introduction

[2] Measuring sea level change and understanding its causes is a major goal in climate research, considering the potentially highly negative consequences of sea level rise under global warming. According to the Intergovernmental Panel on Climate Change-4th Assessment Report (IPCC-AR4), global mean sea level rise during the 1993–2003 decade amounted to 3.1 ± 0.7 mm/yr (2-sigma uncertainty), with ~50% attributed to thermal expansion and ~40% due to water mass input from ice sheet and glacier ice mass loss [*Bindoff et al.*, 2007]. Since about 2004, slowdown in thermal expansion rate has been reported by a number of investigators using Argo profiling floats data [*Willis et al.*, 2008, 2010; *Levitus et al.*, 2009; *Cazenave et al.*, 2009; *Leuliette and Miller*, 2009; *Llovel et al.*, 2010]. However, estimated rates of rise from the different studies are highly scattered, likely a result of too short time spans of analysis, different data processing strategies, etc. [e.g., *Lyman et al.*, 2010]. Nevertheless, as shown by *Llovel et al.* [2010] using different in situ temperature and salinity databases (mostly from Argo), there is clear evidence of slower rate of steric (i.e., thermosteric plus halosteric) sea level rise in the recent years. Such a result motivated us to investigate further the steric sea level at regional scale and as a function of ocean depth. For that purpose, we study the behavior of the steric sea level over the past few years in the three main ocean basins and estimate the contributions of ocean layers at different depths. We finally look at sea level and mass component in the North Atlantic Ocean.

2. Data Sets

2.1. Satellite Altimetry Data

[3] In this study, we use the Ssalto/duacs multi-mission sea level products provided by CLS/AVISO (downloaded at the website: http://www.aviso.oceanobs.com/en/data/products/sea-surface-height-products/global/msla/index.html). As described on the website, data are provided with two levels of resolution on a Mercator grid: (1) 1/3° × 1/3° and (2) 1° × 1°. Here, we choose the first option resampled on a Cartesian grid at 1/4° × 1/4° resolution. These sea level products are available at weekly interval. The data used in this study span from January 2004 to March 2010. Over the studied time span, the data are principally based on Jason-1 and Jason-2, but Envisat and GFO data are also used with lower weight. Most updated geophysical and environmental corrections have been applied to the data, including the inverted barometer correction (see *Ablain et al.* [2009] for details).

2.2. Argo Data

[4] We consider Argo-based temperature T and salinity S fields of the SCRIPPS Institution of Oceanography database (as shown by *Llovel et al.* [2010], compared to other available data bases, the SCRIPPS data have good temporal coverage, cover a larger depth range and are given at monthly interval). The SCRIPPS data can be downloaded from the http://www.argo.ucsd.edu/Gridded_Field.html website [*Roemmich and Gilson*, 2009]. We have computed thermosteric (T anomalies only), halosteric (S anomalies only) and steric (T plus S anomalies) gridded sea level time series in three different layers (0–300 m, 300–700 m and 700–2000 m depth), over the ocean domain up to 65°N and 65°S of latitude, at monthly interval, on 1° × 1° mesh, over the time span from January 2004 to March 2010.

[5] As no errors are provided with the SCRIPPS T/S data, we have also computed steric/thermosteric/halosteric sea level time series using three additional databases (NOAA, IPRC databases, as by *Llovel et al.* [2010] and JAMSTEC data-

[1]LEGOS, CNES, CNRS, IRD, UPS, Toulouse, France.
[2]Jet Propulsion Laboratory, California Institute of Technology, Pasadena, California, USA.

0094-8276/11/2011GL047411

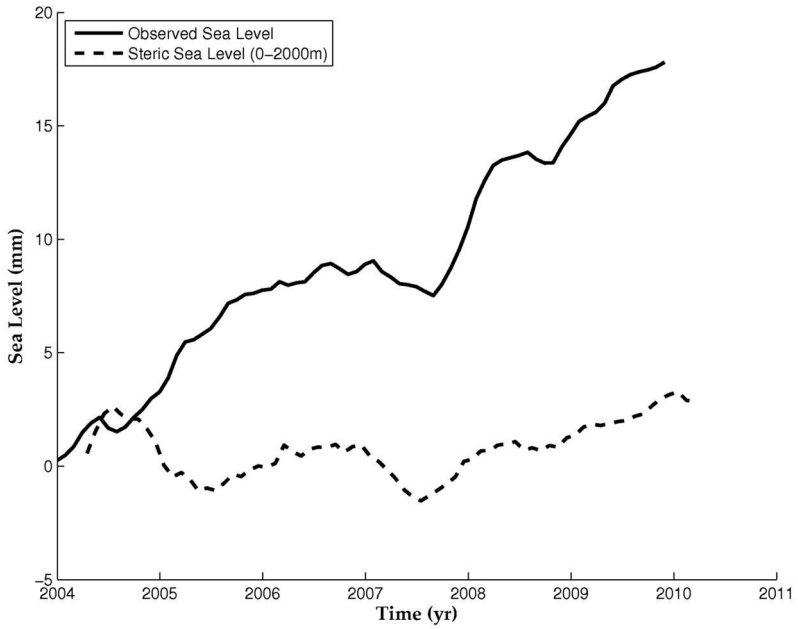

Figure 1. Observed altimetry-based (black curve) and steric (dashed black curve) global mean sea level between 2004–2010 computed between 65°S and 65°N latitude. Seasonal signal removed and 7-month running smoothing applied.

base), and estimated the data errors from the dispersion between the different time series (see *Llovel et al.* [2010] for details).

3. Results

3.1. Region-Depth Steric Sea Level Variations

[6] Figure 1 shows the global mean steric sea level over the time span of analysis (January 2004 to March 2010). The altimetry-based (i.e., observed) global mean sea level is superimposed for comparison. The global mean steric trend (based on T, S data from surface to 2000 m depth) over the period amounts to 0.35 ± 0.3 mm/yr. As mentioned above, the uncertainty is based on the root-mean squares difference between values estimated from individual databases (note that it is compatible with errors provided by *Lyman et al.* [2010], for the ocean heat content from different Argo data bases). In the remainder of the paper, steric/thermosteric/halosteric errors are always based on this approach.

[7] The observed (altimetry-based) rate of sea level rise over the same time span is 2.8 ± 0.4 mm/yr. The 0.4 mm/yr uncertainty is based on that of *Ablain et al.* [2009] from an assessment of all sources of errors affecting the altimetry-derived mean sea level trend.

[8] Figure 2 displays the regional mean steric (Figures 2a–2c) and thermosteric (Figures 2d–2f) sea level over Indian, Pacific and Atlantic ocean sectors in three different layers: 0–300 m (blue curves), 300–700 m (red curves) and 700–2000 m (black curves). The sector boundaries are as defined as follows: Indian Ocean (65°S-30°N latitude, 40°E-110°E longitude); Pacific Ocean (65°S-65°N latitude, 110°E-290°E longitude); Atlantic Ocean (65°S-65°N latitude, 290°E-40°E longitude). Seasonal signals have been removed at each grid mesh through a least squares fit analysis. A 7-month running smoothing has been applied to the time series. Figure 2 reveals a large positive steric trend of the Indian Ocean upper layer (0–700 m). For comparing the trend value to the global mean steric trend, it is necessary to weight it by the ratio of the ocean box area to the total oceanic area considered in this study (±65° latitude). In the following, all quoted trends are weighted trends using the ratio of the considered area to the total area. The weighted trend for the Indian upper layers (0–700 m) amounts to ~1 ± 0.3 mm/yr. The deeper layer (700–2000 m) also shows steric sea level increase but with smaller magnitude. The value for the 0–2000 m depth range is +1.2 ± 0.4 mm/yr. It represents the contribution of the Indian Ocean box to the total steric trend. Comparison with the thermosteric sea level suggests that the steric trend is mainly due to temperature, hence ocean warming. In addition to a positive trend, the upper layer steric/thermosteric sea level (0–300 m) shows large interannual variability associated with the Indian Ocean Dipole – IOD- [*Cai et al.*, 2009; *Schott et al.*, 2009]. The IOD index is superimposed (dashed grey curve) on the thermosteric upper layer curve of the Indian Ocean contribution. The correlation between the two curves is 0.9.

[9] In the Pacific Ocean, the regional mean steric/thermosteric sea level shows small trends both in the upper and deeper layers. Over the 0–2000 m depth range, the Pacific steric trend amounts to 0.35 ± 0.25 mm/yr –weighted value-. Large, ENSO (El Niño-Southern Oscillation)-related interannual variability is observed. The correlation with the Southern Oscillation Index (SOI) superimposed to the thermosteric upper layer curve (dashed grey curve) equals to 0.7. The interannual variability of the recent years steric sea level in the Indian and tropical Pacific was studied in more detail by *Llovel et al.* [2010].

[10] In the Atlantic Ocean, regional mean steric/thermosteric sea level curves show negative trends, especially in the upper layer. Slight negative trends are also seen in the deeper layers. However, unlike the other oceans, the halosteric component (i.e., due to salinity variations) plays a significant role here (not shown), resulting in partial compensation in the steric sea level, likely associated to heat and fresh water, circulation-

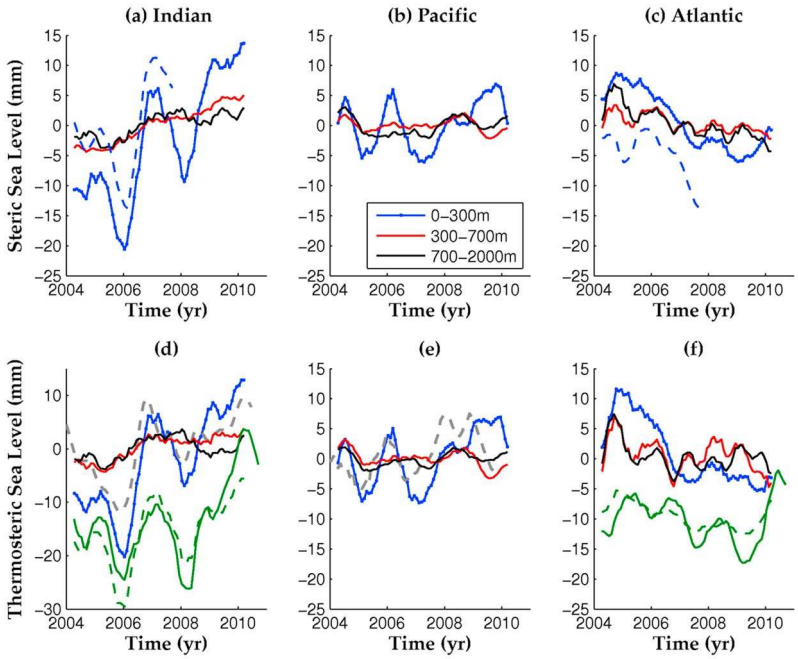

Figure 2. Regional mean steric (upper panels) and thermosteric (lover panels) sea level over 2004–2010, over the Indian, Pacific and Atlantic Ocean boxes for different layers: 0–300 m (blue curves), 300–700 m (red curves) and 700–2000 m (black curves). Seasonal signal removed and 7-month running smoothing applied. Panels are labeled a to f. DRAKKAR-based regional mean steric sea level (0–300 m) are superimposed on panels a and c (dashed blue curves). IOD index and SOI (both grey dashed curves) are superimposed on thermosteric sea level curves for Indian Ocean (panel d) and Pacific Ocean (panel e) respectively. Regional mean SST (dashed green curve) and Argo–based regional thermosteric sea level (over 0–100 m depth, solid green curve) are superimposed in panels d and f.

driven redistribution and fresh water input from land ice melt and river runoff. The Atlantic Ocean weighted steric trend (0–2000 m depth range) amounts to −1.0 ± 0.35 mm/yr.

[11] If we compare the area-weighted steric trends of the three ocean boxes, we note opposite contributions between Indian and Atlantic Oceans (of +1.2 ± 0.4 mm/yr and −1.0 ± 0.35 mm/yr respectively), with near compensation between the two regions. As the Pacific Ocean steric trend is small over the studied period, we get a small value for the total steric trend (of ~0.5 mm/yr) (note that the sum of the three box contributions is slightly larger than the observed total trend of 0.35 mm/yr; this is because the sum of the box areas does not exactly coincide with the total domain). Computed steric and thermosteric weighted trends are summarized in Table 1. The global values are also given.

[12] In order to check whether the apparent warming and cooling of the Indian and Atlantic oceans (hence compensation) may not result from instrumental Argo floats bias, we compared Argo-based thermosteric/steric sea level in these two ocean basins with two types of independent data: (1) the in situ and satellite sea surface temperature (SST) analysis [*Reynolds et al.*, 2002], and (2) the steric sea level from a general ocean circulation model –OGCM- (the DRAKKAR/NEMO -B83 run- model meteorologically forced by the CORE dataset assembled by W. Large [*Large and Yeager*, 2004], and no data assimilation [*Barnier et al.*, 2006; *Dussin et al.*, 2009]). SST data are provided monthly on 1°x1° grids. Data were geographically averaged over the ocean domains defined above over the time span considered in this study. The averaged SST was then compared to Argo-based thermosteric sea level of the 0–100 m upper ocean layer in these two basins. Similarly, we computed the mean steric sea level over the 0–300 m upper ocean layer from the DRAKKAR model outputs (which end in early 2007). Corresponding results are shown in Figures 2a and 2c for DRAKKAR (dashed blue curves) and Figures 2d and 2f for SST (dashed green curves). We note very high correlation (>0.85 for all cases) between Argo-based steric/thermosteric sea level and totally inde-

Table 1. Regional Mean Steric and Thermosteric Sea Level Trends Weighted by the Ratio of the Box Area to the Total Ocean Area for the Indian, Pacific, Atlantic, North Atlantic Oceans and the Sum of the Three Considered Oceans

Jan. 2004–Mar. 2010	Indian Ocean (65°S-30°N, 40°E-110°E)	Pacific Ocean (65°S-650N, 110°E-290°E)	Atlantic Ocean (65°S-65°N, 290°E-40°E	North Atlantic (0-65°N, 290°E-40°E)	Total
Area weighted steric sea level trend (mm/yr) (0–2000 m depth range)	+1.2 ± 0.4	+0.35 ± 0.25	−1.0 ± 0.35	−0.32± 0.25	0.55 ± 0.5
Area weighted thermosteric sea level trend (mm/yr) (0–2000 m depth range)	+1.0 ± 0.4	+0.52 ± 0.25	−0.8 ± 0.35	−0.23 ± 0.25	0.72 ± 0.5

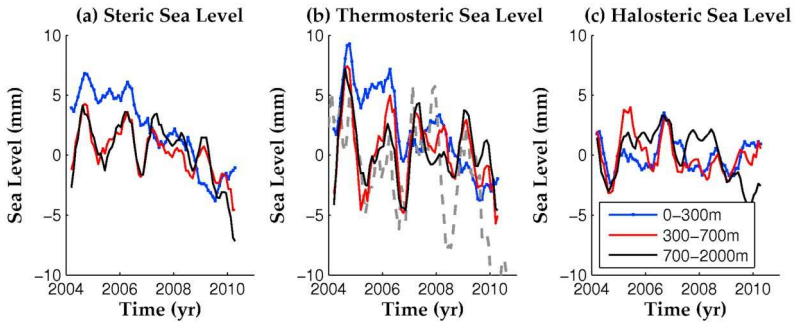

Figure 3. Regional mean (a) steric, (b) thermosteric and (c) halosteric sea level over 2004–2010 over the North Atlantic box at different ocean layers: 0–300 m (blue curves), 300–700 m (red curves) and 700–2000 m (black curves). Seasonal signal removed and 7-month running smoothing applied. NAO (grey dashed curve) is superimposed to thermosteric sea level curves (Figure 3b).

pendent data from an OGCM and SST products. This gives us confidence that the trends reported in the Indian and Atlantic oceans with Argo data are not due to artifacts or instrumental bias of the Argo floats.

3.2. Steric and Mass Components of the Observed Sea Level in the North Atlantic

[13] We now focus on the North Atlantic (equator to 65°N, from 290°E to 40°E longitude). Figures 3a–3c show corresponding steric/thermosteric/halosteric sea level (blue, red and black curves respectively) at the same 3 layers and between 0° to 65° latitude (seasonal signal removed). A clear negative trend is observed in each layer. These short-term trends suggest recent cooling of the region as negative trend is also seen in the thermosteric sea level. The total weighted North Atlantic steric trend (0–2000 m depth range) amounts to -0.32 ± 0.25 mm/yr.

[14] In the lower layers (700–2000 m), steric and thermosteric curves reflect high interannual variability, linked to the North Atlantic Oscillation-NAO (see the NAO index –dashed grey curve- superimposed to the thermosteric curve in Figure 3b).

[15] Figure 4 shows observed, altimetry-based mean sea level over the North Atlantic sector (solid black curve) since 1997. Mean steric (doted-solid blue curve) and thermosteric (solid blue curve) sea level over the same domain are also shown since 2004 (as computed in this study using T, S data down to 2000 m depth). In Figure 4 is also shown the difference (called below 'mass component') between observed (altimetry-based) and steric sea level over the North Atlantic

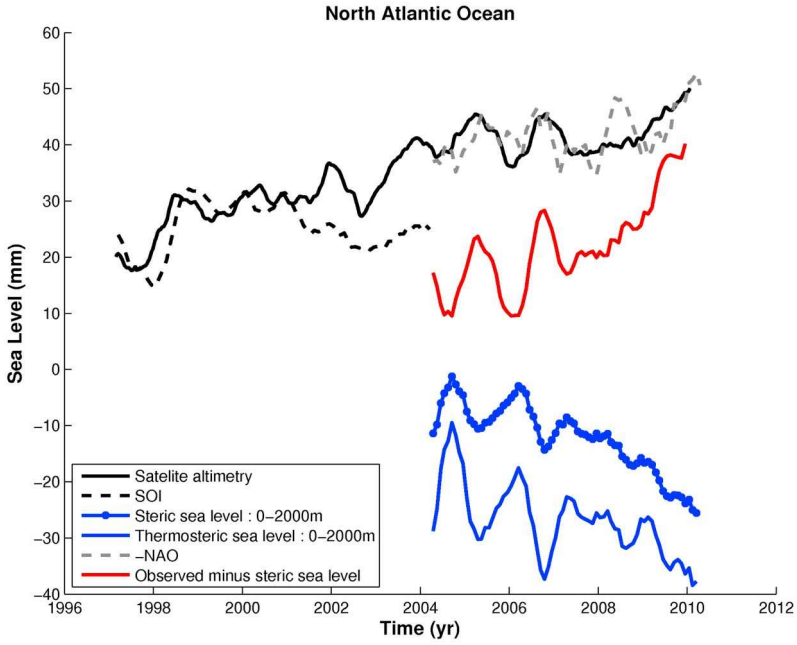

Figure 4. Observed (altimetry-based) mean sea level for the North Atlantic Ocean box (0° to 65°N, 290°E to 40°E) (solid black curve) between 1997–2010; mean steric (doted-solid blue curve), thermosteric sea level (solid blue curve), and mass component (observed minus steric sea level, solid red curve) over the 2004–2010 for the same region. Seasonal signal removed and 7-month running smoothing applied. Steric and thermosteric sea level correspond to the 0–2000 m depth range. Black and grey dashed curves superimposed to observed sea level curve represent SOI and inverse NAO respectively.

sector. The seasonal signal has been removed from all curves and a 7-month smoothing is also applied. While the steric sea level (0–2000 m depth) shows a decreasing trend as discussed above, the mass component shows a positive trend. Both curves appear negatively correlated (correlation coefficient of −0.95).

[16] As shown above, North Atlantic thermosteric sea level is correlated with the NAO index (Figure 3b). We now note that the mass component and the total (altimetry-based) sea level are negatively correlated with NAO during the 2004–2010 time span (positive sea level corresponding to NAO negative phase and inversely). This is illustrated in Figure 4 where the inverse NAO index is superimposed to sea level. Prior to 2004, the North Atlantic sea level is dominantly influenced by ENSO: in Figure 4, we superimposed the Southern Oscillation Index (SOI) (with 7-month smoothing; dashed black curve) to the North Atlantic altimetry-based sea level curve over 1997–2004. The correlation between the two curves amounts to 0.65 between 1997–2001, with positive sea level during La Nina, the ENSO cold phase (corresponding to positive SOI). However the correlation decreases to 0.25 over 1997-2004.

[17] Several previous studies have reported a clear connection between tropical Pacific and tropical North Atlantic sea surface temperature (SST) variability [*Enfield and Mayer*, 1997; *Latif and Grotzner*, 2000] during ENSO events, with warming of the tropical eastern Pacific being associated with warming of the tropical North Atlantic, 4–6 months later [*Giannini et al.*, 2001]. Such tropical North Atlantic SST variability appears in turn to be linked to rainfall conditions over Amazonia [*Yoon and Zeng*, 2010]. Increased rainfall over northeastern Amazonia during La Nina events may eventually extend over the tropical North Atlantic as a result of an eastward shift of precipitation patterns. Increased rainfall over northeastern Amazonia during La Nina events may eventually extend over the tropical North Atlantic as a result of an eastward shift of precipitation patterns, possibly increasing the mass component and sea level. Fresh water input into the tropical Atlantic due to increased runoff from the Amazon River may be another cause, the two effects eventually working concurrently. Further analysis is needed to understand the mechanism responsible for the observed increase in North Atlantic sea level during La Nina events, and more generally the link between tropical Pacific, Amazon hydrology and tropical Atlantic during ENSO events.

[18] While our study suggests some influence of the strong 1997–1999 ENSO event on the North Atlantic sea level, it also reveals that beyond 2004, NAO was the main driver of the interannual variability of the North Atlantic sea level, acting both on the steric and mass components.

4. Conclusion

[19] The present analysis reports different behaviors of the steric sea level depending on the ocean basin over the 2004–2010 time span. The Indian Ocean shows significant ocean warming between 0 and 2000 m depth, while the Atlantic Ocean shows cooling during the same period. In the Atlantic region, slight upper ocean salinity variation is also observed, which suggests large-scale ocean circulation changes and heat and fresh water redistribution are causing the observed steric variations. In the Pacific Ocean, significant trend is noticed and large interannual variability is also observed in the upper layer linked to ENSO events.

[20] Indian Ocean warming and Atlantic Ocean cooling more or less compensate each other during 2004–2010 time span, explaining the recent low observed rate of the steric sea level.

[21] In the North Atlantic, we find that the mass component (deduced from the difference between altimetry-based and steric sea level) is negatively correlated to the steric sea level. We also find that North Atlantic sea level interannual variability was influenced by ENSO during 1997–2004, but since 2004, the NAO influence dominates. Further studies are necessary to understand the mechanisms responsible for these observations.

[22] **Acknowledgments.** The authors thank Marta Marcos and an anonymous reviewer for their helpful comments. The Argo data were collected and made freely available by the international Argo product (http://www.argo.ucsd.edu). The altimeter products were produced by SSALTO/DUACS and distributed by AVISO with support from CNES.

[23] The Editor thanks two anonymous reviewers for their assistance in evaluating this paper.

References

Ablain, M., A. Cazenave, G. Valladeau, and S. Guinehut (2009), A new assessment of the error budget of global mean sea level rate estimated by satellite altimetry over 1993–2008, *Ocean Sci.*, *5*, 193–201, doi:10.5194/os-5-193-2009.

Barnier, B., et al. (2006), Impact of partial steps and momentum advection schemes in a global ocean circulation model at eddy-permitting resolution, *Ocean Dyn.*, *56*, 543–567, doi:10.1007/s10236-006-0082-1.

Bindoff, N., et al. (2007), Observations: Oceanic climate and sea level, in *Climate Change 2007: The Physical Science Basis. Contribution of Working Group I to the Fourth Assessment Report of the Intergovernmental Panel on Climate Change*, edited by S. Solomon et al., pp. 385–432, Cambridge Univ. Press, Cambridge, U. K.

Cai, W., A. Pan, D. Roemmich, T. Cowan, and X. Guo (2009), Argo profiles a rare occurrence of three consecutive positive Indian Ocean Dipole events, 2006–2008, *Geophys. Res. Lett.*, *36*, L08701, doi:10.1029/2008GL037038.

Cazenave, A., K. Dominh, S. Guinehut, E. Berthier, W. Llovel, G. Ramillien, M. Ablain, and G. Larnicol (2009), Sea level budget over 2003–2008: A reevaluation from GRACE space gravimetry, satellite altimetry and Argo, *Global Planet. Change*, *65*, 83–88, doi:10.1016/j.gloplacha.2008.10.004.

Dussin, R., A. M. Treguier, J. M. Moline, B. Barnier, T. Penduff, L. Brodeau, and G. Madec (2009), Definition of the interannual experiment ORCA025-B83 1958–2007, *LPO Rep. 09-02*, Lab. de Phys. des Oceans, Brest, France.

Enfield, D. B., and D. A. Mayer (1997), Tropical Atlantic sea surface temperature variability and its relation to El Niño Southern Oscillation, *J. Geophys. Res.*, *102*, 929–945, doi:10.1029/96JC03296.

Giannini, A., J. C. H. Chiang, M. A. Cane, Y. Kushnir, and R. Seager (2001), The ENSO teleconnection to the tropical Atlantic Ocean: Contributions of the remote and local SSTs to rainfall variability in the tropical Americas, *J. Clim.*, *14*, 4530–4544, doi:10.1175/1520-0442(2001)014<4530:TETTTT>2.0.CO;2.

Large, W., and S. Yeager (2004), Diurnal to decadal global forcing for ocean and sea-ice models: the datasets and flux climatologies, *NCAR Tech. Note NCAR/TN-460+STR*, Natl. Cent. for Atmos. Res., Boulder, Colo.

Latif, M., and A. Grotzner (2000), The equatorial Atlantic oscillation and its response to ENSO, *Clim. Dyn.*, *16*, 213–218, doi:10.1007/s003820050014.

Leuliette, E., and L. Miller (2009), Closing the sea level rise budget with altimetry, Argo and GRACE, *Geophys. Res. Lett.*, *36*, L04608, doi:10.1029/2008GL036010.

Levitus, S., J. I. Antonov, T. P. Boyer, R. A. Locarnini, H. E. Garcia, and A. V. Mishonov (2009), Global ocean heat content 1955–2008 in light of recently revealed instrumentation problems, *Geophys. Res. Lett.*, *36*, L07608, doi:10.1029/2008GL037155.

Llovel, W., S. Guinehut, and A. Cazenave (2010), Regional and interannual variability in sea level over 2002–2009 based on satellite altimetry, Argo float data and GRACE ocean mass, *Ocean Dyn.*, *60*, 1193–1204, doi:10.1007/s10236-010-0324-0.

Lozier, M. S., V. Roussenov, M. S. C. Reed, and R. G. Williams (2010), Opposing decadal changes for the North Atlantic meridional overturning circulation, *Nat. Geosci.*, *3*, 728–734, doi:10.1038/ngeo947.

Lyman, J. M., S. A. Godd, V. V. Gouretski, M. Ishii, G. C. Johnson, M. D. Palmer, D. M. Smith, and J. K. Willis (2010), Robust warming of the global upper ocean, *Nature*, *465*, 334–337, doi:10.1038/nature09043.

Reynolds, R. W., N. A. Rayner, T. M. Smith, D. C. Stokes, and W. Wang (2002), An improved in situ and satellite SST analysis for climate, *J. Clim.*, *15*, 1609–1625, doi:10.1175/1520-0442(2002)015<1609:AIISAS>2.0.CO;2.

Roemmich, D., and J. Gilson (2009), The 2004–2008 mean and annual cycle of temperature, salinity and steric height in the global ocean from the Argo program, *Prog. Oceanogr.*, *82*, 81–100, doi:10.1016/j.pocean.2009.03.004.

Schott, F. A., X. Shang-Ping, and P. McCreary (2009), Indian ocean circulation and climate variability, *Rev. Geophys.*, *47*, RG1002, doi:10.1029/2007RG000245.

Willis, J. K., D. T. Chambers, and R. S. Nerem (2008), Assessing the globally averaged sea level budget on seasonal to interannual time scales, *J. Geophys. Res.*, *113*, C06015, doi:10.1029/2007JC004517.

Willis, J. K., D. P. Chambers, C. Y. Kuo, and C. K. Shum (2010), Global Sea Level Rise recent progress and challenges for the decade to come, *Oceanography*, *23*, 26–35, doi:10.5670/oceanog.2010.03.

Yoon, J.-H., and N. Zeng (2010), An Atlantic influence on Amazon rainfall, *Clim. Dyn.*, *34*, 249–264, doi:10.1007/s00382-009-0551-6.

A. Cazenave and B. Meyssignac, LEGOS, CNES, CNRS, IRD, UPS, 14 av. Edouard Belin, F-31400 Toulouse CEDEX, France.

W. Llovel, Jet Propulsion Laboratory, California Institute of Technology, Pasadena, CA 91125, USA. (william.llovel@jpl.nasa.gov)

2.1.2 Le rôle des variations régionales de la masse de l'océan

Sur la période 1993-2011, les variations régionales de la température de l'océan expliquent une large part de la variabilité régionale du niveau de la mer. Si l'on ajoute les variations régionales de salinité, qui compensent localement une partie de l'effet des variations de température (jusqu'à 25% d'après *Wunsch et al.* [2007]), la variabilité régionale du niveau de la mer observée par altimétrie s'explique encore mieux (voir par exemple *Lombard et al.* [2009]). En effet, le signal résiduel obtenu après avoir soustrait les effets thermostériques et halostériques du niveau de la mer (i.e. signal non-stérique), est très faible entre les latitudes -40° et +40° (compris entre ± 3 mm.a^{-1} en tendance sur la période 1993-2011) et seulement légèrement plus fort aux hautes latitudes (voir Fig. 2.1 et par exemple *Lombard et al.* [2009].

Cependant, les effets stériques n'expliquent pas tout. L'autre contribution majeure à la variabilité du niveau de la mer, la variation de masse de l'océan dûe à la fonte des glaces actuelle et aux échanges d'eau avec les bassins fluviaux, joue aussi un rôle dans la variabilité régionale du niveau de la mer (voir section 1.3 et *Bindoff et al.* [2007]). Mais sa contribution est bien plus faible que celle des effets stériques. Il s'agit d'un signal petit encore difficile à observer. Pour l'estimer, il faut pouvoir déterminer le signal résiduel non-stérique contenu dans le niveau de la mer de manière précise. Cette tâche qui est résumée dans la section 1.5 par les questions scientifiques n°20, 21, 22 et 23 est le sujet de nombreuses recherches au niveau international.

Sur la période récente 2002-2011, nous disposons à la fois de mesures précises du niveau de la mer avec l'altimétrie spatiale et de mesures plus précises de l'expansion thermo-haline des océans entre 0 et 2000m avec le programme Argo. En soustrayant les deux signaux on peut obtenir, de manière indirecte, une mesure de la variabilité du niveau de la mer d'origine non-stérique qui donne accès aux variations régionales de masse de l'océan (car la composante stérique du niveau de la mer provenant des couches de l'océan en dessous de 2000 m est très faible). Sur la période de 2004 à 2011, nous disposons aussi d'une mesure directe des variations de masse de l'océan avec la mission spatiale GRACE. En effet, sur les océans, les variations spatio-temporelles du champ de gravité mesurées par GRACE se convertissent en variations spatio-temporelles de la masse de l'océan avec une résolution spatiale d'environ 300 km x 300 km et une résolution temporelle de $\sim$1 mois. Ceci donne une mesure indépendante et directe des variations régionales de masse de l'océan que l'on peut comparer aux variations non-stériques du niveau de la mer déduites de l'altimétrie combinée avec les données Argo. Si ces deux observations dominées par les variations de la masse de l'océan donnent les mêmes résultats alors on obtiendra une mesure fiable de la variabilité régionale de la masse de l'océan et nous aurons expliqué le bilan du niveau de la mer régional avec ses composantes stériques et massiques (enjeu des questions scientifiques n°22 et 23).

En moyenne globale sur l'océan, il a été montré que les fluctuations saisonnières et inter-annuelles du signal non-stérique (altimétrie moins Argo) du niveau de la mer est en accord avec le signal de masse de l'océan observé par GRACE (voir *Willis et al.* [2008]; *Leuliette and Miller* [2009]; *Cazenave et al.* [2009]).

En variabilité régionale, les différentes estimations des variations de masse de l'océan ne sont pas en accord. Ceci est dû au fait qu'en régional, à l'échelle de la résolution des données Argo, le signal de masse de l'océan est si petit qu'il se confond avec les erreurs de mesures. *Llovel et al.* [2010b] ont estimé le niveau de la mer stérique à partir de 4 jeux de données Argo : les données traitées par CLS, le SCRIPPS et l'IPRC. Ils ont montré que malgré un accord en terme de grandes structures régionales et de variabilité saisonnière, ces données présentent des différences en terme de variabilité inter-annuelle et de tendances sur la période 2004-2008. Ces différences sont telles, que le signal résiduel "Altimetrie moins Argo" est très différent (en terme de variabilité inter-annuelle) quand on utilise un jeu de données Argo ou un autre. Ils ont aussi montré que sur la même période, la variabilité régionale du signal de masse de l'océan calculé avec GRACE diffère des estimations "Altimétrie moins Argo" (voir Fig. 2.3).

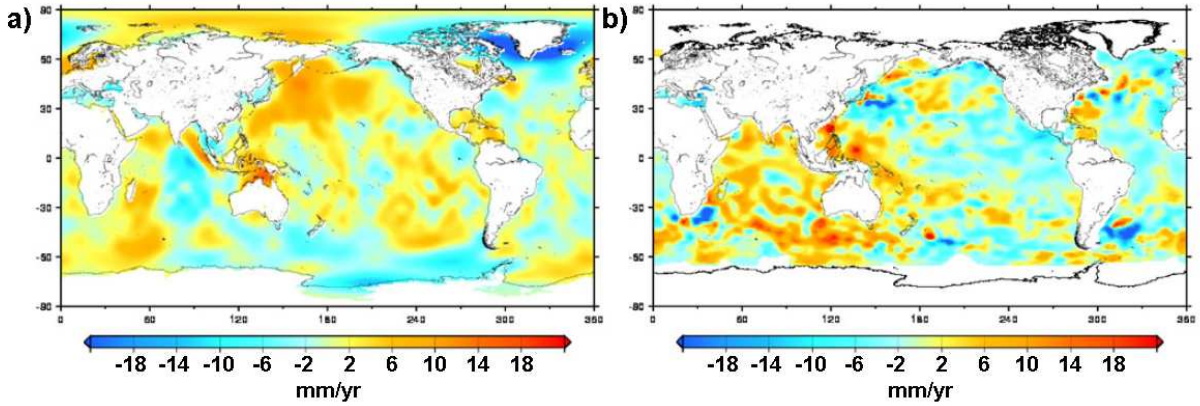

Figure 2.3 – Tendances du signal de masse de l'océan sur la période 2004-2008 (a) mesurées par GRACE et (b) calculées par différence du niveau de la mer mesuré par altimétrie avec le niveau stérique mesuré par les données Argo de CLS. La tendance moyenne globale a été enlevée dans les deux figures. Figure tirée de *Llovel et al.* [2010b]

Les raisons de ces différences entre les estimations de la variabilité régionale de la masse de l'océan ne sont pas claires. Il s'agit peut être du faible échantillonnage spatial Argo dans certaines régions, des incertitudes dans les calculs des données Argo, de la contribution de l'océan profond qui n'est pas prise en compte (en dessous de 2000 m), du mauvais ratio signal sur bruit de GRACE sur les océans ou encore d'une combinaison de ces différents effets (*Llovel et al.* [2010b]). Il apparait aujourd'hui que c'est surtout le mauvais ratio signal sur bruit de GRACE qui est à l'origine des différences observées dans les estimations de la variabilité régionale de la masse de l'océan (*Llovel et al.* [2010b]).

Quelles que soient les différences entre estimations, il est intéressant de noter qu'elles apparaissent quand on cherche à estimer la variabilité régionale de la masse de l'océan avec une forte résolution spatiale de l'ordre 300 km x 300 km. En revanche, quand on moyenne sur l'ensemble de l'océan, on a vu précédemment que les estimations directes et indirectes des variations de masses de l'océan s'accordent en variabilité inter-annuelle. *Fenoglio-Marc et al.* [2006] et *Calafat et al.* [2010] ont montré que ceci était aussi vrai quand on moyennait sur une région plus petite comme la Méditerranée. Ce résultat nous a poussé a regarder dans différentes régions du monde, de la taille de la Méditerranée ou plus grandes, si l'on obtenait aussi un accord entre estimations directes et indirectes des variations de masse

locale de l'océan. C'est le sujet de notre étude "Regional distribution of steric and mass contribution to sea level changes".

Résumé de l'article : "Regional distribution of steric and mass contribution to sea level changes" (l'article original est inséré à la fin de cette section 2.1.2) :
Dans cette étude , nous avons estimé les variations temporelles de la masse océanique moyénnée sur 7 régions différentes du globe entre 2004 et 2008. Les 7 régions sont le Pacifique et l'Atlantique Nord (30°N-50°N), le Pacifique et l'Atlantique équatorial (20°S-20°N), le Pacifique et l'Atlantique Sud (30°S-60°S) et l'océan Indien (10°N-40°S). Nous avons estimé les variations de masse de l'océan dans chaque région, par les deux méthodes : indirecte et directe. Dans la méthode indirecte, nous avons déduit les variations de masse de l'océan en soustrayant à l'altimétrie, les données stériques déduites des mesures hydrographiques in-situ de *Ishii and Kimoto* [2009] ou déduites des données Argo ENACT/ENSEMBLES version2a de *Ingleby and Huddleston* [2007]. Dans la méthode directe, nous avons utilisé les données GRACE RL04 du Center for Space Research. Les résultats de l'étude montrent que, en moyenne sur chaque région, le cycle annuel des variations de masse océanique est cohérent entre les 2 méthodes. Il en est de même pour la variabilité inter-annuelle dans le Pacifique Nord et Sud, l'Atlantic Sud et l'océan Indien. En revanche, les 2 méthodes ne convergent pas dans les régions équatoriales et l'Atlantique Nord. Dans les régions équatoriales cela est dû au mauvais ratio signal sur bruit des données GRACE. Dans le Nord de l'Atlantique cela est dû aux mauvaises estimations du signal thermostérique par les bouées Argo dans des régions de forte variabilité telle que le Gulf Stream. Nous avons aussi étudié la cohérence entre les deux méthodes d'estimations de la masse de l'océan par une analyse en EOF sur chaque région. Les structures spatiales associées aux variations de masse de l'océan sont cohérentes entre les deux méthodes pour le Pacifique Nord et Sud et l'Atlantique Sud. Ceci donnent donc confiance quand aux estimations des variatons de masse dans ces régions. A partir de ces éléments, nous avons pu mettre en évidence l'existence de transferts de masse aux échelles inter-annuelles entre le Nord et le Sud dans le Pacifique et l'Atlantique. Ces transferts semblent se produire en quadrature de phase entre les 2 océans mais ceci reste à confirmer en étudiant une période plus longue que la période 2004-2008.

En résumé, lorsque l'on compare les estimations régionales des variations de masse de l'océan calculées avec GRACE d'une part, et calculées avec l'altimétrie et Argo d'autre part, on trouve un accord pour des échelles spatiales de l'ordre de la taille des bassins océaniques. En dessous, de fortes différences en variabilité inter-annuelle et en tendance apparaissent. Ceci est essentiellement dû au mauvais rapport signal sur bruit des mesures GRACE sur l'océan (l'échantillonnage spatial imparfait des données Argo peut jouer aussi un rôle localement, en particulier dans les régions de forte variabilité océanique ; les variations des courants ou des masses d'eau en dessous de 2000 m peuvent, elles aussi, jouer un rôle). Ce mauvais rapport signal sur bruit empêche une bonne résolution du signal régional de masse de l'océan qui est petit. Ceci apporte de nouveau éléments de réponse à la question scientifique n°23 en mettant en évidence l'existence d'une limite dans les échelles spatiales à partir de laquelle les techniques d'estimation de masse de l'océan ne s'accordent plus. Cela montre que le signal de GRACE mais aussi celui des bouées ARGO doit encore être affiné (technique des Mascons pour GRACE et uniformisation des traitements pour ARGO ?) si l'on veut déterminer précisement le signal régional de masse de l'océan. En particulier, le problème de la détection des signatures spatiales des contributions au signal de masse

de l'océan (question scientifique n°22) reste totalement ouvert car les précisions obtenues aujourd'hui sur la variabilité régionale de la masse de l'océan sont trop faibles.

Dans certains cas très particuliers, cependant, le problème de la signature spatiale ne se pose pas car le signal de masse de l'océan est très fort. C'est le cas par exemple lors des forts évènements ENSO. Lors des évènements El Niño/La Niña, des changements grande échelle dans le régime de précipitation des tropiques génèrent moins/plus de precipitations sur les continents (*Gu and Adler* [2011]). Ceci a pour conséquence de diminuer/augmenter les stocks d'eau continentaux et donc d'augmenter/diminuer la masse totale de l'océan (voir section 1.3.2 et *Llovel et al.* [2011a]). Ces variations de masse sont si fortes, qu'elles dominent la variabilité inter-annuelle du niveau de la mer global. Pour un signal de masse d'une telle intensité il est possible de déterminer précisement sa répartition spatiale dans l'océan.Ceci peut donner des informations sur les processus à l'origine de la variabilité inter-annuelle du niveau de la mer global et de sa covariabilité avec les stocks d'eau continentaux (question scientifique n°20). Nous avons analysé les variations de la répartition spatiale de la masse de l'océan lors du El Niño 1997/1998 dans l'étude intitulée :"Estimating ENSO influence on the global mean sea level during 1993-2010"

Résumé de l'article : "Estimating ENSO influence on the global mean sea level during 1993-2010" (l'article original est inséré à la fin de cette section 2.1.2) :
Dans cette étude nous avons cherché à déterminer comment se répartissait spatialement l'excès de masse d'eau reçu par l'océan lors des évènements El Niño. Cet excès de masse d'eau reçu par l'océan vient des changements grande échelle dans le régime de précipitation des tropiques provoqué par les évènements El Niño. Ceux-ci génèrent plus de precipitations sur les océans (*Gu and Adler* [2011]), ce qui augmente la masse de l'océan en comparaison avec les années normales (*Llovel et al.* [2010a]) durant lesquelles les précipitations se font plus sur les continents(et sont donc stockées en plus grande quantité dans les bassins fluviaux). Comment se répartit cette excès de précipitations dans l'océan ? La masse d'eau supplémentaire se repartit-elle de manière uniforme sur l'ensemble des bassins océaniques ou présente t-elle de la variabilité régionale ? Dans cette étude, nous nous sommes focalisés sur l'évènement El Niño extrême de 1997-1998 pour répondre à ces questions. *Llovel et al.* [2011a] avait montré que le modèle hydrologique ISBA-TRIP, développé par Météo-France, donnait une bonne estimation du transfert de masse d'eau des stocks continentaux vers l'océan lors de l'évènement El Niño 1997-1998. Nous reprenons dans cet article cette estimation basée sur la dynamique des grands bassins fluviaux et nous la comparons à une estimation indépendante de la variation régionale de masse de l'océan. Cette estimation indépendante est obtenue en soustrayant à l'altimétrie, les hauteurs stériques déduites des données hydrographiques de *Ishii and Kimoto* [2009]. Nous analysons ensuite, bassin océanique par bassin océanique, les variations de masse de l'océan afin de déterminer la région la plus impactée par le transfert de masse venant des continents. Dans les bassins Indien et Atlantique, la masse de l'océan ne présente pas d'augmentation significative en 1997-1998 comparé à la variabilité inter-annuelle qui la caractérise sur la période 1993-2010. En revanche dans l'océan Pacifique on observe une très forte augmentation de la masse en 1997 et 1998 suivit d'une diminution en 1999. Un diagramme Latitude-Temps des variations de masse de l'océan sur la Pacifique révèle que cette augmentation de masse est en fait très localisée. Elle se situe sur une unique fine bande de latitude : entre 10°N et 20°N sur toute la largeur du Pacifique. Pour vérifier ce résultat, nous calculons la variation de masse de cette bande de latitude de l'océan Pacifique entre 1997 et 1998. Ceci confirme que cette

petite région concentre quasiment la totalité de l'excès de masse que reçoit l'océan global de la part des continents lors du El Niño 1997-1998. Ce résultat nouveau est surprenant car, contrairement à ce qu'on pouvait attendre, l'excès de masse reçu par les océans entre 1997 et 1998 ne s'est pas répartit uniformément mais se trouve concentré très localement. Comment peut-on expliquer cette observation ? Un bilan d'eau sur la bande 10°N-20°N du Pacifique montre que les vents et les précipitations ne peuvent expliquer à eux seuls cette concentration locale de masse. Il faut prendre en compte les courants océaniques. Les variations du transport dans le détroit de Makassar (qui lie l'océan Indien à l'océan Pacifique), intégrées sur la durée de l'évènement El Niño 1997-1998, montrent un déficit du transport total de masse vers l'océan Indien du même ordre de grandeur que l'accroissement observé entre 10°N et 20°N dans le Pacifique. Ceci suggère que la circulation joue un rôle non négligeable mais la question du mécanisme responsable de telles concentrations d'eau dans le Pacifique Nord en 1997-1998 reste ouverte.

Global and Planetary Change 76 (2011) 206–218

Contents lists available at ScienceDirect

Global and Planetary Change

journal homepage: www.elsevier.com/locate/gloplacha

Regional distribution of steric and mass contributions to sea level changes

Marta Marcos [a,*], Francesc M. Calafat [a], William Llovel [b], Damià Gomis [a], Benoit Meyssignac [b]

[a] IMEDEA (CSIC-UIB), Esporles, Spain
[b] LEGOS, OMP, Toulouse, France

ARTICLE INFO

Article history:
Received 8 July 2010
Accepted 25 January 2011
Available online 3 February 2011

Keywords:
sea level
steric sea level
GRACE
altimetry

ABSTRACT

The contributing factors to regional sea level variability have been explored for the period 2004–2008 based on altimetry observations, hydrographic data and GRACE measurements. The regional averaged annual cycle of the mass contribution to sea level is shown to be highly unsteady. When compared with steric-corrected altimetry, both signals are coherent, though in some regions the coherence analysis is limited by the use of interpolated hydrographic data and in the equatorial regions it is limited by the low signal-to-noise ratio of GRACE data. The closure of regional sea level budgets depends mainly on the GIA correction chosen. A reconstructed global sea level field (with the atmospheric signal eliminated) spanning the second half of the 20th century together with historical hydrographic observations are used to infer the regional mass contribution to sea level rise for the last decades. Results indicate that mass addition from continental ice is the major contributor to regional mean sea level rise for the last decades. In addition, the spatial patterns of mass rates of change point at Greenland as the main source of fresh water input.

1. Introduction

Long-term global sea level changes have been routinely estimated based on tide gauge measurements with a biased spatial distribution. Since 1992 satellite altimetry has revealed a high spatial heterogeneity of sea level changes, with areas experiencing sea level rise up to three times larger than the global rate and others where sea level has dropped (Cazenave and Nerem, 2004; Cazenave and Llovel, 2010). The contributors to long-term global sea level changes are steric changes and mass addition/subtraction. At regional scale we must add the mass displacements due to the mechanical atmospheric forcing and changes in the oceanic circulation, which may play a significant role in those areas where circulation features are important and determine local sea level (e.g., Gulf Stream or Kuroshio). Separating the sources and reducing the uncertainties in the quantification of each contributor to regional sea level changes is of key importance to understand the causes of sea level variations and to infer future changes.

The global sea level budget has been explored by different authors. Willis et al. (2008) did it on the basis of altimetry, in-situ hydrographic data from Argo floats and space gravimetry observations from the Gravity Recovery and Climate Experiment (GRACE) mission between 2003 and 2007. They concluded that while intra- and inter-annual changes inferred from the different observation sets are consistent, the trends computed for the analyzed period do not agree. Conversely, Leuliette and Miller (2009) using the same data for a slightly different period (2004–2007) found statistical agreement between observed sea level rates of change and the addition of the steric and mass components. Cazenave et al. (2009) also found consistency between steric sea level as inferred subtracting GRACE from altimetry and as observed from Argo floats for the period 2004–2008, respectively. Cazenave et al. (2009) pointed to the critical contribution of the Glacial Isostatic Adjustment (GIA) correction that has to be applied to raw GRACE data as one of the reasons for the disagreement between different authors. The GIA correction is based on solid earth models with a particular rheological profile, ice history deglaciation chronology of the late-Pleistocene ice sheets and defined parameters of the visco-elastic properties of the Earth. GIA reflects in the GRACE signal as a long term trend in the gravity field that is not due to the instantaneous redistribution of water over the Earth's surface. It is thus necessary to separate that trend from actual changes in the water content. This linear correction determines to a large extent the rates of change of the ocean mass component inferred from GRACE data. There are currently two broadly used solutions available for such correction, Paulson et al. (2007) and Peltier (2004) models, with very different global rates (1 and 2 mm/yr, respectively) and even larger differences at regional scale. The differences between the two models are analyzed in Peltier (2009), Peltier and Luthcke (2009) and more recently in Chambers et al. (2010). Chambers et al. (2010) have found that the differences are mostly attributed to large trends in predicted degree-2, order-1 geoid coefficients in the Peltier (2009) model. Peltier and Luthcke (2009) attributed these large rates to present-day ice losses. However Chambers et al. (2010) showed that the signals in Peltier's model are inconsistent with the polar motion and rotation feedback theory he claims to be using and considered that these rates are unrealistic.

* Corresponding author.
E-mail address: marta.marcos@uib.es (M. Marcos).

0921-8181/$ – see front matter © 2011 Elsevier B.V. All rights reserved.
doi:10.1016/j.gloplacha.2011.01.007

Also the use of different time-period and processing techniques are partly responsible for the differences found between different studies. For instance, Leuliette and Miller (2009) showed that results were sensitive on how the Argo data are mapped in the early part of the record. This is further exemplified by the fact that, even over the same time-period, Leuliette and Miller (2009) and Cazenave et al. (2009) Argo results differed by 0.5 mm/year.

In this paper we address the quantification of the contributions driving sea level variability regionally rather than globally. When coastal protection and impact assessment are concerned, regional sea level rates of change are of key importance to understand and project how sea level changes will affect a particular area. Given the high spatial heterogeneity of sea level variability the global rates become meaningless in this context. The closure of the regional sea level budget has been explored by fewer authors. Llovel et al. (2010) found a poor agreement between the regional patterns of steric-corrected altimetry and those of the mass contribution inferred from GRACE. Conversely, in the Mediterranean Sea observations of total sea level and its components are reported to be consistent (Fenoglio-Marc et al., 2006; Calafat et al., 2010). In a further step, Calafat et al. (2010) took advantage of this good agreement to infer the mass contribution to Mediterranean mean sea level for the second half of the 20th century, using a reduced-space optimal interpolation of altimetry and tide gauge data to infer total sea level fields for the pre-altimetric period.

In this work we extend the methodology applied in the Mediterranean Sea by Calafat et al. (2010) to different regions worldwide. The independent measures of the mass contribution to sea level provided by GRACE since 2002 are combined with estimates of steric sea level and observed total sea level to explore the regional sea level budgets. The goal of this study is to investigate to which extent regionally averaged mass variations are mimicked by steric-corrected altimetry in different areas and at different temporal scales. Additionally, in order to infer the mass contribution during the last decades of the 20th century we use a global reconstruction of sea level fields together with historical hydrographic observations. Given the assumptions inherent to this methodology a careful uncertainty assessment is carried out.

2. Data sets

2.1. Sea level

Gridded monthly sea level anomalies with a map spacing of $1^\circ \times 1^\circ$ computed from satellite multimission with respect to a seven year mean were obtained from the AVISO data server (http://www.aviso.oceanobs.com). This data set spans the period from October 1992 to present. All geophysical corrections have been applied; the atmospheric correction is applied using the Dynamic Atmospheric Correction currently delivered by AVISO, which consists of using the barotropic model MOG2D (Carrère and Lyard, 2003) to correct frequencies greater than 20 days and the inverted barometer approach otherwise.

The sea level anomaly fields obtained from altimetry data have also been combined with tide gauge records (from which the atmospheric signal has been previously removed) to obtain reconstructed global sea level fields for the period 1950–2003. This field was computed by combining selected 99 tide gauge records (from Llovel et al., 2009) and 11 years of altimetry observations over 1993–2003. The method is based on the reduced space optimal interpolation described by Kaplan et al. (1998, 2000). It uses the spatial structure (EOFs) of the sea level field obtained from the 2-D well resolved spatial fields of altimetry satellite measurement to interpolate the historical measurements from tide gauge records. Following Church et al. (2004), in this run we added a spatially uniform EOF (referred to as EOF0) to the set of EOFs computed from altimetry; the inclusion of this extra EOF is aimed to account for any basin-uniform movement. The global reconstructed sea level fields are mapped on a $(1^\circ \times 1^\circ)$ over the period 1950–2003.

2.2. Steric sea level

Steric sea level fields were computed using two data sets: the Ishii global gridded temperature (T) and salinity (S) climatology (Ishii and Kimoto, 2009) and the ENACT/ENSEMBLES version 2a (EN3) data set (Ingleby and Huddleston, 2007) made available by the Met Office Hadley Centre. The Ishii data set has been produced by objective analysis of in-situ observations and consists of monthly gridded T, S fields with a spacing of $1^\circ \times 1^\circ$; the vertical domain extends down to 700 m, with data on 16 levels. This data base covers the whole second half of the 20th century, namely the period 1945–2006. The steric sea level component has been computed at each grid point by integrating the specific volume down to 700 m. The Ishii climatology includes an estimation of the uncertainties associated with the interpolated T and S gridded fields, which can be propagated to obtain the uncertainty of the steric component.

The EN3 data set has been produced by objective analysis of the T and S profiles of the World Ocean Database'05, the Global Temperature and Salinity Profile Project, Argo and the Arctic Synoptic Basin-Wide Oceanography Project. In the current version (v2a) the Argo profiles with erroneous pressure values according to Willis et al. (2009) and profiles that are suspect of containing errors according to Guinehut et al. (2009) have been rejected. The part of the database used in this work consists on monthly gridded T, S fields with a map spacing of $1^\circ \times 1^\circ$; the vertical domain extends down to 970 m, with data on 24 levels. The time period spanned by this data base is 2002–2008, i.e., it extends to years further than Ishii, which is important when considering the short period spanned by GRACE data.

The computation of the steric component is thus restricted to the upper part of the ocean: 700 m in the case of the Ishii data set and the top 970 m for EN3. The reason why the data bases do not include deeper fields is that below those depths the number of observations decreases significantly, making the interpolation unreliable (Leuliette and Miller, 2009; Dhomps et al., 2010). Dhomps et al. (2010) reported that integrating steric sea level down to 1000 m recovers at least 80% of the total signal worldwide.

2.3. GRACE measurements

Finally the mass contribution has been obtained from measurements provided by the GRACE mission launched in 2002. GRACE measures the variations in the gravity field caused by changes in the water mass of the Earth, then providing an independent measure of the mass contribution to sea level changes. The Level-2 Release-04 (RL04) gravity coefficients computed at the Center for Space Research (CSR) were used to estimate monthly global water mass variations for the period August 2002 to the end of 2008 with a spatial grid of $1^\circ \times 1^\circ$. The data include corrections to specific spherical harmonic coefficients due to solid Earth and ocean tidal contributions to the geopotential. GRACE pre-processing also removes variability from an ocean barotropic model (i.e., the high-frequency ocean mass variations forced by winds and pressure) along with the atmospheric mass. The solid and ocean pole tide are also removed. RL04 coefficients are supplied to degree and order 60. Correlated errors between even or odd Stokes coefficients (C_{lm},S_{lm}) are removed by means of a 5th order polynomial fit (Chambers, 2006). Degree 2, order 0 coefficients from GRACE are replaced with those from the analysis of Satellite Laser Ranging (SLR) data (Cheng and Tapley, 2004). We also restore modeled rates for certain coefficients (degrees 2, 3, and 4 for order 0, and degree 2 for order 1) as discussed in the Processing Standards Documents (Bettadpur, 2007). The last step for obtaining the Stokes coefficients is done by adding back the mean monthly

gravity coefficients of the ocean bottom pressure supplied by the project which were removed in the preprocessing (Flechtner, 2007) and an estimate of degree 1 gravity coefficients (Swenson et al., 2008).

In order to compensate for poorly known short-wavelength spherical harmonic coefficients, gravity coefficients are converted into smoothed maps of surface mass density by means of a Gaussian spatial average (Wahr et al., 1998). Surface mass density is converted to equivalent surface height by dividing it by the density of fresh water. The radius of the Gaussian smoothing function used in this study is 500 km. Because the smoothing is done on global spherical harmonics, any large hydrological signal over land will leak into the ocean signal near the coast. The Climate Prediction Center (CPC) hydrological model has been used to correct the effect of land waters (Fan and van den Dool, 2004). In order to be consistent with GRACE, we have smoothed the hydrology field by using the same spatial averaging applied to GRACE data.

A correction for the Glacial Isostatic Adjustment (GIA) has also been applied. In this work we use the GIA correction field computed by Paulson et al. (2007) and expressed in terms of a mass rate. It is the only solution which is currently publicly available and it has been obtained from http://grace.jpl.nasa.gov/data/pgr. Again, the mass rate estimates were smoothed using a Gaussian averaging function of 500 km radius in order to be consistent with GRACE data.

3. Regional sea level variability during 2002–2008

Sea level anomalies from altimetry and the steric and mass contributions have been compared for the period 2004–2008. Such period has been chosen to ensure that the number of S observations is large enough to compute steric sea level reliably. The Ishii data set is thus restricted to the short period 2004–2006. Despite this limitation it is included in the analysis because it provides an estimation of the uncertainties that will be used later on in the paper. For the purpose of comparison all fields have been filtered using a Gaussian filter of radius 500 km. The steric contribution has been estimated using the two available data sets, referred to simply as Ishii (2004–2006) and EN3 (2004–2008) hereinafter.

3.1. The seasonal cycle

The dominant signal in the time series is the seasonal cycle caused by the warming/cooling of the ocean and the exchange of waters between land and oceans between seasons. Since the sea level seasonal cycle is unsteady in time (Marcos and Tsimplis, 2007) the same period (from 2004 to 2008) has been chosen in all cases for the consistency of comparisons.

The annual cycle of the mass component has been obtained on one hand from GRACE observations and on the other hand from steric-corrected altimetry (Fig. 1), ranging between 0 and 6 cm in both cases (color scales are however defined from 0 to 4 cm for a better visualization of spatial structures). On average the annual cycle represents 25% of the monthly mass signal, reaching values of up to 50% only in the southern ocean, where amplitudes reach 5 cm. According to GRACE observations, maxima values are found around Greenland and in the northernmost Pacific coasts; none of these areas are monitored by the altimetry data used, therefore preventing the comparison with non-steric sea level. Leakage from land hydrology is expected to be very large in this areas and it may generate such signal. For the same reason, larger than average values are also found close to Antarctica, especially around the Antarctic Peninsula. An annual signal larger than average is also obtained in the western equatorial regions of the North Atlantic, likely related to the seasonal variations of large river runoff. Large differences are found between GRACE observations and steric-corrected altimetry at equatorial regions. We suspect this is

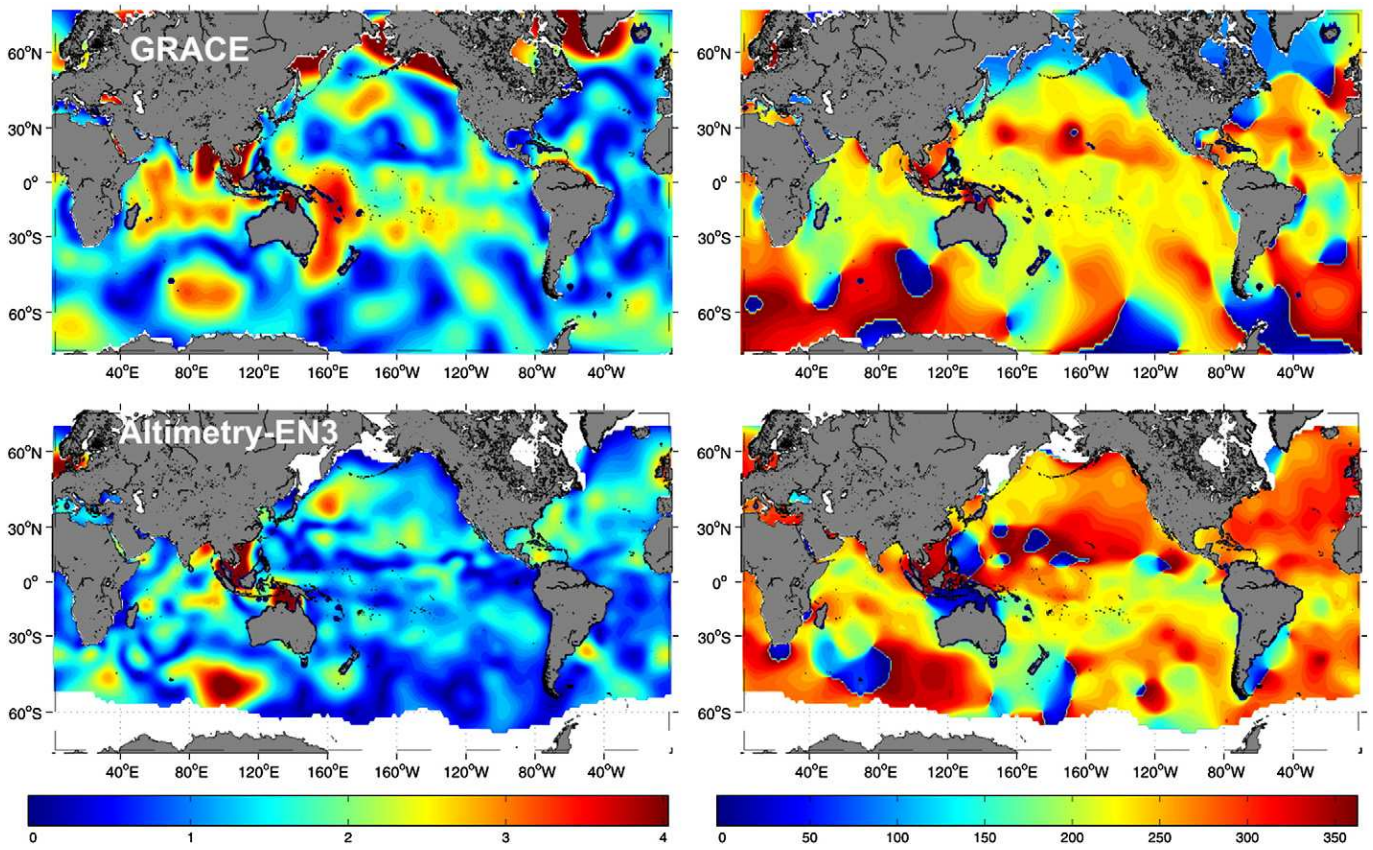

Fig. 1. Mean annual amplitudes (left column) and phases (right column) of the mass component of sea level as observed by GRACE and as inferred from altimetry minus steric sea level. Values are in cm and degrees respectively.

related to different spatial resolution of the data and to the relatively low signal-to-noise ratio of GRACE in the tropics (e.g., Wahr et al., 2004).

3.2. Regional sea level budgets

Regional sea level budgets are explored for seven regions, namely the North, Equatorial and South Pacific and Atlantic Oceans and the Indian Ocean. The mass contributions to sea level changes averaged over each region as observed by GRACE and as inferred from steric-corrected altimetry using Ishii and EN3 climatologies are shown in Fig. 2. The correlation between observed and computed mass for their common periods is quoted for each graph. Time series are dominated by seasonal variations. Correlations are significant almost everywhere with values ranging between 0.4 and 0.8. The exceptions are the north and equatorial Atlantic regions, where correlations are not statistically significant for the longer period 2004–2008. This could be partly attributed to the computation of steric sea level using interpolated data that are biased in such regions with high variability due to the Gulf Stream (Miller and Douglas, 2004). On the other hand in these regions there is a smaller number of valid S profiles which suggests a less reliable steric estimation.

Overall it is fair to say that the two steric sea level data sets are consistent to each other and provide similar correlations between steric-corrected altimetry and mass changes from GRACE.

A large part of the high correlation values is likely due to the dominance of the seasonal cycle, with a major portion of the seasonal cycle controlled by global ocean mass variations, of ± 1 cm. In order to explore the inter-annual consistency of sea level budgets, the mean seasonal cycle is removed from each time series. Results are shown in Fig. 3 (only the steric-corrected altimetry using EN3 is shown for simplicity). De-seasoned time series of mass observations and steric-corrected altimetry have similar variability. Variances are larger for steric-corrected altimetry than for GRACE data only in the south Atlantic (2.1 and 1.2 cm^2 respectively) and in the Indian Ocean (0.9 and 0.5 cm^2 respectively). They are nearly the same everywhere else, ranging between 0.3 and 0.9 cm^2 depending on the region. The RMS of the signals and the RMS of their difference is generally of the same magnitude. The reason is the presence of some large peaks in one of the signals and not in the other.

As expected, correlations have decreased in all the regions when not considering the seasonal cycle (Fig. 3). They become not significant in the equatorial regions and in the North Atlantic. Smoothed time series obtained with a 6-month running average are also plotted in Fig. 3. Linear trends from deseasoned time series are

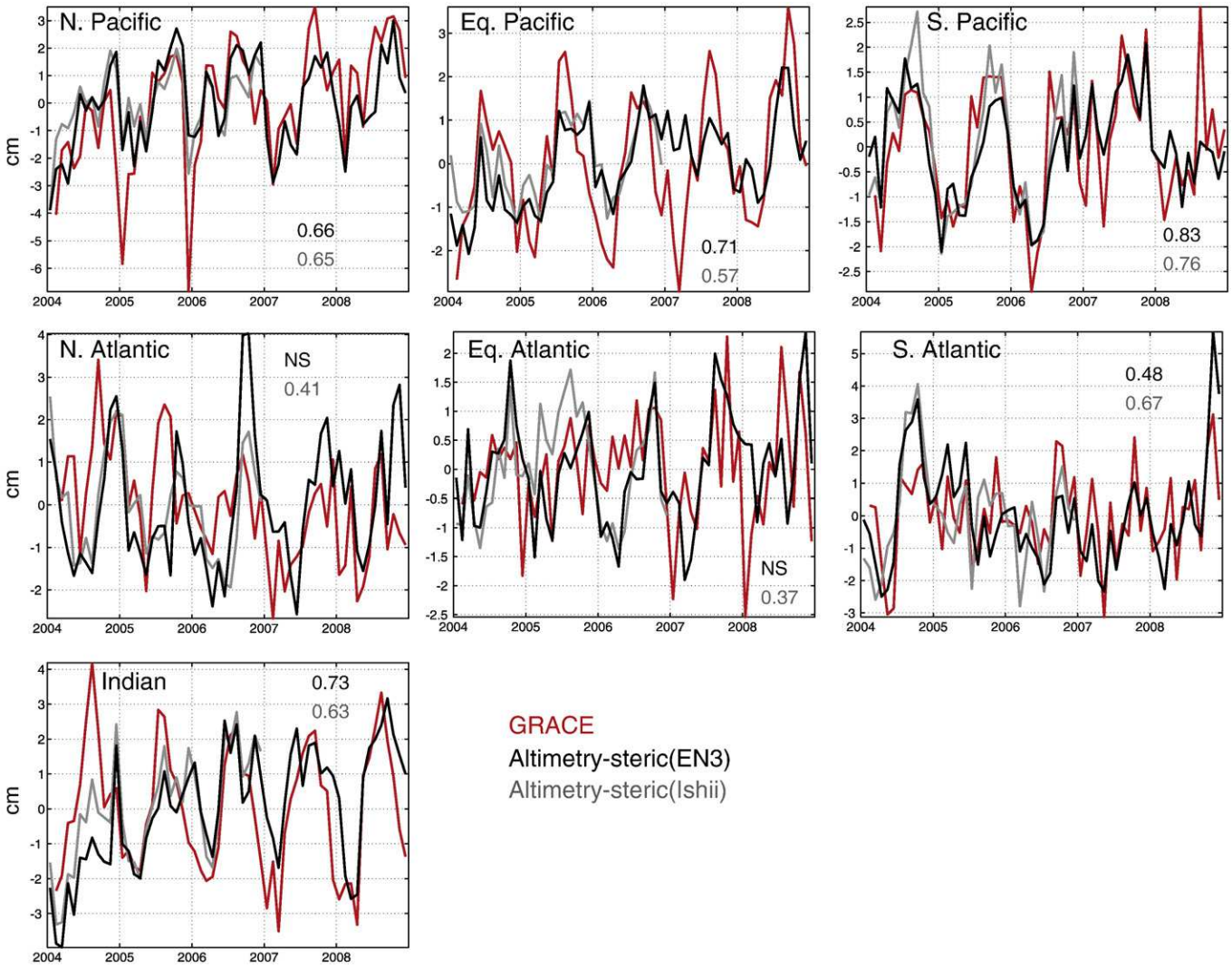

Fig. 2. Comparison between the measured (from GRACE) and inferred (altimetry minus steric component) mass contribution to sea level for different regions. North regions are defined between latitudes 30°N–50°N, equatorial between 20°S–20°N, and south 60°S–30°S. The correlation between both curves is quoted in the right low corner of each graph when significant at the 99% confidence level (NS otherwise).

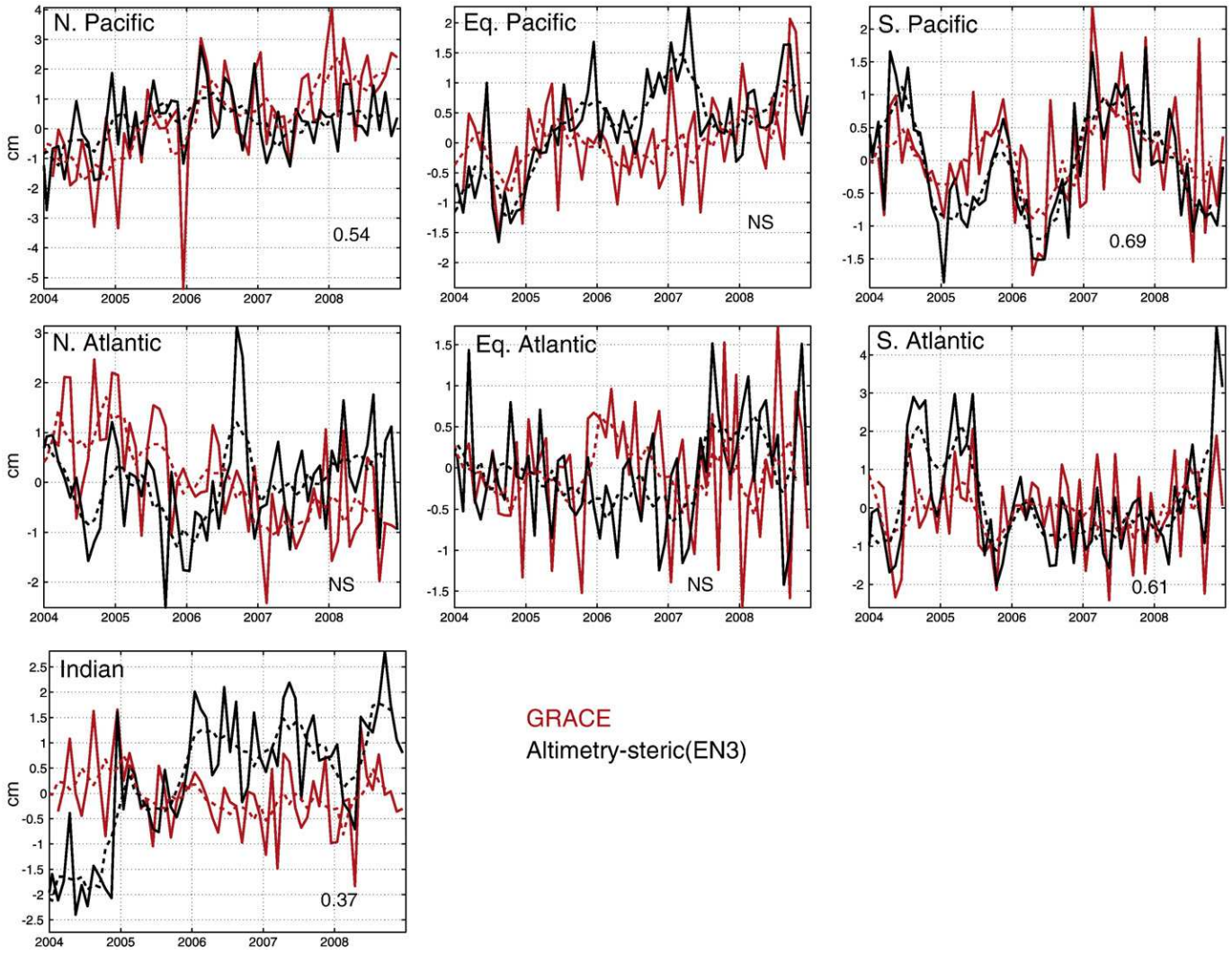

Fig. 3. Steric-corrected altimetry obtained using the EN3 data base (black lines) and mass contribution from GRACE (red lines) de-seasoned (solid) and filtered with a 6-months running mean (dashed). Correlation coefficients are quoted for each region.

quoted in Table 1 together with uncertainties as given by standard errors.

In the North Pacific region, inter-annual changes of steric-corrected altimetry and GRACE observations are fairly correlated (0.54) and both show positive linear trends. GRACE time series present a relative minimum in 2006, in agreement with the results of Chambers and Willis (2008) for a similar but smaller region of the North Pacific. These authors found a trend of about 9 mm/yr for a different period (2003–mid 2007). In our case the GRACE trend for 2004–2008 is 6.7 ± 1.1 mm/yr. Song and Zlotnicki (2008) suggested that ocean bottom pressure below the sub-polar gyre of the North Pacific correlates with tropical ENSO episodes, resulting in below average ocean bottom pressure shortly after an event and above average shortly before. Fig. 4a represents smoothed and detrended GRACE observations averaged over the North Pacific altogether with the multivariate ENSO index (Wolter and Timlin, 1998). Two strong ENSO events took place during the GRACE period, one in early 2003 and one in 2007 (see Fig. 4). Despite there is not statistically significant correlation between the two curves, GRACE observations are qualitatively consistent with Song and Zlotnicki (2008) hypothesis for these both events. This was already partly confirmed by Chambers and Willis (2008), but only until mid-2007. The longer GRACE time series used here permits confirming the predicted drop in ocean bottom pressure during 2007, though this does not discard the possibility that such changes can be due to inter-annual variations not related to ENSO episodes.

Table 1
Trends of the regionally-averaged mass contribution to sea level estimated from GRACE and from steric-corrected altimetry (using the EN3 climatology) for the period 2004–2008. Units are in mm/yr.

Region	GRACE	Steric-corrected altimetry
N. Pacific	6.71 ± 1.11	1.72 ± 0.95
Eq. Pacific	1.60 ± 0.66	3.36 ± 0.62
S. Pacific	0.20 ± 0.80	-0.18 ± 0.83
N. Atlantic	-4.91 ± 0.86	0.93 ± 0.87
Eq. Atlantic	0.09 ± 0.71	1.06 ± 0.58
S. Atlantic	0.54 ± 1.11	-1.29 ± 1.26
Indian	-0.80 ± 0.64	6.06 ± 0.95

In the southern Pacific the correlation between observed and inferred mass variations at inter-annual scales reaches 0.7. No significant trends are found in any of the time series (Table 1). Additionally, Fig. 4b evidences the relationship between mass changes in the southern Pacific basin and the ENSO variability, with a correlation of -0.5 at a 6-months lag.

In the Indian Ocean GRACE observations and steric-corrected altimetry show a significant correlation of 0.4. However, large differences are found in their trends (Table 1). While GRACE observes

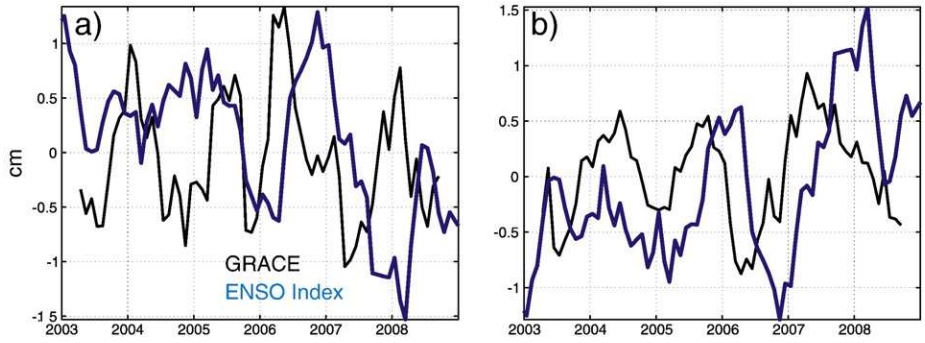

Fig. 4. Detrended and smoothed GRACE observations averaged over the North and South Pacific (black, in cm) and ENSO index (blue).

a trend only slightly different from zero, the value obtained from steric-corrected altimetry is much larger (6.1 ± 1.0 mm/yr). Such discrepancy was already pointed out by Willis et al. (2008). They noted that the large trend observed in altimetry was not visible in steric data, thus pointing at a mass exchange as being the main cause. However, this is not confirmed by GRACE observations. Recent investigations point at new pressure biases in the instruments deployed in the Indian Ocean as the origin of the difference (D. Chambers, personal communication).

Mass exchanges between Atlantic and Pacific regions are plotted in Fig. 5 in order to explore the sub-basin inter-annual variability. Only GRACE time series are used to avoid the unrealistic steric sea level estimates in the north Atlantic region. Chambers and Willis (2008) already demonstrated that inter-annual mass exchanges as large as seasonal variations exist between the Atlantic and Indian basins with the Pacific. Also Stepanov and Hughes (2006) identified mass exchanges between the Southern Ocean and the Pacific (northward 35°S). We therefore focus here in sub-basin exchanges between northern and southern latitudes. Fig. 5 reveals mass exchanges between the target regions. Interestingly, two different regimes of inter-annual barotropic oscillations can be identified. For the period

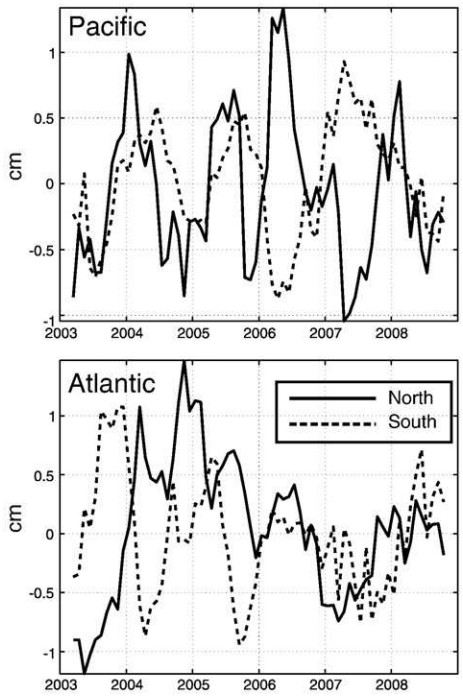

Fig. 5. Detrended and smoothed (with a 6-months running mean) averaged GRACE observations over the northern and southern sub-basins of the Pacific (top) and Atlantic (bottom) Oceans.

2003–2006 the Pacific Ocean oscillates in phase while the north and south Atlantic oscillate out of phase. From 2006 onwards the behavior is the opposite with the Pacific showing clear out of phase signals and the Atlantic oscillating coherently. Whether this shift is an exceptional event or not can only be determined with a longer time series not yet available. The reasons thus remain uncertain and clearly further research is needed to determine its origin.

3.3. Consistency of inter-annual variations

Changes in steric-corrected altimetry and mass variations from GRACE at inter-annual scales are compared on the basis of regional EOFs. The reason why regional analysis has been preferred to global analysis is to account for basin scale mass changes and regional processes without being masked by large scale ocean variations. De-seasoned fields of altimetry and steric sea level from EN3 as well as mass variations from GRACE are used. All fields are filtered using a Gaussian filter of radius 500 km to be consistent with each other. EOFs have been computed for the same seven regions defined above. However, only results for the most interesting areas, namely north and south Pacific and Atlantic Oceans and for the Indian Ocean, are shown (Figs. 6 to 10).

The two leading EOFs of the North Pacific region are shown in Fig. 6. The first EOF explains significantly more variance in the GRACE decomposition (53%) than in the steric-corrected altimetry decomposition (30%), but the patterns are similar. Positive values dominate in the entire domain, being larger in the western area, coinciding with the region where Chambers and Willis (2008) found larger trends. The large trend found in GRACE data is entirely explained by the first EOF (8.4 ± 2.0 mm/yr) and is thus associated to the corresponding spatial pattern. In the second EOF a dipole structure is observed in steric-corrected altimetry, whereas GRACE field presents a track-like pattern and does not represent a physical signal.

In the south Pacific (Fig. 7) the first EOFs explain the same variances in steric-corrected altimetry than in GRACE (30%). A SE–NW gradient is found in the spatial patterns in both cases, although steric-corrected altimetry has larger values in the NW. The linear trends of the temporal amplitudes are large (6 and 11 mm/yr, respectively), despite the trend of the total series is not different from zero. The second EOF also shows similar patterns in the two fields and, in this case, also similar temporal amplitudes. Spatial patterns of mass variations reflect the signature of the El Niño, the dominant climatic mode in the area. Correlations of the first and second amplitudes of GRACE data present statistically significant correlations with ENSO index of 0.6.

The north Atlantic decomposition shows clear discrepancies between steric-corrected altimetry and GRACE spatial EOFs (Fig. 8). The main signal of the steric-corrected altimetry leading EOFs is associated with the Gulf Stream variability. This happens because the use of interpolated gridded data for estimating steric sea level biases

the values with respect to using single T and S profiles (Miller and Douglas, 2004). Therefore the mass contribution in the North Atlantic as inferred from steric-corrected altimetry is not reliable. The temporal amplitude of the first EOF computed from GRACE observations is significantly correlated (0.50) with the East Atlantic pattern (Barnston and Livezey, 1987). This climate pattern is a dominant mode in the North Atlantic consisting in a NE–SW dipole similar to NAO. The pattern of the first EOF presents the same structure. Notably, the first mode is not correlated with the NAO index. We attribute it to the fact that NAO acts over northernmost latitudes.

In the south Atlantic the spatial patterns and the variances explained of the two leading EOFs are consistent between steric-corrected altimetry and GRACE (Fig. 9). The signals found were first identified by Fu et al. (2001) as a free barotropic mode with a length of about 1000 km and a period of 25 days and with strong seasonal and inter-annual variability, on the basis of altimetric measurements and theoretical considerations. Hughes et al. (2007) reported a mode with lower period (20 days) and suggested that its variability is due to interaction between eddies, mean flow and topography rather than to direct atmospheric forcing through pressure and wind. Weijer et al. (2007) found that the flow variability in the Argentine Basin is caused by the excitation of several barotropic normal modes of this basin. The presence of multiple oscillatory basin modes would reconcile the previous frequencies. Interestingly, the first EOF of steric-corrected altimetry clearly reproduces the dipole pattern found by Fu et al. (2001) and later on confirmed by Weijer et al. (2007).

In the Indian Ocean the largest feature of the GRACE decomposition is found in the north-eastern part of the domain and is related to the gravity variations generated by the Sumatra earthquake in 2004 (Fig. 10) (Han et al., 2010); it is thus not reproduced by the steric-corrected altimetry. The spatial patterns of the first EOF, accounting for nearly the same amount of variance for the two data sets, present in both cases larger values in the eastern part of the domain. However, structures in steric-corrected altimetry are smaller and do not appear in GRACE. The second EOF of the GRACE decomposition shows marked track-like structures.

In summary, at inter-annual scales the steric-corrected altimetry is consistent with observations of mass changes in the north and south Pacific and in the south Atlantic. Results are not conclusive for equatorial areas and are clearly non-consistent in the north Atlantic, especially near the Gulf Stream. In the Indian Ocean, despite averaged time series are significantly correlated (Fig. 3) and the amplitudes of the leading EOF present the same variability (Fig. 10), the spatial patterns are clearly different. Therefore we have considered the two fields as non-consistent in this region.

4. Regional sea level changes during 1950–2003 and mass contribution

In those regions where steric-corrected altimetry and GRACE data are consistent at interannual time scales, the mass contribution to sea level changes during the second half of the 20th century may in principle be estimated by subtracting the steric contribution from total sea level. For past decades (1950–2003), total sea level is available through the reconstruction described in Section 2.1 (Llovel et al., 2009), which approaches altimetry from 1993 onwards. The reliability of the reconstructed fields is limited by the steadiness of the spatial patterns obtained during the altimetric period and by the uneven distribution of tide gauge stations. However, previous studies have demonstrated the ability of such methodology to capture the regional sea level variability both globally (Church et al., 2004; Llovel et al., 2009) and regionally (Calafat and Gomis, 2009; Calafat et al., 2010).

Steric sea level is obtained integrating the Ishii T and S climatologies down to 700 m depth for the period 1945–2006. The uncertainty in the steric component can be estimated from the uncertainties associated with the monthly T and S fields. In a first step, the error associated with the specific volume is computed by

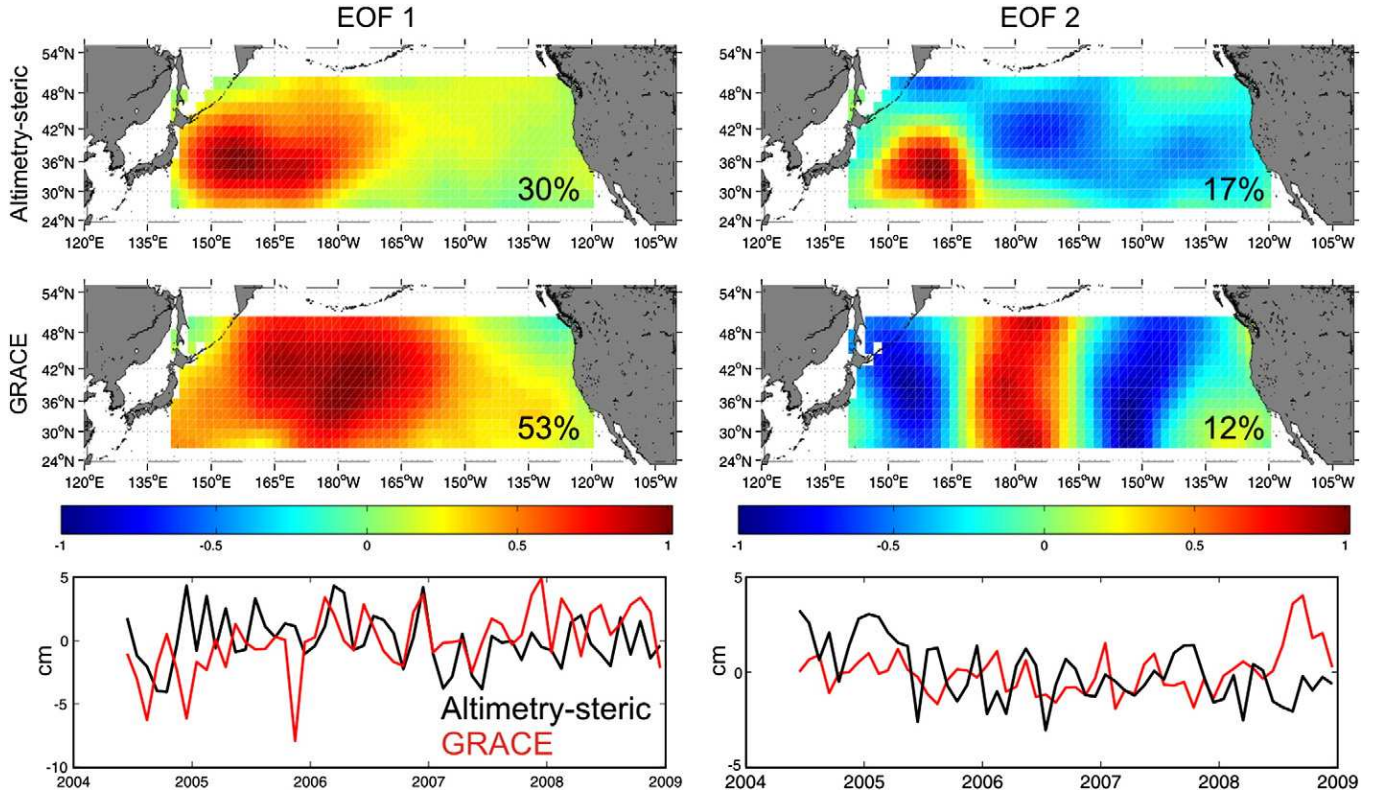

Fig. 6. First and second normalized EOFs of the northern Pacific decomposition for steric-corrected altimetry (top) and GRACE observations (middle). The corresponding amplitudes are shown in the bottom graphs.

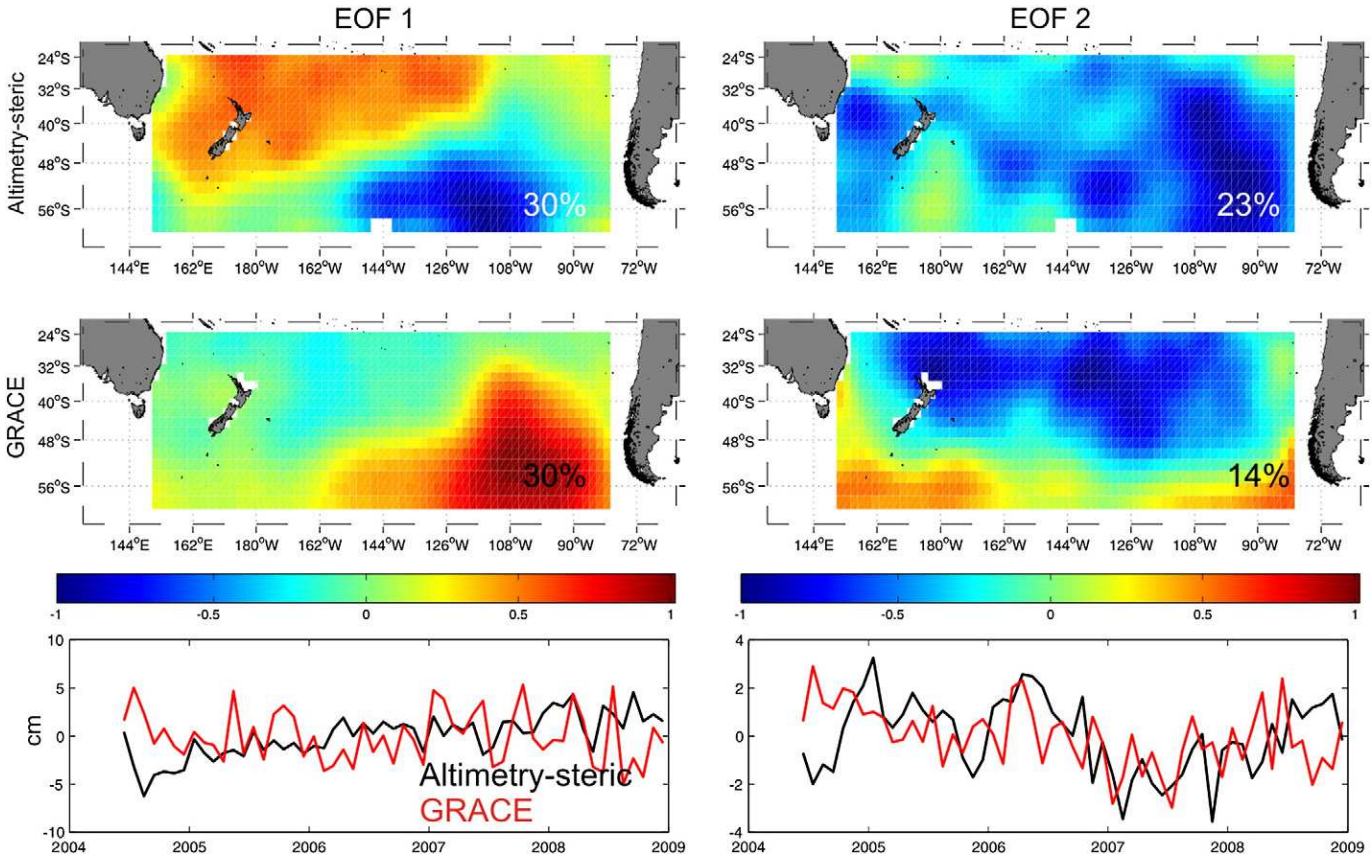

Fig. 7. As in Fig. 7, but for the southern Pacific region.

propagating the errors in T and S. To compute the error in the steric sea level we assume the worst scenario: that the error of the specific volume is vertically correlated and, therefore, the effect of the vertical integration is an error accumulation, rather than an error cancelation. The result will therefore be an upper boundary for the steric error. In a second step we estimate the error associated with the spatial mean steric sea level for each region, assuming in this case that errors are spatially uncorrelated; this is surely not true for small scales (adjacent grid points suffer from similar errors), but there is no reason to believe that errors are correlated at regional scale. More details on the methodology can be found in Calafat et al. (2010). Results yield typical error values between ± 0.7 and ± 1.6 cm for yearly regional averages, being larger at the beginning of the period, when observations are scarcer.

This methodology has of course some limitations. Firstly, those areas where it has been demonstrated that steric sea level estimated from interpolated data is not a good approximation must be discarded. This is the case of the North Atlantic and the Indian Ocean. Also the coverage and quality of measurements of the thermohaline properties of the ocean diminishes backwards in time. In particular, the interpolation of the scarce salinity measurements cannot be considered very reliable and thus only thermosteric changes can be accounted for. This in turn introduces further uncertainties in the steric estimation, but they are considered to have a small impact, since T changes dominate steric sea level variability everywhere except in the north Atlantic (Antonov et al., 2002). A further limitation comes from the fact that thermosteric sea level is integrated down to 700 m, which implies that the contribution of deeper layers to thermal expansion is neglected. Finally, the interpolation method for T data also introduces uncertainties, though they are provided for the Ishii climatology.

In order to account, as accurately as possible for these limitations, we have carried out a careful determination of linear trends and their associated uncertainties: linear trends are computed using an MM-regression estimator (Yohai, 1987), which is robust against outliers and allows including time-varying random errors. These random errors are in our case the uncertainties related to interpolation errors explained above. For more details see Appendix A.

If the errors associated with the variables have constant variance and there are no outliers in the data, then ordinary least squares (OLS) and robust estimators will lead to similar estimates for both the coefficients and the standard errors. However in the presence of errors having non-constant variance (heteroskedasticity), OLS will underestimate standard errors. Moreover if data also suffer from outliers, the coefficient estimates can be seriously biased. A robust standard error consistently estimates the true standard error even for data that suffer from heteroskedasticity and outliers. In order to illustrate this we have computed the thermosteric sea level trend for the North Pacific for the period 1945–2006 by means of both an OLS and an MM-regression estimator. For the OLS we have obtained a trend of -0.09 ± 0.04 mm/yr. In the case of the MM-estimator we have taken into account the uncertainties associated with the thermosteric sea level (which we know are larger at the beginning of the period, i.e., they suffer from heteroskedasticity). The thermosteric sea level trend obtained from the MM-estimator is -0.20 ± 0.05 mm/yr.

Regional sea level trends and their uncertainties for all regions except the north Atlantic and the Indian Ocean are listed in Table 2. Regional trends of total sea level vary between 1.5 and 1.7 mm/yr according to the sea level reconstruction. Values for thermosteric sea level are much smaller everywhere, ranging between 0.03 and 0.58 mm/yr. The remaining observed sea level rise is attributed to two factors: the thermal expansion of the deeper layers and the changes in ocean bottom pressure caused by mass variations. Regarding the contribution of the deep layers, Guinehut et al. (2006) used Argo data and sea level anomalies from altimetry to

conclude that the differences between both data sets when steric sea level is computed with respect to a reference level at 700 m and at 1500 m is less than 10%.

It turns out, therefore, that the contribution of water mass changes dominates sea level changes in all regions. Our approach yields trends varying between 1.05 ± 0.07 mm/yr in the equatorial Atlantic and 1.57 ± 0.07 mm/yr in the north Pacific (Table 2). These values represent between 65% and 96% of the total observed regional sea level rise.

5. Discussion and final remarks

Comparisons among sea level from altimetry, steric sea level estimated from hydrographic data bases and ocean mass changes observed by GRACE have shown that the annual cycle of the ocean mass is in general well approximated by steric-corrected altimetry. Regionally averaged seasonal cycles are highly unsteady in time and represent only a small fraction of the total seasonality observed in sea level, in agreement with Llovel et al. (2010). At inter-annual scales the correlation between inferred and measured regional mass variations is smaller. We have also found that regional ocean mass variability is significantly larger than global changes, similarly to what happens with total and steric sea level. Besides the fact that steric-corrected altimetry has better resolution than GRACE observations, two other reasons have been identified for the weaker consistency between the two fields at inter-annual scales. The first one is related with the GRACE processing errors. The low signal-to-noise ratio of GRACE data prevents from making satisfactory comparisons with steric-corrected altimetry, in agreement with Llovel et al. (2010). This problem is at least partially overcome when working with regionally averaged sea level. We have found significant correlations in the north and south Pacific, in the south Atlantic and in the Indian Ocean. Conversely, results are not satisfactory in equatorial regions and in the north Atlantic. The second reason for the lack of consistency is the inability of interpolated T and S data to account for steric sea level in areas with large variability such as the Gulf Stream region.

The comparison of mass variations among different regions has revealed the exchange of ocean mass between northern and southern latitudes in the Atlantic and Pacific Oceans at inter-annual time scales. Furthermore such exchanges occur out of phase between the two oceans, although the short length of the GRACE time series prevents from drawing definitive conclusions with respect to the underlying mechanisms that drive this variability.

The consistency between regional steric-corrected altimetry and GRACE observations has been examined through the EOFs analysis and has revealed similar patterns of oscillation in the North and South Pacific and in the South Atlantic. In the latter moreover the barotropic mode of the Argentine basin is the main pattern in both data sets. The second EOF of GRACE data often reflects track-like patterns.

Linear trends of the mass contribution to sea level computed by GRACE data are highly dependent on the GIA correction applied. Further work is clearly needed to reconcile the currently available GIA

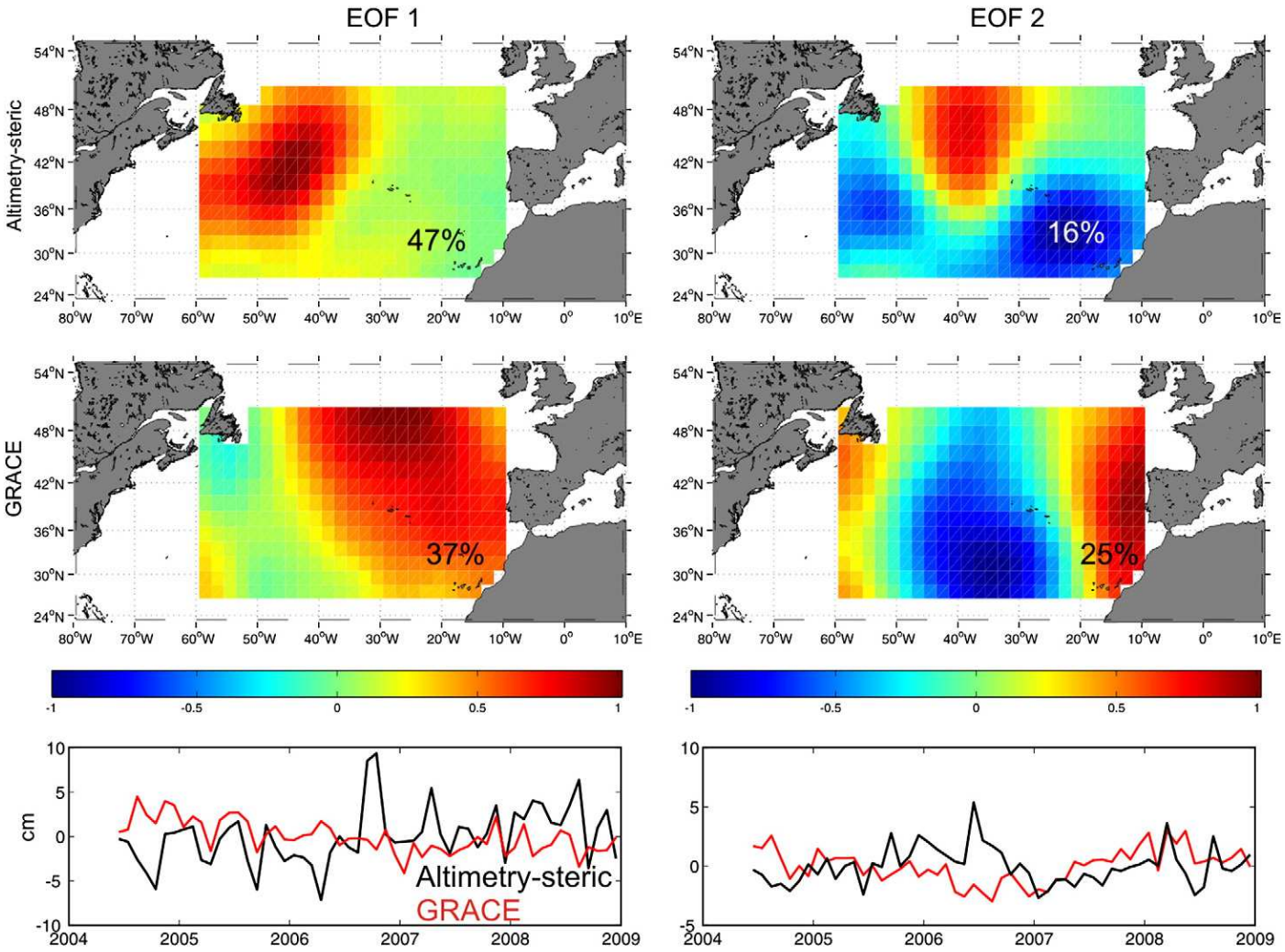

Fig. 8. As in Fig. 7, but for the North Atlantic region.

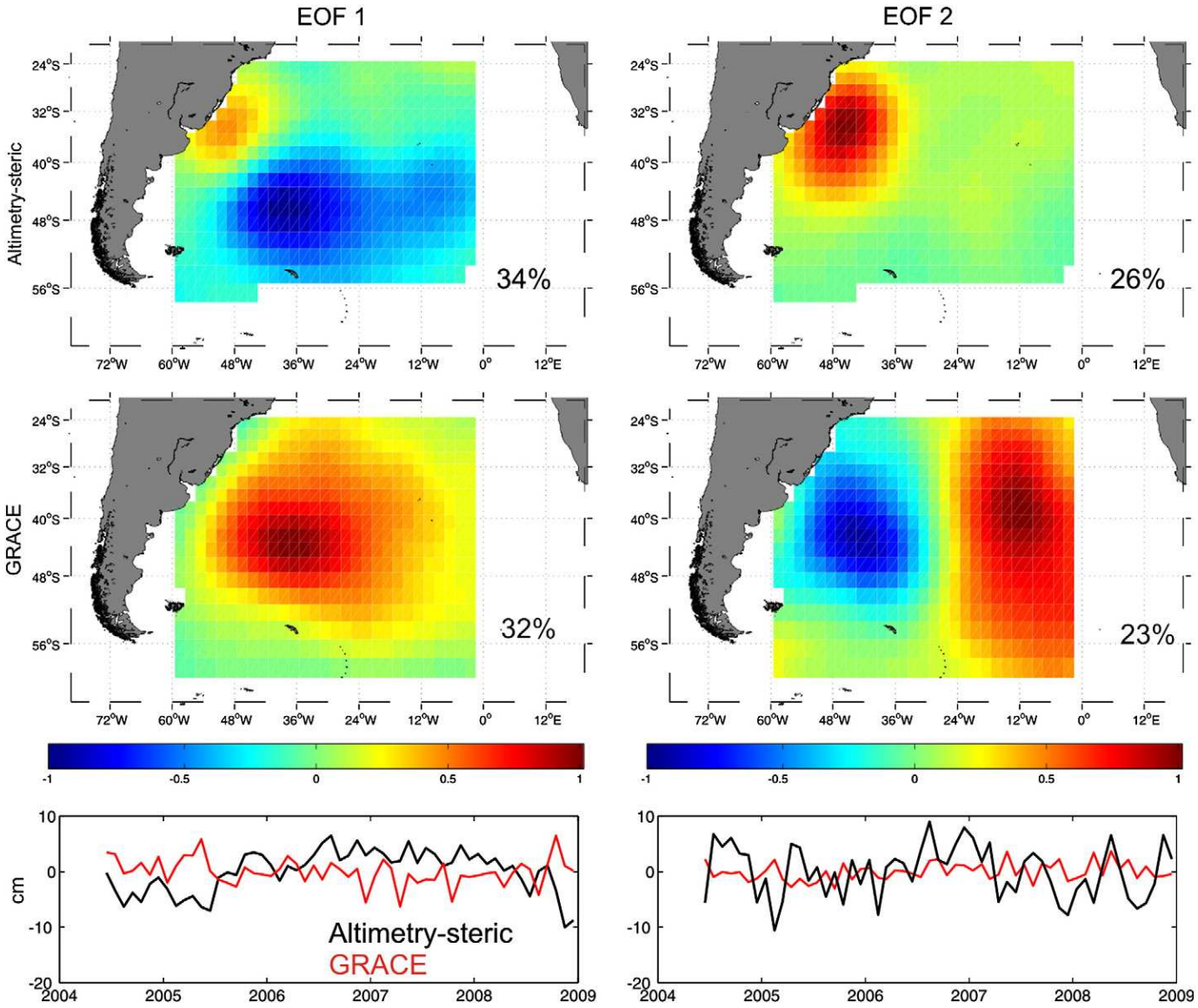

Fig. 9. As in Fig. 7, but for the South Atlantic region.

corrections provided by Paulson et al. (2007) and Peltier (2009). Regional sea level budgets cannot be closed using any of the two corrections, but the agreement is higher in most regions when using the correction chosen for this work (the one by Paulson et al., 2007).

Regarding longer term trends, comparisons of the thermal expansion of the top 700 m against total sea level rise for last decades indicates that the former is a minor contributor to the latter in all regions worldwide. Assuming that the thermal expansion of the layers deeper than 700 m is much smaller than that of the top layers, we conclude that the mass addition is the main contributor to regional mean sea level rise during the second half of the 20th century. This applies to all the regions examined, indicating that the origin of the observed mass increases is not a redistribution of ocean mass between regions, but a net global increase resulting from fresh water addition due to melting of glaciers and ice-sheets.

Our result is in agreement with Miller and Douglas (2004), who pointed at mass increase as the dominant factor in global mean sea level rise during the past century based on tide gauge observations and hydrography. Conversely, this result contrasts with the global average obtained by Domingues et al. (2008), who estimated a contribution of about 0.8 mm/yr of mass addition of a total sea level rise of 1.6 ± 0.2 mm/yr for the period 1961–2003. Their estimate of the thermosteric contribution of the upper 700 m is 0.52 ± 0.08 mm/yr, which is about 50% larger than the 0.31 ± 0.07 mm/yr given by Ishii et al. (2006) and the 0.33 mm/yr given by Antonov et al. (2005) for the period 1955–2003, also for the upper 700 m. Part of the disagreement may be caused by the fact that Domingues et al. (2008) assumed a linear increase in the rate of change of the contribution of Greenland and Antarctic ice sheets, despite the very little information available to constraint these values. Moreover, they used a deep-ocean thermosteric contribution of 0.2 mm/yr, that is, 40% of their estimate for the thermosteric contribution of the upper 700 m; this is in contradiction with the results obtained by Guinehut et al. (2006), who concluded that the contribution of the layers deeper than 700 m is much less important. If only the upper-ocean thermosteric contribution is taken into account, then the mass contribution is of the order of 1.1 mm/yr when using the estimate given by Domingues et al. (2008) and about 1.3 mm/yr when using the estimates given by Ishii et al. (2006) and Antonov et al. (2005). These estimates are in better agreement with our results.

When quantifying the mass contribution to long term regional sea level rise in terms of non-steric sea level, the computation of the regional steric component is a significant source of uncertainty. The other source is the reconstruction used to represent total sea level

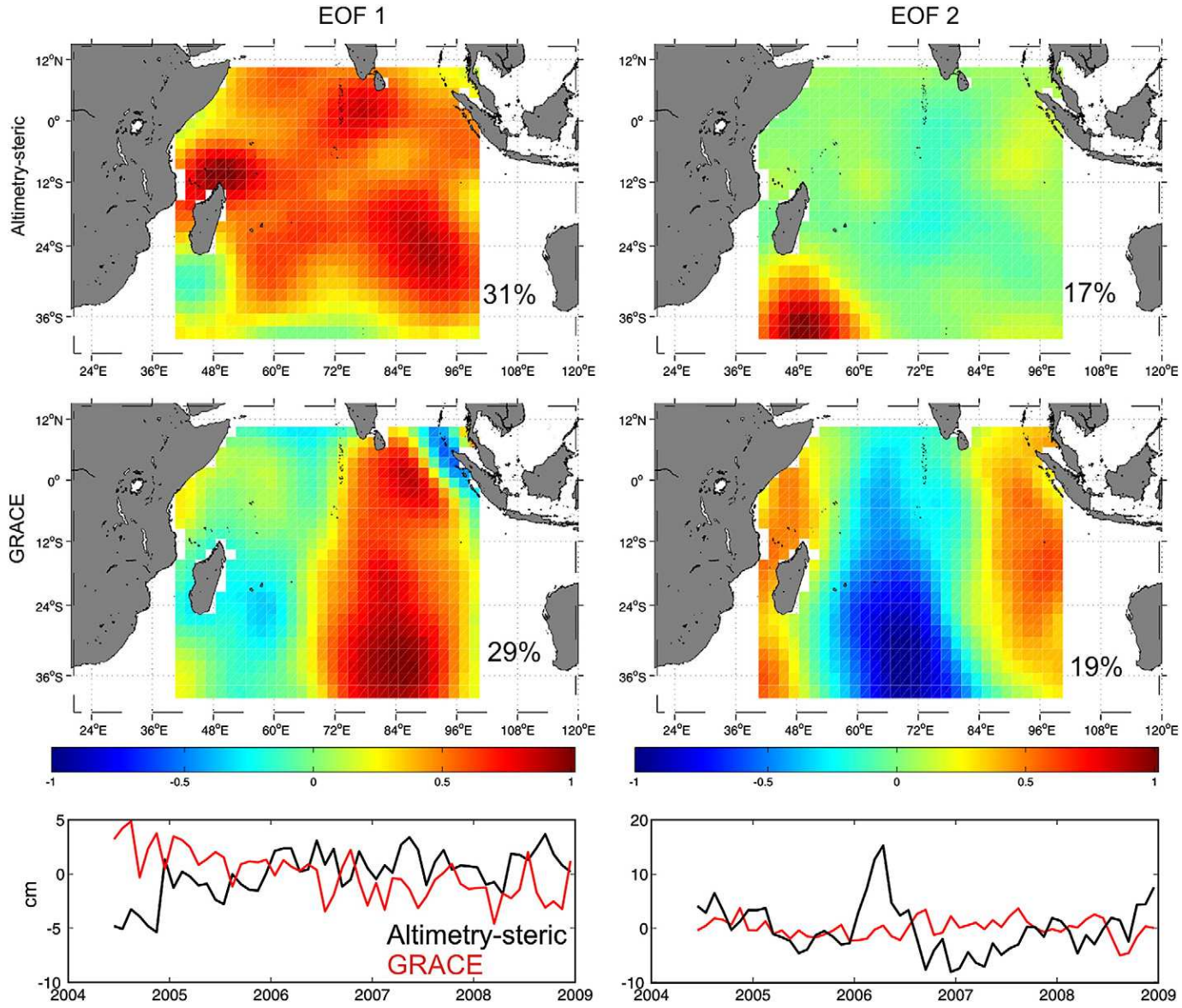

Fig. 10. As in Fig. 7 but for the Indian Ocean.

fields for the pre-altimetric period. Trends in reconstructed sea level are determined by the set of selected tide gauges and by the optimal interpolation method. Thus different spatial distribution of the tide gauge records can lead to small differences in regional sea level trends. Indeed, a region with many tide gauges will be strongly constrained by the optimal procedure to fit the tide gauge records, while regions with a sparse tide gauge distribution will be less constrained and can show differences, particularly at small scales. Further differences can be obtained depending on whether a full covariance matrix error is used or not for the interpolation. Despite all these uncertainty sources, however, the conclusion on the small fraction of the observed sea level rise accounted for by the thermosteric contribution remains unchanged.

An interesting question that remains open is whether the spatial pattern of the mass contribution to long term sea level rise can provide information on the sources of such fresh water input. Recently, Stammer (2008) derived the response of the ocean circulation to enhanced fresh water input associated with melting ice-sheets using an ocean general circulation model. He established that the dynamic response to ice melting implies the development of Kelvin and Rossby waves that propagate the sea surface height anomalies into the ocean basins at different time scales. According to Stammer (2008) results, the dynamic response would be much larger than the gravity response to the melting of continental glaciers and ice sheets. The latter induces spatial gradients of sea level due to the change of the geoid height, with lower than mean values close to the melting location and higher values in the far field (Mitrovica et al., 2001; Tamisiea et al., 2001). The linear trends of the mass contribution to sea level obtained for the period 1950–2003 are mapped in Fig. 11. Our results show striking similarities with the maps of sea surface height anomalies derived from the melting of Greenland (see Fig. 6 in

Table 2
Linear trends of total and thermosteric sea level and the difference between them.

	Reconstruction (total sea level)	Thermosteric	Total − thermosteric
N. Pacific	1.63 ± 0.04	0.03 ± 0.07	1.57 ± 0.07
Eq. Pacific	1.69 ± 0.04	0.24 ± 0.07	1.41 ± 0.08
S. Pacific	1.52 ± 0.03	0.14 ± 0.04	1.41 ± 0.04
Eq. Atlantic	1.63 ± 0.03	0.58 ± 0.07	1.05 ± 0.07
S. Atlantic	1.60 ± 0.02	0.22 ± 0.05	1.39 ± 0.05

Stammer, 2008). The coherence between both spatial patterns points at Greenland as the major source of fresh water input during the second half of the 20th century. However, given the limitations inherent to the interpolation of hydrographic data and to the use of reconstructed sea level field, further research is needed to ensure this point.

Acknowledgments

This work has been carried out in the framework of the VANIMEDAT2 project (CTM2009-10163-C02-01) funded by the Spanish Marine Science and Technology Program and by the Plan-E of the Spanish Government. F. M. Calafat acknowledges an FPI grant and M. Marcos acknowledges a "Ramón y Cajal" contract, both funded by the Spanish Ministry of Education. Altimetry data have been provided by AVISO (http://www.aviso.oceanobs.com/). GRACE data have been obtained from the Physical Oceanography Distributed Active Archive Center (PO.DAAC) (http://podaac.jpl.nada.gov/grace/). Authors are grateful to Prof. A. Cazenave for her constructive comments and to Dr. Don Chambers for his review of an earlier version of the paper.

Appendix A

Linear trends are computed using an MM-regression estimator (Yohai, 1987) calculated with an initial S-estimate (Rousseeuw and Yohai, 1984). The MM-regression estimator is computed with loss functions in Tukey's bi-square family. The tuning constants have been chosen to obtain simultaneous 50% breakdown-point and 95% efficiency when the errors are normally distributed. The S-estimate has been computed by means of the fast algorithm for S-regression estimates developed by Salibian-Barrera and Yohai (2006). While MM-estimators are robust against outlying observations and heteroskedasticity, standard errors estimates also need to be reliable, in the sense of not being overly biased by the presence of outliers and heteroskedasticity. In order to understand the importance of this point, let us consider the regression model

$$y_i = \vec{x}_i'\beta_0 + \sigma\varepsilon_i,\ i = 1,\ \ldots, n$$

where y_i are independent observations, $\vec{x}_i$ are the predictor variables, β_0 is the unknown regression coefficient to be estimated, ε_i are random errors, and n is the number of observations. Ideally, one would like to assume that the distribution of the data follows some specific symmetric distribution (F_0) such as the standard normal distribution. To allow for the occurrence of outliers and other departures from the classical model, we will assume that the actual distribution F takes the form

$$F = (1-\varepsilon)F_0 + \varepsilon\tilde{F}$$

where $0 \le \varepsilon < \frac{1}{2}$ and $\tilde{F}$ is an arbitrary and unspecified distribution. Under this assumption, the interpolation errors associated with the steric sea level (see Section 2.1) can be taken into account to obtain a robust estimate of the errors associated with the linear trends by simply adding an error term of the form $\tilde{\varepsilon}_i N(0,1)$, where $\tilde{\varepsilon}_i$ is the error associated with the ith observation and $N(0,1)$ is the standard normal distribution with mean 0 and unity variance. Steric sea level errors do not have constant variance, mainly due to the fact that the number of observations is larger at the end of the period than at the beginning, and therefore the actual distribution of y_i is of the form of F. In the cases that the errors $\tilde{\varepsilon}_i$ are not known we set them equal to 0, and therefore, the estimates of the standard errors are associated with natural variability and unknown random errors.

The standard error of robust estimates can be estimated using their asymptotic variances. However, the asymptotic distribution of MM-estimates has mainly been studied under the assumption that $F = F_0$, which does not strictly hold in many situations. In order to obtain robust estimates of the errors associated with the trends, we have used the fast bootstrap method proposed by Salibian-Barrera (2006), which yields a consistent estimate for the variance of the trend under general conditions. The simulation used to approximate the bootstrap distribution consists of bootstrapping the residuals of the MM-estimate.

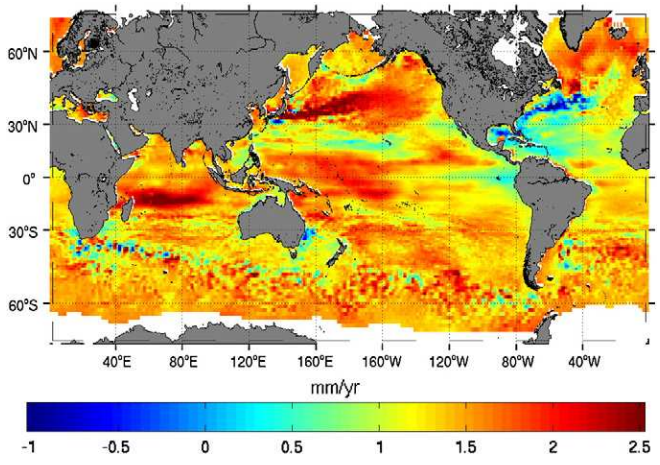

Fig. 11. Linear trends of the mass contribution to sea level rise for the period 1950–2003 inferred from the difference between reconstructed sea level and the thermosteric contribution.

References

Antonov, J.I., Levitus, S., Boyer, T.P., 2002. Steric sea level variations during 1957–1994: importance of salinity. J. Geophys. Res. 107 (C12), 8013. doi:10.1029/2001JC000964.
Antonov, J.I., Levitus, S., Boyer, T.P., 2005. Thermosteric sea level rise, 1955–2003. Geophys. Res. Lett. 32, L12602. doi:10.1029/2005GL023112.
Barnston, A.G., Livezey, R.E., 1987. Classification, seasonality and persistence of low-frequency atmospheric circulation patterns. Mon. Wea. Rev. 115, 1083–1126.
Bettadpur, S., 2007. Level-2 Gravity Field Product User Handbook, GRACE 327–734, CSR Publ. GR-03–01, Rev 2.3. University of Texas at Austin, 19 pp.
Calafat, F.M., Gomis, D., 2009. Reconstruction of Mediterranean sea level fields for the period 1945–2000. Glob. Planet. Change 66 (3–4), 225–234. doi:10.1016/j.gloplacha.2008.12.015.
Calafat, F.M., Marcos, M., Gomis, D., 2010. Mass contribution to the Mediterranean Sea level variability for the period 1948–2000. Glob. Planet. Change 73, 193–201.
Carrère, L., Lyard, F., 2003. Modeling the barotropic response of the global ocean to atmospheric wind and pressure forcing—comparisons with observations. Geophys. Res. Lett. 30 (6), 1275. doi:10.1029/2002GL016473.
Cazenave, A., Llovel, W., 2010. Contemporary sea level rise. Annu. Rev. Mar. Sci. 2, 145–173. doi:10.1146/annurev-marine-120308-081105.
Cazenave, A., Nerem, R.S., 2004. Present-day sea level change: observations and causes. Rev. Geophys. 42, RG3001.
Cazenave, A., Dominh, K., Guinehut, S., Berthier, E., Llovel, W., Ramillien, G., Ablain, M., Larnicol, G., 2009. Sea level budget over 2003–2008: a reevaluation from GRACE space gravimetry, satellite altimetry and Argo. Glob. Planet. Change 65, 83–88.
Chambers, D.P., 2006. Evaluation of new GRACE time-variable gravity data over the ocean. Geophys. Res. Lett. 33 (17), L17603. doi:10.1029/2006GL027296.
Chambers, D.P., Willis, J.K., 2008. Analysis of large-scale ocean bottom pressure variability in the North Pacific. J. Geophys. Res. 113, C11003. doi:10.1029/2008JC004930.
Chambers, D.P., Wahr, J., Tamisiea, M., Nerem, R.S., 2010. Ocean mass from GRACE and Glacial Isostatic Adjustment. J. Geophys. Res. 115, B11415. doi:10.1029/2010JB007530.
Cheng, M., Tapley, B.D., 2004. Variations in the Earth's oblateness during the past 28 years. J. Geophys. Res. 109, B09402. doi:10.1029/2004JB003028.
Church, J.A., Coleman, R., Lambeck, K., Mitrovika, J.X., 2004. Estimates of the regional distribution of sea level rise over the 1950–2000 period. J. Climate 17, 2609–2625.
Dhomps, A.-L., Guinehut, S., Le Traon, P.-Y., Larnicol, G., 2010. A global comparison of Argo and satellite altimetry observations. Ocean Sci. Discuss. 7, 995–1015. doi:10.5194/osd-7-995-2010.
Domingues, C.M., Church, J.A., White, N.J., Glecker, P.J., Wijffels, S.E., Barker, P.M., Dunn, J.R., 2008. Improved estimates of upper-ocean warming and multi-decadal sea level rise. Nature 453, 1090–1094. doi:10.1038/nature07080.
Fan, Y., van den Dool, H., 2004. Climate Prediction Center global monthly soil moisture data set at 0.5_ resolution for 1948 to present. J. Geophys. Res. 109, D10102. doi:10.1029/2003JD004345.

Fenoglio-Marc, L., Kusche, J., Becker, M., 2006. Mass variation in the Mediterranean Sea from GRACE and its validation by altimetry, steric and hydrologic fields. Geophys. Res. Lett. 33, L19606. doi:10.1029/2006GL028651.

Flechtner, F. (2007), AOD1B Product Description Document for product Releases 01 to 04, GRACE 327–750, CSR publ. GR-GFZ-AOD-0001 Rev. 3.1, University of Texas at Austin, 43 pp.

Fu, L.-L., Cheng, B., Qiu, B., 2001. 25-day period large-scale oscillations in the Argentine Basin revealed by the TOPEX/Poseidon altimeter. J. Phys. Ocean 31, 506–517.

Guinehut, S., Le Traon, P.-Y., Larnicol, G., 2006. What can we learn from Global Altimetry/Hydrography comparisons? Geophys. Res. Lett. 33, L10604. doi:10.1029/2005GL025551.

Guinehut, S., Coatanoan, C., Dhomps, A.-L., Le Traon, P.-Y., Larnicol, G., 2009. On the use of satellite altimeter data in Argo quality control. J. Atmos. Oceanic Technol. 26 (2), 395–402.

Han, Weiqing, Meehl, Gerald A., Rajagopalan, Balaji, Fasullo, John T., Hu, Aixue, Lin, Jialin, Large, William G., Wang, Jih-wang, Quan, Xiao-Wei, Trenary, Laurie L., Wallcraft, Alan, Shinoda, Toshiaki, Yeager, Stephen, 2010. Patterns of Indian Ocean sea-level change in a warming climate. Nat. Geosci. doi:10.1038/ngeo901.

Hughes, C.W., Stepanov, V.N., Fu, L.-L., Barnier, B., Hargreaves, G.W., 2007. Three forms of variability in Argentine Basin ocean bottom pressure. J. Geophys. Res. 112, C01011. doi:10.1029/2006JC003679.

Ingleby, B., Huddleston, M., 2007. Quality control of ocean temperature and salinity profiles-historical and real time data. J. Mar. Syst. 65, 158–175. doi:10.1016/j.jmarsys.2005.11.019.

Ishii, M., Kimoto, M., 2009. Reevaluation of historical ocean heat content variations with time-varying XBT and MBT depth bias corrections. J. Oceanogr. 65, 287–299.

Ishii, M., Kimoto, M., Sakamoto, K., Iwasaki, S., 2006. Steric sea level changes estimated from historical ocean subsurface temperature and salinity analyses. J. Oceanogr. 62, 155–170.

Kaplan, A., Cane, M.A., Kushnir, Y., Clement, A.C., 1998. Analyses of global sea surface temperatures 1856–1991. J. Geophys. Res. 103, 18567–18589.

Leuliette, E.W., Miller, L., 2009. Closing the sea level rise budget with altimetry, Argo, and GRACE. Geophys. Res. Lett. 36, L04608. doi:10.1029/2008GL036010.

Llovel, W., Cazenave, A., Rogel, P., Lombard, A., Nguyen, M.B., 2009. Two-dimensional reconstruction of past sea level (1950–2003) from tide gauge data and an Ocean General Circulation Model. Clim. Past 5, 217–227.

Llovel, W., Guinehut, S., Cazenave, A., 2010. Regional and interannual variability in sea level over 2002–2009 based on satellite altimetry, Argo float data and GRACE ocean mass. Ocean Dyn. 60, 1193–1204.

Marcos, M., Tsimplis, M.N., 2007. Variations of the seasonal sea level cycle in southern Europe. J. Geophys. Res. 112, C12011. doi:10.1029/2006JC004049.

Miller, L., Douglas, B.C., 2004. Mass and volume contributions to twentieth-century global sea level rise. Nature 428, 406–409.

Mitrovica, J.X., Tamisiea, M.E., Davis, J.L., Milne, G.A., 2001. Recent mass balance of polar ice sheets inferred from patterns of global sea-level change. Nature 409, 1026–1029.

Paulson, A., Zhong, S., Wahr, J., 2007. Inference of mantle viscosity from GRACE and relative sea level data. Geophys. J. Int. 171 (2), 497–508.

Peltier, W.R., 2004. Global glacial isostasy and the surface of the Ice-Age Earth: the iCE-5 G(VM2) model and GRACE. Annu. Rev. Earth Planet. Sci. 32, 111–149. doi:10.1146/annurev.earth.32.082503.144359.

Peltier, W.R., 2009. Closure of the budget of global sea level rise over the GRACE era: the importance and magnitudes of the required corrections for global glacial isostatic adjustment. Quatern. Sci. Rev. 28, 1658–1674.

Peltier, W.R., Luthcke, S.B., 2009. On the origins of Earth rotation anomalies: new insights on the basis of both "paleogeodetic" data and Gravity Recovery and Climate Experiment (GRACE) data. J. Geophys. Res. 114, B11405. doi:10.1029/2009JB006352.

Rousseeuw, P.J., Yohai, V.J., 1984. Robust regression by means of S-estimators. In: Franke, J., Hardle, W., Martin, D. (Eds.), Robust and Nonlinear Time Series. : Lecture Notes in Statistics., vol. 26. Springer, Berlin, pp. 256–272.

Salibian-Barrera, M., 2006. Bootstrapping MM-estimators for linear regression with fixed designs. Stat. Probabil. Lett. 76, 1287–1297.

Salibian-Barrera, M., Yohai, V.J., 2006. A fast algorithm for S-regression estimates. J. Comput. Graph. Stat. 15 (2), 414–427.

Song, Y.T., Zlotnicki, V., 2008. Subpolar ocean-bottom-pressure oscillation and its links to the tropical ENSO. Int. J. Remote Sens. 29 (21), 6091–6107.

Stepanov, V.N., Hughes, C.W., 2006. Propagation of signals in basin-scale ocean bottom pressure from a barotropic model. J. Geophys. Res. 111, C12002. doi:10.1029/2005JC003450.

Stammer, D., 2008. Response of the global ocean to Greenland and Antarctic ice melting. J. Geophys. Res. 113, C06022. doi:10.1029/2006JC004079.

Swenson, S., Chambers, D.P., Wahr, J., 2008. Estimating geocenter variations from a combination of GRACE and ocean model output. J. Geophys. Res. 113, B08410. doi:10.1029/2007JB005338.

Tamisiea, M., Mitrovica, J.X., Milne, G.A., Davies, J.L., 2001. Global geoid and sea level changes due to present day ice-mass fluctuations. J. Geophys. Res. 106 (B12), 30849–30863.

Wahr, J., Molenaar, M., Bryan, F., 1998. Time variability of the Earth's gravity field: Hydrological and oceanic effects and their possible detection using GRACE. J. Geophys. Res. 103(B12), 30, 205–230, 229. doi:10.1029/98JB02844.

Wahr, J., Swenson, S., Zlotnicki, V., Velicogna, I., 2004. Time-variable gravity from GRACE: first results. Geophys. Res. Lett. 31, L11501. doi:10.1029/2004GL019779.

Weijer, W., Vivier, F., Gille, S.T., Dijkstra, H.A., 2007. Multiple oscillatory modes of the Argentine Basin. Part I: statistical analysis. J. Phys. Oceanogr. 37, 2855–2868. doi:10.1175/2007JPO3527.1.

Willis, J.K., Chambers, D.P., Nerem, R.S., 2008. Assessing the globally averaged sea level budget on seasonal to interannual timescales. J. Geophys. Res. 113, C06015. doi:10.1029/2007JC004517.

Willis, J.K., Lyman, J.M., Johnson, G.C., Gilson, J., 2009. In situ data biases and recent ocean heat content variability. J. Atmos. Oceanic Technol. 26 (4), 846–852.

Wolter, K., Timlin, M.S., 1998. Measuring the strength of ENSO events — how does 1997/98 rank? Weather 53, 315–324.

Yohai, V.J., 1987. High breakdown-point and high efficiency robust estimates for regression. Ann. Statist. 15, 642–656.

Estimating ENSO influence on the global mean sea level over 1993-2010

A. Cazenave[1], O. Henry[1], S. Munier[1], T. Delcroix[1], A.L. Gordon[3]

B. Meyssignac[1], W. Llovel[2], H. Palanisamy[1], M. Becker[4]

(1) LEGOS, OMP, Toulouse, France
(2) JPL, Pasadena, USA
(3) LDEO, Columbia University, USA
(4) UMR Espace-DEV/UAG, Cayenne, French Guiana

Marine Geodesy Special Issue
Submitted 13 January 2012
Accepted 27 April 2012

Abstract

The global mean sea level (GMSL) shows positive/negative anomalies during El Nino/La Nina events. In a previous study, we showed that GMSL and total land water storage variations are inversely correlated, with lower-than average total water storage on land and higher-than-average GMSL during El Nino. This result is in agreement with the observed rainfall deficit/excess over land/oceans during El Nino (and vice versa during La Nina). It suggests that the positive GMSL anomaly observed during El Nino is likely due to an ocean mass rather than thermal expansion increase. Here, we analyse the respective contribution of the Atlantic, Indian and Pacific oceans to the interannual (ENSO-related) GMSL anomalies observed during the altimetry era (i.e., since 1993) with an emphasis on the 1997/1998 El Nino event. For each oceanic region, we compute the steric contribution, and remove it from the altimetry-based mean sea level to estimate the ocean mass component. We find that mass change of the tropical Pacific ocean, mainly in the region within 0°-25°N, is responsible for the observed 1997/1998 ENSO-related GMSL anomaly, and almost perfectly compensates the total land water deficit during the 1997/1998 El Nino.

Key words: Sea level, steric sea level, ocean mass change, ENSO, satellite altimetry, water cycle

1. Introduction

On interannual to multidecadal time scales, global mean sea level (GMSL) variations can be explained by ocean thermal expansion and water mass variations (due to land ice melt and land water storage changes) (e.g., Bindoff et al., 2007). Over the altimetry era (1993-2010), the rate of GMSL rise amounts to 3.2 +/- 0.4 mm/yr (e.g., Ablain et al., 2009, Nerem et al., 2010) and is rather well explained by ocean thermal expansion (by ~30%) and land ice loss (~60%) (e.g., Cazenave and Llovel, 2010, Church et al., 2011). So far however, little attention has been given to explain the origin of the GMSL interannual variability. For the altimetry era, Nerem et al. (2010) noticed that detrended GMSL changes are correlated to ENSO (El Nino-Southern Oscillation) occurrences, with positive/negative sea level anomalies observed during El Nino/La Nina. This is illustrated in Fig.1a showing detrended altimetry-based GMSL over 1993-2010 and the Multivariate ENSO Index (MEI, Wolter and Timlin, 1998). The correlation between the two monthly data sets is rather modest (equal to 0.4) for the whole time span, but it reaches 0.7 when the calculation is performed over the 1997-1998 period including the very strong record-breaking 1997/1998 El Nino event. This suggests that ENSO influences either ocean thermal expansion or ocean mass (or both). Interestingly, Llovel et al. (2011a) reported that the interannual GMSL variations are inversely correlated to interannual variations in global land water storage, with a tendency for a deficit land water storage during El Nino events (and vice versa during La Nina). This was shown through a global water mass conservation approach using GRACE (Gravity Recovery and Climate Experiment) space gravimetry data and the ISBA-TRIP (Interactions between Soil, Biosphere and Atmosphere –Total Runoff Integrating Pathways) global hydrological model developed at MeteoFrance (Alkama et al., 2010) to estimate land water storage changes over the altimetry era.

Continental waters are continuously exchanged between atmosphere, land and oceans through vertical and horizontal mass fluxes (precipitation, evaporation, transpiration of the vegetation, surface runoff and underground flow). Conservation of total water mass in the climate system at interannual time scale (neglecting to a first approximation, the atmospheric reservoir as in Llovel et al., 2011a) leads to :

$$\Delta M_{ocean} \approx - \Delta M_{LW} \quad (1)$$

where ΔM_{ocean} and ΔM_{LW} represent changes with

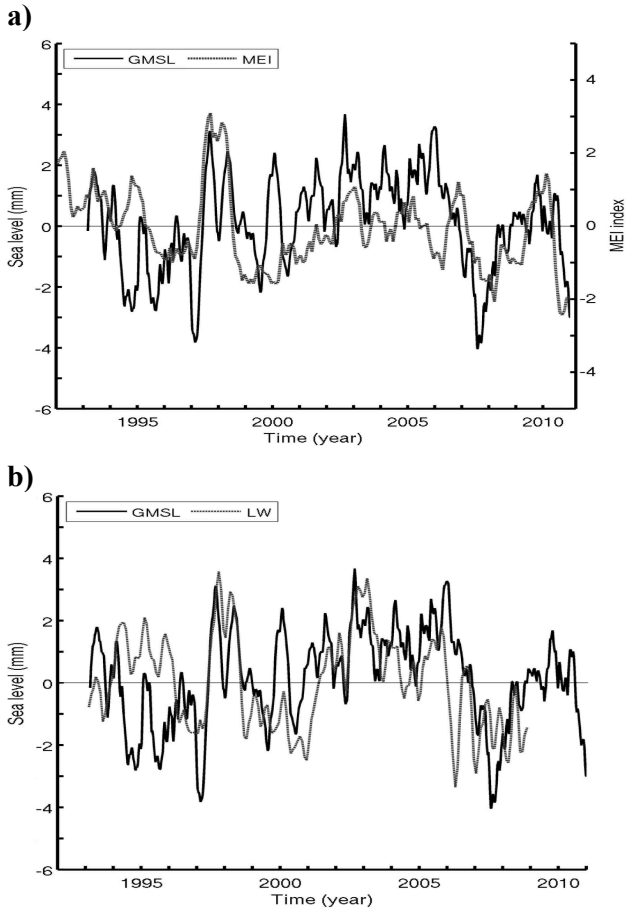

Fig.1: (a) Detrended altimetry-based global mean sea level (GMSL, solid line) and Multivariate ENSO Index (MEI, dotted line). Positive MEI values denote El Nino periods, and negative values La Nina periods (b) Detrended altimetry-based global mean sea level (GMSL, solid line) and reversed (i.e., multiplies by -1) total land water storage from the ISBA-TRIP model expressed in equivalent sea level (LW, dotted line).

time of ocean mass and total land water storage due to total fresh water input/output from precipitation, evaporation-transpiration and runoff. Total land water storage change can be further expressed in terms of equivalent sea level change by simply dividing the total continental water volume change by the mean surface of the oceans and changing its sign (i.e., multiplying by -1 to reflect the fact that less water on land corresponds to more water in the oceans, and inversely). Fig.1b shows the total land water storage change over 1993-2008 (an update of Llovel et al., 2011; see section 2.3), expressed in equivalent sea level, superimposed to the detrended GMSL. We can note the good quantitative agreement between the two curves, in particular during the 1997/1998 El Nino event. This result is not surprising as it is known that during an El Nino, there is more rain over the oceans and less rain on land as reported by several studies (e.g., Dai and Wigley, 2000, Gu et al., 2007, Gu and Adler, 2011).

The fact that the positive 1997/1998 GMSL anomaly is quantitatively well explained by the negative total land water storage anomaly suggests that there is almost perfect water mass compensation between ocean and land during that period, and that other processes (e.g., ocean heat storage change) are negligible.

In the present study, we investigate this issue further and intend to determine whether the total ocean water mass excess noticed during El Nino is uniformly distributed over the oceans or not. If not, we want to know which ocean basin and/or region are mainly responsible for the ENSO-related GMSL anomalies. For that purpose, we consider the altimetry time span (since 1993), but mostly focus the discussion on the 1997/1998 ENSO event. We compute the detrended mean sea level in different oceanic regions, estimate the steric component (thermal expansion plus salinity effects) using in situ ocean temperature and salinity data, and deduce the ocean mass component for each region (from the difference between altimetry-based mean sea level and steric sea level). We find that it is the north tropical Pacific region that mostly contributes to the observed (anti) correlation between interannual GMSL and global land water storage during ENSO. We further estimate the water budget of the ocean-atmosphere system over the north Pacific region, considering the time derivative of ocean mass, precipitation P, evaporation E, and transport of water in and out the considered region. Finally we discuss potential processes causing the tropical North Pacific mass anomaly during ENSO.

2. Datasets

2.1 Sea level data

For the altimetry-based sea level data, we use the DT-MSLA "Ref" series provided by Collecte Localisation Satellite (CLS; http://www.aviso.oceanobs.com/en/data/products/sea-surface-height-products/global/msla/index.html). This data set is used over the time span from January 1993 to December 2010. It is available as 1/4°×1/4° Mercator projection grids at weekly interval from a combination of several altimetry missions (Topex/Poseidon, Jason-1 and 2, Envisat and ERS 1 and 2). Most recently improved geophysical corrections are applied to the sea level data (see Ablain et al., 2009 for details).

2.2 Steric data

Steric sea level is estimated using an updated version (v6.12) of in situ ocean temperature and salinity data from Ishii and Kimoto (2009) (called hereafter IK09). The IK09 temperature data are corrected for the XBT depth bias. The temperature and salinity data are available at monthly interval over 16 depth levels ranging from the ocean surface down to 700 m depth, on a global 1° x 1° grid from 1955 to 2009. Steric sea level anomalies are computed over the 0-700 m depth range for the period January 1993 to December 2009. The deep ocean contribution cannot be accounted for since hydrographic data below 700 m are too sparse, noting however that recent studies showed that almost all interannual variability in steric sea level in confined in the upper 300 - 500 m of the ocean (e.g., Llovel et al., 2011b). At global scale, salinity does not contribute to the GMSL, but this is not true at regional scale. This is why here we account for salinity in this study.

2.3 ISBA-TRIP global hydrological model

To estimate global land water storage, we use the ISBA-TRIP global hydrological model developed at MeteoFrance. The ISBA land surface scheme calculates time variations of surface energy and water budgets. Soil hydrology is represented by three layers: a thin surface layer (1cm) included in the rooting layer and a third layer to distinguish between the rooting depth and the total soil depth. The soil water content varies with surface infiltration, soil evaporation, plant transpiration and deep drainage. ISBA uses a comprehensive parameterization of sub-grid hydrology to account for heterogeneity of precipitation, topography and vegetation within each grid cell. It is coupled with the TRIP (Total Runoff Integrating Pathways) module (Oki and Sud, 1998). TRIP is a simple river routing model converting daily runoff simulated by ISBA into river discharge on a global river channel network here defined at 1° by 1° resolution. Details on the ISBA-TRIP model can be found in Decharme et al. (2006) and Alkama et al. (2010). The outputs of the ISBA-TRIP model cover the period January 1950 to December 2008, with values given at monthly interval on a 1°x1° grid. They are based on a forced mode run, with global meteorological forcing provided by the Princeton University on a 3-hourly time step and 1° resolution. We updated by two additional years (up to December 2008) the total land water storage computation done by Llovel et al. (2011a) using the ISBA-TRIP model. The whole land surface has been considered. The reversed total (i.e., whole land area-averaged) land water storage curve shown in Fig.1b (estimated from ISBA-TRIP model and

expressed in sea level equivalent) has not been detrended (unlike the GMSL curve) because the land water storage trend is negligible. The correlation between the two curves is 0.4 over the whole period. It increases to 0.70 when considering the 1997-1998 time span (El Nino event).

2.4 Precipitation, evaporation and wind stress data

Precipitation P and evaporation E data used in this study are based on different data sets. For precipitation, we used products from the Global Precipitation Climatology Project (GPCP, Adler et al., 2003) and Climate Prediction Center Merged Analysis of Precipitation (CMAP, Xie & Arkin, 1997). For evaporation, we used the Objectively Analyzed air-sea Fluxes product (OAFlux, Yu and Weller, 2007) and the Hamburg Ocean Atmosphere Parameters and Fluxes from Satellite Data (HOAPS, Anderson et al., 2007). We also used reanalysis products from the European Centre for Medium-Range Forecast (ECMWF) ERA-Interim data (Simmons et al., 2007) which provides both precipitation and evaporation data. To give more confidence in the inferred net precipitation (P-E), we also estimated (P-E) using other parameters of the atmospheric moisture budget, namely precipitable water P_{water} and moisture flux divergence divQ (as done in several global- and regional-scale studies; e.g., Syed et al., 2009; Sahoo et al., 2011). This was performed through the relationship:

$$P\text{-}E = -(dP_{water}/dt + divQ) \quad (2)$$

The P_{water} and divQ data were provided by the ECMWF ERA-Interim and the National Centers for Environmental Prediction / National Center for Atmospheric Research (NCEP/NCAR, Kalnay et al., 1996) data bases.

All these data sets provide monthly global data on regular grids (resolution from 0.5° to 2.5° depending on the data set) in units of mm/month. All gridded data are further expressed in terms of monthly averages over the period January 1993 to December 2009.

2.5 Filtering, averaging, weighting, smoothing and data uncertainties

As we focus here on the interannual variability, for all data sets, we remove the seasonal signal at each mesh of all gridded fields (i.e., before area-averaging), through a least-squares adjustments of 6-month and 12-month period sinusoids. Mean time series are obtained by geographical averaging applying a cosine (latitude) weighting. To each spatially averaged time series, we also remove a linear trend over the 1993-2009 time span. A 3-month running filter is further applied.

Estimate of data uncertainties depends on the data set. For altimetry-based sea level data, uncertainty of 3-month area-averaged sea level data is estimated to ~1 mm (assuming a 4 mm error for 10-day mean values; see Ablain et al., 2009). The steric sea level error is estimated from the difference between the IK09 and Levitus et al. (2009) steric data sets. We find a mean error of ~1.5 mm for the 3-month globally area-averaged steric sea level data. A similar approach is conducted to infer the P-E error using the differences between direct P and E estimates as well as indirect estimates from the atmospheric water balance equation (see section 4.1).

3. Results: Contributions of thermal expansion and mass component to the mean sea level in the Atlantic, Indian and Pacific oceans, 1993-2010

We computed the spatially-averaged altimetry-based and steric sea level, as well as mass component (i.e., the difference between altimetry-based mean sea level and steric component, assuming that the deep ocean contribution is negligible) over the: (1) Atlantic ocean (70°W to 20°E; 60°S to 60°N latitude), (2) Indian ocean (20°E to 120°E, 60°S to 30°N), and (3) Pacific ocean (120°E to north and south America coasts, 60°S to 60°N). Figures 2a-c show the relative contributions of the Atlantic, Indian, and Pacific oceans to the interannual GMSL, as well as corresponding steric and ocean mass components. The term ‘relative contributions’ means that each curve is weighted by the ratio between the surface of the considered area and the whole ocean surface (hereafter called ‘area weighting’).

The contributions of the Atlantic, Indian and Pacific sea level to the GMSL display significant interannual variability, with mean standard deviations of 1.1, 1.4 and 1.2 mm, respectively. Atlantic and Indian oceans show positive sea level anomalies peaking in 1998/early 1999, likely related to the La Nina phase that followed the 1997/1998 El Nino. These sea level anomalies are likely of thermal origin as the steric component closely follows the observed sea level. The correlation between mean sea level and steric sea level over 1997-1998 is 0.75 and 0.67 for the Atlantic and Indian oceans respectively, reinforcing the fact that during this El Nino period, the sea level anomaly in these two basins has mostly a steric origin.

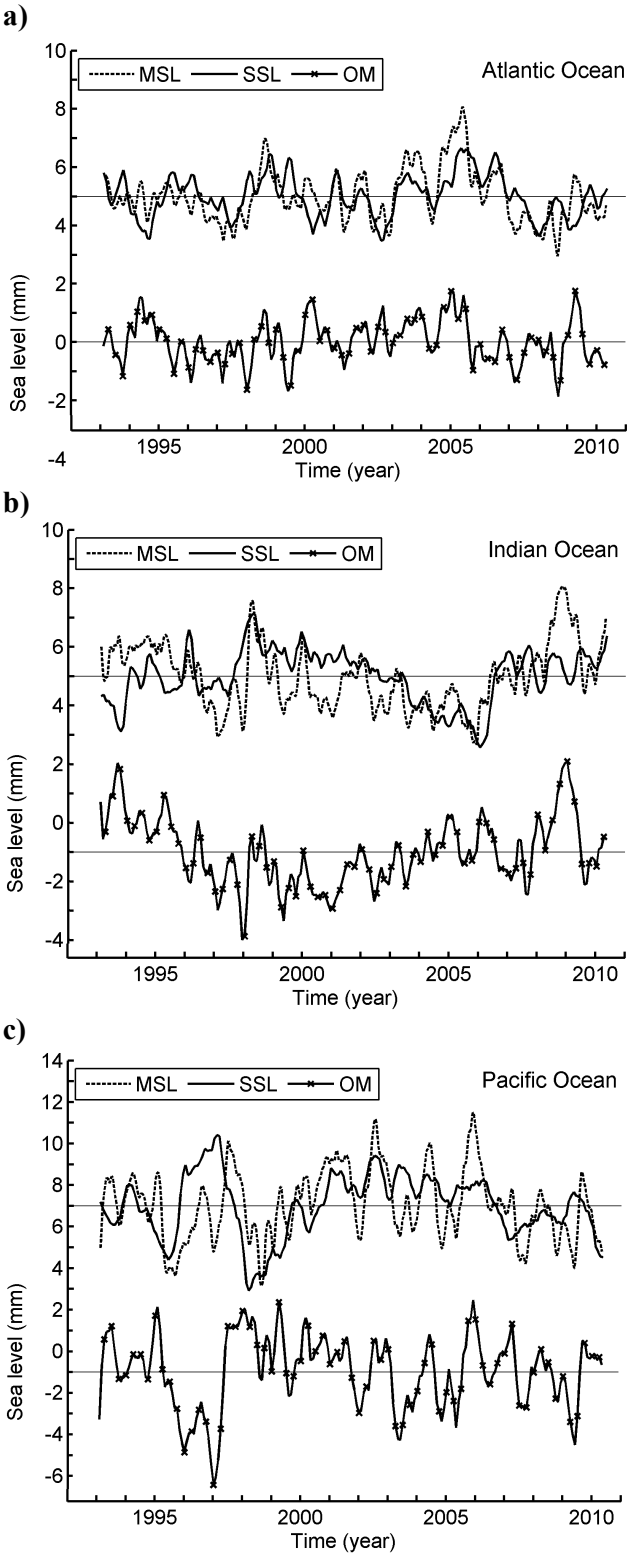

Fig.2: Contribution of the (a) Atlantic, (b) Indian, and (c) Pacific basins to the global mean sea level: area-averaged mean sea level (MSL, dotted line), area-averaged mean steric sea level (SSL, solid line) and ocean mass component (difference between the former two) (OM, solid line with crosses). See text for basin boundaries. Units are mm (sea level equivalent). The MSL/SSL and OM time series are shifted vertically for clarity. Note that the time series are area-weighted (i.e., multiplied by the ratio between the surface of considered region and the whole ocean surface).

In late 1997/early 1998, the Pacific steric sea level is negative while the observed sea level is slightly positive. The correlation between the mean sea level and steric sea level is only 0.2 over 1997-1998, contrasting with the higher correlation values discussed above for the Atlantic and Indian oceans. The Pacific mass component presents a large negative anomaly in 1997 followed by a steep rise and a positive anomaly in early 1998. This result suggests that the 1997/1998 GMSL anomaly could be located in the Pacific Ocean.

To further infer the exact location of this mass anomaly, we computed the zonally-averaged (from 120°E to the American coasts) time-latitude diagram of the Pacific ocean mass anomalies (considering 1° wide latitudinal bands). The diagram is shown in Fig.3. It displays a positive anomaly in the ~10°S-20°N latitude band during the 1994/1995 El Nino, followed another positive anomaly during the 1997/1998 El Nino, located in the 5°S-30°N latitude band, and with an amplitude of ~20 mm. The mass anomalies of this tropical band are then weaker or even slightly negative during the remaining time period that includes both El Nino and La Nina events. .

From the diagram presented in Fig.3, we may conclude that the main 1997/1998 ENSO-related Pacific Ocean mass anomaly seen in Fig.2c is located in the 5°S-30°N latitudinal band. To further detail the importance of such an anomaly, the top inset in Fig. 3 represents the (reverse) total land water storage time series expressed in equivalent sea level (as in Fig. 1b), and the right-hand side inset shows the correlations (computed over the 1993-2008 and 1996-2000 time spans; respectively black and red curves) between the land water time series and the Pacific mass anomalies within successive 1° latitudinal bands. The right hand side curves shows that positive correlations are obtained in the north tropical domain, with correlation maxima (reaching 0.8) around the equator, 10°N and 20°N. In the following, we consider the 0°-25°N latitudinal band for the tropical Pacific mass anomaly. But tests have shown that considering slightly different bands (e.g., 5°S-25°N or 0°-30°N) leads to essentially similar results. Note also that considering a longitude area as of 100°E instead of 120°E (i.e., including the South China Sea) does not change these results.

To determine the zonal extension of the 0°-25°N mass anomaly, we computed a longitude-time diagram of the mass anomalies. It is shown in Fig.4.

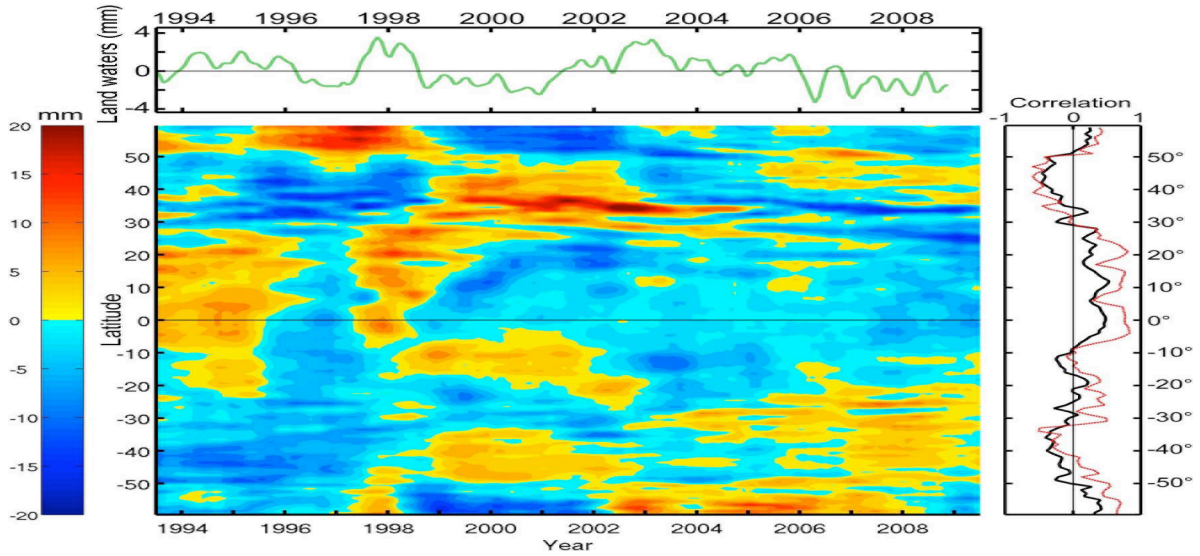

Fig.3: Time-Latitude diagram of the zonally-averaged (from 120°E to the American coasts) Pacific ocean mass component. Values have been smoothed with a 6-month running mean for clarity. Units: mm (sea level equivalent). The top curve represents the reversed total land water storage time series expressed in equivalent sea level, as in Fig. 1b. The right-hand side black and red curves are the correlations as a function of latitude between the land water storage curve (in equivalent sea level) and Pacific ocean mass in successive 1° wide latitudinal bands over the whole time span and over 1996-2000, respectively.

In Fig.4, we observe a band of positive mass anomalies during the 1997/1998 El Nino extending from about 120°E-140°E to the coast of America. In contrast, we note a band of negative anomalies located in the central tropical Pacific during the 1999/2000 La Nina.

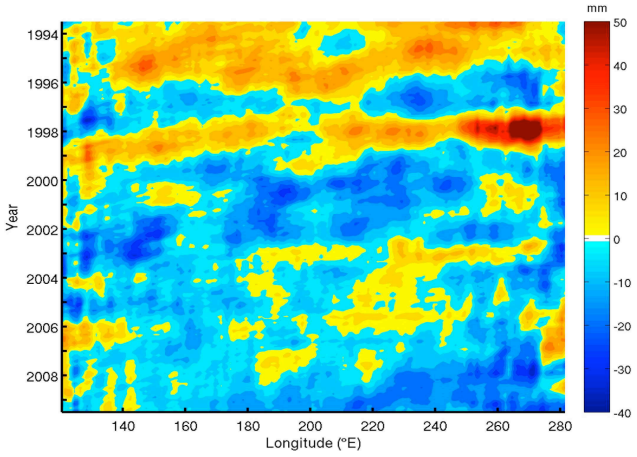

Fig.4: Longitude-time diagram of meridionally-averaged Pacific ocean mass component (data averaged in latitude between 0° and 25°N). Values have been smoothed with a 6-month running mean for clarity.

To check whether the north tropical Pacific mass anomaly quantitatively correlates with (i.e., is compensated by) the total land water storage change, we restricted the analysis done for Fig.2c to the 0°-25°N tropical Pacific. The corresponding altimetry-based sea level, steric sea level and ocean mass time series are shown in Fig.5 (with area-weighting). On the ocean mass curve we have superimposed the (reversed) total land water curve (expressed in equivalent sea level). We note an overall good agreement, and a quasi perfect quantitative agreement during the 1997/1998 El Nino, indicating that total land water deficit during that El Nino is almost totally compensated by an increase of the north tropical Pacific ocean mass. The correlation between north tropical Pacific Ocean (0°-25°N) mass and land water storage (expressed in equivalent sea level) amounts to 0.91 over 1997-1998 (considering slightly different latitudinal bands for the ocean mass averaging, e.g., 0°-30°N, has negligible influence on the shape of the curve shown in Fig.5, as well as on the correlation).

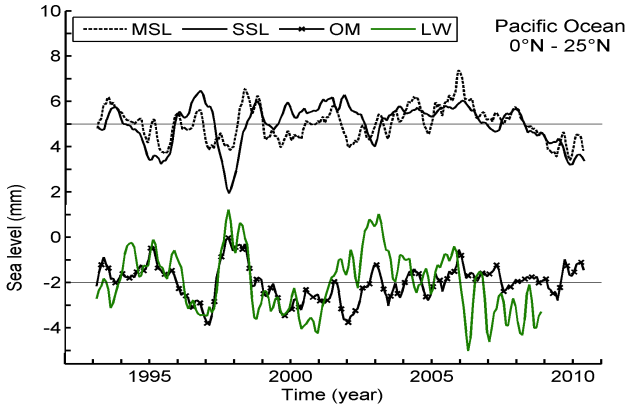

Fig.5: Contribution of the tropical north Pacific (0-25°N) to the GMSL: mean sea level, MSL (dotted line), steric sea level, SSL (solid line) and ocean mass component (difference between the former two), OM (solid line with crosses). The reversed total land water time series (expressed in equivalent sea level) LW (green curve) is superimposed. The MSL/SSL, OM/LW time series are shifted vertically for clarity.

4. Discussion

In the previous section, we showed that the 1997/1998 positive anomaly of the (detrended) GMSL is largely due to an excess of mass located in a zonal band of the north tropical Pacific Ocean between ~0° and 25°N latitude. We also showed that this north tropical Pacific mass excess quantitatively compensates the total land water storage deficit observed during that El Nino event.

The question now is: which process causes the 1997/1998 El Nino-related north tropical Pacific mass positive anomaly?

A budget analysis of all terms involved in the mass conservation equation would be necessary to solve that question. While this is not possible with the observation data we have in hand, we do believe instructive to present tentative explanations that may stimulate ocean modellers and/or new ideas. In the following, we examine successively different terms of the mass budget equation over the north tropical Pacific Ocean (0°-25°N).

Given our definition of the north tropical Pacific in terms of area (i.e., between 0°-25°N latitude, and ~120°E to the American coasts) its mass changes can be due to variations of surface P-E, river runoff (R), and water mass transports across the open boundaries. The mass balance equation can then be written as :

$$dOM/dt = P-E+R + Inflow/Outflow \quad (3)$$

In equation (3), dOM/dt is the time derivative of the north tropical Pacific ocean mass (area defined above). The term called 'Inflow/Outflow' (denoted I/O in the following) represents transport of water in and out the considered domain (counted positive when entering the domain). The I/O term results from: (1) flow across the equator via the interior pathway and the western boundary current, (2) flow across the 25°N parallel, and (3) flow at the western boundary (i.e., the Indonesian throughflow -ITF-, Gordon, 2005). Note that R in Eq.(3) can be neglected as no major river flow into the considered region.

In the following two sub sections, we estimate the two dominant terms of the right-hand side of the water budget equation (equation 3 above), i.e., net precipitation (P-E) (sub-section 4.1) and Inflow/Outflow (I/O; sub-section 4.2). Corresponding analysis is performed over the 0°-25°N tropical Pacific.

4.1 (P-E) changes over the north tropical Pacific Ocean (0°-25°N)

ENSO events produce large scale anomalies of the atmospheric circulation in the tropics, with direct effects on precipitation (e.g., Dai and Wigley, 2000, Trenberth et al., 2002, Neelin et al., 2003, Smith et al., 2006). Warm ENSO events (El Nino) give rise to more rainfall over the oceans and less rainfall over land, with opposite variations during cold events (La Nina) (Gu et al., 2007). Gu et al. (2007) and Gu and Adler (2003, 2011) showed that strong positive/negative precipitation anomalies affect tropical ocean/land during ENSO warm phases, with oceans/land responses being always opposite in sign. They also showed that the ENSO-related total precipitation signal in the tropics (ocean plus land) is weak. Dai and Wigley (2000) and Curtis and Adler (2003) further showed how precipitation patterns evolve in the tropical Pacific during the ENSO development. For example, El Nino produces positive precipitation anomalies in the central equatorial Pacific that move eastward and southward as the event matures.

We computed P-E time series using the different meteorological data sets described in section 2.4. Fig.6a shows the P-E time series over the 0°-25°N tropical Pacific from the different data sets between 1993 and 2009. This graph clearly shows a high correlation between the different computations (mean standard deviation of 0.44 mm/month over the whole period) and particularly during the 1997/1998 El Nino event. Fig.6b compares the net precipitation mean (averaging all individual time series) and associated standard deviation (red curve and shading) with the dOM/dt time series (blue curve). Their difference is shown in Fig. 6c. Fig.6b indicates a reasonably good correlation between mean net precipitation and dOM/dt (correlation of 0.58) during the whole time span. However, we also note that during the 1997/1998 El Nino peak, dOM/dt is less negative than P-E. The difference curve (Fig.6c) indeed shows a large positive residual peaking in early 1998, indicating that there is no compensation between dOM/dt and P-E, thus that the I/O term appearing in equation 3 may not be neglected. The result shown in Fig.6c corroborates the fact that changes in net precipitation cannot to be directly responsible for the north tropical Pacific mass anomaly because of fast water spreading at the surface by the ocean currents (see Huang et al., 2005).

4.2 Mass transport into and out from the north tropical Pacific Ocean (0-25°N)

In the following, we examine the inflow/outflow term of the north tropical Pacific water budget.

Fig.7 shows the I/O term (difference between dOM/dt and P-E) over the north tropical Pacific (0-

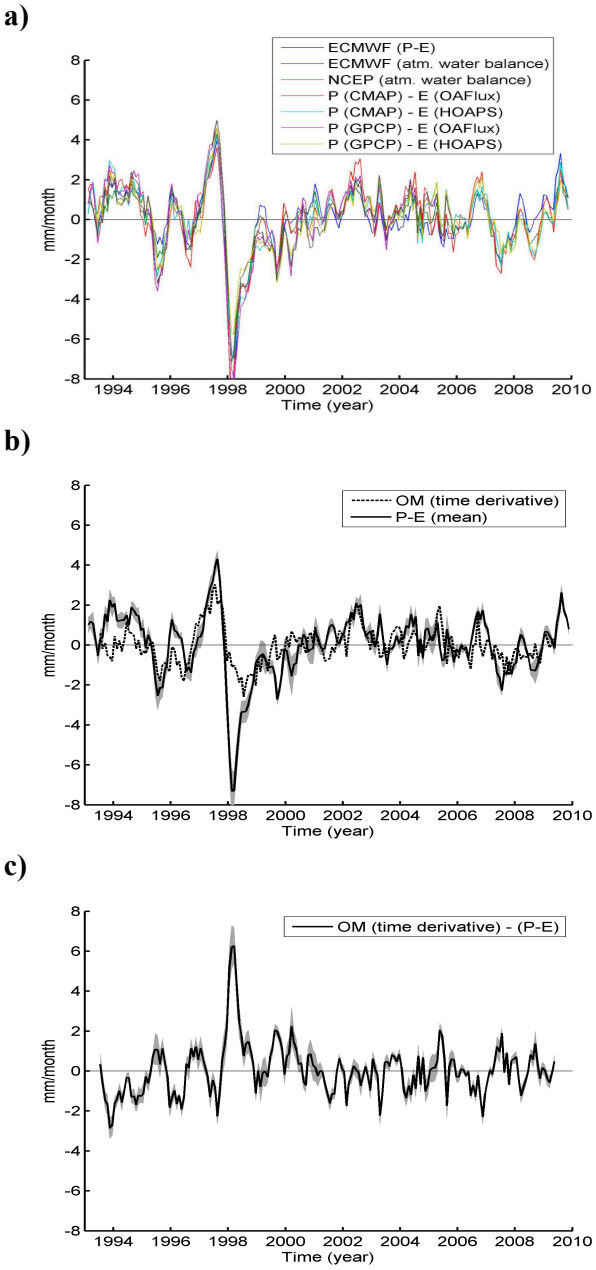

Fig.6: (a) Direct and indirect (from atmospheric water balance) estimates of net P-E over the north Pacific Ocean (0°-25°N) from different meteorological data sets. (b) Time derivative of the mass component (dotted line) and mean P-E (solid line) values averaged over the North Pacific Ocean (0°-25°N). (c) Difference time series between the time derivative of the North Pacific ocean mass component and mean (P-E). Shadings in Fig.6a and 6b represent spreading the P-E estimates. Unit: mm/month.

25°N) (same as Fig.6c but over 1996-2000 only to enhance the 1997/1998 ENSO period) on which is superimposed the negative I/O (i.e., -I/O) term computed as the difference between dOM/dt and P-E over the whole Indian ocean and whole south Pacific domain (0°-60°S). Looking at Fig.7, we clearly see a high anti-correlation (-0.95) between the inflow/outflow terms of these two regions. Fig. 7 also shows the I/O term over the northern part of the north Pacific Ocean (25°N-60°N). The corresponding curve is rather flat, with very small interannual variations compared to the two other curves, indicating that water transfers in/out the 25°N parallel are almost balanced.

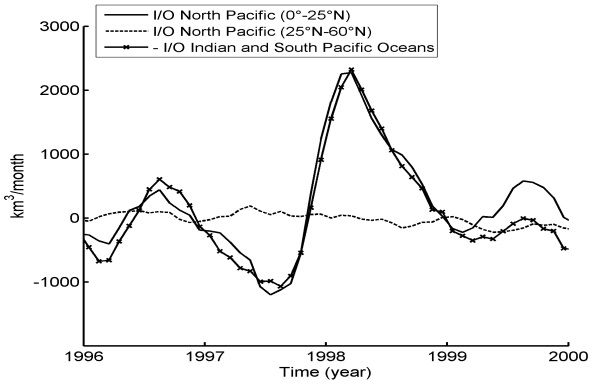

Fig. 7: Time series of the difference (term I/O in Eq. 3) between the time derivative of the ocean mass component and (P-E) for the north tropical Pacific ocean (0°-25°N) (solid line) and (solid line with crosses) the Indian ocean plus south Pacific domain. Note that the sign of the red curve has been reversed to ease the comparison. The dotted line represents the I/O term across the 25°N parallel in the north Pacific. Units are in km^3/month (i.e., data are multiplied by the areas of the considered domains).

The reported anti-correlation between the inflow/outflow terms of the north tropical Pacific (0-25°N) and the combined Indian ocean plus south Pacific domain suggests that the water exchanges with the Atlantic Ocean at the eastern and western boundaries are also compensated.

The above two results suggests that the positive mass anomaly in the north tropical Pacific is linked to flow variations across the equator via the interior pathway and the western boundary current, and/or variations of the Indonesian throughflow (ITF). Let us briefly discuss the latter possibility.

The Makassar Strait located between Borneo and Sulawesi is the main channel for the ITF, carrying about 80% of the total ITF, which amounts to 15 Sv (Sv=10^6 m^3/s) (Gordon et al. 2010). On average, the depth-integrated transport at the Makassar Strait is on the order of 8-12 Sv (Gordon, 2005; Gordon et al. 2008) but interannual variability of the ITF associated with ENSO has been reported (e.g., England and Huang, 2005, Vranes and Gordon, 2005). From in situ measurements, Susanto and Gordon (2005) showed that during the calendar year 1997, the Makassar transport was 7.9 Sv, falling to less than 5 Sv during the peak of the 1997/1998 El Nino. During the 2004-2006 period, the Makassar Strait throughflow averaged 11.6 Sv as observed by the INSTANT program. During this

period the ENSO phase was generally that of El Niño (with a brief La Niña phase in early 2006), though substantially subdued relative to the 1997/1998 event. The 2004-2006 Makassar Strait transport averaged 11.6 Sv (Gordon et al. 2008, Gordon et al., 2010). During the 2007-2010 period, when the ENSO phase shifted towards La Niña, a single current measuring mooring in Makassar Strait observed elevated southward velocity, with an estimated transport of 13 to 14 Sv (Gordon et al., 2012). Surface water from the tropical Pacific is lost as the Mindanao Current leaks into the ITF, i.e., not all of the Mindanao Current turns eastward to feed into the Pacific's North Equatorial Counter Current. In this way, the ITF does act to redistribute the mass input from rainfall. Gordon et al. (2012) showed that the leakage of surface water from the Mindanao Current into the ITF is reduced during El Niño when the surface layer is drawn more from the 19°N Luzon Strait throughflow, to enter Makassar Strait from the South China Sea. During La Nina, the Luzon Strait throughflow goes to near zero allowing greater surface layer inflow from the Mindanao. Such water transport changes are related to large-scale wind field changes over the Pacific and Indian Oceans during ENSO (e.g., Godfrey, 1996).

Reduced ITF of a few Sv, if not compensated by flow variations across the equator, is of the right order of magnitude to explain the north tropical Pacific mass excess observed during the 1997/1998 El Nino peak. In effect, a crude calculation shows that 1 Sv reduction over 1 month corresponds to a water volume of 2600 km^3 remaining in the north tropical Pacific, while the observed mass excess in this region corresponds to ~1500 km^3.

The above results may suggest that the 1997/1998 El Nino event could be related to an important variation of the water mass transfer between the north tropical Pacific Ocean (0°-25°N) and Indian and South Pacific oceans. In particular, a reduction of the ITF possibly combined with an intensification of water transfers from the south Pacific could have led to an important water mass increase in the north tropical Pacific region. Even though this study does not allow us to discriminate between the relative roles of these contributions, we cannot exclude that that an important part of the water transport variations may have occurred at the Makassar Strait. Further quantitative analyses are required to confirm this, for example using ocean general circulation model outputs.

5. Conclusion

The results presented in this study confirm that interannual variability of the GMSL has essentially a water mass origin, as the interannual GMSL is highly inversely correlated with total land water storage change, in particular during ENSO events. Focusing on the large positive GMSL anomaly observed during the 1997/1998 El Nino, we show that this anomaly is largely due to a mass excess of the north tropical Pacific (located between 0°-25°N in latitude and ~120°E to the American coasts in longitude). We also show that the ocean-atmosphere water budget computed over the north tropical Pacific (0°-25°N) is not closed during the 1997/1998 El Nino peak if the inflow/outflow terms are not accounted for. The north tropical Pacific mass excess associated with this El Nino event is consistent with the reduced depth-integrated water transport at the Makassar Strait (the Indonesian Throughflow) previously reported during the 1997/1998 El Nino, although we cannot exclude that flow across the equator via the interior pathway and the western boundary current also play some role. Further analyses are required however to quantitatively confirm or infirm this conclusion.

A similar investigation should be performed for La Nina events, during which important drops of the GMSL are observed. This was the case for example in 2007/2008 and 2010/2011. It will be interesting to determine whether the transport at the Makassar Strait is also a good candidate to explain the GMSL variability, as well as to assess the potential role of meridional mass transports across the equator. In line with our observation-based results, a precise quantification of all processes responsible for the GMSL at the ENSO time scale will be conducted with the help of ocean general circulation model outputs.

Acknowledgements

O. Henry, S. Munier, W. Llovel, and H. Palanisamy are supported respectively by a European grant in the context of the Monarch Project, a Post-Doctoral grant from CNES, a Post-Doctoral grant from JPL/NASA, and the French ANR 'CECILE' project . A.L. Gordon research is supported by the National Science Foundation grant OCE-0725935. This is Lamont-Doherty contribution number 7545. We thank H. Douville, B. Decharme and R. Alkama for providing us with the ISBA-TRIP model outputs.

References

Ablain M., A. Cazenave, S. Guinehut and G. Valladeau (2009). A new assessment of global mean sea level from altimeters highlights a reduction of global slope from 2005 to 2008 in agreement with in-situ measurements, *Ocean Sci.,* 5(2), 193-201.

Adler, R.F., Huffman, G.J., Chang, A., Ferraro, R., Xie, P.P., Janowiak, J., Rudolf, B., Schneider, U., Curtis, S., Bolvin, D., Gruber, A., Susskind, J., Arkin, P. and Nelkin, E. (2003). The version-2 global precipitation climatology project (GPCP) monthly precipitation analysis (1979-present). *Journal of Hydrometeorology* 4, 1147–1167.

Alkama R., B. Decharme, H. Douville, A. Voldoire, S. Tyteca, P. Le Moigne, M. Becker, A. Cazenave, J. Sheffield (2010): Global evaluation of the ISBA-TRIP continental hydrological system Part 1: Comparison to GRACE Terrestrial Water Storage estimates and in-situ river discharges, *J. of Hydromet*., 583-600, doi:10.1175/2010JHM1211.

Andersson, A., Bakan, S., Fennig, K., Grassl, H., Klepp, C. and Schulz, J. (2007). Hamburg Ocean Atmosphere Parameters and Fluxes from Satellite Data – HOAPS-3 – monthly mean. *World Data Center for Climate electronic publication*.

Bindoff N. , J. Willebrand, V. Artale, A. Cazenave, J. Gregory, S. Gulev, K. Hanawa, C. Le Quéré, S. Levitus, Y. Nojiri, C.K. Shum, L. Talley, A. Unnikrishnan (2007).Observations: oceanic climate and sea level. In: *Climate change 2007: The physical Science Basis. Contribution of Working Group I to the Fourth Assessment report of the Intergouvernmental Panel on Climate Change* [Solomon S., D. Qin, M. Manning, Z. Chen, M. Marquis, K.B. Averyt, M. Tignor and H.L. Miller (eds.)]. Cambridge University Press, Cambridge, UK, and New York, USA.

Cazenave A. and W. Llovel (2010). Contemporary sea level rise, *Annual Review in Marine Science,* 2, 145-173.

Chambers D. (2011), ENSO-correlated fluctuations in ocean bottom pressure and wind-stress curl in the North Pacific, *Ocean Dynamics*, 8, 1631-1655.

Church, J.A., N.J. White, L.F. Konikow, C.M. Domingues, J.G. Cogley, E. Rignot, J.M. Gregory, M.R. van den Broeke, A.J. Monaghan, and I. Velicogna (2011). Revisiting the Earth's sea‐level and energy budgets from 1961 to 2008, *Geophys. Res. Lett.*, 38, L18601, doi:10.1029/2011GL048794.

Curtis S; and Adler R.F. (2003), Evolution of El Nino-precipitation relationships from satellites and gauges, *J. Geophys. Res*., 108, 4153, doi:10.1029/2002JD002690.

Dai A. and Wigley T.M.L (2000), Global patterns of ENSO-induced precipitation, *Geophys. Res. Lett.*, 27, 9, 1283-1286.

Decharme B., and H. Douville (2006). Introduction of a sub-grid hydrology in the ISBA land surface model. *Climate Dyn*., **26**, 65–78.

England M. and F. Huang (2005). On the interannual variability of the Indonesian throughflow and its linkage with ENSO, *J. Clim*., 18, 1435-1444.

Giannini A, Chiang JCH, Cane MA, Kushnir Y, Seager R (2001) The ENSO teleconnection to the tropical Atlantic Ocean: contributions of the remote and local SSTs to rainfall variability in the tropical Americas, *J Clim*, 14, 4530–4544.

Godfrey J.S. (1996) The effect of the Indonesian throughflow on ocean circulation and heat exchange with the atmosphere: A review, *J. Geophys. Res*., 101, C5, 12,217-12,237.

Gordon, A.L., R.D. Susanto, and A.L. Field (1999) Throughflow within Makassar Strait. *Geophys. Res. Lett*., 26(21): 3325-3328.

Gordon A.L. (2005) Oceanography of the Indonesian seas and their throughflow, *Oceanography*, 18, n°4, 14-27.

Gordon, A. L.; R. D. Susanto; A. Ffield; B. A. Huber; W. Pranowo; S. Wirasantosa (2008) "Makassar Strait Throughflow, 2004 to 2006", *Geophys. Res. Letters*, 35, L24605, doi:10.1029/2008GL036372.

Gordon, A.L., Sprintall, J., Van Aken, H.M., Susanto, D., Wijffels, S., Molcard, R., Ffield, A., Pranowo, W., Wirasantosa, S. (2010) "The Indonesian Throughflow during 2004-2006 as observed by the INSTANT program." "Modeling and Observing the Indonesian Throughflow",

Guest Editors: A. L. Gordon and V.M. Kamenkovich, Dynamics of Atmosphere and Oceans vol(50) 115-128

Gordon, A. L., B. A. Huber, E. J. Metzger, R. D. Susanto, H. E. Hurlburt, T. R. Adi (2012) "South China Sea Throughflow Impact on the Indonesian Throughflow", *Geophys. Res. Lett.* (in revision).

Gu G., Adler R.F., Huffman G.J., and Curtis S. (2007), Tropical rainfall variability on interannual to interdecadal and longer time scales derived from the GPCP monthly products, *J. Climate*, , 20, 4033-4046.

Gu G. and Adler R.F. (2011), Precipitation and temperature variations on the interannual time scale : assessing the impact of ENSO and volcanic eruptions, *J. Climate*, 24, 2258-2270.

Huang BY, Mehta VM, Schneider N. (2005) Oceanic response to idealized net atmospheric freshwater in the Pacific at the decadal time scale. *J. Phys. Oceanography*, 35(12):2467–2486. doi:10.1175/JPO2820.1.

Ishii M and Kimoto M. (2009), Reevaluation of historical ocean heat content variations with varying XBT and MBT depth bias corrections, *Journal of Oceanography,* 65, 287-299.

Kalnay, E., Kanamitsu, M., Kistler, R., Collins, W., Deaven, D., Gandin, L., Iredell, M., Saha, S., White, G., Woollen, J., Zhu, Y., Chelliah, M., Ebisuzaki, W., Higgins, W., Janowiak, J., Mo, K.C., Ropelewski, C., Wang, J., Leetmaa, A., Reynolds, R., Jenne, R. and Joseph, D. (1996). The NCEP/NCAR 40-year reanalysis project. *Bulletin of the American Meteorological Society* 77, 437–471.

Levitus S, Antonov JI, Boyer TP, Locarnini RA, Garcia HE, Mishonov AV, (2009) Global ocean heat content 1955–2008 in light of recently revealed instrumentation problems. *Geophys Res Lett*, 36:L07608. doi:10.1029/2008GL037155.

Llovel W,Becker M,Cazenave A,Jevrejeva S,Alkama R,Decharme B, Douville H,Ablain M and Beckley B. (2011a). Terrestrial waters and sea level variations on interannual time scale, *Global Planet. Change*, 75, 76-82. doi:10.1016/j.gloplacha.2010.10.008.

Llovel W., Meyssignac B. and Cazenave A., (2011b), Steric sea level variations over 2004-2010 as a function of region and depth: inference on the mass component variability of the North Atlantic, *Geophys. Res. Lett*., 38, L15608, doi: 101029/2011GL047411.

Neelin J.D., Chou C. and Su H. (2003), Tropical drought regions in global warming and El Nino teleconnections, *Geophys. Res. Lett*., 30, 2275, doi:10.1029/2003GL018625.

Nerem, R. S., D. P. Chambers, C. Choe, and G. T. Mitchum (2010), Estimating Mean Sea Level Change from the TOPEX and Jason Altimeter Missions, *Marine Geodesy*, 33 (1), . 435-446.

Oki T. and Y. C. Sud (1998). Design of Total Runoff Integrating Pathways (TRIP)- A global river channel network. *Earth Interactions*, **2**. Issue 1, 1-37.

Preisendorfer R W (1988) Principal Component Analysis in Meteorology and Oceanography. Vol. 17, Developments in Atmospheric Science, Elsevier, Amsterdam.

Sahoo A. K., M. Pan, T. J. Troy, R. K. Vinukollu, J. Sheffield and E. F. Wood (2011), Reconceiling the global terrestrial water budget using satellite remote sensing, in press, *Remote Sensing of Environment*.

Simmons A., Uppala S.,Dee D. , and Kobayashi S. (2007), Era-interim: New ECMWF reanalysis products from 1989 onwards. ECMWF, Newsletter 110 - Winter 2006/07.

Smith T.M., Yin X. And Gruber A. (2006), Variations in annual global precipitation (1979-2004), based on the Global Preipitation Climatology Project 2.5° analysis, *Geophys. Res. Lett*., 33, L06705, doi: 10.1029/2005GL025393.

Susanto, R. D. and A. L. Gordon (2005). Velocity and Transport of the Makassar Strait Throughflow. *J. Geophys. Res*., 110, Jan C01005, doi:10.1029/2004JC002425.

Syed, T. H., J. S. Famiglietti and D. P. Chambers (2009), GRACE-Based Estimates of Terrestrial Freshwater Discharge from Basin to Continental Scales, Journal of *Hydrometeorology*, 10, 22-40.

Trenberth K.E., Caron J.M., Stepaniak D.P. and Worley S., (2002), Evolution of El Nino-Southern Oscillation and global atmospheric surface temperatures, *J. Geohpys. Res*., 107, 4065, doi:10.1029/2000JD000298.

Vranes K. and A.L. Gordon (2005). Comparison if Indonesian Troughflow Transport observations, Makassar Strait to eastern Indian Ocean, *Geophys. Res. Lett*., 32, L10606, doi:10.1029/2004GL022158.

Wolter, K., and M.S. Timlin (1998) Measuring the strength of ENSO - how does 1997/98 rank? *Weather*, 53, 315-324

Xie, P.P. and Arkin, P.A. (1997). Global precipitation: A 17-year monthly analysis based on gauge observations, satellite estimates, and numerical model outputs. *Bulletin of the American Meteorological Society* 78, 2539–2558.

Yu, L. and Weller, R.A., 2007. Objectively analyzed air-sea heat fluxes for the global ice-free oceans (1981-2005). *Bull. Amer. Meteorol. Soc*. 88, 527-+.

2.2 Durant les dernières décennies : depuis 1950

2.2.1 Les estimations du niveau de la mer en 2 dimensions depuis 1950 par les modèles d'océan

Les mesures précises du niveau de la mer faites par les satellites altimétriques remontent au mois d'octobre 1992. Avant cette date, les seules mesures précises dont on dispose proviennent des marégraphes. L'échantillonage spatial des mesures du niveau de la mer avant 1993 est donc extrêmement peu dense comparé à aujourd'hui. De plus pour des raisons historiques, cet échantillonnage est largement biaisé vers l'hémisphère Nord et présente très peu de mesures dans l'hémisphère Sud (voir section 1.2.1). Il est donc impossible d'obtenir une estimation raisonnable du niveau de la mer en 2 dimensions pour les dernières décennies sur la base des seules données marégraphiques.

Pour contourner ce problème, une première approche, consiste à analyser les sorties des modèles de circulation océanique (OGCM). Deux types d'OGCM permettent d'estimer la circulation océanique des dernières décennies : les modèles forcés par une réanalyse atmosphérique comme le modèle DRAKKAR (*Bernard et al.* [2006]; *Dussin et al.* [2009]; *Penduff et al.* [2010]) ou les modèles qui assimilent des données océaniques (réanalyses océaniques), comme SODA (*Carton and Giese* [2008]), MERCATOR-GLORYS2V1 (*Ferry et al.* [2011]) ou ORAS4 (réanalyse océanique de l'ECMWF, *Balmaseda et al.* [2008]). Les modèles d'océan et les réanalyses déduisent le niveau de la mer en 2 dimensions de la somme des composantes thermostériques et halostériques de chaque colonne d'eau auxquelles s'ajoute une petite composante barotrope locale (qui se calcule à partir des variations de la pression au fond de l'océan). Ceci permet de déterminer une estimation des composantes thermostériques et halostériques du niveau de la mer en 2-D dans le passé, cohérente d'une part avec les équations de Navier - Stokes et d'autre part avec le forçage atmosphérique imposé au modèle pour les OGCM forcés ou avec les données assimilées (température, salinité, niveau de la mer, etc...) pour les réanalyses.

Les OGCM différent principalement entre eux par leur schéma d'intégration des équations de Navier et Stokes, leur résolution spatiale et temporelle et leur forçage atmosphérique. Les réanalyses peuvent en plus différer par leur schéma d'assimilation (3DVAR, interpolation optimale ou séquentiel) et par les jeux de données qu'ils assimilent. DRAKKAR et MERCATOR-GLORYS2V1 utilisent le modèle d'équation de Navier et Stokes NEMO (*Madec* [2008]) tandis que SODA est basé sur POP (*Carton and Giese* [2008]) et ORAS sur HOPE (*Wolff et al.* [1997]). Les résolutions spatiales sont aussi différentes, allant du $1/4^\circ$ pour DRAKKAR et MERCATOR-GLORYS2V1, à 1° pour ORAS4 en horizontal et de 75 niveaux verticaux pour DRAKKAR et MERCATOR-GLORYS2V1 à 29 pour ORAS4. En revanche les différents modèles utilisent souvent un forçage atmosphérique basé sur ERA-40 (SODA, ORAS4 et DRAKKAR) corrigé de plusieurs biais (en particulier dans les précipitations) car il a l'avantage de couvrir de manière homogène une longue période : 1958-2002. Sur la periode récente (depuis 1979), la réanalyse atmosphérique ERA interim est une alternative utilisée par MERCATOR-GLORYS2V1 par exemple. Enfin les réanalyses assimilent des profils de température et de salinité issus des bases de données hydrographiques (e.g. *Boyer et al.* [2009]; *Ingleby and Huddleston* [2007]) ainsi que des données de température de surface de l'océan issues

des observations spatiales : c'est le cas de SODA, ORAS et MERCATOR-GLORYS2V1. Certaines réanalyses assimilent aussi les données altimétriques depuis octobre 1992 comme MERCATOR-GLORYS2V1 et ORAS.

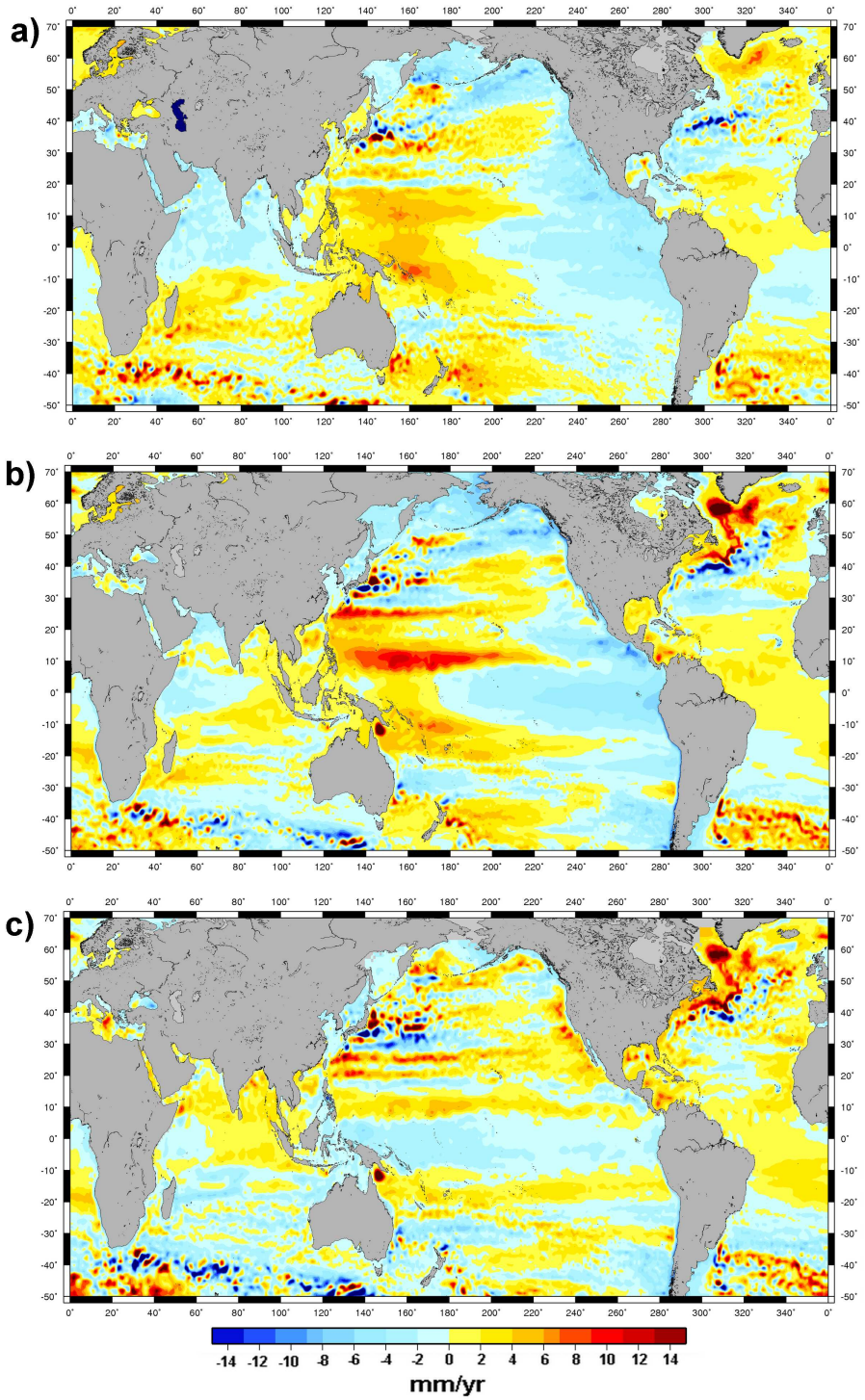

Figure 2.4 – a) Tendances du niveau de la mer observé par altimétrie sur la période 1993-2007. La tendance globale de 3.2 mm.a^{-1} a été retirée. b) Tendances du niveau de la mer modélisées par DRAKKAR dans le run ORCA025-B83 sur la période 1993-2007. La tendance globale de 3.2 mm.a^{-1} a été retirée. c) Différence entre la Fig. 2.4.b et la Fig. 2.4.a.

Sur la période altimétrique, les OGCM forcés et les réanalyses reproduisent les grandes structures des tendances du niveau de la mer observées ainsi que la variabilité inter-annuelle (voir *Lombard et al.* [2009] et Fig. 2.4a,b pour DRAKKAR, *Carton et al.* [2005] pour SODA). Ils confirment sur cette période, l'origine thermostérique de la variabilité régionale du niveau de la mer et le rôle prédominant joué par le vent dans la redistribution de la chaleur dans l'océan. Régionalement, l'accord des OGCM forcés et des réanalyses avec l'altimétrie est moins bon. Dans les hautes latitudes, et les régions où la circulation est particulièrement complexe (comme autour de l'arc Indonésien par exemple), les modèles ne parviennent pas encore à représenter le niveau de la mer tel qu'il est observé depuis 1993 (voir par exemple Fig.2.4 pour DRAKKAR).

Avant 1993, les modèles et les réanalyses s'accordent encore globalement sur les grandes structures de la variabilité régionale du niveau de la mer (comparer par exemple les tendances du niveau de la mer modélisées par DRAKKAR dans le run ORCA025-B83 sur la période 1958-2007, Fig. 2.6a, avec les tendances de SODA pour la même période, Fig. 2.6b). Cependant, ils présentent aussi des différences importantes en régional quand on les compare entre eux (voir Fig.2.6c) ou avec les observations marégraphiques (voir par exemple Fig.2.5 pour la réanalyse ORAS4). Ceci est dû au fait que plus on remonte dans le passé, plus les données atmosphériques ou océaniques sont rares et moins précises. Les forçages imposés aux OGCM sont donc de moins bonne qualité et les reanalyses bénéficient de moins de données à assimiler. De plus, l'état de l'océan dans les années 1950, utilisé pour initialiser les simulations, est aussi mal connu.

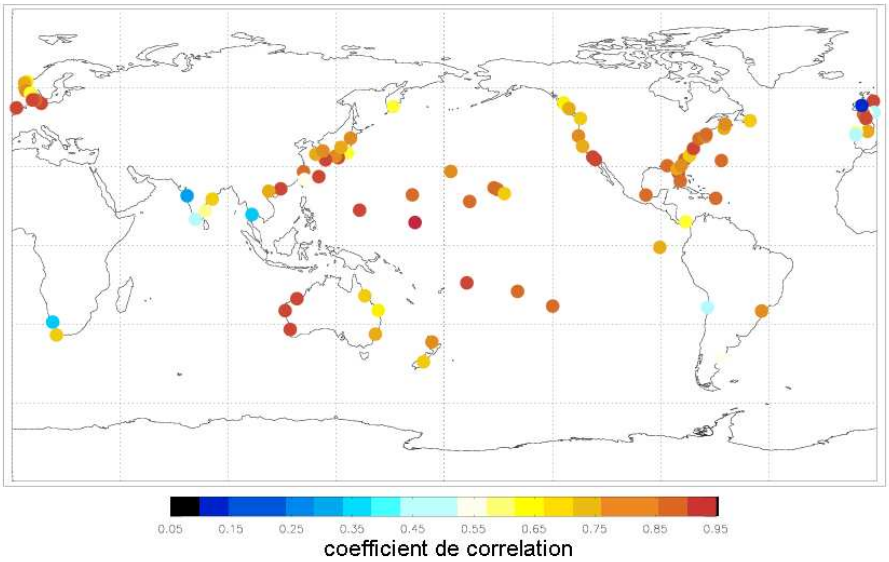

Figure 2.5 – Correlation entre la réanalyse ORAS4 de ECMWF avec une selection de 99 marégraphes répartis sur le globe. La corrélation est calculée sur la période 1960-2009.

En résumé, les OGCM forcés et les réanalyses s'accordent pour montrer que sur les 60 dernières années, les structures de la variabilité régionale du niveau de la mer sont très différentes de celles que l'on observe sur la période altimétrique et qu'elles sont 3 à 4 fois plus faibles en terme de tendance. Ils montrent aussi que, sur cette période, c'est la contribution thermostérique, modulée par le vent, qui explique la variabilité régionale du niveau de la mer (*Köhl and Stammer* [2008]) en particulier dans l'océan Pacifique

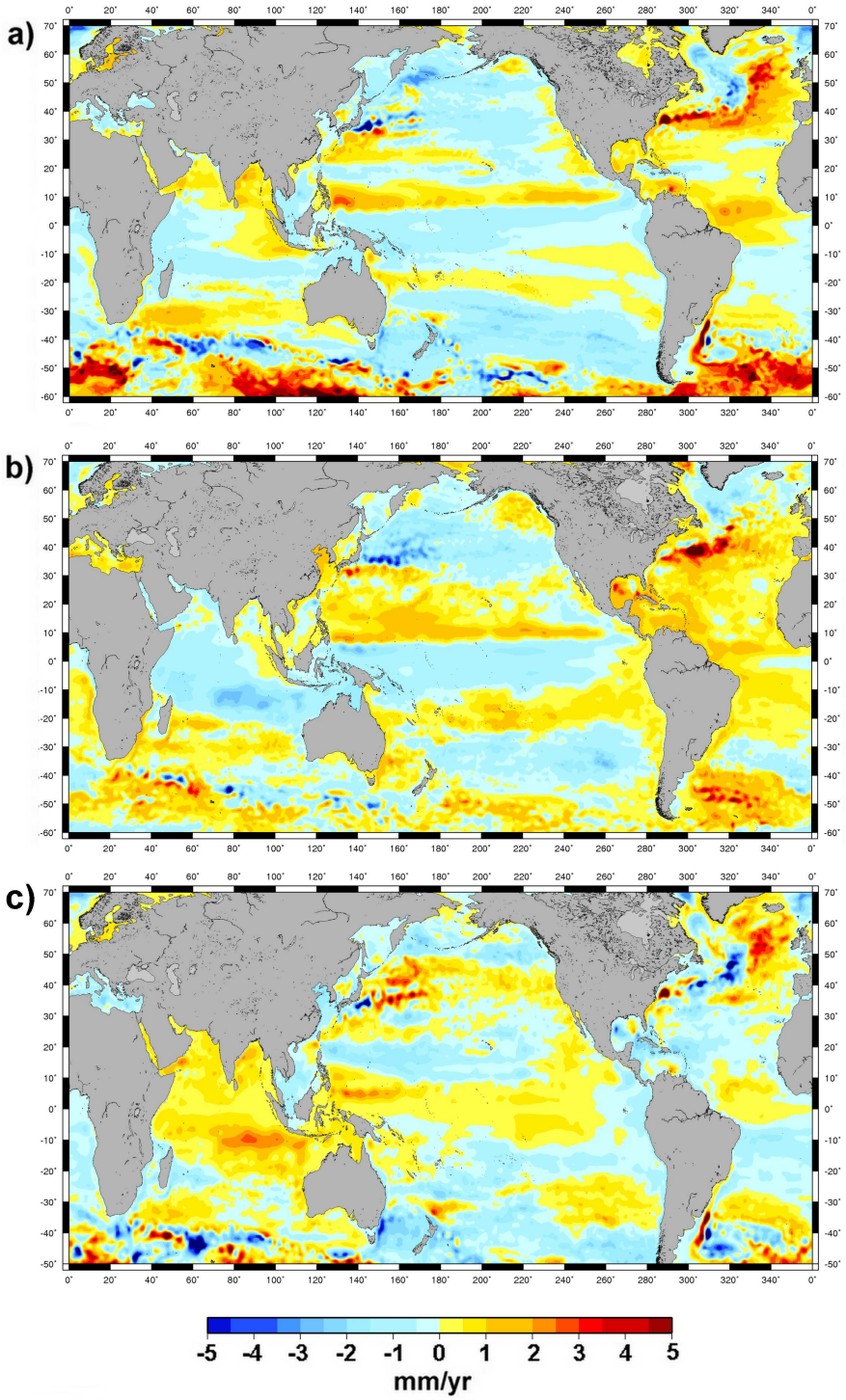

Figure 2.6 – a) Tendances du niveau de la mer modélisées par DRAKKAR (run ORCA025-B83) sur la période 1958-2007. b) Tendances du niveau de la mer modélisé par SODA sur la période 1958-2007. c) Différence entre la Fig. 2.6a et la Fig. 2.6b. Les tendances globales ont été retirées.

(*Timmermann et al.* [2010]) et l'océan Indien (*Han et al.* [2010]). En régional, sur les 60 dernières années, on trouve encore de forte différences entre les modèles mais aussi entre les modèles et les mesures marégraphiques.

2.2.2 Les méthodes de reconstruction basées sur les fonctions empiriques orthogonales

Depuis quelques années, il existe une autre approche pour calculer les variations du niveau de la mer en 2 dimensions au cours des dernières décennies. Celle-ci s'appuie sur les données marégraphiques et d'autres informations venant de l'altimétrie ou des OGCMs. Cette approche que l'on nomme "reconstruction", combine l'information des enregistrements marégraphiques avec les structures spatiales du niveau de la mer déduites de l'altimétrie ou des OGCM (e.g. *Chambers et al.* [2002]; *Church et al.* [2004]; *Berge-Nguyen et al.* [2008]; *Llovel et al.* [2009]; *Church and White* [2011]; *Hamlington et al.* [2011]; *Ray and Douglas* [2011]; *Meyssignac et al.* [2012]). Contrairement à l'approche basée sur les sorties de modèles d'océan ou de réanalyses, les reconstructions ne permettent pas de séparer les composantes thermostériques et halostériques du niveau de la mer. En revanche, comme elles intègrent des mesures marégraphiques, elles apportent en théorie, plus d'information sur la variabilité régionale. En principe, elles devraient permettre de reconstruire la variabilité régionale du niveau de la mer complète, i.e avec les contributions stériques et non-stériques (dûes aux variations de masse de l'océan) au niveau de la mer. En ce sens, cette approche est complémentaire de la précédente.

La méthode de reconstruction du niveau de la mer en 2 dimensions :

Les reconstructions du niveau de la mer s'appuient sur la méthode d'interpolation optimale développée par *Kaplan et al.* [1998, 2000]. Au cours de ma thèse j'ai développé une telle méthode. Elle consiste à utiliser des EOFs représentatives des modes principaux de la variabilité du niveau de la mer, pour interpoler spatialement les enregistrements marégraphiques. Ceci permet d'obtenir, en sortie, le niveau de la mer en 2 dimensions sur toute la période couverte par les marégraphes utilisés. La méthode se décompose en 2 étapes.

La première étape consiste à calculer les modes spatiaux principaux de variabilité du niveau de la mer. Ces modes principaux sont typiquement par exemple la composante spatiale des EOF du niveau de la mer (on pourrait aussi prendre la composante spatiale des CEOF du niveau de la mer comme *Hamlington et al.* [2011] ou encore n'importe quel autre jeu de vecteurs spatiaux linéairement indépendants et représentatifs des modes de variabilité principaux du niveau de la mer). Ils sont calculés à partir de champs de hauteur de mer spatialement bien résolus comme par exemple les données altimétriques ou les sorties d'OGCM. Supposons que ce champ de hauteur soit décrit par les valeurs temporelles de hauteur de mer en m points géographiques $(x_1, ..., x_m)$, à n dates distinctes $(t_1, ..., t_n)$. Nous l'appelons $Z = Z(x_1, ..., x_m, t_1, ..., t_n) = Z(x, t)$ et nous l'écrivons sous la forme d'une matrice de $\mathbb{R}(m, n)$ dans laquelle chacune des m lignes est la série temporelle de hauteur de mer en x_m aux dates $t_1, ..., t_n$:

$$Z(x,t) = \begin{pmatrix} z(x_1,t_1) & ... & z(x_1,t_n) \\ \vdots & \ddots & \vdots \\ z(x_m,t_1) & ... & z(x_m,t_n) \end{pmatrix}$$

La décomposition en EOF de Z correspond à sa décomposition en valeurs singulières. Elle sépare Z en mode propre spatiaux U (matrice de $\mathbb{R}(m, m)$), valeurs propres associées L

(matrice diagonale de $\mathbb{R}(m,n)$) et composantes principales V^{t} (matrice de $\mathbb{R}(n,n)$) de la manière suivante :

$$Z(x,t) = U(x).L.V^{\mathrm{t}}(t)$$

Dans cette écriture, U contient la structure spatiale du signal tandis que $L.V^{\mathrm{t}}$ est sa modulation temporelle. Pour être plus précis, la colonne k de U, i.e. $u_k(x_1,...,x_m)$, est le $k$ième mode propre spatial de Z dont la modulation temporelle est la ligne k de $\alpha = L.V^{\mathrm{t}}$, i.e. $\alpha_k(t_1,...,t_n)$. Ainsi Z s'écrit en séparant les variables espace et temps de la manière suivante :

$$Z(x,t) = U(x).\alpha(t) = \sum_{k=1}^{m} u_k(x)\alpha_k(t).$$

Cette écriture de Z permet d'isoler les modes spatiaux principaux de variabilité du niveau de la mer dans le terme U.

Lorsqu'on utilise les sorties d'un OGCM comme champ de hauteur de mer spatialement bien résolus pour faire ce calcul, on s'attend à ce que U (structure spatiale du signal) soit raisonnablement représentatif des modes de variabilité de l'océan car U dépend essentiellement de la physique implémentée. En revanche, α (la modulation temporelle des structures spatiales) est très sensible aux forçages et aux données éventuellement assimilées par l'OGCM. Or ces données présentent de nombreuses incertitudes en particulier quand on remonte dans le temps du fait de l'échantillonnage qui devient mauvais. Pour cette raison on trouve encore des différences significatives entre les OGCM et les données marégraphiques sur les dernières décennies. La méthode de *Kaplan et al.* [1998, 2000] permet dans la deuxième étape de recalculer un nouveau $\alpha(t) = \widetilde{\alpha}(t)$ à partir des données marégraphiques et de reconstruire ainsi un niveau de la mer en 2 dimensions sur les dernières décennies plus cohérent avec les mesures. Il est de la forme :

$$\widetilde{Z}(x,t) = U(x).\widetilde{\alpha}(t). \tag{2.1}$$

Lorsqu'on utilise l'altimétrie comme champ de hauteur de mer spatialement bien résolu pour faire le calcul des modes principaux de variabilité du niveau de la mer, le problème est différent. Dans ce cas U et α sont, bien sûr, cohérents avec les mesures mais α couvre une periode plus courte (1993-2011) que celle sur laquelle nous cherchons à estimer la variabilité régionale (dernières décennies). La méthode de *Kaplan et al.* [1998, 2000] permet de recalculer à partir des données marégraphiques (dans la deuxième étape) un nouveau $\alpha(t) = \widetilde{\alpha}(t)$ qui couvre toute la période des marégraphes. En ce sens la méthode de *Kaplan et al.* [1998, 2000] permet d'"étendre" les données altimétriques dans le passé sur les dernières décennies. Le niveau de la mer 2D "étendu" ou reconstruit sur les dernières décennies prend aussi la forme de $\widetilde{Z}$ de l'équation 2.1.

Comment calcule-t-on $\widetilde{\alpha}$ pour déduire le niveau de la mer reconstruit ? Dans la deuxième étape de la méthode de *Kaplan et al.* [1998, 2000], le calcul de $\widetilde{\alpha}$ se fait avec les données marégraphiques. Nous disposons en général d'un petit nombre de marégraphes (au plus quelques centaines) répartis autour du globe. Appelons E le petit sous ensemble des points géographiques $(x_1,...,x_m)$ pour lesquels nous avons un enregistrement marégraphique et $\widetilde{Z}_E(t)$ le champ de hauteur de la mer en ces points aux dates couvertes par les marégraphes. De fait, nous cherchons $\widetilde{\alpha}(t)$ afin de déterminer le champ reconstruit $\widetilde{Z}(x,t) = U(x).\widetilde{\alpha}(t)$

et nous connaissons seulement $\widetilde{Z}(x \in E, t) = \widetilde{Z}_E(t)$. Le meilleur $\widetilde{\alpha}(t)$ que nous pouvons calculer est donc celui qui donne le $\widetilde{Z}(x,t)$ le plus proche de $\widetilde{Z}_E(t)$ sur le sous ensemble E. Au sens des moindres carré il s'agit de celui qui minimise la distance entre $\widetilde{Z}_E(t)$ et la projection de $\widetilde{Z}(x,t)$ sur E. C'est le $\widetilde{\alpha}$ qui minimise la fonction suivante :

$$S(\widetilde{\alpha}) = \|H.U.\widetilde{\alpha} - Z_E\|^2 = (H.U.\widetilde{\alpha} - Z_E)^{\mathrm{t}}.(H.U.\widetilde{\alpha} - Z_E)$$

où H est la matrice de projection de $(x_1, ..., x_m)$ sur E. La solution de ce problème de minimisation est bien connue et nous donne l'expression de $\widetilde{\alpha}$:

$$\widetilde{\alpha}(t) = (U^{\mathrm{t}}.H^{\mathrm{t}}.H.U)^{-1}.U^{\mathrm{t}}.H^{\mathrm{t}}.Z_E$$

De cette expression nous déduisons directement le niveau de la mer 2D reconstruit. Il prend la forme suivante :

$$\widetilde{Z}(x,t) = U.(U^{\mathrm{t}}.H^{\mathrm{t}}.H.U)^{-1}.U^{\mathrm{t}}.H^{\mathrm{t}}.Z_E$$

Les variantes de la méthode que l'on trouve dans la littérature :

Dans la littérature, les champs de hauteur de mer spatialement bien résolus utilisés dans les reconstructions viennent de l'altimétrie ou d'un OGCM. Ces champs sont corrigés des corrections usuelles (marées, baromètre inverse, etc). De plus à chaque série temporelle est enlevée sa moyenne sur une période fixe afin d'obtenir les variations du niveau de la mer par rapport à une surface moyenne de la mer (que l'on assimile au géoïde). Les séries temporelles corrigées de cette moyenne sont appelées anomalies de hauteur de mer (sea level anomaly -SLA- en anglais). C'est à partir de ces SLA que les méthodes de reconstructions sont appliquées. Il existe quelques nuances entre les différentes reconstructions que nous avons résumées sur la Fig. 2.7.

Le schéma de reconstruction le plus répandu (*Chambers et al.* [2002]; *Berge-Nguyen et al.* [2008]; *Llovel et al.* [2009]; *Hamlington et al.* [2011]) est celui qui consiste tout d'abord à soustraire aux SLA la tendance moyenne globale du niveau de la mer observée et ensuite à suivre la méthode de *Kaplan et al.* [1998, 2000] décrite plus haut. Nous appelons cette méthode la méthode A (voir Fig. 2.7). Dans certains cas (e.g. *Chambers et al.* [2002]), la méthode de *Kaplan et al.* [1998, 2000] est appliquée directement aux SLA sans en soustraire auparavant la tendance moyenne (ceci est fait en particulier pour les études qui ne cherchent pas à reproduire précisement les cartes de tendance du niveau de la mer ni la tendance globale). Il s'agit là d'une nuance de la méthode A que l'on nomme méthode A'.

Il existe un autre schéma de reconstruction (*Church et al.* [2004]; *Church and White* [2011]; *Ray and Douglas* [2011]; *Meyssignac et al.* [2011, 2012]) qui vise en particulier à reconstruire précisément les variations du niveau de la mer global. L'idée de cette variante est d'introduire dans la reconstruction un mode uniforme (que l'on nomme mode 0) qui permet la reconstruction des variations temporelles du niveau global et en particulier sa tendance. Ceci permet d'une part de déterminer précisément la modulation en temps du niveau global et d'autre part cela isole ce signal uniforme des autres modes reconstruits. Ainsi on empêche que ce signal non-orthogonal aux différents EOFs et très fort dans le cas du niveau de la mer (tendance de 3.2 mm.a^{-1} entre 1993-2011) ne se décompose sur l'ensemble des modes et ne pollue la reconstruction. Pour appliquer cette méthode il faut ajouter à la matrice des vecteurs propres spatiaux U, un vecteur uniforme $(1, ..., 1)^{\mathrm{t}}$ pour restituer le

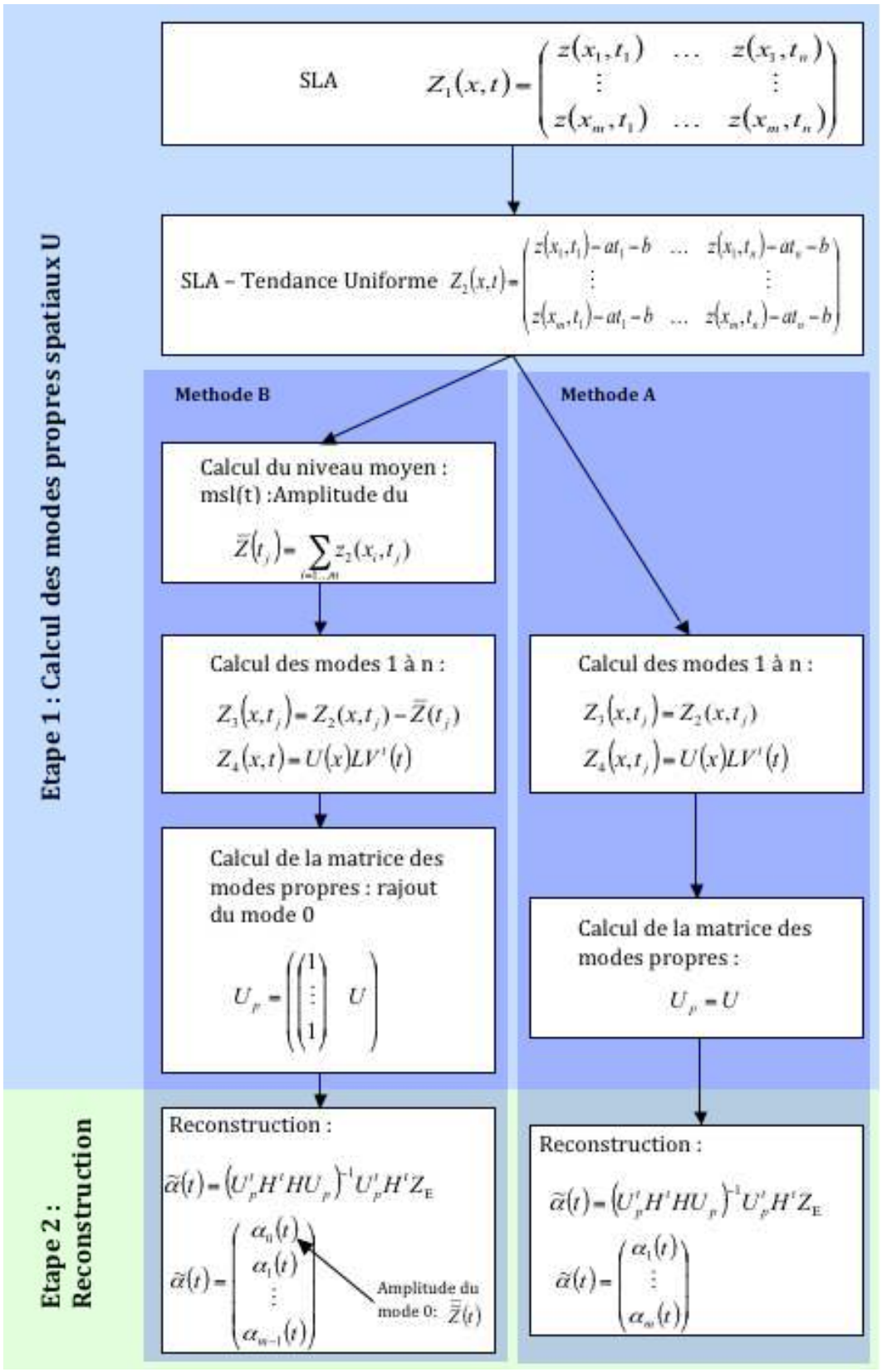

Figure 2.7 – Schéma résumant les différentes techniques de reconstruction 2D du niveau de la mer dans la litterature.

mouvement moyen dans la minimisation par moindre carré : $\widetilde{\alpha}(t) = (U^{\mathrm{t}}H^{\mathrm{t}}HU)^{-1}U^{\mathrm{t}}H^{\mathrm{t}}Z_E$. Cependant, pour s'assurer que les autres modes de la matrice U ne sont pas redondants avec le mode uniforme supplémentaire, il faut les avoir calculés non pas à partir des champs SLA directement (i.e. $Z(x,t)$) mais à partir des champs SLA auxquels on a soustrait le niveau moyen global (i.e. $Z(x,t) - \overline{Z}(t)$). Le détail des calculs est donné dans la Fig. 2.7. Dans la suite, on appelle cette méthode la méthode B. Sa variante qui s'applique directement sur les SLA au lieu de s'appliquer sur les SLA privé de leur tendance moyenne est appelée méthode B'.

Historique des reconstructions 2D du niveau de la mer :

Kaplan et al. [1998, 2000] développèrent leur méthode pour reconstruire dans le passé les températures de surface de l'océan à partir des donnés satellites et des nombreuses données in-situ qui remontent jusqu'au XIX$^{\text{ème}}$ siècle. *Chambers et al.* [2002] furent les premiers à proposer une adaptation de cette méthode au niveau de la mer pour reconstruire les basses fréquences du niveau de la mer global jusqu'en 1952. Dans leur étude, ces auteurs soulignent la difficulté de reconstruire les tendances du niveau de la mer puisqu'il s'agit d'un signal intense avec une importante composante uniforme qui se décompose sur l'ensemble des modes propres spatiaux des EOF et modifie la reconstruction. Pour cette raison, ils ont adopté la methode A' (voir Fig. 2.7) et n'ont pas traité le problème des tendances du niveau de la mer. 2 ans plus tard, *Church et al.* [2004] proposèrent la méthode du mode 0 (méthode B, voir Fig. 2.7) pour isoler dans la reconstruction le niveau de la mer global et sa tendance. Ils proposèrent donc une reconstruction 2D du niveau de la mer complète (avec les tendances) selon la méthode B à partir d'EOFs calculées sur 8 ans d'altimétrie de 1993 à 2001.

Avec la publication de cette première reconstruction du niveau de la mer régional depuis 1950, s'est posé la question de la validité du niveau de la mer reconstruit. Pour être applicable, la méthode de *Kaplan et al.* [1998, 2000] fait une hypothèse forte sur les EOFs utilisés dans l'interpolation spatiale des marégraphes. Elle suppose qu'elles sont représentatives des modes principaux de variabilité du niveau de la mer en 2D sur l'ensemble de la période couverte par les marégraphes (voir equation 2.1) qui est typiquement de 60 ans (1950 à 2010). Mais sur cette période nous manquons d'informations pour connaitre ces principaux modes de variabilité 2D. *Church et al.* [2004] ont utilisé les EOFs du niveau de la mer calculées avec les données altimetriques sur la courte période 1993-2001 (8 ans) pour représenter ces modes de variabilité en supposant que ces modes sont stationnaires au cours du temps et qu'ils peuvent être représentatifs de modes de variabilité plus longs (de l'ordre de 60 ans). C'est une hypothèse très forte et pas forcément valide comme le soulignent *Berge-Nguyen et al.* [2008] et *Llovel et al.* [2009]. Pour cette raison, ces derniers auteurs proposent une nouvelle reconstruction 2D, mais avec des EOFs calculés sur une période plus longue afin de mieux représenter les basses fréquences dans le signal du niveau de la mer. *Berge-Nguyen et al.* [2008] ont utilisé les données hydrographiques in-situ (i.e. l'expansion thermique) sur la période 1950-2003 pour calculer les EOFs en s'appuyant sur l'hypothèse que le niveau de la mer régional est largement dominé par sa composante stérique. *Llovel et al.* [2009] ont utilisé, quant à eux, les sorties SLA d'un OGCM (OPA/CERFACS) sur la période 1960-2003. Dans les 2 cas, ces auteurs ont été forcés d'utiliser la méthode A (voir Fig. 2.7), car la tendance globale des données stériques ou du modèle OGCM est soit faible soit

nulle (par construction pour certains OGCM) en comparaison avec la tendance globale du niveau de la mer sur les dernières décennies.

L'utilisation d'EOFs plus longs par *Berge-Nguyen et al.* [2008]; *Llovel et al.* [2009] a donné des résultats significativement différents de ceux de *Church et al.* [2004] comme le montrent *Ray and Douglas* [2011]. Ceci a soulevé des interrogations sur la fiabilité des reconstructions 2D du niveau de la mer et a remis en question les estimations de la variabilité régionale du niveau de la mer dans le passé (question n°6 de la section 1.5). De plus, comme cette question se trouvait remise en cause, cela jetait aussi le doute sur toutes les questions scientifiques attenantes, comme celles qui concernent la variabilité multi-décennale des structures spatiales du niveau de la mer (questions n°7, 8, 9) ou les impacts de la montée du niveau de la mer à l'échelle climatique (question n°21, 22, 28, 29).

Pour faire le point sur ce problème, nous avons comparé, de manière homogène, les différentes méthodes de reconstructions existantes afin d'évaluer leurs performance en terme d'estimation de la variabilité régionale du niveau de la mer dans le passé. Nous avons aussi développé l'utilisation de la méthode B dans le cas des reconstructions basées sur OGCM pour les améliorer. Enfin nous avons proposé une nouvelle reconstruction 2D moyenne. C'est le sujet de l'article : "An Assessment of Two-Dimensional Past Sea Level Reconstructions Over 1950-2009 Based on Tide-Gauge Data and Different Input Sea Level Grids"

Résumé de l'article : "An Assessment of Two-Dimensional Past Sea Level Reconstructions Over 1950-2009 Based on Tide-Gauge Data and Different Input Sea Level Grids" (l'article original est inséré à la fin de cette section 2.2) :
Dans cette étude, nous comparons 3 méthodes de reconstruction du niveau de la mer sur la période 1950-2010. Les 3 méthodes utilisent le même processus de reconstruction (la méthode B, voir Fig. 2.7) et le même jeu de 91 marégraphes répartis sur le globe avec 60 ans de données de 1950 à 2010. Mais chacune utilise des données différentes de niveau de la mer pour le calcul des EOFs : la première utilise le modèles d'océan forcé DRAKKAR (run ORCA025-B83 sur la période 1958-2007), la seconde utilise la réanalyse SODA (version 2.0.2 qui couvre la période 1958-2007) et la troisième utilise l'altimétrie de 1993 à 2009. Avec la reconstruction basée sur DRAKKAR, nous testons d'abord l'influence du nombre et de la longueur des EOFs utilisés sur le niveau de la mer reconstruit. En comparant avec des marégraphes non utilisés dans la reconstruction, nous montrons que les meilleurs résultats sont obtenus quand on utilise environ 15 EOFs (entre 10 et 20) de la longueur la plus grande possible (i.e. 40 ans au moins pour les modèles d'océan et 17 ans pour l'altimétrie). Sur cette base nous comparons les 3 méthodes. Elles font apparaitre des résultats similaires en ce qui concerne la reconstruction du niveau de la mer global entre 1950 et 2010. De même, la variabilité régionale reconstruite est similaire pour les 3 méthodes dans les tropiques. En revanche nous trouvons des différences significatives aux moyennes et hautes latitudes. La variabilité régionale reconstruite apparait donc très sensible au choix des données utilisées pour le calcul des EOFs. Il est donc difficile de se fier à l'une ou l'autre reconstruction. Seule la comparaison locale avec des marégraphes non utilisés dans la reconstruction permet, lors d'études régionales, de déterminer celle qui présente les meilleures performances. Nous proposons aussi, comme cela se fait généralement avec les modèles de climat, une reconstruction moyenne en calculant la moyenne des 3 reconstructions basées sur DRAKKAR, SODA et l'altimétrie. Comme pour les modèles de climat, cette reconstruction moyenne a l'avantage d'atténuer les défauts majeurs de chaque recon-

struction et de représenter le signal qui fait consensus entre les 3 reconstructions. Une piste pour obtenir une meilleure reconstruction serait de faire la moyenne d'un grand nombre de reconstructions basées sur différents modèles et réanalyses.

En résumé, cet article apporte de nouveaux éléments de réponse à la question scientifique n°6 sur l'estimation de la variabilité régionale du niveau de la mer dans le passé. Tout d'abord il montre que les 8 ans d'altimétrie utilisés par *Church et al.* [2004] sont trop courts pour permettre de reconstruire les basses fréquences du niveau de la mer, il faut au moins 15 ans de données. Ceci explique, en particulier, les différences fortes observées entre les reconstructions de *Church et al.* [2004] et *Llovel et al.* [2009] qui avaient semé le doute sur les reconstructions. De plus, l'article montre que les 17 ans d'altimétrie donnent déjà des résultats comparables à ceux que l'on obtient avec 40 ans d'EOFs calculés à partir d'OGCM (avec la méthode B). Ceci réconcilie en partie les résultats obtenus par les différentes méthodes de reconstruction 2D. En ce sens, la question de l'utilisation des OGCM ou de l'altimetrie dans les reconstructions 2D, n'est pas tranchée par cette étude. Il apparait que les deux méthodes présentent des avantages et seule la comparaison locale avec des marégraphes permet de déterminer la meilleure méthode sur une région donnée. Mais les différences sont faibles et plutôt que de chercher à départager les 2 méthodes, l'article propose une nouvelle voie pour répondre à la question scientifique n°6. Cette voie consiste à moyenner un grand nombre de reconstructions faites avec des EOFS à partir d'observations et d'OGCM pour bénéficier des avantages de chaque méthode. La première solution proposée à la fin de l'article (basée sur seulement 3 reconstructions) est prometteuse.

La technique de reconstruction 2D appliquée à un autre problème :

On a utilisé jusqu'ici la méthode de reconstruction pour estimer le niveau de la mer en 2 dimensions à partir de données historiques avec une faible densité spatiale (les marégraphes). Mais cette méthode peut se généraliser à toute autre variable pour laquelle on dispose aussi d'un jeu de données historiques éparses. *Kaplan et al.* [1998], par exemple, a utilisé une méthode similaire pour reconstruire en 2D les températures de surface de l'océan à partir des données historiques XBT, CTD et des EOFs déduites des mesures satellites. *Smith et al.* [1998]; *Kaplan et al.* [2000] ont reconstruit de la même manière les champs de pression à la surface de la mer sur le Pacifique tropical et en global. Dans un article récent intitulé "Past terrestrial water storage (1980-2008) in the Amazon Basin reconstructed from GRACE and in situ river gauging data", nous proposons d'appliquer aussi cette méthode pour reconstruire en 2 dimensions les variations du stock d'eau du bassin Amazonien entre 1980 et 2008.

Résumé de l'article : "Past terrestrial water storage (1980-2008) in the Amazon Basin reconstructed from GRACE and in situ river gauging data".(l'article original est inséré à la fin de cette section 2.2) :
Le bassin Amazonien joue un rôle important dans le cycle global de l'eau et dans les variations du niveau de la mer. En effet, *Llovel et al.* [2010b] ont montré que les variations inter-annuelles du niveau de la mer global s'expliquaient par la somme des variations des stocks d'eau des 32 plus grands bassins fluviaux du monde (voir section 1.3.2b). Parmi eux, l'Amazone joue un rôle prépondérant. A lui seul, il explique une large part de l'interannualité dans le niveau de la mer global entre 1993 et 2005. Dans cet article nous proposons

une reconstruction en 2 dimensions du stock d'eau du bassin Amazonien entre 1980 et 2008. Pour cela nous utilisons, d'une part, 30 ans de données in-situ de 58 stations réparties sur le bassin Amazonien qui mesurent le niveau local des fleuves. *Xavier et al.* [2010] ont montré que, à un facteur multiplicatif prés, ces enregistrements sont cohérents avec les mesures de GRACE du stock d'eau local intégré sur la verticale (humidité des sols + eau de surface + eau souterraine). Ainsi après redimensionnement, les stations in-situ fournissent 30 ans d'enregistrements du stock d'eau local en 58 endroits de l'Amazone. D'autre part nous utilisons les données GRACE qui fournissent une mesure 2D du stock d'eau du bassin Amazonien depuis 2002. Pour reconstruire le contenu total en eau du bassin Amazonien en 2D, nous interpolons les mesures in-situ avec les EOFs de GRACE calculées entre 2003 et 2008 (selon la méthode de *Kaplan et al.* [1998, 2000]). Ceci donne le stock d'eau du bassin amazonien reconstruit sur 30 ans avec une résolution de 300 km x 300 km en mensuel. La reconstruction ne fait pas apparaitre de tendances à long-terme dans le stock d'eau Amazonien total et elle confirme l'influence dominante des modes ENSO et PDO sur sa variabilité inter-annuelle à multi-décennale. Cette reconstruction, basée uniquement sur des données, est complémentaire des approches classiques d'estimation des stocks d'eau qui se font par bilan hydrologique à l'échelle des bassins. Elle offre de nouvelles perspectives pour la reconstruction en 2D des stocks d'eau des grands bassins fluviaux du monde.

Surv Geophys
DOI 10.1007/s10712-011-9171-x

An Assessment of Two-Dimensional Past Sea Level Reconstructions Over 1950–2009 Based on Tide-Gauge Data and Different Input Sea Level Grids

B. Meyssignac · M. Becker · W. Llovel · A. Cazenave

Received: 8 August 2011 / Accepted: 23 December 2011

Abstract We compare different past sea level reconstructions over the 1950–2009 time span using the Empirical Orthogonal Function (EOF) approach. The reconstructions are based on 91 long (up to 60 years) but sparsely distributed tide-gauge records and gridded sea level data from two numerical ocean models over 1958–2007 (the DRAKKAR/NEMO model without data assimilation and the simple ocean data assimilation ocean reanalysis-SODA-) and satellite altimetry data over 1993–2009. We find that the reconstructed global mean sea level computed over the $\sim$60-year-long time span little depends on the input spatial grids. This is unlike the regional variability maps that appear very sensitive to the considered input spatial grids. Using the DRAKKAR/NEMO model, we test the influence of the period covered by the input spatial grids and the number of EOFs modes used to reconstruct sea level. Comparing with tide-gauge records not used in the reconstruction, we determine optimal values for these two parameters. As suggested by previous studies, the longer the time span covered by the spatial grids, the better the fit with unused tide gauges. Comparison of the reconstructed regional trends over 1950–2009 based on the two ocean models and satellite altimetry grids shows good agreement in the tropics and substantial differences in the mid and high latitude regions, and in western boundary current areas as well. The reconstructed spatial variability seems very sensitive to the input spatial information. No clear best case emerges. Thus, using the longest available model-based spatial functions will not necessarily give the most realistic results as it will be much dependent on the quality of the model (and its associated forcing). Altimetry-based reconstructions

B. Meyssignac (✉) · M. Becker · W. Llovel · A. Cazenave
Laboratoire d'Etudes en Géophysique et Océanographie Spatiale, Toulouse, France
e-mail: benoit.meyssignac@legos.obs-mip.fr

Present Address:
M. Becker
ESPACE-DEV UMR 228 IRD/UM2/UR/UAG, Université Antilles-Guyane, Cayenne, France

Present Address:
W. Llovel
Jet Propulsion Laboratory, Pasadena, CA, USA

Published online: 24 January 2012

(with 17-year long input grids) give results somewhat similar to cases with longer model grids. It is likely that better representation of the sea level regional variability by satellite altimetry compensates the shorter input grids length. While waiting for much longer altimetry records, improved past sea level reconstructions may be obtained by averaging an ensemble of different model-based reconstructions, as classically done in climate modelling. Here, we present such a 'mean' reconstruction (with associated uncertainty) based on averaging the three individual reconstructions discussed above.

Keywords Reconstructed sea level · Tide gauges · Satellite altimetry · Ocean general circulation models · Spatial variability

1 Introduction

Sea level rise is a critical issue of global climate change because of its potential huge impacts on coastal areas (Nicholls 2010). Tide-gauge measurements indicate that, during the twentieth century, the mean rate of sea level rise has been on the order of 1.6–1.8 mm/year (Church and White 2006, 2011; Jevrejeva et al. 2006, 2008; Holgate 2007; Woppelmann et al. 2009; Wenzel and Schroeter 2010; Ray and Douglas 2011). Since the beginning of the 1990s, sea level is measured by high-precision satellite altimetry with global coverage. The satellite observations have shown that sea level does not rise uniformly but displays characteristic spatial trend patterns (see Fig. 1 showing the altimetry-based spatial trend patterns over 1993–2009, with a uniform global mean trend of 3.2 mm/year removed). For example, since early 1993 (the beginning of the high-precision altimetry era), the rate of sea level rise in the western tropical Pacific, southern Ocean and part of the north Atlantic has been 3–4 times faster than the global mean rise of

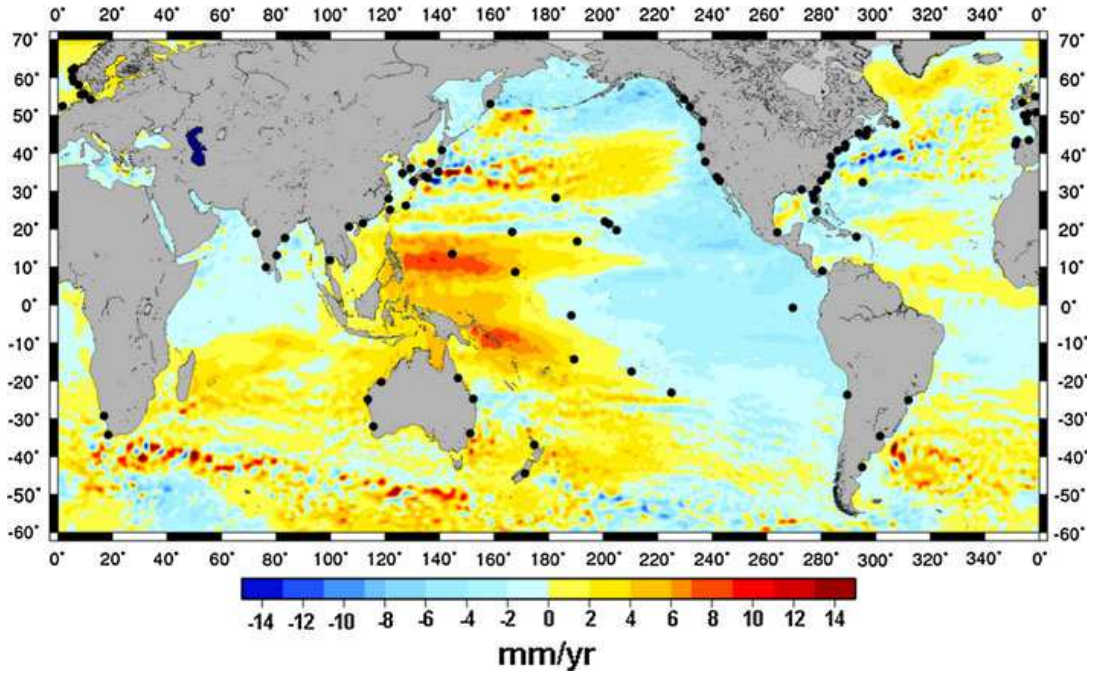

Fig. 1 Spatial trend patterns in sea level from satellite altimetry (1993–2009). A uniform trend of 3.2 mm/year has been removed. Locations of the 91 tide gauges used for the reconstructions are indicated by *black dots*

3.2 ± 0.5 mm/year (Ablain et al. 2009; Nerem et al. 2010). In other regions (e.g., the eastern Pacific), the rate has been slower. These large deviations from the global mean show the importance of estimating and understanding the regional variability of sea level change. This is indeed essential when assessing the potential impacts of sea level rise in coastal areas.

While a number of recent studies focussed on the global mean rise and its causes for the past few decades or altimetry era (e.g., Cazenave and Llovel 2010; Moore et al. 2011; Church et al. 2011), less attention has been given to the regional variability. It is known from previous studies based either on in situ hydrographic data or ocean general circulation models (OGCMs) that the regional variability in sea level is mainly of steric origin (i.e. due to thermal expansion and salinity changes) (Levitus et al. 2005; Lombard et al. 2005; Wunsch et al. 2007; Kohl and Stammer 2008). Other phenomena such as circulation changes due to polar ice melt (Stammer 2008; Stammer et al. 2011) or gravitational effects and visco-elastic response of the solid Earth to last deglaciation and ongoing land ice melt also cause regional variability (e.g., Peltier 2004; Milne et al. 2009; Mitrovica et al. 2009) but corresponding signals are currently smaller than the steric one and have not yet been clearly detected.

It has been shown as well (e.g., Lombard et al. 2005; Levitus et al. 2005; Meyssignac et al. 2011a) that trend patterns in thermal expansion fluctuate with time and space in response to the main modes of variability of the climate system (El Nino-southern Oscillation/ENSO, Pacific Decadal Oscillation/PDO, North Atlantic Oscillation/NAO, Indian Ocean Dipole/IOD, etc.). Thus the high correlation between observed and steric regional variability in sea level over the altimetry era suggests that the altimetry-based spatial trend patterns are not long-lived features, but rather reflect natural modes of ocean variability. Prior to the altimetry era, there is no direct way for measuring globally the regional variability in sea level. However, different approaches can inform about the spatial sea level trend patterns over the last 5–6 decades: (1) Ocean General Circulation Models (OGCMs) and ocean reanalyses (i.e. OGCMs with data assimilation) (e.g., Carton and Giese 2008; Kohl and Stammer 2008) and (2) two-dimensional (2-D) past sea level reconstructions (e.g., Chambers et al. 2002a, b; Church et al. 2004; Berge-Nguyen et al. 2008; Llovel et al. 2009 Church and White 2011; Ray and Douglas 2011; Hamlington et al. 2011). Analysis of corresponding sea level gridded time series can inform on the spatio-temporal variability of past sea level and on the characteristic lifetime of the trend patterns. OGCMs and ocean reanalyses deduce sea level from the sum of the thermosteric (effect of temperature) and halosteric (effect of salinity) components, to which is added a small barotropic component. This allows to follow the temporal behaviour of both temperature and salinity contributions. This is unlike the sea level reconstructions that do not separate these contributions. However, being partly based on tide-gauge observations, the reconstructions may in principle carry more information on the regional variability factors than OGCMs and thus can be viewed as complementary to the latter.

The present study is dedicated to past sea level reconstructions. Its objective is to investigate the influence of the chosen spatial modes used to constrain the reconstruction and the period covered by the corresponding gridded sea level time series. For that purpose, we use three different sea level gridded products (hereafter called input grids) derived from (1) a purely physical ocean circulation model without data assimilation (DRAKKAR/NEMO ocean model, DRAKKAR Group 2007), (2) an ocean reanalysis (SODA, Carton and Giese 2008) and (3) satellite altimetry data. We show that the nature and period of the input spatial grids have strong impact on the reconstructed spatial patterns. Comparison with tide-gauge data not used in the reconstructions leads us to conclude that depending on

the region, some cases perform better than others. But no single case appears to be able to perform better at the planetary scale.

Section 2 describes the reconstruction methodology as used in previous reconstruction studies. Section 3 describes the data and input grids used in this study. Results and discussion are presented in Sects. 4 and 5.

2 Reconstruction Methodology

Several previous studies have developed past (last 50–60 years or last century) sea level reconstructions either globally (e.g., Chambers et al. 2002a, b; Church et al. 2004; Berge-Nguyen et al. 2008; Llovel et al. 2009; Church and White 2011; Hamlington et al. 2011; Ray and Douglas 2011) or regionally (e.g., Calafat and Gomis 2009; Meyssignac et al. 2011b). The method used in most previous studies (as well as in the present one) is based on the reduced optimal interpolation described by Kaplan et al. (1998, 2000). It consists of 2 steps. In the first step, an Empirical Orthogonal Function (EOF) decomposition (Preisendorfer 1988; Toumazou and Cretaux 2001) of a 2-D sea level field (generally from satellite altimetry but also from OGCMs or ocean reanalyses) is done. This decomposition allows to separate the spatially well-resolved sea level signal (here represented by a matrix H, with m lines for each spatial point and n columns for each date) into spatial modes (EOFs) and their related temporal amplitude as follows:

$$H(x, y, t) = U(x, y)\alpha(t) \tag{1}$$

In Eq. 1, $U(x, y)$ stands for the spatial modes and α(t) for their temporal amplitudes. Assuming that the spatial modes $U(x, y)$ are stationary with time, the reconstructed sea level field $H_R(x, y, t)$ covering a period (here 1950–2009) longer than the $H(x, y, t)$ fields has an EOF decomposition as follows:

$$H_R(x, y, t) = U(x, y)\alpha_R(t) \tag{2}$$

where $\alpha_R(t)$ represents the new temporal amplitudes of the EOFs over 1950–2009.

The second step consists of computing these new amplitudes over the whole period 1950–2009 using in situ (tide gauge-based) sea level records. This is done at each time step, through a least-squares procedure which gives the optimal linear combination of the EOFs that fits the tide-gauge records at the tide-gauge locations.

In the first step, the EOF modes and amplitudes of the 2-D sea level grids are computed through a singular value decomposition approach, such that:

$$H = USV^T \tag{3}$$

where $U(x, y)$ is defined as above, S is a diagonal matrix containing the singular values of H, and V represents the temporal eigenmodes. At this stage, the amplitude of the EOF modes can be simply written as $\alpha(t) = SV^T$. Conceptually, each EOF k (kth column of $U(x, y)$ multiplied by the kth line of $\alpha(t)$:$U_k(x, y).\alpha_k(t)$) is a spatio-temporal pattern of sea level variability that accounts for a percentage of the total variance of the sea level signal.

The low-order EOFs (eigenvectors of the largest singular values) explain most of the variance and contain the largest spatial scales of the signal. The higher-order EOFs contain smaller spatial scale patterns and are increasingly affected by noise. Besides, their amplitude is less well resolved by the least-squares procedure, because the sparse tide-gauges coverage does not allow resolving small-scale patterns. Consequently, to be

efficient, the sea level reconstruction uses only a subset of the M lowest-order EOFs (the optimal number of EOFs has been estimated by comparison of the reconstructed sea level with observations; see below).

The data matrix H can be written as follows:

$$H_M = U_M(x, y)\alpha(t) \tag{4}$$

where $\alpha(t) = S_M V_M^T$ is the matrix of the amplitude of the M lowest EOFs. Following Kaplan et al. (2000), in the second step, the amplitude at each time step over the time span of in situ records is obtained by minimizing the cost function:

$$S(\alpha) = \left(PU_M\alpha - H^0\right)^T R^{-1}\left(PU_M\alpha - H^0\right) + \alpha^T\Lambda^{-1}\alpha \tag{5}$$

In Eq. 5, H^0 is the in situ (tide gauge-based) observed sea level, P is a projection matrix equal to 1 when and where in situ data are available and 0 otherwise. Λ is a diagonal matrix of the largest eigen-values of the covariance matrix. The term $\alpha^T\Lambda^{-1}\alpha$ represents a constraint on the EOF spectrum of the solution. It prevents the least-squares procedure to be contaminated by remaining high-frequency noise (it filters out non-significant solutions that display too much variance at grid points without nearby observations). R is the error covariance matrix. It is given by $R = PU_{N-M}\Lambda_{N-M}U_{N-M}^T P^T + D$. The first term of R contains the covariance of the truncated modes (the index 'N–M' indicates the omitted eigenvectors and eigenvalues). It accounts for errors due to the truncation of the set of EOFs to the first M EOFs. D accounts for the instrumental error. We have assumed here a spatially uncorrelated instrumental error so D is the identity matrix multiplied by the instrumental error variance. Amplitudes of the variance used for each reconstruction are indicated below.

When Eq. 5 is solved, it provides the reconstructed amplitude α_R of the EOFs. The least-squares inversion gives an analytical expression of α_R as follows:

$$\alpha_R(t) = QU_M^T P^T R^{-1} H^0(t) \tag{6}$$

$$\text{with} \quad Q = \left(U_M^T P^T R^{-1} PU_M + \Lambda^{-1}\right)^{-1}$$

When solving Eq. 6, two problems further arise. First, because tide-gauge data are expressed relative to their own local datum that is not cross-referenced over the globe, the solution may not necessarily be consistent with the 2-D sea level grid reference surface (from OGCM or altimetry data). To cope with this problem, Church et al. (2004) solved Eq. 6 for changes in α_R between adjacent time steps. It is also the procedure applied in the present study. Instead of computing α_R, we compute $\Delta\alpha_R(t_n) = \alpha_R(t_n) - \alpha_R(t_{n-1})$ thanks to the equation $\Delta\alpha_R = QU_M^T P^T R^{-1}\Delta H^0$. This provides for each time step, the changes in amplitude of α_R which are independent from the tide-gauge local references. Then α_R itself is recovered by summing backward in time $\Delta\alpha_R$ and equalizing the mean amplitude of α_R to the mean amplitude of α (amplitude of the EOF of the OGCM or altimetry data) over the common period. With this procedure, the consistency between the reference surfaces of tide gauges and 2-D sea level grids (from OGCM or altimetry) is ensured.

Another issue in global sea level reconstructions is the large spatially averaged sea level signal (of about 1.7–1.8 mm/year since about 1950; e.g., Church and White 2006, 2011; Woppelmann et al. 2009). This signal, which is contained in the tide-gauge data, is hard to capture and recover from a truncated set of orthogonal EOFs deduced from 2-D gridded sea level (see Christiansen et al. 2010). Hence, following Church et al. (2004) and the results of Christiansen et al. (2010), a spatially uniform EOF (also called EOF0, as in

Church et al. 2004) is added to the set of EOFs in order to represent the time-varying spatially averaged signal of the global ocean in the past. An advantage of this procedure is to avoid pouring the strong past global-averaged sea level signal in different EOFs and perturbing the reconstruction process (e.g., Kaplan et al. 2000).

The final reconstructed gridded sea level is obtained by multiplying the set of M EOFs plus the EOF0 with their reconstructed amplitude:

$$H_R = U_M(x, y).\alpha_R(t) \tag{7}$$

Other authors have performed past sea level reconstructions using different basis functions. For example, Hamlington et al. (2011) use cyclostationary EOFs as basis functions. Unlike classical EOFs, cyclostationary EOFs are periodic and can capture cyclostationary signals such as the annual signal into a single mode. This enables reconstructing the annual signal along with the interannual signal through a unique process.

3 Data Sets Used in this Study

In this study, we used a set of 91 tide-gauge records selected from the Permanent Service for Mean Sea Level (PSMSL) database (http://www.psmsl.org/about_us/news/2010/new_website.php, Woodworth and Player 2003). These records were optimally interpolated (as explained above) with EOFs computed from three different input grids: (1) the ORCA025-B83 run of the DRAKKAR/NEMO model (Barnier et al. 2006; Dussin et al. 2009), (2) the SODA ocean reanalysis (Carton and Giese 2008) and (3) the 17-year long satellite altimetry data set. These data sets are described here after in this section.

3.1 Tide-Gauge Records

We use monthly mean sea level data from the Revised Local Reference (RLR) tide-gauge records of the PSMSL (downloaded in May 2011). A very careful selection of sites has been realized. From the whole set of data available, we consider records at least 35-year long over 1950–2009. Compared with the 99 records considered in Llovel et al. (2009), here we use only 91 records, deleting a number of tide-gauge records with suspect behaviour. In effect, for a number of reasons, gaps and discontinuities may affect the tide-gauge time series (e.g., changes in instrumentation, earthquakes or any other natural or anthropogenic factors). When small gaps (<3 consecutive years) are observed in the tide-gauge record, we reintroduced missing data by linearly interpolating the time series. Outliers were detected using the Rosner's test (Rosner 1975) and removed. Annual and semi-annual cycles were removed (before gap-filling) through a least-squares fit of 12-month and 6-month period sinusoids. At a few sites, recent data (i.e. up to 2009) are lacking in the PSMSL data base. Thus, we completed these tide-gauge time series using altimetry data (22 sites are concerned). To do so, the following constraints have been considered: (1) availability of altimetry measurement at less than 1 degree from the tide-gauge position; and (2) overlapping period of at least 5 years between tide-gauge records and altimetry data (this overlap length was deduced from the Bonnet's formula, Bonett and Wright (2000), in order to insure a correlation >0.9 between the two data sets). The closest altimetry record to the tide-gauge position has been used to complete the tide-gauge sea level time series. We corrected the tide-gauge time series for the inverted barometer response of sea level to atmospheric loading using surface pressure fields from the National

Centres for Environmental Prediction (NCEP; Kalnay et al. 1996, http://www.ncep.noaa.gov/). Tide-gauge data were also corrected for the Glacial Isostatic Adjustment (GIA) effect using the ICE5G-VM2 model from Peltier (2004). As we focus here on interannual to multidecadal time scales, we averaged monthly tide-gauge time series to obtain annual averages. Figure 1 shows the distribution of the tide-gauge sites used in this study (superimposed to the altimetry sea level trend map over 1993–2009). Name, location and data length of the 91 tide gauges are summarized in Table 1. Tide-gauge records completed by altimetry data are those that end before 2009.

3.2 Input Sea Level Grids

To compute the EOFs needed to reconstruct past sea level, three input sea level grids were considered: from the DRAKKAR/NEMO OGCM (without data assimilation) over 1958–2007, from the SODA ocean reanalysis over 1958–2007 and the altimetry-based gridded sea level over 1993–2009. These data sets are briefly presented below.

3.2.1 The DRAKKAR/NEMO Ocean General Circulation Model

The DRAKKAR NEMO model is based on the free surface ocean circulation model NEMO version 2.3 (Madec 2008). We used the outputs of the ORCA025-B83 model configuration (Barnier et al. 2006; Dussin et al. 2009; Penduff et al. 2010). This is a global eddy-admitting ocean/sea-ice simulation that does not assimilate any observational data (e.g., satellite altimetry or in situ hydrographic data). It is very close to the simulation ORCA025-G70 analysed and proved to be consistent with altimetry by Lombard et al. (2009). It has the same horizontal and vertical resolution (46 levels with steps from 6 m at the surface to 250 m at the bottom). The main difference with ORCA025-G70 is the forcing function. ORCA025-B83 is forced by the more realistic hybrid 'DRAKKAR forcing set 4.1' surface forcing described in details by Brodeau et al. (2010). This forcing is based on the CORE data set assembled by W. Large (Large and Yeager 2004), the ECMWF (European Centre for Medium-Range Weather Forecast) ERA 40 reanalysis (Uppala et al. 2005) and the ECMWF operational analyses for the recent years. The simulation was started on the 1st January 1958, with initial conditions for salinity and temperature derived from the Levitus et al. (2005) data set for middle and low latitudes, from the Polar Science Center Hydrographic climatology for the high latitudes (Steele et al. 2001) and from the MEDATLAS climatology (Jourdan et al. 1998) for the Mediterranean sea. Initial conditions for sea-ice were taken from the month of January of the 10th year of ORCA025-G45b (a previous run with a climatological CORE forcing).

In the ORCA025-B83 simulation, the time-varying globally averaged sea level is not properly reproduced because it has been simulated on the basis of the Boussinesq approximation which enforces the total ocean volume (rather than mass) to remain constant. In particular, as shown by Greatbatch (1994), no spatially uniform steric sea level changes can be reproduced by such a model (even though the free surface evolution allows simulating correctly the net freshwater surface fluxes at both regional and global scale). For this reason, prior to the computation of the EOFs, we removed the time-varying globally averaged sea level from each sea surface height time series of the simulation. By doing this, we get a consistent set of EOFs, which are representative of the regional variability in sea level. Indeed, as shown by Greatbatch (1994) (apart from the unrealistic global uniform sea level changes), regional variations are properly reproduced by such a free surface model. Concerning the reconstruction process, the fact that the set of EOFs does not

Table 1 Name, location (degrees of latitude North, and longitude East, being positive), length and percentage of gaps of the tide-gauge series selected from the PSMSL for the reconstructions

ID	Station name	Location		Years of data		Percentage of gaps (max. gap size in months)	Altimetry data used for supplemented the time series or filling the gap
		Longitude	Latitude	Start	End		
1	North Shields	−1.43	55.00	1950	2009	15% (43)	–
2	St. Petersburg	−82.62	27.77	1950	2009	0% (0)	–
3	St. Georges/Esso Pier	−64.70	32.37	1950	2009	9% (41)	–
4	Alesund	6.15	62.47	1951	2009	2% (2)	–
5	Maloy	5.12	61.93	1950	2009	7% (26)	–
6	Bergen	5.30	60.40	1950	2009	3% (6)	–
7	Stavanger	5.73	58.97	1950	2009	3% (16)	–
8	Tregde	7.57	58.00	1950	2009	2% (6)	–
9	Warnemunde 2	12.08	54.18	1950	2009	0% (2)	–
10	Lowestoft	1.75	52.47	1955	2009	6% (12)	–
11	Portsmouth	−1.12	50.80	1961	2009	4% (6)	–
12	Devonport	−4.18	50.37	1961	2009	4% (4)	–
13	Newlyn	−5.55	50.10	1950	2009	1% (4)	–
14	Brest	−4.50	48.38	1952	2009	0% (1)	–
15	Santander I	−3.80	43.47	1950	2009	3% (3)	–
16	La Coruna I	−8.40	43.37	1950	2009	3% (2)	–
17	Vigo	−8.73	42.23	1950	2009	1% (4)	–
18	Port Nolloth	16.87	−29.25	1959	2009	23% (72)	–
19	Simons Bay	18.43	−34.18	1957	2009	17% (49)	–
20	Ko Lak	99.82	11.80	1950	2009	4% (12)	–
21	Zhapo	111.83	21.58	1959	2009	1% (1)	–
22	Kanmen	121.28	28.08	1959	2009	1% (2)	–
23	Petropavlovsk-Kamchatsky	158.65	52.98	1957	2009	0% (1)	–
24	Aburatsubo	139.62	35.15	1950	2009	1% (1)	–
25	Kushimoto	135.78	33.47	1957	2009	1% (2)	–
26	Komatsushima	134.58	34.00	1958	2009	1% (3)	–
27	Misumi	130.45	32.62	1957	2009	3% (5)	–
28	Naha	127.67	26.22	1966	2009	0% (1)	–
29	Wajima	136.90	37.40	1950	2009	4% (12)	–
30	Asamushi	140.87	40.90	1954	2009	1% (5)	–
31	Townsville I	146.83	−19.25	1959	2009	0% (1)	–
32	Bundaberg, Burnett Heads	152.38	−24.77	1966	2009	2% (4)	–
33	Fremantle	115.75	−32.07	1950	2009	2% (3)	–
34	Carnarvon	113.65	−24.90	1965	2009	13% (38)	–
35	Port Hedland	118.57	−20.32	1966	2009	6% (10)	–
36	Guam	144.65	13.43	1950	2009	6% (14)	–
37	Kwajalein	167.73	8.73	1950	2009	2% (2)	–
38	Wake Island	166.62	19.28	1950	2009	7% (17)	–

Table 1 continued

ID	Station name	Location		Years of data		Percentage of gaps (max. gap size in months)	Altimetry data used for supplemented the time series or filling the gap
		Longitude	Latitude	Start	End		
39	Pago Pago	−170.68	−14.28	1950	2009	7% (24)	–
40	Midway Island	−177.37	28.22	1950	2009	6% (14)	–
41	Nawiliwili Bay, Kauai Island	−159.35	21.97	1955	2009	1% (3)	–
42	Honolulu	−157.87	21.32	1950	2009	0% (0)	–
43	Hilo, Hawaii Island	−155.07	19.73	1950	2009	0% (0)	–
44	Papeete-B, Soc.IS.	−149.57	−17.53	1975	2009	2% (7)	–
45	Prince Rupert	−130.33	54.32	1950	2009	1% (2)	–
46	Bella Bella	−128.13	52.17	1961	2009	3% (2)	–
47	Victoria	−123.37	48.42	1950	2009	1% (1)	–
48	Crescent City	−124.20	41.75	1950	2009	2% (9)	–
49	San Francisco	−122.47	37.80	1950	2009	0% (0)	–
50	Los Angeles	−118.27	33.72	1950	2009	2% (6)	–
51	San Diego	−117.17	32.72	1950	2009	2% (9)	–
52	Veracruz	−96.12	19.18	1953	2009	7% (27)	–
53	Magueyes Island	−67.05	17.97	1955	2009	4% (12)	–
54	Pensacola	−87.22	30.40	1950	2009	2% (5)	–
55	Cedar Key II	−83.03	29.13	1950	2009	6% (20)	–
56	Key West	−81.80	24.55	1950	2009	1% (8)	–
57	Charleston I	−79.93	32.78	1950	2009	0% (0)	–
58	Wilmington	−77.95	34.23	1950	2009	2% (6)	–
59	Hampton Roads	−76.33	36.95	1950	2009	0% (0)	–
60	Baltimore	−76.58	39.27	1950	2009	2% (12)	–
61	New York	−74.02	40.70	1950	2009	1% (4)	–
62	Newport	−71.33	41.50	1950	2009	2% (10)	–
63	Boston	−71.05	42.35	1950	2009	1% (5)	–
64	Halifax	−63.58	44.67	1950	2009	3% (4)	–
65	Charlottetown	−63.12	46.23	1950	2009	6% (4)	–
66	St. Johns, Nfld.	−52.72	47.57	1957	2009	8% (36)	–
67	Sydney, Fort Denison 2	151.23	−33.85	1950	2009	0% (2)	–
68	Saint John, N.B.	−66.07	45.27	1950	1999	6% (5)	Yes
69	Puerto Madryn	−65.03	−42.77	1957	2000	10% (39)	Yes
70	Mumbai/ Bombay	72.83	18.92	1950	1994	2% (4)	Yes
71	Balboa	−79.57	8.97	1950	2003	1% (3)	Yes
72	Auckland II	174.77	−36.85	1950	2000	3% (6)	Yes
73	Mayport	−81.43	30.40	1950	2000	0% (2)	Yes
74	Lyttelton II	171.27	−44.40	1950	2000	10% (47)	Yes
75	Dublin	−6.22	53.35	1950	2001	1% (3)	Yes

Table 1 continued

ID	Station name	Location		Years of data		Percentage of gaps (max. gap size in months)	Altimetry data used for supplemented the time series or filling the gap
		Longitude	Latitude	Start	End		
76	Hondau	106.80	20.67	1957	2001	0% (1)	Yes
77	Johnston Island	−169.52	16.75	1950	2003	5% (15)	Yes
78	Rikitea	−134.95	−23.13	1969	2003	6% (7)	Yes
79	Fredericia	9.77	55.57	1950	2006	2% (3)	Yes
80	Esbjerg	8.43	55.47	1950	2006	3% (12)	Yes
81	Cananeia	−47.93	−25.02	1954	2006	3% (17)	Yes
82	Santa Cruz	−90.32	−0.75	1978	2006	4% (10)	Yes
83	Cochin (Willingdon IS.)	76.27	9.97	1950	2007	8% (12)	Yes
84	Chennai/Madras	80.30	13.10	1952	2007	10% (24)	Yes
85	Vishakhapatnam	83.28	17.68	1950	2007	16% (39)	Yes
86	Mokpo	126.40	34.78	1960	2009	1% (1)	–
87	Pohang	129.40	36.02	1972	2009	0% (1)	Yes
88	Keelung II	121.73	25.13	1956	1995	1% (7)	Yes
89	Antofagasta 2	−70.40	−23.65	1950	2006	7% (8)	Yes
90	Palermo	−58.36	−34.60	1950	2009	0% (0)	–
91	Kanton	−171.72	−2.80	1950	2006	15% (45)	Yes

contain any globally uniform sea level component is not an issue because an extra EOF (the globally uniform EOF called EOF0, see Sect. 2) is added to the set of EOFs to capture from the tide-gauge records the missing time-varying uniform sea level (see Sect. 2 for more details). The spatial sea level trend patterns over 1958–2007 from the DRAKKAR/ NEMO/ ORCA025-B83 model are presented in Fig. 2a.

3.2.2 The SODA Ocean Reanalysis

In this study, we also used the ocean reanalysis SODA 2.0.2 that span over the period 1958 to 2007. This reanalysis is based on an optimal interpolation described by Carton and Giese (2008). The ocean general circulation model, POP2.0.1 (see Carton and Giese 2008, for details), has a horizontal resolution of 0.4° in longitude and 0.25° in latitude, and 40 vertical levels with a resolution of about 10 m in the upper 100 m. For this study, we used the monthly mean oceanic variables interpolated on a horizontal grid of 0.5°× 0.5°. In SODA 2.0.2, POP2.0.1 is forced by ERA-40 daily wind stresses and heat fluxes. It assimilates hydrographic data from the WOD05 hydrographic data base (Levitus et al. 2005), but it does not assimilate satellite altimetry data. Sea level outputs are computed diagnostically using a linearized continuity equation valid for small ratios of sea level to fluid depth (Carton and Giese 2008).

The spatial sea level trend patterns over 1958–2007 from the SODA reanalysis are presented in Fig. 2b.

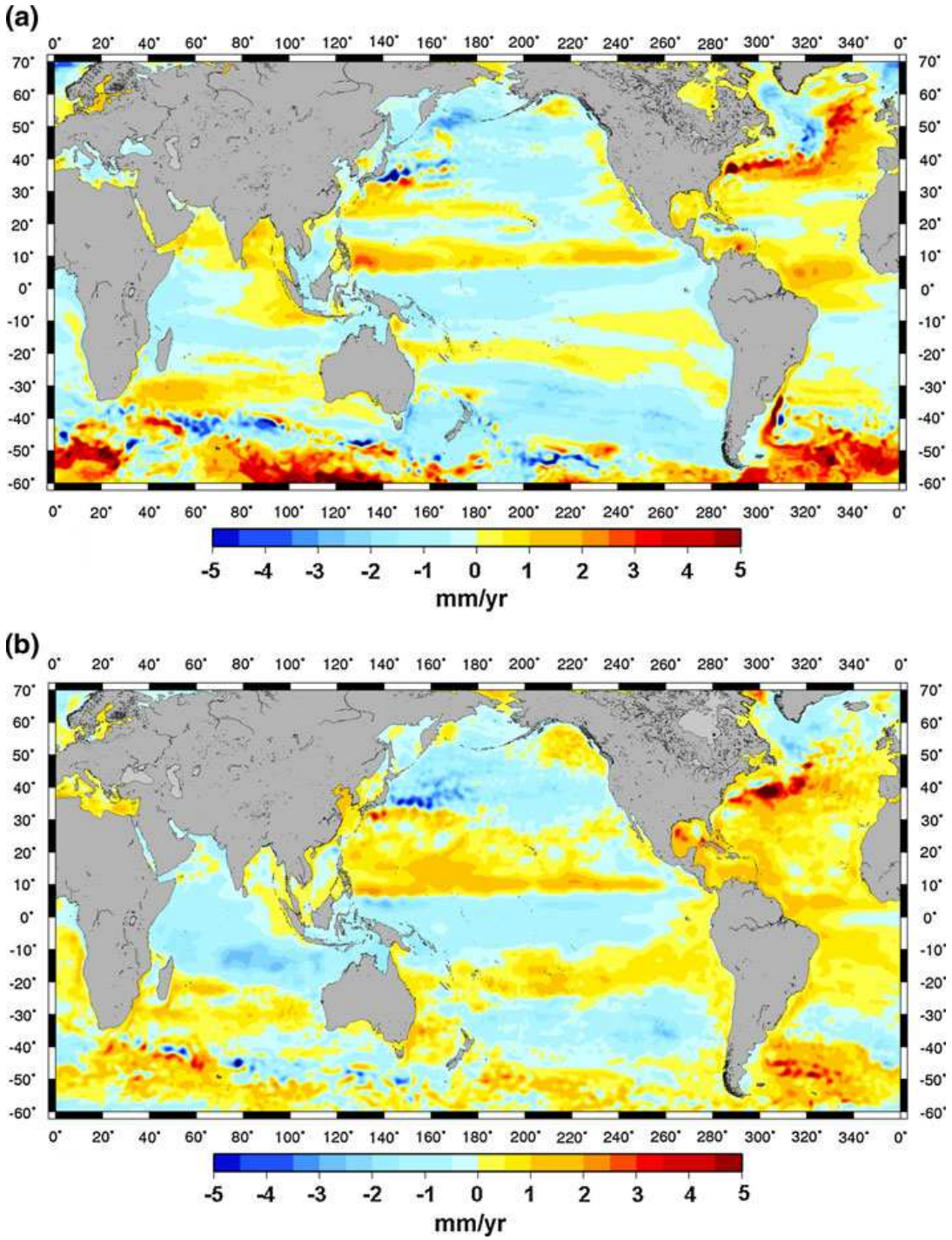

Fig. 2 Spatial trend patterns in sea level over 1958–2007 from **a** the DRAKKAR/NEMO ocean model and **b** the SODA reanalysis

3.2.3 The Altimetry Data Set

For the altimetry data, we used the DT-MSLA "Ref" series provided by Collecte Localisation Satellite (CLS; http://www.aviso.oceanobs.com/en/data/products/sea-surface-height-products/global/msla/index.html). This data set was used over the time span from January 1993 to December 2009. It is available as 1/4° × 1/4° Mercator projection grids at weekly

intervals. The DT-MSLA "Ref" series are based on the combination of several altimetry missions, namely: Topex/Poseidon (T/P), Jason-1 and 2, Envisat, and ERS-1 and ERS-2. It is a global homogenous inter-calibrated data set based on global crossover adjustment using T/P and then Jason-1 as reference missions. Moreover, the use of a recently updated orbit solution for Jason-1 and T/P (GSFC—Goddard Space Flight Center-orbit computed with the ITRF2005 terrestrial reference frame; Altamimi et al. 2007) allows to remove previous heterogeneity between global hemispheric mean sea level trends (Ablain et al. 2009). Usual geophysical corrections are applied: solid Earth and ocean tides, wet and dry troposphere, ionosphere (see Ablain et al. 2009 for more details) and inverted barometer (Carrere and Lyard 2003) corrections.

4 2-D Reconstructed Sea Level Over 1950–2009

We reconstructed 2-D sea level grids at yearly intervals over 1950–2009 using the three input sea level grids (DRAKKAR/NEMO, SODA and altimetry) described above. The same area (50°S to 70°N) was considered for each input sea level grids to ensure consistency between the reconstructions. The input sea level grids were also yearly averaged before the reconstruction process because here we are mostly interested in the interannual to multidecadal timescales. Thus, all reconstructions are based on yearly data sets.

For reconstructions based on altimetry, we considered an instrumental error variance of 4 cm^2 to compute the error covariance matrix (see Sect. 2). For reconstructions based on OGCM, there is no instrumental error but instead we consider a data error. The data error has been derived from the variance of the differences between the OGCM and the altimetry yearly data sets over their overlapping period 1993–2007. This gives a data error variance of 15.2 cm^2 for SODA and 10.9 cm^2 for DRAKKAR. These values are introduced in the error covariance matrix for the OGCM-based reconstructions.

Several reconstructions were computed to estimate the sensitivity of the reconstructed sea level with respect to two key points of the reconstruction process: (1) the number of EOF modes used in the reconstruction and (2) the period covered by the input grids used to compute the EOFs. All together, 87 different reconstructions were produced: 42 reconstructions for the DRAKKAR and SODA cases (6 series of 7 reconstructions based on 10, 15, 20, 25, 30 and 35 modes) with EOFs computed over 7 different time spans of the OGCM runs: 50 years (1958–2007), 43 years (1965–2007), 40 years (1968–2007), 38 years (1970–2007), 30 years (1978–2007), 28 years (1980–2007), and 20 years (1988–2007), plus 3 reconstructions for the altimetry cases based on 10, 15 and 17 modes, with EOFs computed over the 17-year-long time span.

4.1 Spatial trend Patterns and Modes of Variability (EOFs) of the Reconstructed Sea Level Over 1950–2009

Figure 3a presents reconstructed spatial trend patterns over 1950–2009 for three cases: (1) EOFs from DRAKKAR/NEMO over 1958–2007—case 1, (2) EOFs from SODA over 1958–2007—case 2 and (3) EOFs from altimetry over 1993–2009—case 3 (here 15 modes are used for the reconstructions; this number of modes optimizes the results as discussed in Sect. 4.2).

Some features common to the two model-based reconstructions (cases 1 and 2) are seen in Fig. 3a; for example, the patterns in the Pacific, Indian, Austral and south Atlantic oceans. However, differences are noticed in the tropical Atlantic and North Atlantic south of Greenland. The altimetry-based reconstructed trends agree better with SODA (case 2)

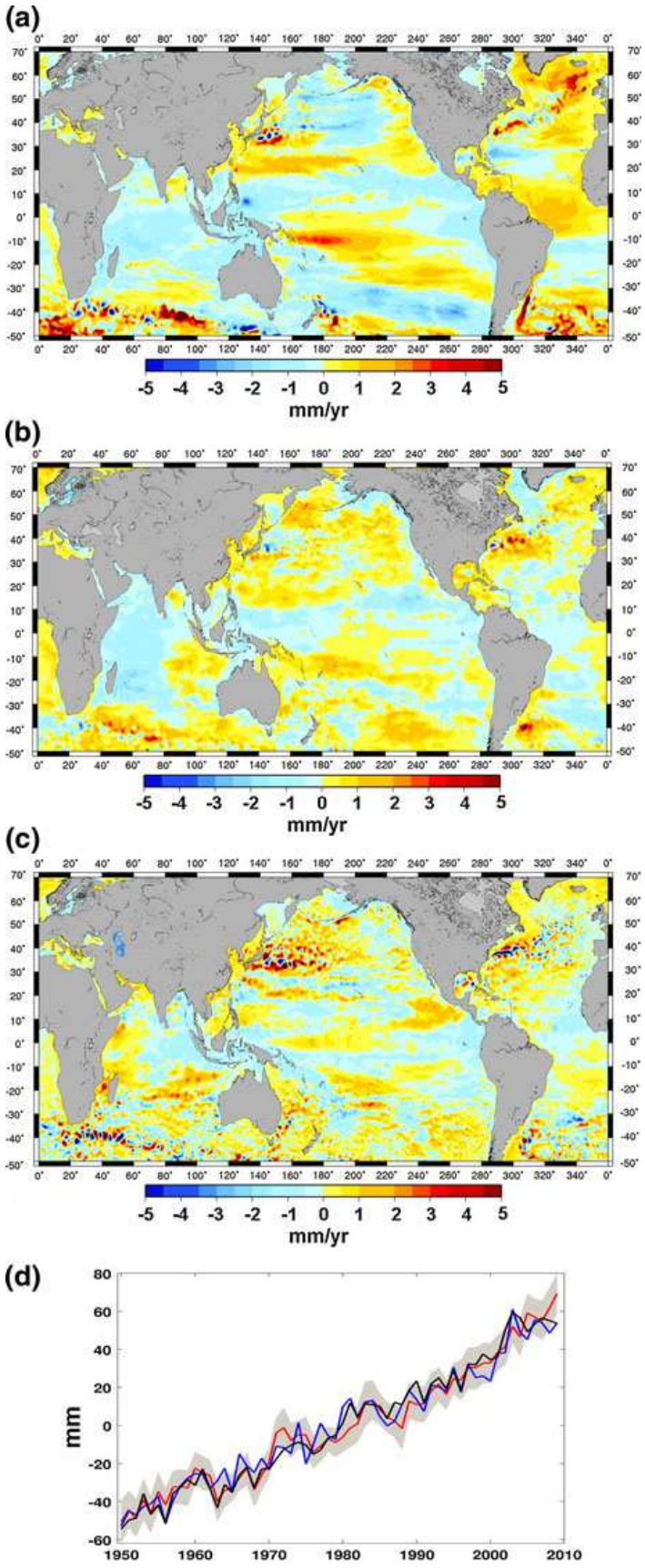

Fig. 3 Reconstructed spatial trends in sea level over 1950–2009 (15 first modes) based on: **a** EOFs of DRAKKAR/NEMO over 1958–2007, **b** EOFs of SODA over 1958–2007, **c** EOFs of satellite altimetry over 1993–2009. **d** The reconstructed global mean sea level since 1950 for the 3 reconstructions (*black curve* DRAKKAR/NEMO; *red curve* SODA; *blue curve* altimetry). The *grey shaded zone* represents the uncertainty of the altimetry-based reconstructed global mean sea level

than DRAKKAR/NEMO (case 1). We note that the DRAKKAR/NEMO reconstruction has locally higher amplitudes than the other two reconstructions.

Unlike the spatial patterns, the global mean sea level curves over 1950–2009 from the 3 reconstructions agree rather well (see Fig. 3d). Curves for the two model-based reconstructions (cases 1 and 2) fall within the uncertainty of the altimetry-based reconstructed sea level curve. This uncertainty was estimated from the quadratic sum of formal errors derived from the inversion process and tide-gauge data errors. The latter were estimated from a bootstrap method (Efron and Tibshirani 1993) for standard errors of yearly tide-gauge-based sea level values with a significance level—SL >95%. It dominates the total error.

The three global mean sea level curves present very similar trends over 1950–2009, 1.8 mm/year for the DRAKKAR/NEMO and altimetry-based reconstructions and 1.7 mm/year for the SODA-based reconstruction. Global mean interranual to decadal variability also correlates fairly well. The detrended global mean sea level from the DRAKKAR/NEMO-based reconstruction shows a correlation of 0.66 with the SODA-based reconstruction and 0.62 with the altimetry-based reconstruction.

We performed an EOF decomposition of the reconstructed grids over 1950–2009 for the three cases (note that the EOF decomposition of reconstructed sea level is not expected to be similar to that of the spatial input grids because new temporal amplitudes have been estimated). The global mean sea level was removed before the EOF decomposition. The 3 leading modes (EOF1/2/3) of each case (i.e. DRAKKAR-/NEMO-, SODA- and altimetry-based reconstructions) are shown in Fig. 4. The EOF1 temporal curves of the DRAKKAR-/NEMO- and altimetry-based reconstructions display an upward trend. For the DRAKKAR/NEMO reconstruction, the interranual variability of this curve correlates significantly (0.52 SL >99%) with the PDO index (e.g., Zhang et al. 1997) after $\sim$1975, showing an influence of the Pacific ocean on the leading mode over the last decades. It is not the case for the altimetry reconstruction because no similar significant correlation could be found with its EOF1 temporal curve. Noting that the spatial patterns of both EOF1 s closely resemble the trend patterns shown in Fig. 3, we conclude that this mode reflects the sea level signature of a low frequency signal. (of pseudo periodicity longer than the 60-year-long time span considered in this study). The EOF1 of the SODA reconstruction displays different characteristics. First, its temporal curve increases only after 1980, and second, its spatial pattern does not resemble the trend patterns shown in Fig. 3. Rather, it seems closer to an ENSO-like pattern. The temporal curve correlates well (0.62 with SL >99%) with the Southern Oscillation index (SOI) (difference of atmospheric pressure between Darwin, Australia, and Tahiti, French Polynesia: a proxy of ENSO), revealing the influence of ENSO. Unlike EOF1 s, EOF2 spatial patterns of the 3 reconstructions compare fairly well. Their temporal curves show significant influence from the Pacific region: EOF2 of the DRAKKAR/NEMO reconstruction correlates well with the PDO index before 1975 (0.65 with SL >99%), EOF2 of the SODA reconstruction correlates well with the SOI over 1950–2009 (0.67 with SL >99%) and EOF2 of the altimetry reconstruction correlates well with the PDO index over 1950–2009 (0.64 with SL >99%). Finally, EOF3s of the three reconstructions agree reasonably well each other. They all show significant correlation with the El Nino Modoki Index (EMI), a proxy of a different type of ENSO events marked by a warming of the central Pacific instead of the East Pacific (Ashok and Yamagata 2009). However, the correlation is reasonable for the DRAKKAR/NEMO reconstruction (0.54 with SL >99%) and weak for the SODA (0.30 with SL = 0.99%) and altimetry-based (0.34 with SL = 99%) reconstructions.

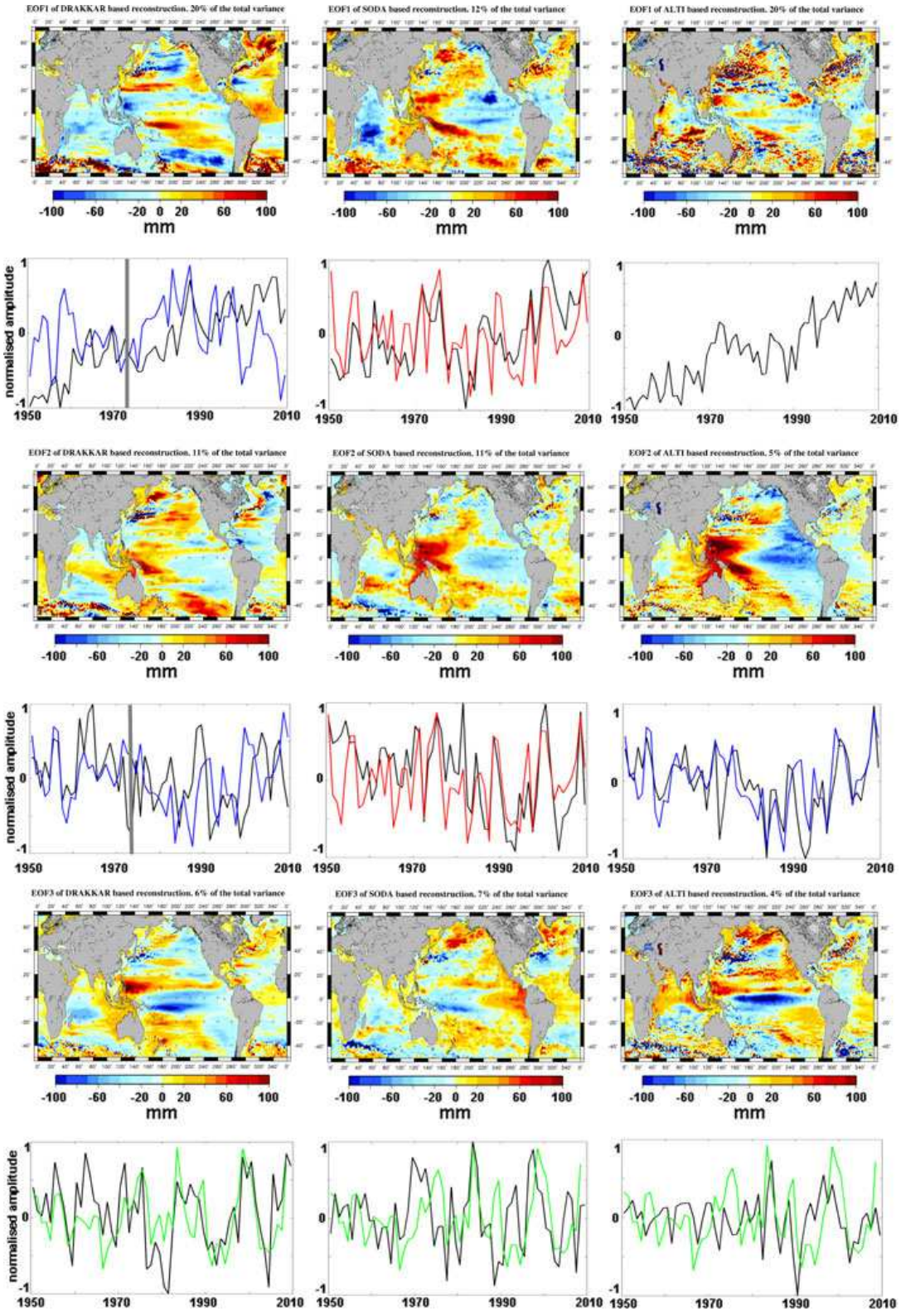

Fig. 4 EOFs modes 1 (*top panels*), 2 (*middle panels*) and 3 (*bottom panels*) of the reconstructed sea level heights based on EOFs of DRAKKAR/NEMO (1958–2007) (*left column*), SODA (1958–2007) (*middle column*) and altimetry (1993–2009) (*right column*). The global mean sea level was removed before the EOF decomposition. The reconstructions are based on 15 EOF modes. Superimposed to the temporal amplitudes (*black curves*) are plotted the PDO index (*blue*), the SOI index (*red*) and the EMI index (*green*)

Looking at Fig. 4, we note that DRAKKAR/NEMO- and altimetry-based reconstructions roughly capture similar signals, in particular a low-frequency signal. A similar low-frequency signal had been previously reported by Llovel et al (2009) in their sea level reconstruction over 1950–2003 using the OPA/NEMO ocean reanalysis (a version of the NEMO model with data assimilation; see Llovel et al. 2009 for details). The DRAKKAR/NEMO- and altimetry-based reconstructions also display in their EOF3 some imprint of the El Nino Modoki type event, in particular in recent years where the amplitude of the EOF3 gets higher. On the other hand, the SODA-based reconstruction seems to be dominated by the classical ENSO signal. It captures as well in its EOF3 some imprint of the El Nino Modoki type events, in particular in the recent years.

These three reconstructions use the same set of tide gauges but different input spatial grids. Thus, the differences noticed both in reconstructed spatial trend patterns and EOF decompositions likely reflect the dominant influence of these input spatial functions. Several factors may play a role, among them the quality of the sea level grids (e.g., the respective performance of the DRAKKAR/NEMO and SODA ocean models) and the period covered by the EOFs were used to do the reconstruction (50 years for DRAKKAR/NEMO and SODA, and 17 years for altimetry). We examine below the influence of the latter factor (in addition to that of the number of EOF modes used for the reconstruction).

4.2 Optimization of the Number of EOF Modes Used for the Reconstruction and Length of Input Sea Level Grids

In this section, we examine the effect of the number of EOF modes used for the reconstruction and the length of the input sea level grids. To find the optimal case, we perform two kind of comparisons: (1) we compare locally reconstructed and observed sea level time series over the time span of data availability at tide gauges not used in the reconstruction (91 reconstructions are completed, omitting one gauge at a time; we then compare at each corresponding site the reconstructed and observed sea level time series) and (2) we compare global reconstructed trends with (observed) altimetric trends over 1993–2009. For that purpose, we only consider the DRAKKAR/NEMO reconstruction. For the reconstruction, two parameters were varied: the number of modes (10, 15, 20, 25 and 30 modes were considered) and the length of the input grids to compute the EOFs (50 years, 40 years, 30 years and 20 years; the final year is always 2007, meaning that the time span of the input grids starts in 1958, 1968, 1978 and 1988, respectively).

Figure 5 shows the reconstructed trend maps over 1950–2009 with 50-year, 40-, 30- and 20-year long DRAKKAR/NEMO EOFs (with 15 and 20 modes). At global scale, these different reconstructions are consistent with each other except in the southern oceans south of 45°S. This region is actually not constrained by any tide gauge since the lowest latitude tide gauge we use is located at 44°S. For that reason, the reconstructed fields in the high latitude southern oceans are not very reliable. At regional scale, some discrepancies are noticed. The two reconstructions using 30- and 20-year long EOFs show a larger positive pattern in the southern tropical Pacific with lower amplitude than in the other reconstructions. It should be noticed as well that the 15-mode reconstructions based on 40- and 30-year long EOFs show a negative pattern south of Greenland that is not seen in the other reconstructions. To decide which case provides the best results, we present below different validations.

4.2.1 Validation with Independent Tide Gauges and Optimization of the Mode Number and EOF Length

Because in the reconstruction, we used all long, high-quality tide-gauge records available in the PSMSL data base, none were left for validation of the reconstruction. Thus, as in Llovel et al. (2009), we removed one by one each tide-gauge record, and then performed 91 new reconstructions with only 90 tide-gauge time series and compared at the left tide-gauge site reconstructed and observed sea level. Figure 6a shows the mean correlation between reconstructed time series and tide-gauge records over their overlapping time span as a function of input grid length and number of modes while Fig. 6b shows the standard deviation (rms) of the differences between reconstructed trends and tide-gauge trends over their overlapping time span. Both figures clearly show that 25-, 30- and 35-mode reconstructions perform less well than 10-, 15- and 20-mode reconstructions. We also note that the smallest rms is obtained for the longest input grid lengths (>40 years). The differences between 10 and 15 modes is very small but the 15-mode reconstruction seems to perform better in terms of reconstructed interannual variability since it shows slightly higher mean correlation with tide-gauge records when using long EOFs (see Fig. 6a). In the following, we consider 15 modes as optimal. In addition, reconstructions based on longest EOFs time span seem to perform better.

4.2.2 Validation with Altimetry Data Over the Altimetry Time Span (1993–2009)

Another method to validate the reconstructions and determine the optimal number of modes and EOF temporal length is to compare the reconstructed fields with observed (from altimetry) sea level over the altimetry time span (1993–2009). Mean correlation between reconstructed time series and observed time series over 1993–2009 at each grid mesh over the whole oceanic domain are shown in Fig. 6c as a function of number of modes and EOF temporal length. Root mean squares of the differences between reconstructed and observed trends over 1993–2009 at each grid mesh are also shown in Fig. 6d. As for the validation with tide gauges, we find that the highest mean correlation and lowest rms are obtained for 10–15–20 modes. In terms of trend rms, the impact of the EOF period is barely visible. In terms of mean correlation, we find here that on these short time scales (1993–2009), reconstructions with short EOF periods (<20 years) perform better. This is unlike the result obtained by comparison with independent tide gauges over the long period 1950–2009 (see Fig. 6a). But this is not surprising because these reconstructions are based on 20-year-long EOFs over 1988–2007 for which the modelled sea level coincides very well with altimetry used here for verification. Note that for long EOF periods (>40 years), best results in terms of both mean correlation and trend differences are obtained for the 10–15 modes reconstructions.

To summarize, the above comparisons indicate that the $\sim$15 mode case (i.e. between 10 and 20 modes) optimizes the reconstruction when the whole time span 1950–2009 is considered. This is due to the fact that higher modes contain more noise while small scale features can not be resolved during the inversion process because of the too sparse tide-gauge data. Hence, using too many modes makes the reconstructions noisy and increases artificially the amplitude of the regional variability. In addition, the 15-mode reconstructions are optimized when the input grids time is sufficiently long (roughly >30–40 years).

On the basis of the results shown on Fig. 6, the reconstruction that seems to give the best results is the 15-mode reconstruction based on 50-year long EOFs.

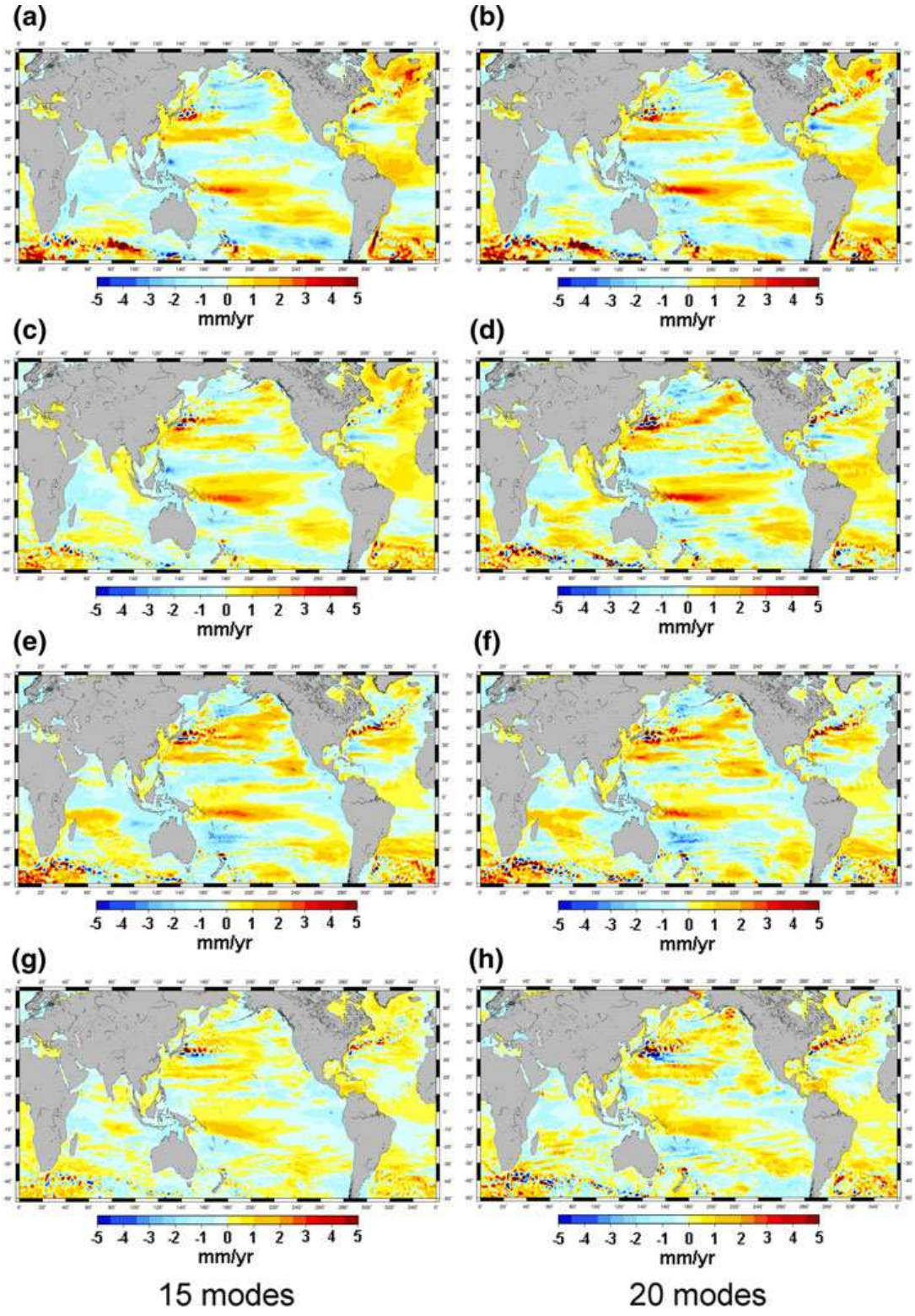

Fig. 5 Spatial trend patterns of the DRAKKAR/NEMO reconstruction (15 and 20 modes) for 50-year EOFS (**a** and **b**), 40-year EOFs (**c** and **d**), 30-year EOFs (**e** and **f**) and 20-year EOFs (**g** and **h**)

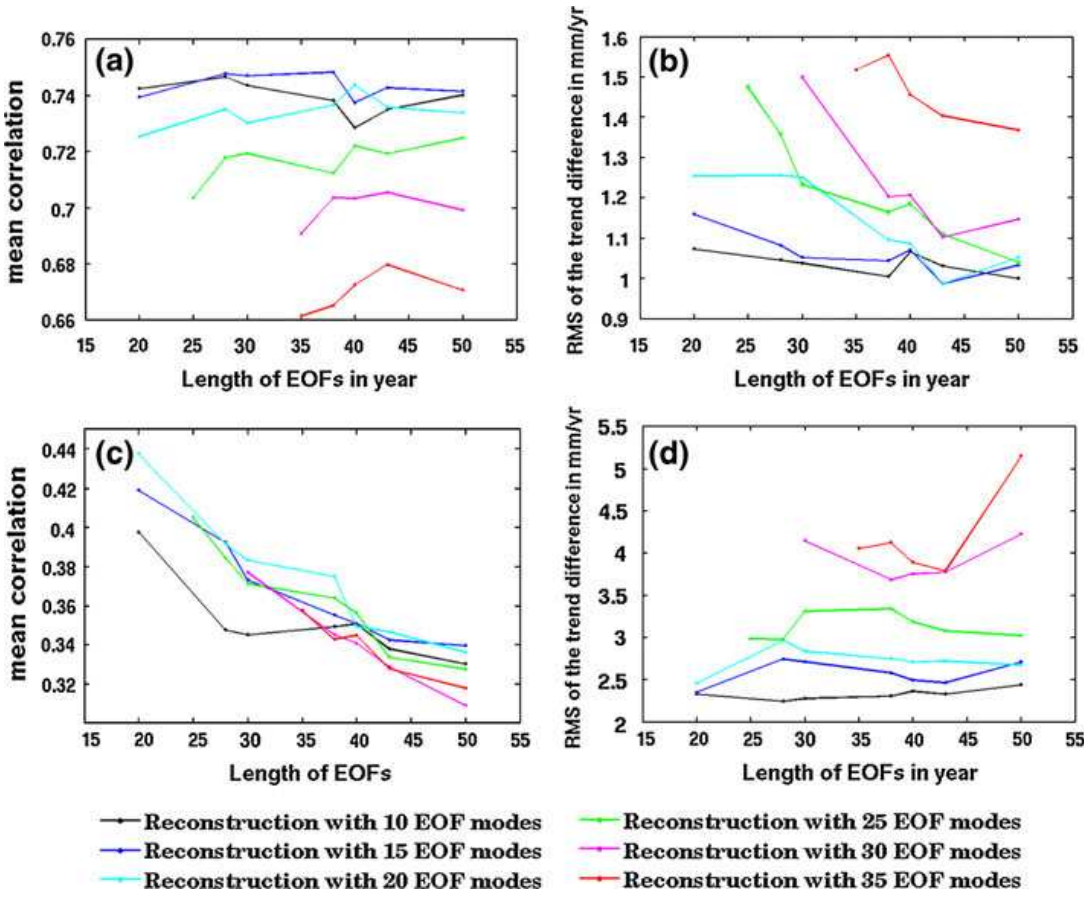

Fig. 6 *Top panels* correlation and rms trend differences between DRAKKAR/NEMO reconstructed sea level time series and each of the 91 tide gauges not used in the reconstruction (91 reconstructions are completed, omitting one gauge at a time; we then compare at each corresponding site the reconstructed and observed sea level time series), *bottom panels* correlation and trend differences between DRAKKAR/NEMO reconstructed sea level time series and altimetry. Results are presented for reconstructions using 10 modes (*black curves*), 15 modes (*blue curves*), 20 modes (*cyan curves*), 25 modes (*green curves*), 30 modes (*magenta curves*) and 35 modes (*red curves*). **a** Mean of the 91 correlations between tide gauges and DRAKKAR/NEMO reconstructed sea level time series over 1950–2009 at the tide-gauge location as a function of mode number and EOF length. **b** rms of the 91 differences between tide-gauge records not used in the reconstruction and DRAKKAR/NEMO reconstructed sea level trends over 1950–2009 at the tide-gauge location as a function of mode number and EOF length. **c** Mean of the correlations between satellite altimetry and DRAKKAR/NEMO reconstructed sea level time series over 1993–2009 as a function of mode number and EOF length (the correlations are computed over the 70°N–50°S oceanic domain on 1° × 1° grid meshes). **d** rms of the differences between satellite altimetry and DRAKKAR/NEMO reconstructed sea level trends over 1993–2009 as a function of mode number and EOF length (the differences are computed over the 70°N–50°S oceanic domain on 1° × 1° grid meshes)

4.3 Comparisons Between the Three Reconstructions (DRAKKAR/NEMO, SODA and Altimetry) Over 1950–2009

The results presented in Sect. 4.2 with the DRAKKAR/NEMO EOFs lead us to prefer the 15-mode and 50-year long input grids. A similar option is considered for the SODA input grids. For altimetry, we can only use 17-year long input grids (with 15 modes for the reconstruction). We can now compare the respective performances of these three cases. As for case 1 (DRAKKAR/NEMO EOFs), we compare the performances of the SODA and altimetry reconstructions at each of the 91 tide gauges not used in their respective reconstructions. Figure 7 left panels show histograms of the 91 correlations between

reconstructed and observed time series at tide gauges not used in the reconstruction. The high number of correlations higher than 0.7 (68) and of standard deviations lower than 30 mm (57) gives confidence in the reconstructed fields. The right panels show histograms of the rms differences between these time series. The top panel shows the DRAKKAR/NEMO reconstruction results, the middle one the SODA reconstruction results and the bottom panel the altimetry reconstruction results.

No clear conclusion can be drawn from Fig. 7, as no single case appears to perform better. We note that the SODA histograms spread more than DRAKKAR/NEMO and altimetry histograms but differences are not drastic. The DRAKKAR/NEMO and altimetry reconstructions give roughly similar performances. As noticed above for the EOF decomposition of the reconstructed sea level grids, the DRAKKAR/NEMO- and altimetry-based reconstructions compare better with each other than with the SODA-based reconstruction. The reason for this is unclear. Possibly, each case at its advantages and drawbacks. For example, the models provide longer input sea level grids (50 years compared with the 17-year long altimetry record), allowing better capture of the low-frequency variability. But the dominant modes of sea level variability remain imperfectly simulated by the models, whereas they are likely better reproduced by the altimetry data. In fact, these factors act in producing more or less similar reconstructions.

In Fig. 8 is shown the map of the absolute value of the differences between reconstructed spatial trend patterns over 1950–2009 with DRAKKAR/NEMO (EOFs over 1958–2007, 15 modes) and SODA (EOFs over 1958–2007, 15 modes). The difference signal is low in tropical regions (on the order of 1–2 mm/year) but much higher in the mid and high latitudes, as well as in areas of western boundary currents, likely a result of the poor performance of models in these regions. This is an illustration of less robust reconstructed results in these particular regions whatever the choice of the input model.

5 Mean Reconstruction Based on Averaging of the DRAKKAR/NEMO-, SODA- and Altimetry-Based Reconstructions; Comparison with Published Reconstructions

As classically done in climate modelling, we averaged the three reconstructions discussed above to provide a 'mean' reconstruction. This was done by averaging at each yearly time step the three reconstructed grids. Figure 9a shows spatial trend patterns over 1950–2009 of this 'mean' reconstruction, with the global mean trend (of 1.8 mm/year) included. Figure 9b shows the same map in which the global mean trend has been removed. Figure 9c shows the standard deviation (rms) of the spatial trend patterns of the 'mean' reconstruction. Low rms are observed almost everywhere, except in western boundary current regions, south of Iceland and south-east of Papua New-Guinea . In these areas, the reconstructed signal should be taken with caution, as indicated above.

We compared the spatial trend patterns of our 'mean' reconstruction with those from Hamlington et al. (2011) based on cyclostationary functions. Over the altimetry period, the reconstructed patterns are very similar (and in good agreement with altimetry observations). However, over longer time spans (1950–2001), the patterns look quite different (see Fig. 6 of Hamlington et al. 2011). The exact cause of such a discrepancy, possibly due to the choice of the basis functions, remains to be investigated.

Figure 10 shows the global mean sea level over 1950–2009 based on the 'mean' reconstruction. Its trend amounts to 1.8 $\pm$ 0.1 mm/year. The 0.1 mm/year uncertainty is the formal error. A more realistic error is likely closer to 0.3–0.4 mm/year (e.g., Ray and Douglas 2011 and Church and White 2011 propose a mean trend error of 0.26 and 0.4 mm/

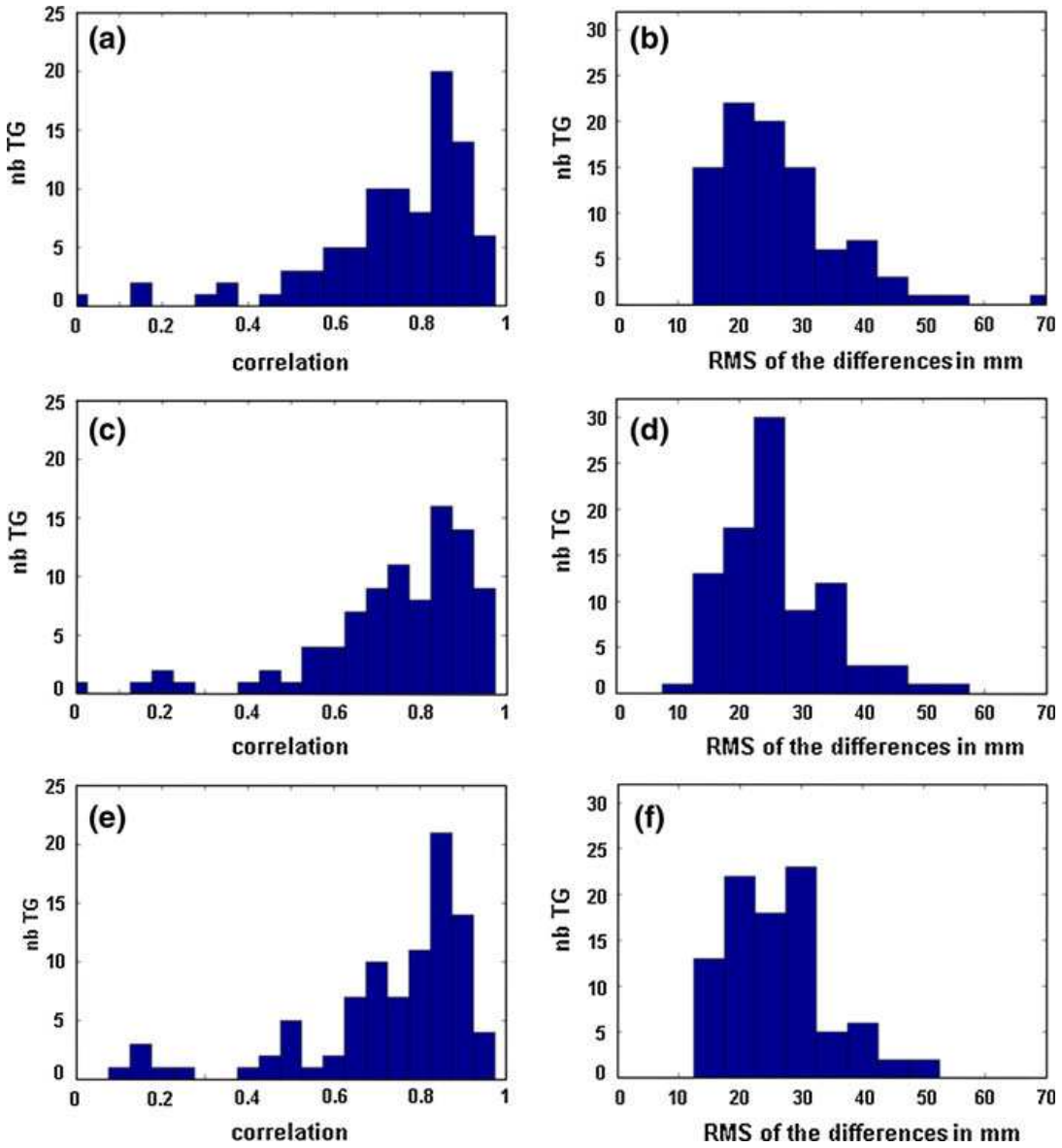

Fig. 7 Performance of the 15-mode reconstructions: (*left*) histogram of the correlations between observed and reconstructed sea level time series at tide-gauge sites not used in the reconstruction (91 sites considered); (*right*) histogram of rms difference (observed minus reconstructed) time series at the tide-gauge locations. **a** and **b** are for the DRAKKAR/NEMO reconstruction (EOFs over 1958–2007, 15 modes) while **c** and **d** are for the SODA reconstruction (EOFs over 1958–2007, 15 modes). **e** and **f** are for the altimetry-based reconstruction (EOFs over 1993–2009, 15 modes)

year, respectively, after accounting for various sources of errors, including GIA uncertainty).

Other published estimates of global mean sea level curves—either based on the reconstruction approach as described here or on other methods—are available in the literature (e.g., Chambers et al. 2002a, b; Church et al. 2004; Holgate 2007; Jevrejeva et al. 2006, 2008; Wenzel and Schroeter 2010; Church and White 2011; Ray and Douglas 2011; Hamlington et al. 2011). In Fig. 10, we have superimposed the global mean sea level curves based on the Church and White (2011) and Hamlington et al. (2011) reconstructions. The global mean sea level from our 'mean' reconstruction agrees very well with that from Church and White (2011) (within the uncertainty computed here as for Fig. 3d), both

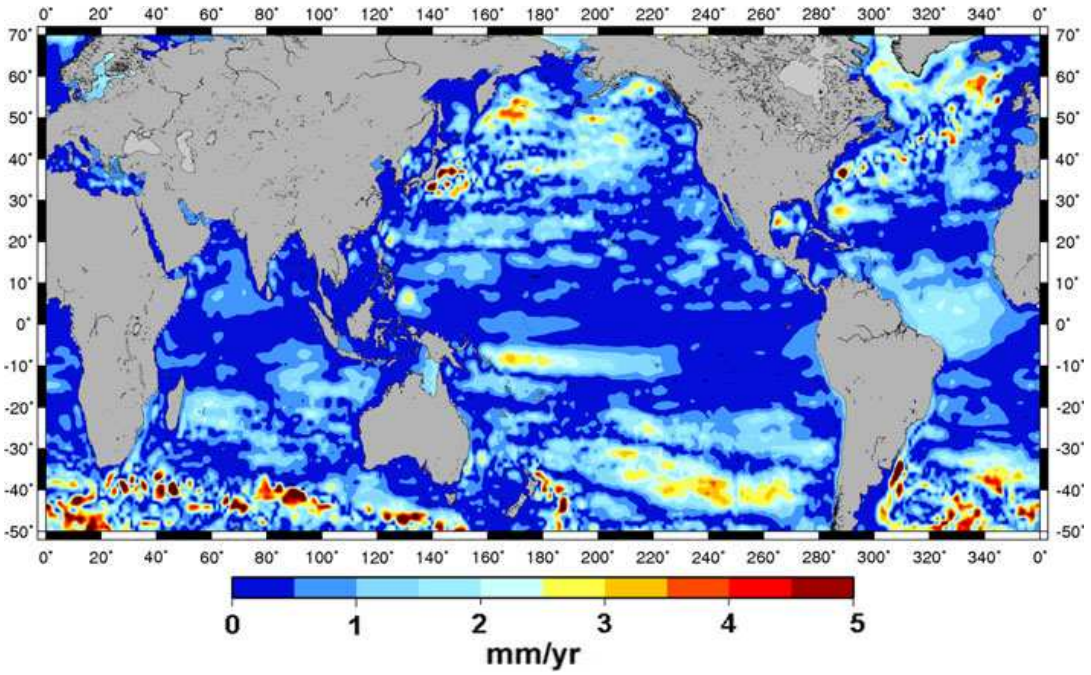

Fig. 8 Map of the absolute value of the differences between reconstructed spatial trend patterns over 1950–2009 with DRAKKAR/NEMO (EOFs over 1958–2007, 15 modes) and SODA (EOFs over 1958–2007, 15 modes)

in terms of interannual variability and trends (a trend of 1.8 mm/year is found with the Church and White data over 1950–2009). The agreement with the Hamlington et al. (2011) curve is not as good. The latter shows a larger trend of 1.95 ± 0.4 mm/year and slightly less interannual variability. Again, the difference may result from the choice of the basis functions.

Overall, the global mean sea level trend of our 'mean' reconstruction is very comparable to most previously published estimates for the second-half twentieth century. For the whole twentieth century, Ray and Douglas (2011)'s reconstruction proposes a value of 1.7 ± 0.26 mm/year quite similar to Church and White (2011) (equal to 1.7 ± 0.2 mm/year for 1900–2009). From a neuronal network technique, Wenzel and Schroeter (2010) found a trend of 1.6 ± 0.25 mm/year between 1900 and 2006.

6 Discussion

In this study, we developed and compared different 2-D sea level reconstructions based on the EOF approach, using different spatial grids as input. An EOF analysis of the reconstructed sea level fields shows a dominant low-frequency signal related to the PDO. Other leading modes are also related to other natural ocean modes, in particular ENSO.

Validation tests dedicated to estimate the influence of the number of EOF modes used for the reconstruction and the period of the input grids show that between 10 and 20 modes and input grids longer than 30–40 years optimize the results. The latter result is not really surprising as it is expected that the longer the input gridded data, the more complete the set of ocean modes of variability be accounted for in the reconstructed signal. The use of 50-year long OGCM grids to compute the input EOFs allows capturing low-frequency

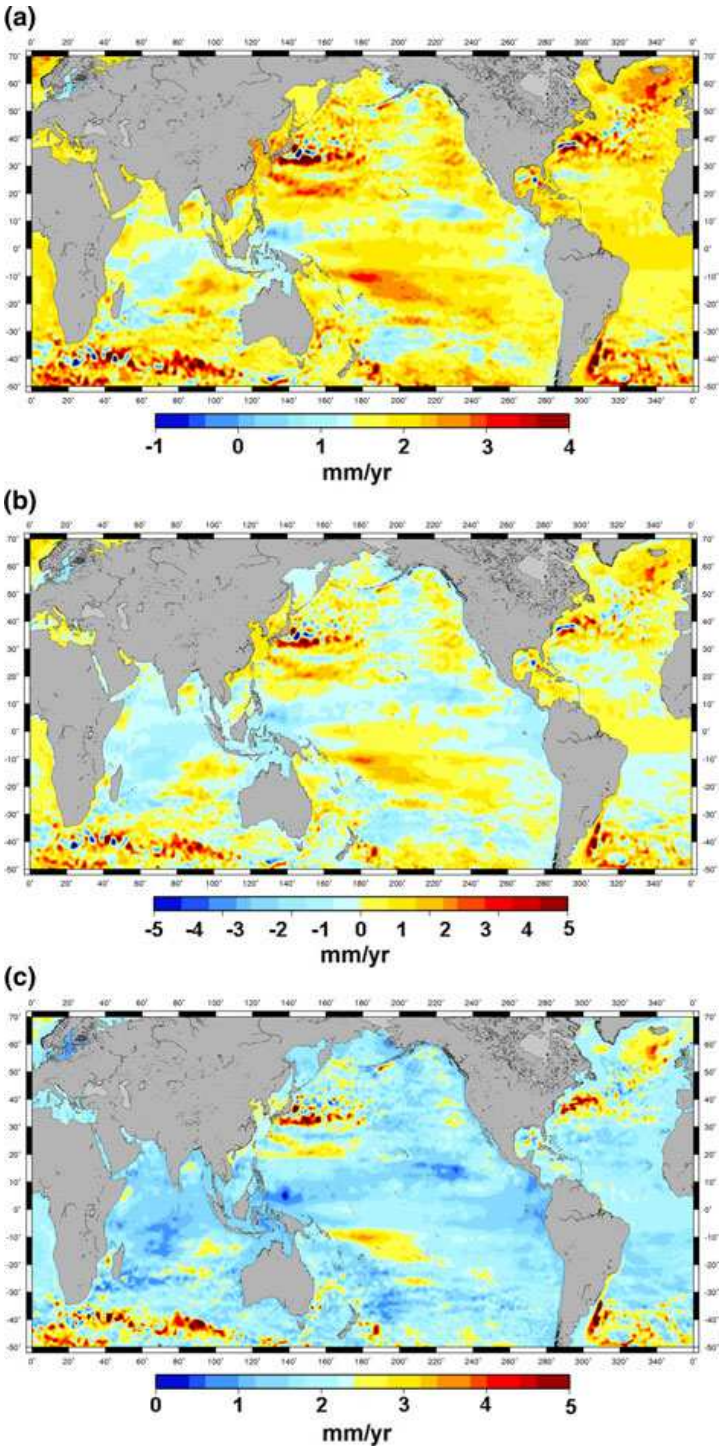

Fig. 9 Mean of the three reconstructions based on DRAKKAR (15 modes, EOF over 1958–2007), SODA (15 modes, EOF over 1958–2007) and altimetry. **a** Trends of the 'mean' reconstruction over 1950–2009. **b** Trends of the 'mean' reconstruction over 1950–2009. The global trend of 1.8 mm/year has been removed. **c** Standard deviation of the trends of the three reconstructions

modes of variability, in particular those related to the PDO. A similar conclusion was drawn by Llovel et al. (2009). However, the results presented above show that the spatial patterns of the reconstructed sea level are influenced by the input spatial grids (see Fig. 8).

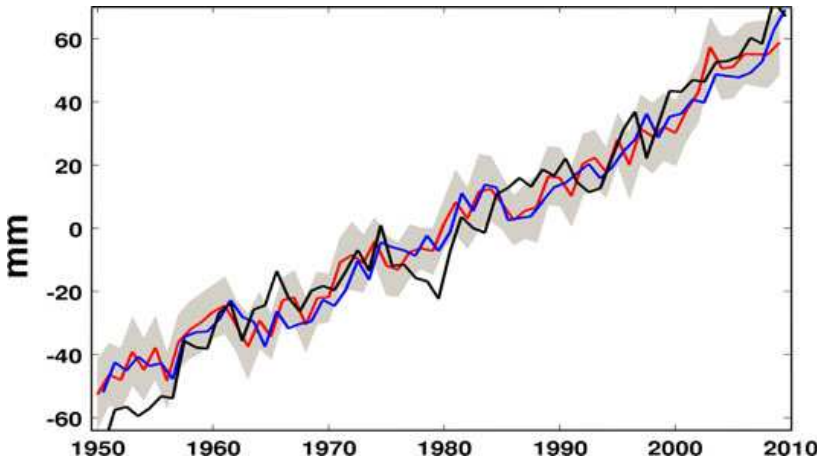

Fig. 10 Global mean sea level from the 'mean' reconstruction over 1950–2009 (*red curve*). We have added the reconstructed global mean sea level over 1950–2009 from Church et al. (2011) (*blue curve*) and Hamlington et al. (2011) (*black curve*). The grey shaded zone represents the uncertainty of the 'mean' reconstructed global mean sea level

The assessment performed in this study also showed that the DRAKKER/NEMO model-based and altimetry-based reconstructions compare rather well with each other (see Fig. 4). This is somewhat unexpected because the altimetry-based reconstruction uses only 17-years of input sea level grids. We interpret this as the result of some kind of compensation between longer input grids (from the model) and a better representation of the sea level variability (from the altimetry data). As a result, more or less similar reconstructions are obtained. Evidently, the best results are to be expected when 50 years of satellite altimetry will be available!

An interesting point is that the reconstructed global mean sea level is fairly independent of the input grids (see Fig. 3d). It appears also relatively independent of the tide-gauge selection. Indeed, we find a reconstructed global mean sea level very close to the Church and White (2011) one based on a different tide-gauge records selection.

Finally, one may wonder whether reconstructing past sea level has any interest provided that several OGCM outputs and ocean reanalyses now available are regularly improving and provide gridded sea level time series since the late 1950 s. While there is no doubt that ocean models improved much in the recent years, some differences are still observed between the models. This is illustrated in Fig. 11 showing the spatial trend difference map over 1958–2007 between DRAKKAR/NEMO and SODA. As for Fig. 8, we note that the difference signal is low in the tropics (on the order of only 1–2 mm/year) but higher in middle and high latitudes, probably reflecting that OGCMs and ocean reanalyses are still imperfect in these regions. Another argument to perform past 2-D sea level reconstructions is the fact that regional variability due to non-steric factors affects sea level. OGCMs and ocean reanalyses simulate steric variability only but not circulation changes due to land water mass addition or GIA or other mass redistribution effects causing solid Earth deformation and gravitational effects. To illustrate this, Fig. 12 shows the spatial trend difference map between the DRAKKAR model outputs over 1993–2007 and observed (altimetry-based) sea level over the same time span. Of course, the residual map seen in Fig. 12 may reflect model uncertainty, but we cannot exclude it also may well contain physical signal of non-steric origin present in the altimetry data but not in the model.

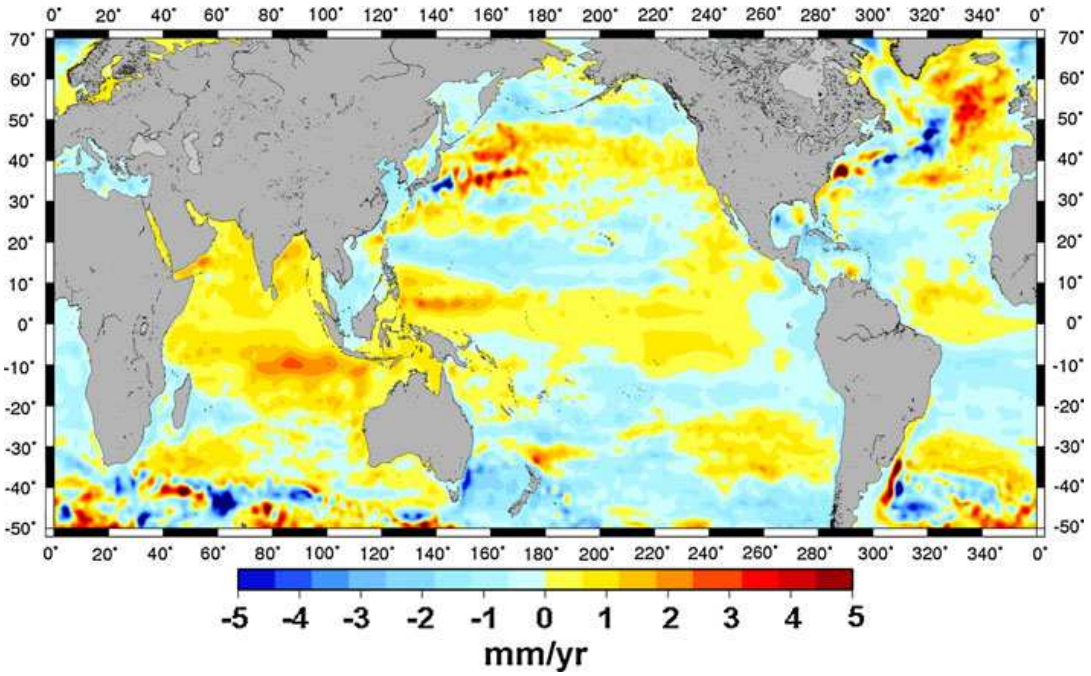

Fig. 11 Spatial trend pattern differences over 1958–2007 between DRAKKAR/NEMO model and SODA reanalysis

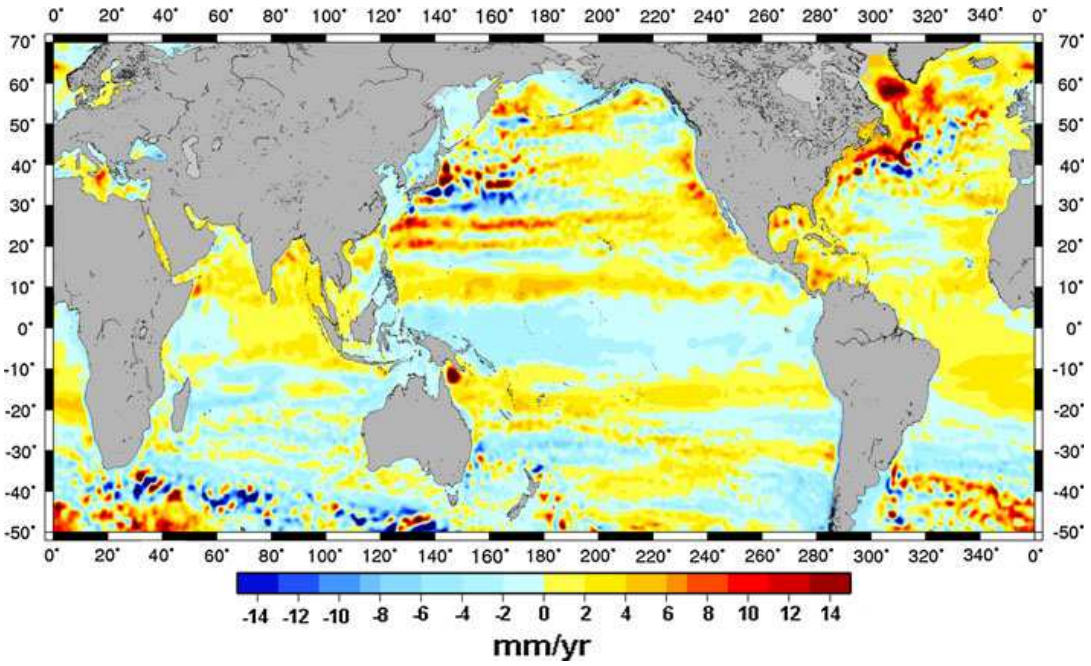

Fig. 12 Spatial trend pattern differences over 1993–2007 between DRAKKAR/NEMO model and altimetry-based sea level

Efforts to develop 2-D past sea level reconstructions are certainly worthwhile pursuing. However, as we have seen in this study, the reconstructed spatial trend patterns are somewhat dependent on the input spatial grids and basis functions. Using a larger number of tide-gauge data with improved spatial coverage may partly solve this problem. But the

tide-gauge coverage will never be good enough to capture all the sea level regional variability.

A potential solution of improvement is to perform 2-D reconstructions with an ensemble of input spatial grids (from different OGCMs and reanalyses) and then deduce a 'mean' reconstruction by averaging the different reconstructions, as done with coupled climate model projections of future regional sea level variability. In this study, we make a first attempt in this direction and produce a 'mean' reconstruction based on averaging reconstructed annual sea level grids from three independent reconstructions. This is a promising solution that should provide more and more realistic past sea level data when a larger set of reconstructions will be available.

Acknowledgments We thank two anonymous reviewers for their useful comments. M. Becker is supported by an ANR CNRS grant number ANR-09-CEP-001-01 (CECILE project). W. Llovel is supported by a NASA Postdoctorate fellowship. The 'mean' reconstructed sea level grids from the present study are available on request.

References

Ablain M, Cazenave A, Valladeau G, Guinehut S (2009) A new assessment of the error budget of global mean sea level rate estimated by satellite altimetry over 1993–2008. Ocean Sci 5:193–201

Altamimi Z, Collilieux X, Legrand J, Garayt B, Boucher C (2007) ITRF2005: a new release of the international terrestrial reference frame based on time series of station positions and earth orientation parameters. J Geophys Res 112:B09401. doi:10.1029/2007JB004949

Ashok K, Yamagata T (2009) Climate change: the El Niño with a difference. Nature 461:481–484. doi:10.1038/461481a

Barnier B, Madec G, Penduff T, Molines JM, Treguier AM, Le Sommer J, Beckmann A, Biastoch A, Böning C, Dengg J et al (2006) Impact of partial steps and momentum advection schemes in a global ocean circulation model at eddy-permitting resolution. Ocean Dyn 56:543–567

Berge-Nguyen M, Cazenave A, Lombard A, Llovel W, Viarre J, Cretaux JF (2008) Reconstruction of past decades sea level using thermosteric sea level, tide gauge, satellite altimetry and ocean reanalysis data. Glob Planet Change 62:1–13

Bonett DG, Wright TA (2000) Sample size requirements for estimating pearson, kendall, and spearman correlations. Psychometrica 65(1):23–28

Brodeau L, Barnier B, Treguier AM, Penduff T, Gulev S (2010) An ERA40-based atmospheric forcing for global ocean circulation models. Ocean Model 31:88–104

Calafat FM, Gomis D (2009) Reconstruction of Mediterranean sea level fields for the period 1945–2000. Glob Planet Change 66:225–234

Carrere L, Lyard F (2003) Modeling the barotropic response of the global ocean to atmospheric wind and pressure forcing—comparisons with observations. Geophys Res Lett 6:1275. doi:10.1029/2002GL016473

Carton JA, Giese BS (2008) A reanalysis of ocean climate using simple ocean data assimilation (SODA). Mon Weather Rev 136:2999–3017

Cazenave A, Llovel W (2010) Contemporary sea level rise. Annu Rev Mar Sci 2:145–173

Chambers DP, Mehlhaff CA, Urban TJ, Nerem RS (2002a) Analysis of interannual and low-frequency variability in global mean sea level from altimetry and tide gauges. Phys Chem Earth 27:1407–1411

Chambers DP, Mehlhaff CA, Urban TJ, Fuji D, Nerem RS (2002b) Low-frequency variations in global mean sea level: 1950–2000. J Geophys Res 107(C4):3026. doi:10.1029/2001JC001089

Christiansen B, Schmith T, Thejll P (2010) A surrogate ensemble study of sea level reconstructions. J Clim 23:4306–4326

Church JA, White NJ (2006) A 20th century acceleration in global sea-level rise. Geophys Res Lett 33:L01602. doi:10.1029/2005GL024826

Church JA, White NJ (2011) Changes in the rate of sea-level rise from the late 19th to the early 21st century. Surv Geophys 1–18. doi:10.1007/s10712-011-9119-1

Church JA, White NJ, Coleman R, Lambeck K, Mitrovica JX (2004) Estimates of the regional distribution of sea-level rise over the 1950 to 2000 period. J Clim 17(13):2609–2625

Church JA, White NJ, Konikow LF, Domingues CM, Cogley JG, Rignot E, Gregory JM, van den Broeke MR, Monaghan AJ, Velicogna I (2011) Revisiting the earth's sea level and energy budgets from 1961 to 2008. Geophys Res Lett. doi:10.1029/2011GL048794

DRAKKAR Group (2007) Eddy-permitting ocean circulation hindcasts of past decades. Clivar Exch 12(3):8–10

Dussin R, Treguier AM, Molines JM, Barnier B, Penduff T, Brodeau L, Madec G (2009) Definition of the interannual experiment ORCA025-B83, 1958–2007. LPO Report 902

Efron B, Tibshirani RJ (1993) An Introduction to the bootstrap. Chapman & Hall, New York

Greatbatch RJ (1994) A note on the representation of steric sea-level in models that conserve volume rather than mass. J Geophys Res 99:12767–12771

Hamlington BD, Leben R, Nerem S, Han W, Kim KY (2011) Reconstructing sea level using cyclostationary empirical orthogonal functions. J Geophys Res. doi:10.1029/2011JC007529

Holgate S (2007) On the decadal rates of sea level change during the twentieth century. Geophys Res Lett 34:L01602. doi:10.1029/2006GL028492

Jevrejeva S, Grinsted A, Moore JC, Holgate S (2006) Nonlinear trends and multiyear cycles in sea level records. J Geophys Res 111:C09012. doi:10.1029/2005JC003229

Jevrejeva S, Moore JC, Grinsted A, Woodworth PL (2008) Recent global sea level acceleration started over 200 years ago? Geophys Res Lett 35:L08715. doi:10.1029/2008GL033611

Jourdan D, Balopoulos E, Garcia-Fernandez MJ, Maillard C (1998) Objective analysis of temperature and salinity historical data set over the Mediterranean Basin, IEEE

Kalnay EC, Kanamitsu M, Kistler R, Collins W, Deaven D, Gandin L, Iredell M, Saha S, White G, Woollen J et al (1996) The NCEP/NCAR 40-year reanalysis project. Bull Am Meteorol Soc 77:437–472

Kaplan A, Cane MA, Kushnir Y, Clement AC, Blumenthal MB, Rajagopalan B (1998) Analyses of global sea surface temperature 1856–1991. J Geophys Res 103:18567–18589

Kaplan A, Kushnir Y, Cane MA (2000) Reduced space optimal interpolation of historical marine sea level pressure: 1854–1992. J Clim 13:2987–3002

Kohl A, Stammer D (2008) Decadal sea level changes in the 50-year GECCO ocean synthesis. J Clim 21:1876–1890

Large W, Yeager S (2004) Diurnal to decadal global forcing for ocean and sea ice models: the datasets and flux climatologies, NCAR Tech. Note NCAR/TN460 + STR, Natl Cent for Atmos Res, Boulder, Colorado

Levitus S, Antonov J, Boyer T (2005) Warming of the world ocean, 1955–2003. Geophys Res Lett 32:L02604. doi:10.1029/2004GL021592

Llovel W, Cazenave A, Rogel P, Lombard A, Bergé-Nguyen M (2009) Two-dimensional reconstruction of past sea level (1950–2003) from tide gauge data and an Ocean General Circulation Model. Clim Past 5:217–227

Lombard A, Cazenave A, Le Traon PY, Ishii M (2005) Contribution of thermal expansion to present-day sea level rise revisited. Glob Planet Change 47:1–16

Lombard A, Garric G, Penduff T (2009) Regional patterns of observed sea level change: insights from a 1/4A degrees global ocean/sea-ice hindcast. Ocean Dyn 59(3):433–449

Madec G (2008) NEMO reference manual, ocean dynamics component: NEMO-OPA. Preliminary version. Note du Pole de modélisation, Institut Pierre-Simon Laplace (IPSL), France, pp 1288–1619

Meyssignac B, Salas y Melia D, Becker M, Llovel W, Cazenave A (2011a) Tropical Pacific spatial trend patterns in observed sea level: internal variability and/or anthropogenic signature? Clim Past (in review)

Meyssignac B, Calafat SM, Somot S, Rupolo V, Stocchi P, Llovel W, Cazenave A (2011b) Two-dimensional reconstruction of the Mediterranean sea level over 1970–2006 from tide gauge data and regional ocean circulation model outputs. Glob Planet Change 77:49–61

Milne G, Gehrels WR, Hughes C, Tamisiea M (2009) Identifying the causes of sea level changes. Nat Geosci 2:471–478

Mitrovica JX, Gomez N, Clark PU (2009) The sea-level fingerprint of West Antarctic collapse. Science 323:753

Moore JC, Jevrejeva S, Grinsted A (2011) The historical sea level budget. Ann Glaciol 52959

Nerem RS, Chambers DP, Choe C, Mitchum GT (2010) Estimating mean sea level change from the TOPEX and Jason altimetermissions. Mar Geodesy 33(1):435–446

Nicholls RJ (2010) Impacts of and responses to sea level rise. In: Church J, Woodworth P, Aarup T, Wilson WS (eds) Understanding sea level rise and variability. Wiley-Blackwell, New York

Peltier WR (2004) Global glacial isostasy and the surface of the ice-age earth: the ICE-5G (VM2) model and GRACE. Annu Rev Earth Planet Sci 32:111–149

Penduff T, Juza M, Brodeau L, Smith G, Barnier B, Molines J, Treguier A, Madec G (2010) Impact of global ocean model resolution on sea-level variability with emphasis on interannual time scales. Ocean Sci 6:269–284

Preisendorfer RW (1988) Principal component analysis in meteorology and oceanography. Developments in atmospheric science, vol 17. Elsevier, Amsterdam

Ray R, Douglas B (2011) Experiments in reconstructing twentieth-century sea levels. Prog Oceanogr 91: 496–515

Rosner B (1975) On the detection of many outliers. Technometrics 17:221–227

Stammer D (2008) Response of the global ocean to Greenland and Antarctica melting. J Geophys Res 113:C06022. doi:10.1029/2006JC001079

Stammer D, Agarwal N, Herrmann P, Kohl A, Mechoso CR (2011) Response of a coupled ocean-atmosphere model to Greenland melting. Surv Geophys 32:621–642. doi:10.1007/s10712-011-9142-2

Steele M, Morley R, Ermold W (2001) PHC: a global ocean hydrography with a high quality Arctic Ocean. J Clim 14:2079–2087

Toumazou V, Cretaux JF (2001) Using a Lanczos eigensolver in the computation of empirical orthogonal functions. Mon Weather Rev 129:1243–1250

Uppala SM, da CostaBechtold V, Fiorino M, Gibson JK, Haseler J, Hernandez A, Kelly GA, Li X, Onogi K, Saarinen S, Sokka N, Allan RP, Andersson E, Arpe K, Balmaseda MA, Beljaars ACM, van de Berg L, Bidlot J, Bormann N, Caires S, Chevallier F, Dethof A, Dragosavac M, Fisher L, Fuentes M, Hagemann S, Hólm E, Hoskins BJ, Isaksen L, Janssen PAEM, Jenne R, McNally AP, Mahfouf J-F, Morcrette JJ, Rayner NA, Saunders RW, Simon P, Sterl A, Trenberth KE, Untch A, Vasiljevic D, Viterbo P, Woollen J (2005) The ERA-40 re-analysis. Q J Roy Meteorol Soc 131:2961–30128

Wenzel M, Schroeter J (2010) Reconstruction of regional mean sea level anomalies from tide gauges using neural networks. J Geophys Res 115:C08013. doi:10.1029/2009JC005630

Woodworth PL, Player R (2003) The permanent service for mean sea level: an update to the 21st century. J Coastal Res 19:287–295

Woppelmann G, Letetrel C, Santamaria A, Bouin MN, Collilieux X, Altamimi Z, Williams SDP, Martin Miguez B (2009) Rates of sea-level change over the past century in a geocentric reference frame. Geophys Res Lett 36:L12607. doi:10.1029/2009GL038720

Wunsch C, Ponte RM, Heimbach P (2007) Decadal trends in sea level patterns: 1993–2004. J Clim. doi: 10.1175/2007JCLI1840.1

Zhang Y, Wallace JM, Battisti DS (1997) ENSO-like interdecadal variability: 1900–93. J Clim 10: 1004–1020

Hydrol. Earth Syst. Sci., 15, 533–546, 2011
www.hydrol-earth-syst-sci.net/15/533/2011/
doi:10.5194/hess-15-533-2011

Hydrology and Earth System Sciences

Past terrestrial water storage (1980–2008) in the Amazon Basin reconstructed from GRACE and in situ river gauging data

M. Becker[1], **B. Meyssignac**[1], **L. Xavier**[1,2], **A. Cazenave**[1], **R. Alkama**[3], **and B. Decharme**[3]

[1]LEGOS/GOHS, UMR 5566/CNES/CNRS/UPS/IRD, Toulouse, France
[2]COPPE/UFRJ, Rio de Janeiro, Brazil
[3]Météo-France, CNRS, GAME, CNRM/GMGEC/UDC, Toulouse, France

Received: 28 September 2010 – Published in Hydrol. Earth Syst. Sci. Discuss.: 15 October 2010
Revised: 13 January 2011 – Accepted: 27 January 2011 – Published: 9 February 2011

Abstract. Terrestrial water storage (TWS) composed of surface waters, soil moisture, groundwater and snow where appropriate, is a key element of global and continental water cycle. Since 2002, the Gravity Recovery and Climate Experiment (GRACE) space gravimetry mission provides a new tool to measure large-scale TWS variations. However, for the past few decades, direct estimate of TWS variability is accessible from hydrological modeling only. Here we propose a novel approach that combines GRACE-based TWS spatial patterns with multi-decadal-long in situ river level records, to reconstruct past 2-D TWS over a river basin. Results are presented for the Amazon Basin for the period 1980–2008, focusing on the interannual time scale. Results are compared with past TWS estimated by the global hydrological model ISBA-TRIP. Correlations between reconstructed past interannual TWS variability and known climate forcing modes over the region (e.g., El Niño-Southern Oscillation and Pacific Decadal Oscillation) are also estimated. This method offers new perspective for improving our knowledge of past interannual TWS in world river basins where natural climate variability (as opposed to direct anthropogenic forcing) drives TWS variations.

1 Introduction

Terrestrial water storage (hereafter noted as TWS) is an important component of the global and continental water cycle. TWS refers to the total amount of water integrated over depth, stored in a catchment area. It is comprised of surface waters, soil moisture and underground waters. In some regions, TWS also includes snow. Variation of TWS with time t is linked to accumulated precipitation (P), evapotranspiration (ET), surface and subsurface runoff (R) within a given area or basin, through the water balance, written as:

$$\frac{d(\mathrm{TWS})}{dt} = P - \mathrm{ET} - R \quad (1)$$

Quantification of TWS variability and change is difficult because limited ground water level and soil moisture observations are available, and often are simply inadequate or inexistent (e.g., Rodell and Famiglietti, 1999; Shiklomanov et al., 2002; Alsdorf et al., 2007; Liu and Yang, 2010; Liu et al., 2009) at basin or smaller scales.

Global and regional hydrological models developed for water resources assessment and climate research purposes provide an alternative to missing in situ measurements (e.g., Döll et al., 2003; Milly and Shmakin, 2002, Rodell et al., 2004). Some of these models compute the water and energy balance at the Earth' surface, yielding – among other parameters, temporal variations of the total water storage in response to prescribed forcing (solar radiation and precipitation) and variations of near-surface atmospheric conditions. Since 2002, the Gravity Recovery and Climate Experiment (GRACE) space mission provides gridded time series of TWS at monthly or sub-monthly interval, with a resolution of ∼300–400 km (Tapley et al., 2004; Wahr et al., 2004) and a precision of ∼2 cm in equivalent water height (EWH) (in the following EWH refers to spatially distributed water storage while TWS refers to water storage averaged over a given area). GRACE provides a highly valuable new data set that allows studying water storage change over large river basins worldwide, complementary to precipitation, in situ river level and discharge data. However the GRACE lifetime is still short and does not allow studying past decade variability of

Correspondence to: M. Becker
(melanie.becker@legos.obs-mip.fr)

TWS. Only hydrological model outputs can be used for that purpose.

We have developed a novel method to reconstruct 2-dimensional (i.e., gridded) TWS over the past decades (since 1980). The method is similar to that classically used to reconstruct past atmospheric or oceanic fields such as marine sea level pressure (Kaplan et al., 2000), sea surface temperature (Smith and Reynolds, 2003) and sea level (Chambers et al., 2002; Church et al., 2004; Llovel et al., 2009; Calafat and Gomis, 2009). The method developed in the present study combines spatial information on TWS from GRACE (over 2003–2008) with multi-decade-long (over 1980–2008) but sparse river level time series based on in situ gauges. The past reconstructed TWS grids cover the 1980–2008 period. The method is applied to the Amazon Basin and is focussed on interannual variability.

Compared to classical reconstructions applied to atmospheric or oceanic data sets which combine grids and sparse records of the same physical quantity (e.g., surface atmospheric pressure or sea level), here this is not the case as we combine gridded TWS from GRACE with in situ river level records. River level is a component of the total TWS, related in a nonlinear way to inundation extent and thus surface water volumes. However, in the Amazon Basin, previous studies (e.g., Xavier et al., 2010; Vaz de Almeida, 2009) have shown that at seasonal and interannual time scales, river water level fluctuations can locally be correlated to TWS (as observed by GRACE). Such a correlation suggests that, at these time scales, TWS (including underground waters) and surface waters co-vary in a similar way. In the present study, we take advantage of this correlation at the interannual time scale and compute a scaling factor between river level and GRACE-based TWS over the GRACE time span (since 2002). This allows us to construct virtual multi-decade long TWS time series at the gauging sites for further combination of 2-D TWS grids from GRACE (of limited time duration) with sparse but long virtual TWS time series (based on the re-scaled river level time series). The final products are gridded (i.e., 2-D) time series of past TWS.

2 Data

2.1 In situ river level data

In this study, we use water level data from the in-situ gauging stations instead of river discharge data because it is one of the TWS components, unlike discharge. Since direct measurements of discharge in river channels can be time-consuming and costly, flow is commonly estimated indirectly by means of a curve relating stage (river level) to discharge (Clarke, 1999). Hence, uncertainties of stage measurements and rating curve method increase the final uncertainty. Using river level data is thus more straightforward (but note that our reconstruction method would also work with discharge data).

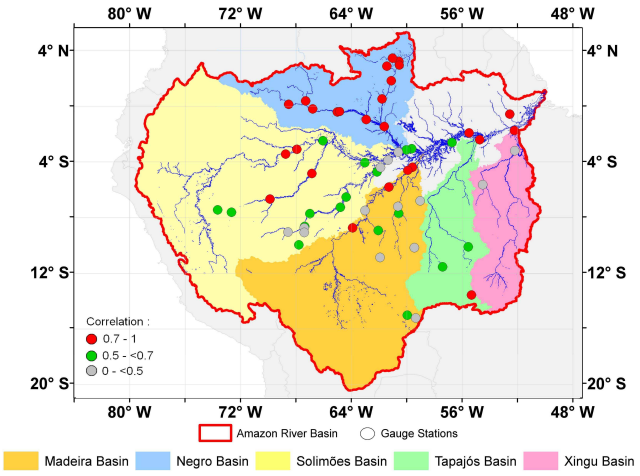

Fig. 1. Amazon River watershed with its main sub-basins. Location of the in situ river stages is indicated by dots. The red dots are the stations used in the reconstruction over 1980–2008 and correspond to a correlation coefficient $\geq$0.7 with GRACE TWS and in-situ level data over 2003–2008. The stations with a correlation coefficient in the range (0.5–0.7) are in green dots and in grey dots for a correlation coefficient $<$0.5.

We considered 58 in situ gauge sites with almost continuous water level time series over 1980–2008. The data are available from the Brazilian water agency ANA – Agência Nacional de Águas- network (www.ana.gov.br). The location of the 58 sites is shown in Fig. 1. The river level time series are located on the Amazon River and on some of its tributaries. They cover the period from January 1980 to December 2008 and are given at monthly interval. Only time series with gaps smaller than 2 consecutive years are considered (see Table 1). These gaps are then filled by linear interpolation. This dataset is subjected to outlier analysis in order to identify and remove extreme values that may lead to an incorrect interpretation of the data. In the present study, outliers are detected using the Rosner's test (Rosner, 1975). As we focus here on interannual to multidecadal time scales, we removed the seasonal cycles from in-situ river level data. The seasonal cycles in these data was removed by fitting sinusoids with periods of 12 and 6 months, before filling the gaps.

2.2 GRACE TWS data

The GRACE space mission, jointly developed by NASA and DLR (German Space Agency), was launched on 17 March 2002. It utilizes a state-of-the-art technique to measure temporal variations of the Earth's gravity field by tracking through a K-band ranging (KBR) system, the inter-satellite range and range rate between two coplanar, low altitude satellites (GRACE A and B) (Tapley et al., 2004). In addition, each satellite is equipped with a SuperSTAR Accelerometer, GPS receiver/antenna, Star Cameras, and

Table 1. Characteristics of the in-situ river level stations: location (latitude, longitude), name of the sub-basin, percentage of gaps in the record over 1980–2008 and maximum of consecutive months missing in the record (in the brackets, "–" means that no month is missing). Correlation GRACE-based TWS data over 2003-2008 (SL > 99%) and corresponding scaling factor. We average three pairs of in situ stations (ID: 6, 17 and 24) because these stations are in the same 1° × 1° GRACE pixel.

ID	Location (lat, lon)		Sub-basin	Percentage of gaps 1970–2008 (maximum gap in months)		Correlation with GRACE data 2003–2008	Scaling factor
1	−0.57	−52.57	–	2%	(3)	0.8	6
2	−1.92	−55.51	–	1%	(1)	0.7	7
3	−2.62	−56.73	–	10%	(21)	0.6	10
4	−3.06	−56.73	–	8%	(16)	0.6	11
5	−8.75	−63.92	Madeira	–	(–)	0.8	29
6	−4.39 −4.9	−59.6 −60.03	Madeira	2% 4%	(5) (7)	0.8	13
7	−5.82	−61.3	Madeira	7%	(14)	0.7	20
8	−8.93	−62.06	Madeira	8%	(17)	0.6	12
9	−15.01	−59.96	Madeira	9%	(9)	0.5	5
10	−7.71	−60.59	Madeira	1%	(2)	0.5	12
11	−7.21	−60.65	Madeira	5%	(3)	0.4	–
12	−10.87	−61.94	Madeira	8%	(19)	0.4	–
13	−10.17	−59.46	Madeira	12%	(12)	0.4	–
14	−7.5	−63.02	Madeira	4%	(10)	0.3	–
15	−6.8	−59.04	Madeira	3%	(3)	0.2	–
16	−15.22	−59.35	Madeira	7%	(11)	0.1	–
17	2.87 2.83	−61.44 −60.66	Negro	3% 7%	(5) (8)	0.9	5
18	0.51	−61.79	Negro	5%	(4)	0.9	12
19	−1.46	−61.63	Negro	2%	(4)	0.8	9
20	3.21	−60.57	Negro	11%	(6)	0.8	7
21	3.44	−61.04	Negro	16%	(17)	0.8	6
22	−0.97	−62.93	Negro	2%	(4)	0.8	8
23	1.82	−61.12	Negro	8%	(23)	0.8	8
24	−0.48 −0.42	−64.83 −65.02	Negro	3% –	(5) (–)	0.8	10
25	−0.2	−66.8	Negro	–	(–)	0.8	16
26	0.13	−68.54	Negro	9%	(8)	0.8	14
27	0.37	−67.31	Negro	2%	(5)	0.8	18
28	−3.14	−60.03	Negro	–	(–)	0.5	11
29	−3.45	−68.75	Solimões	2%	(5)	0.8	26
30	−3.1	−67.94	Solimões	3%	(3)	0.8	23
31	−6.68	−69.88	Solimões	9%	(10)	0.7	25
32	−4.84	−66.85	Solimões	5%	(5)	0.7	22
33	−7.72	−67	Solimões	2%	(3)	0.6	20
34	−6.54	−64.38	Solimões	5%	(4)	0.6	20
35	−2.49	−66.06	Solimões	7%	(14)	0.6	22
36	−9.97	−67.8	Solimões	2%	(7)	0.6	18
37	−7.45	−73.66	Solimões	4%	(4)	0.6	7
38	−7.63	−72.66	Solimões	3%	(3)	0.5	26
39	−7.26	−64.8	Solimões	3%	(5)	0.5	24
40	−4.73	−62.15	Solimões	15%	(20)	0.5	19
41	−4.06	−63.03	Solimões	5%	(7)	0.5	21
42	−8.65	−67.38	Solimões	6%	(11)	0.5	–
43	−8.74	−67.4	Solimões	10%	(7)	0.4	–
44	−3.31	−60.61	Solimões	1%	(2)	0.4	–
45	−3.88	−61.36	Solimões	7%	(14)	0.4	–
46	−4.41	−61.9	Solimões	7%	(6)	0.4	–
47	−9.07	−67.4	Solimões	12%	(11)	0.3	–
48	−9.04	−68.58	Solimões	7%	(12)	0.2	–
49	−13.56	−55.33	Tapajós	6%	(4)	0.6	8
50	−2.41	−54.74	Tapajós	5%	(12)	0.7	6
51	−11.54	−57.42	Tapajós	4%	(2)	0.6	5
52	−10.11	−55.57	Tapajós	7%	(14)	0.5	7
53	−1.75	−52.24	Xingu	7%	(5)	0.7	3
54	−3.21	−52.21	Xingu	1%	(5)	0.3	–
55	−5.65	−54.52	Xingu	9%	(9)	0.2	–

Laser Retro Reflector. The GRACE Science Data System uses measured inter-satellite range and range rate data, along with ancillary data, to estimate monthly (or sometimes sub-monthly) time series of global Earth's gravity fields (Bettadpur, 2007; Flechtner, 2007).

Time variable GRACE global gravity solutions are provided by three GRACE data processing centers of the Science Data System (SDS): Center for Space Research (CSR) at the University of Texas at Austin, the Geoforschungszentrum (GFZ) in Potsdam, and the NASA Jet Propulsion Laboratory (JPL). The GRACE solutions are distributed by NASA PODAAC (http://podaac.jpl.nasa.gov/grace/). Other groups external to SDS also provide GRACE solutions, e.g., the Goddard Space Flight Center (NASA; Rowlands et al., 2002), the Delft Institute of Earth Observation and Space Systems (DEOS; Klees et al., 2008), the Groupe de Recherche de Geodesie Spatiale (GRGS; Lemoine et al., 2007), among others. The GRACE monthly (or sub monthly) solutions are generally expressed in the form of spherical harmonic coefficients of the geoid height, up to some maximum degree (typically between 60 and 100, corresponding to wavelengths of ∼400 to 700 km). Gridded time series are also available, in general expressed in terms of EWH. Since the beginning of the mission, different GRACE solutions releases have been made available by the SDS groups, with improved quality from release to release. Here we use GRACE products (release 2) computed by the Groupe de Recherche de Geodesie Spatiale – GRGS (Bruisma et al., 2009). These are monthly EWH solutions provided as $1° \times 1°$ global grids from January 2003 through December 2008. As we focus here on interannual to multidecadal time scales, we removed the seasonal cycle from the gridded GRACE EWH by fitting sinusoids with periods of 12 and 6 months at each grid mesh.

We selected GRACE-based EWH data over the Amazon Basin. For small basins, it is necessary to correct for a leakage factor (due to gravitational signal from outside the considered basin; Chambers, 2006). However over the Amazon Basin, the leakage correction is ∼5% of the seasonal signal (Chen et al., 2007; Ramillien et al., 2008; Xavier et al., 2010). To confirm this result, we estimated the leakage error on the Amazon Basin following Klees et al. (2007) and Longuevergne et al. (2009). Outputs from the Global Land Data Assimilation System (GLDAS-NOAH) (Rodell et al., 2004) has been considered as an a-priori information to compute the leakage error over the period 2003–2008. We obtain a leakage error of about 5% of the seasonal cycle, as in previous studies, and around 3% of the interannual signal. As we focus here on the interannual variability, we conclude that the leakage error is negligible.

Figure 2 shows the first three leading modes of the Empirical Orthogonal Function (EOF) decomposition (Preisendorfer, 1988) of gridded TWS based on GRGS GRACE data over 2003-2008. The EOF mode 1 is dominated by a strong positive signal affecting the Negro subbasin and a small area in the southern part of the basin. The EOF mode 2 suggests

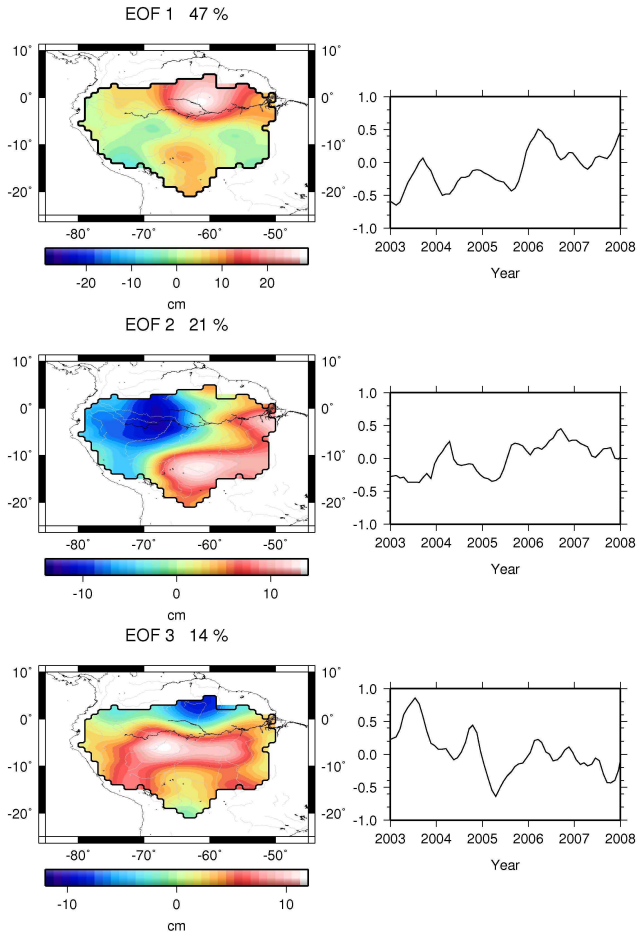

Fig. 2. EOF analysis of TWS from GRACE data over 2003–2008. Spatial patterns of the EOF decomposition of TWS. The three modes are arranged from top to bottom. The principal components are given in the right.

that the Amazon Basin is divided into two main hydrological zones (west and east). The EOF mode 3 shows the mid-2005 drought that affected the centre and the western part of the basin (Chen et al., 2009). These EOF results are very similar to those obtained by Xavier et al. (2010), who made an EOF decomposition of TWS from the CSR GRACE solutions filtered by Chambers (2006).

3 Relationship between GRACE-based TWS and in situ river levels

The first step of the analysis consists of expressing interannual river level data in terms of local EWH time series, taking advantage of the local correlation existing between in situ river level and GRACE-based TWS measurement at the river gauge location. Xavier et al. (2010) investigated this correlation and showed it is quite significant along the Amazon

River, and in the Madeira and Negro sub basins, in particular at interannual time scale.

We computed the regression function between in situ river level and GRACE-based EWH time series (annual cycle removed), averaging all in situ river level records available in each $1° \times 1°$ GRACE pixel (in order to not weight over pixels that contain more than one in situ station). The actual GRACE resolution is closer to ∼300 km (e.g., Schmidt et al., 2008) but tests made by averaging the in situ data in grid mesh of $3° \times 3°$ did not show significant difference in the reconstruction results. Computing the regression slope between the two data sets is equivalent to computing the ratio (called scaling factor) between the standard deviations of both river level and GRACE EWH time series (after removing their mean). The correlations and the scaling factors for each of 55 in-situ river level stations are gathered in Table 1 (see Fig. 1 for their location). Figure 3 shows in situ water level and GRACE EWH for a subset of 16 sites, chosen for their wide distribution across the basin (note that when 3 sites are located inside a single 1° 1° GRACE mesh, only mean location and mean river level time series are shown in Fig. 3; in these plots, river level time series are expressed in EWH using the computed scaling factor over span 2003–2008). From Table 1 and Fig. 3, we observe significant correlation on interannual time scale between the two data sets (river level and total TWS) at a given location. We also checked that the time series of the EOF decomposition of both GRACE and gauges are consistent over the GRACE period (not shown here).

Using the scaling factor computed over the validation period 2003–2008, TWS virtual records were then reconstructed backward in time (back to 1980) from the river level time series. In the reconstruction we only use in situ river levels that do verify a correlation higher than 0.7 with the closest GRACE data point. Only 23 sites verify the correlation among a total of 55. This may result from a different hydrodynamic behaviour between total water storage and surface waters (possibly because of the presence of seasonal floodplains; Alsdorf et al., 2000; or confluence with a tributary). In situ virtual TWS records used to reconstruct the past 2-D TWS fields will have in common that they are dominated by their surface water component variability. For the Negro subbasin Frappart et al. (2008) confirmed that the surface water component is not negligible in the interannual TWS, which is almost equally partitioned between surface water and the combination of soil moisture and groundwater. We cannot exclude that in other regions of the Amazon Basin, the relationship does not hold. At first sight, this could bias the reconstruction process. Actually this is not the case, as we will see below (see method in Sect. 4) since the functions (EOFs) used to interpolate the virtual records in the reconstruction process are statistical modes of the total TWS variability that intrinsically take into account the co-variability of the different layers of the soil at different places (the method optimally interpolates virtual TWS records that are all dominated by their surface waters). In other (not correlated) areas, reconstructed spatial patterns will be based on the statistical information contained in GRACE TWS grids (provided that these patterns are stationary; see discussion below).

4 Method

The method used to reconstruct past (over 1980–2008) TWS in 2-dimension over the Amazon Basin is based on the reduced optimal interpolation described by Kaplan et al. (2000) and used by Church et al. (2004) to reconstruct past sea level. This method has 2 steps. In the first step an EOF decomposition (Preisendorfer, 1988; Toumazou and Cretaux, 2001) of the GRACE-based TWS grids is done. This decomposition allows to separate the GRACE signal (here represented by a matrix **H**, with m lines for each spatial point and n columns for each date) into spatial modes (EOFs) and their related temporal amplitude as follow:,

$$\mathbf{H}(x,y,t) = U(x,y)\,\alpha(t). \quad (2)$$

In this equation $U(x,y)$ stands for the spatial modes and $\alpha(t)$ for their amplitude over the GRACE period. Assuming that the spatial modes $U(x,y)$ are stationary in time, we deduce that the reconstructed TWS field of the Amazon Basin over the long period 1980–2008 (called here $\mathbf{H}_{\mathrm{R}}(x,y,t)$) has an EOF as follow:

$$\mathbf{H}_R(x,y,t) = U(x,y)\,\alpha_{\mathrm{R}}(t). \quad (3)$$

where $\alpha_R(t)$ represents the new amplitudes of the EOFs over 1980–2008.

The second step consists of computing the new amplitudes $\alpha_{\mathrm{R}}(t)$ over the whole period 1980–2008 thanks to the in situ virtual TWS records. It is done through a least squares optimal procedure that minimizes the difference between the reconstructed field and the in situ virtual TWS records at the in situ gauge locations.

In the first step, the EOF modes and amplitudes of the GRACE data set matrix **H** are computed through a singular value decomposition approach, such that:

$$\mathbf{H} = U\mathbf{S}V^T \quad (4)$$

where $U(x,y)$ still stands for the EOF spatial modes, **S** is a diagonal matrix containing the singular values of **H** and V represents the temporal eigen modes. At this stage the amplitude $\alpha(t)$ of the EOF modes can be simply written as $\alpha(t) = \mathbf{S}V^T$. Conceptually, each EOF k (k-th column of $U(x,y)$ multiplied by the k-th line of $\alpha(t)$: $U_k(x,y)\alpha_k(t)$) is a spatio-temporal pattern of TWS variability that accounts for a percentage of the total variance of the TWS signal **H**. As stated in Eq. (2), the computation of the EOFs is purely statistical and has no information on the layers of the soil involved in the local variance of the EOFs. This information is actually randomly distributed in each EOFs so that each one of them carries variability that comes from all the layers. Obviously if at a location $(x_{\mathrm{s}},\ y_{\mathrm{s}})$ the total signal $\mathbf{H}(x_{\mathrm{s}},\ y_{\mathrm{s}})$

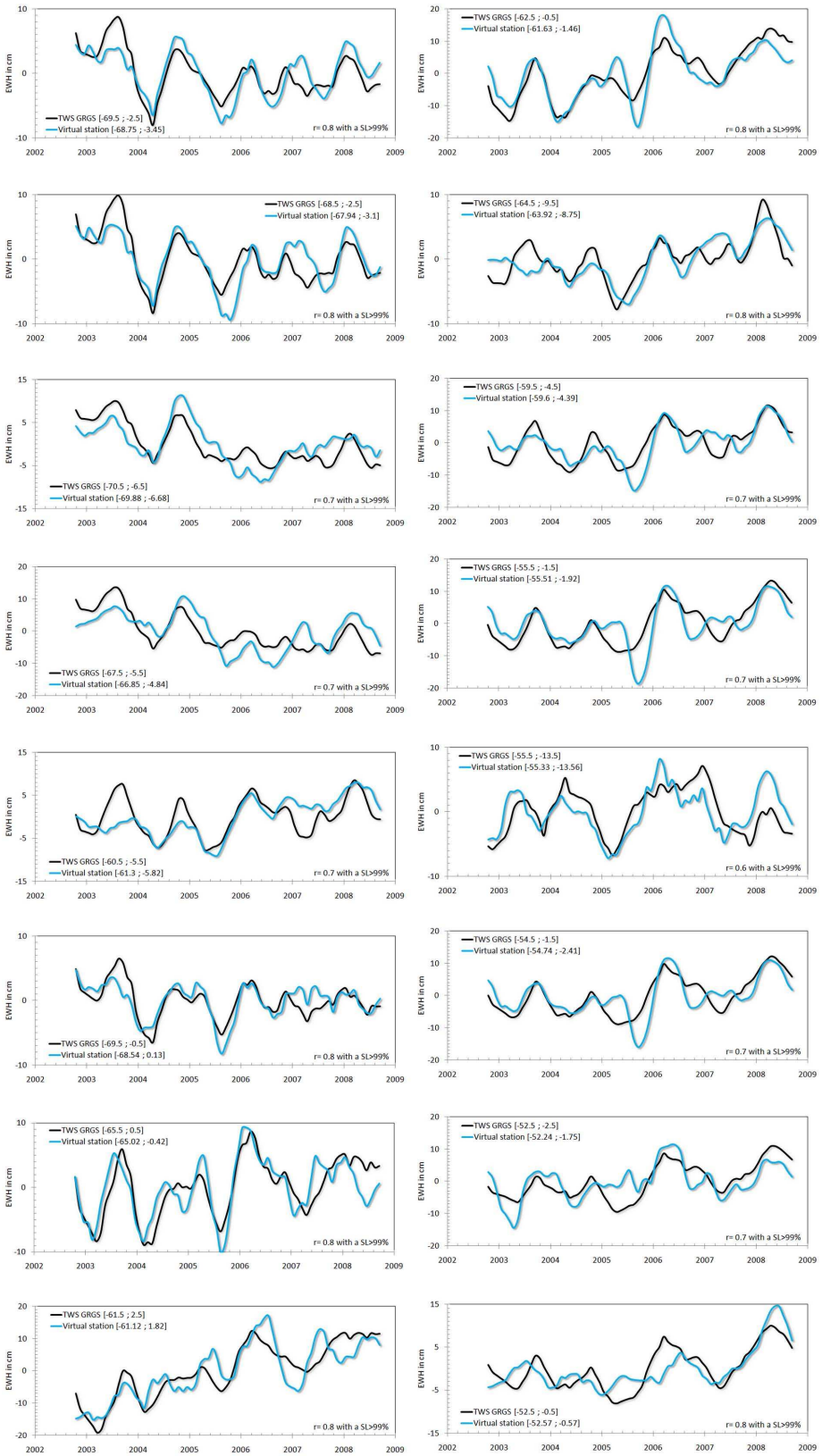

Fig. 3. Scaled EWH for in situ station. The figure shows the scaling result for some in situ stations (see red dots on Fig. 1 for locations). The TWS from GRACE over 2003–2008 period is plotted in black lines and the in situ river levels scaled in EWH over the same period are in blue lines. r is the correlation coefficient and SL its significance level.

is dominated by its surface water component, then for each EOF k, the signal $U_k(x_s,\ y_s)$ will also be dominated by the surface water. But at the same time, for other points $(x_j,\ y_j)$ where this is not the case, then $U_k(x_j,\ y_j)$ will carry variability from other layers. The $U_k(x, y)$ modes intrinsically take into account the co-variability of the different layers of the soil at different locations.

The low-order EOFs (eigenvectors of the largest singular values) explain most of the variance and contain the largest spatial scales of the signal. The higher-order EOFs contain smaller spatial scale patterns and are increasingly affected by noise. Besides, their amplitude is decreasingly well resolved by the least squares procedure because the sparseness of the set of in situ gauges does not allow to resolve too small scale patterns. Consequently, to be efficient, the TWS reconstruction over the Amazon Basin uses only a subset of the M lowest-order EOFs (the best fit between maximum variance explained and minimum noise perturbation led us to choose $M = 3$, which accounts for 79% of the total variance of the GRACE data).

Consequently; the data matrix $\mathbf{H}$ can be written as

$$\mathbf{H}_M\ =\ U_M(x,\ y)\ \boldsymbol{\alpha}(t) \tag{5}$$

where $\boldsymbol{\alpha}(t) = S_M V_M^T$ is the matrix of the amplitude of the M lowest EOFs. Following Kaplan et al. (2000), in the second step, we compute, at each time step over the time span of the in situ records, the amplitudes $\alpha_R(t)$ by minimizing the cost function:

$$\mathbf{S}(\alpha)\ =\ \left(\mathbf{P}U_M\,\alpha\ -\ \mathbf{H}^0\right)^T\ \mathbf{R}^{-1}\ \left(\mathbf{P}U_M\,\alpha\ -\ \mathbf{H}^0\right) \tag{6}$$
$$+\ \alpha^T\ \boldsymbol{\Lambda}^{-1}\,\alpha$$

In Eq. (6) $\mathbf{H}^0$ is the in situ observed TWS, $\mathbf{P}$ is a projection matrix equal to 1 when and where in situ records are available and 0 otherwise and $\boldsymbol{\Lambda}$ is a diagonal matrix of the M largest eigenvalues of the covariance matrix. $\mathbf{R}$ is the error covariance matrix accounting for the data error covariance matrix (instrumental error) and the error due to the truncation of the set of EOFs to only the first M EOFs. The second term on the right hand side of the function is a constraint on the EOF spectrum of the solution. It prevents the least squares procedure to be contaminated by high-frequency noise (it filters out non significant solutions that display too much variance at grid points without nearby observations). The least squares procedure is then applied to the virtual in situ TWS records ($\mathbf{H}^0$) deduced from the in situ water level records. It provides the reconstructed amplitude α_R of the EOFs.

Since virtual TWS records are all relative to their own local datum that are not cross-referenced over the basin, this solution may be polluted by spatial variability of the in situ TWS reference surface not necessarily consistent with the GRACE TWS reference surface. To cope with this problem we solved Eq. (3) for changes in TWS between adjacent steps following Church et al. (2004). Once changes in amplitude have been obtained at each time step, the amplitudes themselves have been recovered integrating backward in time. The integration constants are chosen to equal the reconstructed EOF amplitudes mean to the GRACE EOF amplitude mean over the GRACE measurement period, ensuring consistency between both sets of EOFs. Finally the reconstructed field of TWS over the Amazonian Basin is obtained by multiplying the first three EOFs with their reconstructed amplitude:

$$\mathbf{H}_R\ =\ U_M(x,\ y)\ \alpha_R(t) \tag{7}$$

5 Stationarity of the spatial patterns

Since the spatial structure of EOFs is sensitive to noise in the observational dataset, we use the longest GRACE dataset available. The GRACE record used in this study spans only 6 years between January 2003 and December 2008 (this is somewhat less but not significantly different from the 9 years of TOPEX/Poseidon altimetry data used by Church et al., 2004, to reconstruct past 50 years sea level). However, as full coverage of the Amazon Basin's TWS is only available for the GRACE period, there is no other way to determine TWS spatial patterns. As an alternative, EOFs could have been computed from long hydrological model outputs. But while hydrological models agree rather well in terms of TWS spatial average, they much differ when looking at the spatial patterns.

One possible drawback of using GRACE to compute spatial EOFs is linked to the question of (non) stationarity in time of the spatial patterns. Here, we assume that the EOF spatial patterns of the GRACE TWS capture most of the interannual/decadal variability. To test this stationary assumption (inherent to the method used here), we consider a dataset composed of 23 in situ gauges (black dots in Fig. 4, see below), spanning over the period 1980–2008. We computed the river level EOFs over three interval subsets (2003–2008, 1990–2008 and 1980–2008). Corresponding first 3 leading modes (>80% of the total variance) are shown in Fig. 4. Very little difference is noticed between the three cases. It is striking to see how the EOFs are similar despite the different time span over which they have been computed.

In addition, we computed the EOFs of the monthly $1° \times 1°$ gridded precipitation produced at the Global Precipitation Climatology Center (GPCC) (Rudolf, 1995) over the same three interval subsets (2003–2008, 1990–2008 and 1980–2008). As we focus here on interannual time scale, we removed the seasonal cycle from the gridded GPCC precipitation data. The first 3 leading modes for each case are shown in the Fig. 5. Again, very little difference is noticed between the three cases, suggesting that the shortest time span captures well most of the interannual variability. These results suggest that the main spatial structures are present in the in situ data and in precipitation data over the three periods considered (2003–2008, 1990–2008 and 1980–2008).

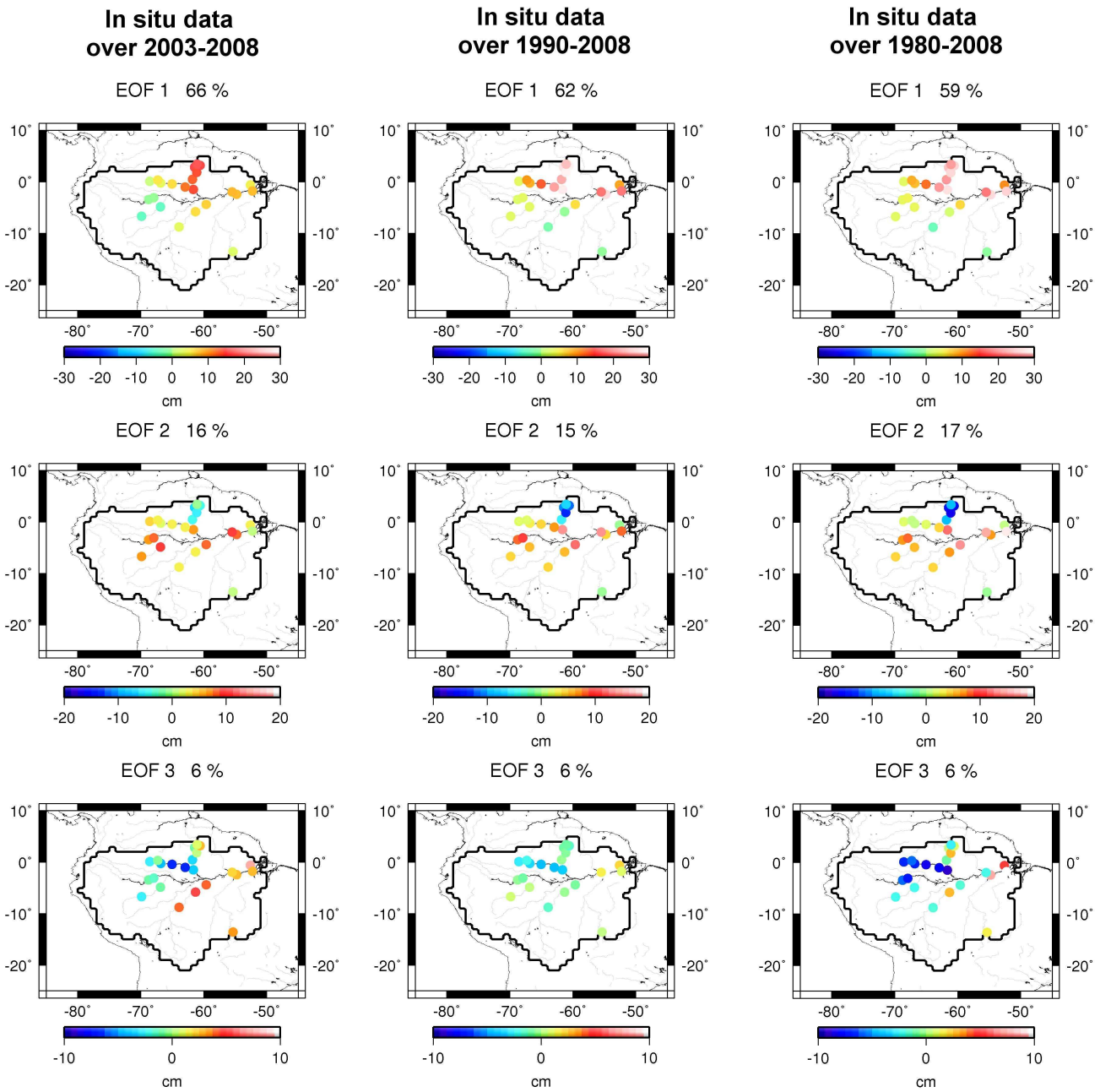

Fig. 4. Spatial patterns of the third EOFs computed from in situ gauges. The black dots correspond to the 23 in situ gauges (the same 23 used in the reconstruction) used for the EOF analysis over 2003–2008 (left panel), 1990–2008 (middle panel) and over 1980–2008 (right panel).

We conclude that surface water patterns (hence TWS fields, because of the reported correlation) and precipitation patterns are quasi stationary with time (at least as far as the early 1980s). Thus the basic assumption of our reconstruction method (stationarity of the spatial EOFs) holds.

6 Reconstruction of past TWS (TWSR): results

We applied the method described in Sect. 4 to the GRACE spatial modes and 23 in situ time series expressed in EWH (seasonal signal removed, as indicated above).

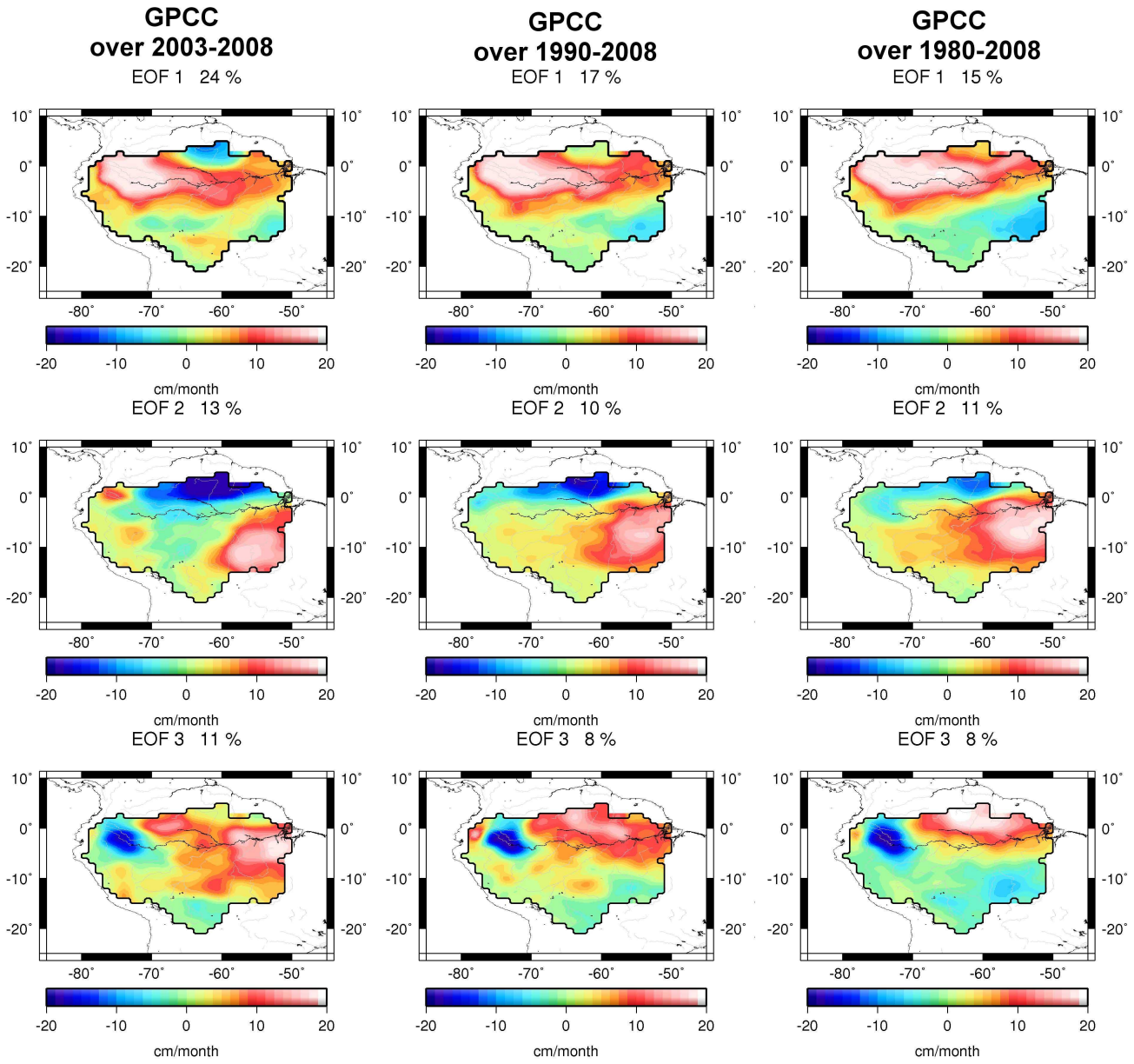

Fig. 5. Spatial patterns of the third EOFs computed from GPCC. EOF analysis over 2003–2008 (left panel), 1990–2008 (middle panel) and over 1980–2008 (right panel).

6.1 Reconstructed TWSR averaged over the Amazon Basin

Figure 6 shows past TWSR (1980–2008) averaged over the Amazon Basin (a 5-month smoothing was applied to the time series; TWSR holds for reconstructed TWS). For comparison, we also show the reconstructed TWSR (with same smoothing) over 1990–2008. For the latter case, a larger number (36) of in situ stations well correlated ($r > 0.7$) with GRACE TWS were available. Hence a larger number of virtual TWS time series could be used. Comparing the two reconstructions shows very little difference, suggesting that the number of virtual stations is not critical, provided that they are well distributed across the basin (see Fig. 1). In Fig. 6 is also shown GRACE-based mean TWS, which superimposes well with the reconstructed curves.

We compared mean TWSR over 1980–2008 with mean TWS computed by the ISBA-TRIP hydrological model. ISBA is a hydrological model that uses the force-restore method to calculate the time variation of the surface energy and water budgets (Noilhan and Planton, 1989). The soil hydrology is represented by three layers: a thin surface layer (1 cm) included in the rooting layer and a third layer to distinguish between the rooting depth and the total

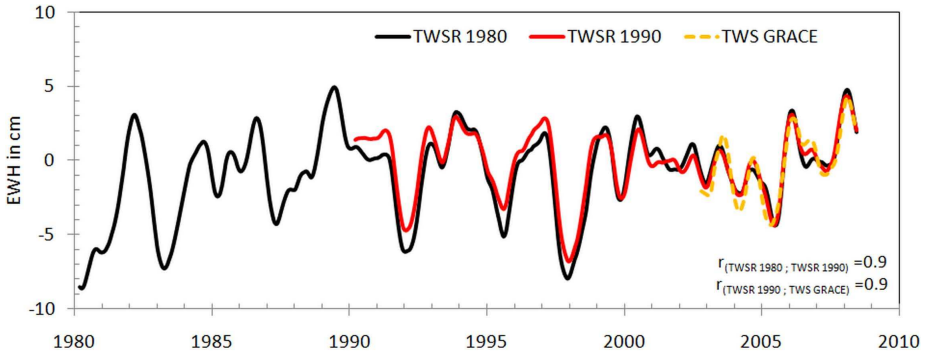

Fig. 6. Basin-averaged of the TWSR. The basin-averaged of the TWSR over 1980–2008 is the black line. The basin-averaged of the TWSR over 1990–2008 is the red line. The TWS GRACE data is superimposed in dot line over 2003–2008. We filtered out the high frequencies using a simple 5-month running mean. r is the correlation coefficient (with a significance level higher than 99%).

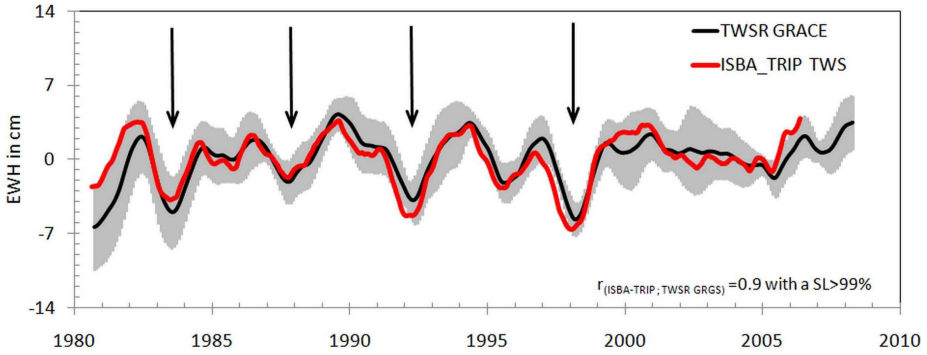

Fig. 7. Basin-averaged of the TWSR comparison with ISBA-TRIP. The basin-averaged of the TWSR is the black line and its error bars are in grey. The error in TWSR computed here is the sum of the error due to the least squares method and the error of the in situ records. This signal accounts for 60% of the total reconstructed signal variance. ISBA-TRIP is in red line. The El Niño events are represented by arrows. We filtered out the high frequencies ($>1\,\mathrm{yr}^{-1}$) using a simple 12-month running mean. r is the correlation coefficient (with a significance level higher than 99%).

soil depth. Several surface water storage compartments as dams, lakes, or groundwater storage are not simulated in the ISBA-TRIP model. The soil water content varies with surface infiltration, soil evaporation, plant transpiration and deep drainage. The infiltration rate is computed as the difference between the through-fall rate and the surface runoff. The through-fall rate is the sum of rainfall not intercepted by the canopy, dripping from the interception reservoir and snowmelt from the snow pack. ISBA also uses a comprehensive parameterization of sub-grid hydrology to account for the heterogeneity of precipitation, topography and vegetation within each grid cell (Decharme and Douville, 2007). TRIP -Total Runoff Integrating Pathways- was developed by Oki and Sud (1998). It is a simple runoff routine model used to convert the daily runoff simulated by 1° by 1° resolution. The ISBA-TRIP version used in this study is driven by prescribed atmospheric forcing using monthly precipitation data from the Global Precipitation Climatology Center (GPCC) Full Data Product V4 (Alkama et al., 2010; Decharme et al., 2010). The temporal resolution of this data set in 1 month. A fair comparison with GRACE observations requires that ISBA fields be spatially filtered in a similar way. To do this, ISBA-TRIP TWS gridded fields were expanded in spherical harmonic (SH) functions. SH coefficients were truncated at degree and order 50 (corresponding to a spatial resolution of ∼400 km). Then, new gridded ISBA-TRIP TWS were computed with the ISBA-TRIP SH truncated at degree 50. TWS based on ISBA-TRIP was averaged over the Amazon Basin, and as for GRACE data. The seasonal signal was removed data were smoothed with a 12-month running mean filter. ISBA-TRIP-based mean TWS for the 1980–2008 period is shown in Fig. 7. In Fig. 7, mean TWSR (as shown in Fig. 6) is superimposed. Looking at Fig. 7, we note that the two time series are well correlated, both in amplitude and timing. The correlation between the two time series amounts to 0.9 (significant at the 99% level), giving confidence in the mean TWSR, since the ISBA-TRIP simulation is based on a totally independent approach. Conversely, this mutual agreement provides another validation of the ISBA-TRIP model (see Alkama et al., 2010). Non account of ground water storage

in ISBA-TRIP could explain the small differences that remain between the two curves. We observe TWS minima during ENSO events (indicated by arrows in Fig. 7), as expected from previously reported correlation between ENSO and rainfall and in situ discharge data over the Amazon Basin (Marengo, 2004; Molinier et al., 2009; Ronchail et al., 2002). The lack of trend in both curves (reconstruction and ISBA-TRIP model) suggests no net gain or loss in total water storage over the Amazonian Basin between 1980 and 2008.

In Fig. 7, the grey zone represents uncertainty in TWSR. This uncertainty is based on the sum of errors due to the least-squares inversion (as presented in Sect. 4) and errors of the in situ records. This latter error is estimated from a bootstrap method for standard errors of the in situ water levels for each month (significant at the 95% level). Actually, the reconstruction method includes additional uncertainties. For example, the scaling factor between in situ river level and GRACE-based TWS may introduce some uncertainty. Indeed, river level may be more closely tied to the surface wetness condition than to groundwater (or TWS). Another source of error possibly be due to precipitation events in upstream areas, may affect downstream water levels with some time delay due to water transport. GRACE measurements have also their own uncertainty. As a matter of fact, GRACE-based TWS is not a point measurement (as it is the case for river level) but represents an average over a much larger region (of about 300 km size). All these uncertainties will affect the precision of the reconstruction but they are very difficult to estimate. They have been neglected here. Thus the grey zone likely underestimates of the actual uncertainty.

6.2 Spatial patterns of TWSR

We have analysed the spatial patterns of the 2-D TWSR fields over 1980–2008 and 1990–2008, through an EOF decomposition approach. Results are shown in Fig. 8. The spatially constant mode (EOF0, around 60% of the total variance for each TWSR) which represents the interannual variability of the mean TWSR over the Amazon Basin from 1980–2008 is that shown in Figs. 6 and 7.

Figure 8 shows the first three EOF modes of the TWSR fields over the two time spans (1990–2008 and 1980–2008). Recall that the 1990–2008 reconstruction is based on a larger set of in situ station than the 1980–2008 one (36 versus 23). Looking at the spatial pattern maps and at the temporal curves, we note quite good agreement between the two reconstructions (1990–2008 and 1980–2008), as previously noticed for the mean TWSR. On EOF1 (26% and 25% of the total variance) temporal curve, we have superimposed the Southern Oscillation Index (SOI; mean sea-level pressure difference between Tahiti and Darwin), a proxy of ENSO. Correlation between SOI and TWS mode 1 is high ($r = 0.7$ with a SL $>99\%$). In the north-eastern region, including the Negro sub-basin, and in the Madeira basin, where EOF1 exhibits a strong positive anomaly in the spatial map, minima in local TWS correspond to negative SOI (warm phase of ENSO). In contrast, a negative correlation can be observed locally between SOI and TWS mode 1 in the Tapajos and the Xingu sub-basins. Studies have shown that precipitation over the northeastern part of the Amazon Basin is largely controlled by ENSO (Zeng, 1999; Marengo, 1992; Espinoza et al., 2009). Thus, a positive correlation between mean TWS and SOI is expected, as our result indeed shows.

Studies provided diagnostic evidence of ENSO low frequency modulation (McCabe and Dettinger, 1999; Gutzler et al., 2002), in particular by the Pacific Decadal Oscillation (PDO) (Mantua et al., 1997). The PDO index is defined as the leading principal component of the North Pacific monthly sea surface temperature variability. The PDO is a long-lived El Niño–like pattern of Pacific climate variability. In the cool (warm) phases of PDO, the central and northwest Pacific sea surface temperature (SST) is warm (cold) and the SST at the coast of the North America is of cold (warm) SST. In Fig. 8, is displayed the EOF2 temporal curve of TWS with the PDO index superimposed. Correlation between PDO and TWS EOF2 is significant ($r = -0.5$ with a SL $>99\%$). In the whole eastern Amazon Basin, where the spatial EOF2 mode shows a negative pattern, local TWSR temporal variability is negatively correlated to the PDO index, while in the Negro and the Solimões sub-basins a positive correlation is observed.

The spatial pattern and temporal curve of the EOF3 in Fig. 8 reflect the recurrent droughts that affect the centre of the Amazon Basin, in particular the main river. These are indicated by arrows on the temporal curve. The well publicized 2005 drought is clearly visible. It has been reported to be one of the most intense droughts of the past 100 years in the Amazon Basin (Marengo et al., 2008; Zeng et al., 2008; Chen et al., 2009), but the TWSR mode 3 seems to indicate that the 1980 and 1998 droughts had even stronger impact in terms of basin total water storage depletion. Drought events in 1983 and 1998 occurred during El Niño years, unlike in 1980, 1992, 1995 and 2005.

7 Conclusions

The present study has established for the first time direct, observation-based, estimate of TWS spatiotemporal variability over the Amazon Basin for the past $\sim$3 decades. It is only based on TWS observations from GRACE and (re-scaled) in situ water levels. TWSR appears able to depict interannual to multidecadal variability in water storage and associated spatial patterns. Such an approach is complementary to traditional methods, e.g., moisture convergence method (Zeng, 1999; Masuda et al., 2001) or PER method, where the key input variables are observed precipitation P and runoff R and estimated evaporation ET. In these methods, the authors apply the basin water budget equation to diagnose the long-term variability of total TWS (Zeng et al., 2008).

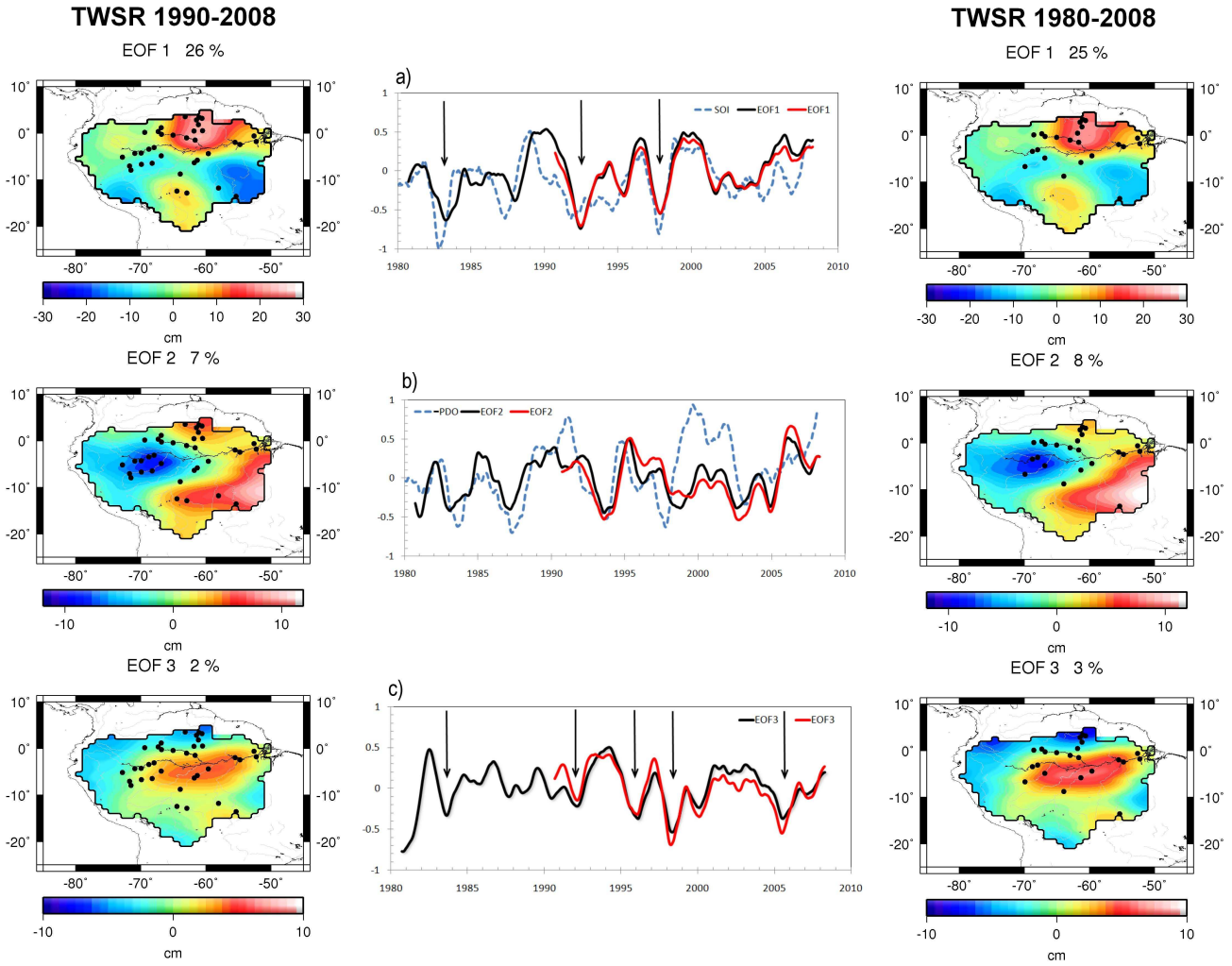

Fig. 8. EOF analysis of TWSR. The left panel shows the EOF analysis for the TWSR over 1990–2008. The locations of the 36 in situ stations used for the reconstruction are indicated by black dots. The right panel shows the EOF analysis for the TWSR over 1980–2008. The locations of the 23 in situ stations used for the reconstruction are indicated by black dots. The middle panel shows the EOFs' time series computed on the TWSR over 1990–2008 in red line and in black line over 1980–2008, and superimposed **(a)**the scaled SOI index (dash line) and the El Niño events (arrows), **(b)** the inverse scaled PDO index (dash line) and **(c)** the drought events (arrows). We filter out the high frequencies ($>1\,\mathrm{yr}^{-1}$) using a simple 12-month running mean.

The observed timing and regional distribution of the TWSR over the Amazonian Basin during ∼30 years shows no long-term trend and confirms the dominant influence of ENSO and PDO. In addition, recurrent drought events affecting the centre of the basin are also well reproduced. The approach developed in this study offers interesting perspective for improving our knowledge of past TWS in many river basins over the world where climate variability is the main driver of TWS change. However, it will be less easily applicable in river basins which have been strongly affected by anthropogenic forcing over the GRACE period, such as in northern India. Indeed, in these basins, GRACE measurement may be impacted by the recent ground water mining used for crop irrigation (Rodell et al., 2009; Tiwari et al., 2009). Thus GRACE EOFs will exhibit the spatial signature of this recent anthropogenic forcing and will be inappropriate to reconstruct past TWS variability in such regions. Some caution should then be highlighted in order that imprint of such events in GRACE data be not erroneously extrapolated backward in time.

Acknowledgements. M. Becker and R. Alkama were supported by the CYMENT project of the RTRA "Sciences et Technologies pour l'Aéronautique et l'Espace" STAE. L. Xavier has been supported by a grant of Brazilian agency CAPES (Coordenação de Aperfeiçoamento de Pessoal de Nível Superior).

Edited by: J. Liu

The publication of this article is financed by CNRS-INSU.

References

Alkama, R., Decharme, B., Douville, H., Becker, M., Cazenave, A., Sheffield, J., Voldoire, A., Tyteca, S., and Le Moigne, P.: Global evaluation of the ISBA-TRIP continental hydrologic system, Part 1: a two-fold constraint using GRACE terrestrial water storage estimates and in situ river discharges, J. Hydrometeorol., 11, 583 - 600, 2010.

Alsdorf, D. E., Melack, J. M., Dunne, T., Mertes, L. A. K., Hess, L. L., and Smith, L. C.: Interferometric radar measurements of water level changes on the Amazon floodplain, Nature, 404, 174–177, 2000.

Alsdorf, D. E., Rodriguez, E., and Lettenmaier, D. P.: Measuring surface water from space, Rev. Geophys., 45, 1–24, 2007.

Bettadpur, S.: CSR Level-2 Processing Standards Document for Product Release 04, GRACE 327-742, The GRACE Project, Center for Space Research, University of Texas at Austin, 2007.

Bruinsma, S., Lemoine, J.-M., Biancale, R., and Vales, N.: CNES/GRGS 10-day gravity field models (release 2) and their evaluation, Adv. Space Res., 45, 587–601, 2009.

Calafat, F. M. and Gomis, D.: Reconstruction of Mediterranean sea level fields for the period 1945–2000, Global Planet. Change, 66, 225–235, 2009.

Chambers, D. P.: Evaluation of new GRACE time-variable gravity data over the ocean, Geophys. Res. Lett., 33, L17603, doi:10.1029/2006GL027296, 2006.

Chambers, D. P., Mehlhaff, C. A., Urban, T. J., Fujii, D., and Nerem, R.: S. Low-frequency variations in global mean sea level: 1950–2000, J. Geophys. Res., 107, 3026, 2002.

Chen, J. L., Wilson, C. R., Famiglietti, J. S., and Rodell, M.: Attenuation Effects on Seasonal Basin-Scale Water Storage Change From GRACE Time-Variable Gravity, J. Geodesy, 81(4), 237–245, doi:10.1007/s00190-006-0104-2, 2007.

Chen, J. L., Wilson, C. R., Tapley, B. D., Yang, Z. L., and Niu, G. Y.: 2005 drought event in the Amazon River basin as measured by GRACE and estimated by climate models, J. Geophys. Res., 114, B05404, doi:10.1029/2008JB006056, 2009.

Church, J. A., White, N. J., Coleman, R., Lambeck, K., and Mitrovica, J. X.: Estimates of the regional distribution of sea level rise over the 1950–2000 period, J. Climate, 17, 2609–2625, 2004.

Clarke, R. T.: Uncertainty in the estimation of mean annual flood due to rating-curve in definition, J. Hydrol., 22(1–4), 185–190, doi:10.1016/S0022-1694(99)00097-9, 1999.

Decharme, B. and Douville, H.: Global validation of the ISBA sub-grid hydrology, Clim. Dynam., 29, 21–37, 2007.

Decharme, B., Alkama, R., Douville, H., Becker, M., and Cazenave, A.: Global Evaluation of the ISBA-TRIP Continental Hydrological System, Part II: Uncertainties in River Routing Simulation Related to Flow Velocity and Groundwater Storage, J. Hydrometeorol., 11, 601–617, 2010.

Döll, P., Kaspar, F., and Lehner, B.: A global hydrological model for deriving water availability indicators: model tuning and validation, J. Hydrol., 270, 105–134, 2003.

Espinoza Villar, J. C., Ronchail, J., Guyot, J. L., Cochonneau, G., Naziano, F., Lavado, W., De Oliveira, E., Pombosa, R., and Vauchel, P.: Spatio-temporal rainfall variability in the Amazon basin countries (Brazil, Peru, Bolivia, Colombia, and Ecuador), Int. J. Climatol., 29(11), 1574–1594, 2009.

Flechtner, F.: GFZ Level-2 Processing Standards Document for Product Release 04, GRACE, Department 1: Geodesy and Remote Sensing, GeoForschungszentrum Potsdam, Flechtner, 2007.

Frappart, F., Papa, F., Famiglietti, J. S., Prigent, C., Rossow, W. B., and Seyler, F.: Interannual variations of river water storage from a multiple satellite approach: A case study for the Rio Negro River basin, J. Geophys. Res., 113, D21104, doi:10.1029/2007JD009438, 2008.

Gutzler, D. S., Kann, D. M., and Thornbrugh, C.: Modulation of ENSO-based long-lead outlooks of southwestern US winter precipitation by the Pacific Decadal Oscillation, Weather Forecast., 17, 1163–1172, 2002.

Kaplan, A., Kushnir, Y., and Cane, M. A.: Reduced space optimal interpolation of historical marine sea level pressure: 1854–1992, J. Climate, 13, 2987–3002, 2000.

Klees, R., Zapreeva, E. A., Winsemius, H. C., and Savenije, H. H. G.: The bias in GRACE estimates of continental water storage variations, Hydrol. Earth Syst. Sci., 11, 1227–1241, doi:10.5194/hess-11-1227-2007, 2007.

Klees, R., Liu, X., Wittwer, T., Gunter, B. C., Revtova, E. A., Tenze, R., Ditmar, P., Winsemius, H. C., and Savenije, H. H. G.: A comparison of global and regional GRACE models for land hydrology, Surv. Geophys., 29, 335–359, 2008.

Lemoine, J. M., Bruinsma, S., Loyer, S., Biancale, R., Marty, J. C., Perosanz, F., and Balmino, G.: Temporal gravity field models inferred from GRACE data, Adv. Space Res., 39(10), 1620–1629, 2007.

Liu, J. and Yang H.: Spatially explicit assessment of global consumptive water uses in cropland: green and blue water, J. Hydrol., 384, 187–197, 2010.

Liu, J., Zehnder, A. J. B., and Yang, H.: Global consumptive water use for crop production: The importance of green water and virtual water, Water Resour. Res., 45, W05428, doi:10.1029/2007WR006051, 2009.

Llovel, W., Cazenave, A., Rogel, P., Lombard, A., and Nguyen, M. B.: Two-dimensional reconstruction of past sea level (1950-2003) from tide gauge data and an Ocean General Circulation Model, Clim. Past, 5, 217–227, doi:10.5194/cp-5-217-2009, 2009.

Longuevergne, L., Scanlon, B. R., and Wilson, C. R.: GRACE Hydrological estimates for small basins: Evaluating processing approaches on the High Plains Aquifer, USA, Water Resour. Res., 46, W11517, doi:10.1029/2009WR008564, 2010.

Mantua, N. J., Hare, S. R., Zhang, Y., Wallace, J. M., and Francis, R. C.: A Pacific interdecadal climate oscillation with impacts on salmon production, B. Am. Meteorol. Soc., 78, 1069–1079, 1997.

Marengo, J. A.: Interannual variability of surface climate in the Amazon basin, Int. J. Climatol., 12, 853–863, 1992.

Marengo, J. A.: Interdecadal variability and trends of rainfall across the Amazon basin, Theor. Appl. Climatol., 78, 79–96, 2004.

Marengo, J. A., Nobre, C. A., Tomasella, J., Oyama, M. D., Sampaio de Oliveira, G., de Oliveira, R., Camargo, H., Alves, L. M., and Brown, I. F.: The drought of Amazonia in 2005, J. Climate, 21, 495–516, 2008.

Masuda, K., Hashimoto, Y., Matsuyama, H., and Oki, T.: Seasonal cycle of water storage in major river basins of the world, Geophys. Res. Lett., 28, 3215–3218, 2001.

McCabe, G. J. and Dettinger, M. D.: Decadal variations in the strength of ENSO teleconnections with precipitation in the western United States, Int. J. Climatol., 19, 1399–1410, 1999.

Milly, P. C. D. and Shmakin, A. B.: Global modeling of land water and energy balances, Part I: The Land Dynamics (LaD) model, J. Hydrometeorol., 3, 283–299, 2002.

Molinier, M., Ronchail, J., Guyot, J. L., Cochonneau, G., Guimaraes, V., and de Oliveira, E.: Hydrological variability in the Amazon drainage basin and African tropical basins, Hydrol. Process., 23, 3245–3252, 2009.

Noilhan, J. and Planton, S.: A simple parameterization of land surface processes for meteorological models, Mon. Weather Rev., 117, 536–549, 1989.

Oki, T. and Sud, Y.: Design of the global river channel network for Total Runoff Integrating Pathways (TRIP), Earth Interact., 2, 1–36, 1998.

Preisendorfer, R. W.: Principal Component Analysis in Meteorology and Oceanography, New York, 1–455, 1988.

Ramillien, G., Bouhours, S., Lombard, A., Cazenave, A., Flechtner, F., and Schmidt, R.: Land water storage contribution to sea level from GRACE geoid data over 2003–2006, Global Planet. Change, 60, 381–392, doi:10.1016/j.gloplacha.2007.04.002, 2008.

Rodell, M. and Famiglietti, J. S.: Detectability of variations in continental water storage from satellite observations of the time dependent gravity field, Water Resour. Res. 35, 2705–2724, 1999.

Rodell, M., Houser, P. R., Jambor, U., Gottschalck, J., Mitchell, K., Meng, C. J., Arsenault, K., Cosgrove, B., Radakovich, J., and Bosilovich, M.: The global land data assimilation system, B. Am. Meteorol. Soc., 85, 381–394, 2004.

Rodell, M., Velicogna, I., and Famiglietti, J. S.: Satellite-based estimates of groundwater depletion in India, Nature, 460, 999–1002, 2009.

Ronchail, J., Cochonneau, G., Moloinier, M., Guyot, J. L., Goretti de Miranda Chaves, A., Guimaraes, V., and De Oliveira, E.: Interannual rainfall variability in the Amazon basin and sea-surface temperatures in the equatorial Pacific and the tropical Atlantic Oceans, Int. J. Climatol., 22, 1663–1686, 2002.

Rosner, B.: On the detection of many outliers, Technometrics, 17, 221–227, 1975.

Rowlands, D. D., Ray, R. D., Chinn, D. S., and Lemoine, F. G.: Short-arc analysis of intersatellite tracking data in a gravity mapping mission, J. Geodesy, 76, 307–316, 2002.

Rudolf, B.: The Global Precipitation Climatology Centre, WMO Bull., 44, 77–78, 1995.

Schmidt, R., Flechtner, F., Meyer, U., Neumayer, K. H., Dahle, Ch., Konig, R., and Kushe, J.: Hydrological signals observed by the GRACE satellites, Surv. Geophys., 29, 319–334, 2008.

Shiklomanov, A. I., Lammers, R. B., and Vorosmarty, C. J.: Widespread decline in hydrological monitoring threatens, Pan-Arctic research, EOS Transact. AGU, 83, 13–16, 2002.

Smith, T. M. and Reynolds, R. W.: Extended reconstruction of global sea surface temperatures based on COADS data (1854–1997), J. Climate, 16, 1495–1510, 2003.

Tapley, B. D., Bettadpur, S., Watkins, M., and Reigber, C.: The gravity recovery and climate experiment: Mission overview and early results, Geophys. Res. Lett., 31, L09607, doi:10.1029/2004GL019920, 2004.

Tiwari, V. M., Wahr, J., and Swenson, S.: Dwindling groundwater resources in northern India, from satellite gravity observations, Geophys. Res. Lett., 36, L18401, doi:10.1029/2009GL039401, 2009.

Toumazou, V. and Cretaux, J. F.: Using a Lanczos eigensolver in the computation of Empirical Orthogonal Functions, Mon. Weather Rev., 129, 1243–1250, 2001.

Vaz De Almeida, F. : Study of the temporal variations of the terrestrial gravitational field from the GRACE mission data: Application in the Amazonian basin, Ph.D. thesis, University of São Paulo, Brazil, 2009.

Wahr, J., Swenson, S., Zlotnicki, V., and Velicogna, I.: Time-variable gravity from GRACE: First results, Geophys. Res. Lett., 31, L11501, doi:10.1029/2004GL019779, 2004.

Xavier, L., Becker, M., Cazenave, A., Longuevergne, L., Llovel, W., and Rotunno Filho, O. C.: Interannual variability in water storage over 2003–2008 in the Amazon Basin from GRACE space gravimetry, in situ river level and precipitation data, Remote Sens. Environ., 114, 1629–1637, 2010.

Zeng, N.: Seasonal cycle and interannual variability in the Amazon hydrologic cycle, J. Geophys. Res.-Atmos., 104, 9097–9106, 1999.

Zeng, N., Yoon, J. H., Mariotti, A., and Swenson, S.: Variability of basin-scale terrestrial water storage from a PER water budget method: The Amazon and the Mississippi, J. Climate, 21, 248–265, 2008.

2.2.3 Résultats des reconstructions et discussion

En résumé, les reconstructions du niveau de la mer sont une alternative aux modèles d'océan forcés et aux réanalyses pour estimer le niveau de la mer en 2 dimensions sur les dernières décennies (depuis 1950).

En ce qui concerne le niveau de la mer global depuis 1950, les différentes reconstructions donnent des résultats similaires en terme de tendance avec une estimation de l'augmentation du niveau de la mer à 1.8 ± 0.2 mm.a^{-1} entre 1950 et 2009 (voir Fig. 2.8). Ceci est en accord avec les études basées sur les marégraphes seulement (voir section 1.2.1). En revanche, elles présentent des différences dans la variabilité inter-annuelle du niveau moyen global de la mer comme cela est illustré sur la Fig. 2.8.

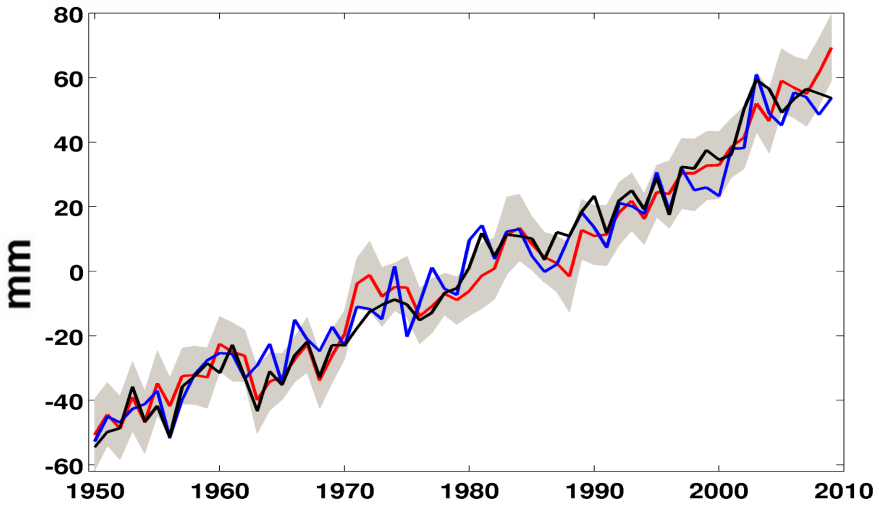

Figure 2.8 – Niveau global de la mer estimé par des reconstructions basées sur DRAKKAR (courbe noire), sur SODA (courbe bleue) et sur l'altimétrie (courbe rouge). La region ombrée est l'incertitude associée à la reconstrucion basée sur l'altimétrie. La tendance sur la periode 1950-2009 est de 1.8 mm.a^{-1}. Figure adaptée de *Meyssignac et al.* [2012].

En variabilité régionale sur la période 1950-2009, les reconstructions s'accordent pour montrer des structures spatiales très différentes de celles observées par altimétrie entre 1993 et 2009, avec des amplitudes 3 à 4 fois plus faibles sur les tendances (voir Fig. 2.9a). Ceci confirme les résultats obtenus avec les modèles d'océan forcés et les réanalyses (voir section 2.2.1). Nous en déduisons que les tendances spatiales observées aujourd'hui par l'altimétrie (Fig. 1.12) ne sont probablement pas stationnaires mais changent avec le temps et l'espace (voir la question scientifique n°8 de la section 1.5 et le chapitre 4). En régional, aux moyennes et hautes latitudes, les reconstructions présentent des différences significatives entre elles. Elles diffèrent aussi régionalement des modèles d'océan forcés et des réanalyses sur la majorité du globe. Ceci montre que l'incertitude sur la variabilité régionale des tendances du niveau de la mer des 60 dernières années reste encore grande. Sur la base des reconstructions uniquement, on peut estimer cette incertitude à environ ±2.5 mm.a^{-1} en tendance (voir Fig. 2.9b). Elle est plus forte encore dans les régions de forte variabilité

comme dans les courants de bord Ouest. In fine, seule la comparaison avec des marégraphes (non-utilisés dans les reconstructions) peut déterminer localement la fiabilité d'une reconstruction car c'est l'unique source de mesure directe du niveau de la mer avant 1993.

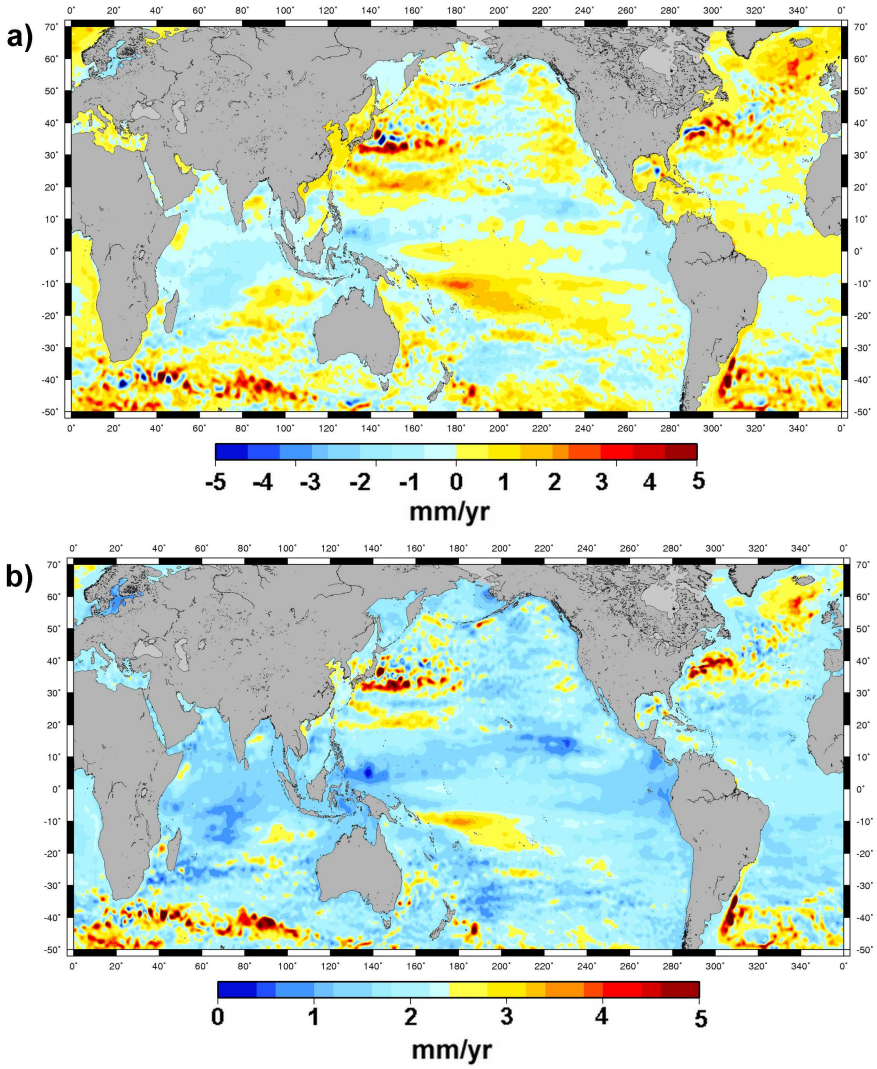

Figure 2.9 – a) Variabilité régionale du niveau de la mer entre 1950 et 2009. Estimation par la reconstruction moyenne de trois reconstructions basées sur DRAKKAR, SODA et l'altimétrie. La tendance uniforme de 1.8 mm.a^{-1} a été retirée. b) Incertitude sur la variabilité régionale du niveau de la mer entre 1950 et 2009. Estimation par écart type entre les trois reconstructions basées sur DRAKKAR, SODA et l'altimétrie. Figure adaptée de *Meyssignac et al.* [2012]

Lorsque l'on cherche à estimer la variabilité régionale du niveau de la mer sur les dernières décennies, chacune des deux approches (modèles d'océan ou reconstructions) présente des avantages et des inconvénients. Les reconstructions ont l'avantage de faire intervenir directement des mesures marégraphiques dans leur processus d'estimation du niveau de la mer. Ceci permet, en principe, de reconstruire la variabilité régionale totale du niveau de la mer et non sa seule composante stérique comme c'est le cas pour les modèles d'océan. De plus cela garantit en général que les reconstructions donnent des résultats cohérents avec les mesures marégraphiques au voisinnage des marégraphes. En

revanche, contrairement aux modèles, les reconstructions ne permettent pas de séparer les rôles respectifs de la température et de la salinité dans la variabilité régionale du niveau de la mer.

Le fait d'avoir maintenant 2 approches différentes pour estimer la variabilité régionale du niveau de la mer dans le passé est un avantage en soi : en les comparant on peut obtenir des informations sur les composantes du niveau de la mer régional. Parmi les différentes reconstructions présentées plus haut, les reconstructions qui utilisent les EOFs de l'altimétrie sont particulièrement intéressantes car elles n'utilisent que des données (altimétrie + marégraphes) pour estimer le niveau de la mer. En ce sens, elle produisent une sorte d' "observation" de la variabilité régionale du niveau de la mer sur les dernières décennies qui est totalement indépendante des modèles d'océan. L'inter-comparaison de ces quasi-observations avec les modèles peut apporter de nombreuses informations sur les processus qui dominent la variabilité régionale du niveau de la mer aux échelles inter-annuelles à multi-décennales. Les autres reconstructions qui utilisent les EOFs de modèles présentent aussi un intérêt particulier. Quand on fait la différence avec les sorties du modèle utilisé dans la reconstruction, on obtient un signal résiduel qui montre l'information apportée par les marégraphes en sus de celle du modèle, dans la variabilité régionale du niveau de la mer reconstruite. Cette information est en principe représentative du signal non-stérique de l'océan (e.g. masse de l'océan) qui n'est pas simulé dans les modèles mais qui se trouve dans les enregistrements marégraphiques. Elle peut donc fournir des informations sur les variations régionales inter-annuelles et multi-décennales de la masse de l'océan. Cependant, pour cela, il faut encore attendre que les modèles d'océan et les reconstructions atteignent des précisions plus grandes.

Chapitre 3

Le niveau de la mer dans trois régions vulnérables durant les dernières décennies

Dans la deuxième partie de cette thèse, nous nous sommes intéressés aux questions scientifiques du groupe (d) (voir section 1.5) qui portent sur les impacts de la montée du niveau de la mer dans les régions côtières. L'augmentation du niveau de la mer est l'un des problèmes majeurs posés par le réchauffement climatique global car elle menace les régions côtières et les populations qui y habitent. Les conséquences de la montée du niveau de la mer sur le littoral sont bien connues (*Nicholls et al.* [2007]). De manière immédiate, cela se traduit par la submersion des terres basses, des inondations plus fréquentes et plus fortes sur les côtes et la salinisation des eaux de surface. A plus long terme, lorsque le littoral s'ajuste aux nouvelles conditions océaniques, on observe une érosion accélérée des côtes et des intrusions d'eau de mer dans les aquifères. Les écosystèmes tels que les marais maritimes et les mangroves déclinent si les apports sédimentaux ne compensent pas la montée de l'eau (*Nicholls et al.* [2007]). Tous ces éléments se traduisent par des pertes socio-économiques directes et indirectes considérables (*Nicholls* [2010]).

Pour estimer ces impacts de la montée du niveau de la mer, il est nécessaire de connaitre précisément pour chaque région l'augmentation du niveau de la mer relatif, c'est à dire du niveau de la mer par rapport à la côte (enjeu de la question scientifique n°28). Le niveau de la mer relatif contient 2 termes. C'est la somme du niveau de la mer local induit par les variations climatiques (cette composante étant elle-même constituée de 2 composantes : la hausse moyenne globale du niveau de la mer plus la variabilité régionale) et du mouvement vertical de la côte.

Grâce aux reconstructions développées dans la première partie de cette thèse, nous avons une estimation du premier terme sur plus de 50 ans avec une fine résolution spatiale. En revanche, très peu d'information sont disponibles sur le second terme. Les mouvements de la côte suivent les mouvements de la croûte terrestre locale. Ils ont pour origine soit des processus géologiques locaux (tels que la compaction sédimentaire, le GIA, l'activité tectonique, etc) soit les activités anthropiques (subsidence du sol suite au pompage de l'eau et des hydrocarbures souterrains, drainage des régions deltaiques, etc). Les modèles

de GIA donnent sur tout le globe des estimations du mouvement vertical de la croûte induit par la dernière déglaciation (voir Fig. 1.20) mais on ne dispose pas d'estimation globale des mouvements de la croûte induits par les autres effets. Localement, sur les sites équipés de balises GPS, on peut obtenir une mesure du mouvement vertical local total.

Dans cette deuxième partie de ma thèse nous nous sommes focalisés sur 3 régions identifiées comme sensibes au réchauffement global : le Pacifique tropical, la mer Méditerrannée et l'océan Arctique. Pour chaque région nous avons évalué les tendances du niveau de la mer total (hausse moyenne globale plus variabilité régionale) sur les dernières décennies pour tenter de répondre à la question scientifique n°28 (qui porte sur l'estimation des variations du niveau de la mer relatif). Là où nous avons trouvé des mesures GPS, nous avons aussi estimé le mouvement local de la croûte terrestre afin de fournir une estimation des variations du niveau de la mer relatif total sur les 60 dernières années dans les régions côtières et permettre ainsi l'étude des impacts de la hausse du niveau de la mer qui est l'enjeu des questions scientifiques n°29 et 30.

3.1 Le Pacifique Tropical

Les îles du Pacifique sont pArcticulièrement vulnérables à la montée du niveau de la mer car elles présentent souvent une densité de population forte et une très faible élévation au dessus du niveau de la mer. Par exemple Funafuti, un atoll des Tuvalus a une densité de population de 1870 hab.km^{-2} et s'élève seulement entre 0 et 5m au dessus du niveau de la mer. De plus ces îles sont souvent sujettes a des mouvements de subsidence de la croûte dûs à l'activité tectonique locale (isostasie thermique de la croûte océanique par exemple, *Pirazzoli* [1995]) ou à l'activité anthropique (pompage de l'eau douce souterraine, urbanisation, etc, *Webb and Kench* [2010]). Ces facteurs combinés entre eux font de cette région l'une des plus exposées aux risques associés à la montée du niveau de la mer (*Nicholls and Cazenave* [2010]). A propos des îles Tuvalu, le 4$^{\text{ème}}$ rapport du GIEC précise qu'elles sont menacées de submersions significatives voire de disparition totale au cours du XXI$^{\text{ème}}$ siècle (*Mimura et al.* [2007]).

Sur la période altimétrique on observe une forte augmentation du niveau de la mer dans l'Ouest du Pacifique (voir Fig. 3.1). En tendance, sur la période 1993-2010, le niveau de la mer y a augmenté à un rythme de 9 à 14 mm.a^{-1}, i.e. 3 à 4 fois plus vite que la moyenne globale sur la même période (voir Fig.1.12a). C'est l'augmentation la plus forte observée dans le monde par l'altimétrie. Elle a été attribuée à une augmentation de l'intensité des vents d'Est sur la région au cours des années 1990 (*Timmermann et al.* [2010]; *Merrifield and Maltrud* [2011]).

Cependant, avec seulement 18 ans d'altimétrie, il est difficile de savoir si cette augmentation est représentative des variations du niveau de la mer au cours des 60 dernières années car dans l'océan Pacifique tropical ces variations sont loin d'être linéaires. Elles présentent une très forte variabilité inter-annuelle (environ ±20 cm dans l'Ouest du Pacifique) avec une périodicité de 2 à 6 ans liée à l'oscillation ENSO et aussi une forte variabilité multi-décennale entre -10°N et +10°N comme le montre les marégraphes, l'altimétrie et les

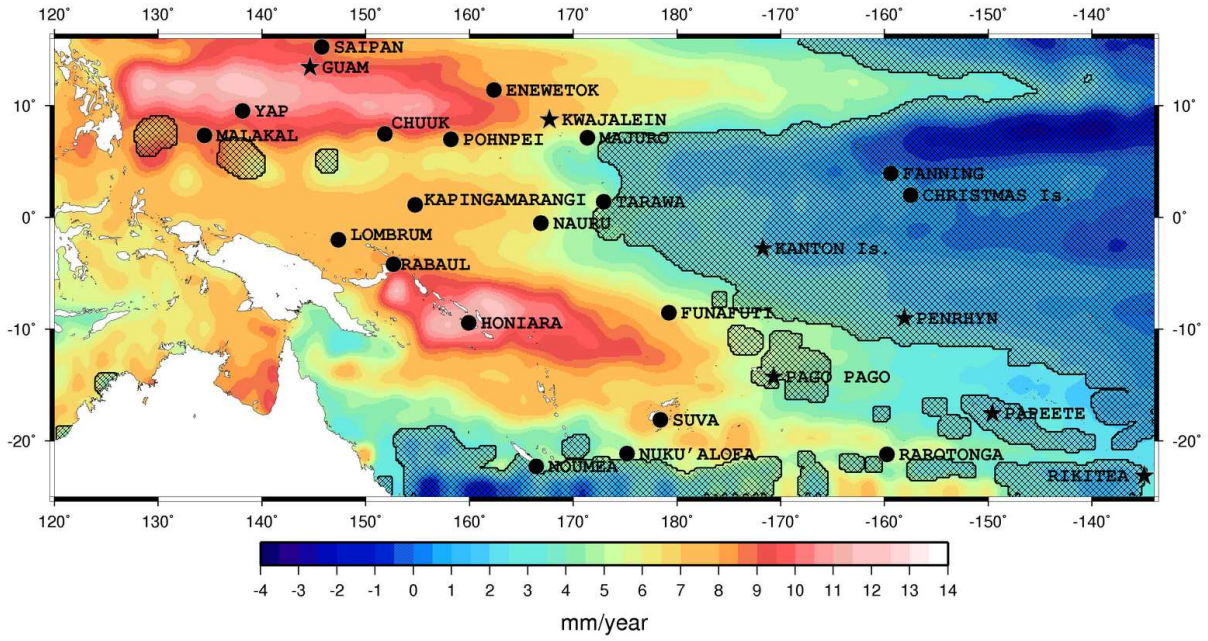

Figure 3.1 – Tendances du niveau de la mer mesurées par altimétrie dans le Pacifique Ouest entre 1993 et 2009. Les régions hachurées indiquent les zones pour lesquelle la courbe du niveau de la mer local diffère significativement d'une droite (pvalue > 0.1). Figure adaptée de *Becker et al.* [2011].

modèles (*Church et al.* [2006]; *Merrifield* [2011]). Nous avons donc proposé d'analyser les variations du niveau de la mer dans cette région avec les reconstructions présentées plus haut dans l'Arcticle intitulé :"Sea level variations at tropical Pacifique islands since 1950"

Résumé de l'Arcticle : "Sea level variations at tropical Pacifique islands since 1950" (l'Arcticle original est inséré à la fin de cette section 3.1).
Dans cette Arcticle, nous analysons la variabilité régionale du niveau de la mer d'origine climatique dans l'Ouest du Pacifique ainsi que le mouvement de la croûte terrestre sur 12 îles équipées de GPS pour estimer localement la montée du niveau de la mer relative sur la période 1950-2009. La variabilité régionale du niveau de la mer est estimée à partir de la reconstruction basée sur le modèle DRAKKAR/NEMO développée dans l'étude *Meyssignac et al.* [2012]. Le mouvement vertical de la croûte est estimée à partir des solutions GPS de *Santamaria-Gomez et al.* [2011],de *Fadil et al.* [2011] et du service GPS international (IGS). Dans un premier temps nous vérifions que la reconstruction représente bien les variations spatio-temporelles du niveau de la mer dans la région, en comparant avec l'altimétrie sur la période 1993-2009 et avec 20 enregistrements marégraphiques non-utilisés dans la reconstruction, sur la période 1950-2009. La reconstruction montre que le niveau de la mer en moyenne sur l'Ouest du Pacifique (20°S-15°N par 120°E-135°W) a augmenté à la vitesse de 1.8 ± 0.5 mm.a^{-1} depuis 1950 en accord avec la moyenne globale. La variabilité régionale est forte dans la région, en pArticulier autour des îles Tuvalus, avec des tendances qui atteignent 4 mm.a^{-1} sur la période 1950-2009. Les variations spatio-temporelles du niveau de la mer s'expliquent par les variations spatio-temporelles de l'expansion thermique et sont fortement liées à l'oscillation ENSO. A l'échelle inter-annuelle, la signature des évènements El Niño/La Niña est très forte de l'ordre de 20 à 30cm. On observe aussi une forte vari-

abilité multi-décennale avec moins d'amplitude dans le signal régional du niveau de la mer avant 1970 et après 2002 et plus d'amplitude entre ces 2 dates. Ceci confirme les résultats de *Church et al.* [2006] pour la période avant 1970. Pour la période après 2002, la baisse d'amplitude observée est liée à l'occurence de El Niño/La Niña modoki (*Ashok et al.* [2007]) plutôt que de El Niño/La Niña classiques (*Behera and Yamagata* [2010]). Ceci suggère que la variabilité multi-décennale observée dans le niveau de la mer à l'Ouest du Pacifique s'expliquerait par des variations dans la nature des évènements El Niño/La Niña plutôt que dans leur amplitude. L'analyse des séries GPS nous a permis d'estimer de manière fiable le mouvement vertical local de la croûte pour 9 îles de la région : Guam, Pohnpei, Roratonga, Nauru, Funafuti, Pago Pago, Papeete, Noumea et Tarawa. Pour chacune de ces îles, le mouvement vertical n'est pas négligeable en comparaison avec la montée locale du niveau de la mer. Ceci montre que lorsqu'on estime le niveau de la mer relatif, il est essentiel de prendre en compte à la fois les facteurs climatiques qui influencent le niveau de la mer et les autres facteurs qui influencent les mouvements de la croûte. Pour Guam, Pohnpei et Roratonga, nous trouvons une montée du niveau de la mer relatif en accord (avec les barres d'erreur) avec la montée du niveau de la mer global (1.8 $mm.a^{-1}$). En revanche, pour Nauru, Funafuti, Pago Pago, Papeete, Noumea et Tarawa elle est significativement supérieure. Pour Funafuti elle est pArcticulièrement forte et s'élève à 5 $mm.a^{-1}$ sur la période 1950-2009 confirmant les inquiétudes de la population locale. Il est à noter que plus de 15% de cette élévation est dûe à la subsidence locale de l'île dont l'origine est en partie l'activité anthropique (voir *Webb and Kench* [2010]).

Global and Planetary Change 80-81 (2012) 85–98

Contents lists available at SciVerse ScienceDirect

Global and Planetary Change

journal homepage: www.elsevier.com/locate/gloplacha

Sea level variations at tropical Pacific islands since 1950

M. Becker [a,*], B. Meyssignac [a], C. Letetrel [b], W. Llovel [c], A. Cazenave [a], T. Delcroix [a]

[a] LEGOS, UMR5566/CNES/CNRS/UPS/IRD, Toulouse, France
[b] LIENSs, UMR6250/CNRS/University of La Rochelle, France
[c] Jet Propulsion Laboratory, Caltech, Pasadena, USA

ARTICLE INFO

Article history:
Received 1 April 2011
Accepted 9 September 2011
Available online 18 September 2011

Keywords:
sea level rise
sea level variability
tide gauge
satellite altimetry
ENSO
Pacific Islands

ABSTRACT

The western tropical Pacific is usually considered as one of the most vulnerable regions of the world under present-day and future global warming. It is often reported that some islands of the region already suffer significant sea level rise. To clarify the latter concern, in the present study we estimate sea level rise and variability since 1950 in the western tropical Pacific region (20°S–15°N; 120°E–135°W). We estimate the total rate of sea level change at selected individual islands, as a result of climate variability and change, plus vertical ground motion where available. For that purpose, we reconstruct a global sea level field from 1950 to 2009, combining long (over 1950–2009) good quality tide gauge records with 50-year-long (1958–2007) gridded sea surface heights from the Ocean General Circulation Model DRAKKAR. The results confirm that El Niño-Southern Oscillation (ENSO) events have a strong modulating effect on the interannual sea level variability of the western tropical Pacific, with lower/higher-than-average sea level during El Niño/La Niña events, of the order of ±20–30 cm. Besides this sub-decadal ENSO signature, sea level of the studied region also shows low-frequency (multi decadal) variability which superimposes to, thus in some areas amplifies current global mean sea level rise due to ocean warming and land ice loss. We use GPS precise positioning records whenever possible to estimate the vertical ground motion component that is locally superimposed to the climate-related sea level components. Superposition of global mean sea level rise, low-frequency regional variability and vertical ground motion shows that some islands of the region suffered significant 'total' sea level rise (i.e., that felt by the population) during the past 60 years. This is especially the case for the Funafuti Island (Tuvalu) where the "total" rate of rise is found to be about 3 times larger than the global mean sea level rise over 1950–2009.

1. Introduction

Sea level rise is a major consequence of global warming, which threatens many low-lying, highly populated coastal regions of the world. The western tropical Pacific Island Region (hereafter called PIR), defined here as the area located between 20°S and 15°N latitude, and 120°E and 135°W longitude, is usually considered as one of the most vulnerable world regions under future sea level rise (Nicholls and Cazenave, 2010). This region is indeed characterized by volcanic archipelagos composed of low-lying islands and atolls where climate-related sea level rise may amplify other stresses caused by natural phenomena (e.g., vertical ground motions due to tectonics and volcanism, as well as occurrence of extreme events like storm surges) or human activities (e.g., ground subsidence due to ground water and/or oil extraction, urbanization, etc.) (Nicholls et al., 2007). In many cases (e.g., the Tuvalu and Kiribati island chains), much of the land altitude above present mean sea level rarely exceeds 5 m. The combination of low elevation, small island size, sensitivity to change in boundary conditions (coastal sea level, waves and currents) and in some cases, high population density, is a matter of concern, as there is little doubt that sea level will continue to rise in the future (IPCC, 2007). Regularly, the media highlight the case of tropical island inhabitants, referring them as the first climatic refugees of current global warming. For example, in the Tuvalu islands, it is common to hear that people already see the impacts of sea level rise (Nicholls et al., 2007) and that the situation will worsen in the future.

Tide gauge observations indicate that global mean sea level rose at an average rate of ~1.7 mm/yr since 1950 (Church and White, 2006; Jevrejeva et al., 2006; Holgate, 2007). Satellite altimetry reports faster global mean sea level rise since 1993, of 3.3 +/− 0.4 mm/yr (Leuliette et al., 2004; Nerem et al., 2006, 2010; Ablain et al., 2009). However, sea level rise is far from being spatially uniform. Global coverage of satellite altimetry data shows that in the western tropical Pacific region, sea level rose at a rate up to 3–4 times larger than the global mean between 1993 and 2010 (Cazenave and Llovel, 2010; Nerem et al., 2010). Unfortunately, the satellite altimetry record is still too short to conclude that the PIR also displays on the long-term (e.g., since 1950), rates of sea level rise several times higher than the global

* Corresponding author at: 18 Av. E. Belin, 31400 Toulouse, France. Tel.: +33 5 61 33 30 03.
E-mail address: melanie.becker@legos.obs-mip.fr (M. Becker).

0921-8181/$ – see front matter © 2011 Elsevier B.V. All rights reserved.
doi:10.1016/j.gloplacha.2011.09.004

mean. In addition, in situ tide gauge measurements (Wyrtki, 1985; Mitchum and Lukas, 1990), satellite altimetry (Merrifield et al., 1999), and modeling results (Busalacchi and Cane, 1985) have shown that the El Niño-Southern Oscillation (ENSO) phenomenon has strong impact on the interannual variability of sea level in that region. In the PIR, El Niño/La Nina events correspond to sea level lows/highs of ~20–30 cm compared to normal conditions.

In the present study, we estimate sea level change and variability in the PIR since 1950. We then assess the total rate of change at selected PIR islands, as a result of the climatic signal (uniform-global mean-sea level rise plus regional variability) and vertical ground motion. The objective of this work is indeed to determine the amount of "total" sea level change effectively felt by the populations over the last ~60 years. For that purpose, we developed a past sea level reconstruction from 1950 to 2009 (this is an update of an earlier work by Llovel et al., 2009, with a few methodological improvements — see Section 2.3). The reconstruction method combines nearly one hundred, long (1950–2009) good quality tide gauge records with 50-year-long (1958–2007) gridded sea surface height fields from an Ocean General Circulation Model (OGCM), the DRAKKAR model without data assimilation (Barnier et al., 2006; Madec, 2008; Dussin et al., 2009). Sea level is reconstructed globally over a 60-year long time span (1950–2009) (Meyssignac et al., 2011), but here we focus on the PIR and analyze the reconstructed regional variability superimposed to the uniform global mean sea level rise. The reconstructed sea level is compared to 27 tide gauge records available at PIR island sites equipped with tide gauges (in general, these tide gauge records do not cover the whole 60 years, and just a few of them, 7 out of 27, were used in the global sea level reconstruction). When possible, we also estimate vertical crustal motions deduced from GPS (Global Positioning System) solutions. This allow us to estimate the "total" sea level rise felt locally at a few PIR islands, i.e., the climatic components (global mean rise plus regional variability) and ground motion. We focus on Funafuti (Tuvalu Islands) because it is there that the largest total sea level rise is observed over the 1950–2009 time span.

The paper is organized as follows. In Section 2 we describe the data sets used in this study and present the past sea level reconstruction. In Section 3, we analyze sea level spatial patterns in the PIR over 1950–2009 (the 60-year long reconstruction). In Section 4, we analyze three distinct sub-regions under ENSO influence and compare tide gauge-based, reconstruction-based and satellite altimetry-based sea level variations. We present the main results and address the question "how past and recent sea level changes have locally affected the PIR?". In Section 5, we determine the "total" sea level trend due to the climatic component (uniform global mean rise plus regional variability), and vertical ground motion using GPS solutions. Section 6 summarizes our main results and conclusions.

2. Data

2.1. Satellite altimetry

For the altimetry data, we use the DT-MSLA "Ref" series provided by Collecte Localisation Satellite (CLS; http://www.aviso.oceanobs.com/en/data/products/sea-surface-height-products/global/msla/index.html). This data set is used over the time span from January 1993 to December 2009. It is available as 1/4°×1/4° Mercator projection grids at weekly interval. The DT-MSLA "Ref" series are based on the combination of several altimetry missions, namely: Topex/Poseidon (T/P), Jason-1 and 2, Envisat and ERS 1 and 2. It is a global homogenous inter-calibrated data set based on a global crossover adjustment using T/P and then Jason-1 as reference missions. Moreover, the use of recent orbit solutions for Jason-1 and T/P (GSFC—Goddard Space Flight Center-orbit computed with the ITRF2005 terrestrial reference frame; Altamimi et al., 2007) allows to remove previous heterogeneity between global hemispheric mean sea level trends (Ablain et al., 2009). ERS satellite orbits are also improved using the approach developed by Le Traon et al. (1998) and Ducet et al. (2000). Usual geophysical corrections are applied: solid Earth, ocean and pole tides, wet and dry troposphere, ionosphere (see Ablain et al., 2009 for more details) and inverted barometer (Carrere and Lyard, 2003; Volkov et al., 2007).

2.2. Tide gauges

We use monthly mean sea level data from 27 tide gauge stations (listed in Table 1) included in the Revised Local Reference data set of the Permanent Service for Mean Sea Level (PSMSL; Woodworth and Player, 2003, http://www.pol.ac.uk/psmsl). We consider only tide gauges that have at least 30 years of data between 1950 and 2009. Note that only tide gauge records covering the whole studied period, 1950–2009, were considered to perform the global sea level reconstruction (see Section 2.3). Where necessary, the PSMSL records were extended through 2009 using fast delivery data from the University of Hawaii Sea Level Center (UHSLC; http://ilikai.soest.hawaii.edu/uhslc). At 12 sites (Saipan, Yap, Pohnpei, Majuro, Kanton, Tarawa, Rabaul, Funafuti, Kapingamarangi, Christmas, Rikitea and Rarotonga), recent data are lacking in both PSMSL and UHSLC. Thus we completed the tide gauge time series using altimetry data beyond 1993. For that purpose, we interpolated the gridded altimetry data in a radius of 1° around the tide gauge position. Then the missing tide gauge data were replaced by the interpolated altimetry data. This was done only at sites with at least 5-year overlap and a correlation ≥ 0.9 between the tide gauge and altimetry time series. This 5-year overlap is deduced from the Bonett's formula (Bonett and Wright, 2000) and is based on a desired Pearson's correlation coefficient of 0.9 ± 0.1, with 95% level of confidence (for more details on the method, see Bonett and Wright, 2000).

Tide gauge location (latitude, longitude) and data length are listed in Table 1. We corrected the tide gauge time series for the inverted barometer response of sea level to atmospheric loading using surface pressure fields from the National Centers for Environmental Prediction (NCEP) (Kalnay et al., 1996) (data available at http://www.ncep.noaa.gov/). Tide gauge data were also corrected for the Glacial Isostatic Adjustment — GIA — effect using the ICE5G-VM4 model from Peltier (2004). The GIA correction is small in the PIR and ranges between −0.1 mm/yr and −0.3 mm/yr. Thus using this particular GIA model versus another has little impact of the sea level results.

For a number of reasons (changes in instrumentation, earthquakes or other natural of anthropogenic factors; see Becker et al., 2009), gaps and discontinuities may affect the tide-gauge time series. When small gaps (≤ 4 consecutive years) are observed in the tide-gauge record, we reintroduce missing data by linearly interpolating the time series. Outliers were detected using the Rosner's test (Rosner, 1975) and removed. Annual and semi-annual cycles were removed through a least-squares fit of 12-month and 6-month period sinusoids. In a last step, to be consistent with the time resolution of the sea level reconstruction (see Section 2.3), we averaged monthly tide gauge time series to obtain annual averages.

2.3. Past sea level reconstruction

Several previous studies have attempted to reconstruct past decade sea level in two dimensions (2-D), combining sparse but long tide gauge records with global gridded (i.e., 2-D) sea level (or sea level proxies) time series of limited temporal coverage (Smith, 2000; Chambers et al., 2002; Church et al., 2004; Berge-Nguyen et al., 2008; Llovel et al., 2009; Ray and Douglas, 2010; Church and White, 2011). Satellite altimetry available since 1993 has shown that sea level is not rising uniformly. But altimetry-based spatial trend patterns essentially reflect decadal variability rather than low-frequency trends because the altimetry record is still short. Thus on longer time spans, regional sea level trends are expected to be

Table 1
Locations, time spans and sea-level trends for the PIR tide gauges when the tide gauges are extended by altimetry. The correlation coefficient and the root mean square with the annual reconstructed sea level (RESL) are given for the tide gauge time span. The RESL trends and errors from 1950 to 2009 are also given in the two last columns. The symbol * corresponds to significant trends (p-value<0.1). Stars ★ correspond to tide gauges used in the reconstruction.

Station group	Station	Tide-gauge										RESL (tide gauge time span)		RESL 1950–2009	
		Lon	Lat	Start	End (extended by altimetry)		Span (yr)	% of gap (maximum length in months)	Trend (mm/yr)	Error (mm/yr)	Corr. coef. With RESL	Root Mean square (cm)	Trend (mm/yr)	Error (mm/yr)	Trend (mm/yr)	Error (mm/yr)
G1	Saipan	145.75	15.23	1979	(2004)	2009	31	16 (24)	3.1*	1.1	0.7	4.9	3.6 *	1.0	1.5 *	0.6
	Guam ★	144.65	13.43	1950		2009	60	6 (14)	1.9 *	0.5	0.9	2.5	1.4 *	0.6	1.4 *	0.6
	Yap	138.13	9.52	1970	(2005)	2009	40	8 (28)	1.3	1.1	0.9	3.8	1.3	1.1	0.7	0.7
	Malakal	134.47	7.33	1970		2009	40	5 (5)	2.0	1.2	0.8	5.3	−0.4	1.2	−0.1	0.7
	Chuuk Is.	151.85	7.45	1950		1995	46	11 (23)	0.6	0.6	0.8	3.8	0.1	0.7	1.1 *	0.6
	Pohnpei	158.23	6.98	1974	(2004)	2009	36	0 (0)	3.0 *	0.9	0.8	3.8	1.6 *	0.9	1.4 *	0.6
	Kwajalein ★	167.73	8.73	1950		2009	60	1 (2)	2.2 *	0.3	0.9	2.9	1.2 *	0.6	1.2 *	0.6
	Enewetok	162.35	11.37	1951		1972	22	0 (0)	0.5	1.5	0.9	2.8	−1.0	1.5	1.4 *	0.6
	Majuro	171.37	7.10	1969	(2001)	2009	41	8 (16)	3.7 *	0.6	0.6	5.0	1.8 *	0.8	1.4 *	0.6
G2	Lombrum	147.37	−2.04	1995		2009	15	6 (10)	5.9 *	2.8	0.8	5.1	5.4 *	2.9	1.4 *	0.6
	Nauru	166.90	−0.53	1974		1994	21	7 (3)	−0.1	2.0	0.8	3.7	1.7	1.7	2.3 *	0.6
	Tarawa	172.93	1.37	1988	(1997)	2009	22	24 (7)	3.4 *	1.8	0.9	4.8	1.7 *	1.5	2.2 *	0.6
	Kapingamarangi	154.78	1.10	1979	(2008)	2009	31	7 (7)	3.1 *	1.0	0.9	3.7	2.5 *	1.2	1.9 *	0.6
	Rabaul	152.18	−4.20	1966	(1997)	2009	44	17 (45)	1.5	0.9	0.7	6.3	1.8 *	0.9	1.7 *	0.7
	Honiara	159.95	−9.43	1974		2009	36	2 (4)	2.1	1.4	0.7	7.9	3.4 *	1.5	3.2 *	0.8
	Funafuti	179.22	−8.53	1978	(2001)	2009	32	4 (3)	4.4 *	1.3	0.8	8.3	4.1 *	1.7	4.7 *	0.7
	Penrhyn ★	201.93	−9.02	1978		2009	32	5 (7)	2.5 *	0.9	0.7	6.7	1.1 *	1.1	3.5 *	0.6
	Pago Pago ★	189.32	−14.28	1950		2009	60	7 (24)	2.4 *	0.4	0.9	2.2	2.5 *	0.6	2.5 *	0.6
	Kanton ★	188.28	−2.80	1950	(2007)	2009	60	17 (31)	0.9 *	0.3	0.7	3.8	2.1 *	0.6	2.1 *	0.6
	Fanning	200.62	3.90	1973		1987	15	7 (3)	1.4	3.4	0.7	3.9	0.5	2.2	1.5 *	0.6
	Christmas Is.	202.52	1.98	1974	(2003)	2009	36	5 (5)	1.1	1.0	0.9	4.2	1.0	0.9	1.8 *	0.6
	Papeete ★	210.43	−17.53	1976		2009	34	3 (7)	2.7 *	0.5	0.8	4.4	2.8 *	0.7	2.9 *	0.5
G3	Suva	178.43	−18.13	1990		2009	20	7 (6)	6.0 *	1.5	0.6	5.1	3.6 *	0.9	1.2 *	0.5
	Nuku'alofa	184.80	−21.13	1990		2009	20	1 (1)	5.8 *	1.8	0.6	5.0	5.3 *	1.1	1.2 *	0.6
	Noumea	166.43	−22.30	1967		2003	37	7 (12)	0.5	0.5	0.4	4.2	0.7	0.8	0.5 *	0.6
	Rikitea ★	225.05	−23.13	1970	(2003)	2009	40	10 (7)	2.1 *	0.4	0.6	4.0	2.5 *	0.6	2.5 *	0.5
	Rarotonga	200.23	−21.20	1977	(2001)	2009	33	3 (2)	3.7 *	0.7	0.7	4.2	3.4 *	0.7	1.8 *	0.5

different (see, for example, Bindoff et al., 2007). Numerical ocean models and ocean reanalyses have been developed in the recent years and eventually could be used to study past regional variability in sea level. While the models agree rather well with each other over the altimetry era (since 1993), they may diverge prior to that period because of lesser quality of the meteorological forcing in the past. Moreover, they are not available before the late 1950s/early 1960s. Finally, 'true' regional sea level contains other signal than that simulated by ocean models (among others, the global mean sea level rise signal to which the regional variability is superimposed, in general not provided by the ocean models, and GIA-related regional variability). These are the main arguments for developing 2-D sea level reconstructions which combine several types of information.

We previously developed such a method (Berge-Nguyen et al., 2008; Llovel et al., 2009) and here use an updated version (Meyssignac et al., 2011) of these earlier works. Let us briefly describe the method. It is based on the reduced optimal interpolation described by Kaplan et al. (2000). It consists of combining long tide gauge records with a time-varying linear combination of EOF-based (Empirical Orthogonal Functions; Preisendorfer, 1988; Toumazou and Cretaux, 2001) spatial patterns derived from 2-D sea level grids (in general of shorter duration than the tide gauge records). These sea level grids are based on either satellite altimetry or outputs from an OGCM. The method has 2 steps. In the first step, an EOF decomposition of the sea level grids is performed over their time span of availability. This decomposition allows separating the spatially well resolved signal of the gridded data into spatial modes (EOFs) and associated temporal amplitudes. The second step consists of computing new temporal amplitudes of the EOFs over the longer period covered by the selected tide gauge records. This is done through a least-squares optimal procedure that minimizes the difference between the reconstructed fields and the tide gauge records at the tide gauge locations. In Llovel et al. (2009), the 2-D sea level grids were based on 44-yr long outputs of the OPA/NEMO ocean model. The option of using OGCM outputs rather than satellite altimetry grids (as in Church et al., 2004 and Church and White, 2011) was dictated by the fact that spatial sea level patterns observed during the relatively short altimetry time span are likely not stationary in time but fluctuate at frequencies related to the internal modes of variability of the climate system (e.g., ENSO, NAO—North Atlantic Oscillation, PDO—Pacific Decadal Oscillation) (e.g., Bindoff et al., 2007). Thus, as shown in Berge-Nguyen et al. (2008) and Llovel et al. (2009), to correctly capture the decadal/multidecadal variability of the spatial patterns, it is preferable to use sea level grids of longer duration than available from satellite altimetry (see Llovel et al., 2009). Here, we refine Llovel et al.'s (2009) reconstruction, with 3 major improvements: (1) As in Church et al. (2004), Christiansen et al. (2010) and Church and White (2011), we account for a covariance matrix of data errors and perform a specific treatment for the so-called EOF0 (the global mean sea level component); this significantly improves the quality of the sea level reconstruction; (2) we update the tide gauge data set of Llovel et al. (2009) in order to reconstruct sea level up to 2009 (instead of 2003); the new reconstruction thus provides global 2-D sea level grids from January 1950 to December 2009; (3) instead of using the OPA/NEMO OGCM of 2° resolution only, we now use a higher-resolution (1/4°) OGCM: the ORCA025-B83 run over 1958–2007 of the DRAKKAR/NEMO model (Barnier et al., 2006; Madec, 2008; Dussin et al., 2009). This is a purely physical version of the model that does not assimilate any observational data. The ORCA025-B83 run uses the DFS4.1 atmospheric forcing (Brodeau et al., 2010). Penduff et al. (2010) showed that ocean models with higher resolution bring substantial improvements in their representation of the sea level spatial variability, in particular at interannual time scales. We use 91 long tide gauge records from the PSMSL for the reconstruction. One problem with tide gauge records is that measurements are made in local datum that varies from one site to another. By working with derivatives, this problem can be overcome. Here we choose a different approach consisting of subtracting from each sea level record a mean value computed over the 1950–2009 time span (note that most of the 91 tide gauge records are almost complete over this 60-yr long time span; when gaps are observed, we linearly interpolate the missing data). The tide gauge data are corrected for the inverted barometer and GIA as explained in Section 2.2. Annual and semi-annual cycles are also removed and yearly-averages are computed. Fig. 1 shows the distribution of the 91 tide gauge sites superimposed on a

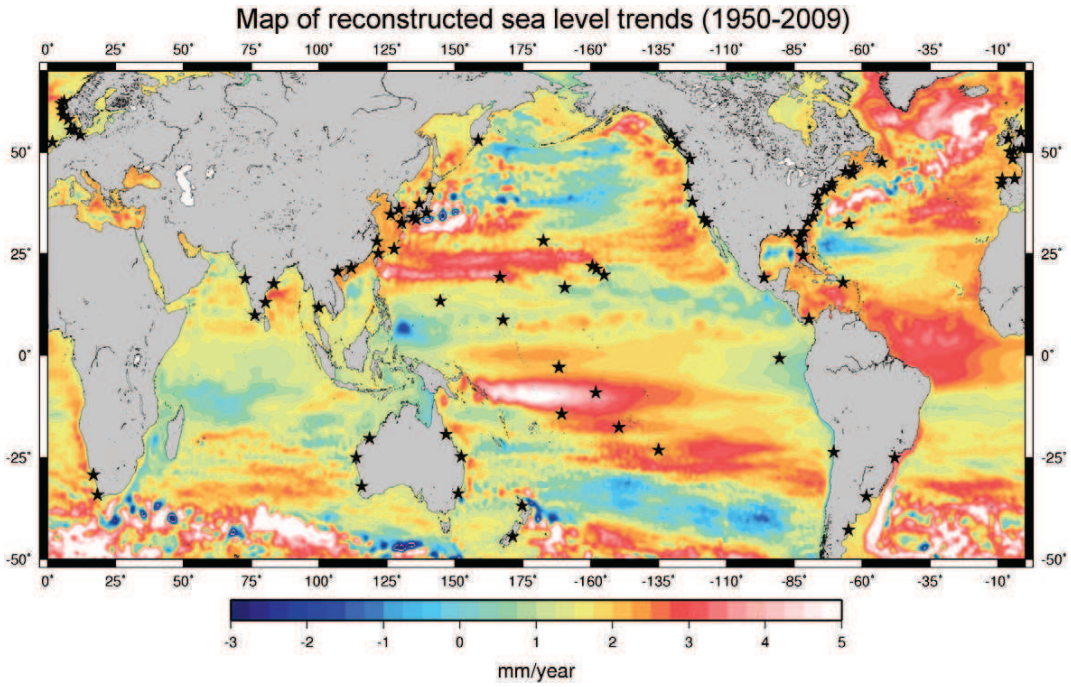

Fig. 1. Location map of the 91 tide gauges (stars) used in the global sea level reconstruction. The background map shows the sea level trends over 1950–2009 from DRAKKAR-based reconstruction of sea level (uniform trend of 1.8 mm/yr included).

global map of reconstructed sea level trends over 1950–2009. The reconstructed trends shown in Fig. 1 include the uniform global mean sea level trend (deduced from the reconstruction and equal to 1.8 ± 0.5 mm/yr) plus the regional trends.

As previously done in Llovel et al. (2009), this new reconstruction was validated at global scale by comparison with independent tide gauges not used in the reconstruction process. For this validation, we perform 91 new reconstructions leaving out successively each one of the 91 tide gauge records (thus each of these new 91 reconstructions now uses a set of 90 tide gauges). For each ignored tide gauge, we compare the reconstructed sea level time series at the tide gauge site with the observed data. 70% of the reconstructed sea level time series present a correlation coefficient with the observed sea level >0.8 (95% confidence level) (28% have a correlation between 0.5 and 0.7). This is a better score than in Llovel et al. (2009). We computed the root mean squared (rms) differences between (detrended) reconstructed sea level and observed sea level time series. 75% of the rms differences between detrended tide gauge-based and reconstructed sea level time series are below 30 mm (compared to only 60% in Llovel et al., 2009), again indicating significant improvement compared to the previous reconstruction.

Locally, we estimate the uncertainty of reconstructed sea level trends over the 1950–2009 time span on the order of 0.5 mm/yr. This uncertainty is based on the sum of errors due to the least-squares method and errors of the tide gauge records. This latter error is estimated from a bootstrap method (Efron and Tibshirani, 1993) for standard errors of the tide gauge records for each year (significant at the 95% level).

Another way to check the validity of the new reconstruction is to look at reconstructed sea level trends over the altimetry period (here 1993–

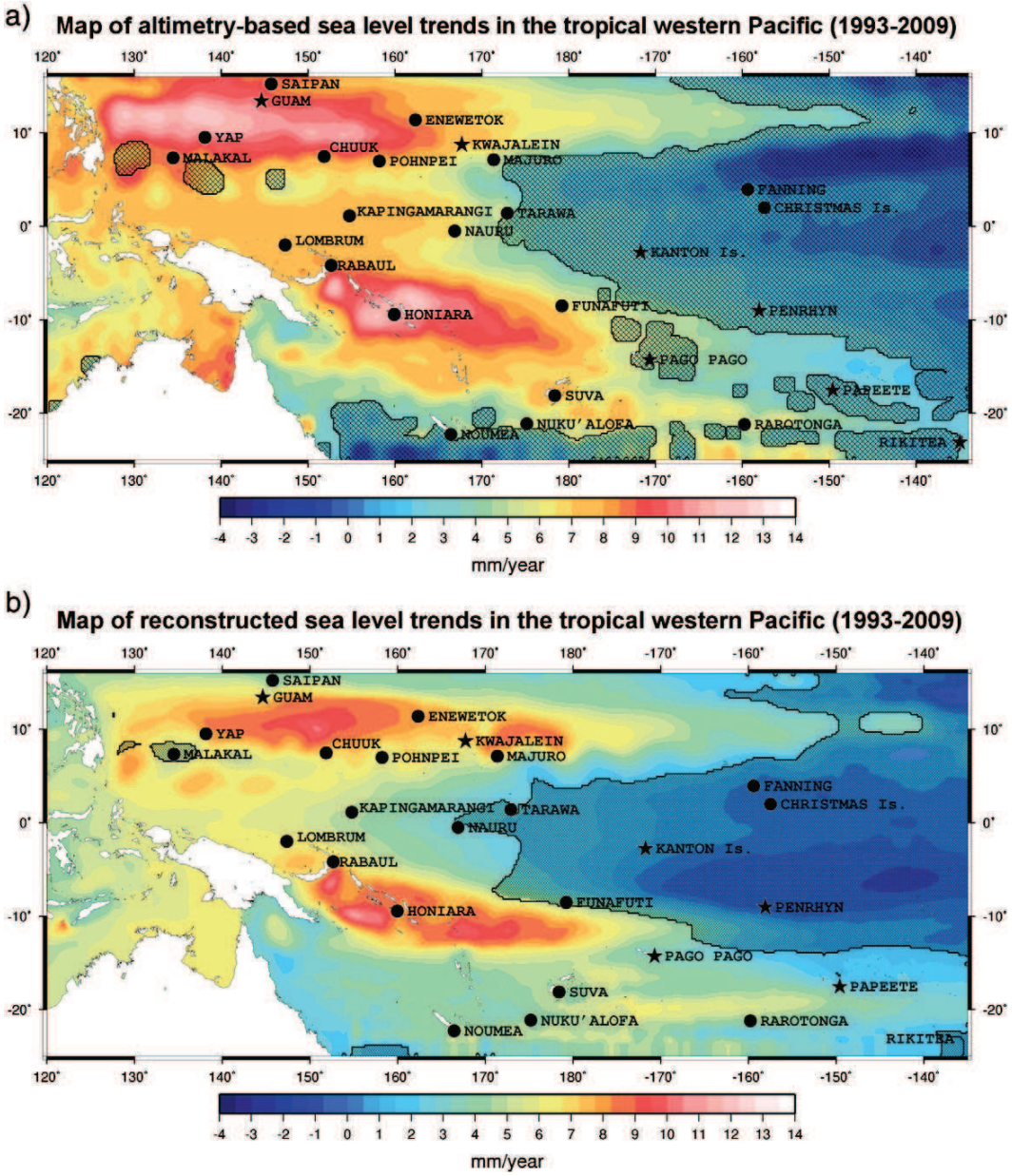

Fig. 2. (a) Altimetry-based sea level trend patterns in the PIR over 1993–2009 on which are superimposed the 27 tide gauges used in this study. (b) Reconstructed sea level trend patterns in the PIR over 1993–2009. Stars correspond to the 7 tide gauges used in the global reconstruction. The hatched areas correspond to non-significant trends (p-value>0.1).

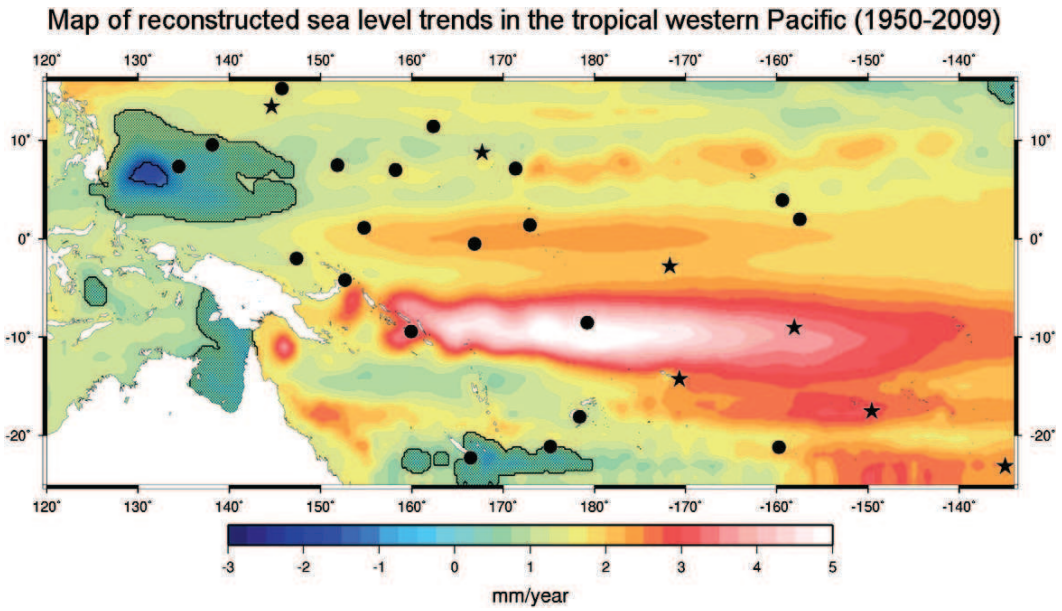

Fig. 3. Map of the PIR interannual sea level trends from the reconstruction over 1950–2009. Locations of the 27 tide gauges (black circles and stars) used in this study are superimposed. Stars correspond to the 7 tide gauges used in the global reconstruction. The hatched areas correspond to non-significant trends (p-value>0.1).

2009) and compare with altimetry data for which we trust the spatial trend patterns. This is illustrated in Fig. 2a and b which presents altimetry-based and reconstructed sea level trend patterns over the study area (PIR) for 1993–2009 (the 27 tide gauge sites of the studied region are also shown on these maps). Visual inspection indicates that the two maps agree well. The altimetry trend map shows slightly higher amplitude than the reconstruction at some maxima/minima. This results from the fact that reconstruction is based on a limited set of EOF modes, which acts as a low-pass filter. The rms between the two spatial trend patterns over the PIR amounts 1.8 mm/yr. This is a very satisfactory result considering the trend amplitudes in the PIR region (in the range of − 4 mm/yr to + 14 mm/yr over 1993–2009).

In Section 4, we discuss in more detail the performance of the reconstruction in the PIR and compare tide gauge records with reconstructed sea level (both in terms of trend and interannual variability) at tide gauge sites not used in the reconstruction. We also show in Section 5 that available tide gauge data in the PIR reflect (thus confirm) the regional trend variability deduced from the reconstruction. This represents an additional validation of the reconstruction at the scale of the studied region.

In the following, we call RESL the annual reconstructed sea level over 1950–2009.

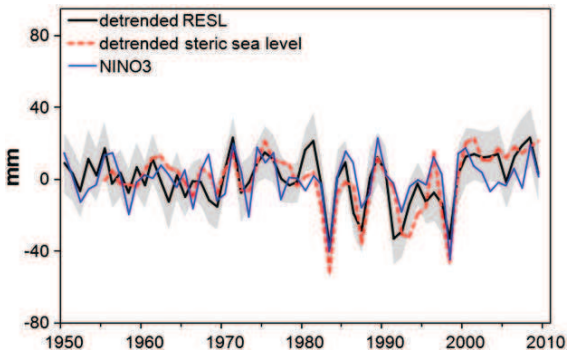

Fig. 4. Reconstructed and steric mean sea level time series for 1950–2009. The detrended RESL is the black line and its uncertainty is in gray. The detrended steric sea level is the red line. The inverse NINO3 index (shifted by half a year) is superimposed in blue. (For interpretation of the references to color in this figure legend, the reader is referred to the web version of this article.)

2.4. Steric sea level

In situ ocean temperature and salinity measurements provide an important information about the causes of regional sea level change (Levitus et al., 2005; Lombard et al., 2005). Regional ocean circulation changes, which are reflected in ocean temperature and salinity changes through depth, drive sea surface height variations by several decimeters regionally. In this work, we computed the annual-mean steric sea level anomalies for the period 1955–2009, using data from the 2009 World Ocean Database (WOD09) from the National Oceanographic Data Center (NODC; Levitus et al., 2009; expendable bathy-thermograph — XBT — measurements corrected for fall rate bias; http://www.nodc.noaa.gov/OC5/indprod.html). The NODC temperature data are available over 16 depth levels ranging from the ocean surface to 700 m on a global $1^\circ \times 1^\circ$ grid from 1955 to 2009. Steric sea level anomalies were computed over the 0–700 m depth range (although we do not account for salinity, in the following we use the term steric sea level for the thermal expansion component). We removed the annual and semi-annual cycles and computed annual averages of steric sea level over the 1950–2009 time span.

2.5. Vertical land motion based on GPS precise positioning

A few tide gauge sites of the studied region are collocated with GPS stations for which published solutions of vertical land motions are available. Here we consider three GPS solutions: the Santamaría-Gómez et al. (2011) (http://www.sonel.org/-GPS-.html) and Fadil et al. (2011) solutions — hereafter called ULR4 and F2011, plus the combined solution provided by the re-processing of the International GPS Service (IGS) (http://acc.igs.org/reprocess.html; called REPRO1). All solutions are expressed in the ITRF2005 reference frame (Altamimi et al., 2007). REPRO1 is based on 11 individual solutions, including that from Santamaría-Gómez et al. (2011). It is available as combined position time series at weekly interval.

3. 'Long-term' trends and ENSO signature in sea level

3.1. Spatial trend patterns during 1993–2009 and 1950–2009

Over the period January 1993 to December 2009, the PIR mean sea level trend amounts to 4.9 ± 0.7 mm/yr. However, high contrast is observed between western and eastern parts of the region as illustrated in Fig. 2a. In effect, the western part of the PIR shows positive sea level rise with two maxima (in the range 10–14 mm/yr) around 12°N, 125°E to 160°E and around 10°S, 150°E to 165°E. The largest rates of rise since 1993 are observed in Micronesia (Yap, Malakal and Chuuk islands), at Mariana Islands (Saipan and Guam islands), in Papua New Guinea Islands (Rabaul city) and Solomon Islands (Honiara city), with a strong maximum of 11 ± 3 mm/yr in the latter region. As shown in previous studies (e.g., Lombard et al., 2005; Bindoff et al., 2007), spatial trend patterns shown in Fig. 2a likely reflect interannual variability rather than long term trends. Thus on time spans longer than the altimetry era, spatial trend patterns should be different. This is indeed the case, as illustrated in Fig. 3 which presents spatial sea level trend patterns for 1950–2009 over the PIR from the reconstruction (global mean sea level rise included). While on average over the past 60 years, the PIR mean trend from the RESL amounts to 1.8 ± 0.5 mm/yr (a value similar to the global mean sea level rate of rise; Church and White, 2011 and our global reconstruction), locally, the maxima can reach up to ~5 mm/yr. The trend uncertainty is estimated from the quadratic sum of the error due to the reconstruction method and the formal error of least-squares linear regression. Fig. 3 displays zonal-type patterns with a succession of sea level trend maxima, in particular around 10°S, an area that includes the islands of Funafuti and Penrhyn.

3.2. The ENSO signature in past sea level

Fig. 4. shows geographically averaged RESL over the PIR between 1950 and 2009, after removing the 1.8 mm/yr mean trend over the region. In Fig. 4, the gray zone represents RESL uncertainty. This uncertainty is based on the quadratic sum of errors due to the reconstruction method and errors of the tide gauge records. This latter error is estimated from a bootstrap method (Efron and Tibshirani, 1993) for standard errors of the tide gauge records for each year (significant at the 95% level).

Fig. 4 also presents the detrended steric sea level averaged over the PIR. The trend of the steric sea level at PIR, on the order of 0.3 mm/yr, is much lower than the RESL mean trend, in agreement with previous findings (e.g., Miller and Douglas, 2004). On the other hand, we note a high correlation (r = 0.8) at interannual time scale between detrended RESL and steric sea level, with relative minima corresponding to the 1958–59, 1965–66, 1969–70, 1972–73, 1976–77, 1982–83, 1986–87, 1992–94, and 1997–98 El Niño events. This high correlation confirms that interannual variability of both thermal expansion and sea level is driven by ENSO (e.g., Bindoff et al., 2007). This is highlighted by superimposing the Niño 3 index (NINO3 hereafter). NINO3 is a proxy of ENSO, defined as the mean sea surface temperature averaged over the 150°W–90°W, 5°N–5°S area of the eastern equatorial Pacific. We note a high anti-correlation (r = −0.6) at interannual time scale between detrended RESL and NINO3 shifted by half a year (there is indeed a 6-month delay due to the eastward propagation of the El Niño-related sea level anomaly between the PIR and the NINO3 region, as shown in Delcroix, 1998).

To capture the characteristics of the regional sea level variability over the PIR, we performed an EOF decomposition of the reconstructed sea level data over 1950–2009, removing to the RESL fields, the 1.8 mm/yr mean trend over the PIR. Similarly, an EOF decomposition has been performed with the steric sea level fields (mean steric trend over the PIR removed).

Fig. 5 shows EOF modes 1 and 2 (called EOF1 and EOF2 hereafter) of RESL and steric sea level since 1950. RESL EOF2 (29% of the total variance) is highly correlated with the steric EOF1 (41% of the total variance). The correlation between the temporal curves amounts to 0.8. RESL spatial EOF1 (34% of the total variance) closely resembles RESL trend patterns over 1950–2009. Its correlation with the steric EOF2 (22% of the total variance) is lower than for EOF1 (equal to

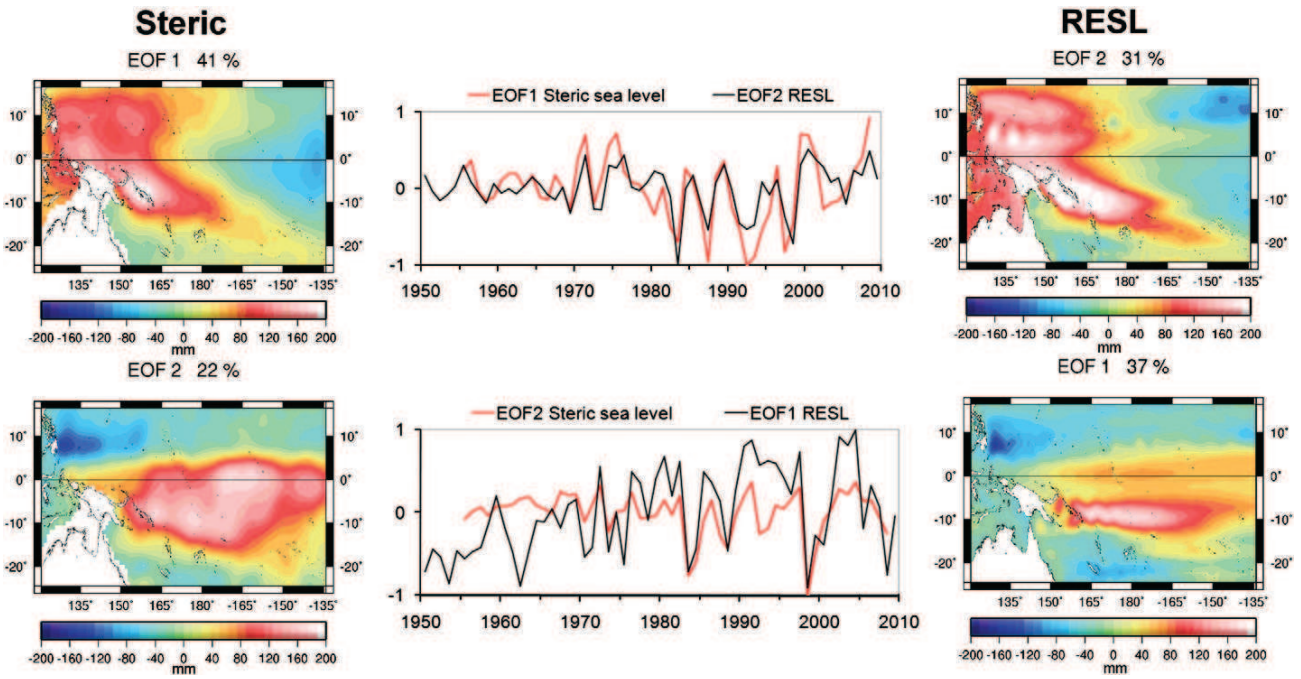

Fig. 5. EOF1 and EOF2 decomposition of reconstructed and steric sea level for 1950–2009. Left/right panels show the spatial patterns of the first two RESL/steric sea level EOF modes. In the middle panel, temporal time series of the two first EOF modes are plotted in black for the RESL and in red for the steric sea level. (For interpretation of the references to color in this figure legend, the reader is referred to the web version of this article.)

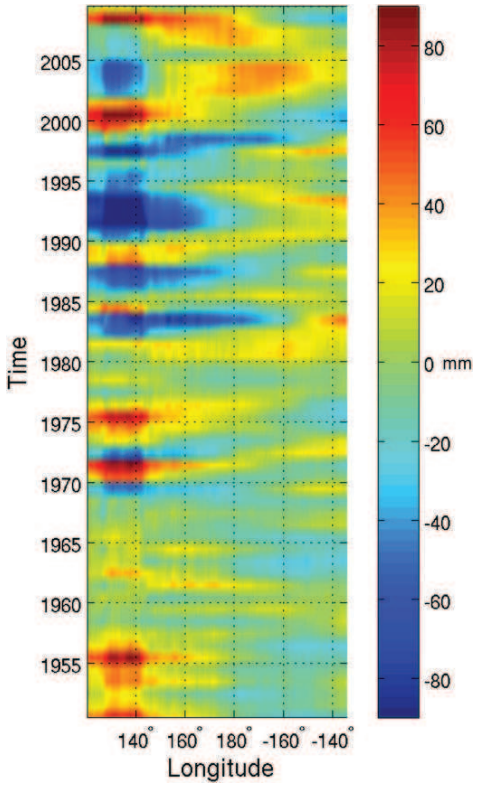

Fig. 6. Longitude–time diagram of detrended yearly-averaged reconstructed sea level from 1950 to 2009. Detrended RESL data are averaged between 20°S and 15°N.

0.5). The temporal curves show large negative anomalies associated with ENSO events, confirming that during El Niño events, sea level is lower-than-average in the western part of the region. The 10°S–10°N latitudinal band displays the well-known zonal seesaw in sea level at the ENSO frequency, as previously documented from scattered tide gauge data (Wyrtki, 1984), Geosat and T/P satellite altimetry data (Chao et al., 1993; Hendricks et al., 1996), in situ temperature data (Zhang and Levitus, 1996), XBT-derived dynamic topography (Delcroix, 1998), and model outputs (Busalacchi and Cane, 1985; Zebiak and Cane, 1987). This EOF analysis confirms that ENSO events have a strong modulating effect on the PIR sea level variability, with a tendency for low sea level during El Niño events and high sea level during La Niña events. Besides the sub-decadal ENSO signature, the temporal curves also show some low-frequency (multi decadal) variability. This EOF analysis also confirms that spatial patterns in sea level are mostly of thermal origin.

3.3. Longitudinal variability in PIR sea level

Fig. 6 shows a longitude–time diagram of RESL averaged between 20°S–15°N (mean PIR trend removed). The maximum variability clearly appears in the western part of the domain, with an alternation of positive and negative sea level anomalies at the ENSO frequency. In qualitative agreement with Fig. 4, negative anomalies (in blue) occur during the 1969–70, 1972–73, 1976–77, 1982–83, 1986–87, 1992–94, 1997–98, and 2002–2004 El Niño events. In contrast, positive anomalies (in red) show up during the 1955–56, 1962–63, 1967, 1971–72, 1973–75, 1988–89, 1996, 1999–2001 and 2008 La Nina events. It is interesting to note that positive sea level anomalies are concentrated in a small longitudinal band, between 120°E and 140°E, i.e., in the Philippines and the western part of Papua New Guinea region, while the signal weakens eastward. The diagram shown in Fig. 6 also suggests an intensification of La Niña-related sea level anomalies since about 1970. The analysis highlights the regions most at risk because of anomalous high sea levels during various ENSO cold phases. For example, it is evident from Fig. 6 that the Pacific islands west of the dateline show particularly high sea levels during La Niña. Since 2002, Fig. 6 shows repeated increased sea levels in the central basin (between 160°W and 160°E), likely related to the 2002–2003, 2003–2004, 2009–2010 El Niño Modoki events (Ashok et al., 2007; Weng et al., 2007; Behera and Yamagata, 2010). El Niño Modoki events induce positive sea level anomalies confined in the central Pacific near the dateline rather than in the eastern part of the tropical Pacific as for conventional ENSO (Bosc and Delcroix, 2008; Kug et al., 2009). This longitude–time diagram confirms that sea level interannual variability in the PIR is driven by ENSO, including its low frequency modulation. The results also suggest an amplification of the ENSO signature since 1970 and the hint for an increased occurrence of El Niño Modoki-type signature events since 2002 in the PIR.

4. Sea level time series at the tropical Pacific Islands from tide gauges, reconstruction and satellite altimetry

We now consider tide gauge data along with reconstructed sea level over 1950–2009 at the 27 tide gauge sites shown in Fig. 2. In Fig. 7, we superimpose tide gauge-based and reconstructed sea level over their respective time span. We also superimpose altimetry-based sea level interpolated at the tide gauge sites since 1993. Oceanographic considerations as well as EOF patterns from Fig. 5 lead us to consider three groups of sea level stations as follows: [15°N–5°N] roughly corresponding to the meridional extension of the North Equatorial Current, [5°N–18°S] corresponding to the South Equatorial Current, and [18°S–20°S], an area situated on the southward rim of the south Pacific subtropical gyre. These 3 sub-regions are called hereafter: G1, G2 and G3 respectively. As noted above, only 7 tide gauge records were used in the global reconstruction (Guam, Chuuk island, Kwajalein, Pago Pago, Kanton, Papeete and Rikitea) while the remaining 20 tide gauges were not. Thus at these 20 sites, we can test the quality of the reconstruction looking at the correlation with the tide gauge data, in particular at interannual time scale. This is in addition to the global validation presented in Section 2.3. Table 1 summarizes correlations as well as sea level trends from the RESL and tide gauge data sets.

For the G1 region, where the Saipan, Guam, Yap, Malakal, Chuuk, Pohnpei, Kwajalein, Enewetok and Majuro islands are located, the average correlation between RESL and observed sea level from tide gauges (not used in the reconstruction) is 0.8. The mean rms difference between tide gauges and RESL amounts to 3.9 cm. Some discrepancies between RESL and tide gauge are noted for the trends (see Table 1). This may result from the fact that tide gauge data have been corrected for GIA only and also due to the uncertainties of the RESL. In effect, if the tide gauge sites are affected by land subsidence (due to ground water pumping for example), such effects were not corrected for. Thus GIA-corrected-only tide gauge trends may not everywhere agree with RESL trends. This question will be addressed in Section 5. Besides, the reconstructed sea level trends have their own uncertainty (of the order of 0.5 mm/yr; see Section 2.3). Another tide gauge trend uncertainty results from the shortness of the tide gauge records.

Fig. 7. Sea level curves at tide gauge sites since 1950. Time series of reconstructed sea level (black), tide-gauge (red) and altimetry (blue). The dashed blue line corresponds to tide gauge records supplemented using altimetry data. The time series are arranged in 3 groups: G1 [15°N–5°N], G2 [5°N–18°S] and G3 [18°S–20°S]. (For interpretation of the references to color in this figure legend, the reader is referred to the web version of this article.)

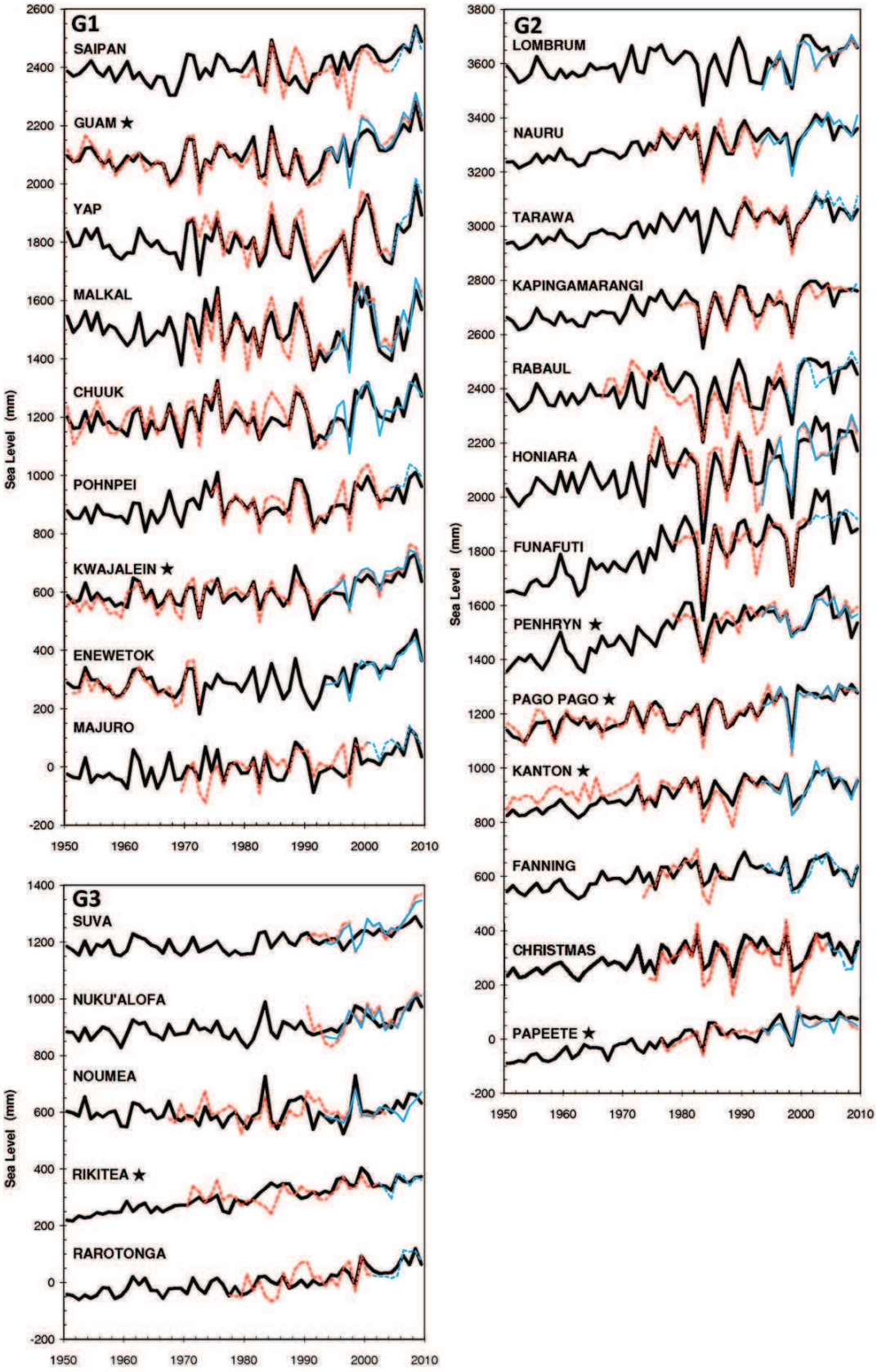
G1
SAIPAN
GUAM ★
YAP
MALKAL
CHUUK
POHNPEI
KWAJALEIN ★
ENEWETOK
MAJURO
G2
LOMBRUM
NAURU
TARAWA
KAPINGAMARANGI
RABAUL
HONIARA
FUNAFUTI
PENHRYN ★
PAGO PAGO ★
KANTON ★
FANNING
CHRISTMAS
PAPEETE ★
G3
SUVA
NUKU'ALOFA
NOUMEA
RIKITEA ★
RAROTONGA
Sea Level (mm)
1950
1960
1970
1980
1990
2000
2010

The mean (detrended) RESL time series for the G1 region is shown in Fig. 8a (RESL mean rise over 1950–2009 in G1 amounts to 1.1 ± 0.6 mm/yr). We observe a clear negative correlation ($r = -0.6$) between detrended mean sea level and NINO3 shifted by half a year (see above and Delcroix, 1998). As previously noted by Church et al. (2006), interannual sea level variability beyond 1970 is greater than prior to 1970. This was quantified by calculating the standard deviation of interannual anomalies: sea level has an average interannual variability of 3 cm before 1970, and 6 cm after 1970. For example at Malakal, the 1997–1998 ENSO event was accompanied by a decrease in sea level followed by an abrupt increase. For the period 1997–1998, the positive sea level anomaly at Malakal reached ~26 cm (~20 cm at Yap and Chuuk islands).

In the G2 region which includes the Lombrum, Nauru, Kapingamarangi, Rabaul, Honiara, Funafuti, Kanton, Pago Pago, Fanning, Christmas Island, Penrhyn, Papeete and Tarawa islands, the average correlation between RESL and tide gauge (not used in the reconstruction) sea level is 0.8 (Table 1). The mean rms difference between tide gauges and RESL is ~5 cm. The mean RESL trend over the G2 region amounts to 2.6 ± 0.6 mm/yr for 1950–2009. At Funafuti and Penrhyn, the RESL trends amount to 4.7 ± 0.7 mm/yr and 3.5 ± 0.6 mm/yr respectively. Fig. 8b shows detrended mean RESL of the G2 sub-region and NINO3 (shifted by half a year, Delcroix, 1998). A negative correlation of $r = -0.6$ is reported. RESL interannual variability in the G2 region can be roughly divided into three phases: before the 1982–1983 El Niño, during 1982–2001 and after 2001, a period of prevailing El Niño Modoki events. The interannual standard deviation of RESL in G2 is 6 cm for the period 1982–2001, i.e., 1.4 times more than over the other two periods. At Funafuti, the negative sea level anomaly during the 1982–1983 ENSO reaches −35 cm. There, the interannual standard deviation of RESL is ~5 cm for the period 1950–1981, ~9 cm for the period 1982–2009. We observe also that the time series at the three sites of Honiara, Funafuti and Penrhyn are very similar, probably due to their location near the South Equatorial Ridge (Noye and Grzechnik, 2001).

In the G3 region which includes the Suva, Nuku'Alofa, Rarotonga, Rikitea and Noumea islands, the average correlation between detrended RESL (mean RESL trend in G3 amounts to 1.5 ± 0.5 mm/yr over 1950–2009) and tide-gauge-based sea level (not used in the reconstruction) is 0.6. Tide gauge record and RESL trends are in good agreement over their overlapping time span (except at Suva). The mean difference between tide gauges and RESL time series is ~4.5 cm. Fig. 8c shows detrended RESL. The mean interannual standard deviation in G3 is on the order of 2 cm.

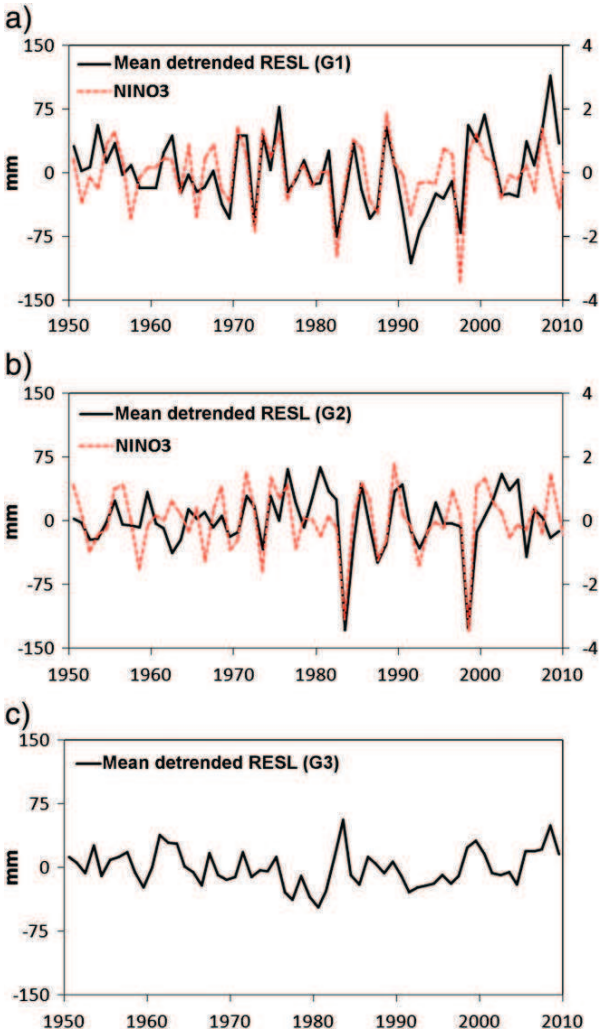

Fig. 8. Detrended mean RESL curves in each of the 3 regions: a) G1 [15°N–5°N], b) G2 [5°N–18°S] and c) G3 [18°S–20°S] with the superimposed inverse NINO3 (right axis) shifted by half a year.

5. Total sea level trend (climatic components and vertical ground motions) at tide gauge sites

In the previous section, we discussed the interannual/decadal/multidecadal variability and trends of the reconstructed sea level time series at the island sites of the PIR. We now examine vertical ground motions that affect locally tide gauge measurements. In effect, tide gauges are affected by ground motions while the reconstruction is supposed to reflect the 'climatic' signal only (global mean trend plus regional variability). Note that this is not totally true because to reconstruct past sea level, we used tide gauge data corrected for GIA only (see Section 2). If natural or anthropogenic ground subsidence also affects a given tide gauge site used in the reconstruction, such effects were not corrected for. However, in the studied region, only 7 over 27 tide gauges contributed to the global reconstruction. Moreover the reconstructed trend at a given site results from two components: (1) global mean trend (equal to 1.8 mm/yr) due to global warming (through ocean warming and land ice melt) and (2) regional trends. As shown by several previous studies (e.g. Timmermann et al., 2010), the latter component mainly results from wind-driven steric sea level regional variability and is supposed to be related to internal modes of variability of the climate system. Thus, we expect that at island sites not used in the reconstruction, the reconstructed trend is essentially of climate origin (with some uncertainty of course) and is little contaminated by unrelated vertical ground motions.

In this section we examine the 'total' trend at the tide gauges collocated with GPS stations. For that purpose, we now use tide gauge records not corrected for GIA. In effect, our purpose is to compare tide gauge trends with the combination of reconstructed (i.e., 'climatic') sea level trends and GPS-based vertical rates (that include the GIA component). By 'total' trend, we mean the 'climatic' components as derived from the reconstruction (i.e., the global mean rise plus the regional trend), to which we subtract the 'local' component due to vertical ground motion (negative/positive vertical ground motion, i.e., subsidence/uplift, gives rise to relative sea level rise/drop; thus to obtain the total sea level trend, we subtract vertical ground motion). The 'total' trend should reflect the sea level change felt by the population locally. We first discuss vertical ground motions and then the climatic and total trends.

5.1. Vertical ground motions from GPS

In the PIR, 12 tide gauges are collocated with GPS stations: Guam, Funafuti, Kwajalein, Lombrum, Nauru, Noumea, Pago-Pago, Papeete, Pohnpei, Rarotonga, Saipan and Tarawa. The distance between the tide gauge and the GPS antenna is given in Table 2. If the GPS time series show spurious jumps or curious behavior, we then discard the corresponding data (e.g., Saipan, Kwajalein, Lombrum and Nauru). The ULR4 (Santamaría-Gómez et al., 2011) and F2011 (Fadil et al., 2011) solutions directly provide vertical rates. This is unlike the REPRO1 solution which consists of weekly position time series. To compute REPRO1 vertical rates and their uncertainties, we use the maximum likelihood estimation (MLE) technique using the CATS software (Williams, 2008). A combination of power-law plus variable white noise model provides the most likely stochastic description of REPRO1 GPS position time series. This result is consistent with former results (e.g., Mao et al., 1999; Santamaría-Gómez et al., 2011). The estimated spectral indexes are close to −1, indicating flicker noise. On this assumption, the average noise levels are 0.4 ± 0.1 mm and 5.6 ± 1.1 mm/yr^0.25 for the variable white- and power law noises, respectively.

Vertical rates and associated uncertainties are given in Table 2 for the three GPS solutions. Looking at Table 2, we note that vertical rates are in general negative, evidencing ground subsidence (hence apparent sea level rise). At Guam, estimated rates are positive but the REPRO1 time series (not shown) suggests spurious behavior before 2002, which is confirmed in the ULR4 solution too (figure available on http://www.sonel.org/-GPS-.html). The REPRO1 rate at Guam is estimated over the period 2002–2010 as in F2011, while ULR4 consider the total 1996–2010 time span despite the spurious behavior observed in the time series. Whatsoever, the positive rates from the three GPS solutions are consistent within their error bars and are not statistically different. At Saipan, the REPRO1 time series shows a large data gap and a big jump, making it somewhat suspect. This is not visible in the corresponding ULR4 time series. We remove this station from our analysis. Note that both Guam and Saipan are located at the forefront volcanic arc of the Marianna trench, thus may be subject to strong volcanic and tectonic deformations. At Pohnpei, the ULR4 time series shows some large data gaps, making it somewhat suspect. At Kwajalein, both the REPRO1 and ULR4 time series show a large data gap and ground subsidence around −3 mm/yr, but we suspect a shift around year 2000. Thus we prefer not to consider it. At Nauru, the three solutions are in good agreement. Although the corresponding time series are short (5–6 years), we decide to keep this station. At Funafuti, the REPRO1 time series shows strong interannual variability and significant dispersion is noticed between the three solutions. While the ULR4 and F2011 solutions agree well and report subsidence rates of −0.7 mm/yr and −0.9 mm/yr, the REPRO1 solution gives a rate of nearly zero. This is surprising as the three solutions are based on similar GPS data length. At Lombrum, the REPRO1 time series shows spurious gaps between 2004 and 2008, which is confirmed in the ULR4 solution too. This GPS time series is thus discarded. At Pago Pago, the REPRO1 time series shows spurious data after mid-2008, whereas ULR4 and F2011 rates are calculated from mid-2001 to 2009. At Papeete and Noumea, the REPRO1 and F2011 estimates are in close agreement but differ from the ULR4 estimate. At Rarotonga, ULR4 and F2011 rates are negative while the REPRO1 rate is positive for the same period. But the differences between the estimated rates are not statistically significant. At Tarawa, the REPRO1 time series shows strong interannual variability, and significant dispersion is noticed between the three solutions. The ULR4 time series shows spurious data between 2004 and 2006. Some other discrepancies are observed between the REPRO1, ULR4 and F2011 solutions, probably due to the different processing techniques used by each group. In summary, close inspection of the GPS solutions leaves us with only 9 stations: Guam, Pohnpei, Nauru, Funafuti, Pago Pago, Papeete, Noumea, Rarotonga and Tarawa. In the following, we use for each station the weighted mean vertical

Table 2
GPS rates (from REPRO1, ULR4 and F2011, and weighted mean of the three solutions), reconstruction rates accounting for land motion (weighted mean) and tide gauge rates (non GIA corrected). The symbol − corresponds to unavailable or missing value or non-significant trend. Stars ★ correspond to tide gauges used in the global reconstruction.

Collocated tide gauge station	GPS				REPRO1			ULR4			F2011			Weighted mean (REPRO1, ULR4, F2011)		RESL–Weighted mean 1950–2009		RESL–Weighted mean (tide gauge time span)		Tide gauge (non GIA corrected)		
	Acronym of the GPS site	Lon	Lat	Dist. (km)	Vertical velocity (mm/yr)	Error (mm/yr)	Span (yr)	Vertical velocity (mm/yr)	Error (mm/yr)	Span (yr)	Vertical velocity (mm/yr)	Error (mm/yr)	Span (yr)	Vertical velocity (mm/yr)	Error (mm/yr)	Trend (mm/yr)	Error (mm/yr)	Trend (mm/yr)	Error (mm/yr)	Span (yr)	Trend (mm/yr)	Error (mm/yr)
Guam ★	GUAM	144.9	13.5	28	0.4	0.3	7.8	0.4	0.3	13.0	0.1	0.6	7.5	0.4	0.2	1.0	0.7	1.0	0.9	60	2.1	0.5
Pohnpei	POHN	158.2	6.9	2.5	−0.3	0.3	6.4	−1.7	0.6	5.7	−1.0	0.7	6.4	−0.6	0.2	2.0	0.6	2.2	1.1	36	3.2	0.9
Kwajalein ★	KWJ1	167.7	8.7	1.2	−3.1	0.6	6.3	−2.7	0.9	6.4	−	−	−	−	−	−	−	−	−	60	−	−
Nauru	NAUR	166.9	−0.5	3	−1.3	0.4	4.5	−1.1	0.8	5.5	−1.5	0.7	6.3	−1.3	0.3	3.6	0.6	3.0	1.8	21	−	−
Funafuti	TUVA	179.2	−8.5	2.5	0.0	0.2	7.8	−0.9	0.3	7.0	−0.7	0.7	7.4	−0.4	0.2	5.1	0.7	4.5	1.9	32	4.5	1.3
Lombrum	PNGM	147.4	−2.0	0.9	−0.1	0.9	8.5	−1.3	0.4	6.6	−	−	−	−	−	−	−	−	−	15	−	−
Pago Pago ★	ASPA	−170.7	−14.2	7	−0.1	0.2	6.5	−0.6	0.2	7.4	−2.0	0.9	8.1	−0.4	0.1	2.9	0.6	2.9	0.8	60	2.5	0.4
Papeete ★	THTI	−149.6	−17.5	6	−0.3	0.2	11.5	−0.7	0.4	10.5	−0.3	0.4	11.4	−0.4	0.2	3.3	0.6	3.2	0.9	34	2.9	0.5
Noumea	NOUM	166.4	−22.1	3.6	−2.7	0.4	9.2	−1.6	0.3	9.2	−2.9	0.6	9.2	−2.1	0.2	2.6	0.6	2.8	1.0	37	−	−
Rarotonga	CKIS	−159.8	−21.1	3.5	0.6	0.3	8.0	−0.3	0.5	7.3	−0.1	0.7	8.1	0.3	0.2	1.5	0.6	3.1	0.9	33	3.9	0.7
Saipan	CNMR	145.7	15.1	0.6	−0.9	0.5	4.6	0.3	0.5	5.4	−	−	−	−	−	−	−	−	−	31	−	−
Tarawa	KIRI	172.9	1.3	1.6	0.3	0.5	7.2	−0.8	0.5	6.4	−0.5	0.7	7.2	−0.3	0.3	2.5	0.6	2.0	1.6	22	−	−

rate computed from the three GPS solutions (i.e., the average of the three rate values weighted by their respective inverse squared uncertainty).

5.2. 'Total' sea level rise

We now compare trends from the (non GIA corrected) tide gauge records (supposed to reflect the total rate, i.e., climatic components and vertical land motion), from the reconstruction ('climatic' components) and from the GPS solutions (vertical rates). We consider only the tide gauge records with at least 30 years of data and with a significant trend (p-value>0.1, i.e., result not significant at the 0.1 significance level). This leads us to not consider the tide gauge trends at Tarawa and Noumea stations (see Tables 1 and 2). In Table 2, the (non GIA corrected) tide gauge trends are computed over their available data spans while the reconstruction trends are given for both the whole 1950–2009 time span and the generally shorter tide gauge time span. GPS trends are estimated with a few years of data only but as done in many previous studies (e.g., Woppelmann et al., 2007), we make the assumption that they reflect long term vertical rates (of course we are aware of the fact that this may not be totally true and we cannot exclude that some factors — e.g., atmospheric or hydrological loading may produce decadal/multidecadal variability). In the following, the quoted uncertainty on the 'total' sea level trend is based on the quadratic sum of the reconstruction method error, the formal error of the least-squares linear regression and the (realistic) error of the GPS solution.

Fig. 9a shows tide gauge-based and RESL–GPS (i.e., from the reconstruction and land motion) trends for Guam, Pohnpei, Funafuti, Pago Pago, Papeete and Rarotonga, computed over each tide gauge time span (as summarized in Table 2). We note that the two types of trend agree within their respective uncertainties. Fig. 9a also confirms the important regional variability, with significantly different trends from one site to another. The largest trend is seen at Funafuti both in the tide gauge data and RESL–GPS.

Fig. 9b shows RESL–GPS trends and associated uncertainty over 1950–2009 at the 6 tide gauge sites as in Fig. 9a, plus at Nauru, Noumea and Tarawa (the latter 3 tide gauges records were not considered in Fig. 9a for the reasons discussed above). In Fig. 9b, the global mean sea level trend and its uncertainty range are also shown. From Fig. 9b (see also Table 2), we note that at Guam and Rarotonga, the 'total' sea level trend based on the reconstruction including the vertical land motion is below the global mean sea level rise of the past 60 years while Pohnpei total trend is slightly above (although, in the three cases, total trend falls within the uncertainty range of the global mean trend). At the 6 remaining sites, total trends are above the global mean sea level rise, with one clear outsider: Funafuti where the total sea level trend since 1950 amounts to ~5 mm/yr.

5.3. The Funafuti case

Sea-level change at the Tuvalu islands has been the subject of several previous studies (Hunter, 2002; Eschenbach, 2004; Church et al., 2006; Yamano et al., 2007; Aung et al., 2009). The nine major islands of the Tuvalu archipelago are all highly sensitive to climate change. In effect, the islands are very low-lying, their morphology is entirely dependent on coral growth, and they have shallow freshwater lenses which are easily depleted during drought episodes. They also have high population density. The largest of the Tuvalu islands is Funafuti, a near-continuous ring of 33 islets, each just 20 m to 400 m wide, around a central lagoon of 20 km diameter. With a land area of 2.8 km^2, Funafuti atoll supports a population of approximately 5000 people (Government of Tuvalu, 2006). Over the past few decades, Funafuti has seen an influx of migrants from outer islands (Mortreux and Barnett, 2009). Tuvalu has no streams or rivers, and therefore, almost no drinkable water. Rising sea level already adversely impacts traditional fresh water sources. Moreover, there is a crop livelihood decline due to soil salinity (Patel, 2006). All these factors have influenced people to migrate from other islands to Funafuti.

The Funafuti tide gauge is located on a jetty on the islet of Fongafale. The atoll encloses a lagoon roughly 15 km in diameter, in which the tide gauge is located. Therefore, the tide gauge is relatively sheltered from the deep ocean. At Funafuti, we get a total rate of sea level rise of ~5.1 ± 0.7 mm/yr (considering the weighted mean of the ULR4, F2011 and REPRO1 solutions). Because of the regional variability component, the amount of sea level rise really felt by the population is almost three times the global mean rate of sea level rise over the past half century. Over the last 60 years, this corresponds to a total sea level elevation of ~30 ± 4 cm. This result allows us to better understand why the Tuvalu (Funafuti) population feels highly threatened by global warming and sea level rise, as often reported by the world media.

6. Conclusion

In this study, we determined past sea level variability and change in the western tropical Pacific using a 2-D past sea level reconstruction.

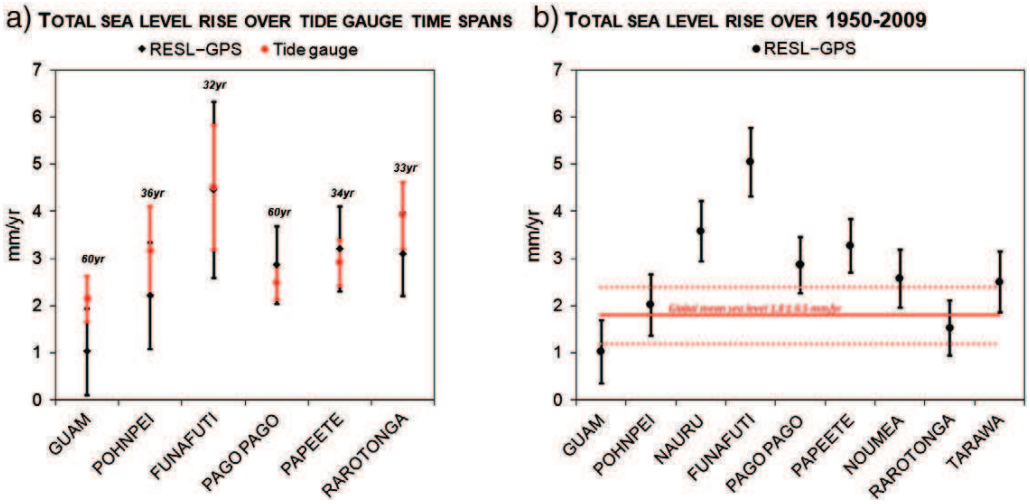

Fig. 9. Left panel: total sea level rise at Guam, Pohnpei, Funafuti, Pago Pago, Papeete and Rarotonga estimated over the tide gauge time spans (red: from tide gauge data, black: RESL-GPS); Right panel: total sea level rise at Guam, Pohnpei, Nauru, Funafuti, Pago Pago, Papeete, Noumea, Rarotonga and Tarawa estimated over 1950-2009 from RESL-GPS. The horizontal lines represent the global mean sea level trend over this period and its associated uncertainty.

We observe that over 1950–2009, spatial trend patterns are quite different from those observed over the altimetry era (1993–2009). Over the time span 1950–2009, sea level in the PIR is characterized by a strong positive trend pattern, almost centered on the Tuvalu islands. We find that sea level in the PIR displays important regional variability driven by ENSO events. We show that ENSO events have a strong modulating effect on the PIR sea level variability, with a tendency for low sea level during El Niño events and high sea level during La Niña events. Moreover, besides the sub-decadal ENSO signature, our results also show some low-frequency variability in PIR sea level, seen in the steric sea level as well. Our results suggest an amplification of the ENSO signature since 1970 and the hint for an increased occurrence of El Niño Modoki-type signature events since 2002 in the PIR. However, this regional variability has different characteristics depending on the sub-regions. For the G1 sub-region [15°N–5°N], the reconstructed sea level rise over 1950–2009 amounts to 1.1 ± 0.6 mm/yr. In this sub-region, we observe a clear negative correlation between detrended mean sea level and NINO3 index (with 6-month shift). For the G2 sub-region [5°N-18°S], the reconstructed sea level trend amounts to 2.6 ± 0.6 mm/yr for 1950–2009. A negative correlation with NINO3 index is reported (with 6-month shift). In this sub-region, the interannual variability can be roughly divided into three phases: before the 1982–1983 El Niño, during 1982–2001 and after 2001, a period of prevailing El Niño Modoki events. For the G3 region [18°S–20°S], the reconstructed sea level rise over 1950–2009 amounts to 1.5 ± 0.5 mm/yr.

In the study, we also estimate the total rate of sea level change at selected PIR islands, as a result of the climate-related sea level change (uniform-global mean-sea level rise plus regional variability) and vertical land motion. This allows us to determine the amount of "total" sea level change effectively felt by the populations over the last ~60 years. We find that at Guam, Pohnpei and Rarotonga, the 'total' sea level trend based on the reconstruction and GPS vertical land motion, is within the uncertainty range of the global mean sea level rise of ~1.8 mm/yr since 1950. At Nauru, Funafuti, Pago Pago, Papeete, Noumea, and Tarawa, the 'total' sea level trend is significantly above the global mean. At Funafuti, the total rate of sea level rise is found to be ~5 mm/yr over the last 60 years. This corresponds to a sea level elevation of ~30 cm during this time span. These results corroborate that at this particular location, sea level rise – as felt by the population – is no longer the question. The question now is how well prepared the low-lying Pacific Islands will be in a world affected by these global changes.

The above results clearly demonstrate the utmost importance of two factors when considering global warming-related sea level rise threat: regional variability and land motion. Regional variability that is superimposed to the global mean sea level rise may either diminish or amplify the latter by a substantial amount. For the past 60 years, at some islands of the western tropical Pacific like Papeete and Funafuti, the regional amplification is in the range 70%–150%. Vertical land motion, which more often consists of local subsidence rather than uplift, is another factor of amplification of the relative sea level rise. This was recently discussed by Ballu et al. (2011) for the Torres islands (north Vanuatu, southwest Pacific). Using GPS precise positioning, these authors clearly demonstrate that during the past ~two decades, earthquake-related vertical land motion led to large subsidence (of about −10 mm/yr), almost doubling the absolute, climate-related sea level rise. They judiciously warn against interpreting natural hazards affecting these remote islands as the only consequence of global warming-related climate change. This concern clearly applies to other regions, in particular the low-lying islands of the tropical Pacific. At Funafuti, ground subsidence increases the climate-related sea level rise by about 10%. At Papeete, this amplification is about 15% but at Noumea, ground subsidence is by far dominating the climate-related sea level change. As concluded by Ballu et al. (2011), climate change adaptation in low-lying small islands must identify other potentially risky factors than uniformly rising sea level, namely regional variability and land subsidence and account for them when developing mitigation and adaptation projects.

Acknowledgments

We would like to thank two anonymous reviewers for very helpful comments that led to significant improvement of the manuscript. We also thank G. Woppelmann (LIENSs, CNRS) and F. Perosanz (DTP, CNES) for kindly helping us for the GPS section. The altimeter products were produced by SSALTO/DUACS and distributed by AVISO with support from CNES. M. Becker and C. Letetrel are supported by an ANR CNRS grant number ANR-09-CEP-001-01 (CECILE project). W. Llovel is supported by a NASA Postdoctorate fellowship. The SONEL data assembly center is also acknowledged for providing a comprehensive access to GPS data at tide gauges, and assistance for the latest ULR solution.

References

Ablain, M., Cazenave, A., Valladeau, G., Guinehut, S., 2009. A new assessment of the error budget of global mean sea level rate estimated by satellite altimetry over 1993–2008. Ocean Science 5, 193–201.

Altamimi, Z., Collilieux, X., Legrand, J., Garayt, B., Boucher, C., 2007. ITRF2005: a new release of the International Terrestrial Reference Frame based on time series of station positions and Earth Orientation Parameters. Journal of Geophysical Research 112, B09401. doi:10.1029/2007JB004949.

Ashok, K., Behera, S.K., Rao, S.A., Weng, H., Yamagata, T., 2007. El Niño Modoki and its possible teleconnection. Geophysical Research Letters 112, C11007. doi:10.1029/2006JC003798.

Aung, T., Singh, A., Prasad, U., 2009. Sea level threat in Tuvalu. American Journal of Applied Sciences 6, 1169–1174.

Ballu, V., Bouin, M.N., Simeoni, P., Crawford, W.C., Calmant, S., Bore, J.M., Kana, T., Pelletier, B., 2011. Comparing the role of absolute sea level rise and vertical tectonic motions in coastal flooding, Torres Islands (Vanuatu). PNAS. doi:10.1073/pnas.1102842108.

Barnier, B., Madec, G., Penduff, T., Molines, J.M., Treguier, A.M., Le Sommer, J., Beckmann, A., Biastoch, A., Böning, C., Dengg, J., et al., 2006. Impact of partial steps and momentum advection schemes in a global ocean circulation model at eddy-permitting resolution. Ocean Dynamics 56, 543–567.

Becker, M., Karpytchev, M., Davy, M., Doekes, K., 2009. Impact of a shift in mean on the sea level rise: application to the tide gauges in the Southern Netherlands. Continental Shelf Research 29, 741–749.

Behera, S., Yamagata, T., 2010. Imprint of the El Niño Modoki on decadal sea level changes. Geophysical Research Letters 37, L23702. doi:10.1029/2010GL045936.

Berge-Nguyen, M., Cazenave, A., Lombard, A., Llovel, W., Viarre, J., Cretaux, J.F., 2008. Reconstruction of past decades sea level using thermosteric sea level, tide gauge, satellite altimetry and ocean reanalysis data. Global and Planetary Change 62, 1–13.

Bindoff, N.L., Willebrand, J., Artale, V., Cazenave, A., Gregory, J., Gulev, S., Hanawa, K., Le Quere, C., Levitus, S., Nojiri, Y., et al., 2007. Observations: oceanic climate change and sea level. Climate Change 2007: The Physical Science Basis. In: Solomon, S., Qin, D. (Eds.), Contribution of Working Group I to the Fourth Assessment Report of the Intergovernmental Panel on Climate Change. M. Cambridge University Press, Cambridge.

Bonett, D.G., Wright, T.A., 2000. Sample size requirements for estimating Pearson, Kendall, and Spearman correlations. Psychometrica 65 (1), 23–28.

Bosc, C., Delcroix, T., 2008. Observed equatorial Rossby waves and ENSO-related warm water volume changes in the equatorial Pacific Ocean. Journal of Geophysical Research 113, C06003. doi:10.1029/2007JC004613.

Brodeau, L., Barnier, B., Treguier, A.M., Penduff, T., Gulev, S., 2010. An ERA40-based atmospheric forcing for global ocean circulation models. Ocean Modelling 31, 88–104.

Busalacchi, A.J., Cane, M.A., 1985. Hindcasts of sea level variations during the 1982–83 El Niño. Journal of Physical Oceanography 15, 213–221.

Carrere, L., Lyard, F., 2003. Modeling the barotropic response of the global ocean to atmospheric wind and pressure forcing - comparisons with observations. Geophysical Research Letters 6, 1275. doi:10.1029/2002GL016473.

Cazenave, A., Llovel, W., 2010. Contemporary sea level rise. Annual Review of Marine Science 2, 145–173.

Chambers, D.P., Mehlhaff, C.A., Urban, T.J., Nerem, R.S., 2002. Analysis of interannual and low-frequency variability in global mean sea level from altimetry and tide gauges. Physics and Chemistry of the Earth 27, 1407–1411.

Chao, Y., Halpern, D., Perigaud, C., 1993. Sea surface height variability during 1986–1988 in the Tropical Pacific Ocean. Journal of Geophysical Research 98 (C4), 6947–6959. doi:10.1029/92JC02984.

Christiansen, B., Schmith, T., Thejll, P., 2010. A surrogate ensemble study of sea level reconstructions. Journal of Climate 23, 4306–4326.

Church, J.A., White, N.J., 2006. A 20th century acceleration in global sea-level rise. Geophysical Research Letters 33, L01602. doi:10.1029/2005GL024826.

Church, J.A., White, N.J., 2011. Changes in the rate of sea-level rise from the late 19th to the early 21st century. Surveys in Geophysics 1–18. doi:10.1007/s10712-011-9119-1.

Church, J.A., White, N.J., Coleman, R., Lambeck, K., Mitrovica, J.X., 2004. Estimates of the regional distribution of sea level rise over the 1950–2000 period. Journal of Climate 17, 2609–2625.
Church, J.A., White, N.J., Hunter, J.R., 2006. Sea-level rise at tropical Pacific and Indian Ocean islands. Global and Planetary Change 53, 155–168.
Delcroix, T., 1998. Observed surface oceanic and atmospheric variability in the tropical Pacific at seasonal and ENSO timescales: a tentative overview. Journal of Geophysical Research 103 (C9), 18611–18633.
Ducet, N., Le Traon, P.Y., Reverdin, G., 2000. Global high-resolution mapping of ocean circulation from TOPEX/Poseidon and ERS-1 and-2. Journal of Geophysical Research 105 (C8), 19,477–19,498. doi:10.1029/2000JC900063.
Dussin, R., Treguier, A.M., Molines, J.M., Barnier, B., Penduff, T., Brodeau, L., Madec, G., 2009. Definition of the Interannual Experiment ORCA025-B83, 1958–2007. LPO Report 902.
Efron, B., Tibshirani, R.J., 1993. An Introduction to the Bootstrap. Chapman & Hall.
Eschenbach, W., 2004. Tuvalu not experiencing increased sea level rise. Energy & Environment 15, 527–543.
Fadil, A., Barriot, J., Sichoix, L., Ortega, P., Willis, P., 2011. Evidence for a slow subsidence of the Tahiti Island from GPS, DORIS, and combined satellite altimetry and tide gauge sea level records. Comptes Rendus Geosciences 343 (5), 331–341. doi:10.1016/j.crte.2011.02.002.
Government of Tuvalu, 2006. Census of Population and Housing Central Statistics Division.
Hendricks, J.R., Leben, R.R., Born, G.H., Koblinsky, C.J., 1996. Empirical orthogonal function analysis of global TOPEX/POSEIDON altimeter data and implications for detection of global sea level rise. Journal of Geophysical Research 101 (C6), 14,131–14,145. doi:10.1029/96JC00922.
Holgate, S.J., 2007. On the decadal rates of sea level change during the twentieth century. Geophysical Research Letters 34, L01602. doi:10.1029/2006GL028492.
Hunter, J.R., 2002. A Note on Relative Sea Level Change at Funafuti, Tuvalu, Antarctic Cooperative Research Centre. University of Tasmania, p. 25http://staff.acecrc.org.au/~johunter/tuvalu.pdf.
Intergovernmental Panel on Climate Change (IPCC), 2007. Climate Change 2007: The Physical Science Basis. In: Solomon, S., et al. (Ed.), Contribution of Working Group I to the Fourth Assessment Report of the Intergovernmental Panel on Climate Change. Cambridge Univ. Press, Cambridge, U. K. available at http://ipcc-wg1.ucar.edu/wg1/wg1-report.html.
Jevrejeva, S., Grinsted, A., Moore, J.C., Holgate, S., 2006. Nonlinear trends and multiyear cycles in sea level records. Journal of Geophysical Research 111, C09012. doi:10.1029/2005JC003229.
Kalnay, E.C., Kanamitsu, M., Kistler, R., Collins, W., Deaven, D., Gandin, L., Iredell, M., Saha, S., White, G., Woollen, J., et al., 1996. The NCEP/NCAR 40-year reanalysis project. Bulletin of the American Meteorological Society 77, 437–472.
Kaplan, A., Kushnir, Y., Cane, M.A., 2000. Reduced space optimal interpolation of historical marine sea level pressure: 1854–1992. Journal of Climate 13, 2987–3002.
Kug, J.S., Jin, F.F., An, S.I., 2009. Two types of El Niño events: cold tongue El Niño and warm pool El Niño. Journal of Climate 22, 1499–1515.
Le Traon, P.Y., Nada, F., Ducet, N., 1998. An improved mapping method of multisatellite altimeter data. Journal of atmospheric and oceanic technology 15, 522–534.
Leuliette, E., Nerem, R., Mitchum, G., 2004. Calibration of TOPEX/Poseidon and Jason altimeter data to construct a continuous record of mean sea level change. Marine Geodesy 27, 79–94.
Levitus, S., Antonov, J., Boyer, T., 2005. Warming of the world ocean, 1955–2003. Geophysical Research Letters 32, L02604. doi:10.1029/2004GL021592.
Levitus, S., Antonov, J.I., Boyer, T.P., Locarnini, R.A., Garcia, H.E., Mishonov, A.V., 2009. Global ocean heat content 1955–2008 in light of recently revealed instrumentation problems. Geophysical Research Letters 36, L07608. doi:10.1029/2008GL037155.
Llovel, W., Cazenave, A., Rogel, P., Lombard, A., Bergé-Nguyen, M., 2009. Two-dimensional reconstruction of past sea level (1950–2003) from tide gauge data and an Ocean General Circulation Model. Climate of the Past 5, 217–227.
Lombard, A., Cazenave, A., Le Traon, P.Y., Ishii, M., 2005. Contribution of thermal expansion to present-day sea-level change revisited. Global and Planetary Change 47, 1–16.
Madec, G., 2008. NEMO reference manual, ocean dynamics component: NEMO-OPA. Preliminary Version. Note du Pole de modélisation, Institut Pierre-Simon Laplace (IPSL), France, pp. 1288–1619.
Mao, A., Harrison, C.G.A., Dixon, T.H., 1999. Noise in GPS coordinate time series. Journal of Geophysical Research 104, 2797–2816.
Merrifield, M., Kilonsky, B., Nakahara, S., 1999. Interannual sea level changes in the tropical Pacific associated with ENSO. Geophysical Research Letters 26 (21), 3317–3320. doi:10.1029/1999GL010485.
Meyssignac, B., Becker, M., Llovel, W., Cazenave, A., 2011. An Assessment of Two Dimensional Past Sea Level Reconstructions over 1950–2009 Based on Tide Gauge Data and Different Input Sea Level Grids Submitted. Surveys in Geophysics.
Miller, L., Douglas, B.C., 2004. Mass and volume contributions to twentieth-century global sea level rise. Nature 428, 406–409. doi:10.1038/nature02309.
Mitchum, G.T., Lukas, R., 1990. Westward propagation of annual sea level and wind signals in the Western Pacific Ocean. Journal of Climate 3, 1102–1110.
Mortreux, C., Barnett, J., 2009. Climate change, migration and adaptation in Funafuti, Tuvalu. Global Environmental Change 19, 105–112.
Nerem, R.S., Leuliette, E., Cazenave, A., 2006. Present-day sea-level change: a review. Comptes Rendus Geosciences 338, 1077–1083.
Nerem, R.S., Chambers, D.P., Choe, C., Mitchum, G.T., 2010. Estimating mean sea level change from the TOPEX and Jason Altimeter Missions. Marine Geodesy 33, 435–446.
Nicholls, R.J., Cazenave, A., 2010. Sea-level rise and its impact on coastal zones. Science 328, 1517.
Nicholls, R.J., Wong, P.P., Burkett, V.R., Codignotto, J.O., Hay, J.E., McLean, R.F., Ragoonaden, S., Woodroffe, C.D., 2007. Coastal systems and low-lying areas. Climate Change 2007: impacts, adaptation and vulnerability. Fourth Assessment Report of the Intergovernmental Panel on Climate Change, pp. 315–356.
Noye, J., Grzechnik, M., 2001. Sea-level Changes and Their Effects. World Scientific Pub Co Inc.
Patel, S.S., 2006. A sinking feeling. Nature 440, 734–736.
Peltier, W.R., 2004. Global glacial isostasy and the surface of the ice-age Earth: the ICE-5G (VM2) model and GRACE. Annual Review of Earth and Planetary Sciences 32, 111–149.
Penduff, T., Juza, M., Brodeau, L., Smith, G., Barnier, B., Molines, J., Treguier, A., Madec, G., 2010. Impact of global ocean model resolution on sea-level variability with emphasis on interannual time scales. Ocean Science 6, 269–284.
Preisendorfer, R.W., 1988. Principal component analysis in meteorology and oceanography. Developments in Atmospheric Science, vol. 17. Elsevier (425 pp.).
Ray, R.D., Douglas, B.C., 2010. Experiments in reconstructing twentieth-century sea levels. American Geophysical Union, Fall Meeting 2010, abstract #G51D-03.
Rosner, B., 1975. On the detection of many outliers. Technometrics 17, 221–227.
Santamaría-Gómez, A., Bouin, M.N., Collilieux, X., Wöppelmann, G., 2011. Correlated errors in GPS position time series: implications for velocity estimates. Journal of Geophysical Research 116, B01405. doi:10.1029/2010JB007701.
Smith, T.M., 2000. Tropical Pacific sea level variations (1948–98). Journal of Climate 13, 2757–2769.
Timmermann, A., McGregor, S., Jin, F.F., 2010. Wind effects on past and future regional sea level trends in the Southern Indo-Pacific. Journal of Climate 23, 4429–4437.
Toumazou, V., Cretaux, J.F., 2001. Using a Lanczos eigensolver in the computation of empirical orthogonal functions. Monthly Weather Review 129, 1243–1250.
Volkov, D.L., Larnicol, G., Dorandeu, J., 2007. Improving the quality of satellite altimetry data over continental shelves. Journal of Geophysical Research 112, C06020. doi:10.1029/2006JC003765.
Weng, H., Ashok, K., Behera, S.K., Rao, S.A., Yamagata, T., 2007. Impacts of recent El Niño Modoki on dry/wet conditions in the Pacific rim during boreal summer. Climate Dynamics 29, 113–129.
Williams, S.D.P., 2008. CATS: GPS coordinate time series analysis software. GPS Solutions 12 (2), 147–153. doi:10.1007/s10291-007-0086-4.
Woodworth, P.L., Player, R., 2003. The permanent service for mean sea level: an update to the 21st century. Journal of Coastal Research 19, 287–295.
Woppelmann, G., Martin Miguez, B., Bouin, M.-N., Altamimi, Z., 2007. Geocentric sea-level trend estimates from GPS analyses at relevant tide gauges world-wide. Global and Planetary Change 57 (3–4), 396–406.
Wyrtki, K., 1984. The slope of sea level along the equator during the 1982/1983 El Niño. Journal of Geophysical Research 89 (C6), 10,419–10,424. doi:10.1029/JC089iC06p10419.
Wyrtki, K., 1985. Water displacements in the Pacific and the genesis of El Nino Cycles. Journal of Geophysical Research 90 (C4), 7129–7132. doi:10.1029/JC090iC04p07129.
Yamano, H., Kayanne, H., Yamaguchi, T., Kuwahara, Y., Yokoki, H., Shimazaki, H., Chikamori, M., 2007. Atoll island vulnerability to flooding and inundation revealed by historical reconstruction: Fongafale Islet, Funafuti Atoll, Tuvalu. Global and Planetary Change 57, 407–416.
Zebiak, S.E., Cane, M.A., 1987. A model El Nino-Southern Oscillation. Monthly Weather Review 115, 2262–2278.
Zhang, R.H., Levitus, S., 1996. Structure and evolution of interannual variability of the tropical Pacific upper ocean temperature. Journal of Geophysical Research 101 (C9), 20,501–20,524. doi:10.1029/96JC01805.

3.2 La mer Méditerranée

La mer Méditerrannée compte 46000 km de côtes dont 54% sont rocheuses et 46% de type sédimentaire. Le marnage y dépasse rarement les 30 cm rendant la côte pArticulièrement sensible aux évènements extrêmes en cas de montée du niveau de la mer. En effet, le marnage étant faible, l'augmentation du niveau de la mer se reporte directement sur le niveau maximum atteint lors des évènements extrêmes. Ainsi les évènements extrêmes atteignant une hauteur donnée sont d'autant plus fréquents en Méditerrannée que le niveau de la mer augmente (*Nicholls and Hoozemans* [1996]). Par exemple, sur la côte Egyptienne, une augmentation du niveau moyen de la mer Méditerranée de 0.3 m a pour conséquence de rendre 100 fois plus fréquent les évènements qui font ponctuellement augmenter le niveau de la mer de 0.5 m (voir la courbe de fréquence des inondations sur la côte Egyptienne Fig.3.2). Ceci expose les côtes Méditerranéennes à des inondations bien plus fréquentes à mesure que le niveau de la mer augmente en pArticulier sur les côtes sédimentaires et dans les marais maritimes qui sont peu élevés par rapport au niveau de la mer.

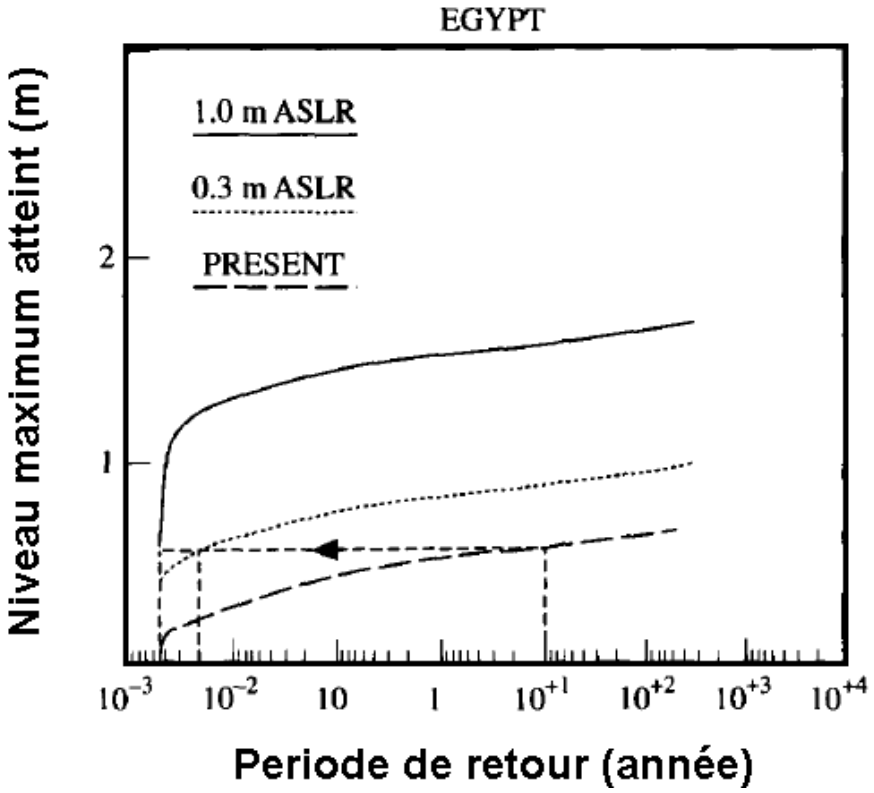

Figure 3.2 – Courbe de la fréquence des inondations sur la côte Egyptienne en fonction de l'augmentation du niveau de la mer. En ordonnée se trouve le niveau maximum atteint par l'eau au dessus du niveau moyen de la mer au cours des évènements extrêmes. En abscisse se trouve la fréquence d'occurence des évènements extrêmes. En trait pointillé : courbe calculée pour le niveau moyen de la méditerranée actuel. En point : courbe calculée pour le niveau moyen de la Méditerranée actuel augmenté de 0.3 m. En trait plein : courbe calculée pour le niveau moyen de la Méditerranée actuel augmenté de 1.0 m. Figure adaptée de *Nicholls and Hoozemans* [1996].

De plus, la Méditerranée est située sur une zone tectoniquement active (zone de convergence de la plaque Africaine avec la plaque Eurasienne) si bien que toute la côte Méditerranéenne est affectée par des mouvements verticaux importants (en pArcticulier dans sa partie orientale, *Bennett and Hreinsdottir* [2007]; *Antonioli et al.* [2009]) qui intensifient en de nombreux endroits la montée relative du niveau de la mer (Nord de la mer Adriatique, Delta du Nil, Nord de la mer Tyrennienne etc, voir par exemple *Braitenberg et al.* [2011]; *Fenoglio-Marc et al.* [2012]). Enfin la côte Méditerranéenne concentre plus de 150 millions d'habitants. Elle attire chaque année environ 200 millions de touristes (i.e. un tiers du nombre de touristes dans le monde) signifiant qu'elle concentre aussi une très forte infrastructure touristique et une activité économique considérable.

Ces différents éléments font de la côte Méditerranéenne l'une des côtes les plus vulnérables au monde, en pArcticulier sur sa partie Africaine où les protections contre les inondations sont rares (*Nicholls and Cazenave* [2010]). La région du delta du Nil est un exemple typique des situations les plus exposées que l'on trouve autour de la Méditerrannée. Elle concentre à elle seule 25 millions d'habitants (30% de la population Egyptienne), 40% des ressources agricoles et halieutiques de l'Egypte et 50% de ses ressources industrielles (*Frihy et al.* [2010]). De plus elle fait face à une augmentation du niveau de la mer de 1.8 $mm.a^{-1}$ depuis 1950 (*Marcos and Tsimplis* [2007]; *Calafat and Gomis* [2009]) tandis que la croûte terrestre locale est en subsidence suite au drainage du Delta (*Stanley and Warne 1993, Frihy 2010*).

Pour estimer les risques auxquels s'exposent les différentes régions du pourtour Meditérranéen comme le delta du Nil nous avons cherché à calculer la variabilité régionale du niveau de la mer en Méditerranée sur les dernières décennies.

3.2.1 Estimation locale du niveau de la mer depuis 1970

Sur les 18 dernières années, l'altimétrie montre que le niveau de la mer moyen en Mer Méditerranée présente une variabilité inter-annuelle très forte avec des amplitudes de plus de 100 mm d'une année sur l'autre. De même, la variabilité régionale est très forte avec des tendances très négatives dans la mer Ionienne et fortement positive dans la mer Egée et le bassin Levantin sur la période 1993-2006. Ces tendances sont la signature de l'"Eastern Mediterranean Transient" (EMT) : un changement de circulation en Mer Ionienne et dans le bassin Levantin dans les années 1990 qui a fortement marqué la variabilité du niveau de la mer Méditerranéen sur la décade 1993-2003 (*Roether et al.* [2007] par exemple). L'EMT est caractérisé par un changement dans la production des eaux profondes du bassin Levantin et de leurs caractéristiques thermo-halines. Au cours du $XX^{ème}$ siècle, elles se sont formées en mer Adriatique, mais au début des années 1990 ces eaux profondes ont été supplantées par des eaux plus denses provenant de mer Egée et qui se sont formées suite a plusieurs évènements climatiques inhabituels (*Beuvier et al.* [2010]). Parmis ces évènements déclencheurs, on compte un changement de circulation dans les bassins Ionien et Levantin (*Malanotte-Rizzoli et al.* [1999]; *Samuel et al.* [1999]), une convection hivernale extrême en mer Egée lors de l'hiver 1987 et l'occurence de deux hivers très froids consécutifs en 1992 et 1993 (*Josey* [2003]; *Beuvier et al.* [2010]). Ce changement de production d'eau profonde a fortement impacté la circulation Méditerranéenne à tel point qu'il domine la variabilité

régionale du niveau de la mer dans les bassins Ionien et Levantin sur la période 1993-2006 (*Tsimplis et al.* [2009]; *Vera et al.* [2009]).

En résumé, durant la période altimétrique, la variabilité du niveau de la mer est dominée par un évènement exceptionnel : l'EMT. Un tel évènement ne s'est très probablement pas produit entre 1950 et 1990 (*Beuvier et al.* [2010]). Ceci fait que les observations altimétriques sont pArcticulièrement peu représentatives de la variabilité du niveau de la mer Méditerranée aux cours des dernières décennies.

Les reconstructions globales, développées dans la section 2.2.2, ne donnent pas non plus d'informations fiables sur la variabilité du niveau de la mer en Méditerranée depuis 1950. Ceci est dû à 2 raisons. D'une part, comme la Méditerranée est un bassin semi fermé, elle est dominée par ses propres modes de variabilité océanique (comme l'EMT par exemple) qui sont largement découplés des modes de variabilité globaux qui ont servi à l'interpolation spatiale des marégraphes dans le processus de reconstruction. En conséquence l'interpolation réalisée dans les reconstructions globales donne des résultats biaisés pour la Méditerranée. D'autre part, sachant ce fait, nous n'avons pas utilisé de marégraphes Méditerranéens dans les reconstructions globales pour éviter de polluer en retour les reconstructions globales avec des informations spécifiques à la Méditerranée. Il n'y a donc aucune information marégraphique remontant à 1950 concernant la Méditerranée dans les reconstructions globales.

En conséquence nous avons développé des reconstructions spécifiques à la Méditerranée pour estimer sa variabilité régionale aux échelles inter-annuelles et multi-décennales. Pour cela nous avons suivi une méthodologie similaire à celle de l'étude *Meyssignac et al.* [2012] tout en l'adaptant aux spécificités du bassin Méditerranéen. C'est le sujet de l'Arcticle : "Two-dimensional reconstruction of the Mediterranean sea level over 1970-2006 from tide gage data and regional ocean circulation model outputs".

Résumé de l'Arcticle : "Two-dimensional reconstruction of the Mediterranean sea level over 1970-2006 from tide gage data and regional ocean circulation model outputs" (l'Arcticle original est inséré à la fin de cette section 3.2).
Dans cette étude nous développons 3 reconstructions différentes du niveau de la mer en Méditerranée sur la période 1970-2006. Pour les 3 reconstructions nous utilisons le même jeu de 13 marégraphes répartis autour du bassin. En revanche, nous utilisons pour chacune, une base de données différente pour estimer les EOFs du niveau de la mer qui permettent d'interpoler spatialement les marégraphes sur la période 1970-2006. Pour la première reconstruction nous utilisons des EOFs calculées à partir des données altimétriques sur la période 1993-2005. Ces données couvrent une période courte et fortement marquée par l'évènement EMT qui est pArcticulier aux années 1990, comme on a vu plus haut. Ceci peut donner trop de poids au mode de variabilité EMT dans la reconstruction multi-décennale (voir section 2.2.2). Pour cette raison, nous utilisons pour les 2 autres reconstructions, des EOFs calculées sur une période plus longue (1970-2002) à partir de modèles. Pour la deuxième reconstruction, les EOFs sont calculées à partir du modèle d'océan NEMOMED8 forcé par la réanalyse atmosphérique ARPERA (*Beuvier et al.* [2010]; *Herrmann et al.* [2010]). Pour la troisième reconstruction, les EOFs sont calculées à partir du modèle couplé atmosphère-océan PROTHEUS SYSTEM (*The PROTHEUS Group et al.* [2009]). Nous comparons ensuite ces 3 reconstructions entre elles et avec la reconstruction de *Calafat and Gomis*

[2009] basée sur un jeu de marégraphe distinct et des EOFs déduites de l'altimétrie (sur une période plus courte, de 1993 à 2001). L'ensemble des 4 reconstructions est aussi évalué de manière indépendante par comparaison avec les données altimétriques sur la période 1993-2000 et avec 7 marégraphes indépendants couvrant la période complète 1970-2006. Les 4 reconstructions donnent des résultats similaires et cohérents avec les données en terme de variabilité inter-annuelle et multi-décennale. Les meilleurs résultats sont obtenus pour la reconstruction basée sur le modèle NEMOMED8 (en pArcticulier dans le bassin Ionien où l'EMT a une forte influence, voir Fig. 3.3). Elle montre que la variabilité régionale semble avoir été dominée par l'impact de la NAO jusqu'en 1992 date à laquelle s'est manifesté l'EMT. En ce qui concerne le niveau moyen de la Méditerranée, les 4 reconstructions donnent aussi des résultats très similaires avec une forte baisse autour des années 1975, une hausse de plus de 30 mm en 1995 et une tendance de 1.4 mm.a^{-1} entre 1970 et 2000. En revanche, en terme de tendances sur la période 1970-2006, les résultats divergent entre les reconstructions. Ceci est dû à la forte variabilité inter-annuelle du niveau de la mer en Méditerranée (de l'ordre de $\pm$ 100 mm d'une année sur l'autre) qui empêche d'obtenir des tendances significatives sur une periode de seulement 36 ans. Il est quand même intéressant de noter que les 4 reconstructions s'accordent pour donner des tendances régionales du niveau de la mer relativement faibles sur la période 1970-2006 : entre -3 mm.a^{-1} et +3 mm.a^{-1}. Ceci est remarquablement faible comparé aux tendances régionales du niveau de la mer que l'on peut trouver autour du globe sur la même période : entre -7 mm.a^{-1} et +7 mm.a^{-1}.

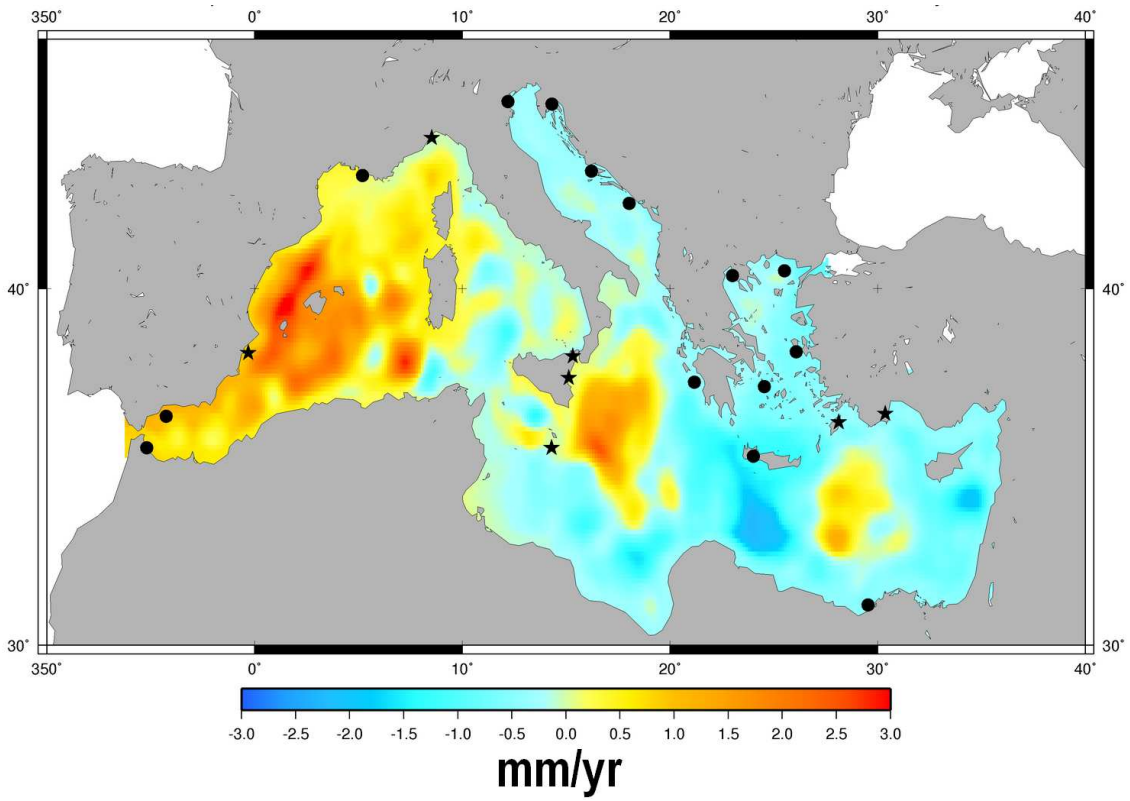

Figure 3.3 – Tendances du niveau de la mer reconstruites avec les marégraphes (indiqués par les points noirs) et les EOFs du modèle NEMOMED8 entre 1970 et 2009. Figure adaptée de *Meyssignac et al.* [2011].

3.2.2 Bilan de masse de la mer Méditerrannée sur les dernières décennies

Les reconstructions du niveau de la mer en Méditerranée nous ont montré que le niveau moyen du bassin avait augmenté à la vitesse de 1.4 $mm.a^{-1}$ entre 1970 et 2006. Cette vitesse est légèrement plus faible que celle du niveau de la mer global sur la même période (*Marcos and Tsimplis* [2008]; *Calafat and Gomis* [2009]). Dans le même temps, les reconstructions montrent une variabilité régionale en tendance assez faible. En effet, les tendances régionales ne s'écartent pas plus de $\pm 3 mm.a^{-1}$ de la moyenne du bassin. Ainsi dans toute la Méditerranée, c'est la tendance moyenne du bassin qui domine le signal local d'augmentation du niveau de la mer. Dans ce contexte, le niveau moyen du bassin et sa tendance semblent les éléments les plus importants à estimer et à comprendre, en pArcticulier pour les études d'impact.

Nous avons donc cherché à calculer les composantes stérique et massique du niveau de la mer Méditerranée pour estimer leur contribution à la hausse du niveau moyen du bassin. Sur la période 1970-2006, le niveau de la mer stérique moyenné sur la Méditerranée présente 2 phases : une baisse de 1970 à 1990 (-1 $mm.a^{-1}$) suivi d'une hausse entre 1990 et 2006 (1.2 $mm.a^{-1}$). Ces variations décennales sont dûes principalement à des variations de température moyenne du bassin (les variations de salinité ont été faibles aux échelles décennales depuis 1970 même si elles présentent une forte inter-annualité). Sur la période complète de 1970 à 2006 les variations décennales du niveau de la mer stérique se compensent, si bien que la tendance moyenne stérique est quasiment nulle. La tendance de 1.4 $mm.a^{-1}$ du niveau de la mer moyen sur la même période s'explique donc par l'augmentation de la masse d'eau en Méditerranée (*Calafat et al.* [2010]; *Fenoglio-Marc et al.* [2012]). C'est ce dernier point que nous analysons en proposant un bilan de masse complet de la mer Méditerranée entre 1970 et 2006 dans l'Arcticle intitulé "Decadal variability of net water flux at the Mediterranean sea Gibraltar Strait "

Résumé de l'Arcticle : "Decadal variability of net water flux at the Mediterranean sea Gibraltar Strait " (l'Arcticle original est inséré à la fin de cette section 3.2). Dans cette étude nous estimons tout d'abord les variations de masse de la Méditerranée entre 1970 et 2006 à partir de la reconstruction développée plus haut dans l'étude *Meyssignac et al.* [2011]. Pour cela nous soustrayons à la reconstruction basée sur NEMOMED8 le niveau de la mer stérique calculé à partir des données hydrographiques in-situ globales de *Ishii and Kimoto* [2009] ou régionales de MEDAR/MEDATLAS (*Rixen et al.* [2005]). Nous validons ces estimations sur la dernière decennie par comparaison avec les données GRACE et les données altimétriques corrigées du même niveau stérique. Nous estimons ensuite les différents facteurs qui font varier la masse de la Méditerranée. 5 facteurs ont un impact sur la masse d'eau du bassin : l'évaporation, les précipitations, le débit des fleuves affluents et les débits aux détroits de Bosphore et de Gibraltar. La somme des débits des fleuves et du débit au détroit de Bosphore forme une contribution faible à la masse de la Méditerranée. Elle est d'un ordre de grandeur inférieur aux autres contributions (*Mariotti et al.* [2002]). Même si elle est négligeable, nous l'estimons avec le modèle couplé atmosphère-océan Protheus System (*The PROTHEUS Group et al.* [2009]). Pour l'évaporation et les précipitations, nous disposons d'estimations qui remontent aux années 1950 grâce au réanalyses atmosphériques. Nous choisissons les bases de données OAFlux (*Yu et al.*

[2008]), REOFS (*Smith et al.* [2008]) et GPCP (*Adler et al.* [2003]) pour les calculer. En revanche nous ne disposons pas de mesures du débit à Gibraltar sur la période 1970-2006. Nous proposons donc de calculer cette contribution à l'aide des autres contributions à la masse de la Méditerranée en supposant le bilan de masse du bassin comme fermé. Ceci nous donne la première estimation publiée du débit à Gibraltar entre 1970 et 2006 basée sur des mesures uniquement (excepté pour la faible contribution du débit des fleuves et du détroit de Bosphore obtenue à partir d'un modèle). Nous validons ensuite notre bilan de masse par comparaison avec le modèle Protheus System. L'estimation du débit à Gibraltar s'avère en accord avec celle du modèle ce qui donne confiance au bilan de masse de la mer Méditerranée que nous proposons. Ceci nous permet de mettre en évidence que la tendance du niveau de la mer en Méditerranée entre 1970 et 2006 s'explique par une augmentation de masse. Aux échelles décennales, en revanche, les variations de masse apparaissent faibles car le débit au détroit de Gibraltar compense les variations de masse dûes aux précipitations et à l'évaporation à la surface du bassin. Ceci est moins vrai aux échelles inter-annuelles pour lesquelles les variations de masse sont plus fortes. A ces échelles le débit des fleuves semble jouer un rôle non négligeable.

Global and Planetary Change 77 (2011) 49–61

Contents lists available at ScienceDirect

Global and Planetary Change

journal homepage: www.elsevier.com/locate/gloplacha

Two-dimensional reconstruction of the Mediterranean sea level over 1970–2006 from tide gage data and regional ocean circulation model outputs

B. Meyssignac [a,*], F.M. Calafat [b], S. Somot [c], V. Rupolo [d], P. Stocchi [e], W. Llovel [a], A. Cazenave [a]

[a] LEGOS/CNES, 14, Avenue E. Belin, 31400 Toulouse, France
[b] IMEDEA (CSIC-UIB), Miquel Marques, 21, Esporles 07190, Mallorca, Baleares, Spain
[c] Météo-France/CNRS, CNRM-GAME, 31057 Toulouse cedex, France
[d] ACS-CLIM MOD, ENEA, Bldg F19, Room 112 Sp. 91 CR Casaccia, Via Anguillarese 301, 00060 Santa Maria di Galeria, Rome, Italy
[e] DEOS, Faculty of Aerospace Engineering, TUDelft, Delft, The Netherlands

ARTICLE INFO

Article history:
Received 19 January 2011
Accepted 22 March 2011
Available online 29 March 2011

Keywords:
sea level
Mediterranean Sea
reconstruction
interannual sea level variability
altimetry
tide gages
empirical orthogonal functions
Eastern Mediterranean Transient

ABSTRACT

Two-dimensional reconstructions of the Mediterranean sea level corrected for the atmospheric effects are proposed at monthly interval over the period 1970–2006 using 14 tide gage records and 33-year long (1970–2002) sea level grids from the NEMOMED8 regional ocean circulation model (NM8) and the PROTHEUS System Atmosphere–Ocean coupled model (PS). They are compared with a similar reconstruction using decade-long sea level grids from altimetry (Topex/Poseidon and Jason1) and a published reconstruction by Calafat and Gomis (2009). Tests with extra tide gages, not used in the computation, show that interannual variability is better captured when using long (33-year) spatial grids. In particular the NM8-based reconstruction reproduces better the sea level variability at all independent tide gages. An empirical Orthogonal Function decomposition of this reconstruction over 1970–2006 shows that the temporal curve of the two first modes are highly correlated with the North Atlantic Oscillation. We note in particular different behaviors over the 1970–1994 and 1994–2006 time spans. Results suggest that the North Atlantic Oscillation forcing modified the spatial patterns of the Mediterranean sea level around the year 1993 close to the date of occurrence of the Eastern Mediterranean Transient (a major change in the deep water formation of the Levantine and Ionian basin that occurred in the early 1990s).

1. Introduction

Long term sea level rise is a critical issue of the global climate change because of its potential huge impacts (IPCC 2007). It has been extensively studied in recent years in order to understand the driving mechanisms of its spatial and temporal variability. Since 1993, sea level is accurately monitored by satellite altimetry (i.e. Topex/Poseidon, Jason1, Jason2 and Envisat among others) with a global coverage and a short revisit time. These observations have shown that sea level does not rise uniformly. In some regions it rises faster than the global average while in others, the rise is slower (Bindoff et al., 2007). Cabanes et al. (2001), and then Lombard et al. (2005) showed that most of these regional variations could be explained by the geographical variations of ocean thermal expansion although some other processes may also play a role in regional sea level trends (e.g. the solid Earth response to the last deglaciation, Milne et al., 2009). A number of studies have shown that spatial trend patterns in thermal expansion are not stationary but fluctuate in space and time in response to forcing modes of the coupled Atmosphere–Ocean system, such as ENSO (El Nino-Southern Oscillation), PDO (Pacific Decadal Oscillation), NAO (North Atlantic Oscillation) and others (Lombard et al., 2005; Bindoff et al., 2007). Thus the regional variability seen by satellite altimetry over 1993–2009 is likely not representative of the past few decades.

However it is important to know past regional variability and understand how it changes with time on interannual/decadal/multi-decadal time scales. This helps to understand the local dominant modes of variability and assess the potential regional impacts of sea level rise. It is particularly important in vulnerable populated area such as the Mediterranean basin. Unfortunately, for the past decades, there are no direct basin-scale observations informing on spatial trend patterns in Mediterranean sea level. In this study, we develop a reconstruction method of past Mediterranean sea level (since 1970) that combines long tide gage records of limited spatial coverage with 2-D sea level patterns based either on satellite altimetry or on runs from Regional Ocean circulation Models (here after noted ROM) (see Section 2 below for the description of the models). Gridded time series that cover the whole Mediterranean basin over the tide gage records time span are obtained as a result, giving some information on the past spatial trend patterns variability in Mediterranean sea level.

* Corresponding author at: LEGOS, 14 Avenue Edouard Belin, 31400 Toulouse, France. Tel.: +33 5 61 33 29 90; fax: +33 5 61 25 32 05.
E-mail address: benoit.meyssignac@legos.obs-mip.fr (B. Meyssignac).

0921-8181/$ – see front matter © 2011 Elsevier B.V. All rights reserved.
doi:10.1016/j.gloplacha.2011.03.002

Such a reconstruction method has previously been developed for the global sea level over the past 50 years by Church et al. (2004) and Llovel et al. (2009). For the Mediterranean sea, a regional reconstruction is also available from Calafat and Gomis (2009) (hereafter C&G). They used the optimal interpolation method of Kaplan et al. (2000) (as used in Church et al., 2004) to interpolate the long tide gage records with the spatial patterns of the 2-D sea level grids from altimetry. In this study we expand the earlier work of C&G by reconstructing with the same method, the atmospheric-corrected Mediterranean sea level variability. Indeed, C&G did not correct the sea level data for the inverted barometer – IB – effect (the response of the sea surface to atmospheric pressure). In the Mediterranean sea, this signal is strong (Tsimplis and Josey (2001), Marcos and Tsimplis (2007)). If one is interested in the climate variability signal only, it should be removed. By making use of atmospheric-corrected Mediterranean sea level we get a closer view of the long-term, non-meteorological influence on the Mediterranean sea level. The study by C&G used as well spatial patterns (spatial component of the EOFs of the sea level, see Section 2) deduced from satellite altimetry over a limited time span (13 years: 1993–2006), a period affected by the strong change in the central and eastern Mediterranean circulation that occurred in the early 1990s: the Eastern Mediterranean Transient (EMT hereafter) (Roether et al., 1996; Klein et al., 1999; Lascaratos et al., 1999; Theocharis et al., 1999; Zervakis et al., 2004; Roether et al., 2007). The EMT is characterized by a change in the Eastern Mediterranean deep water characteristics. For almost the entire 20th century, these deep waters were of Adriatic origin, and in the early 1990s they were formed in the Aegean Sea after some climatic events; among them, a change in the surface circulation of the Ionian and Levantine basin (Malanotte-Rizzoli et al., 1999; Samuel et al., 1999; Theocharis and Kontoyiannis, 1999), an intense winter convection in the Aegean Sea in 1987 and two successive very cold winters in the Aegean Sea in 1992 and 1993 (Josey, 2003; Beuvier et al., 2010). The EMT impacted the Mediterranean circulation during the 1990 and still has an influence nowadays (Roether et al., 2007). It seems to be responsible for a change of surface circulation from anti-cyclonic to cyclonic in the Ionian basin in 1998 (Tsimplis et al., 2009; Vera et al., 2009) and may have interannual to interdecadal impacts on sea level variability as suggested by Tsimplis et al. (2005). In particular the EMT is likely to have strongly impacted the Mediterranean sea level patterns over the short altimetry period, making them exceptional and poorly representative of the past decades patterns. This non-stationarity of the sea level patterns in time and space can alter the reconstruction of the past sea level (see Llovel et al., 2009). By making use of short term sea level spatial patterns from altimetry that are dominated by the EMT, C&G reconstruction may be too much influenced by this exceptional event which seems to have occurred once in the XXth century (Beuvier et al., 2010). In this study, in addition to a reconstruction based on short term sea level patterns deduced from altimetry (like in C&G), we develop two other reconstructions on the basis of long-term sea level patterns deduced from models instead of altimetry on the assumption that they better capture the decadal variability of the spatial trend patterns.

The long-term sea level patterns are computed from long runs of ROM of the Mediterranean basin: the ARPERA-forced NEMOMED8 model (Sevault et al., 2009; Beuvier et al., 2010; Herrmann et al., 2010) (NM8 here after) and the coupled model PROTHEUS SYSTEM (Artale et al., 2009) (PS here after). These long-term model outputs (we took 33 years of simulation; between 1970 and 2002 because the PS model ends in 2002, see below) are used with the hope that they provide better representative sea level patterns of the whole reconstructed period 1970–2006 (instead of only the EMT period). The resulting reconstructions are compared to an altimetry-based reconstruction computed with the same tide gage dataset, and with the C&G reconstruction corrected a posteriori for the Inverse Barometer – IB – effects over the common period (i.e. 1970–2000).

The advantage of the approach proposed in this study is twofold: (1) the direct reconstruction of the IB-corrected sea level variability should ensure a reliable reconstruction of the low residual sea level variability only influenced by non-meteorological effect in the Mediterranean region, (2) the 33-year long coverage of the ROM grids in principle minimizes the possible non stationarity of the spatial patterns during the altimetry period (because of the exceptional EMT event).

The structure of the work is as follows. We first select and process the data used to carry out the 3 reconstructions (i.e. the tide gage dataset and the 2-D sea level grids from altimetry and the two ROMs. See Section 2). The methodology of sea level reconstruction is presented in Section 3. In Section 4, the results of the three reconstructions over 1970–2006, in terms of Empirical Orthogonal Functions (EOFs) and maps of spatial trends, are given and validated by comparisons with altimetry and extra tide gage records not used in the reconstruction processes. All results are summarized, discussed and compared in Section 5 before the conclusion.

2. Datasets processing

2.1. Tide gage records

The tide gage records used for the reconstruction were selected among the monthly sea level series available from the database of the Permanent Service for Mean Sea Level (PSMSL) (Woodworth and Player, 2003). The longest continuous records were chosen to get the longest reconstruction. Only 10 records longer than 40 years were available while a minimum of 13 records is needed to get a consistent reconstruction (see Section 4). The best trade-off between longest time span and minimum number of tide gage records made us finally select 13 records from the PSMSL database that span the 36 years period: 1970–2006. All these records are on the north coast of the Mediterranean. To compensate this geographical bias, an extra tide gage record from Alexandria (Egypt) over 1970–2006 was added. The Alexandria record is incomplete in the PSMSL database. However, an updated record was provided to us by O. Frihy of the Coastal Research Institute at Alexandria (Frihy et al., 2010). The tide gage dataset used for the reconstruction had finally 14 records sparsely distributed around the Mediterranean.

The location of the 14 tide gages is shown in Fig. 1 (black dots). All records (except Alexandria) are Revised Local Reference (RLR) data. The RLR label ensures that the records do not contain datum shifts resulting from re-leveling adjustments reported by the PSMSL datum history. In this study the reduction to common reference datum is useless since the reconstruction process uses changes in tide gage sea level instead of absolute tide gage sea level (see Section 3) but jumps in the records would have undoubtly an impact on the decadal reconstructed sea level variability if not corrected. For this reason, the Alexandria record was checked with a shift detector based on the generalized likelihood ratio statistic developed by Becker et al. (2009) to verify that no datum shifts was to be found over the 1970–2006 period. Moreover we checked that the updated Alexandria tide gage record (Frihy et al., 2010) is consistent with the Alexandria record from the PSMSL over the common period 1970–1989. Among the 13 records left, some presented gaps larger than 2 years: Soudhas (Greece), Siros (Greece) and Marseille (France). For the Soudhas that ends in 2002, and the Siros record that has a gap of 13 years between 1984 and 1997, PSMSL provides some extra data called metric record: the term “metric” refers to non-RLR records in the PSMSL database. So we completed them until 2006 with their respective metric record. The RLR records were concatenated with their respective metric record ensuring that the global mean equaled the mean of the long RLR record. The Marseille RLR record only shows a small gap of ~2.5 years between 1996 and 1999. Following the same approach, we completed this gap with the Toulon record since these records show a very high correlation of 0.90 (at a significance level (SL) of more than 99%) over the common time span. For the Venezia (Punta della Salute) record ending in 2000, no metric record was actually available from PSMSL but the Italian tide gage network (www.idromare.it) provides data that covers the period 1986 to 2010. We completed the Venezia RLR

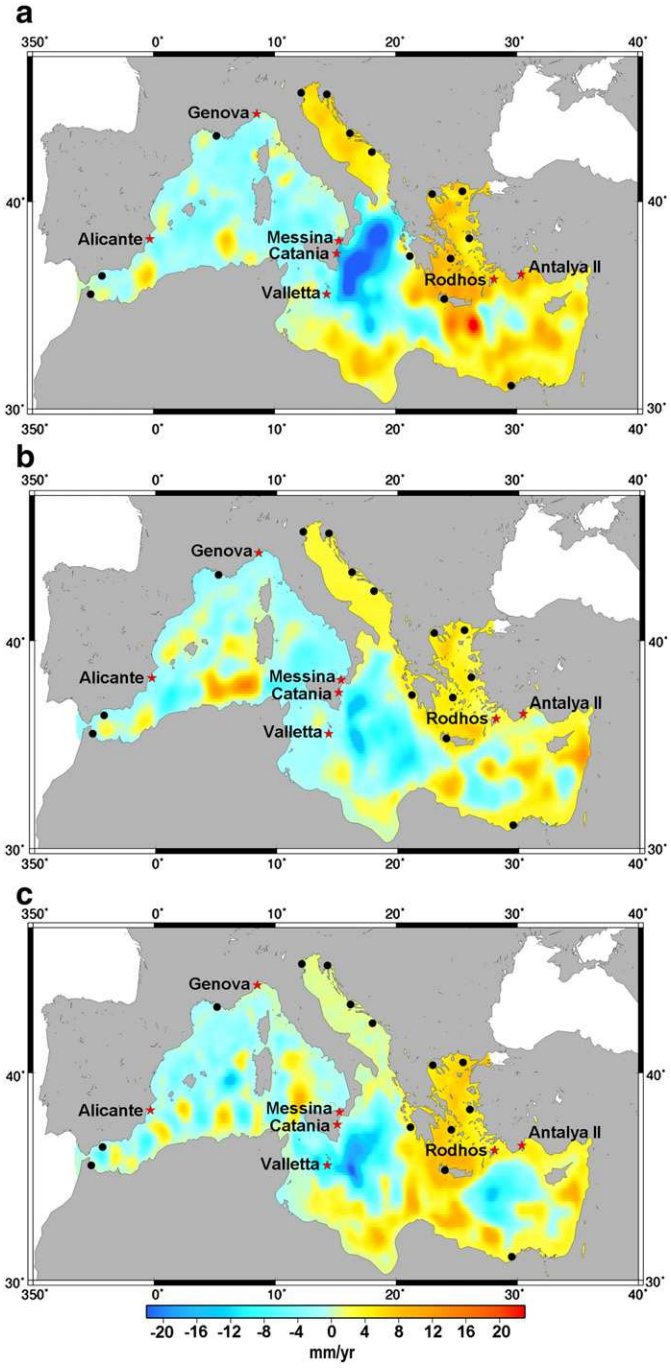

Fig. 1. Trend maps over 1993–2000 from altimetry (a), PS (b) and NM8 (c).

record using data from Idromare website concatenating the two datasets. The Malaga tide gage record span the whole reconstruction period but it shows an unrealistic large trend of 13.9 mm/yr over the period 1993–2010 while the RLR records of its neighbor tide gages present much lower trends, of the order of 6 mm/yr (6.0 mm/yr for Algeciras, 6.6 mm/yr for Tarifa over the same period). The new tide gage situated in Malaga (so called Malaga II in the PSMSL database) shows a similar trend of 6.0 mm/yr. When comparing both tide gages (Malaga and Malaga II), it appears that they fit well over the period 1993.0–1996.5 but beyond the data gap of 1997, the Malaga record drifts upward at a rate of 9.6 mm/yr with respect to the Malaga II record. Assuming that the record of Malaga II is more reliable (its trend over 1993–2010 is consistent with Tarifa and Algeciras) we replaced the record of Malaga by the record of Malaga II over the common period 1993–2010, ensuring that over the period of agreement (1993.0–1996.5) the two records agree. In each of the 14 records, the small gaps that remained (smaller than 2 years) were filled in with a linear interpolation.

To focus on the interannual and decadal time scale of the sea level variability, before filling the gaps and applying the IB correction, we removed from the records the annual and semi annual signal through a harmonic analysis. The analysis was done on the common period 1970–2006 to allow the fitting of a consistent signal in the dataset since the annual cycle is not constant in time (Marcos and Tsimplis, 2007).

The tide gage data were corrected from the static inverted barometer response (IB) of sea level to atmospheric loading using surface pressure fields from the National Centers for Environmental Project (NCEP) (Kalnay et al., 1996).

Tide gages measure sea level relative to the ground, hence also register vertical ground motions. For comparison or combination with altimetry-based sea level data (which are free from ground motions), vertical displacements need to be corrected for. While most tide gage analyses account for the Glacial Isostatic Adjustment (GIA hereafter) whose correction is available from models (Peltier, 2004; Stocchi and Spada, 2009), other contributions such as tectonics, volcanism, sediment load for which little quantitative information is available, are generally neglected. Nevertheless estimates of the total vertical displacements at some tide gage sites have been obtained thanks to GPS techniques (Steigenberger et al., 2006; Woppelmann et al., 2007, 2009). In this study we use land motion estimates by Woppelmann et al. (2009), to correct the tide gages of Marseille, Venezia, Dubrovnik and Ceuta of their vertical displacement. For other tide gages, where these corrections were not available, we only took into account the GIA effect using the model of Stocchi and Spada (2009).

2.2. Satellite altimetry dataset

To estimate the spatial structure of Mediterranean sea level variability, the first option was to use the AVISO satellite altimeter dataset (as in C&G). Weekly high resolution maps of sea level anomalies refined over the Mediterranean Sea were obtained from AVISO (http://www.aviso.oceanobs.com) on a 1/8° regular grid for the 13 year period January 1993–December 2005 (http://www.aviso.oceanobs.com/en/data/products/sea-surface-height-products/regional/m-sla-mediterranean/index.html). We used the DT-MSLA "Ref" series computed at CLS by combining several altimeter missions, namely: Topex/Poseidon, Jasons1 and 2, Envisat and ERS 1 and 2. It is a global homogenous intercalibrated dataset based on global crossover adjustment (Le Traon and Ogor, 1998) using Topex/Poseidon and then Jason1 as reference missions. The Mediterranean DT-MSLA "Ref" series are a subsampled dataset filtered and corrected from the long wavelength error (Le Traon et al., 1998) with specific regional criteria dedicated to the Mediterranean basin. These data are corrected from tides, wet/dry troposphere and ionosphere (see Ablain et al., 2009 for more details). The IB correction has also been applied in order to minimize aliasing effects (Volkov et al., 2007) through the MOG2D barotropic model correction (Carrere and Lyard, 2003) that includes the dynamic ocean response to short-period (<20-day) atmospheric wind and pressure forcing and the static IB correction at periods above 20-day (see Carrere and Lyard, 2003 for details).

We removed the annual and semi annual signal from the dataset through a harmonic analysis over the whole period (January 1993–December 2007). We corrected as well the altimeter-derived sea level from the GIA correction provided by Stocchi and Spada (2009) over the Mediterranean Sea. At this regional scale, the GIA correction value is of the order of −0.24 mm/yr (between −0.26 mm/yr and −0.22 mm/yr).

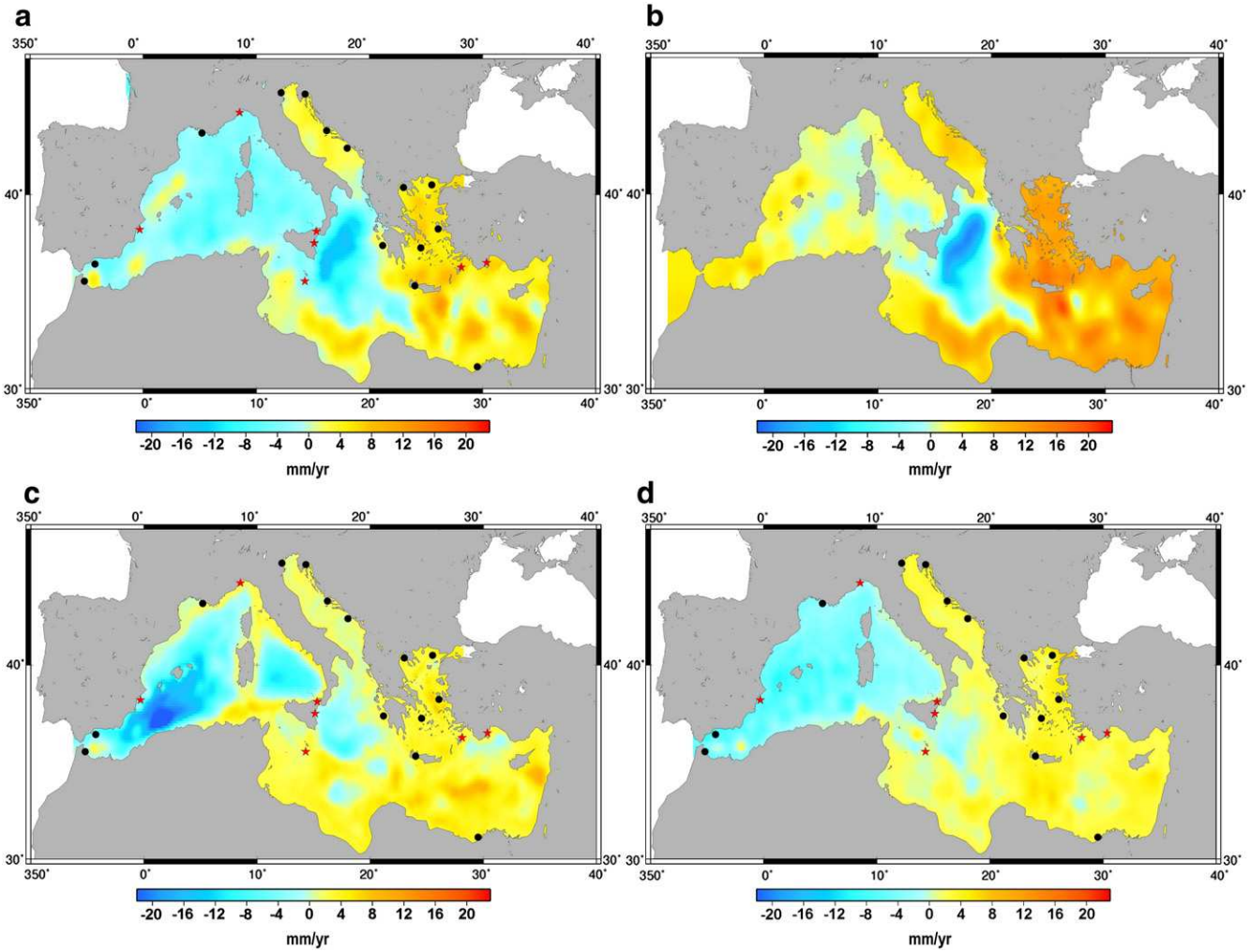

Fig. 2. Trend maps over 1993–2000 from altimetry-based reconstruction (a), Calafat reconstruction (b), PS-based reconstruction (c) and NM8-based reconstruction (d).

2.3. Mediterranean circulation models outputs

As an alternative option to capture the long-term (~20 year periods) spatial structures of Mediterranean sea level variability, we tested the reconstruction with gridded sea level fields obtained from two different ROM simulations: NM8 (Sevault et al., 2009; Beuvier et al., 2010) and PS (Artale et al., 2009).

2.3.1. The NM8 model

The high resolution model NM8 is a Mediterranean configuration of the NEMO ocean model (Madec, 2008). It has an horizontal resolution of 1/8°×1/8° and a vertical resolution of 43 non-uniform levels (with a resolution varying from 6 m at the surface and 200 m at the bottom). The evolution of the surface of the sea is parametrized by a filtered free-surface (Roullet and Madec, 2000). During the simulation, the volume of the Mediterranean sea is kept constant by redistribution of the evaporated water in the Atlantic buffer zone. The model was used in a simulation over the 1961–2008 period from which we extracted the 33 year period: 1970–2002 (this 33 year simulation will be referred here in after as the NM8 simulation) (Herrmann et al., 2010).

The atmospheric forcing is based on a dynamical downscaling of the ERA40 (Uppala et al., 2005) and of the ECMWF reanalysis filtered at the ERA40 resolution after year 2001. This dynamical downscaling is based on a spectral nudging technique that constrains the large scales (>250 km) of the prognostic variables (air temperature, wind components and logarithm of the surface pressure) to follow the ERA40 chronology and that lets the smaller scales (from 250 km to 50 km) free to develop. The spatial filtering of the ECMWF analysis fields and the non-nudging of the humidity field allow keeping as much as possible a temporal consistency in 2001. The downscaling used in this simulation is named ARPERA (Herrmann and Somot, 2008; Herrmann et al., 2010), it was carried out by the climate model ARPEGE-Climate (Déqué and Piedelievre, 1995). It allows getting high resolution (50 km along the horizontal directions) forcing with a real temporal chronology over the Mediterranean basin. Here the daily mean fields of momentum, fresh water flux (Evaporation minus Precipitations) and net heat flux from ARPERA were used to force NM8 ensuring that NM8 is driven by high resolution air-sea fluxes, homogeneous over the simulation duration (no changes in the ARPEGE configuration between 1970 and 2006) with a realistic interannual variability. The NM8 simulation was forced by climatologic interannual values for the river runoff fluxes, the Black sea inflow and the Atlantic boundary conditions when available or climatologic values otherwise (see Herrmann et al., 2010 for more details). The simulation used here started in August 1960 after a 15-year spin-up under the 1960s atmosphere conditions. The initial conditions were also representative of the 1960s following data from Rixen et al. (2005). Besides a careful overall validation of the NM8 simulation, it has been proved that the NM8 simulation forced by ARPERA air–sea fluxes gives a very realistic representation of the EMT event in the 1990s (Beuvier et al., 2010) and of the Western Mediterranean Deep Water formation (Herrmann et al., 2010). This

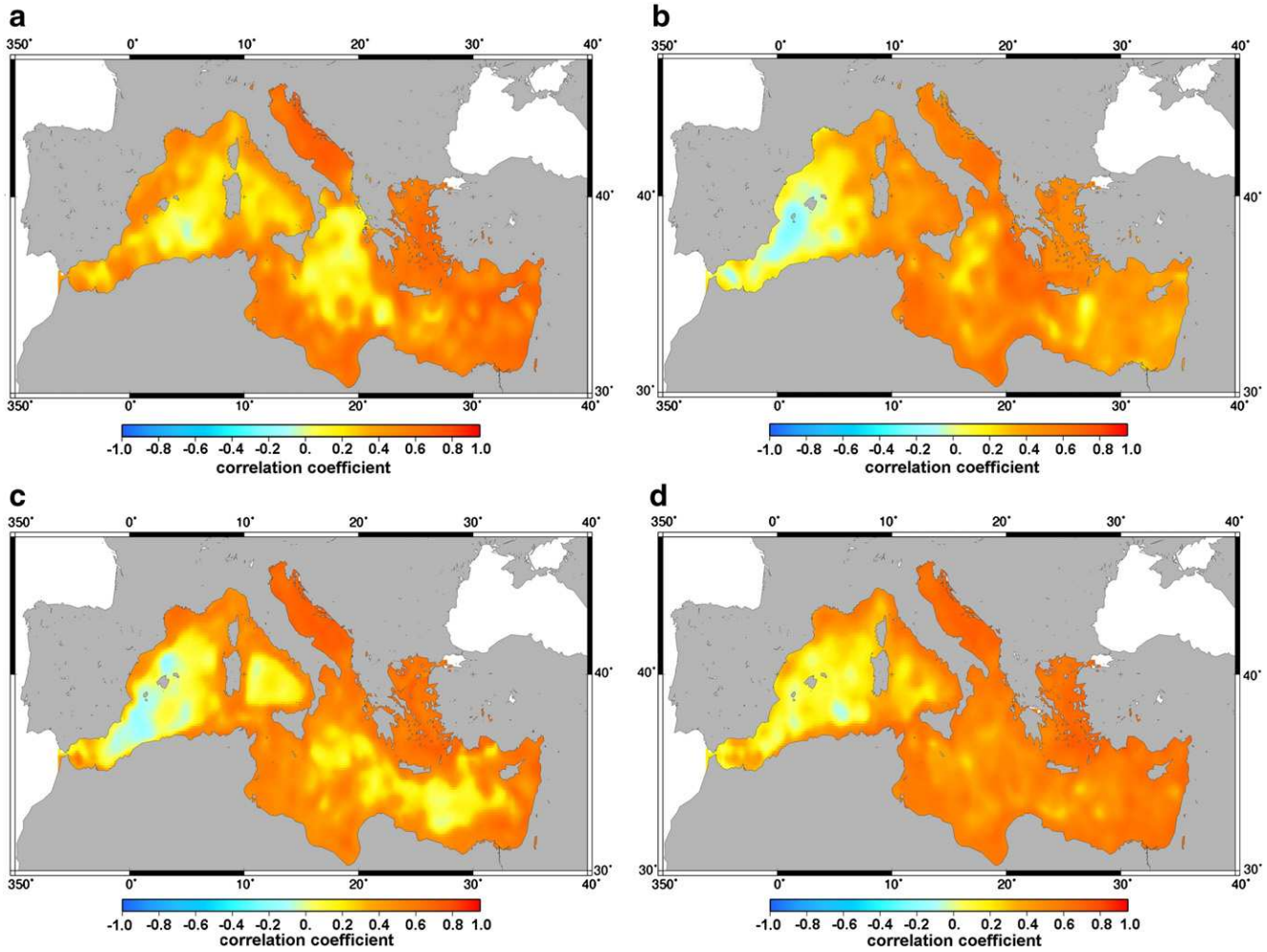

Fig. 3. Correlation maps over 1993–2000 between altimetry and our altimetry-based reconstruction (a), C&G reconstruction (b), PS-based reconstruction (c) and NM8-based reconstruction (d).

version of NM8 includes the coding of the sea level including the absolute steric sea level but excluding the pressure effect and the changes in the Atlantic Ocean sea level.

2.3.2. The PS model

The PS model is an Atmosphere–Ocean regional climate model for the Mediterranean basin. It is composed of the RegCM3 atmospheric regional model (Pal et al., 2007) and a Mediterranean configuration of the MITgcm ocean model (Artale et al., 2009) coupled through the OASIS3 coupler (Valcke and Redler, 2006). In the current study, we only use the outputs of the ocean component of PS that is to say The MITgcm model. It is a free-surface model with $1/8° \times 1/8°$ horizontal resolution and 42 non-uniform vertical levels (with a resolution varying from 10 m at the surface and 300 m at the bottom). The volume of the Mediterranean sea is kept constant during the 37 year simulation as in NM8 but since the freshwater forcing (Evaporation minus Precipitation minus river runoff) is applied as a virtual salt flux, here the net volume transport through the Strait of Gibraltar is zero. Atmospheric forcing (wind stress, heat fluxes, evaporation and precipitation) is computed by the RegCM3 (RegCM3 is a 3-dimensional, sigma coordinate hydrostatic regional climate model with a uniform horizontal resolution of 30 km). Only the river runoff fluxes are climatologic values computed apart (Struglia et al., 2004). The inflow from the Black sea is considered as an extra river flux. In this simulation the lateral boundary conditions are supplied by the ERA40 reanalysis (Uppala et al., 2005) while the MITgcm component provides the Sea Surface Temperature (SST) field.

The PS run starts in 1958 and ends in 2002. For consistent comparisons with the NM8 model, we extracted from this simulation the 33 years period 1970–2002.

From both simulations, total sea level change is computed as the sum of circulation and steric components. The circulation sea level change is given by the surface deformation while the steric sea level change is deduced at each grid point from the vertical integration of the specific volume anomaly caused by temperature and salinity anomalies. When computing global mean sea level from ocean reanalyses, it is classical to apply a basin-averaged, time-varying factor corresponding to the uniform steric effect (as explained by Greatbatch, 1994). However, here this correction is useless because we remove the total basin-average time varying sea level from the models (and the altimetry when it is used). Indeed we only use the spatial patterns of the sea level from the models (or the altimetry) to interpolate the tide gage records and reconstruct the past Mediterranean sea level. Moreover since we are only interested in the interannual to multidecadal sea level fluctuations, the annual and semi annual signals were removed as well from both sea level fields through an harmonic analysis over the whole period January 1970–December 2002.

Fig. 1 shows the trends over 1993–2000 of the sea level computed from a) altimetry, b) the PS run and c) the NM8 run. The very good agreement between the three maps confirms that the two ROM runs reproduce well the Mediterranean sea level at least over the last decade. The signal in the ROM runs appears slightly smaller but the negative patterns of the Western and Ionian basin and the positive pattern of the Aegean basin are consistent with the altimetry.

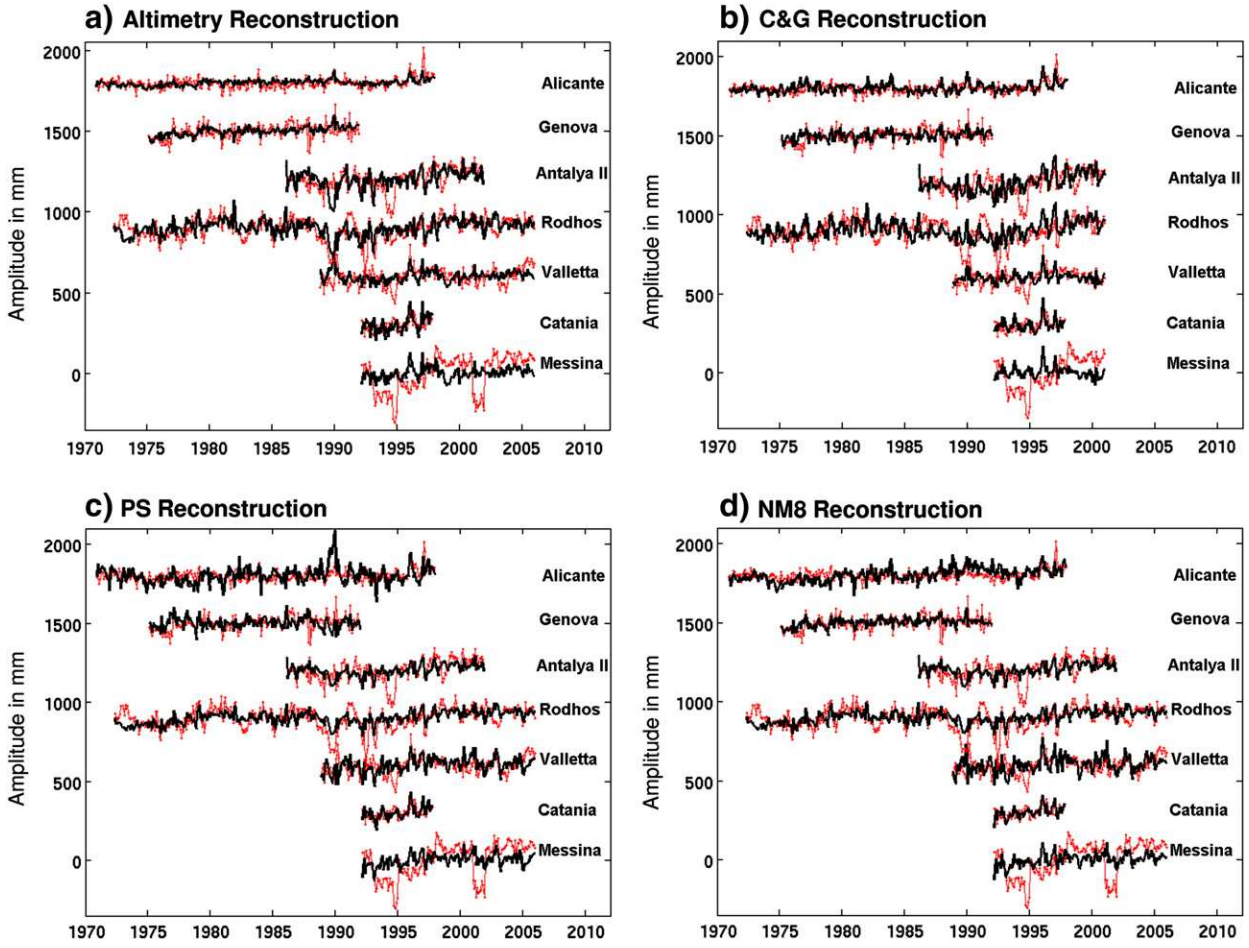

Fig. 4. Comparison of the altimetry reconstruction (a), Calafat reconstruction (b), PS-based reconstruction (c) and NM8-based reconstruction (d) with the tide gages of Alicante, Genova, Antalya II, Rodhos, Valletta, Catania and Messina (from top to bottom on the figure).

3. Reconstruction methodology

The method used to reconstruct past (over 1970–2006) sea level in 2 dimensions over the Mediterranean Basin is based on the reduced optimal interpolation described by Kaplan et al. (2000) and used by Church et al. (2004) and C&G to reconstruct past sea level. The idea consists in interpolating in 2-D the long tide gage records thanks to a time varying linear combination of the spatial patterns of a 2-D sea level grid (either Altimetry or ROMs). This method has 2 steps. In the first step an EOF decomposition (Preisendorfer, 1988; Toumazou and Cretaux, 2001) of a 2-D sea level grid (from altimetry or a Regional Circulation Model) is done. This decomposition allows to separate the spatially well resolved signal (here represented by a matrix H, with m lines for each spatial point and n columns for each date) into spatial modes (EOFs) and their related temporal amplitude as follow:

$$H(x,y,t) = U(x,y)\alpha(t). \quad (1)$$

In this equation $U(x,y)$ stands for the spatial modes and $\alpha(t)$ for their amplitude. Assuming that the spatial modes $U(x,y)$ are stationary in time (see the discussion below), we deduce that the reconstructed sea level field of the Mediterranean basin over the long period 1970–2006 (called here $H_R(x,y,t)$) has an Empirical Orthogonal Decomposition as follow:

$$H_R(x,y,t) = U(x,y)\alpha_R(t)$$

where $\alpha_R(t)$ represents the new amplitudes of the EOFs over 1970–2006.

The second step consists of computing the new amplitudes over the whole period 1970–2006 thanks to the tide gage records. It is done through a least square optimal procedure that minimizes the difference between the reconstructed field and the tide gage records at the tide gage locations.

In the first step, the EOF modes and amplitudes of the 2-D sea level grids are computed through a singular value decomposition approach, such that:

$$H = USV^t \quad (2)$$

where $U(x,y)$ still stands for the EOF spatial modes, S is a diagonal matrix containing the singular values of $H$and Vrepresents the temporal eigen modes. At this stage the amplitude of the EOF modes can be simply written as $\alpha(t) = SV^T$. Conceptually, each EOF k (kth column of $U(x,y)$ multiplied by the kth line of $\alpha(t)$:$U_k(x,y).\alpha_k(t)$) is a spatio-temporal pattern of sea level variability that accounts for a percentage of the total variance of the sea level signal.

The low-order EOFs (eigenvectors of the largest singular values) explain most of the variance and contain the largest spatial scales of the signal. The higher-order EOFs contain smaller spatial scale patterns and are increasingly affected by noise. Besides, their amplitude is decreasingly well resolved by the least squares procedure because the sparseness of the set of in situ gages does not allow resolving too small scale patterns. For efficiency, the reconstruction over the Mediterranean basin uses a subset of the Mlowest-order EOFs (the best fit between maximum variance explained and minimum noise perturbation led us to choose $M = 3$, which account for at least 69% of

Table 1
Correlation and trend's differences between the independent tide gage records (indicated by stars on the maps and shown in Fig. 1) and the corresponding reconstructed time series. Correlations and trend differences are computed over 2 different periods: until 2001 to be able to compare them with the reconstruction of Calafat and Gomis and until 2006 to have the correlations over the whole reconstructed time span. All the correlations computed have a significance level higher than 99% (except for the correlation between the C&G reconstruction and the Messina record).

Name of the tide gage	Calafat and Gomis reconstruction		Altimetry-based reconstruction				PS-based reconstruction				NM8-based reconstruction			
	Corr	Trend	Correlation		Trend difference in mm/yr		Correlation		Trend difference in mm/yr		Correlation		Trend difference in mm/yr	
	→2001	diff→2006	→2001	→2006	→2001	→2006	→2001	→2006	→2001	→2006	→2001	→2006	→2001	→2006
Alicante	0.67	−0.3±0.4	0.59	0.59	−0.1±0.4	−0.1±0.4	0.44	0.44	0.0±0.7	−0.1±0.7	0.50	0.50	1.9±0.5	1.9±0.5
Genova	0.54	−1.8±1.0	0.49	0.49	0.2±1.1	0.2±1.1	0.42	0.41	−3.4±1.1	−3.4±1.1	0.59	0.59	−1.1±1.0	−1.1±1.0
Antalya II	0.48	1.8±2.3	0.43	0.46	−1.6±2.3	−2.2±2.1	0.47	0.51	−2.5±2.0	−3.0±1.8	0.46	0.50	−2.6±2.1	−3.1±1.8
Rodhos	0.39	1.07±0.9	0.57	0.55	0.3±0.7	0.0±0.6	0.55	0.54	1.6±0.7	1.1±0.6	0.56	0.55	1.3±0.7	0.8±0.5
Valletta	0.45	−2.8±2.1	0.25	0.27	−3.8±2.5	−2.1±1.4	0.36	0.40	2.9±2.6	0.2±1.5	0.32	0.39	0.7±2.8	−0.5±1.6
Catania	0.54	−6.9±4.9	0.51	0.51	3.2±6.6	3.2±6.6	0.67	0.67	0.2±4.7	0.1±4.7	0.69	0.69	−0.4±4.2	−0.4±4.2
Messina	−0.08	−27.4±6.6	0.10	0.16	−23.6±6.8	−12.4±3.7	0.30	0.28	−17.5±6.8	−11.7±3.6	0.31	0.32	−18.1±6.7	−11.0±3.6

the total variance of the sea level grid data). Consequently, the data matrix H can be written as:

$$H_M = U_M(x,y).\alpha(t)$$

where $\alpha(t) = S_M V_M^T$ is the matrix of the amplitude of the Mlowest EOFs. Following Kaplan et al. (2000), in the second step, we compute, at each time step over the time span of the in situ records, the amplitudes by minimizing the cost function:

$$S(\alpha) = \left(PU_M\alpha - H^0\right)^T R^{-1}\left(PU_M\alpha - H^0\right) + \alpha^T\Lambda^{-1}\alpha \quad (3)$$

In $S(\alpha)$, H^0 is the sea level observed by the tide gages, $P$is a projection matrix equal to 1 when and where in situ records are available and 0 otherwise and $\Lambda$is a diagonal matrix of the largest eigenvalues of the covariance matrix. R is the error covariance matrix accounting for the data error covariance matrix (instrumental error) and the error due to the truncation of the set of EOFs to only the first M EOFs. The second term on the right hand side of the function is a constraint on the EOF spectrum of the solution. It prevents the least squares procedure to be contaminated by high-frequency noise (it filters out non significant solutions that display too much variance at grid points without nearby observations). The least squares procedure is then applied to the virtual in situ tide gage records (H^0). It provides the reconstructed amplitude α_R of the EOFs.

Since tide gage records are all relative to their own local datum that are not cross-referenced over the basin, this solution may be polluted by spatial variability of the in situ tide gage records reference surface not necessarily consistent with the altimetry reference surface or the ROM reference surface. To cope with this problem, we have solved Eq. (3) for changes in sea level between adjacent steps following Church et al. (2004). Once changes in amplitude have been obtained at each time step, the amplitudes themselves have been recovered, integrating backward in time. The integration constants are chosen to equal the reconstructed EOF amplitudes mean to the 2-D gridded sea level EOF amplitude mean over the 2-D gridded sea level field period, ensuring consistency between both sets of EOFs.

Another issue with sea level reconstruction in the Mediterranean basin is the strong basin-average signal of the Mediterranean basin. This signal, that is contained in the tide gages, is hardly captured by the few EOFs we use. The reason is that before the computation of the EOFs, for each gridded times series (the 2 ROMs and the altimetry) we have removed the basin-averaged time varying sea level (see Section 2) so the set of EOFs we use is not adapted to reconstruct any basin average sea level. Hence, as in Church et al. (2004), we added in the set of EOFs a spatially uniform EOF (so called EOF0 in Church et al., 2004 and in C&G) to capture, from the tide gages, the basin-averaged signal of the Mediterranean in the past. An advantage of this procedure is that it avoids pouring the strong basin-average sea level signal in different EOFs. Note that tests carried out with and without the EOF0 resulted in almost the same reconstructions.

Finally the reconstructed field of sea level is obtained by multiplying the first three EOFs plus the EOF0 with their reconstructed amplitude:

$$H_R = U_M(x,y)\cdot\alpha_R(t) \quad (4)$$

At this point, the correction for the atmospheric effects of the tide gage dataset and the altimetry dataset appears particularly important because of the sparsely distribution of the tide gage data set. Indeed, changes over time in atmospheric pressure patterns can be misrepresented with such a sparse network of tide gages biased toward the north of the Mediterranean basin. For example if atmospheric pressure patterns had a bias toward the north in the past this would be misinterpreted as a change in past global Mediterranean sea level although it is not the case. As discussed above, beyond 20-day periods, the correction applied to account for the ocean response to atmospheric forcing is the static IB (1 mbar corresponds to 1 cm sea level). It is known that in the Mediterranean Sea, there is a slight low-frequency non static component. However this effect remains small (a few% of the static part) and for the purpose of the present study can be neglected (F. Lyard, personal communication).

4. Reconstructed sea level

4.1. Validation over the altimetry period

A first way to check the validity of the reconstructions is to look at the reconstructed sea level over the altimetry period and check that the reconstructed spatial trend patterns and variability are similar to the observed one by the altimetry. Fig. 2 shows the spatial trend maps (uniform trend removed) over 1993–2000 (because the C&G reconstruction ends in December 2000) of the altimetry-based reconstruction (Fig. 2a), the C&G reconstruction (see Fig. 2b) and from the two ROM-based reconstructions (Fig. 2c and d). For this comparison, the C&G reconstruction was a posteriori corrected for the IB effect. This was done by simply removing at each time step, NCEP IB grids to the C&G reconstructed sea level.

We note a good agreement between the spatial trend patterns of the reconstructed maps and satellite altimetry presented in Fig. 1a. Our altimetry reconstruction and the C&G reconstruction are very close to each other and they are very consistent with the satellite altimetry signal (Fig. 1a) as expected. The only difference that can be noticed is the lower negative pattern in the Ionian Sea in our altimetry reconstruction. To a lesser extent, the two ROM-based reconstructed trend patterns are consistent as well with the satellite altimetry patterns in each basin but they show a lower negative pattern in the Ionian Sea and a lower positive pattern in the Aegean Sea.

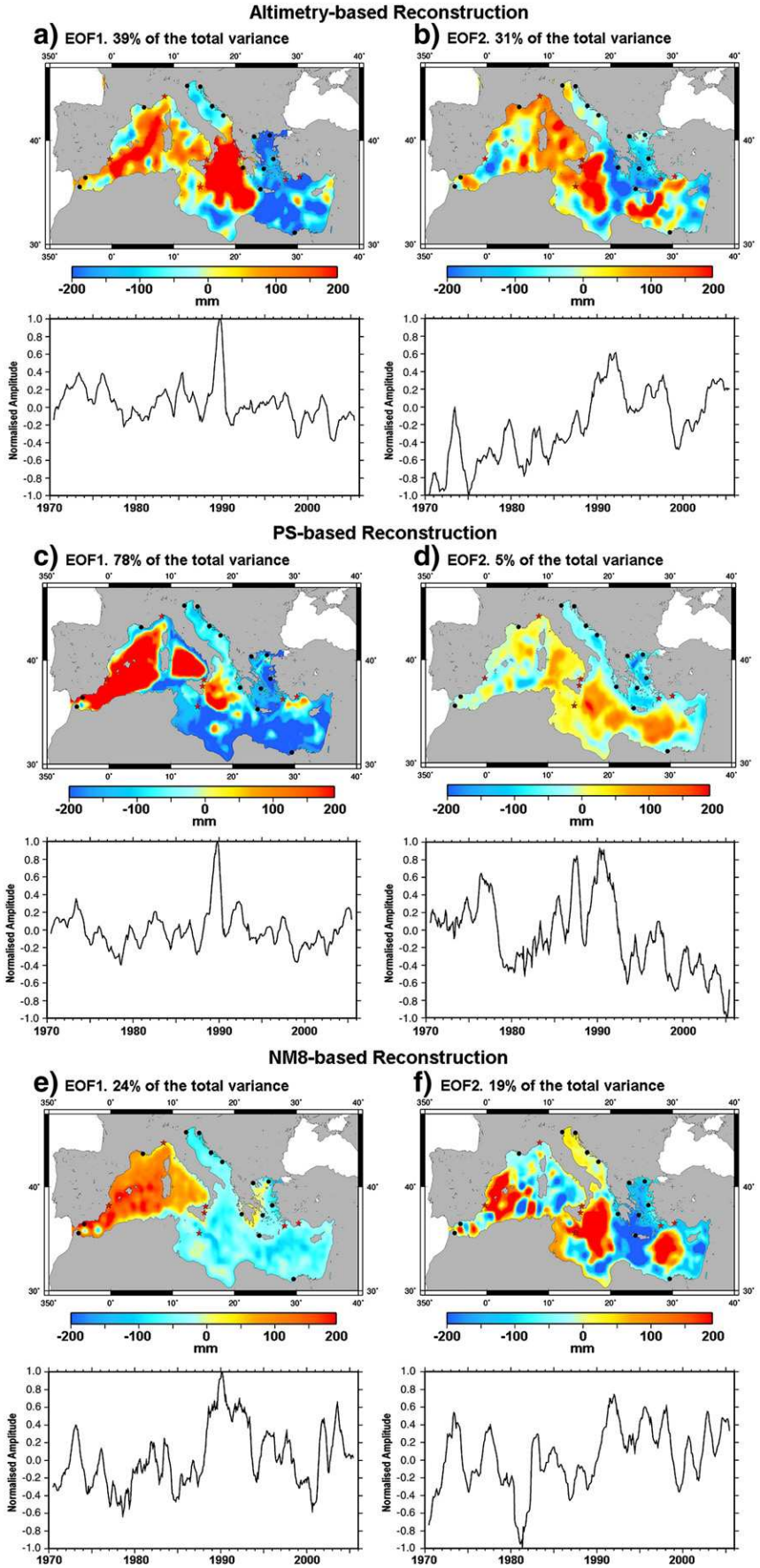

Fig. 5. EOF decomposition over 1970–2006 of the reconstructions. a) and b) show the modes 1 and 2 of the altimetry-based reconstruction. c) and d) show the modes 1 and 2 of the PS-based reconstruction and e) and f) show the modes 1 and 2 of the NM8-based reconstruction. The temporal curves have been smoothed with a 12-month running mean.

We compare as well the reconstructed sea level variability with the observed one over the same period 1993–2000. To do so, we computed, at each grid point, the correlation between the reconstructed time series and the observed altimetry time series over the period 1993–2000. The results are presented in Fig. 3. All reconstructions present positive significant correlations in the central and eastern Mediterranean basins. Correlations are less good in the western basin. C&G reconstruction (Fig. 3b) shows particularly good correlations in the Ionian basin while our altimetry-based reconstruction (Fig. 3a) performs less in this region. This is probably due to the fact that C&G used the tide gage of Valletta over 1989–2000 to do their reconstruction: it must have constrained better their reconstructed variability in this region. Nevertheless our altimetry-based reconstruction seems to perform slightly better in the western basin. It is probably linked to the choice of the tide gages in this region as well. The reconstruction that performs the best in terms of reproduced variability over 1993–2000 appears to be the NM8-based reconstruction (Fig. 3d). The geographically averaged correlations for each case amount to 0.46 for our altimetry based reconstruction, 0.49 for the C&G reconstruction, 0.44 for the PS-based reconstruction and 0.50 for the NM8-based reconstruction. This clearly shows the ability of the model-based reconstructions (especially the NM8-based reconstruction) to reproduce reliably the past sea level variability.

4.2. Validation with tide gage records

Another way to validate the reconstructions over the whole period 1970–2006 is to compare the reconstructed sea level fields with tide gage records that were not taken into account in the reconstruction process.

Note that the coastal tide gage records we use are monthly averages and contain potential contributions from regional or local coastal processes (e.g. local variability of narrow shelf currents, flooding events, wind-forced coastal waves, etc.) as well as land motion unrelated to the signal we are attempting to reconstruct here. Moreover, with the reconstructed sea level fields, the optimal interpolation method uses only part of the total sea level grids variance to reconstruct the total sea level. Consequently, we expect to reconstruct only part of the total observed variance of the tide gage records but it should be representative of the reconstruction validity.

Fig. 4 shows the comparison of the reconstructed fields with 7 tide gage records that were not used in our reconstruction. These are the Alicante and Genova records in the western basin (data from the PSMSL database), the Valletta, Catania and Messina records in the Ionian Sea (data from the Italian tide gage network (www.idromare.it)) and the Rodhos and the Antalya II records in the eastern basin (data from PSMSL). Location of the tide gages is indicated in Fig. 1 (black stars). For each record, we applied the same corrections as explained earlier in Section 2.1: the annual and semi annual signals were removed, and IB and GIA corrections were applied. In Fig. 4, observed tide gage records are plotted in red and reconstructions at the gages location are in black. Table 1 sum up the correlation and the trend differences computed on the basis of this figure. Fig. 4 and Table 1 illustrate the strengths and weaknesses of each of the reconstructions (and of the tide gage records as well):

- In the western Mediterranean, 2 long RLR records from PSMSL, Alicante and Genova, are available to check the reconstructions. Their variability is fairly well reproduced (correlation ~0.5) by both altimetry reconstructions (C&G reconstruction and our reconstruction) (Fig. 4a and b and Table 1 columns 2 and 4). Alicante record variability is exceptionally well reproduced (correlation of 0.67) by the C&G reconstruction certainly because this record is used in their reconstruction process. The trends appear consistent with each other except at Genova for the C&G reconstruction that underestimates its trend by 1.8 mm/yr. Looking at the ROM and our altimetry reconstruction over the whole period (until 2006) (Fig. 4b, c and d and Table 1 columns 5, 9 and 13) the NM8 reconstruction appears to perform better in term of interannual variability.
- The variability at Antalya II is quite well reproduced by both altimetry reconstructions with a similar correlation of ~0.45 (Fig. 4a and b and Table 1 columns 2 and 4) but the C&G reconstruction shows a significantly lower correlation for the Rodhos record (correlation of 0.39) than ours (correlation of 0.57). The model reconstructions (Fig. 4c and d and Table 1 columns 9 and 13) appear homogenous over the Levantine basin with correlations of ~0.5 with both tide gage records (as for the altimetry reconstruction) (Fig. 4a and Table 1 column 5).
- In the Ionian basin, unfortunately we could not find long records to check the reconstructions. The longest available record is the RLR record of Valletta from PSMSL over 1989–2006. Two additional records could be found in the Ionian basin, the Catania and Messina record from the Idromare database (www.idromare.it). These are actually too short to give a reliable verification of the reconstructed trend but they give interesting insights on the interannual variability of the Ionian sea level. The Messina record was selected because of its interesting location. However, it should be taken with caution since it shows many suspicious jumps (in particular in 1998) as previously noticed by Fenoglio-Marc et al. (2004). The two altimetry reconstructions (Fig. 4a and b and Table 1 columns 2 and 4) show very similar correlations with the tide gage records except for the Valletta record that shows higher correlation with the C&G reconstruction (probably because this record was used in the C&G reconstruction). Over 1970–2006, the model reconstructions show consistent, and higher correlations at all tide gages in the Ionian basin than the altimetry reconstruction (Fig. 4a, c and d and column 5, 9 and 13 of Table 1). They show an exceptionally high correlation of 0.68 with the Catania record. As for the trend of the Valletta record it is actually well resolved only by the ROM reconstructions while it is strongly underestimated by the altimetry reconstruction (column 6, 10 and 14 of Table 1).

4.3. Mediterranean sea level variability

In Fig. 5, we present, the 2-D reconstructed fields based on the altimetry dataset, the PS and the NM8 runs respectively. We have performed an EOF decomposition over the whole reconstructed time span 1970–2006 for the three fields. Only the first 2 modes (EOF1 and EOF2) are presented because they account for the largest percentage of the total variance of the signal. The temporal curves have been smoothed with a 12-month running mean in order to emphasize the interannual variability. EOF modes 1 of each of the three reconstructions (Fig. 5a, c and e) – 39, 78 and 24% of total variance respectively – show no trend and a maximum in 1990 in its temporal amplitude. EOF modes 2 (31, 5 and 19% of total variance respectively, see Fig. 5b, d and f) exhibit high and low frequency signal (period ~15 years) over 1970–2006. The EOF spatial patterns differ from one reconstruction to another. We note strong similarities between EOF mode 1 patterns of each reconstruction, with a global dipole marked by a positive pattern in the Western basin and a negative pattern in the Levantine basin. Nevertheless they differ in the Ionian Sea: the NM8 reconstruction shows a negative pattern whereas the altimetry reconstruction shows a positive one and the PS reconstruction a pattern somehow between the both. Concerning the EOF mode 2 patterns, the three reconstructions are fairly consistent in the Ionian and Levantine basin with a strong positive anomaly in the Ionian and Levantine Sea and negative one in the Agean Sea. In the western basin, the altimetry-based and the PS-based reconstructions agree well, with a dipole positive in the eastern part while the NM8-based reconstruction patterns are inversed there. In Fig. 6, the reconstructed basin-average sea level (i.e., the EOF0 of each reconstruction) is shown and compared to the satellite altimetry sea level over 1993–2006. As for the EOFs, it has been smoothed by a 12-month running mean to emphasize the interannual to decadal variability. The four reconstructed sea level curves show the same decadal variability.

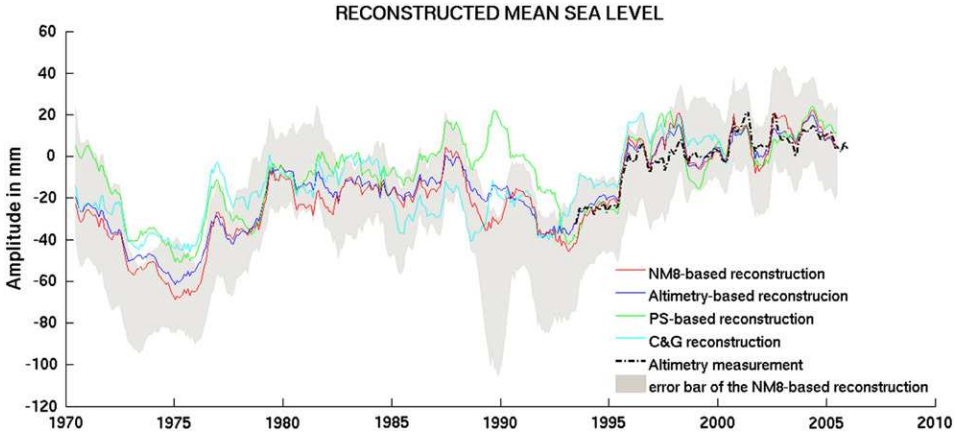

Fig. 6. Basin-average sea level from Satellite altimetry (black dashed line), our altimetry-based reconstruction (blue plain line), the C&G reconstruction (cyan plain line), the PS-based reconstruction (green plain line) and the NM8-based reconstruction (red plain line). The temporal curves have been smoothed with a 12-month running mean.

Their interannual variability is very similar as well over the periods 1970–1985 and 1994–2006. But some differences appear between 1985 and 1995: the PS-based reconstructed basin average sea level shows a high level that does not appear in the other reconstructions. Over the altimetry era, all reconstructions show a mean sea level similar to the observed, altimetry-based global mean sea level. In Fig.6, the gray zone represents the uncertainty in the NM8-based reconstructed mean sea level. This uncertainty is based on the sum of errors due to the least-squares inversion (as presented in Section 3) and errors of the in situ records. This latter error is estimated from a bootstrap method (Efron and Tibshirani, 1993) for standard errors of the in situ water levels for each month (significant at the 95% level).

5. Discussion

The altimetry-based reconstruction developed in this study has been compared with the C&G one over the period 1970–2000 only, because the C&G reconstruction stops in December 2000. We note very similar correlations between the two altimetry-based reconstructions and the tide gage records (Table 1, columns 1 and 3). It suggests that the two altimetry reconstructions are consistent and that the techniques used in C&G and the present study, end up with very close results. This means that removing IB before the reconstruction (this study) or after has little impact on the results.

The Valletta record cannot actually be considered as an independent reference to compare with the two altimetry reconstructions since it is used in C&G reconstruction (between 1995 and 2000) and not in the other (by using only tide gage records that spanned the whole period 1970–2006 and excluding others like Valletta, we ensured the reconstruction to be homogenous over the whole time span). As for the Rhodos record it is not clear why it shows higher correlation with our altimetry reconstruction. An explanation could be that our reconstruction is more constrained in the Levantine basin thanks to the use of the Alexandria record. But this remains to be confirmed.

Considering the reconstructed variability of the basin-averaged Mediterranean sea level, the consistency of the two altimetry reconstructions, while the tide gage dataset differ, gives confidence in the robustness of the results presented by C&G and in this study. However, the spatial trend maps do not match as well (see Fig. 7). The two methods lead to the same basin-averaged trend of ~1.1 mm/yr over 1970–2000 (1.0 mm/yr and 1.2 mm/yr for C&G and this study respectively) but differ in the trend patterns. The two reconstructions show the same geometry in the trend patterns (positive pattern in the Ionian Sea and in the Tyrrhenian Sea) but the C&G reconstruction exhibits lower variability. The comparison of the reconstructions with independent long tide gage record (Table 1) tend to show that in the western basin the trends of our altimetry-based reconstruction are closer to the trends observed at tide gages (see columns 3 and 6 of Table 1 for the Alicante and the Genova records). In the eastern basin, the C&G reconstruction tend to overestimate the trends by ~1 mm/yr while our altimetry reconstruction tend to underestimate the trend at Antalya, as shown by the comparison with the Antalya and the Rodhos tide gage trends. In the Ionian basin the tide gage trends used for the validation are not reliable because of too short records. Both reconstructions seem to underestimate the trend at Valletta, but we cannot extrapolate for the rest of the Ionian Sea.

The three reconstructions presented here (altimetry and ROM based) have been computed by the same process (same tide gage dataset). They only differ by the initial sea level grids used to estimate the spatial variability statistics of the Mediterranean sea level. Looking at the correlations (Table 1, columns 5, 9 and 13) we note a good consistency of the three reconstructed sea level fields: the correlations of each reconstruction with independent tide gages never differ by more than 0.2 from one another. Looking more carefully, both model reconstructions appear particularly consistent since their correlations with tide gages do not differ by more than 0.06, except for the Genova record which has a surprising very low correlation with the PS reconstruction. Hence the two models give similar reconstructed interannual variability. This point gives confidence in the robustness of the model-based reconstruction process. Among the three reconstructions, even if they show similar results, the NM8 reconstruction shows the highest correlations with the test tide gages.

At sub-basin scale, the conclusion is less clear. Some discrepancies appear among the reconstructions. While in the eastern basin, the three reconstructions have similar correlations with the test tide gages, in the western basin, the NM8 and the altimetry reconstruction show higher correlation (see columns 5, 9 and 13 of Table 1 for the Antalya and Rodhos records).

It is in the Ionian Sea where the highest discrepancies can be seen: both model reconstructions show significant higher correlation with the test tide gages of Valletta, Catania and Messina than the altimetry reconstruction. As said earlier, the Ionian basin waters have been strongly impacted by the EMT. This event impacted the Mediterranean circulation during the 1990s until now (Roether et al., 2007) and seems to be responsible for a change in surface circulation, from anti-cyclonic to cyclonic in the Ionian basin in 1998 (Vera et al., 2009). This change in circulation is characterized by the very strong negative pattern in the Ionian Sea that can be seen in the trend maps of the models and the altimetry over the period 1993–2000 (see Fig. 2) (Vera et al., 2009). This exceptional signal dominates the altimetry EOFs since the altimetry dataset only cover the EMT-period (i.e. since 1993). It is less strong in both model-based reconstructions because they capture a long term

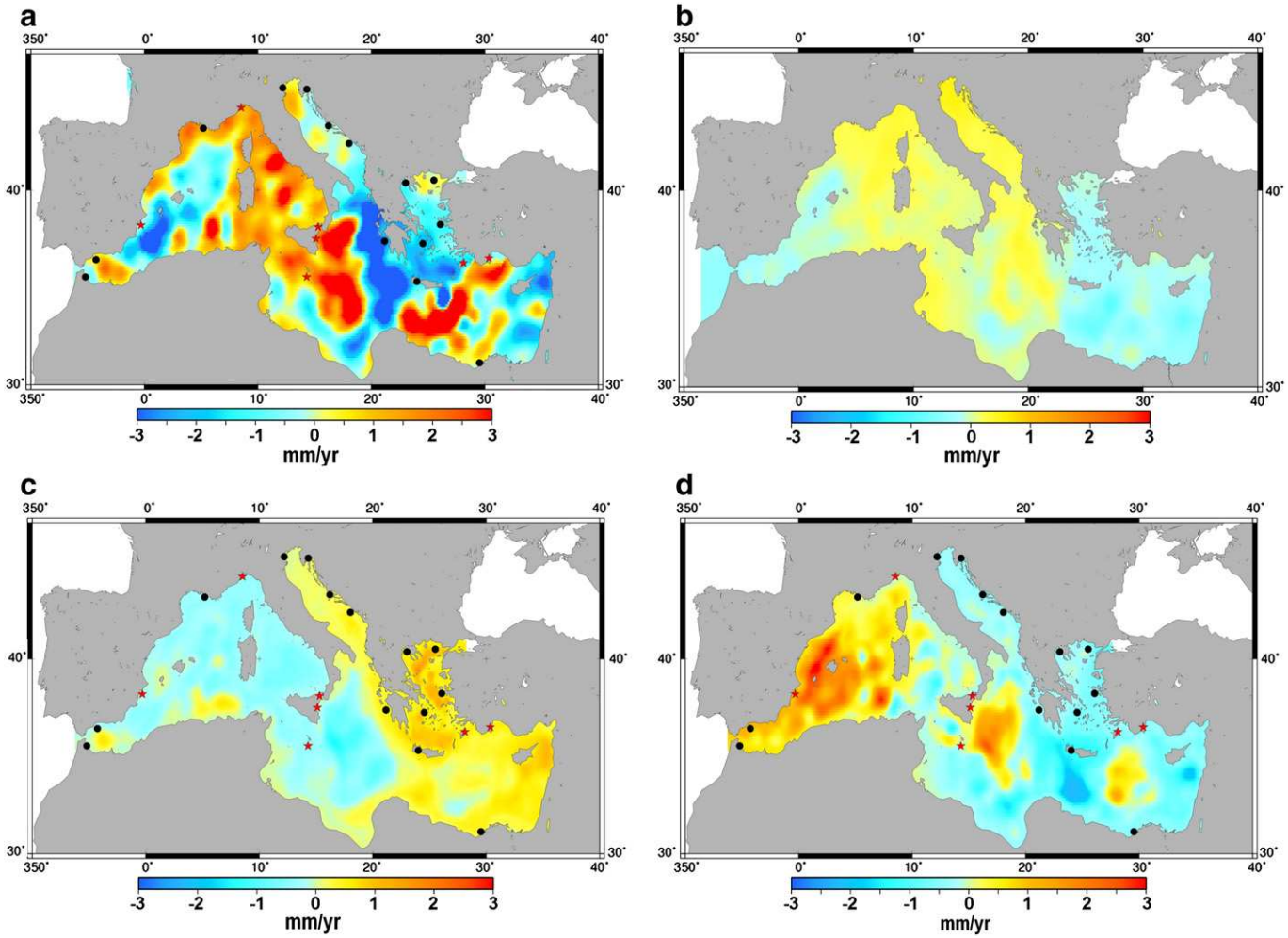

Fig. 7. Map of sea level trends over 1970–2006 of a) the altimetry reconstruction., b) the C&G reconstruction, c) the PS reconstruction and d) the NM8 reconstruction. For each map we have removed the basin-averaged sea level trend computed over 1970–2006 which is of 1.2 mm/yr for the altimetry reconstruction, 1.0 for the C&G reconstruction, 0.8 mm/yr for the PS reconstruction and 1.4 mm/yr for the NM8 reconstruction.

signal not dominated by the EMT event. This could explain the difference of correlations between the reconstructions in the Ionian basin. Looking at Fig. 4a, c and d, the model-based reconstructions appear indeed to better reconstruct the signal prior to the 1990s for the Valletta record for example.

In terms of trends over the period 1970–2000, the three reconstructions of this study plus C&G present strong discrepancies. Only the ROM reconstructions appear to properly reconstruct the Valletta record trend (Table 1 column 15). In the western basin the altimetry-based reconstruction (of this study) is the only one that seems to reproduce both the Genova and Alicante trends. In the eastern basin the trends of Rodhos and Antalya II are not captured by any reconstruction despite their proximity. This point highlights the sensitivity of this region.

The NM8 reconstruction shows better interannual to decadal reconstructed variability so it was used as the reference reconstruction to investigate the potential past influence of some forcing modes of the coupled Atmosphere–Ocean system on the Mediterranean sea level. Fig. 8 compares the amplitude of EOF1 and of the negative EOF2 of the NM8 reconstruction with the North Atlantic Oscillation – NAO – index. For the NAO index we used the monthly index from the Climate Analysis Section NCAR at Boulder, USA (Hurrell, 1995) based on the difference of normalized sea level pressure between Ponta Delgada (Azores) and Reykjavik (Iceland). The NAO index was smoothed by a 12-month running mean and compared to the EOFs of the NM8 reconstruction (smoothed as well by the 12-month running mean). It turns out that before ~1993.5 (date indicated by a gray bar in Fig. 8), the EOF1 temporal curve of the NM8 reconstruction shows a correlation with the NAO index of up to 0.60 (with a significance level >0.99) while over the period 1993.5–2006 the correlation gets down to −0.37. On the other hand, after ~1993.5 the negative EOF2 temporal curve of the NM8 reconstruction shows a high correlation with NAO index of 0.54 (with a SL >0.99) while over the period 1970–1993.5 it only amounts to −0.30. It is interesting to note that the correlation with NAO switches from EOF1 to EOF2 at the epoch of the EMT occurrence.

6. Conclusions

Concerning the interannual/decadal variability of the Mediterranean sea level, the overall agreement of the reconstructions with each other and with the test tide gage records gives confidence in the reconstructed sea level fields. The comparison of model-based reconstructions and altimetry-based reconstructions confirms this robustness since they agree on global scale. At sub-basin scale, the ROM-based reconstructions (especially the NM8-based reconstruction) perform better in the Ionian basin than altimetry-based, and this is probably due to a too strong representation of the EMT event in the altimetry EOFs. This point highlights the advantage of using long ROM

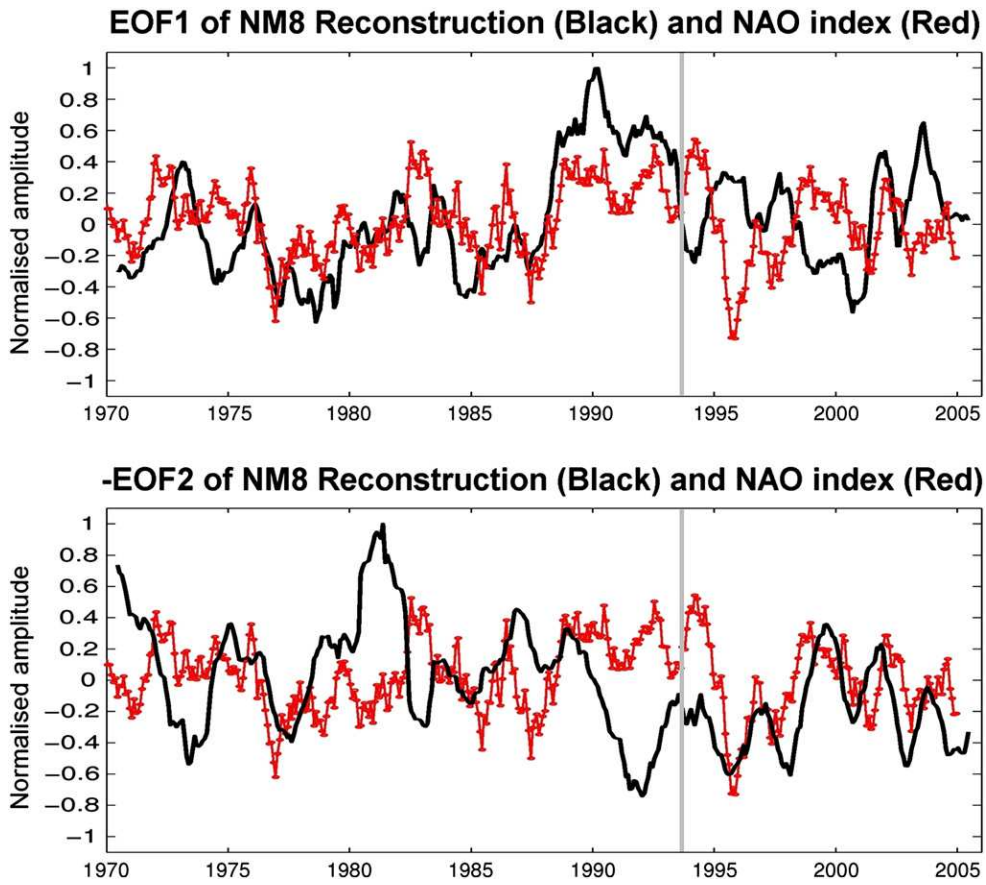

Fig. 8. Comparison of the amplitudes of the NM8 reconstruction EOFs with the NAO index. Top: Amplitude of EOF1 in black and NAO index in red. Bottom: Inverse of the amplitude of EOF2 in black and NAO index in red. The gray line indicates the date 1993.5. The temporal curves have been smoothed with a 12-month running mean.

runs for reconstructing sea level as they capture long-term ocean spatial structure and better reconstruct past sea level.

In term of trends over 1970–2000, no agreement was found between the different reconstructions: the reconstructed fields show trends that differ from the long tide gage record trends by up to 2 mm/yr. The main reason of this difference is probably linked to the Mediterranean sea level interannual to multidecadal variability (of more than 100 mm from one year to the next see Fig. 4). Thus the records are too short to precisely estimate trends. Nevertheless the results suggest that the ROM-based reconstructions give the better trend estimate in the Ionian Sea while the altimetry reconstructions seem to be closer to real trends in the western basin. To sum up, the NM8-based reconstruction shows the highest correlation with test tide gages. The mean sea level trend reproduced by the NM8 reconstruction is of 1.4 mm/yr (over 1970–2000).

Gomis et al. (2008) and Marcos and Tsimplis (2008) >showed that the NAO drove the atmospheric-induced (wind stress + atmospheric pressure) sea level variability in the Mediterranean basin between 1960 and 1990. Here the comparison of the NM8 reconstruction EOFs with the NAO index suggests that between 1970 and the beginning of the 1990s, NAO forcing strongly impacts as well the IB-corrected Mediterranean sea level variability. But since then, NAO forcing has modified its impact on the sea level spatial patterns. The strong impact of the basin-scale water mass redistribution after the EMT event that lasted at least a decade probably plays some role (Herrmann et al., 2010). This redistribution could have had an impact on the steric component (East–west gradient) and on the circulation component (Ionian Sea) at decadal time scale. But the mechanism for this needs further investigation. In particular, further study using sensitivity runs with regional ocean models has to be done to better attribute the Mediterranean sea level variability in the 90s.

Acknowledgments

We would like to thank our colleague O. Frihy of the Coastal Research Institute at Alexandria for kindly providing us with the Alexandria tide gage record and S. Zerbini for providing us with the tide gage records of the idromare dataset. We would like to thank as well Florence Sevault (Météo-France, CNRM-GAME) for developing, maintaining and running the NEMOMED8 regional ocean model. A special thank to Volfango Rupolo who contributed to this work with his enthusiasm for science and with his happiness. Unfortunately, it has been our last chance to collaborate with him on this earth as he passed away on April 2010.

Finally we are very grateful to L. Fenoglio-Marc for her thorough review and to an anonymous reviewer for his/her useful comments.

We would like to acknowledge the support and financial contribution of the Topo-Europe programme and CECILE programme.

References

Ablain, M., Cazenave, A., Valladeau, G., Guinehut, S., 2009. A new assessment of the error budget of global mean sea level rate estimated by satellite altimetry over 1993–2008. Ocean Sci. 5, 193–201.

Artale, V., Calmanti, S., Carillo, A., Dell'Aquila, A., Herrmann, M., Pisacane, G., Ruti, P.M., Sannino, G., Struglia, M.V., 2009. An atmosphere–ocean regional climate model for

the Mediterranean area: assessment of a present climate simulation. Ocean Modelling 30, 56–72.
Becker, M., Karpytchev, M., Davy, M., Doekes, K., 2009. Impact of a shift in mean on the sea level rise: application to the tide gauges in the Southern Netherlands. Continental Shelf Res. 29, 741–749.
Beuvier, J., Sevault, F., Herrmann, M., Kontoyiannis, H., Ludwig, W., Rixen, M., Stanev, E., Beranger, K., Somot, S., 2010. Modelling the Mediterranean Sea interannual variability during 1961–2000: focus on the Eastern Mediterranean Transient (EMT). J. Geophys Res. 115, C08017. doi:10.1029/2009JC005850.
Bindoff, N.L., Willebrand, J., Artale, V., Cazenave, A., Gregory, J.M., Gulev, S., Hanawa, K., Le Quéré, C., Levitus, S., Nojiri, Y., Shum, C.K., Talley, L.D., Unnikrishnan, A.S., 2007. Observations: oceanic climate change and sea level. Climate Change 2007: The Physical Science Basis. Cambridge University Press, pp. 385–432.
Cabanes, C., Cazenave, A., Le Provost, C., 2001. Sea level change from Topex-Poseidon altimetry for 1993–999 and possible warming of the southern oceans. Geophys. Res. Lett. 28, 9–12.
Calafat, F.M., Gomis, D., 2009. Reconstruction of Mediterranean sea level fields for the period 1945–2000. Glob. Planet. Change 66, 225–234.
Carrere, L., Lyard, F., 2003. Modeling the barotropic response of the global ocean to atmospheric wind and pressure forcing — comparisons with observations. Geophys. Res. Lett. 6, 1275. doi:10.1029/2002GL016473.
Church, J.A., White, N.J., Coleman, R., Lambeck, K., Mitrovica, J.X., 2004. Estimates of the regional distribution of sea level rise over the 1950–2000 period. J. Clim. 17, 2609–2625.
Déqué, M., Piedelievre, J.P., 1995. High-resolution climate simulation over Europe. Clim. Dyn. 11, 321–339.
Efron, B., Tibshirani, R.J., 1993. An Introduction to the Bootstrap. Chapman & Hall.
Fenoglio-Marc, L., Groten, E., Dietz, C., 2004. Vertical land motion in the Mediterranean sea from altimetry and tide gauge stations. Marine Geodey 27, 683–701.
Frihy, O.E., Deabes, E.A., Shereet, S.M., Abdalla, F.A., 2010. Alexandria-Nile Delta coast, Egypt: update and future projection of relative sea-level rise. Earth Environment Science 2, 253–273. doi:10.1007/s12665-009-0340-x.
Gomis, D., Ruiz, S., Sotillo, M.G., Alvarez-Fanjul, E., Terradas, J., 2008. Low frequency Mediterranean sea level variability: the contribution of atmospheric pressure and wind. Glob. Planet. Change 63, 215–229.
Greatbatch, R.J., 1994. A note on the representation of steric sea-level in models that conserve volume rather than mass. J. Geophys. Res. 99, 12767–12771.
Herrmann, M.J., Somot, S., 2008. Relevance of ERA40 dynamical downscaling for modeling deep convection in the Mediterranean Sea. Geophys. Res. Lett. 35, L04607. doi:10.1029/2007GL032442.
Herrmann, M., Sevault, F., Beuvier, J., Somot, S., 2010. What induced the exceptional 2005 convection event in the northwestern Mediterranean basin? Answers from a modeling study. J. Geophys. Res. 115, C12051. doi:10.1029/2010JC006162.
Hurrell, J.W., 1995. Decadal trends in the North Atlantic Oscillation — regional temperatures and precipitations. Science 269, 676–679.
Josey, S.A., 2003. Changes in the heat and freshwater forcing of the eastern Mediterranean and their influence on deep water formation. J. Geophys. Res. 108, 3237–3255. doi:10.1029/2003JC001778.
Kalnay, E., Kanamitsu, M., Kistler, R., Collins, W., Deaven, D., Gandin, L., Iredell, M., Saha, S., White, G., Woollen, J., Zhu, Y., Chelliah, M., Ebisuzaki, W., Higgins, W., Janowiak, J., Mo, K.C., Ropelewski, C., Wang, J., Leetmaa, A., Reynolds, R., Jenne, R., Joseph, D., 1996. The NCEP/NCAR 40-year reanalysis project. Bull. Amer. Meteor. Soc. 77, 437–471.
Kaplan, A., Kushnir, Y., Cane, M.A., 2000. Reduced space optimal interpolation of historical marine sea level pressure: 1854–1992. J. Clim. 13, 2987–3002.
Klein, B., Roether, W., Manca, B.B., Bregant, D., Beitzel, V., Kovacevic, V., Luchetta, A., 1999. The large deep water transient in the Eastern Mediterranean. Deep Sea Res. I. 46, 371–414.
Lascaratos, A., Roether, W., Nittis, K., Klein, B., 1999. Recent changes in deep water formation and spreading in the eastern Mediterranean Sea: a review. Progress in Oceanography 44, 5–36.
Le Traon, P.Y., Nadal, F., Ducet, N., 1998. An improved mapping method of multisatellite altimeter data. J. atmospheric oceanic technology 15, 522–534.
Le Traon, P.Y., Ogor, F., 1998. ERS-1/2 orbit improvement using TOPEX/POSEIDON: the 2 cm challenge. J. Geophys. Res. 103, 8045–8057.
Llovel, W., Cazenave, A., Rogel, P., Lombard, A., Nguyen, M.B., 2009. Two-dimensional reconstruction of past sea level (1950–2003) from tide gauge data and an Ocean General Circulation Model. Climate of the Past 5, 217–227.
Lombard, A., Cazenave, A., DoMinh, K., Cabanes, C., Nerem, R.S., 2005. Thermosteric sea level rise for the past 50 years; comparison with tide gauges and inference on water mass contribution. Glob. Planet. Change 4, 303–312.
Madec, G., 2008. Nemo ocean engine. Note du pôle modélisation no. 27. IPSL France. ISSN n°1288–1619.
Malanotte-Rizzoli, P., Manca, B.B., d'Alcala, M.R., Theocharis, A., Brenner, S., Budillon, G., Ozsoy, E., 1999. The Eastern Mediterranean in the 80s and in the 90s: the big transition in the intermediate and deep circulations. Dynamics of Atmospheres and Oceans 29, 365–395.
Marcos, M., Tsimplis, M.N., 2007. Variations of the seasonal sea level cycle in southern Europe. J. Geophys. Res. 112, C12011. doi:10.1029/2006JC004049.
Marcos, M., Tsimplis, M.N., 2008. Coastal sea level trends in southern Europe. Int. J. Geophys. 175, 70–82.
Milne, G.A., Gehrels, W.R., Hughes, C.W., Tamisiea, M.E., 2009. Identifying the causes of sea-level change. Nature Geoscience 2, 471–478.
Pal, J.S., Giorgi, F., Bi, X.Q., Elguindi, N., Solmon, F., Gao, X.J., Rauscher, S.A., Francisco, R., Zakey, A., Winter, J., Ashfaq, M., Syed, F.S., Bell, J.L., Diffenbaugh, N.S., Karmacharya, J., Konare, A., Martinez, D., da Rocha, R.P., Sloan, L.C., Steiner, A.L., 2007. Regional climate modeling for the developing world — the ICTP RegCM3 and RegCNET. Bull. Amer. Meteor. Soc. 88, 1395–1409.
Peltier, W.R., 2004. Global glacial isostasy and the surface of the ice-age earth: the ice-5G (VM2) model and grace. Ann. Rev. Earth Planet. Sci. 32, 111–149.
Preisendorfer, R.W., 1988. Principal component analysis in meteorology and oceanography. Developments in Atmospheric Science, vol. 17. Elsevier. 425 pp.
Rixen, M., Beckers, J.M., Levitus, S., Antonov, J., Boyer, T., Maillard, C., Fichaut, M., Balopoulos, E., Iona, S., Dooley, H., Garcia, M.J., Manca, B., Giorgetti, A., Manzella, G., Mikhailov, N., Pinardi, N., Zavatarelli, M., 2005. The western Mediterranean deep water: a proxy for climate change. Geophys. Res. Lett. 32, L12608. doi:10.1029/2005GL022702.
Roether, W., Manca, B.B., Klein, B., Bregant, D., Georgopoulos, D., Beitzel, V., Kovacevic, V., Luchetta, A., 1996. Recent changes in eastern Mediterranean deep waters. Science 271, 333–335.
Roether, W., Klein, B., Manca, B.B., Theocharis, A., Kioroglou, S., 2007. Transient Eastern Mediterranean deep waters in response to the massive dense-water output of the Aegean Sea in the 1990s. Progress in Oceanography 74, 540–571.
Roullet, G., Madec, G., 2000. Salt conservation, free surface, and varying levels: a new formulation for ocean general circulation models. J. Geophys. Res. 105, 23927–23942.
Samuel, S., Haines, K., Josey, S., Myers, P.G., 1999. Response of the Mediterranean Sea thermohaline circulation to observed changes in the winter wind stress field in the period 1980–1993. J. Geophys. Res. 104, 7771–7784.
Sevault, F., Somot, S., Beuvier, J., 2009. A regional version of the NEMO ocean engine on the Mediterranean sea: NEMOMED8 user's guide. Note de centre no 107, CNRM, Toulouse, France.
Steigenberger, P., Rothacher, M., Dietrich, R., Fritsche, M., Rulke, A., Vey, S., 2006. Reprocessing of a global GPS network. J. Geophys. Res. 111, B05402. doi:10.1029/2005JB003747.
Stocchi, P., Spada, G., 2009. Influence of glacial isostatic adjustment upon current sea level variations in the Mediterranean. Tectonophysics 474, 56–68.
Struglia, M.V., Mariotti, A., Filograsso, A., 2004. River discharge into the Mediterranean Sea: climatology and aspects of the observed variability. J. Clim. 17, 4740–4751.
Theocharis, A., Nittis, K., Kontoyiannis, K., Papageorgiou, E., Balopoulos, E., 1999. Climatic changes in the Aegean Sea influence the Eastern Mediterranean thermohaline circulation (1986–1997). Geophys. Res. Lett. 26, 1617–1620.
Theocharis., A., Kontoyiannis, K., 1999. Interannual variability of the circulation and hydrography in the Eastern Mediterranean (1986–1995). In: Kluwer Academic Publishing (Ed) NATO Sciences Series. Dordrecht, The Netherlands pp453–464.
Toumazou, V., Cretaux, J.F., 2001. Using a Lanczos eigensolver in the computation of empirical orthogonal functions. Mon. Weather Rev. 129, 1243–1250.
Tsimplis, M.N., Josey, S., 2001. Forcing of the Mediterranean Sea by atmospheric oscillations over the North Atlantic. Geophys. Res. Lett. 28, 803–806.
Tsimplis, M.N., Alvarez-Fanjul, E., Gomis, D., Fenoglio-Marc, L., Perez, B., 2005. Mediterranean Sea level trends: atmospheric pressure and wind contribution. Geophys. Res. Lett. 20, L20602. doi:10.1029/2005GL023867.
Tsimplis, M.N., Marcos, M., Colin, J., Somot, S., Pascual, A., Shaw, A.G.P., 2009. Sea level variability in the Mediterranean Sea during the 1990s on the basis to two 2d and one 3d model. J. Marine Systems. 18, 109–123. doi:10.1016/j.jmarsys.2009.04.003.
Uppala, S.M., Kallberg, P.W., Simmons, A.J., Andrae, U., Bechtold, V.D., Fiorino, M., Gibson, J.K., Haseler, J., Hernandez, A., Kelly, G.A., Li, X., Onogi, K., Saarinen, S., Sokka, N., Allan, R.P., Andersson, E., Arpe, K., Balmaseda, M.A., Beljaars, A.C.M., Van De Berg, L., Bidlot, J., Bormann, N., Caires, S., Chevallier, F., Dethof, A., Dragosavac, M., Fisher, M., Fuentes, M., Hagemann, S., Holm, E., Hoskins, B.J., Isaksen, L., Janssen, P.A.E.M., Jenne, R., McNally, A.P., Mahfouf, J.F., Morcrette, J.J., Rayner, N.A., Saunders, R.W., Simon, P., Sterl, A., Trenberth, K.E., Untch, A., Vasiljevic, D., Viterbo, P., Woollen, J., 2005. The ERA-40 re-analysis. Quarterly J. Royal Meterological Society 131, 2961–3012.
Valcke, S., Redler, R., 2006. OASIS3 user guide. PRISM support Initiative report no 4. 60 pp.
Vera, J.D., Criado-Aldeanueva, F., Garcia-Lafuente, J., Soto-Navarro, F.J., 2009. A new insight on the decreasing sea level trend over the Ionian basin in the last decades. Glob. Planet. Change 68, 232–235.
Volkov, D.L., Larnicol, G., Dorandeu, J., 2007. Improving the quality of satellite altimetry data over continental shelves. J. Geophys. Res. 112, C06020. doi:10.1029/2006JC003765.
Woodworth, P.L., Player, R., 2003. The permanent service for mean sea level: an update to the 21st century. J. Coast. Res. 19, 287–295.
Woppelmann, G., Miguez, B.M., Bouin, M.N., Altamimi, Z., 2007. Geocentric sea-level trend estimates from GPS analyses at relevant tide gauges world-wide. Glob. Planet. Change 57, 396–406.
Woppelmann, G., Letetrel, C., Santamaria, A., Bouin, M.N., Collilieux, X., Altamimi, Z., Williams, S.P.D., Martin Miguez, B., 2009. Rates of sea level change over the past century in a geocentric reference frame. Gephys. Res. Lett. 36, L12607. doi:10.1029/2008GL038720.
Zervakis, V., Georgopoulos, D., Karageorgis, A.P., Theocharis, A., 2004. On the response of the Aegean sea to climatic variability: a review. Int. J. Climat. 24, 1845–1858.

Global and Planetary Change 100 (2013) 1–10

Contents lists available at SciVerse ScienceDirect

Global and Planetary Change

journal homepage: www.elsevier.com/locate/gloplacha

Decadal variability of net water flux at the Mediterranean Sea Gibraltar Strait

L. Fenoglio-Marc [a,*], A. Mariotti [b], G. Sannino [c], B. Meyssignac [d], A. Carillo [c], M.V. Struglia [c], M. Rixen [e]

[a] Institute of Physical Geodesy, Technical University Darmstadt, Petersenstrasse 13, D-64287 Darmstadt, Germany
[b] National Oceanic and Atmospheric Administration, Office of Oceanic and Atmospheric Research (NOAA/OAR), 1315 East/West Hwy, Silver Spring, MD 20910, USA
[c] Italian Agency for Energy and Environment (ENEA), Climate Project - Ocean Modelling Unit, Via Anguillarese 301, S.M. di Galeria, I-00060, Roma, Italy
[d] LEGOS/CNES, 14, Avenue E. Belin, 31400 Toulouse, France
[e] World Meteorological Organisation, 7bis, avenue de la Paix, CH-1211 Geneva, Switzerland

ARTICLE INFO

Article history:
Received 15 October 2011
Accepted 23 August 2012
Available online 30 August 2012

Keywords:
Gibraltar net water flux
Ocean mass change
Sea-level
Water cycle

ABSTRACT

Long-term variability of the net water flux into the Mediterranean Sea at the Gibraltar Strait over the period 1960–2009 is explored based on an approach combining multiple observational datasets and results from a regional climate model simulation. The approach includes deriving Gibraltar net inflow from the application of the Mediterranean Sea water budget equation using observationally based estimates of mass variation, evaporation, precipitation and simulated river discharge and Bosphorus Strait water fluxes. This derivation is compared with results from a simulation using the PROTHEUS regional ocean–atmosphere coupled model considering both individual water cycle terms and overall Gibraltar water flux.

Results from both methodologies point to an increase in net water flux at Gibraltar over the period 1970–2009 ($0.8 +/- 0.2$ mm/mo per year based on the observational approach). Simulated Gibraltar net water flux shows decadal variability during 1960–2009 including a net Gibraltar water flux decrease during 1960–1970 before the 1970–2009 increase.

Decadal variations in net evaporation at the sea-surface, such as the increase during 1970–2009, appear to drive the changes in net inflow at Gibraltar, while river runoff and net inflow at the Bosphorus Strait have a modulating effect. Mediterranean Sea mass changes are seen to be relatively small compared to water mass fluxes at the sea surface and do not show a long-term trend over 1970–2009. The Atlantic Multi-decadal Oscillation (AMO) and the North Atlantic Oscillation (NAO) are relevant indirect influences on net water flux at Gibraltar via the influence they bear on regional evaporation, precipitation and runoff.

1. Introduction

As the Mediterranean Sea is a semi-enclosed basin, connected with the open Atlantic Ocean only at the Gibraltar Strait, the fluxes of water and salt through this Strait bear a major influence on the state of the Sea with impacts on the mass, salt and energy budgets. A net water inflow at Gibraltar (G) results from incoming fresh and cool Atlantic water and outflowing warm and salty Mediterranean water. Climatologically, net inflow of water at Gibraltar primarily balances the vertical loss of water at the sea-surface (water fluxes through the Bosphorus Strait (B) and river discharge (R) also contribute to balance the surface water loss; e.g. Mariotti et al., 2002). Recent research has shown that decadal changes in net Mediterranean Sea evaporation have characterized the 1958–2006 period, with an overall increase in net evaporation resulting in a substantial increase in sea-surface water loss (Criado-Aldeanueva et al., 2010; Mariotti, 2010). An open question is whether this increased water loss has induced increases in the net water inflow at Gibraltar or whether there have been changes in Mediterranean Sea water mass. In fact, while the Mediterranean thermohaline circulation is sustained by the atmospheric forcing, its intensity is controlled by the narrow and shallow Strait of Gibraltar via hydraulic control processes (Sannino et al., 2007, 2009a). While measurements of the Mediterranean water outflow through Gibraltar have been collected over short time periods (Sanchez-Roman et al., 2009, Soto-Navarro et al., 2010), there are no long-term direct measurements of net water fluxes. Model simulations have been utilized to improve the understanding of the processes that regulate water fluxes at Gibraltar, with very high-resolution models now able to represent much of the complexity characterizing the dynamics of the Strait and simulate realistic Gibraltar flows (Sannino et al., 2009a; Sanchez-Garrido et al., 2011). It is interesting to note that a common assumption in state-of-art Mediterranean Sea models used for these studies is the "equilibrium condition" which forces the net flow at Gibraltar to strictly compensate the freshwater lost at the sea-surface (e.g. Tonani et al., 2008). Here we stress that such an assumption has still not been verified by specific observations.

Nowadays, changes in Mediterranean Sea mass are directly measured by the satellite gravimetric mission GRACE. These measurements, available over the interval 2002–2010, are usually expressed in terms of changes in equivalent water thickness, i.e. water mass

* Corresponding author.
E-mail address: fenoglio@ipg.tu-darmstadt.de (L. Fenoglio-Marc).

0921-8181/$ – see front matter © 2012 Elsevier B.V. All rights reserved.
http://dx.doi.org/10.1016/j.gloplacha.2012.08.007

changes per surface area (with 1 mm water column corresponding to 1 kg/m^2 if a density of 1 g/cm^3 is assumed). Mediterranean Sea water mass change values may also be derived from sea level change, provided the steric component of the sea level change can be estimated. In this case the water mass change is directly expressed as water thickness (volume). Recent studies have compared indirect estimates of Mediterranean Sea water mass derived from sea-level by way of steric-corrected satellite altimetry with those based on GRACE satellite mass retrievals. Results indicate a good agreement and a Mediterranean Sea mass increase during the last decade (Calafat et al., 2010; Fenoglio-Marc et al., 2012b).

Mediterranean sea level variability has been shown to be affected by the variability of the North Atlantic Oscillation (NAO; Hurrell et al., 2003) mainly through the impact of atmospheric sea-level pressure changes (Tsimplis and Josey, 2001). Although these results collectively suggest long-term variations in Mediterranean Sea mass and sea-level, and large-scale atmospheric influences, to our knowledge how long-term changes in fresh water fluxes may have affected Gibraltar water fluxes is yet to be explored. The level of accuracy of the satellite-based measurements calls for a re-examination of many conventional approximations often taken for granted (Greatbatch and Lu, 2001).

The goal of this work is to study the decadal variations in net water flux at the Strait of Gibraltar over the period 1960–2009 based on a combined observational-modelling approach and to indirectly explore the correctness of the "equilibrium condition" assumption made in state-of-art models. First, Gibraltar water flux is derived indirectly from the water budget equation based on observational estimates of Mediterranean Sea mass changes (from steric-corrected sea-level estimates and GRACE mass retrievals), regional precipitation and evaporation. Next, an independent estimate of the Gibraltar water flux is obtained from a numerical simulation by a regional ocean–atmosphere climate model. Lastly, potentially important factors regulating long-term Gibraltar flux changes are discussed. The paper is organized as follows: overall data and methodology are described in Section 2; results pertaining Mediterranean Sea mass and Gibraltar water flux variability are presented in Section 3; conclusions are in Section 4.

2. Methodology and data

The net water inflow through Gibraltar (G), may be estimated on the basis of the water budget equation for the Mediterranean Sea:

$$G = E - (P + R + B) + \partial M/\partial t \quad (1)$$

with E being sea-surface evaporation, P precipitation over the sea; R river discharge into the sea from the Mediterranean catchment; B net water influx from the Black Sea at the Bosphorus Strait; $\partial M/\partial t$ the rate of Mediterranean Sea water mass (M) change (see also Fenoglio-Marc et al., 2012b; Grayek et al., 2010). (Note that changes in Mediterranean Sea mass due to salinity changes are not accounted for in this water budget equation). As all quantities in Eq. (1) represent a volume variation, they can be expressed as basin-uniform sea level change in units of mm/mo, We apply Eq. (1) to derive G based on observational estimates of $\partial M/\partial t$, E and P. $\partial M/\partial t$ may be derived as the difference of water mass-induced sea level averaged over the sea (S_{mass}) at two following time-steps (Fenoglio-Marc et al. (2007)), as well as estimated from GRACE gravity solutions. In contrast, the independent results from the model simulation are based on the model's assumption, so it is interesting to see how these results compare with the observational estimate of G and whether they can contribute to a qualitative description of long-term variability in Gibraltar water fluxes.

All the quantities in Eq. (1) are estimated indirectly (as explained in the following) and it is clearly a challenge to define long-term changes and uncertainties of any of these quantities, let alone the resulting G estimate. Nevertheless, we attempt to estimate errors of annual mass-induced sea level S_{mass} and derivated quantities, namely $\partial M/\partial t$ and G. These error estimates are based on either the root mean square (RMS) difference between the various datasets available for a given quantity, or on error propagation considering the various components contributing to a given estimated quantity (see Table 1 for a summary of data used in this study; Tables 2–5 for associated error estimates). The first method reflects the spread of the datasets, but unknown systematic errors may remain. We account for the temporal autocorrelation of a time series, by using its effective sample size based on the lag-1 autocorrelation coefficient (Santer et al., 2000). The correlation between time-series and its double-sided significance are evaluated. Linear regression is used to estimate the linear trend and its error. We further assess the trend significance by applying the t-test to the ratio between the estimated trend and its error (Fenoglio-Marc et al., 2011). In the error propagation we consider the components to be uncorrelated (Fenoglio-Marc et al., 2006, 2012b).

2.1. Mediterranean Sea water mass derivation

During August 2002–December 2009, Mediterranean water mass-induced sea level (S_{mass}) may be estimated directly from satellite-based gravity observations retrieved by the GRACE satellite mission (S^g_{mass} hereafter; Flechtner, 2007; Fenoglio-Marc et al., 2006). Note that since GRACE measures gravity, a priori mass changes detected by GRACE include both the effect of water and salt changes. Over the longer 1970–2009 period, S_{mass} may be also estimated indirectly from Eq. (2), by correcting the total sea level (S_{tot}) for its steric component (S_{ster}) so as to account only for water mass induced sea-level (S_{mass}):

$$S_{mass} = S_{tot} - S_{ster} \quad (2)$$

During 1993–2009, S_{tot} is evaluated from satellite altimetry data (S^{alti}_{tot}). For this derivation we have used along-track data of the Topex/Poseidon, Jason-1, Jason-2 and Envisat altimetry missions from the RADS database (Naeije et al., 2008) and applied the conventional geophysical corrections accounting for the ocean response to atmospheric wind and pressure forcing (atmospheric loading on the sea surface) via the Dynamic Atmospheric Correction (DAC). Grids of 0.5 degrees have been computed and used to evaluate the sea level basin average. Prior to the altimetry era, starting from 1970 S_{tot} is derived based on a reconstruction developed by Meyssignac et al. (2011) (hereafter MBMED11). Comparing the MBMED11 basin averaged reconstruction (S^{reco}_{tot}) with a

Table 1
List of data. For the seven fields used in this study : temperature (T), salinity (S), sea level (S_{tot}), mass-induced sea level (S_{mass}), evaporation (E), precipitation (P), sea level pressure (SLP) the name of the database together with its time interval, spatial and temporal resolutions are given. For the T and S fields the maximum depth and the number of levels are given in addition.

Database name	Field	Time interval	Grid	Depth (m)	Levels	Time sampling
Medar/Medatlas	T, S	1945–2002	0.2°×0.2°	4000	25	1 yr
Ishii v6.7	T, S	1945–2006	1°×1°	700	16	30 days
MFSTEP/ICBM	T, S	2000–2009	1°×1°	3850	31	30 days
GRACE	$S_{mass,}$	2002–2009	300 km			30 days
altimetry	S_{tot}	1993–2009	0.5°×0.5°			30 days
MBMED11	S_{tot}	1970–2009	0.5°×0.5°			30 days
Protheus	E	1958–2001	30 km			30 days
OAFLUX	E	1958–2009	1°×1°			30 days
Protheus	P	1958–2001	30 km			30 days
GPCP	P	1979–2009	2.5°×2.5°			30 days
REOFS	P	1960–2009	5°×5°			30 days
HadSLP	SLP	1960–2009	5°×5°			30 days

Table 2
Correlation (Corr), root mean square difference (RMSD), number of samples (N) and level of significance of correlation (Significance) of annual time-series in common interval (Time Interval). Units are mm for sea-level (S) quantities and mm/mo for precipitation/evaporation rates and rate of mass change ∂M/∂t. For sea level the component type is indicated by the subscript (tot: total sea level; ster: steric sea level; thermo-ster: thermo-steric sea level; halo-ster: halo-steric sea level; mass: mass induced sea level). The superscript indicates the dataset used (e.g. alti: altimetric sea level; reco: reconstructed sea level etc.; see text). For precipitation and evaporation the datasets used are indicated by the subscript.

		Corr	RMSD	N	Time interval	Significance (%)
S_{tot}^{alti}	S_{tot}^{reco}	0.98	4.0	13	1993–2002	99
S_{tot}^{reco}	$S_{tot}^{reco\_alti}$	0.95	9.0	13	1993–2002	99
S_{ster}^{ishii}	S_{ster}^{medar}	0.57	12.0	57	1945–2002	99
$S_{thermo\text{-}ster}^{ishii}$	$S_{thermo\text{-}ster}^{medar}$	0.82	5.1	57	1945–2002	99
$S_{halo\text{-}ster}^{ishii}$	$S_{halo\text{-}ster}^{medar}$	0.36	12.0	57	1945–2002	99
$S_{mass}^{reco\text{-}ishii}$	$S_{mass}^{reco\text{-}medar}$	0.80	15.0	33	1970–2002	99
$\partial M/\partial t^{\ reco\text{-}ishii}$	$\partial M/\partial t^{\ reco\text{-}medar}$	0.71	1.4	32	1970–2002	99
P_{gpcp}	P_{reofs}	0.41	4.9	23	1979–2001	95
$E_{oaflux}-P_{gpcp}$	$E_{oaflux}-P_{reofs}$	0.67	5.0	23	1979–2001	99

reconstruction based on satellite altimetry ($S_{tot}^{reco\_alti}$; Meyssignac et al., 2011) one finds a good agreement with a correlation 0.95 and RMS differences 9 mm (see Table 2). The advantage of the MBMED11 reconstruction, compared to an alternative one by Calafat and Gomis (2009), is the use of the long-term sea level patterns deduced from a 33-year long run of the ARPERA-forced NEMOMED8 ocean model (Sevault et al., 2009) instead of a 13-year long altimetry record as in Calafat and Gomis (2009), which enables to better capture Mediterranean sea level decadal variability of specific interest to our study (Meyssignac et al., 2011).

We compute the steric component of sea level $S_{ster,}$ taking into account both the effects of temperature (S_{thermo_ster}) and salinity (S_{halo_ster}). Temperature and salinity fields are obtained from two gridded climatologies: the regional Medar/Medatlas (Rixen et al., 2005; available yearly 1970–2002) and the global Ishii (Ishii and Kimoto, 2009; available monthly 1970–2006); and also from the MFSTEP oceanographic model (Tonani et al., 2008; 2002–2009). We integrate from the surface down to the maximum depth with available data (see Table 4). It is noted that models routinely provide potential temperature (Fofonoff, 1977), while climatologies give in-situ temperature; this is accounted for in our analysis concerning the estimation of steric heights.

We compute annual basin means of $S_{ster,}$ S_{tot}, and their difference S_{mass} to derive its rate of change ∂M/∂t. The overlap between the GRACE-based mass estimate S_{mass}^{g} and the indirect sea-level-based mass derivations (two separate ones from altimetry and reconstruction) over the common 2002–2009 period allows a comparison of the various methods as a mean to gain a sense of the uncertainties associated to the mass estimates (see Table 3 for comparisons; Calafat et al., 2010; Fenoglio-Marc et al., 2012). It is worth noticing that over the common period, the GRACE mass change estimate (including both water and salt mass changes) is found to be largely similar to the indirect sea-level based derivation which only includes the effect of water mass changes in virtue of the steric correction (see Section 3.1). This suggests that, at least for this period, mass changes measured by GRACE were mostly water induced.

Table 3
Correlation (Corr), root mean square difference (RMSD), number of samples (N) and level of significance of correlation (Significance) of observed and simulated annual time-series in 1979–2001 (n = 23).

Simulated	Observed	Corr	RMSD (mm/mo)	Significance (%)
$E_{protheus}$	E_{oaflux}	0.50	4.2	99
$P_{protheus}$	P_{gpcp}	0.78	2.8	99
$P_{protheus}$	P_{reofs}	0.15	5.8	50
$E_{protheus}-P_{protheus}$	$E_{oaflux}-P_{gpcp}$	0.63	6.2	99
$E_{protheus}-P_{protheus}$	$E_{oaflux}-P_{reofs}$	0.46	5.6	95
$G_{protheus}$	$E_{oaflux}-P_{gpcp}+\partial M/\partial t$	0.44	7.0	95
$G_{protheus}$	$E_{oaflux}-P_{reofs}+\partial M/\partial t$	0.59	5.6	99
$G_{protheus}$	$E_{oaflux}-P_{reofs}-R-B+\partial M/\partial t$	0.66	6.0	99

Table 4
Annual errors of basin averages. Methods are RMS difference (RMSD) and error propagation (EP) in (mm) or (mm/mo) as indicated in Table 2. Bold values have been selected to provide the final error estimate for G from EP.

	Annual error	Source
$S_{tot}^{\ alti}$	3	RMSD of $S_{tot}^{\ alti}$
$S_{tot}^{\ reco}$	**6**	EP, Meyssignac et al., 2011
S_{tot}	4	RMSD of $S_{tot}^{\ alti}$ and $S_{totl}^{\ reco}$ (Table 2)
	6	**Selected for EP**
S_{ster}	12	RMSD of S_{ster}
	15–25	EP
	15	**Selected for EP**
$S_{mass}^{\ alti\text{-}ster}$	12	EP of $S_{tot}^{\ alti}$ & S_{ster}
$S_{mass}^{\ reco\text{-}ster}$	**16**	EP of $S_{tot}^{\ reco}$ & S_{ster},
S_{mass}	15	RMSD using various S_{ster} (Table 2)
S_{mass}^{g}	7	**EP of GRACE**
	16	**Selected for EP**
$\partial M/\partial t^{\ reco\text{-}ster}$	**23**	EP of $S_{mass}^{\ reco\text{-}ster}$
	1.5	RMS diff. of solutions (Table 2)
$\partial M/\partial t^{\ g}$	10	EP of $S_{mass}^{\ g}$
	23	**Selected for EP**
E	4.2–4.8	Yu et al., 2008
	4	RMSD of E datasets (Table 2)
	5	**Selected for EP**
P	9–12	Adler et al., 2012
	6	RMSD of P datasets (Table 2)
	10	**Selected for EP**
E-P	11	EP
	6	RMSD of E-P datasets (Tables 2,3)
	11	**Selected for EP**
R	**2**	STD of R
B	**2**	STD of B
G	25	EP including all components
	11	EP of E-P, neglect R, B, ∂M/∂t
	7	RMSD of results

2.2. Observational evaporation and precipitation data

Both oceanic evaporation and precipitation are challenging quantities to derive, as neither is directly observed. Mariotti (2010) provides a recent intercomparison of estimates for the Mediterranean Sea from various datasets and methodologies over the period since the

Table 5
Standard deviation (STD), trend and its significance of observed and simulated water cycle parameters in 1979–2001.

	STD (mm/mo)	Trend (mm/mo)/yr	Significance (%)
$E_{protheus}$	3.3	0.03 +/− 0.08	–
$P_{protheus}$	4.1	−0.13 +/− 0.13	75
$R_{protheus}$	2.0	−0.10 +/− 0.06	90
$B_{protheus}$	2.2	−0.00 +/− 0.06	–
$G_{protheus}$	7.9	0.34 +/− 0.22	90
$(E-P)_{protheus}$	5.7	0.15 +/− 0.14	75
$(R+B)_{protheus}$	3.4	−0.10 +/− 0.11	75
$(E-P-R-B)_{protheus}$	8.5	0.25 +/− 0.20	75
E_{oaflux}	6.9	0.43 +/− 0.09	99
P_{gpcp}	4.0	−0.31 +/− 0.13	99
$E_{oaflux}-P_{gpcp}$	8.2	0.74 +/− 0.13	99
$E_{oaflux}-P_{gpcp}-(R+B)_{protheus}$	6.9	0.84 +/− 0.20	99
$\partial M/\partial t$	1.6	−0.09 +/− 0.13	99
$E_{oaflux}-P_{gpcp}-(R+B)_{protheus}+\partial M/\partial t$	9.1	0.74 +/− 0.23	99
$E_{oaflux}-P_{gpcp}+\partial M/\partial t$	8.4	0.66 +/− 0.14	99

late-1950s and allows qualitative insights into the uncertainties associated with Mediterranean Sea E and P estimates. In this study, we choose to use selected estimates of E and P among those analyzed by Mariotti (2010) rather than explore the full range of estimates available, while keeping in mind the range of uncertainties highlighted by the Mariotti (2010) study. For evaporation over the period 1958–2006, we use the derivation from the air–sea fluxes dataset OAFLUX, which objectively synthesizes surface meteorology obtained from satellite products (including SSM/I, Quick Scatterometer (QuikSCAT), Advanced Very High Resolution Radiometer (AVHRR), Tropical Rainfall Measuring Mission (TRMM)) and model NCEP re-analyses (Yu et al., 2008). For precipitation over 1979–2006, we consider data from the Global Precipitation Climatology Project (GPCP; Adler et al., 2003). Back in time, for the period 1960–2006 we use a reconstruction of oceanic precipitation (REOFS hereafter; Smith et al., 2008), which aims at capturing the large-scale features of global precipitation. Estimated OAFLUX evaporation error for the Mediterranean Sea is 4.2–4.8 mm/mo (5–6 Wm^2 or more conservatively 5–8 Wm^2; Yu et al., 2008). Estimated GPCP precipitation error is 9–12 mm/mon for GPCP (0.3–0.4 mm/d; Adler et al., 2012). No error estimate is available for REOFs (see Table 4 for intercomparison of error estimates).

2.3. Climate model simulation

We consider results from a regional ocean–atmosphere coupled model simulation with the PROTHEUS system (Artale et al., 2010). The PROTHEUS system includes the RegCM3 atmospheric regional model (Pal et al., 2007) and the MED-MITgcm ocean model (Marshall et al., 1997; Sannino et al., 2009b), that are coupled through the OASIS3 coupler (Valcke and Redler, 2006). It is a hydrostatic ocean model that uses the Boussinesq approximation (volume-conserving condition) (Song and Hou, 2006). As the volume of water in the model domain is conserved by model's construction the volume of water lost from the Mediterranean basin is balanced by means of a positive flux of water over the Atlantic box (see Carillo et al., 2012 for a complete validation of the ocean model). The experiment considered here is a simulation of climate variability in the European-Mediterranean domain over the period 1958–2001 at a spatial resolution of 30 km for the atmospheric component and $1/8° \times 1/8°$ for the oceanic model. The model includes the Interactive RIver Scheme (IRIS) that computes river discharge from runoff (Dell'Aquila et al., 2012). The oceanic and the atmospheric models exchange coupling fields (SST, wind stress components and total heat and salt fluxes) every 6 h. Surface natural boundary conditions are used for the oceanic model which treats $P+R-E$ as a real fresh water flux.

The ocean component is initialized with MEDATLAS II data (MEDAR Group, 2002), then a 40 year spin-up is performed using a 3D relaxation of temperature and salinity to the climatological values. ERA40 re-analyses (Uppala et al., 2005) are used as atmospheric lateral boundary conditions. The two-way exchange through the Strait of Gibraltar is achieved by means of 3D relaxation of salinity and temperature toward the climatological monthly Levitus data (Levitus, 1982), in a box composed by 30 grid points located west of Gibraltar. The PROTHEUS net water flux at Gibraltar is computed as the volume transport through a latitudinal section, derived as difference of the two-way exchange given in Fig. 3S.

Since observational estimates of R and B times series for the period 1970–2009 are not available, we consider R, B values from the PROTHEUS simulation as observational surrogates, to be used in the water budget equation (Eq. 1) to derive G, together with data from observational datasets. However the modeled terms are roughly an order of magnitude smaller than E (Mariotti et al., 2002), hence are second order factors in the estimation of G. Because of the different assumptions in the simulated G versus the indirectly observationally derived G, comparing the two allows to both corroborate independently derived G estimates and also explore whether the model's condition is indeed a realistic assumption.

2.4. Climatic indices

We consider various climatic indices to explore the role of large-scale climate phenomena on long-term G variability as it relates to other water cycle changes. Specifically, the December–March (DJFM) station-based NAO index calculated as the normalized pressure difference between Gibraltar and South West Iceland [Jones et al., 1997]; and the annual AMO index available from NOAA/OAR Physical Science Division calculated as the de-trended area-weighted average of North Atlantic (0° to 70°N) Sea Surface Temperature (SST) (available since 1856) (Enfield et al., 2001). To compare with the NAO index, we consider DJFM means of Mediterranean mean P, R and $\partial M/\partial t$, and compute six-years running means to focus on long-term variability. In this analysis, we also include monthly mean sea-level pressure from the HadSLP2 dataset (SLP), combining land and marine pressure observations (Allan and Ansell, 2006). In the comparison with the AMO index, we consider six-year running means of annual values. Annual mean anomalies are relative to the period 1979–2001, as this is the common period of availability for all data used.

3. Results

3.1. Mediterranean Sea mass variability

Fig. 1 shows anomalies of annual mean basin-averaged sea-level in 1970–2009, as derived from the altimeter measurements (S_{tot}^{alti}) and the sea-level reconstruction (S_{tot}^{reco}). Over the 1970–2005 period, reconstructed sea-level displays both interannual and decadal variations with relative minima observed around 1975 and 1994. The monthly error associated with the reconstructed basin-averaged sea-level estimated by a bootstrap method (Efron and Tibshirani, 1993) is about 20 mm and significant at the 95% level (see Meyssignac et al., 2011 for more details). The corresponding annual mean error is 6 mm. The annual mean error of the altimetric basin-averaged sea level is 3 mm based on a RMS difference between data sets (Table 4, see also Fenoglio-Marc et al., 2012). Overall, there is very good consistency for basin averaged sea-level between the altimeter estimates and the reconstructed estimates, which reinforces confidence in the sea-level reconstruction for the earlier period. Over the common interval 1993–2005, yearly mean sea-level estimates from the reconstruction and from the altimeter observations are in good agreement with a 0.98 correlation and 4 mm RMS difference (Tables 2, 4). We finally assume a value of 6 mm for the error of the combined sea level S_{tot}, to account for the lower accuracy of the

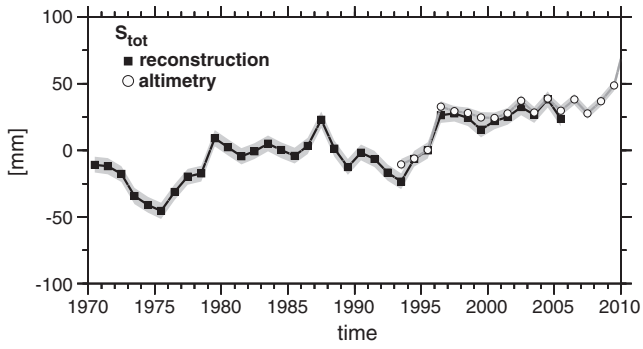

Fig. 1. Yearly mean sea level anomaly in the Mediterranean Sea over the period 1970–2009 derived from multi-satellite altimetry (circle) and from MBMED11 reconstruction (square) with error bounds corresponding both to the RMS difference of input data (gray shadow).

reconstruction before the altimeter era (Table 4). The overall trend of the combined sea level S_{tot} over 1970–2009 is 1.9 +/− 0.2 mm/yr.

Fig. 2 shows the annual basin average anomalies of the steric component (S_{ster}) derived from the Medar/Medatlas and from the Ishii gridded climatologies. Over the common interval 1945–2002 correlation and RMS difference between the two derivations are 0.57 and 12 mm, with correlation significant at the 99% level (Table 2). The RMS difference mainly arises from the difference in halo-steric components, which are still significantly correlated at the 99% level (correlation and RMS difference of 0.36 and 12 mm, respectively). The thermo-steric components ($S_{thermo\text{-}ster}$) are more similar (correlation and RMS difference are 0.81 and 5 mm respectively). These differences can be partly attributed to the different depths covered by the Ishii and Medar/Medatlas datasets (maximum depths available are 700 m and 4000 m respectively) and partly attributed to the different values of temperature and salinity in the databases. As results do not change significantly when integrating Medar/Medatlas to 600 m only (see Fig. 2) we may conclude that this second reason holds.

The RMS-based error of 12 mm derived above is our first estimate of the error of the steric component (Table 4). Another estimate is obtained from the grid of statistical errors associated to each Medar/Medatlas grid (Rixen et al., 2005). The error of the basin average of temperature (T) and salinity (S) for different intervals in depths has been computed from the grid of statistical errors. The error associated with the specific volume has been evaluated as:

$$\varepsilon(\alpha) = \left|\frac{\partial\alpha(S.T.P.)}{\partial S}\right|\varepsilon(S) + \left|\frac{\partial\alpha(S.T.P.)}{\partial T}\right|\varepsilon(T)$$

where $\varepsilon(T)$and $\varepsilon(S)$are the objective analysis errors associated to T and S and are function of time and space. A Monte-Carlo approach is used to perturb $\varepsilon(T)$ and $\varepsilon(S)$ so as to obtain the associated specific volume anomaly. The gridded temperature and salinity fields were perturbed within the range of its associated temperature and/or salinity uncertainty so as to infer total, thermo and halosteric uncertainty; 100 members were sufficient to make the algorithm converge. Steric anomalies were directly confronted to the unperturbed reference.

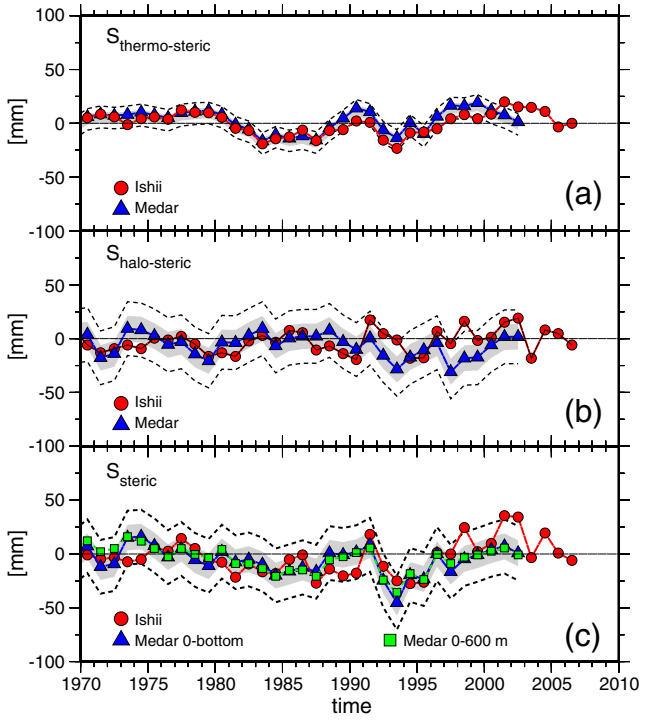

Fig. 2. Yearly mean thermo-steric (a), halo-steric (b), total steric (c) sea level anomalies in the Mediterranean Sea over the period 1970–2006 from Ishii version 6.7 (circle) and Medar/Medatlas integrated until 4000 meter depth (triangle). In c) Medar/Medatlas integrated until 600 (square) is shown in addition. Error bounds computed from Medar/Medatlas (dashed line) and corresponding both to the RMS difference of input data (gray shadow) are given.

Fig. 1S (additional material) shows basin averages of temperature and salinity data averaged over different intervals of depths together with the corresponding uncertainty. Being the variability range of temperature and salinity higher at the surface than at depth, and despite the lower amount of data at deeper levels, the uncertainty of the data decreases with depth. The uncertainties of the basin averages are between 0.1 and 0.2 °C in the first 150 m and lower than 0.1 °C below 150 m. Uncertainties are higher at both ends of the 1945–2002 period due to the lower amount of observations available to the objective analysis.

The volume uncertainty derived from a Monte Carlo perturbation of temperature and/or salinity for year 1995 (3-year running window) is illustrated in Fig. 2S. The steric uncertainty contributions are mainly located in deep ocean basins, as uncertainties are then integrated over larger depths. The halo-steric uncertainties dominate and reach 10 mm in the top 600 m and 15–25 mm in the complete water column (Table 4). This is mainly due to the scarcity of salinity data in the (eastern) Mediterranean. Results for other years in the 1960–1995 period are qualitatively similar. In summary, results suggest that the total steric anomaly uncertainties are lower than 25 mm for the whole water column. The uncertainty is lower near to the surface and is less than 5 mm for the 0–150 m layer, less than 10 mm for the 150–600 m layer and less than 15 mm for the 600–4000 m layer. It is however well known that theoretical errors provided by the objective analysis techniques usually underestimates actual errors, therefore errors could be higher. We observe that the error estimated for Medar/Medatlas is larger than the error derived for RMS difference of data. We finally assume a value of 15 mm for the error of the combined steric sea level S_{ster} (Table 4). The two different estimates of the steric component are quite consistent (Fig. 2, c). They show a tendency for the steric component to decrease from 1970 until the mid-1990s and increase thereafter (considering Ishii data, trends are −1.02 +/− 0.34 mm/yr during 1970–1990 and 1.19 +/− 0.8 mm/yr during 1990–2006).

As described in previous section, the steric component of basin-averaged sea level (as shown in Fig. 2) is used in combination with basin-averaged sea-level estimates (as shown in Fig. 1) to derive basin-averaged Mediterranean water mass variations S_{mass}. Fig. 3 shows annual mean basin-average Mediterranean Sea water mass anomalies over the period 1970–2009 based on the multiple sea-level and steric components estimates described above. Overall the various estimates depict a quite consistent behavior during the periods for which the data overlap both on interannual and longer timescales. Specifically, the correlation and RMS differences between the mass derivations considering the two different steric corrections of the sea-level reconstruction are 0.8 and 15 mm, respectively, with correlation statistically significant at the 99% confidence level (Table 2). Nevertheless there are differences among these estimates, highest differences are found in mid-1970s and early 1990s, which are however within the error bars based on Fig. 2.

Mass estimates from the Ishii steric-corrected sea-level reconstruction and the Ishii steric-corrected altimetry values are in particularly good agreement during 1993–2006. Similarly there is very good agreement between the mass estimates from the MFSTEP steric-corrected altimetry and the direct mass retrievals from GRACE for the most recent period (Fig. 3). As previously mentioned, the agreement between GRACE and the steric-corrected reconstructions during the period of overlap suggests that the mass changes measured by GRACE are primarily water mass induced. Relative minima occur in the mid-1970s, the early 1990s and early in the 2000s. Over the long-term, considering the period since 1970s, Mediterranean Sea water mass is seen to increase (this is consistent with

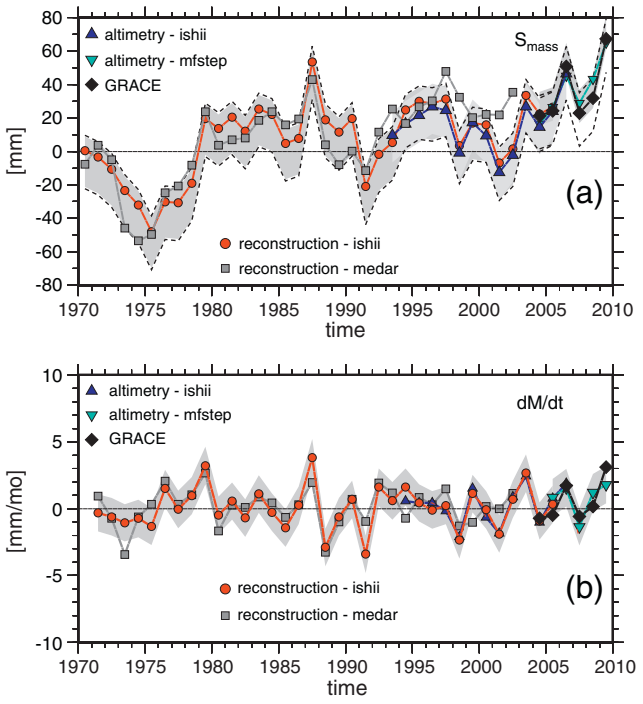

Fig. 3. Yearly mass-induced sea level anomaly in Mediterranean Sea (a) and its time derivative (b) over the period 1970–2009. Shown are estimates based on the steric-corrected sea-level reconstruction using two different steric corrections (squares for Medar/Medatlas and circles for Ishii), on the steric-corrected sea-level altimetry using two different steric corrections (inverted triangles from MFSTEP and triangles from Ishii) and on GRACE-based mass retrievals (diamonds). Bounds in (a) correspond both to error propagation of components (dashed line) and to RMS difference of solutions derived from input data in Figs. 1 and 2 (gray shadow). In (b) only bounds corresponding to RMS of solutions are shown.

Calafat et al., 2010). The trend over the period 1970–2006 is 0.88 +/− 0.33 mm/yr based on the reconstruction corrected for the Ishii steric component. Considering the extended time series (1970–2009), that combines the reconstruction- and the GRACE-based S_{mass}, the trend is 1.1 +/− 0.3 mm/yr.

The estimate of the annual error of the mass-induced sea-level S_{mass}, derived by error propagation from the errors of S_{tot} and S_{ster} is 16 mm (dashed line in Fig. 3a), in very good agreement with the above obtained RMS difference-based error of 15 mm (shaded bounds in Fig. 3.a). The annual error of GRACE-derived mass-induced sea-level S_{mass} is smaller (7 mm, see also Fenoglio-Marc et al., 2012). We finally assume a value of 16 mm for the annual error of the combined mass-induced sea-level S_{mass} over 1970–2009 (Table 4).

Finally, the annual mean water mass change ∂M/∂t (the term that actually enters Eq. 1) is derived over 1970–2009 as the difference of the combined mass-induced sea level S_{mass} at two following time steps (Fig. 3b). The timeseries shows interannual ∂M/∂t values of up to 3–4 mm/mo, its standard deviation is 1.8 mm (1.6 mm in 1979–2001, see Table 5). The overall ∂M/∂t mean is 0.14 mm/mo as there is an overall mass increase over the period of consideration. However there is no significant ∂M/∂t trend over the period of consideration (trend value for the ∂M/∂t based on mass estimates from the reconstruction and Ishii steric correction is 0.018 +/− 0.024 mm/mo per year). It is interesting to note that ∂M/∂t is small, as it is indeed often assumed to be according to the "equilibrium condition"; hence based on the water budget equation (Eq. 1) we find a first order compensation between G and other terms of Mediterranean Sea water cycle, primarily E and P (another common assumption).

We obtain for ∂M/∂t an annual error of 23 mm, from error propagation of S_{mass}. The annual error of the GRACE-based mass-induced sea-level ∂M/∂t is smaller (10 mm). Also the RMS difference of the various estimates of ∂M/∂t derived from various sea-level and steric data is significantly smaller (1.5 mm) (Table 4). The standard deviation of ∂M/∂t is 1.6 mm and therefore much smaller than its error.

3.2. Gibraltar water flux variability

Next, remaining Mediterranean Sea water cycle terms are considered in order to close the water budget (Eq. 1) and derive G variability over the period 1960–2010 (see Fig. 4; see Tables 2,3 for correlation and RMS difference of the yearly time-series and Table 5 for a comparison of observed and simulated trends over the period). Both observational and PROTHEUS-simulated estimated annual mean anomalies relative to the period 1979–2001 are considered for comparison (as available). Note that the PROTHEUS simulation is forced at the atmospheric boundaries by ERA40 reanalyses, independent from the observational estimates presented here. Mediterranean Sea averaged evaporation from OAFLUX data shows an initial decrease 1960 to the mid-1970s, followed by an increase up until the most recent period (trend over 1979–2001 is 0.43 +/− 0.09 mm/mo per year; see Mariotti, 2010 for more discussion on decadal variability of Mediterranean Sea evaporation). PROTHEUS-simulated evaporation shows a similar decadal variability over the whole period, with basically no increase during 1979–2001 (Fig. 4.a)

GPCP precipitation shows a negative trend over the period 1979–2001 (−0.31 +/− 0.13 mm/mo per year), similarly to the

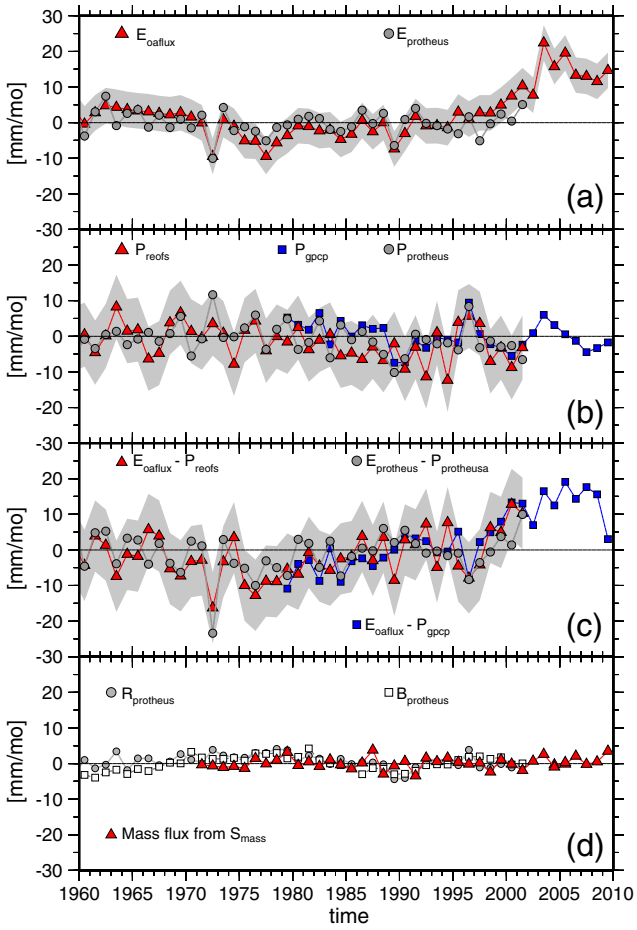

Fig. 4. Yearly anomalies of Mediterranean Sea water cycle components in water budget equation (Eq. 1) during 1960–2009 relative to the period 1979–2001. From top to bottom: Evaporation (a), Precipitation (b), E-P (c), Bosphorus water flux, river discharge and time derivative of mass-induced sea level (Fig. 3b) (d) from model simulations (gray) and observations. Legend specifies data source. Error bounds in (a–b–c) correspond to the RMS difference of data input from databases (gray shadow).

PROTHEUS-simulated one except the latter is smaller and weakly significant (Fig. 4.b). REOF reconstruction also shows a precipitation decrease during 1979–2001 that is similar to GPCP but in the context of a long-term decrease during the period since 1960 (see also Mariotti, 2010). Correlation and RMS difference of the GPCP and REOF precipitation yearly values are 0.4 and 4.9 mm/mo respectively, correlation is significant at the 95% level (Table 2). The correlation of simulated and observed evaporation and precipitation quantities are all significant, except for precipitation from REOFS (Table 3). Their RMS differences are 4 mm/mo for evaporation and 6 mm/mo for precipitation (Table 3); we adopt these values as the RMS-based errors for the two quantities (see Table 4). We finally assume an error of 5 mm/mo and 10 mm/mo for the two quantities, thus error propagation gives a result of 11 mm/mo for E-P.

Based on the observational estimates, the combination of the evaporation increase seen in OAFLUX data and precipitation decrease seen in GPCP gives a significant increase in net evaporation (E-P) over the period 1979–2001 (Fig. 4.c). Observationally derived trend over 1979–2001 is 0.74 +/− 0.13 mm/mo per year. Simulated net evaporation trend is also seen to be positive, albeit weakly significant. The GPCP/OAFLUX E-P estimates indicate that the increase has been continuing up until the recent period (trend over 1979–2009 is 0.79 +/− 0.1 mm/mo per year). Error propagation gives a result of 11 mm/mo for E-P (Table 4), while the RMS-based error computed from various datasets is lower than 6.2 mm/mo (Tables 2, 3).

Since observational river discharge and Bosphorus water flux anomalies are not available for the period of investigation, we consider the simulated quantities as a surrogate (in any case, as previously discussed these are second order terms in Eq. 1). Simulated river discharge shows a significant negative trend over 1979–2001 (−0.1 +/− 0.06 mm/mo per year; Table 5), consistent with simulated precipitation behavior. Simulated water flux at the Bosphorus Strait does not indicate a significant trend. Relying on a single run of a single model we cannot attribute an error bar to such estimate, however this fact does not impair our results, as the river runoff is, together with the Bosphorus the smallest term in Eq. (1) and does not exceed the 20% of the E-P budget (Mariotti et al., 2002). This relationship holds also in our analysis (see Table 5) between the standard deviations of the R and B simulated time-series (2 and 2.2 respectively) and of E-P observed (8.2 mm/mon) and simulated (5.7 mm/mo) (Table 5). A similar relationship holds for the rate of mass change ∂M/∂t (Fig. 4.d), as the standard deviation of ∂M/∂t is 1.6 mm/mo (Table 5) and therefore smaller than for all the other components in Eq. (1).

Combining observational E and P estimates with simulated R and B, we obtain estimates of the overall mean fresh water budget anomalies that have characterized the Mediterranean Sea over 1979–2001. Interannual anomalies are of the order of 5–10 mm/mo with a linear trend over 1979–2001 of 0.84 +/− 0.20 mm/mo per year (this trend value is based on GPCP precipitation, OAFLUX evaporation and simulated R and B), that is a linear increase of about 19 mm/mo in total over this period. The corresponding simulated fresh water budget quantity also shows an increase, however trend value is smaller than observed (0.25 +/− 0.20 mm/mo per year or about 6 mm/mo in total over this period). Error propagation gives an error of 11 mm/mo for E-P-R-B, if we neglect the errors of R and B. If we assume for R and B an error equal to their standard deviation (2 mm/mo, Table 4), the resulting error is not significantly different.

Finally, we combine the fresh water budget changes discussed above with mass changes ∂M/∂t as derived in the previous section to depict Gibraltar water flux (G) variability during 1960–2009 based on the application of the water budget equation (Eq. 1) (see Fig. 5).

All G estimates, whether combining observational and PROTHEUS-simulated terms or derived purely from the PROTHEUS simulation, show an overall increase in the net water flux at Gibraltar since the mid-1970s. It is worth underlying that a priori the observationally derived G and the PROTHEUS simulated G could be quite different, because of the assumptions built-in the model, in primis the "equilibrium condition" assumption. The best agreement with the model is obtained when all components of Eq. (1) are included (correlation and RMS difference are 0.66 and 6 mm, see Table 3); neglecting R and B, the correlation drops to 0.59, with significance level still 99%. If one neglects R and B, and derives G purely based on observations (using estimated ∂M/∂t, OAFLUX evaporation and precipitation from either GPCP or REOFs), one still finds an increase in G since the mid-1970s that is consistent with the PROTHEUS simulated G estimate. Based on the combined observational/modeling approach we find for G a linear trend over the period 1979–2001 of 0.74 +/− 0.23 mm/mo per year (see Table 5), that is a linear increase of about 16 mm/mo over this period. The linear trend is even higher (0.80 +/− 0.21 mm/mo per year) when the recent years are included (period 1970–2009) even neglecting the contribution of R and B.

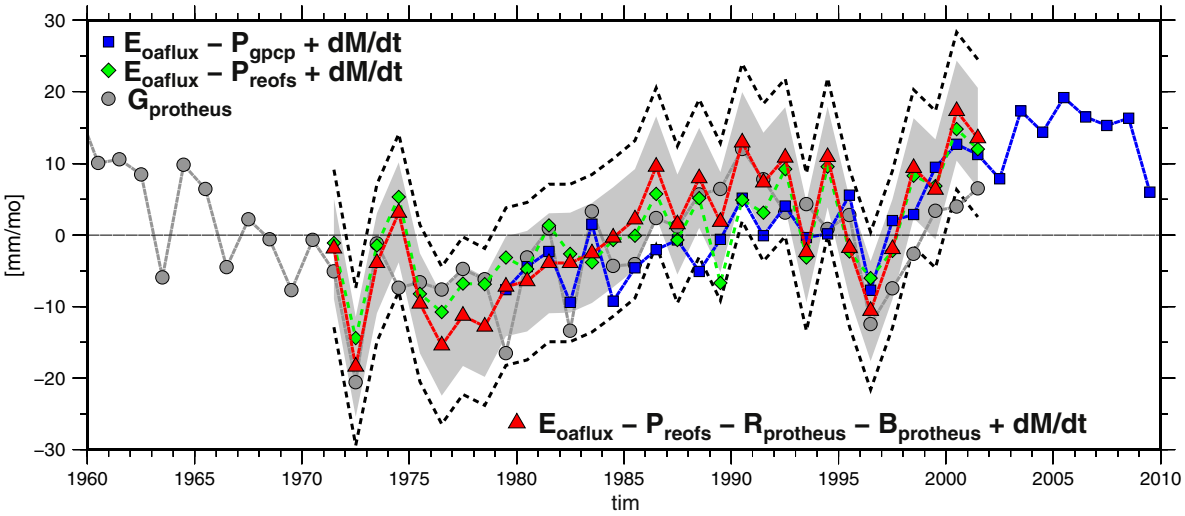

Fig. 5. Estimates of Gibraltar water flux anomalies during the period 1960–2010 (reference period is 1979–2001). Shown are yearly values from the PROTHEUS model simulation (circle) and from the water budget equation using observational estimates of E, P, ∂M/∂t and simulated R and B (triangle), and similar estimates neglecting R + B (square, diamond). E is from OAFLUX, P is from the REOFS and from GPCP, ∂M/∂t is from the steric corrected sea-level reconstruction using Ishii data. Error bounds correspond to the annual uncertainties given for E, P, E-P in Table 4. Bounds correspond both to error propagation of components including only E, P (black dashed line) and to RMS difference of solutions including all components in Fig. 4 (gray shadow).

Simulated G values give similar qualitative results, however with a 50% smaller trend (0.34 +/− 0.22 mm/mo per year or about 8 mm/mo over 1979–2001, see Table 5). Over the longer 1960–2000 period, the simulation indicates that the above mentioned G increase is in the context of broader decadal variations, with a decrease during 1960–1970 before the most recent increase; a similar result is found considering observational G estimates (based on REOFS P, OAFLUX E and ∂M/∂t, but neglecting B and R). This variability is seen to have been primarily forced by precipitation and evaporation over the Mediterranean Sea, as variations in mass in the basin have been found to be comparatively small (consistently with previous knowledge). Results suggest that the increase in the fresh water loss at the sea-surface, as also found by Mariotti (2010), is compensated mainly by an increase in water fluxes at Gibraltar, with little change in ∂M/∂t. As previously noted, this is an assumption built-in the PROTHEUS model (as in most state-of-art Mediterranean Sea models), which we find *a posteriori* to be well verified by the observational ∂M/∂t estimates.

The accuracy of the Gibraltar Strait flow is almost independent from the accuracy of the rate of change of mass in the basin, river runoff and the Bosphorus strait flow, as their magnitude is small when compared to the effect of evaporation and precipitation on the resulting Gibraltar net flux. The error estimate of G, derived by error propagation from each component in Table 4, is 25 mm. This value is 3 times larger than the RMS difference (7 mm) of the various solutions obtained for G from the available data and models. For a realistic error estimate only the errors in E and P are considered and give an error of 11 mm/mo for the Gibraltar Strait flow.

3.3. Large-scale influences

In order to gain some insights on the mechanisms driving the long-term Gibraltar water flux changes described above, we explore the relationship with major large-scale climate phenomena known to have had significant influence on decadal climate variability over the Mediterranean region (Mariotti and Dell'Aquila, 2012). Fig. 6a shows the DJFM means of the NAO index (NAO_{DJFM}) and Mediterranean mean P, R and sea level pressure (SLP), with a 6-year moving average applied (see Table 6 for correlation values among the various time-series). Consistently with previous studies, the NAO shows a significant negative correlation with regional precipitation (−0.70 based on REOFS). In addition we also find a significant negative correlation with regionally averaged simulated river-discharge (−0.77; as also shown by Struglia et al. (2004), based on observational river discharge). All correlations are significant at the 99% level. Observed NAO variability during 1960–2009, with a well-known long-term increase during the 1960s to the early 1990s (Hurrell, 1995), has resulted in a precipitation and river discharge decrease during winter with an overall effect on annual means of these water cycle quantities. This in turn has contributed to increase the Mediterranean Sea fresh water budget (E-P-R) and related water fluxes at Gibraltar based on results from this work.

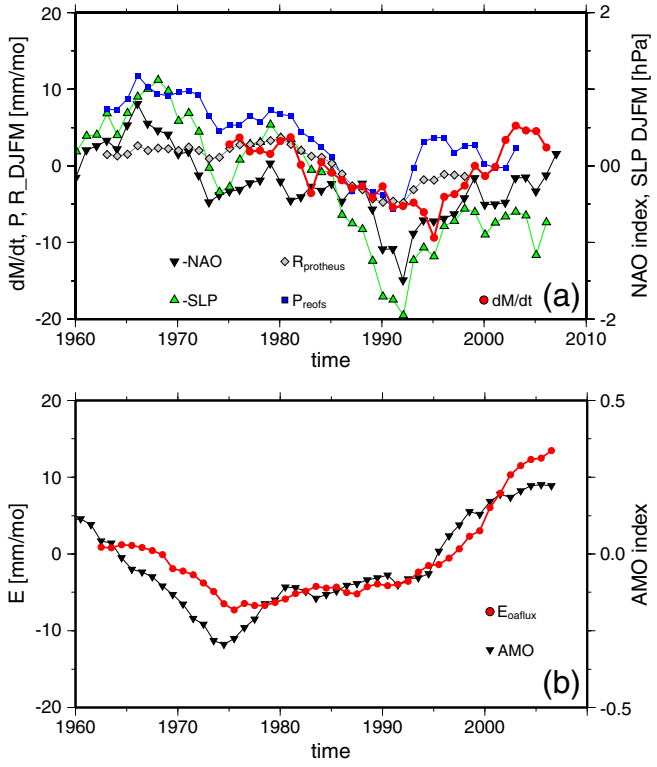

Fig. 6. Influence of large-scale climate modes on Mediterranean water mass budget components. DJFM yearly values of NAO index and anomalies of P, R sea level pressure, ∂M/∂t (note: the signs of the NAO and SLP are reversed) (top panel) and yearly values of the AMO index and of OAFLUX evaporation anomalies (bottom panel). For all, a six-year running mean is shown to focus on long-term anomalies.

Table 6
Correlation and significance of climatic index with variables in 1970–2006. For sea level the component type is indicated by the subscript (tot: total sea level; ster: steric sea level; thermo-ster: thermo-steric sea level; halo-ster: halo-steric sea level; mass: mass induced sea level).

Climatic index	Field	Correlation	Significance (%)
NAO_{DJFM}	∂M/∂t	0.64	99
NAO_{DJFM}	SLP (HadSLP)	0.81	99
NAO_{DJFM}	P_{reofs}	−0.70	99
NAO_{DJFM}	$R_{protheus}$	−0.77	99
AMO	E_{oaflux}	0.9	99

Previous studies have suggested the NAO also impacts Mediterranean sea-level owing to the inverse barometer effect (IB) (e.g. as described by Tsimplis and Josey, 2001). However in our study the altimeter data have been corrected for direct atmospheric effects including the IB and the PROTHEUS model does not simulate the effect of pressure. Therefore the effects of the NAO through local pressure have been removed and should not impact estimated mass changes and Gibraltar fluxes. However, for DJFM, we find an anti-correlation between the NAO index and regionally averaged sea level pressure SLP (−0.81) and also a significant anti-correlation between the NAO and Mediterranean rate of mass change ∂M/∂t (−0.64). These results suggests that the NAO may affect the mass component of sea level S_{mass} through mechanisms associated to redistribution of water, other than the atmospheric pressure changes. Those mechanisms could be associated to winds near the Gibraltar strait (Menemenlis et al., 2007) and to ocean circulation. However, these hypotheses need to be substantiated by targeted process studies.

Recent studies have shown a significant connection between Mediterranean Sea SST and the AMO, as well a connection between regional surface air temperature and the AMO particularly during the summer season (Marullo et al., 2011; Mariotti and Dell'Aquila, 2012). Because of the impact temperature can have on the humidity gradient and sea surface evaporation, we investigate the linkage between the AMO and Mediterranean Sea evaporation variability. Fig. 6b, shows 6-years running means of OAFLUX annual Mediterranean Sea evaporation anomalies together with those of the AMO index. We find significant positive correlation between evaporation and the AMO (0.9) which is consistent with the thermodynamical linkage hypothesized above. Again, this speculated connection needs to be investigated by further studies using different evaporation datasets and in-depth analyses of the thermodynamic changes associated with AMO variability in the Mediterranean. If confirmed, our study suggests that the impact of AMO variability on Mediterranean Sea is not only confined to Mediterranean SST (as also suggested

by Mariotti and Dell'Aquila, 2012) but also affects the sea more broadly with evaporation-driven changes in Gibraltar water fluxes.

4. Conclusions

We have explored the long-term variability of net water flux into the Mediterranean Sea at the Gibraltar Strait over the period 1960–2009 based on an approach combining multiple observational datasets and results from a regional climate model simulation. The approach includes deriving Gibraltar water fluxes from the application of the full Mediterranean Sea water budget equation using observationally based estimates of mass variation (from GRACE satellite and indirect derivations from steric-corrected sea level changes from altimetry and a sea-level reconstruction), evaporation, precipitation and simulated river discharge and Bosphorus Strait water fluxes. This derivation is compared with results from a simulation using the PROTHEUS regional ocean–atmosphere coupled model considering both individual water cycle terms and overall Gibraltar water flux.

Based on observational estimates of Mediterranean Sea mass, we find that its changes are relatively small compared to water fluxes at the sea surface and with no long-term trend over 1970–2009. Hence, the "equilibrium condition" assumption, common to many Mediterranean Sea models is indeed a reasonable one. As a result, decadal variations in net evaporation (E-P) at the sea-surface drive changes in net inflow at Gibraltar as dictated by the water budget equation, while changes in river runoff and net inflow at the Bosphorus Strait have a secondary modulating effect. Estimates from this approach have been compared to the PROTHEUS simulated Gibraltar Strait water fluxes over the period 1960–2001. Results from both methodologies point to an increase in net water flux at Gibraltar over the period 1970–2009 ($0.8 +/- 0.2$ mm/mo per year based on the observational approach) primarily resulting from an increase in evaporation and a decrease in precipitation during this period. Above mentioned G increase over 1970–2009 is in the context of broader decadal including a net Gibraltar water flux decrease during 1960–1970 before the 1970–2009 increase, as found in both observations and the model simulation.

The accuracy of the Gibraltar Strait flow is virtually independent from the accuracy in the rate of change of mass in the basin, river runoff and Bosphorus strait flow, as their effect on the resulting Gibraltar net flux is small compared to the effect of evaporation and precipitation. Uncertainties associated with variations of evaporation and precipitation, underlying the observational derivation of Gibraltar fluxes, are particularly hard to quantify when dealing with decadal timescales. By means of data intercomparison, Mariotti (2010) showed that although differences exist in the amplitude of the evaporation increase from the mid-1990 to late 2010s, this increase is a robust feature of all analyzed datasets; similarly precipitation decrease from the mid-1970 to the mid-1990s is also a robust feature seen in various observational datasets. Hence, the increase in Gibraltar water fluxes over this period we derive based on observational datasets is also likely to be a robust feature although the exact amplitude of the increase needs to be further investigated. An additional boost in confidence in the results for G, is given by the fact that the PROTHEUS system independently simulates decadal G variability that is qualitatively similar to that derived from observations. *A priori*, because of the model's built-in assumptions (*in primis* the "equilibrium condition" assumption), the observational and model G derivations could have significantly differed. *A posteriori* we find that they don't because, as we find in our observational analysis, the equilibrium assumption is indeed a reasonable one.

Our investigation points to an important role for large-scale climate variability, specifically the Atlantic Multi-decadal Oscillation (AMO) and the North Atlantic Oscillation (NAO) climate modes, in driving observed Gibraltar fluxes which needs to be further investigated. These climate modes appear to influence net water flux at Gibraltar indirectly via the influence they bear on regional evaporation, precipitation and runoff.

Supplementary data to this article can be found online at http://dx.doi.org/10.1016/j.gloplacha.2012.08.007.

Acknowledgments

We thank L. Li and an anonymous reviewer for their comments that helped to significantly improve our manuscript. We acknowledge A. Cazenave for helpful discussions, M. Tsimplis and A. Shaw for support in providing the Medar/Medatlas data. This study was partly carried out in the frame of the projects STREMP funded by the DFG/SPP1257 and TOPO-EUROPE funded by the EU. The PROTHEUS model simulation has been performed as part the CIRCE Integrated Project, funded under the European Commission's Sixth Framework Program.

References

Adler, R.F., et al., 2003. The version-2 Global Precipitation Climatology Project (GPCP) monthly precipitation analysis (1979–present). Journal of Hydrometeorology 4, 1147–1167.

Adler, Robert F., Guojun, Gu., Huffman, George J., 2012. Estimating Climatological Bias Errors for the Global Precipitation Climatology Project (GPCP). Journal of Applied Meteorology and Climatology 51, 84–99. http://dx.doi.org/10.1175/JAMC-D-11-052.1.

Allan, R., Ansell, T., 2006. A new globally complete monthly historical gridded mean sea level pressure dataset (HadSLP2): 1850–2004. Journal of Climate 19 (22), 5816–5842.

Artale, V., et al., 2010. An atmosphere–ocean regional climate model for the Mediterranean area: assessment of a present climate simulation. Climate Dynamics 35, 721–740.

Calafat, F., Gomis, D., 2009. Reconstruction of Mediterranean sea level fields for the period 1945–2000. Global and Planetary Change 66, 225–234. http://dx.doi.org/10.1016/j.gloplacha.2008.12.015.

Calafat, F.M., Marcos, M., Gomis, D., 2010. Mass contribution to Mediterranean Sea level variability for the period 1948–2000. Global and Planetary Change 73, 193–201. http://dx.doi.org/10.1016/j.gloplacha.2010.06.002.

Carillo, A., Sannino, G., Artale, V., Ruti, P.M., Calmanti, S., Dell'Aquila, A., 2012. Steric sea level rise over the Mediterranean Sea: present climate and scenario simulations. Climate Dynamics. http://dx.doi.org/10.1007/s00382-012-1369-1.

Criado-Aldeanueva, F., Soto-Navarro, X., Garcia-Lafuente, J., 2010. Seasonal and interannual variability of surface heat and freshwater fluxes in the Mediterranean Sea: budgets and exchange through the Strait of Gibraltar Int. Journal of Climatology. http://dx.doi.org/10.1002/joc.2268.

Dell'Aquila, A., Calmanti, S., Ruti, P., Struglia, M.V., Pisacane, G., Carillo, A., Sannino, G., 2012. Impacts of seasonal cycle fluctuations in an A1B scenario over the Euro-Mediterranean region. Climate Research 52, 135–157. http://dx.doi.org/10.3354/cr01037.

Efron, B., Tibshirani, R.J., 1993. An introduction to the Bootstrap. Chapman & Hall, CRC Monographs on Statistics & Applied Probability.

Enfield, D.B., et al., 2001. The Atlantic Multidecadal Oscillation and its relationship to rainfall and river flows in the continental U.S. Geophysical Research Letters 28, 2077–2080.

Fenoglio-Marc, L., Kusche, J., Becker, M., Fukumori, I., 2007. Comments on "On the steric and mass-induced contributions to the annual sea level variations in the Mediterranean Sea" by D. Garcia et al. Journal of Geophysical Research 112, C12018. http://dx.doi.org/10.1029/2007JC004196.

Fenoglio-Marc, L., Braitenberg, C., Tunini, L., 2012a. Sea level variability and trends in the Adriatic Sea in 1993–2008 from tide gauges and satellite altimetry. Physics and Chemistry of the Earth 40–41, 47–58. http://dx.doi.org/10.1016/j.pce.2011.05.014.

Fenoglio-Marc, L., Rietbroek, R., Grayek, S., Becker, M., Kusche, J., Stanev, E., 2012b. Water mass variation in the Mediterranean and Black Sea. Journal of Geodynamics 59–60, 168–182. http://dx.doi.org/10.1016/j.jog.2012.04.001.

Fenoglio-Marc, L., Kusche, J., Becker, M., 2006. Mass variation in the Mediterranean Sea from GRACE and its validation by altimetry, steric and hydrologic fields. Geophysical Research Letters 33, L19606. http://dx.doi.org/10.1029/2006GL026851.

Flechtner F. (2007) GFZ level-2 processing standards documents for level-2 product release 4, GRACE 327–743, Rev. 1.0.

Fofonoff, 1977. Computation of potential temperature of sea water for an arbitrary reference pressure. Deep Sea Research 24, 489–491.

Grayek, S., Stanev, E., Kandilarov, R., 2010. On the response of Black Sea o external forcing: altimeter data and numerical modelling. Ocean Dynamics 60, 123–140.

Greatbatch, R.J., Lu, Y., 2001. Relaxing the Boussinesq Approximation in Ocean Circulation Models. Journal of Atmospheric and Oceanic Technology 1911–1923.

Hurrell, J.W., 1995. Decadal trends in the North-Atlantic Oscillation – regional temperatures and precipitation. Science 269 (5224), 676–679.

Hurrell, J.W., et al., 2003. The North Atlantic Oscillation: Climate Significance and Environmental Impact. p. 279.

Ishii, M., Kimoto, M., 2009. Reevaluation of Historical Ocea Heat Content Variations with Time-Varying XBT and MBT Depth Bias Corrections. Journal of Oceanography 65, 287–299.
Jones, P.D., et al., 1997. Extension to the North Atlantic Oscillation using early instrumental pressure observations from Gibraltar and south-west Iceland. International Journal of Climatology 17 (13), 1433–1450.
Levitus, S., 1982. Climatological Atlas of the World Ocean. NOAA Professional Paper 13. U.S. Government Printing Office, Washington D.C. 173pp.
Mariotti, A., 2010. Recent Changes in the Mediterranean Water Cycle: A Pathway toward Long-Term Regional Hydroclimatic Change? Journal of Climate 23.
Mariotti, A., Dell'Aquila, A., 2012. Decadal climate variability in the Mediterranean region: roles of large scale forcing and regional processes. Climate Dynamics. http://dx.doi.org/10.1007/s00382-011-1056-7.
Mariotti, A., Struglia, M.V., Zeng, N., Lau, K.M., 2002. The hydrological cycle in the mediterranean region and implications for the water budget of the Mediterranean Sea. Journal of Climate 15, 1674–1690.
Marshall, J., Adcroft, A., Hill, C., Perelman, L., Heisey, C., 1997. A finitevolume, incompressible navier stokes model for, studies of the ocean on parallel computers. Journal of Geophysical Research 102 (C3), 5753–5766.
Marullo, S., Artale, V., Santoleri, R., 2011. The SST multidecadal variability in the Atlantic–Mediterranean region and its relation to AMO. Journal of Climate 24, 4385–4401. http://dx.doi.org/10.1175/2011JCLI3884.1.
MEDAR Group, 2002. Medatlas/2002 Database. Mediterranean and Black Sea Database of Temperature Salinity and Bio-chemical Parameters, Climatological atlas, IFREMER Edition.
Menemenlis, D., Fukumori, J., Lee, T., 2007. Atlantic to Mediterranean Sea level difference driven by winds near Gibraltar Strait. Journal of Physical Oceanography 37, 359–376.
Meyssignac, B., Calafat, F.M., Somot, S., Rupolo, V., Stocchi, P., Llovel, W., Cazenave, A., 2011. Two-dimensional reconstruction of the Mediterranean sea level over 1970–2006 from tide gauge data and regional ocean circulation model outputs. Global and Planetary Change 77 (1–2), 49–61. http://dx.doi.org/10.1016/j.gloplacha.2011.03.002.
Naeije, M., Scharroo, R., Doornbos, E., Schrama, E., 2008. Global altimetry sea-level service: Glass, NUSP-2 report GO 52320 DEO. NIVR/DEOS, Netherlands.
Pal, J.S., Giorgi, F., Bi, X., Elguindi, N., Solmon, F., Gao, X., Rauscher, S., Francisco, R., Zakey, A., Winter, J., Ashfaq, M., Syed, F., Bell, J., Diffenbaugh, N., Karmacharya, J., Konar´e, A., Martinez, D., da Rocha, R., Sloan, L., Steiner, A., 2007. Regional climate modeling for the developing world: the ictp regcm3 and regcnet. Bulletin of the American Meteorological Society 88, 1395–1409.
Rixen, M., Beckers, J.M., Levitus, S., Antonov, J., Boyer, T., Maillard, C., Fichaut, M., Baloupos, E., Iona, S., Dooley, H., Garcia, M.-J., Manca, B., Giorgetti, A., Manzella, G., Mikhailov, N., Pinardi, N., Zavatarelli, M., 2005. The Western Mediterranean Deep Water: a proxy for climate change. Geophysical Research Letters 32, L12608. http://dx.doi.org/10.1029/2005GL022702 (2949-2952).
Sanchez-Garrido, J.C., Sannino, G., Liberti, L., Garcıa-Lafuente, J., Pratt, L., 2011. Numerical Modelling of Three-Dimensional Stratified Tidal Flow Over Camarinal Sill. Strait of Gibraltar, Journal of Geophysical Research, 116, C12. http://dx.doi.org/10.1029/2011JC007093.
Sanchez-Roman, A., Sannino, G., Garcia-Lafuente, J., Carillo, A., Criado-Aldeanueva, F., 2009. Transport estimates at the western section of the Strait of Gibraltar: a combined experimental and numerical modeling study. Journal of Geophysical Research 114, C06002. http://dx.doi.org/10.1029/2008JC005023.
Sannino, G., Carillo, A., Artale, V., 2007. Three-layer view of transports and hydraulics in the Strait of Gibraltar: a three-dimensional model study. Journal of Geophysical Research 112, C03010. http://dx.doi.org/10.1029/2006JC003717.
Sannino, G., Pratt, L., Carillo, A., 2009a. Hydraulic criticality of the exchange flow through the Strait of Gibraltar. Journal of Physical Oceanography 39 (11), 2779–2799. http://dx.doi.org/10.1175/2009JPO4075.1.
Sannino, G., Herrmann, M., Carillo, A., Rupolo, V., Ruggiero, V., Artale, V., Heimbach, P., 2009b. An eddy-permitting model of the Mediterranean Sea with a two-way grid refinement at the Strait of Gibraltar. Ocean Modelling 30 (1), 56–72.
Santer, B.D., Wigley, T.M.L., Boyle, J.S., Gaffen, D.J., Hnilo, J.J., Nychka, D., Parker, D.E., Taylor, K.E., 2000. Statistical significance of trends and trend differences in layer-average atmospheric temperature time series. Journal of Geophysical Research 105 (D6), 7337–7356. http://dx.doi.org/10.1029/1999JD901105.
Sevault, F., Somot, S., Beuvier, J., 2009. A Regional Version of the NEMO Ocean Engine on the Mediterranean Sea: NEMOMED8 User's Guide. Note de centre n°107. CNRM, Toulouse, France.
Smith, T.M., Sapiano, M.R.P., Arkin, P.A., 2008. Historical reconstruction of monthly oceanic precipitation (1900–2006). Atmospheres 113, D17115. http://dx.doi.org/10.1029/2008JD009851.
Song, T., Hou, T., 2006. Parametric vertical coordinate formulation for multiscale Boussinesq, and non-Boussinesq ocean modeling. Ocean Modelling 11, 298–332.
Soto-Navarro, J., Criado-Aldeanueva, F., García-Lafuente, J., Sánchez-Román, A., 2010. Estimation of the Atlantic inflow through the Strait of Gibraltar from climatological and in situ data. Journal of Geophysical Research 115, C10023. http://dx.doi.org/10.1029/2010JC006302.
Struglia, M.V., Mariotti, A., Filograsso, A., 2004. River discharge into the Mediterranean Sea: climatology and aspects of the observed variability. Journal of Climate 17, 4740–4751.
Tonani, M., Pinardi, N., Dobricic, S., Pujol, I., Fratianni, C., 2008. A high-resolution free-surface model of the Mediterranean Sea. Ocean Science 4, 1–14.
Tsimplis, M., Josey, S., 2001. Forcing of the Mediterranean Sea by atmospheric oscillations over the North Atlantic. Geophysical Research Letters 2001 (28), 803–806,5.
Uppala, S.M., KÅllberg, P.W., Simmons, A.J., Andrae, U., Bechtold, V.D.C., Fiorino, M., Gibson, J.K., Haseler, J., Hernandez, A., Kelly, G.A., Li, X., Onogi, K., Saarinen, S., Sokka, N., Allan, R.P., Andersson, E., Arpe, K., Balmaseda, M.A., Beljaars, A.C.M., Berg, L.V.D., Bidlot, J., Bormann, N., Caires, S., Chevallier, F., Dethof, A., Dragosavac, M., Fisher, M., Fuentes, M., Hagemann, S., Hólm, E., Hoskins, B.J., Isaksen, L., Janssen, P.A.E.M., Jenne, R., Mcnally, A.P., Mahfouf, J.-F., Morcrette, J.-J., Rayner, N.A., Saunders, R.W., Simon, P., Sterl, A., Trenberth, K.E., Untch, A., Vasiljevic, D., Viterbo, P., Woollen, J., 2005. The ERA-40 re-analysis. Quarterly Journal of the Royal Meteorological Society 131, 2961–3012.
Valcke, S., Redler, R., 2006. OASIS3 User Guide. PRISM support initiative report, 4. 60 pp.
Yu, L., Jin, X., Weller, R.A., 2008. Multidecade global flux datasets from the Objectively Analyzed Air–Sea Fluxes (OAFlux) Project: Latent and Sensible Heat Fluxes, Ocean Evaporation, and Related Surface Meteorological Variables. Woods Hole Oceanographic Institution OAFlux Project Tech. Rep. OA-2008-01. 64 pp.

3.3 L'océan Arctique

L'Arctique n'est pas une région vulnérable à la montée du niveau de la mer en terme de quantité de population menacée. En effet, la région compte moins de 10 millions d'habitants répartis sur une côte de 45 000 km de long dont une grande partie subit un mouvement vertical ascendant considérable (ce qui donne un niveau de la mer relatif local qui descend) du fait du GIA. En revanche d'un point de vue climatique, c'est une région très sensible au changement climatique global. La région Arctique a connu un réchauffement plus rapide que le reste de la planète sur les dernières décennies qui s'est traduit en pArticulier par une augmentation forte des températures atmosphériques et océaniques, une diminution du volume de glace continentale (en pArticulier au Groenland) et du volume de glace de mer (*Solomon et al.* [2007]). On observe aussi à plus basse latitude la fonte du permafrost, une diminution du volume d'eau de surface (assèchement des lacs Sibériens par exemple) et de la couverture neigeuse (*Solomon et al.* [2007]).

En ce qui concerne l'avenir, les différents modèles de climat s'accordent pour prédire en Arctique la plus forte montée du niveau de la mer d'ici 2100 (voir *Yin et al.* [2010]; *Pardaens et al.* [2011] et section 1.4.2). Ils attribuent cette augmentation à une baisse de la salinité dans l'océan Arctique qui ferait suite à la fonte des glaces de mer et des glaciers du Groenland et à une augmentation des précipitations et du débit des fleuves dans la région.

Les observations passées et récentes montrent que l'étendue des glaces de mer a déjà diminué de plus de 30% au cours des 30 dernières années (voir par exemple *Polyakov et al.* [2012]). De même, de nombreuses études ont montré que le Groenland perd de la masse depuis les années 1990 (au moins) et que cette perte s'est intensifiée (de $\sim$40%) depuis 2003-2004 (voir par exemple *Rignot et al.* [2011]). Enfin les mesures in-situ hydrographiques montrent aussi que la salinité diminue dans l'océan Arctique (*McPhee et al.* [2009]). Ces différents éléments révèlent qu'une partie des processus qui expliquent la montée du niveau de la mer en Arctique au cours du XXI$^{\text{ème}}$ siècle dans les modèles de climat est déjà en train de se réaliser depuis les années 1990, voire plus tôt encore. On peut donc s'attendre à observer une montée du niveau de la mer pArticulièrement rapide en Arctique sur les dernières décennies. C'est ce que nous avons cherché à déterminer dans l'étude intitulée "Tide gauge-based sea level variations since 1950 along the Norvegian and Russian coasts of the Arctic Ocean ; Contribution of the steric component"

Résumé de l'Arcticle : "Tide gauge-based sea level variations since 1950 along the Norvegian and Russian coasts of the Arctic Ocean ; Contribution of the steric component" (l'Arcticle original est inséré à la fin de cette section 3.3).
Dans cette étude nous analysons les données de 62 marégraphes qui se situent sur les côtes Norvégiennes et Russes de l'océan Arctique et qui couvrent une période d'une soixantaine d'années de 1950 à 2009. Sur la période totale, la moyenne des marégraphes indique une augmentation du niveau de la mer en Arctique de 1.6 mm.a^{-1} ce qui est en accord avec la moyenne globale du niveau de la mer. En revanche quand on regarde les variations inter-annuelles à multi-décennales, il apparait que le niveau de la mer est resté stable avec une tendance quasi nulle jusqu'en 1980 puis a augmenté fortement au rythme de 4.2 mm.a^{-1} de 1990 à 2009. Avant 1990 le niveau moyen des marégraphes est fortement corrélé à l'Oscillation Arctique (AO) qui est un mode de variabilité naturel de l'atmosphère sur la

région. Mais après 1990, il augmente fortement et ne suit plus l'AO. L'analyse des données thermostériques et halostériques in situ sur le gyre subpolaire Nord Atlantique, la mer du Nord, du Groenland et de Norvège indiquent aussi un changement significatif autour des années 1995 avec une soudaine augmentation des températures et de la salinité. Ces résultats se confirment le long des côtes Norvégiennes et Russes.

En résumé, sur les 60 dernières années, les marégraphes montrent que le niveau de la mer en Arctique n'a pas augmenté plus vite que la moyenne globale. Cependant ils montrent aussi un changement important vers les années 1995 qui se traduit par une augmentation très forte du niveau de la mer côtier en lien avec une augmentation des températures de la mer. Ces élèments suggèrent un changement dans la variabilité du niveau de la mer en Arctique vers 1995 qui aurait pour origine des modifications régionales de la structure thermo-haline de l'océan. Ces modifications semblent aussi liées à un changement dans les interactions atmosphère-ocean locales car avant 1995 on observait depuis plusieurs décennies une covariabilité du niveau de la mer avec l'AO qui est un mode de variabilité atmosphérique et qu'elle n'est plus visible depuis 1995 dans les données.

Il est intéressant de noter que la covariabilité du niveau de la mer avec l'AO avant 1995 (et l'absence de covariabilité après 1995) est encore vrai lorsque l'on ne considère que les marégraphes du secteur Norvégien ou que les marégraphes du secteur Russe. Ceci tend à montrer que le changement détecté en 1995 se fait à grande échelle. Cependant il est difficile de l'extrapoler à tout le bassin ou de se faire une idée de sa répartition spatiale car la répartition géographique des marégraphes est éparse et très fortement biasée vers l'Est du bassin.

Les nouvelles données altimétriques produites par *Prandi et al.* [in press] sur l'Arctique permettent d'obtenir des mesures qui couvrent une grande partie de l'océan Arctique (jusqu'à 82°N) sur la période 1993-2009. Ces données révèlent une forte variabilité régionale (voir Fig. 3.4) avec des tendances du niveau de la mer élevées au Sud du Groenland et dans le gyre de Beaufort. Mais en moyenne sur le bassin, elles donnent une courbe du niveau de la mer très proche de celle que nous avons obtenue à partir de la moyenne des marégraphes. Cela confirme la portée régionale à l'échelle de l'Arctique, des résultats côtiers que nous avons établis dans l'Arcticle *Henri et al.* [2012]. En pArticulier le changement de régime détecté en 1995 s'est probablement réalisé sur l'ensemble du bassin et pas seulemement le long des côtes ou sur le talus continental. Néanmoins, Il reste difficile de ce faire une idée des changements dans la variabilité 2D du niveau de la mer autour de 1995 avec l'altimétrie seulement car les données débutent en 1993. Pour pallier à ce problème, nous avons donc proposé une reconstruction du niveau de la mer en Arctique. Les reconstructions globales du niveau de la mer en 2 dimensions ne couvrent pas l'océan Arctique car en général les modèles ou les mesures dont sont extraites les EOFs pour l'interpolation spatiale ne couvrent pas cette région. De plus, les reconstructions globales que nous avons effectuées ne prenaient pas en compte les marégraphes de l'Arctique. Nous avons donc développé une reconstruction dédiée à l'océan Arctique en s'appuyant sur les nouvelles données altimétriques de *Prandi et al.* [in press] qui couvrent désormais une large part de l'Arctique et en utilisant les séries marégraphiques traitées dans l'Arcticle présenté plus haut. A la date de soumission de cette thèse les résultats sont encore préliminaires et semblent confirmer ceux de notre étude précédente mais une analyse plus approfondie est nécessaire pour s'en assurer.

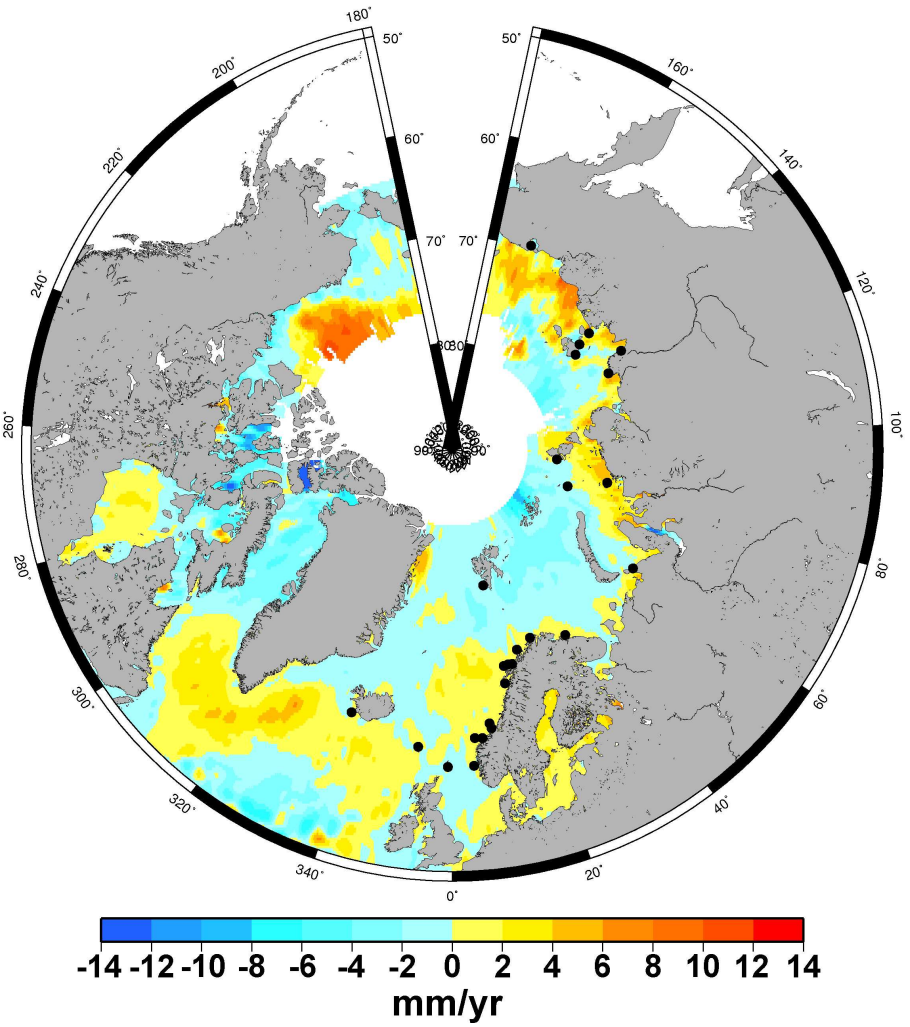

Figure 3.4 – Tendances régionales du niveau de la mer entre 1993 et 2009 estimée à partir des données retraitées de *Prandi et al.* [in press]. La tendance moyenne du bassin de 3.6 mm.a^{-1} a été retirée.

Tide gauge-based sea level variations since 1950 along the Norwegian and Russian coasts of the Arctic Ocean: Contribution of the steric and mass components

O. Henry,[1] P. Prandi,[2] W. Llovel,[3] A. Cazenave,[1] S. Jevrejeva,[4] D. Stammer,[5] B. Meyssignac,[1] and N. Koldunov[5]

Received 28 October 2011; revised 11 May 2012; accepted 13 May 2012; published 27 June 2012.

[1] We investigate sea level change and variability in some areas of the Arctic region over the 1950–2009 period. Analysis of 62 long tide gauge records available during the studied period along the Norwegian and Russian coastlines shows that coastal mean sea level (corrected for Glacial Isostatic Adjustment and inverted barometer effects) in these two areas was almost stable until about 1980 but since then displayed a clear increasing trend. Until the mid-1990s, the mean coastal sea level closely follows the fluctuations of the Arctic Oscillation (AO) index, but after the mid-to-late 1990s the co-fluctuation with the AO disappears. Since 1995, the coastal mean sea level (average of the Norwegian and Russian tide gauge data) presents an increasing trend of ∼4 mm/yr. Using in situ ocean temperature and salinity data down to 700 m from three different databases, we estimated the thermosteric, halosteric and steric (sum of thermosteric and halosteric) sea level since 1970 in the North Atlantic and Nordic Seas region (incomplete data coverage prevented us from analyzing steric data along the Russian coast). We note a strong anti-correlation between the thermosteric and halosteric components both in terms of spatial trends and regionally averaged time series. The latter show a strong change as of ∼1995 that indicates simultaneous increase in temperature and salinity, a result confirmed by the Empirical Orthogonal Function decomposition over the studied region. Regionally distributed steric data are compared to altimetry-based sea level over 1993–2009. Spatial trend patterns of observed (altimetry-based) sea level over 1993–2009 are largely explained by steric patterns, but residual spatial trends suggest that other factors contribute, in particular regional ocean mass changes. Focusing again on Norwegian tide gauges, we then compare observed coastal mean sea level with the steric sea level and the ocean mass component estimated with GRACE space gravimetry data and conclude that the mass component has been increasing since 2003, possibly because of the recent acceleration in land ice melt.

Citation: Henry, O., P. Prandi, W. Llovel, A. Cazenave, S. Jevrejeva, D. Stammer, B. Meyssignac, and N. Koldunov (2012), Tide gauge-based sea level variations since 1950 along the Norwegian and Russian coasts of the Arctic Ocean: Contribution of the steric and mass components, *J. Geophys. Res.*, *117*, C06023, doi:10.1029/2011JC007706.

1. Introduction

[2] During the past few decades, the Arctic region has warmed at a faster rate than the rest of the globe in response to anthropogenic climate change [*Intergovernmental Panel on Climate Change*, 2007]. Air temperature increase [e.g., *Bekryaev et al.*, 2010; *Chylek et al.*, 2010], sea ice extent and thickness decrease [e.g., *Kwok et al.*, 2009; *Stroeve et al.*, 2007] and Greenland ice sheet mass loss [e.g., *Holland et al.*, 2008; *Steffen et al.*, 2010; *Rignot et al.*, 2011] are now among the most visible effects of global warming in the Arctic region. Other phenomena have been reported as well, such as permafrost thawing [*Lawrence et al.*, 2008], drying of Siberian lakes [*Smith et al.*, 2005], Arctic Ocean surface warming [*Karcher et al.*, 2003; *Polyakov et al.*, 2005], decline in snow cover and lake ice [*Lemke et al.*, 2007], etc.

[3] Several studies have been dedicated to study Arctic sea level along the Russian coastlines [*Proshutinsky et al.*, 2001, 2004, 2007a, 2011]. *Proshutinsky et al.* [2004] estimated sea level change using data from Russian tide gauges released in

[1]LEGOS-OMP, Centre National de la Recherche Scientifique, Toulouse, France.
[2]Collecte Localisation Satellites, Ramonville, France.
[3]Jet Propulsion Laboratory, California Institute of Technology, Pasadena, California, USA.
[4]National Oceanography Centre, Liverpool, UK.
[5]Institute of Marine Sciences, University of Hamburg, Hamburg, Germany.

Corresponding author: O. Henry, LEGOS-OMP, Centre National de la Recherche Scientifique, 14 Ave. Edouard Belin, Toulouse F-31400, France. (olivier.henry@legos.obs-mip.fr)

0148-0227/12/2011JC007706

2003 by the Arctic and Antarctic Research Institute in St Petersburg (Russia). These authors found that over the period 1950–2000, the mean sea level along the Russian coastlines rose at a mean rate of 1.85 mm/yr after correcting for the Glacial Isostatic Adjustment (GIA) process. They estimated the different contributions to this rate of rise. Using an ocean model [*Häkkinen and Mellor*, 1992], they reported a contribution of 35% for the steric effects (due to ocean temperature and salinity variations). Decrease in atmospheric sea level pressure was found to account for 30% of the observed trend while winds had a minor role, accounting for ∼10% to the trend. Since then, the state of the sea level in the Siberian sector of the Arctic Ocean is provided annually by *Proshutinsky et al.* [2007b, 2009, 2011].

[4] In the present study we revisit the sea level variations over the 1950–2009 time span, considering all available tide gauge data in the Arctic sector, north of 55°N. Thus in addition to the Russian tide gauges, we also consider tide gauge data along the Norwegian coastlines (no tide gauge records from the Canadian Arctic region are long enough to be usable). We derive mean sea level time series for these two areas and a combined "mean" sea level time series representative of the whole Eurasian sector of the coastline is produced. The present work differs from previous published studies [e.g., *Proshutinsky et al.*, 2001, 2004] in several aspects: we consider tide gauge data in a larger region (Russian and Norwegian coastlines) and estimate the steric contribution (i.e., the effects of ocean temperature and salinity variations) from observations rather than models using in situ hydrographic measurements from three different databases. Because we focus on the steric component and for the purpose of improved comparison, we correct observed sea level for GIA and atmospheric pressure loading effect. Availability of spatially distributed temperature and salinity data in the North Atlantic and Nordic Seas sectors allows us also to investigate the spatiotemporal variability in steric sea level in that region since 1970. Finally we also present spatially distributed sea level from satellite altimetry since 1993 and perform comparisons with steric data over the altimetry period, and since 2002 with GRACE (Gravity Recovery and Climate Experiment)-based ocean mass.

2. Tide Gauge Sea Level Data From the Norwegian and Russian Sectors

[5] We use monthly Revised Local Reference (RLR) tide gauge records from the Permanent Service for Mean Sea Level (PSMSL) [*Woodworth and Player*, 2003]. Data have been downloaded from http://www.psmsl.org/. These records include 11 sites along the Norwegian coast, 48 sites along the Russian coast and 3 island sites (Reykjavik, Lerwick and Torshavn). Tide gauge data from the Russian sector have been released only a few years ago (2003) and start in the 1950s. These data were used by *Proshutinsky et al.* [2004] but at that time no data beyond 1999 were available. Fortunately, updated (up to 2009) sea level data from the Russian tide gauges are now available in the PSMSL database. Information about the Russian tide gauge data and their accuracy can be found in *Proshutinsky et al.* [2007a].

[6] We consider two sets of data: (1) almost continuous records over the period 1950–2009 (hereafter data set1) and (2) combination of records covering the whole 1950–2009 period and shorter records also starting in the 1950s but ending around year 1990 (data set2). In some cases a few data gaps are observed. If the gap is less than 3 years, we linearly interpolate the missing data. Otherwise we exclude the time series. This leaves us with 27 tide gauge records for data set1 (11 sites along the Norwegian coast, 3 island sites and 13 sites along the Russian coast with almost continuous data over 1950–2009). When adding the Russian tide gauges of data set1 the shorter records all located along the Russian coastlines, we obtain data set2 corresponding to a total of 48 Russian tide gauges time series. Location and site name for the 62 sites are shown in Figure 1 and Tables 1a and 1b.

[7] There are no tide gauges along the Canadian coastlines. In the PSMSL database a few tide gauge records from this region are available but non exploitable. They were much too short and generally affected by multi decade-long gaps. We explored the possibility to collect data in other databases (i.e., Fisheries and Oceans Canada) but could not find usable data for the purpose of the present study.

[8] As we focus here on interannual to multidecadal time scales, we removed the seasonal cycles from the monthly tide gauge sea level time series, by fitting sinusoids with periods of 12 and 6 months (after closing data gaps). As this procedure may not be optimal if seasonal cycles are not purely sinusoidal, we further applied a 12-month running mean smoothing to each tide gauge time series. Figure 2 shows for two tide gauge sites (Bergen, Norway and Anderma, Russia) the raw tide gauge time series, the raw time series after removing the 12-month and 6-month sinusoids and the smoothed time series (after applying a 12-month running mean smoothing to the raw tide gauge data corrected for the 12-month and 6-month cycles).

3. Effects of Glacial Isostatic Adjustment and Atmospheric Pressure on Coastal Sea Level

[9] Because in this study we focus on the steric sea level contribution to observed sea level, the tide gauge data need to be corrected for unrelated effects such as GIA and the effect of atmospheric pressure loading. We examine below these two effects.

3.1. GIA Effect at the Tide Gauge Sites

[10] We corrected the tide gauge-based sea level for GIA. The GIA correction is crucial in the Arctic region because this effect is of the same order of magnitude as (or even larger than) the sea level rates. We used different GIA models: *Peltier*'s [2004, 2009] models with different deglaciation histories (ICE-3G and ICE-5G) and different Earth's mantle viscosity structures (VM2 and VM4). We noticed quite large differences between the models in a number of sites. To illustrate this, Figure 3 compares GIA rates in the Arctic region from the ICE-5G model for the VM2 and VM4 viscosity structures and the ICE-3G model (VM2 viscosity structure). ICE-5G model gives GIA rates of much larger amplitude than ICE-3G. To a lesser degree, some differences are also noticed between the ICE-5G VM2 and VM4 viscosity structures. To discriminate between the various solutions, we decided to choose the model version that minimizes sea level trend differences between tide gauge-based and altimetry-based data during the altimetry period (1993–2009) at the considered tide gauge sites (see section 5).

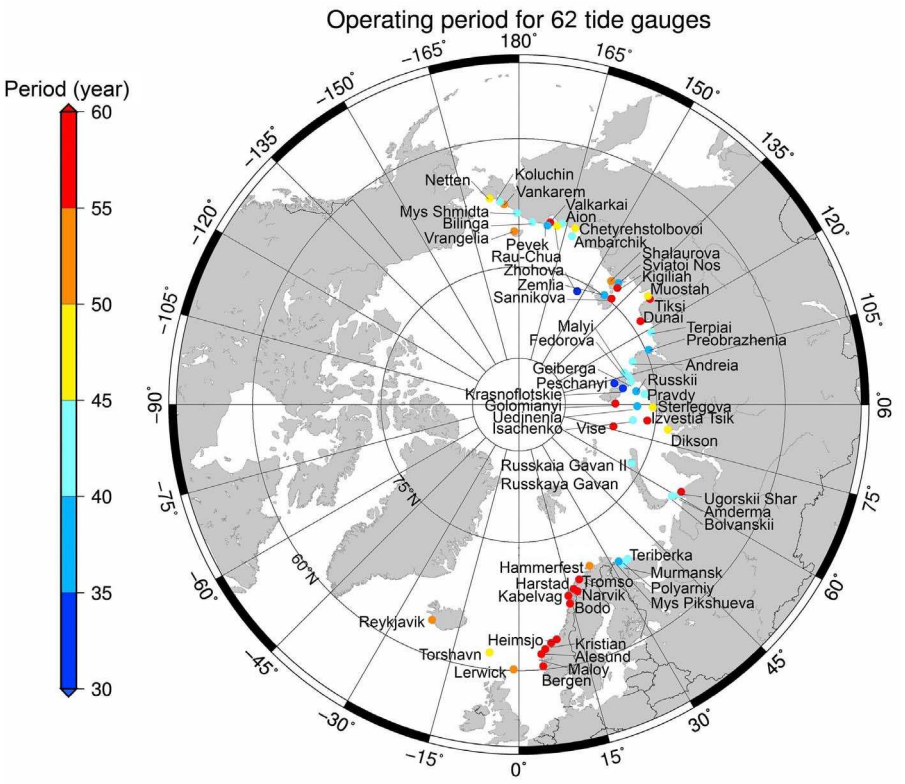

Figure 1. Distribution of the 62 tide gauges available in the Arctic region. Color indicates the length of the record in years as of 1950.

This led us to retain the ICE-5G/VM2 model to correct for GIA the tide gauge records. However, as we can see from Figure 3, differences between ICE-5G/VM2 and ICE-5G/VM4 are small in the Norwegian and Russian sectors, the region of interest in this study. In Tables 1a and 1b GIA trends (ICE5G-VM2 model) at each tide gauge site are given.

[11] Estimating the accuracy of the GIA correction is not an easy task. Some comparisons can be performed at some selected sites of the Norwegian coast between the preferred GIA correction used in this study and GPS-based crustal uplift rates. For example, using GPS precise positioning, *Vestøl* [2006] finds a crustal uplift in the range 1.2 mm/yr – 1.5 mm/yr in the southwesten part of Norway, in reasonable agreement with the ICE5G-VM2 GIA correction for the tide gauge of this area (see Tables 1a and 1b; note the reversed sign because the GIA correction is expressed in terms of equivalent sea level).

3.2. Atmospheric Pressure Loading

[12] *Proshutinsky et al.* [2001, 2004] studied in detail the effects on sea level of atmospheric loading and wind stress at the Russian tide gauge sites, using a 2-D coupled barotropic ocean-ice model (see details in the two references quoted above). Over the period 1950–1990/2000, they found that wind stress was responsible of the high frequency variability but caused insignificant trends in sea level, unlike the atmospheric pressure load that accounted for about 30% of the observed sea level trend. Unlike in *Proshutinsky et al.* [2004], we here do not correct sea level for wind stress effects. Partly this is justified since we are not interested in the high-frequency non static atmospheric response. On the other hand, changing wind-forcing results in a changing circulation which in turn leads to heat redistribution, hence to steric changes, i.e., the signal we are investigating here. Thus our preferred approach is to separately estimate steric changes, and then compare observed sea level with the steric component. On the other hand, we corrected for the static atmospheric pressure loading effect (also called inverted barometer effect, denoted IB hereafter) in the tide gauge records.

[13] To correct for the atmospheric loading effect we used surface pressure fields from the National Centers for Environmental Prediction (NCEP) [*Kalnay et al.*, 1996] (http://www.ncep.noaa. gov/), which are available on a 1.5° × 1.5° grid and at monthly intervals. To correct for the IB effect at the tide gauges sites, we tested three different methods: (1) using pressure data from the nearest grid point of the tide gauge site, (2) computing an average pressure within a 1° radius around the tide gauge, and (3) interpolating gridded pressure data at the tide gauge site. The three methods gave similar results. The IB correction was computed using the classical static correction relating sea level to surface atmospheric pressure [e.g., *Ponte*, 2006]. It should be stressed that this represents only the static response of sea level to atmospheric forcing. It is well known that dynamical effects also exist, in particular at short time scales (periods from hours to weeks) [*Wunsch and Stammer*, 1997]. Thus more realistic sea level responses to atmospheric forcing have been developed [e.g., *Carrère and Lyard*, 2003]. However, in such models, the model response is essentially similar to the static one on time scales longer than

Table 1a. Tide Gauge's Name, Country, Data Length and Location: GIA, IB and Tide Gauge Sea Level Trends at Each Tide Gauge Site (Data Set1)

Station	Country	Start–End Time	Coordinates		GIA ICE5G-VM2 (mm/yr)	IB (mm/yr)	Sea Level Trend (GIA and IB Corrected) (mm/yr)	
			Longitude (°E)	Latitude (°N)			Tide Gauge Operating Period	Altimetry Period
Reykjavik	Iceland	1956–2010	338.07	64.15	−1.23	0.21	3.42	7.43
Torshavn	Faroe Islands	1957–2006	353.23	62.02	1.31	0.37	0.11	4.76
Lerwick	United Kingdom	1950–2010	358.87	60.15	−0.12	0.24	−0.11	3.27
Maloy	Norway	1950–2010	5.12	61.93	−0.71	0.07	1.22	4.27
Bergen	Norway	1950–2010	5.30	60.40	−1.48	0.02	1.81	3.59
Alesund	Norway	1950–2010	6.15	62.47	−0.94	0.14	1.76	3.83
Kristian	Norway	1952–2010	7.73	63.12	−1.49	0.14	0.34	4.06
Heimsjo	Norway	1950–2010	9.12	63.43	−2.24	0.00	0.72	3.85
Bodo	Norway	1950–2010	14.38	67.28	−1.73	0.17	0.30	1.41
Kabelvag	Norway	1950–2010	14.48	68.22	−0.66	0.13	−0.28	2.44
Harstad	Norway	1952–2010	16.55	68.80	−1.12	0.30	−0.05	3.23
Narvik	Norway	1950–2010	17.42	68.43	−2.18	0.12	−0.29	1.67
Tromso	Norway	1952–2010	18.97	69.65	−1.30	0.27	1.09	3.16
Hammerfest	Norway	1957–2010	23.67	70.67	−1.71	0.27	2.33	4.44
Murmansk	Russia	1952–2010	33.05	68.97	−2.10	0.28	5.63	7.49
Amderma	Russia	1950–2009	61.70	69.75	−0.39	0.24	4.24	11.69
Vise	Russia	1953–2009	76.98	79.50	−2.66	0.29	2.62	0.38
Izvestia Tsik	Russia	1954–2009	82.95	75.95	−0.58	0.30	3.04	2.83
Golomianyi	Russia	1954–2009	90.62	79.55	−1.61	0.41	0.36	0.58
Dunai	Russia	1951–2009	124.50	73.93	−0.46	0.26	2.56	12.52
Tiksi	Russia	1950–2009	128.92	71.58	−0.58	0.27	2.06	6.08
Sannikova	Russia	1950–2009	138.90	74.67	−0.49	0.19	1.74	5.01
Kigiliah	Russia	1951–2009	139.87	73.33	−0.55	0.15	0.95	3.32
Aion	Russia	1954–2001	167.98	69.93	−0.36	0.08	0.96	/
Pevek	Russia	1950–2009	170.25	69.70	−0.35	0.07	3.66	8.77
Vrangelia	Russia	1950–2000	181.52	70.98	0.19	0.08	2.32	/
Vankarem	Russia	1950–2002	184.17	67.83	−0.06	0.14	2.78	/

one month. In the Arctic, the situation is more complex as non-static responses have been reported to exist on time scales between one month and one year (F. Lyard, personal communication, 2012). But for the purpose of the present study in which we focus on time scales longer than 1-year, the static response is a good approximation of the atmospheric pressure loading effect (F. Lyard, personal communication, 2012). In Figure 3 are also shown IB trends over the Arctic region (same area as for GIA) over 1950–2009. For this time span, IB trends are on the order of ∼0.5 mm/yr.

[14] In the following, we compute the IB correction at each tide gauge site using method 1. As for tide gauge-based sea level, the seasonal cycles are removed and a 12-month running mean smoothing is applied.

[15] Figure 4 shows individual tide gauge-based sea level time series in the Norwegian and Russian sectors (data set1 only) (seasonal cycles removed and further applying a 12-month running mean smoothing) corrected for GIA (ICE5G-VM2 model), with and without the IB correction. At most stations, the corrected and uncorrected curves show small differences. Accounting for the IB correction in general reduces the amplitude of the interannual variability. IB trends computed for each tide gauge operating period are presented in Tables 1a and 1b. For data set1, IB trends range between 0 and 0.3 mm/yr, except at Golomianyi (Russia) where the trend reaches 0.4 mm/yr.

[16] Tables 1a and 1b summarize tide gauge trends after correcting for GIA and IB over two time spans: the total operating period of each tide gauge and the 1993–2009 satellite operating time span.

3.3. Mean Coastal Sea Level in the Norwegian and Russian Sectors: Trend and Interannual Variability

[17] The coastal "mean" sea level (corrected for GIA and IB) (hereafter called CMSL) is displayed in Figure 5 separately for the Norwegian and Russian sectors (data sets 1 and 2) based on averages of individual time series in each region. The light gray area around each curve represents the uncertainty of the corresponding CMSL. It is computed from the root-mean squared (RMS) difference between individual time series and the mean.

[18] The Norwegian CMSL curve shows a slight downward trend between 1950 and 1975/1980, followed by an upward trend beyond 1980. The Russian CMSL curves (data sets 1 and 2) are rather similar, with an almost flat behavior between 1950 and 1975/1980 followed by an upward trend since then. This upward trend since about 1980 appears common to both Norwegian and Russian coastal regions, and thus seems to be a robust feature. For that reason, we averaged CMSL of the Norwegian and Russian sectors, plus the 3 island time series (i.e., 62 records in total) to obtain an Arctic CMSL over the whole Eurasian sector (in the following, we use the term 'Arctic CMSL' for this regional average). Arctic CMSL and associated uncertainty (computed as indicated above) over 1950–2009 is shown in Figure 6. As for the Norwegian and Russian sectors, the Arctic CMSL displays high interannual variability but almost no trend until the end of the 1970s. Subsequently it shows an increasing trend with two periods of marked rise: between 1980 and 1990 and since about 1995. The Arctic

Table 1b. Tide Gauge's Name, Country, Data Length and Location: GIA, IB and Tide Gauge Sea Level Trends at Each Tide Gauge Site (Data Set2)

Station	Country	Start–End Time	Coordinates		GIA ICE5G-VM2 (mm/yr)	IB (mm/yr)	Sea-Level Trend (GIA and IB Corrected) (mm/yr)	
			Longitude (°E)	Latitude (°N)			Tide Gauge Operating Period	Altimetry Period
Mys Pikshueva	Russia	1955–1990	32.433	69.55	−1.84	0.39	1.48	/
Murmansk II	Russia	1952–1993	33.05	68.967	−2.1	0.38	2.86	/
Murmansk	Russia	1952–2010	33.05	68.967	−2.1	0.28	5.63	7.49
Polyarniy	Russia	1950–1990	33.483	69.2	−1.46	0.23	−0.23	/
Teriberka	Russia	1950–1990	35.117	69.2	−0.7517	0.24	0.75	/
Bolvanskii	Russia	1951–1993	59.083	70.45	−0.79	0.44	3.22	/
Ugorskii Shar	Russia	1950–1989	60.75	69.817	−0.49	0.27	0.84	/
Amderma	Russia	1950–2009	61.7	69.75	−0.39	0.24	4.24	11.69
Russkaia Gavan II	Russia	1953–1993	62.583	76.183	−2.35	0.49	1.49	/
Russkaya Gavan	Russia	1953–1991	62.583	76.2	−2.37	0.31	1.28	/
Vise	Russia	1953–2009	76.983	79.5	−2.66	0.29	2.62	0.38
Dikson	Russia	1950–1997	80.4	73.5	0.19	0.5	1.55	/
Uedinenia	Russia	1953–1995	82.2	77.5	−1.91	0.56	2.11	/
Izvestia Tsik	Russia	1954–2009	82.95	75.95	−0.58	0.3	3.04	2.83
Sterlegova	Russia	1950–1995	88.9	75.417	−0.51	0.55	2.14	/
Isachenko	Russia	1954–1993	89.2	77.15	−1.58	0.65	4.49	/
Golomianyi	Russia	1954–2009	90.617	79.55	−1.61	0.41	0.36	0.58
Pravdy	Russia	1950–1994	94.767	76.267	−1.01	0.52	3.24	/
Russkii	Russia	1951–1989	96.433	77.167	−1.24	0.28	2.61	/
Krasnoflotskie	Russia	1954–1987	98.833	78.6	−0.95	0.04	3.05	/
Geiberga	Russia	1951–1995	101.517	77.6	−0.78	0.55	2.83	/
Peschanyi	Russia	1962–1993	102.483	79.433	−0.22	0.67	3.59	/
Fedorova	Russia	1950–2000	104.3	77.717	−0.47	0.3	1.84	/
Malyi	Russia	1950–1991	106.817	78.083	−0.16	0.43	2.43	/
Andreia	Russia	1951–1999	110.75	76.8	−0.12	0.54	3.3	/
Preobrazhenia	Russia	1951–1991	112.933	74.667	−0.39	0.41	0.45	/
Terpiai	Russia	1956–1998	118.667	73.55	−0.5	0.5	2.24	/
Dunai	Russia	1951–2009	124.5	73.933	−0.46	0.26	2.56	12.52
Tiksi	Russia	1950–2009	128.917	71.583	−0.58	0.27	2.06	6.08
Muostah	Russia	1951–1995	130.033	71.55	−0.58	0.41	3.03	/
Sannikova	Russia	1950–2009	138.9	74.667	−0.49	0.19	1.74	5.01
Kigiliah	Russia	1951–2009	139.867	73.333	−0.55	0.15	0.95	3.32
Sviatoi	Russia	1951–1987	140.733	72.833	−0.56	−0.35	3	/
Zemlia	Russia	1951–1987	142.117	74.883	−0.48	−0.6	3.78	/
Shalaurova	Russia	1950–2001	143.233	73.183	−0.55	0.01	1.18	/
Zhohova	Russia	1950–2000	152.833	76.15	−0.14	0.29	1.91	/
Ambarchik	Russia	1950–1995	162.3	69.617	−0.47	−0.02	3.63	/
Chetyrehstolbovoi	Russia	1951–1994	162.483	70.633	−0.4	−0.03	1.73	/
Rau-Chua	Russia	1950–1989	166.583	69.5	−0.42	−0.04	0.73	/
Aion	Russia	1954–2001	167.983	69.933	−0.36	0.08	0.96	/
Pevek	Russia	1950–2009	170.25	69.7	−0.35	0.07	3.66	8.77
Valkarkai	Russia	1956–1993	170.933	70.083	−0.3	0.15	3.46	/
Billinga	Russia	1953–1995	175.767	69.883	−0.21	0.07	1.92	/
Mys Shmidta	Russia	1950–1994	180.633	68.9	−0.13	0.03	1.86	/
Vrangelia	Russia	1950–2000	181.517	70.983	0.19	0.08	2.32	/
Vankarem	Russia	1950–2002	184.167	67.833	−0.06	0.14	2.78	/
Koluchin	Russia	1950–1991	185.35	67.483	−0.04	0.17	2.54	/
Netten	Russia	1950–1995	188.067	66.967	0.07	0.08	1.92	/

CMSL trend over 1980–2009 amounts to 2.25 +/− 0.26 mm/yr. The latter value compares well with the global mean sea level trend over the same time span (1980–2009) (equal to 2.09 +/− 0.04 mm/yr [*Church and White*, 2011]). On average over the whole 60-year time span (1950–2009), we find a positive Arctic CMSL trend of 1.62 +/− 0.11 mm/yr (after correcting for GIA and IB). For the Russian sector alone, *Proshutinsky et al.* [2004] found a rate of sea level rise of about 1.3 mm/yr over 1954–1989 after correcting for GIA and IB. Over the same time span (1954–1989), our Arctic CMSL trend amounts to 1.70 +/− 0.24 mm/yr. This trend is slightly larger than *Proshutinsky et al.*'s [2004] value, but refers to both Russian and Norwegian coasts.

[19] Considering only the 27 time series of data set1 to construct Arctic CMSL (not shown) gives the same result. Again Arctic CMSL rate is quite similar to the global mean rate over 1950–2009 (1.8 +/− 0.15 mm/yr [*Church and White*, 2011]). Thus so far, Arctic CMSL does not seem to rise faster than the global mean sea level.

[20] As indicated above, strong interannual variability affects Arctic CMSL. On Figure 6, we superimposed the Arctic Oscillation (AO) index to the CMSL curve. The AO is an important climate index of the Arctic region, referring to opposing atmospheric pressure patterns in northern middle and high latitudes. It exhibits a negative phase with

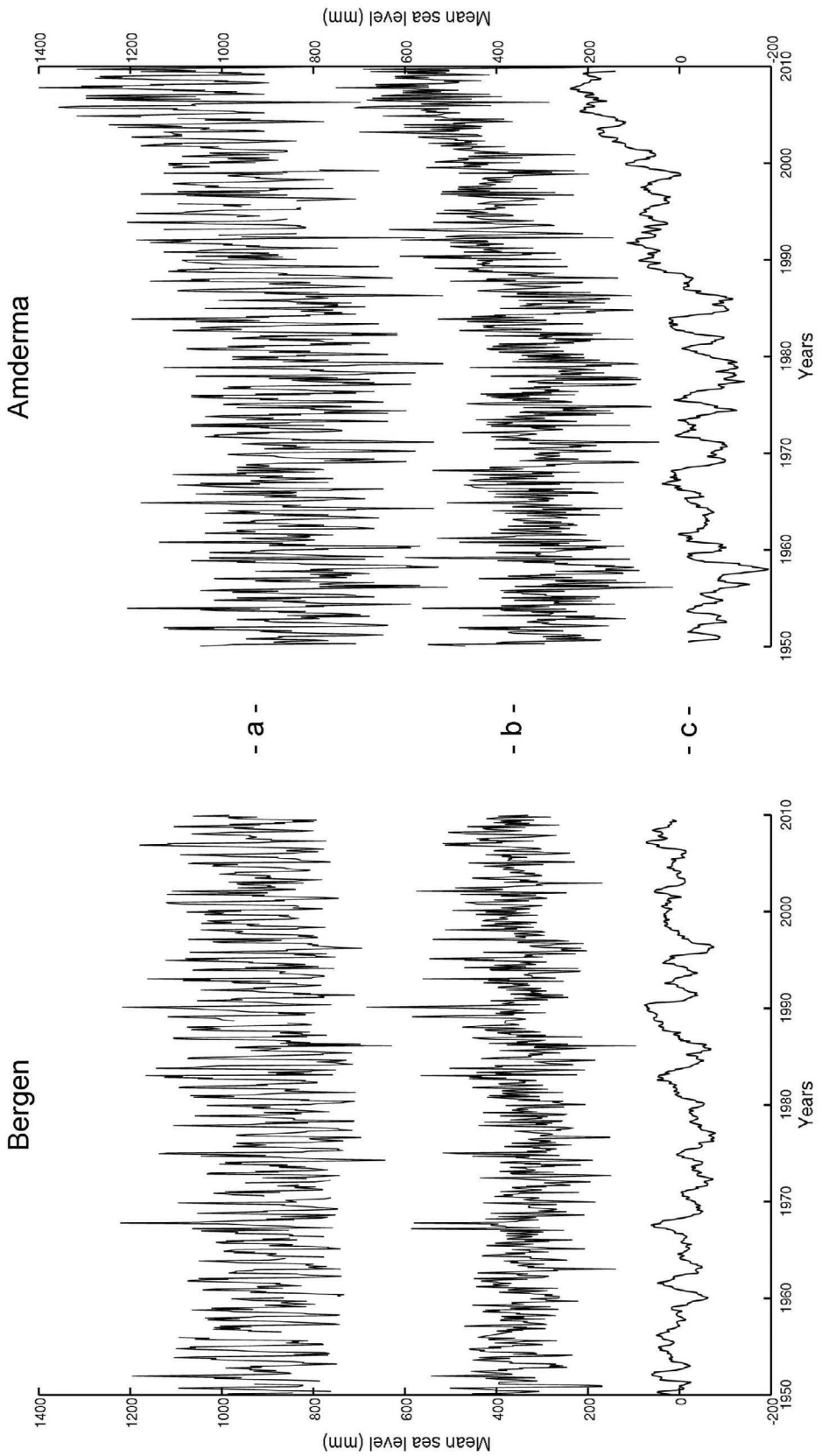

Figure 2. Tide gauge time series at Bergen (Norway) and Amderma (Russia): (a) raw data, (b) raw data minus the 12-month and 6-month sinusoids, and (c) smoothed data (12-month running mean smoothing applied to the middle curve).

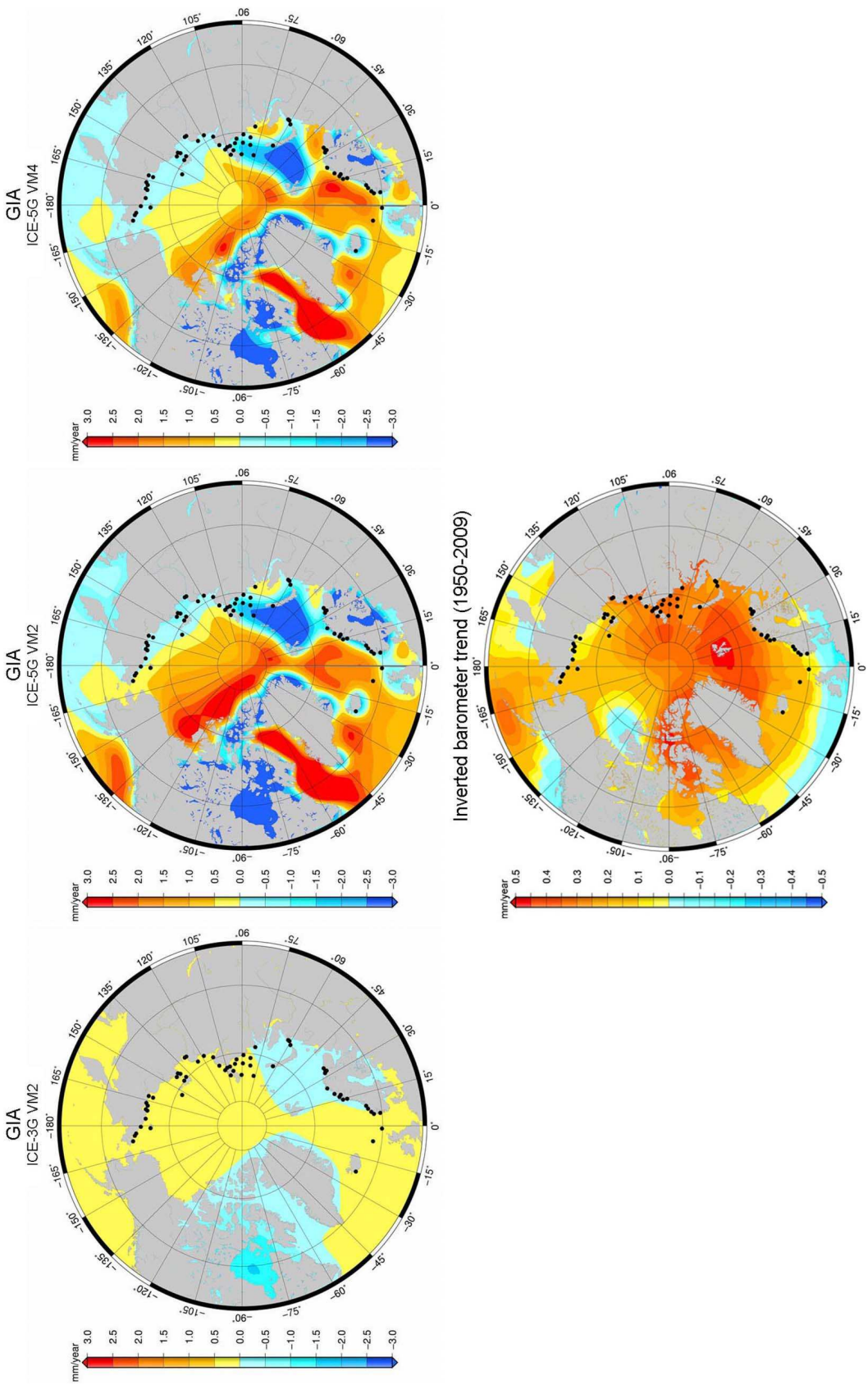

Figure 3. Regional GIA rates (mm/yr) for the ICE-3G/VM2 and ICE-5G-VM2/VM4 models, and IB (inverted barometer) trends over 1950–2009 (mm/yr). Black dots represent the tide gauge sites used in this study.

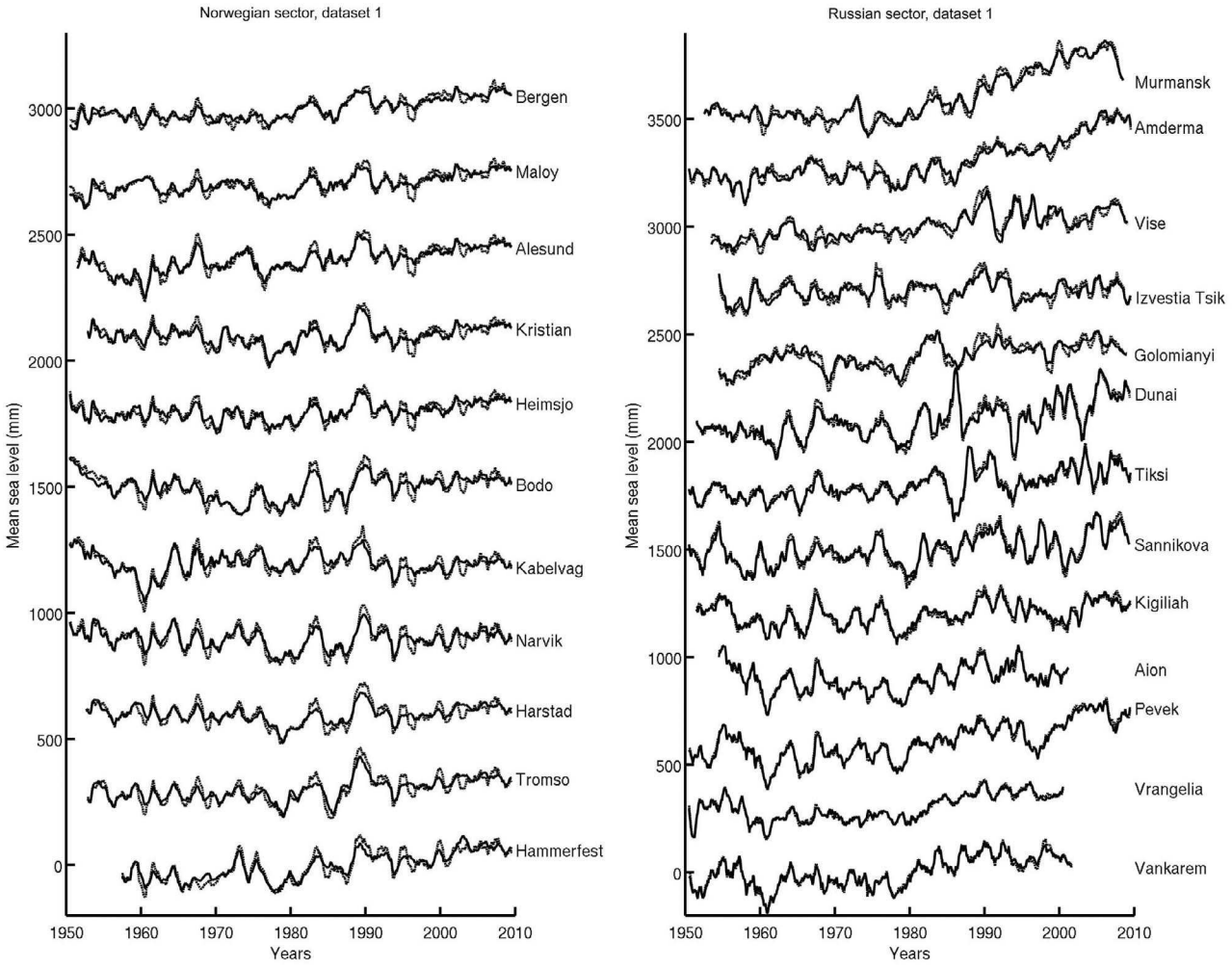

Figure 4. Plots of individual tide gauge time series with (solid line) and without (dashed line) the IB correction over 1950–2009 for the (left) Norwegian sector (11 tide gauges) and (right) Russian sector (13 tide gauges).

relatively high pressure over the polar region and low pressure at midlatitudes, and a positive phase during which the pattern is reversed. Over most of the past century, the AO alternated between its positive and negative phases. Starting in the 1970s, however, the oscillation has tended to stay in the positive phase, with strong positive values in the early 1990s. During the past decade, the AO has been low and much variable. A number of previous studies reported that several meteorological and climatic variables of the Arctic region are highly correlated with the AO index (and with the North Atlantic Oscillation -NAO- [e.g., *Chylek et al.*, 2010]).

[21] Looking at Figure 6, we indeed observe significant correlation between Arctic CMSL curve and AO up to 1995–2000. Most of the large interannual oscillations seen in the CMSL curve, in particular the high positive anomaly in the early 1990s, are also visible in the AO index. The correlation, between 1950 and 1995, amounts to 0.68 (95% confidence). However, surprisingly, beyond the mid-1990s and especially since 2000, the correlation breaks down, even if at interannual time scale, there is still some agreement between the two curves. The Arctic CMSL shows sustained rise since about 1995 while the AO index does not, oscillating between positive and negative values. We performed tests with other climate indices such the NAO but the correlation between CMSL and AO was found higher.

[22] It seems surprising at first look to find a significant correlation between AO and IB-corrected CMSL because AO is purely sea level pressure-based parameter. However, AO also reflects large-scale atmospheric forcing and is a measure of the polar vortex, which defines changes in wind stress and wind direction that may influence the ocean circulation, hence sea level. So far we have just corrected for the purely static IB effect. The observed correlation thus suggests that other factors (e.g., wind stress and associated circulation changes, and ocean mass changes due to land ice melt and possibly river runoff) contribute to the year-to-year variability in CMSL.

[23] The above results indicate that between 1950 and the mid-to-late 1990s, Arctic CMSL was mostly driven by internal climate modes, in particular the AO, possibly through changes in wind stress and associated ocean circulation (although quantitative analyses of the latter effects

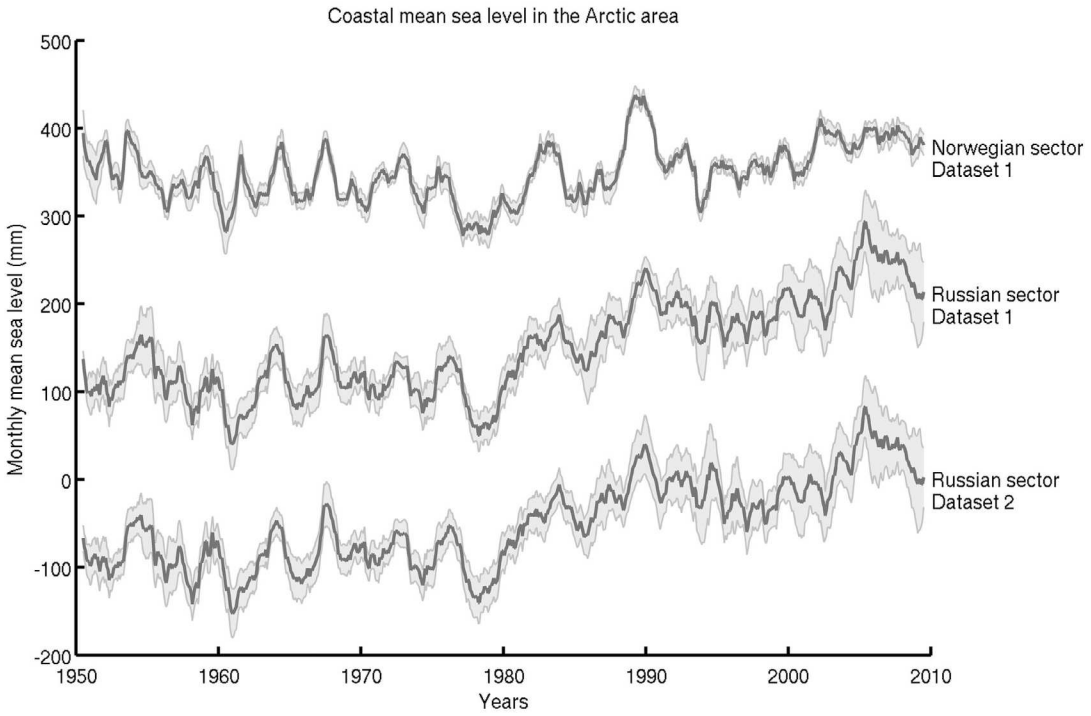

Figure 5. CMSL curves in the Norwegian (data set1) and Russian sectors (data set1 and 2). The light gray zone represents the uncertainty of the CMSL time series.

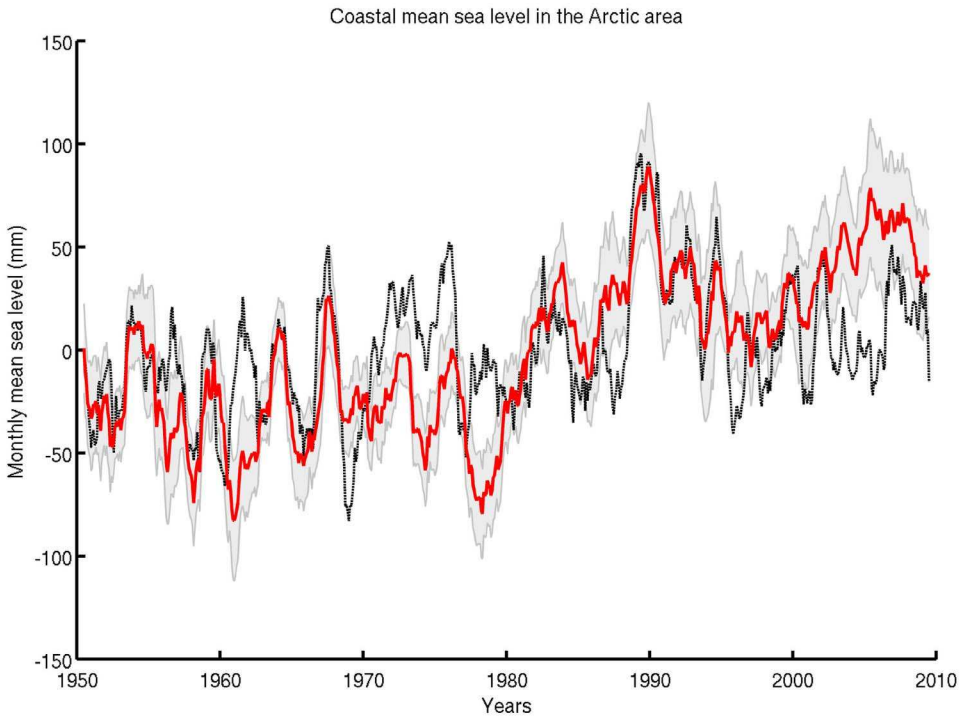

Figure 6. Arctic CMSL curve (red solid curve) and associated uncertainty (light gray zone). Arctic oscillation index is superimposed (black dashed curve).

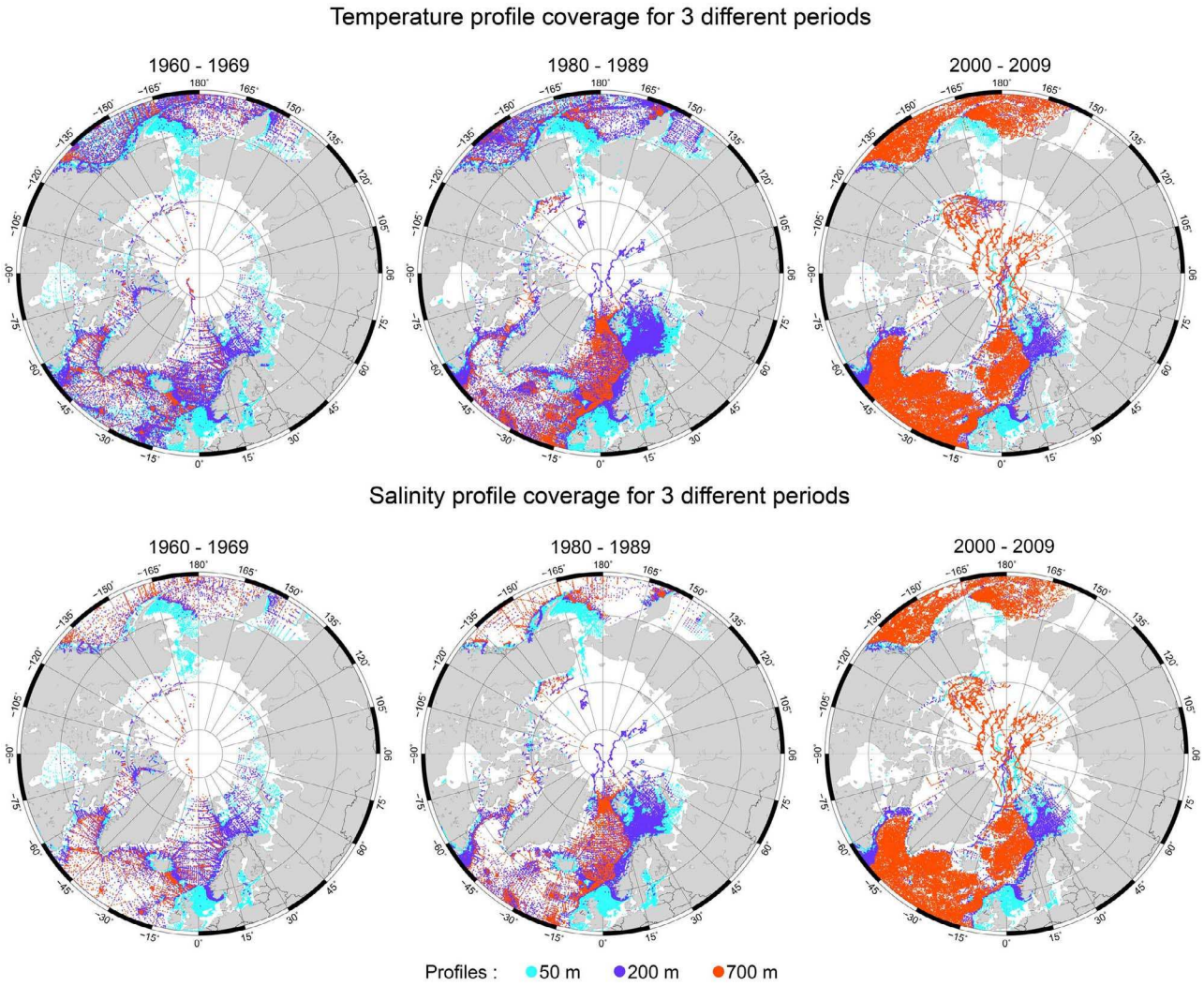

Figure 7. (top) Temperature and (bottom) salinity profile coverage (data from EN3) in the Arctic region for 3 different depth ranges (0–50 m, 0–200 m and 0–700 m) and 3 different periods (1960–1969, 1980–1989 and 2000–2009).

remain to be performed), as well as ocean mass changes. Since the mid-to-late 1990s, Arctic CMSL shows a marked rise of 4.07 +/− 0.65 mm/yr.

4. Steric Sea Level in the North Atlantic and Nordic Seas

4.1. Steric Data

[24] In this section we estimate the contribution of the steric (effect of ocean temperature T (thermosteric component) and salinity S (halosteric component)) sea level to Arctic CMSL. For that purpose, we use T/S data from 3 different databases: the WOD09 [*Levitus et al.*, 2009], the *Ishii and Kimoto* [2009] (called IK09 hereafter) databases and the EN3 database developed by the Met Office/Hadley Centre, UK [*Ingleby and Huddleston*, 2007]. The EN3 database consists of the WOD05 database [*Levitus et al.*, 2005] plus additional T data from the ASBO (Arctic Synoptic Basin-wide Oceanography) project (see NOCS ASBO web page: http://www.noc.soton.ac.uk/ooc/ASBO/index.php) and Argo project. The WOD09 and IK09 databases account for depth-bias corrections on XBT temperature data [e.g., *Wijffels et al.*, 2008], unlike the WOD05 data included in the EN3 gridded database (after this study was started, XBT depth bias corrections were posted along T profiles on the EN3 web site; however, accounting for profile-based depth bias corrections was found beyond the scope of the present study; nevertheless the EN3 database include a large portion of non XBT data which do not suffer from XBT depth-bias). The T/S data from the 3 databases are publicly available at: http://www.nodc.noaa.gov/OC5/indprod.html for WOD09; http://atmphys.nies.go.jp/~ism/pub/ProjD/v6.9/ for IK09; and http://www.metoffice.gov.uk/hadobs/en3/index.html for EN3.

[25] The depth and time coverage of these data is very inhomogeneous in the studied region, leaving much of the Arctic Ocean uncovered. This is illustrated in Figure 7 which shows for three periods (1960–1969, 1980–1989 and 2000–2009) T and S data coverage (from EN3) down to 700 m (coverage is shown for the 0–50 m, 0–200 m and 0–700 m upper ocean layers). The coverage during the 1960s and

earlier is far too sparse and limited to the near surface layers, preventing us to quantify the steric contribution in the whole Arctic and even along the Russian coasts. Before the 1990s, we also note that the data coverage is poor. This leads us to not consider data prior to 1970 and only consider a limited geographical sector bounded by the 75°W–45°E longitudes and the 50°N–80°N parallels.

4.2. Steric Spatial Trend Patterns

[26] For each database, we computed the thermosteric sea level on a 1° × 1° grid at monthly interval since 1970 (at 3-month intervals for WOD09), integrating T anomalies from the surface down to 700 m. For that purpose, we first computed density anomalies at each standard level down to 700 m by considering temperature anomalies and using the classical equation of state of the ocean. Then, we integrated density anomalies at each grid point (using a climatology for the salinity) and each time step to obtain the thermosteric sea level [*Gill*, 1982; *Levitus et al.*, 2005; *Lombard et al.*, 2005].

[27] We also computed the halosteric sea level using salinity anomalies available for the IK09 and EN3 databases (no gridded salinity data are available for WOD09). We followed the same methodology as for the thermosteric sea level but now considering salinity anomalies from the surface down to 700 m and a climatology for the temperature.

[28] Figures 8a and 8c show thermosteric trend patterns computed over 1970–2009 for the IK09 and WOD09 data over the limited region described above. We note that thermosteric spatial trends are positive almost everywhere and very similar in both cases, with higher rates than average south of Iceland, in the Baffin Bay, Greenland and Norwegian seas. Figure 8b shows halosteric spatial trend patterns for IK09. Halosteric trends are moderately negative over the studied area, indicating a slight increase in salinity since 1970. Comparing thermosteric and halosteric trend maps for IK09 shows that the patterns are anticorrelated (with higher magnitude for the thermosteric trends). This anticorrelation between thermosteric and halosteric trend patterns suggests simultaneous increase of both temperature and salinity since 1970 in the North Atlantic and Nordic Seas sector (the two factors having opposite effects on sea level). A similar behavior has been reported in several other regions from in situ hydrographic data and/or ocean circulation modeling [e.g., *Wunsch et al.*, 2007; *Köhl and Stammer*, 2008].

[29] Figure 9 shows the steric (sum of thermosteric and halosteric) trend patterns over 1970–2009 for the IK09 and EN3 data (note that computing the steric sea level by summing the thermosteric and halosteric components or by direct integration of T- and S-related density anomalies gives essentially the same result). The two maps show more or less similar patterns in the North Atlantic and Nordic Seas, in particular along the Norwegian coast. Some difference is noticed however in the Baffin Bay and southwest of Greenland.

4.3. Interannual Variability of the Gridded Steric Data

[30] To investigate the dominant modes of variability of the steric data in the limited region considered above, we performed an EOF (empirical orthogonal function) decomposition [*Preisendorfer*, 1988] of the WOD09 and IK09 gridded thermosteric data over the 1970–2009 time span. Figure 10 (top) shows corresponding first spatial and temporal mode (noted EOF1) for the two thermosteric data. We note that EOF1s (42.9 and 46.1% of the total variance, respectively) are highly correlated both spatially and temporally, and closely resemble the thermosteric trend patterns shown in Figure 8. The temporal curves are also highly correlated. They are flat until 1995 but since then show an upward trend. Figure 10 (bottom) shows EOF1 of IK09 halosteric data decomposition. The anticorrelation noted above for the spatial trend patterns between thermosteric and halosteric components is even more evident in EOF1s. Like EOF1 thermosteric temporal curve, the EOF1 halosteric temporal curve also displays an upward trend as of 1995 (associated with negative spatial trend values), suggesting simultaneous increase of temperature and salinity in the region. To see more clearly the latter behavior, we have averaged the gridded thermosteric (IK09 and WOD09) and halosteric (IK09) data at each time step over the region, and computed the mean thermosteric and halosteric curves. These are shown in Figure 11. We first note that the two thermosteric curves agree well. We also note the strong change and opposite behavior affecting the thermosteric and halosteric curves as of ∼1995.

4.4. Steric Sea Level at the Norwegian Tide Gauges

[31] We computed the steric sea level (thermosteric plus halosteric components) using the IK09 and EN3 data since 1970 at the 11 Norwegian tide gauge sites by interpolating the steric grids at the tide gauge locations (averaging the gridded data within a 1° radius around the tide gauge). Corresponding curves are shown in Figure 12 (top) superimposed to the Norwegian CMSL curve. We first note that both IK09 and EN3 curves are in general good agreement (as previously noticed between IK09 and WOD09 thermosteric components). Although smoother, they correlate also well between 1970 and 2006 with the CMSL curve (correlation of 0.65). However, as of 2006, the steric sea level curves show a downward trend not seen in the CMSL curve. The steric sea level trends over 1970–2006 amounts to 1.63 +/− 0.14 mm/yr and 1.9 +/− 0.17 mm/yr for IK09 and EN3 respectively, a value quite comparable to the CMSL trend over the same time span (of 1.73 +/− 0.23 mm/yr). This suggests that, at least over this time span (1970–2006), observed CMSL rise along the Norwegian coast has a steric origin. However, the interannual variability in steric sea level and Norwegian CMSL are not well correlated, suggesting that the latter is influenced by other factors on such time scales, e.g., wind stress-driven ocean circulation and ocean mass changes.

[32] We computed the residual (observed CMSL minus steric sea level) curve at the Norwegian tide gauges with the IK09 and EN3 data. The corresponding time series over 1970–2006 are shown in Figure 12 (bottom). The AO index is superimposed. The trend of the residual curves over 1970–2006 amount to 0.11 +/− 0.23 mm/yr and −0.17 +/− 0.22 mm/yr for the IK09 and EN3 data, respectively, thus are not significant. On the other hand, the residual curves show important interannual variability moderately correlated with the AO index. Over 1970–2006, this correlation is equal to 0.54 only but at some periods (e.g., around 1990), the sea level residuals and the AO co-vary similarly, possibly reflecting the dynamical response of the sea to wind-forcing. At the end of the studied period (around 2006), the residual curves show an upward trend not seen on

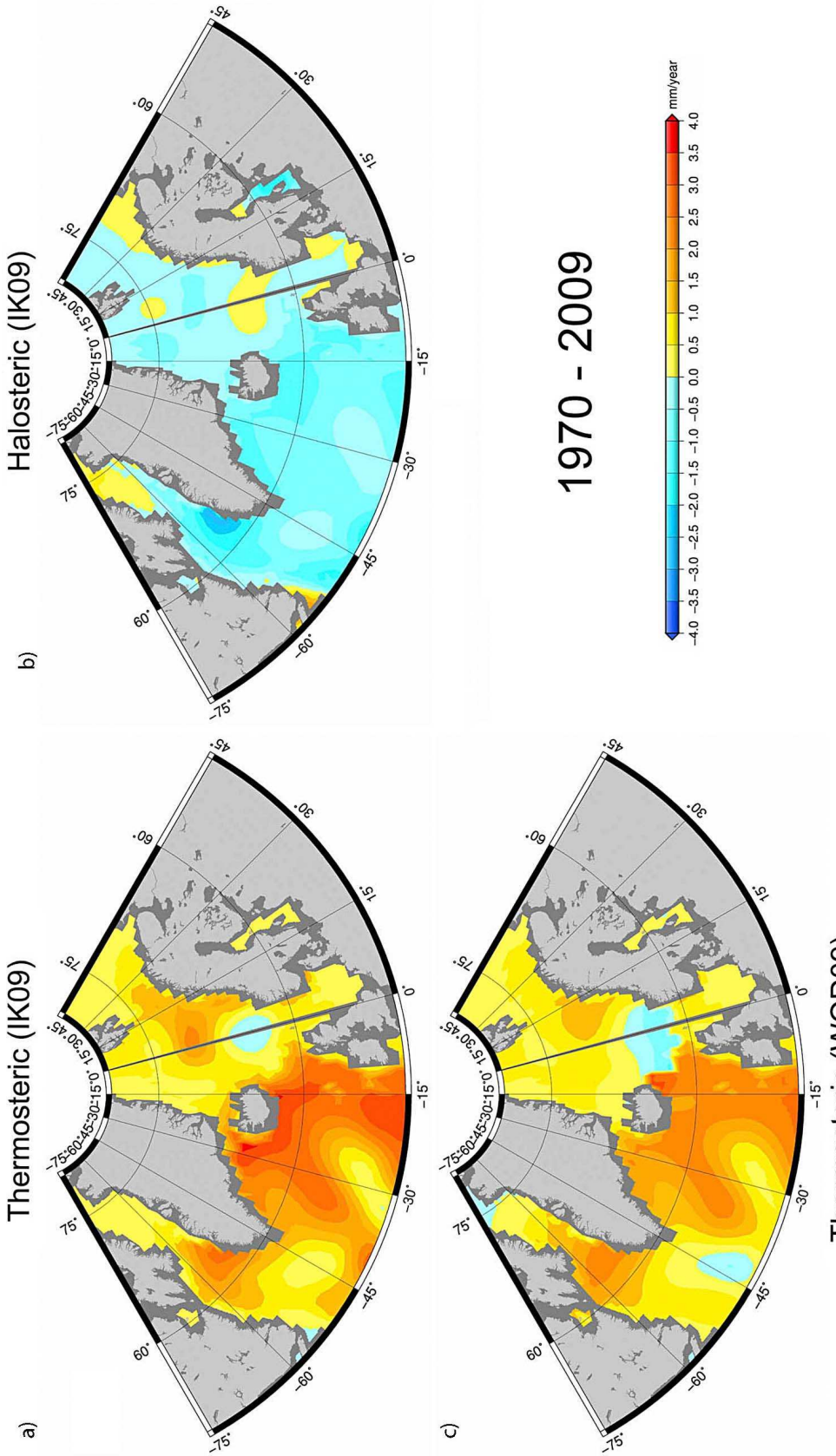

Figure 8. Spatial trend patterns in thermosteric sea level ((a) IK09 and (c) WOD09) for 1970–2009 over the North Atlantic and Nordic sea. (b) The IK09 halosteric trend patterns are also presented. Units: mm/yr.

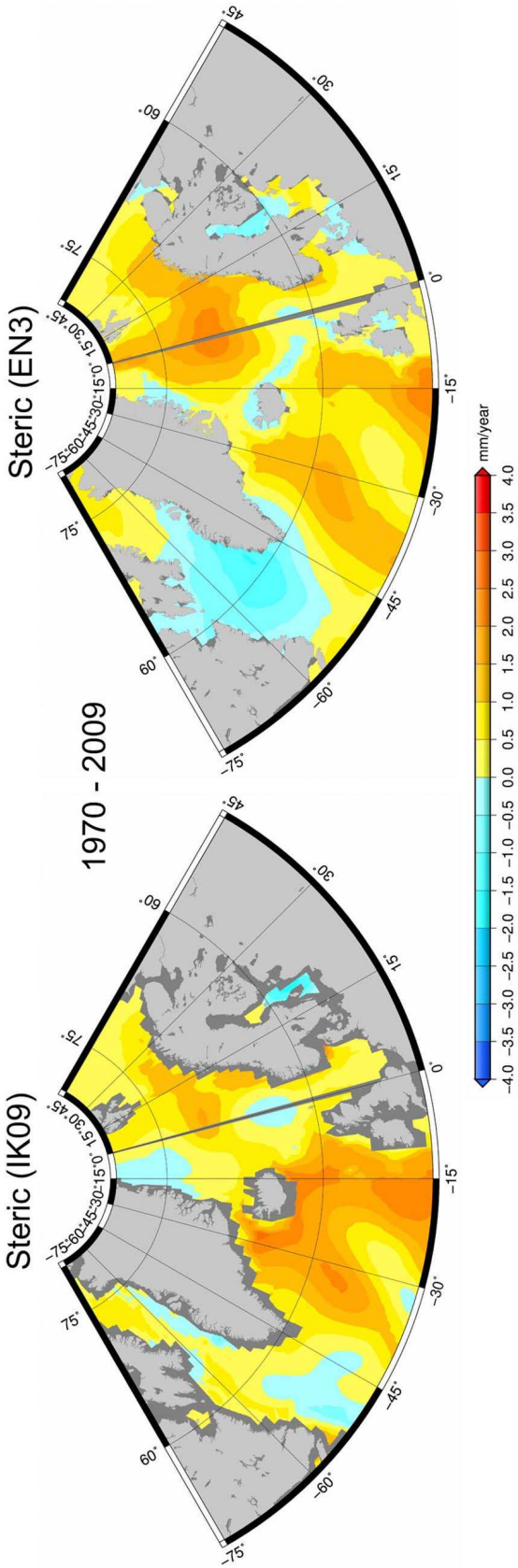

Figure 9. Spatial trend patterns in steric sea level for (left) IK09 and (right) EN3 data for 1970–2009. Units: mm/yr.

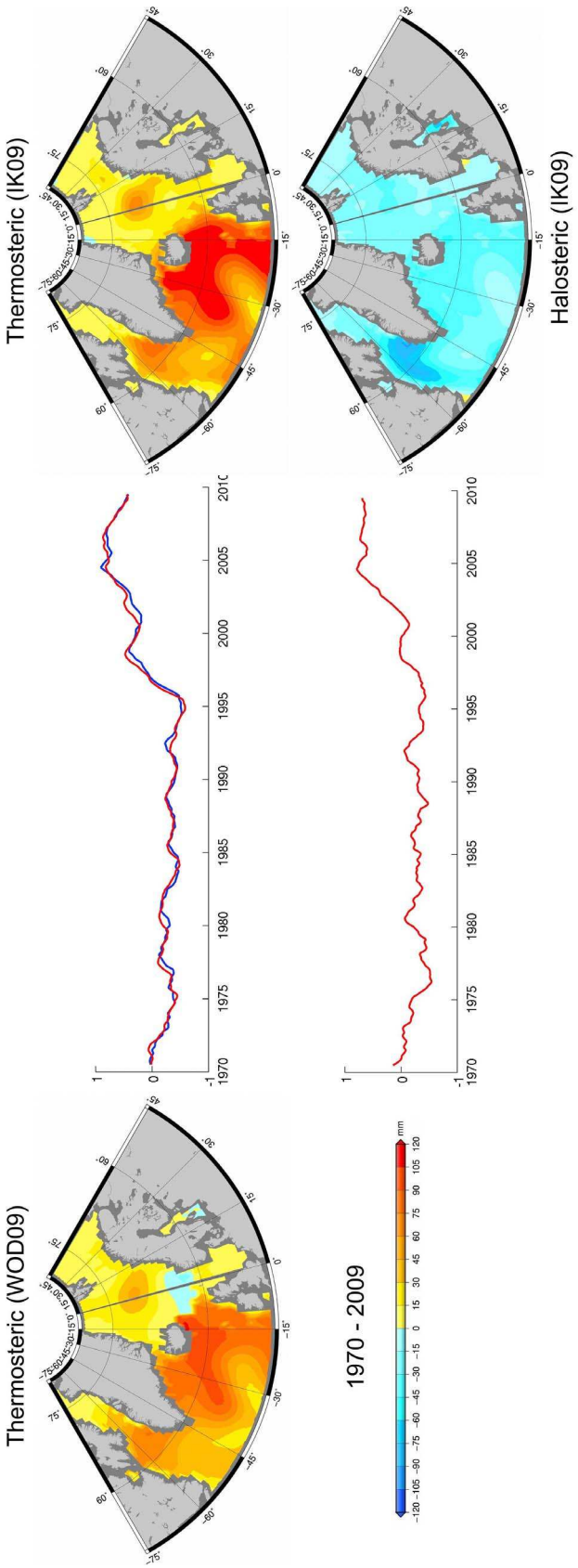

Figure 10. (top) EOF mode 1 of thermosteric sea level for WOD09 (red curve) and IK09 (blue curve) over 1970–2009. (bottom) EOF mode 1 of IK09 halosteric sea level.

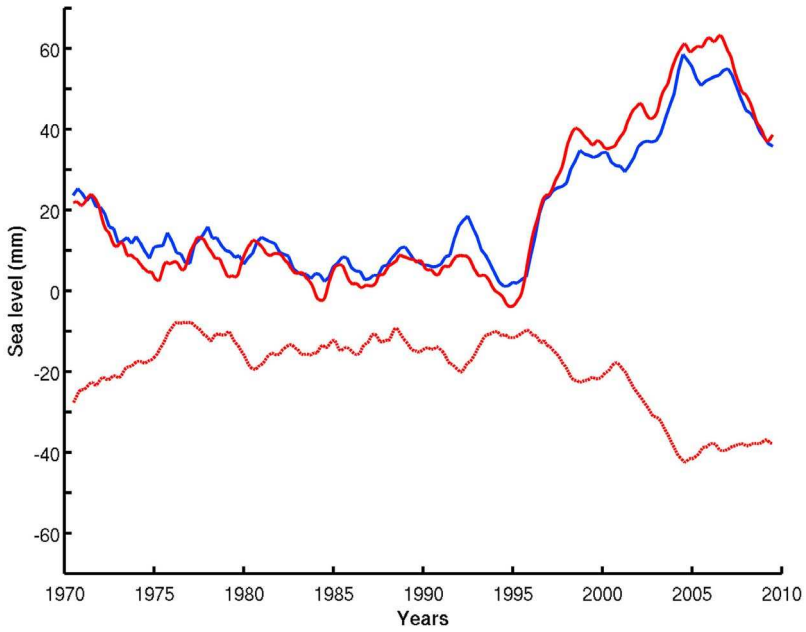

Figure 11. Top curves are regionally averaged thermosteric sea level over 1970–2009 (region as shown in Figures 8 and 9) for IK09 (red curve) and WOD09 (blue curve) data. Bottom curve is regionally averaged halosteric sea level (IK09 data, red curve).

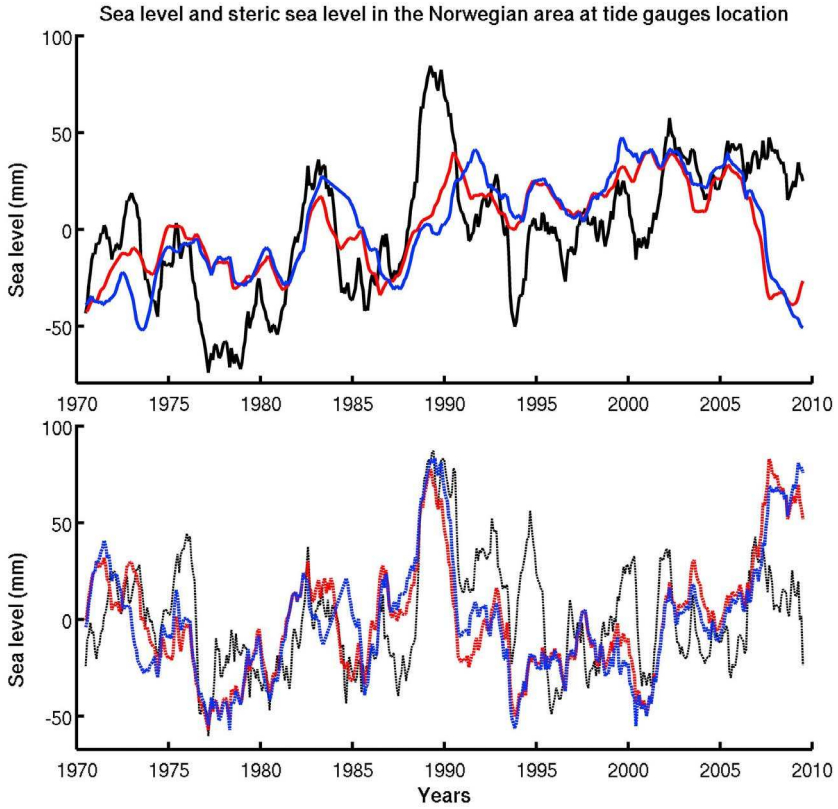

Figure 12. (top) CMSL at the Norwegian tide gauges (black curve) over 1970–2009 on which is superimposed the steric sea level (IK09: red curve and EN3: blue curve) interpolated at the tide gauge sites. (bottom) Residual (observed minus steric) sea level (red and blue curves for IK09 and EN3 respectively). The AO index is superimposed (black-dashed curve).

the AO. This may reveal an increased contribution of the ocean mass component linked to the recently reported acceleration in land ice melt [i.e., *Holland et al.*, 2008; *Steffen et al.*, 2010; *Rignot et al.*, 2011] plus regional water mass redistribution. We will come back to this issue in section 5.

5. Comparison Between Tide Gauge-Based, Altimetry-Based and Steric Sea Level in the North Atlantic and Nordic Seas Over 1993–2009 and Estimate of GRACE-Based Ocean Mass Over 2003–2009

[33] In this section, we take advantage of the availability of gridded altimetry sea level data up to 82°N since 1993 to investigate in more detail the mean and regional sea level in the North Atlantic and Nordic Seas sector and its relationship with the steric sea level. Satellite altimetry measures absolute sea level (i.e., relative to the Earth's center of mass [*Fu and Cazenave*, 2001; *Cazenave and Nerem*, 2004]), thus reflects global/regional changes in ocean water volume (due to density changes and water mass variations) as well as additional factors causing regional variability in sea level such as the deformations of ocean basins in response to land ice melt-induced mass redistribution [*Milne et al.*, 2009; *Tamisiea and Mitrovica*, 2011]. As altimetry-based sea level does not sense vertical crustal motions, it can be compared to tide gauge-based sea level, once the latter is corrected for vertical crustal motions. Here we use the multi mission altimetry data reprocessed by *Prandi et al.* [2012]. This reprocessing improves the data coverage and the quality of the geophysical corrections to apply to the altimetry data in the Arctic region. The details of the data reprocessing is described in *Prandi et al.* [2012]. The inverted barometer correction is applied to altimetry data as for the tide gauge data using the *Carrère and Lyard* [2003] model.

5.1. Spatial Trend Patterns in Altimetry-Based and Steric Sea Level (1993–2009)

[34] We compared the altimetry-based sea level trend patterns with the thermosteric and halosteric spatial patterns (IK09 data) for the 1993–2009 time span over the North Atlantic and Nordic Seas sector. These are shown in Figures 13a–13c. In several areas, e.g., south of Iceland and Greenland and in the Norwegian Sea, the spatial trend patterns of altimetry-based and thermosteric sea level show positive trends. Thermosteric trends have larger amplitude than observed (i.e., altimetry-based) ones, but because of opposite trends in the halosteric component (see Figures 13a–13c), their sum (i.e., the steric component) will better agree with altimetry-based trends. This is indeed the case (although not everywhere), as illustrated in Figures 13d and 13e showing steric trend patterns over 1993–2009 for the IK09 and EN3 data.

[35] We computed residual trend maps (i.e., altimetry-based minus steric trends) with the IK09 and EN3 data over 1993–2009. These are shown in Figure 14. In most areas (northwest and southeast of Greenland, Greenland and Norwegian seas, and along the coasts of Norway), the residual trend patterns roughly agree. Although part of the residual trends may result from uncertainty and imperfect data coverage of T/S data in the region, we cannot exclude that they reflect real non-steric signals, for example ocean mass changes. Since ~2003, the latter are measurable by GRACE space gravimetry data. This is discussed in the next section.

5.2. Tide Gauge-Based, Altimetry-Based, GRACE-Ocean Mass and Steric Sea Level Along the Norwegian Coasts

[36] We interpolated the altimetric grids at the tide gauge locations (as done for the steric sea level in section 4). At the Norwegian tide gauges, the altimetry-based and tide gauge-based sea level time series are highly correlated both in terms of trend and interannual variability, with all correlations >0.9 (not shown). The highest correlation was obtained when the ICE-5G/VM2 GIA correction was used for the tide gauge data. This was the basis for preferring this particular GIA correction (see section 3). We constructed an altimetry-based CMSL along the Norwegian coast averaging individual time series at the 11 tide gauge sites of data set1. The tide gauge and altimetry-based CMSL curves in the Norwegian sector for 1993–2009 are shown in Figure 15 (top). Both curves are highly correlated and show an increasing sea level trend of 3.32 +/− 0.65 mm/yr (from tide gauges) and 4.23 +/− 0.23 mm/yr (from satellite altimetry) over the altimetry period (1993–2009). The trend difference (0.9 mm/yr) is only slightly larger than the tide gauge trend uncertainty. Thus the altimetry data clearly confirm the recent sea level increase in that particular region. We note in passing that the rate of sea level rise in this region is very similar to the global mean rate (of 3.3 mm/yr over 1993–2009 [e.g., *Cazenave and Llovel*, 2010]), a result confirmed by *Prandi et al.* [2012] for the whole Arctic region.

[37] We estimated the ocean mass change along the Norwegian coast as of 2003 using GRACE space gravimetry data [*Wahr et al.*, 2004]. GRACE measures temporal variations of the Earth's gravity field and, over the oceanic domain, provides an estimate of ocean mass changes. Several GRACE products have been released from teams involved in the GRACE project (CSR, JPL and GFZ), each time with substantial improvement [*Chambers*, 2006]. Here we use the CSR 1° × 1° gridded data over the ocean (RL04 release) at monthly interval (available at http://grace.jpl.nasa.gov/data/GRACEMONTHLYMASSGRIDSOCEAN/). These data include an implementation of the carefully calibrated combination of de-stripping and smoothing, with different half-width Gaussian filters (the solutions need to be smoothed because errors increase with wavelength). These gridded ocean GRACE products are corrected for Glacial Isostatic Adjustment using the *Paulson et al.*'s [2007] model. The data used in this study cover the time span from January 2003 to December 2009 and are expressed in sea level equivalent.

[38] We interpolated monthly GRACE-ocean mass grids at the 11 Norwegian tide gauge sites, removed the seasonal signal as for the other data sets and then averaged the 11 individual ocean mass time series. Corresponding GRACE-based averaged ocean mass curve is superimposed to the CMSL curve in Figure 15 (top). Over 2003–2009, the GRACE ocean mass trend is positive and equal to 2.9 +/− 0.66 mm/yr. This is significantly different from the CMSL trend over the same time span (equal to −1.14 +/− 0.21 mm/yr). As the CMSL trend reflects primarily the sum of the steric plus ocean mass trends, this trend difference is not really surprising considering the downward trend seen in the mean

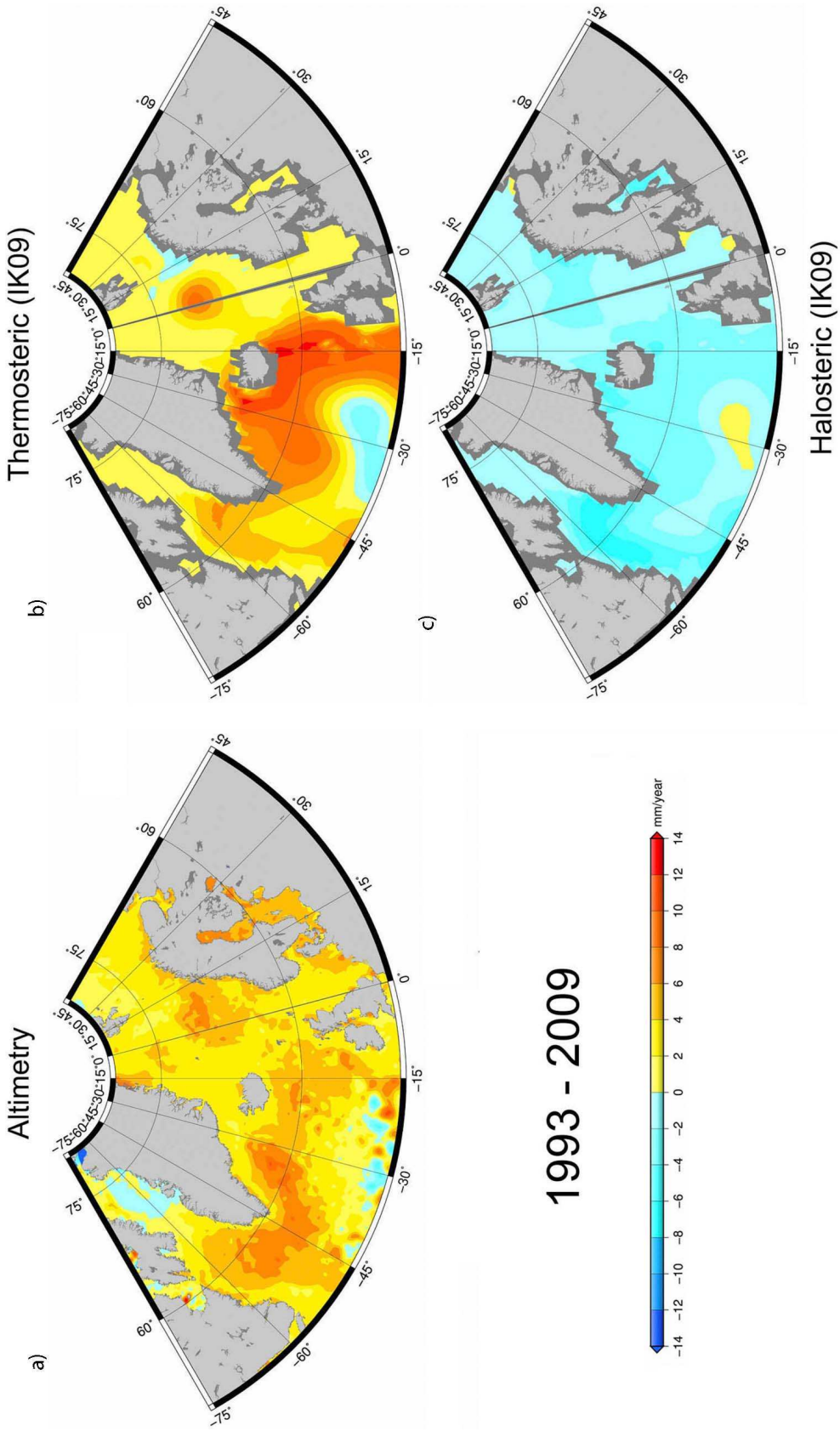

Figure 13. (a) Spatial trend patterns of altimetry-based, (b) thermosteric (IK09), and (c) halosteric (IK09) in the North Atlantic and Nordic Seas region over 1993–2009. Spatial trend patterns in steric sea level over 1993–2009 ((d) IK09 and (e) EN3). Units: mm/yr.

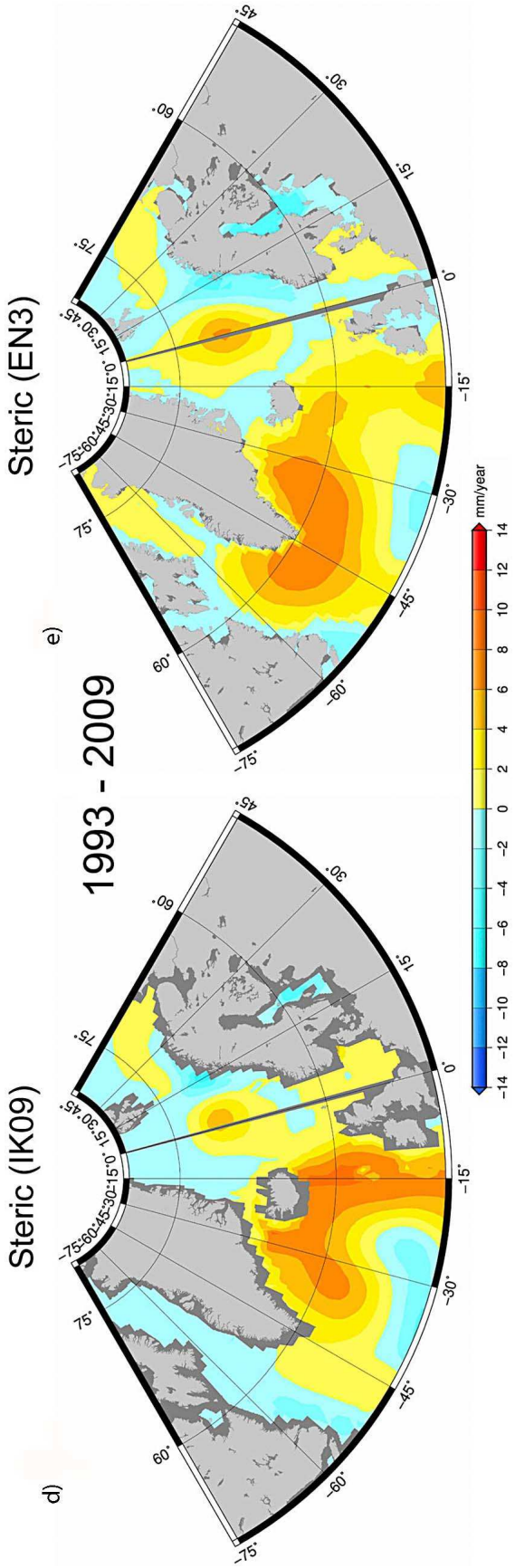

Figure 13. (continued)

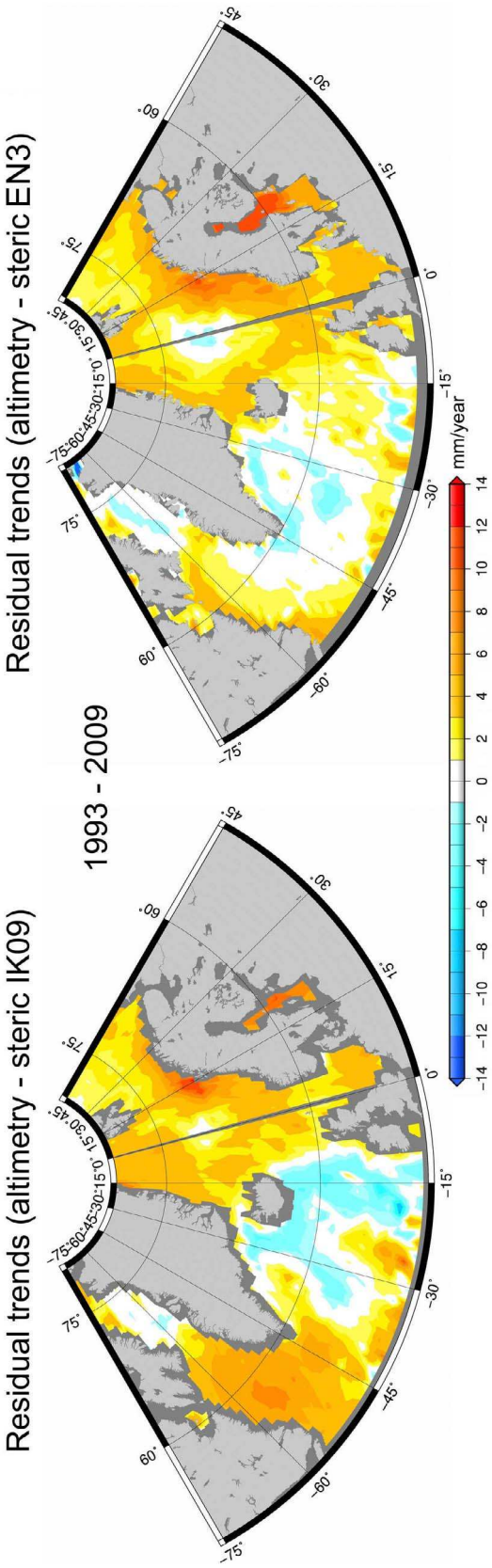

Figure 14. Spatial trend patterns of the residual (altimetric minus steric) sea level in the North Atlantic and Nordic Seas region over 1993–2009 ((left) IK09 and (right) EN3). Units: mm/yr.

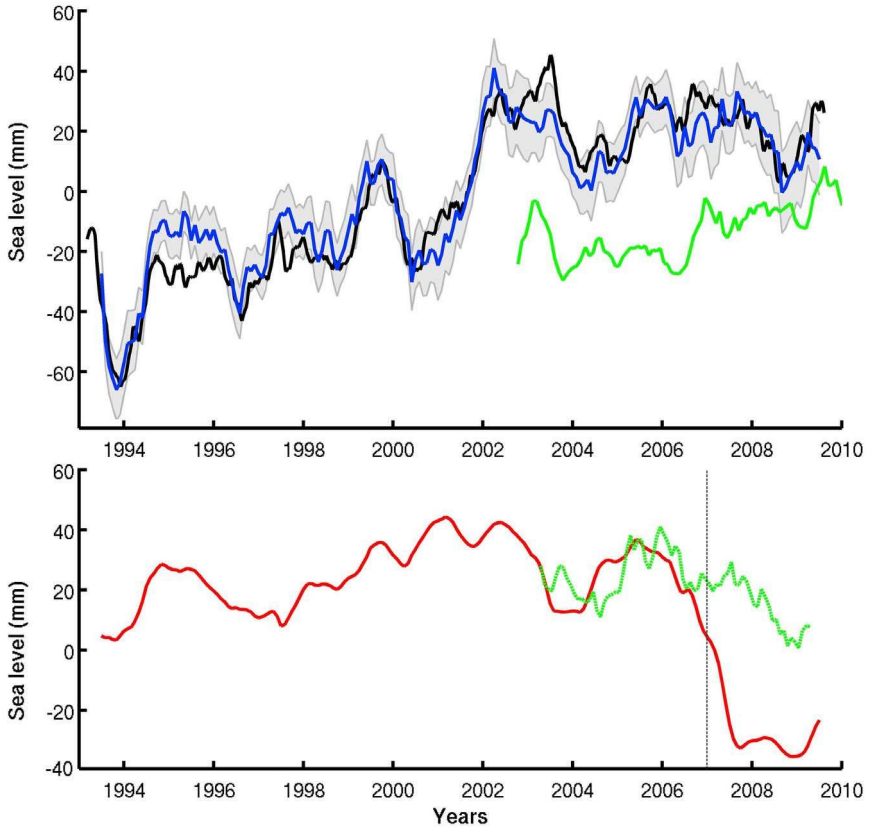

Figure 15. (top) Tide gauge-based (blue curve) and altimetry-based CMSL (black curve) at the Norwegian tide gauge sites over 1993–2009. The green curve represents the GRACE-based ocean mass component averaged at the Norwegian tide gauge sites. (bottom) Mean steric sea level (IK09 data, red curve); the green curve represents the steric component estimated from the difference between tide gauge-based CMSL and GRACE ocean mass. The dashed vertical line corresponds to the date (early 2007) beyond which no ocean temperature data are available along the Norwegian coast.

steric sea level averaged at the Norwegian tide gauges (Figure 12, top). On the other hand, reasonable agreement is observed between CMSL sea level and GRACE-based ocean mass in terms of year-to-year variability.

[39] In Figure 15 (bottom) is shown the difference over 2003–2009 between CMSL and GRACE-based ocean mass averaged at the Norwegian tide gauges. This difference should primarily reflect the steric component. The coastal steric sea level from the IK09 data is also shown over 1993–2009. While both curves show a downward trend over their overlapping time span (2003–2009), the highly negative observed steric trend seems somewhat suspect. This highly negative steric trend may not be real and may simply reflect lack of data in the very recent years. To check this, we looked at the T/S data coverage between 2005 and 2009. This is illustrated in Figure 16 showing yearly coverage in T data for years 2005 to 2009. Figure 16 clearly reveals very poor data coverage along the Norwegian coast over this time span. We note data down to 200 m only in 2005 and 2006. But in 2007, 2008 and 2009, there is no data at all along the Norwegian coast. Thus the interpolated steric curve (Figure 15, bottom) is likely biased low for these years. Besides considering the 2003–2006 time span during which there are some T data, we note that the "CMSL minus GRACE ocean mass" curve closely follows the steric curve, and both trends (equal to 1.41 +/− 0.7 mm/yr and 1.36 +/− 0.4 mm/yr for "CMSL-GRACE ocean mass" and steric sea level respectively over 2003–2006) agree quite well.

6. Discussion

[40] In this study, we estimated the mean sea level over the past ∼60 years along the Norwegian and Russian coasts using good quality tide gauge data. Between 1950 and 1980, coastal sea level did not rise significantly but beyond 1980, it shows a significant upward trend. Estimate of the thermosteric and halosteric sea level since 1970 in a limited sector including the North Atlantic subpolar gyre and the Nordic Seas indicates a strong change around 1995, with simultaneous increase in temperature and salinity. Along the Norwegian coast, a similar behavior is noticed with an increasing trend of observed sea level (from tide gauges and satellite altimetry) since the mid-1995s (note that the downward trend observed in the mean coastal steric sea level as of 2007 is likely an artifact due to a lack of data in this region over the very recent years). We also observe an increase in the GRACE-based averaged ocean mass at the Norwegian coast since 2003. Its positive trend (of 2.9 +/− 0.66 mm/yr over 2003–2009) is somewhat larger than the global mean ocean mass increase due to total land ice melt over about the same time span (of 1.5–2 mm/yr) [e.g., *Church and White*, 2011].

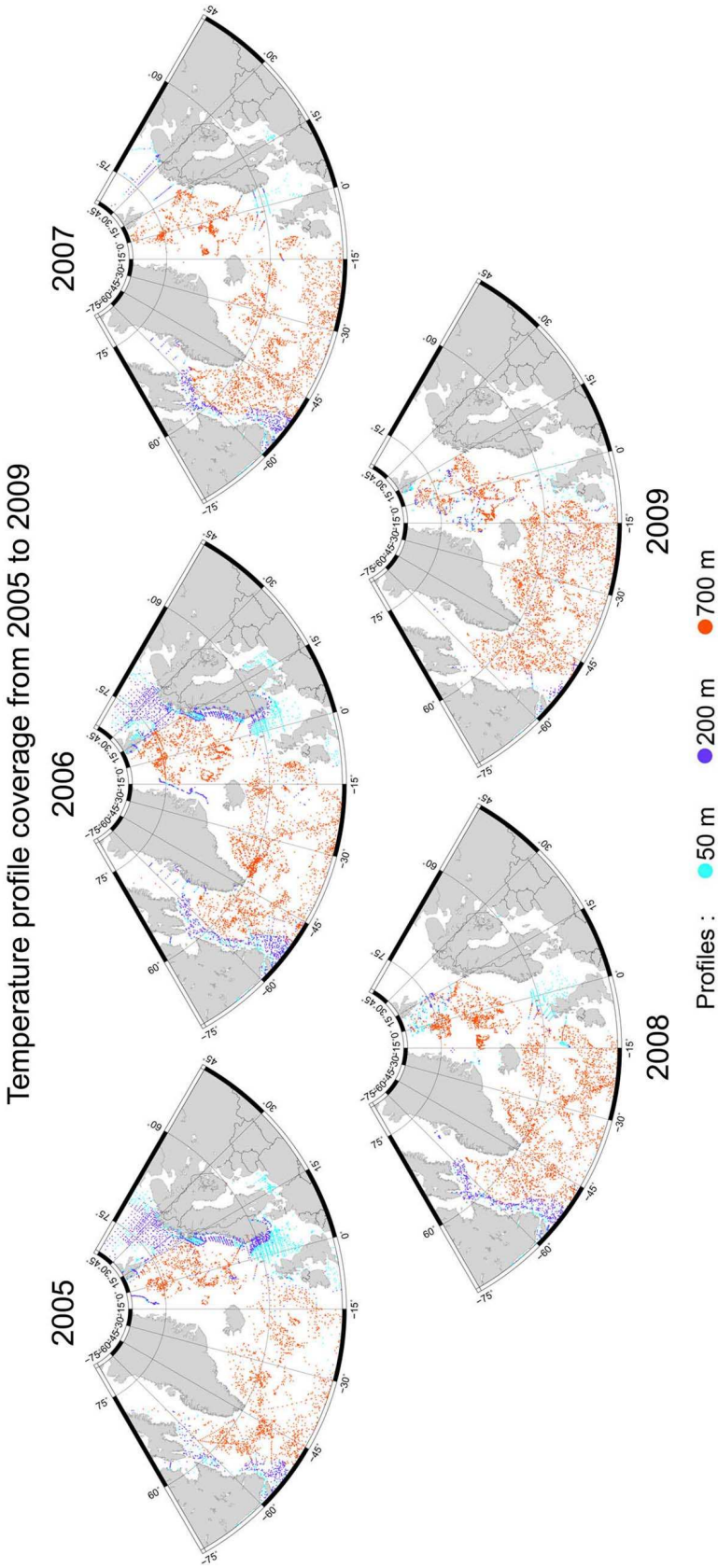

Figure 16. Temperature data coverage (EN3 data down to 700 m) for the years 2005 to 2009 in the North Atlantic and Nordic Seas sector.

It thus includes a regional ocean mass trend component (due to ocean circulation-driven mass redistribution), in addition to the global mean mass trend. Anyway, this ocean mass increase at least partly reflects the recent acceleration reported in ice mass loss from glaciers and ice sheets [e.g., *Steffen et al.*, 2010; *Rignot et al.*, 2011].

[41] The results of the present study show that between 1950 and 1995, sea level along Norwegian and Russian coasts does not display any significant upward trend, while being highly correlated to the AO. On the other hand, since the mid-to-late 1990s, coastal sea level in the Norwegian and Russian sectors has been rising faster during the previous decades. This coincides with strong changes affecting thermosteric and halosteric sea level in the North Atlantic and Nordic Seas, with simultaneous increase in temperature and salinity over the past 15 years.

[42] Recent warming of the Arctic region has been reported by *Karcher et al.* [2003] and *Polyakov et al.* [2005]. These studies observed significant changes in temperature of the Arctic and Nordic Seas during the 1990s. *Rigor and Wallace* [2004] showed that areal coverage of multiyear sea ice decreased even during 1989–1990 when the AO was in extremely high index state. This could be explained by longer ice free periods during summer, the open ocean absorbing more heat, preventing formation of sea ice (positive feedback mechanism). Warming in the Nordic Seas reduces heat loss from the Atlantic water before it enters the Arctic Ocean, with warmer Atlantic water propagating into the Arctic region. *Carton et al.* [2011] investigated the interannual/decadal variability of Atlantic water in the Nordic and adjacent seas. Their analysis shows a succession of four multiyear warm events occurring in the region between 1950 and 2009 (i.e., the same time span as in the present study), the last reported warm event began in the late 1990s and persisted for nearly a decade. Our results clearly show that in the North Atlantic, Nordic Seas and coastal zones of Norway and even Russia, significant changes also affected sea level as of mid-to-late 1990s, in agreement with other recently reported changes in Arctic climate since 1–2 decades [i.e., *Serreze and Barry*, 2011]. This period (last 15 years) may represent a transition in the Earth system evolution as recently suggested by *Peltier and Luthcke* [2009] and *Roy and Peltier* [2011]. Finally our results also show an increase of the ocean mass component along the Norwegian coast, at least partly explained by the recent acceleration in land ice loss as reported by numerous recent studies.

[43] **Acknowledgments.** This work is a contribution to the MONARCH project funded under the 7th Framework Programme of the European Union. O. Henry and P. Prandi are respectively supported by the MONARCH project and a CNES-CLS PhD grant. W. Llovel benefited of a post-doctoral NASA grant. We are very grateful to M. Ishii for useful discussions as well as to Florent Lyard for helpful exchanges about the atmospheric forcing. We thank Dick Peltier as well as the Editor of the Journal and an anonymous reviewer for their numerous and detailed comments that greatly helped us improving the manuscript.

References

Bekryaev, R. V., I. V. Polyakov, and V. A. Alexeev (2010), Role of polar amplification in long-term surface air temperature variations and modern Arctic warming, *J. Clim.*, *23*, 3888–3906, doi:10.1175/2010JCLI3297.1.

Carrère, L., and F. Lyard (2003), Modeling the barotropic response of the global ocean to atmospheric wind and pressure forcing—Comparisons with observations, *Geophys. Res. Lett.*, *30*(6), 1275, doi:10.1029/2002GL016473.

Carton, J. A., G. A. Chepurin, J. Reagan, and S. Häkkinen (2011), Interannual to decadal variability of Atlantic water in the Nordic and adjacent seas, *J. Geophys. Res.*, *116*, C11035, doi:10.1029/2011JC007102.

Cazenave, A., and W. Llovel (2010), Contemporary sea level rise, *Annu. Rev. Mar. Sci.*, *2*, 145–173, doi:10.1146/annurev-marine-120308-081105.

Cazenave, A., and R. S. Nerem (2004), Present-day sea level change: Observations and causes, *Rev. Geophys.*, *42*, RG3001, doi:10.1029/2003RG000139.

Chambers, D. P. (2006), Evaluation of new GRACE time-variable gravity data over the ocean, *Geophys. Res. Lett.*, *33*, L17603, doi:10.1029/2006GL027296.

Church, J. A., and N. J. White (2011), Sea-level rise from the late 19th to the early 21st century, *Surv. Geophys.*, *32*(4–5), 585–602, doi:10.1007/s10712-011-9119-1.

Chylek, P., C. K. Folland, G. Lesins, and M. K. Dubey (2010), Twentieth century bipolar seesaw of the Arctic and Antarctic surface air temperatures, *Geophys. Res. Lett.*, *37*, L08703, doi:10.1029/2010GL042793.

Fu, L. L., and A. Cazenave (2001), *Satellite Altimetry and Earth Sciences: A Handbook of Techniques and Application*, *Int. Geophys. Ser.*, vol. 69, 463 pp., Academic, San Diego, Calif.

Gill, A. E. (1982), *Atmosphere-Ocean Dynamics*, 662 pp., Academic, San Diego, Calif.

Häkkinen, S., and G. L. Mellor (1992), Modeling the seasonal variability of the coupled Arctic ice-ocean system, *J. Geophys. Res.*, *97*, 20,285–20,304, doi:10.1029/92JC02037.

Holland, D. M., R. H. Thomas, B. de Young, M. H. Ribergaard, and B. Lyberth (2008), Acceleration of Jakobshawn Isbrae triggered by warm subsurface ocean waters, *Nat. Geosci.*, *1*, 659–664, doi:10.1038/ngeo316.

Ingleby, B., and M. Huddleston (2007), Quality control of ocean temperature at profiles-huistorical and real-time data, *J. Mar. Syst.*, *65*, 158–175, doi:10.1016/j.jmarsys.2005.11.019.

Intergovernmental Panel on Climate Change (2007), *Climate Change 2007: The Physical Science Basis: Working Group I Contribution to the Fourth Assessment Report of the Intergovernmental Panel on Climate Change*, edited by S. Solomon et al., Cambridge Univ. Press, New York.

Ishii, M., and M. Kimoto (2009), Reevaluation of historical ocean heat content variations with varying XBT and MBT depth bias corrections, *J. Oceanogr.*, *65*, 287–299, doi:10.1007/s10872-009-0027-7.

Kalnay, E. C., et al. (1996), The NCEP/NCAR 40-year reanalysis project, *Bull. Am. Meteorol. Soc.*, *77*, 437–471, doi:10.1175/1520-0477(1996)077<0437:TNYRP>2.0.CO;2.

Karcher, M. J., R. Gerdes, F. Kauker, and C. Koberle (2003), Arctic warming: Evolution and spreading of the 1990s warm event in the Nordic seas and the Arctic Ocean, *J. Geophys. Res.*, *108*(C2), 3034, doi:10.1029/2001JC001265.

Köhl, A., and D. Stammer (2008), Decadal sea level changes in the 50-year GECCO ocean synthesis, *J. Clim.*, *21*(9), 1876–1890, doi:10.1175/2007JCLI2081.1.

Kwok, R., G. F. Cunningham, M. Wensnahan, I. Rigor, H. J. Zwally, and D. Yi (2009), Thinning and volume loss of the Arctic Ocean sea ice cover: 2003–2008, *J. Geophys. Res.*, *114*, C07005, doi:10.1029/2009JC005312.

Lawrence, D. M., A. G. Slater, R. A. Tomas, M. M. Holland, and C. Deser (2008), Accelerated Arctic land warming and permafrost degradation during rapid sea ice loss, *Geophys. Res. Lett.*, *35*, L11506, doi:10.1029/2008GL033985.

Lemke, P., et al. (2007), Observations: Changes in snow, ice and frozen ground, in *Climate Change 2007: The Physical Science Basis: Working Group I Contribution to the Fourth Assessment report of the Intergovernmental Panel on Climate Change*, edited by S. Solomon et al., pp. 337–384, Cambridge Univ. Press, New York.

Levitus, S., J. L. Antonov, and T. P. Boyer (2005), Warming of the world ocean, 1955–2003, *Geophys. Res. Lett.*, *32*, L02604, doi:10.1029/2004GL021592.

Levitus, S., J. L. Antonov, T. P. Boyer, R. A. Locarnini, H. E. Garcia, and A. V. Mishonov (2009), Global ocean heat content 1955–2008 in light of recently revealed instrumentation, *Geophys. Res. Lett.*, *36*, L07608, doi:10.1029/2008GL037155.

Lombard, A., A. Cazenave, P. Y. Le Traon, and M. Ishii (2005), Contribution of thermal expansion to present-day sea-level change revisited, *Global Planet. Change*, *47*(1), 1–16, doi:10.1016/j.gloplacha.2004.11.016.

Milne, G., W. R. Gehrels, C. Hughes, and M. Tamisiea (2009), Identifying the causes of sea level changes, *Nat. Geosci.*, *2*, 471–478, doi:10.1038/ngeo544.

Paulson, A., S. Zhong, and J. Wahr (2007), Inference of mantle viscosity from GRACE and relative sea level data, *Geophys. J. Int.*, *171*, 497–508, doi:10.1111/j.1365-246X.2007.03556.x.

Peltier, W. R. (2004), Global glacial isostasy and the surface of the ice-age Earth: The ICE-5G (VM2) model and GRACE, *Annu. Rev. Earth Planet. Sci.*, *32*, 111–149, doi:10.1146/annurev.earth.32.082503.144359.

Peltier, W. R. (2009), Closure of the budget of global sea level rise over the GRACE era: The importance and magnitudes of the required corrections for global isostatic adjustment, *Quat. Sci. Rev.*, *28*, 1658–1674, doi:10.1016/j.quascirev.2009.04.004.

Peltier, W. R., and S. B. Luthcke (2009), On the origins of Earth rotation anomalies: New insights on the basis of both "paleogeodetic" data and Gravity Recovery and Climate Experiment (GRACE) data, *J. Geophys. Res.*, *114*, B11405, doi:10.1029/2009JB006352.

Polyakov, I. V., et al. (2005), One more step toward a warmer Arctic, *Geophys. Res. Lett.*, *32*, L17605, doi:10.1029/2005GL023740.

Ponte, R. M. (2006), Low-frequency sea level variability and the inverted barometer effect, *J. Atmos. Oceanic Technol.*, *23*(4), 619–629, doi:10.1175/JTECH1864.1.

Prandi, P., M. Ablain, A. Cazenave, and N. Picot (2012), A new estimation of mean sea level in the Arctic Ocean from satellite altimetry, *Mar. Geod.*, in press.

Preisendorfer, R. W. (1988), *Principal Component Analysis in Meteorology and Oceanography*, *Dev. Atmos. Sci. Ser.*, Vol. 17, Elsevier, Amsterdam.

Proshutinsky, A., V. Pavlov, and R. H. Bourke (2001), Sea level rise in the Arctic Ocean, *Geophys. Res. Lett.*, *28*(11), 2237–2240, doi:10.1029/2000GL012760.

Proshutinsky, A., I. M. Ashik, E. N. Dvorkin, S. Häkkinen, R. A. Krishfield, and W. R. Peltier (2004), Secular sea level change in the Russian sector of the Arctic Ocean, *J. Geophys. Res.*, *109*, C03042, doi:10.1029/2003JC002007.

Proshutinsky, A., I. Ashik, S. Häkkinen, E. Hunke, R. Krishfield, M. Maltrud, W. Maslowski, and J. Zhang (2007a), Sea level variability in the Arctic Ocean from AOMIP models, *J. Geophys. Res.*, *112*, C04S08, doi:10.1029/2006JC003916.

Proshutinsky, A., et al. (2007b), The Arctic Ocean, *Bull. Am. Meteorol. Soc.*, *89*, supplement, S86–S89.

Proshutinsky, A., et al. (2009), Ocean, *Bull. Am. Meteorol. Soc.*, *90*, supplement, S99–S102.

Proshutinsky, A., et al. (2011), The Arctic (Ocean), *Bull. Am. Meteorol. Soc.*, *92*(6), supplement, S145–S148.

Rignot, E., I. Velicogna, M. R. van den Broeke, A. Monaghan, and J. Lenaerts (2011), Acceleration of the contribution of the Greenland and Antarctic ice sheets to sea level rise, *Geophys. Res. Lett.*, *38*, L05503, doi:10.1029/2011GL046583.

Rigor, I. G., and J. M. Wallace (2004), Variations in the age of Arctic sea-ice and summer sea-ice extent, *Geophys. Res. Lett.*, *31*, L09401, doi:10.1029/2004GL019492.

Roy, K., and W. R. Peltier (2011), GRACE era secular trends in Earth rotation parameters: A global scale impact of the global warming process?, *Geophys. Res. Lett.*, *38*, L10306, doi:10.1029/2011GL047282.

Serreze, M. C., and R. G. Barry (2011), Processes and impacts of Arctic amplification: A research synthesis, *Global Planet. Change*, *77*(1–2), 85–96, doi:10.1016/j.gloplacha.2011.03.004.

Smith, L. C., Y. Sheng, G. M. MacDonald, and L. D. Hinzman (2005), Disappearing arctic lakes, *Science*, *308*, 1429, doi:10.1126/science.1108142.

Steffen, K. et al. (2010), Cryospheric contributions to sea level rise and variability, in *Understanding Sea-Level Rise and Variability*, edited by J. Church et al., pp. 177–225, Blackwell, Oxford, U. K., doi:10.1002/9781444323276.ch7.

Stroeve, J., M. M. Holland, W. Meier, T. Scambos, and M. Serreze (2007), Arctic sea ice decline: Faster than forecast, *Geophys. Res. Lett.*, *34*, L09501, doi:10.1029/2007GL029703.

Tamisiea, M. E., and J. X. Mitrovica (2011), The moving boundaries of sea level change: Understanding the origins of geographic variability, *Oceanography*, *24*(2), 24–39, doi:10.5670/oceanog.2011.25.

Vestøl, O. (2006), Determination of postglacial land uplift in Fennoscandia from leveling, tide gauges and continuous GPS stations using least-squares collocation, *J. Geod.*, *80*, 248–258, doi:10.1007/s00190-006-0063-7.

Wahr, J., S. Swenson, V. Zlotnicki, and I. Velicogna (2004), Time-variable gravity from GRACE: First results, *Geophys. Res. Lett.*, *31*, L11501, doi:10.1029/2004GL019779.

Wijffels, S. E., J. Willis, C. M. Domingues, P. Barker, N. J. White, A. Gronell, K. Ridgway, and J. A. Church (2008), Changing expendable bathythermograph fall rates and their impact on estimates of thermosteric sea level rise, *J. Clim.*, *21*, 5657–5672, doi:10.1175/2008JCLI2290.1.

Woodworth, P. L., and R. Player (2003), The permanent service for mean sea level: An update to the 21st century, *J. Coastal Res.*, *19*, 287–295.

Wunsch, C., and D. Stammer (1997), Atmospheric loading and the oceanic "inverted barometer" effect, *Rev. Geophys.*, *35*(1), 79–107, doi:10.1029/96RG03037.

Wunsch, C., R. M. Ponte, and P. Heimbach (2007), Decadal trends in sea level patterns: 1993–2004, *J. Clim.*, *20*(24), 5889–5911, doi:10.1175/2007JCLI1840.1.

Chapitre 4

Détection et attribution des variations actuelles du niveau de la mer

Dans la troisième partie de cette thèse, nous nous sommes intéressés à la question scientifique n°10 (voir section 1.5) qui porte sur les causes premières de la variabilité régionale du niveau de la mer. L'enjeu majeur lié à cette question est de savoir si la variabilité régionale du niveau de la mer telle que nous l'observons aujourd'hui (par altimétrie depuis 1993 et par reconstruction 2D depuis 1950) est le résultat de la variabilité naturelle du système climatique ou si l'on peut y détecter l'empreinte des activités anthropiques (émissions de gaz à effet de serre et d'aérosols, occupation des sols).

Les preuves de l'impact des activités anthropiques sur le climat se sont accumulées depuis 1990 et le premier rapport du GIEC (*Houghton et al.* [1990]). A cette époque il y avait encore peu d'observations qui révélaient l'influence de l'homme sur le climat (*Houghton et al.* [1990]). Par la suite, les observations se sont multipliées et les premières études de détection/attribution (D&A) ont vu le jour. Ces études couvrent un champ de recherche récent dont le but est de détecter et d'attribuer dans les observations et les modèles, la réponse du système climatique aux différents forçages extérieurs que sont la variabilité solaire, les éruptions volcaniques, les émissions de gaz à effet de serre dues aux activités humaines et aux changements d'occupation des sols, ainsi que les émissions d'aérosols anthropiques et naturels (par les volcans par exemple). Ces études permettent en particulier d'évaluer l'impact de l'activité anthropique sur le climat. Les premières études D&A furent menées sur les observations de température dans la basse atmosphère, dans les années 1990. Sur la base de leurs résultats, le 3ème rapport du GIEC (*Houghton et al.* [2001]) concluait en 2001 que le signal des gaz à effet de serre était détecté de manière fiable dans la courbe de température atmosphérique globale de la Terre et que la majorité du réchauffement global observé depuis les 50 dernières années était "probablement" lié à l'activité anthropique. Par la suite les études D&A se sont généralisées à d'autres observations (températures de l'océan, vent de surface, etc) et d'autres échelles spatiales (continents, océans) en s'appuyant sur une plus grande variété de modèles de climat et de simulations disponibles (exercice CMIP3). Leurs résultats ont confirmé et renforcé la conclusion du 3ème rapport si bien que le GIEC affirmait en 2007 dans la conclusion du 4ème rapport (*Solomon*

et al. [2007]) que la majorité du réchauffement global (océans et continents inclus) observé depuis les 50 dernières années était "très probablement" dûe à l'augmentation des gaz à effet de serre d'origine anthropique dans l'atmosphère. Depuis 2007, l'impact anthropique sur le climat a commencé à être détecté dans des mesures autres que la température : par exemple dans les mesures de la salinité des océans (*Terray et al.* [2012]; *Durack et al.* [2012]), de la fonte des glaciers de montagne (*Huss and Bauder* [2009]), de la réduction de la surface de la banquise (*Kay et al.* [2011]; *Overland et al.* [2011]) etc. Cependant, jusqu'à aujourd'hui, aucune étude de D&A ne s'est intéressée aux mesures des variations du niveau de la mer si bien qu'il n'y a pas dans la littérature de publications qui établissent un lien direct entre l'activité anthropique et l'augmentation du niveau de la mer.

On trouve néanmoins un certain nombre d'études de D&A qui traitent de chacune des 3 contributions majeures au niveau de la mer : le réchauffement de l'océan (e.g. *Gleckler et al.* [2012]), la fonte des glaciers de montagne (e.g.*Huss et al.* [2010]) et la perte de masse des calottes polaires (*Hanna et al.* [2008]). A travers ces études il est possible de faire un lien indirect entre le réchauffement climatique d'origine anthropique et l'augmentation du niveau de la mer au cours des 50 dernières années. Dans la section 4.1 nous résumons ces études et évaluons les conclusions que l'on peut en tirer en ce qui concerne le niveau de la mer.

On trouve aussi dans la littérature un certain nombre d'études qui reproduisent la hausse du niveau de la mer au cours des dernières décennies, à l'échelle globale ou régionale, avec des modèles et qui montrent que l'on ne peut en reproduire les variations si l'on ne prend pas en compte les émissions de gaz à effet de serre (*Gregory et al.* [2006]; *Jevrejeva et al.* [2009]). Ces études montrent que les variations du niveau de la mer sont compatibles avec les observations actuelles d'augmentation des gaz à effet de serre anthropiques. Cependant elles ne détectent pas et n'attribuent pas ces variations aux gaz à effet de serre anthropiques car elles ne montrent pas que ces variations sont incompatibles avec les autres composantes du système climatique. Le système climatique est un système chaotique qui génère de la variabilité aléatoire à toutes les échelles de temps à travers les réactions du système aux forçages extérieurs (e.g. variabilité solaire, les émissions de gaz à effet de serre, etc) et à travers les interactions à l'intérieur et entre les différentes composantes du système (atmosphère, océan, terres emergées, cryosphère et biosphère) (voir *Hasselmann* [2010]). Les variations du niveau de la mer, même si elles présentent une tendance long terme forte, pourraient être le fruit de la variabilité aléatoire (et chaotique) d'une de ces composantes et donc avoir une autre origine que le réchauffement climatique d'origine anthropique. Dans la section 4.2 nous résumons d'abord les informations apportées par ces études du niveau de la mer avec des modèles qui prennent en compte les gaz à effet de serre. Nous évaluons les conclusions que l'on peut en tirer sur les origines des variations du niveau de la mer en particulier à l'échelle globale. Ensuite nous présentons la première étude de D&A sur le niveau de la mer que nous avons développé et publié en 2012. Elle s'intéresse à la variabilité régionale du niveau de la mer et se focalise sur l'océan Pacifique tropical.

4.1 Détection et attribution des contributions au niveau de la mer

Dans cette section nous résumons les études D&A qui ont traité différentes contributions au niveau de la mer (le réchauffement de l'océan, la fonte des glaciers de montagne et la perte de masse des calottes polaires) et nous évaluons les conclusions que l'on peut en tirer sur l'impact éventuel des activités anthropiques sur le niveau de la mer.

4.1.1 Le réchauffement de l'océan

Les observations montrent que les couches supérieures de l'océan (0-700m) se réchauffent depuis les années 1950 (*Bindoff et al.* [2007]; *Domingues et al.* [2008]; *Levitus et al.* [2009]; *Ishii and Kimoto* [2009]). De plus, ce réchauffement qui représente plus de 90% de l'augmentation de chaleur totale de la Terre depuis les anneés 1950 (voir section 1.3.1 et *Levitus et al.* [2005]; *Church et al.* [2011]) est en accord avec le déséquilibre radiatif de la Terre qui montre que sur la même période, la terre reçoit plus d'énergie du soleil qu'elle n'en emet vers l'espace (*Church et al.* [2011]; *Hansen et al.* [2011]).

Plusieurs études ont démontré statistiquement que la majorité de ce réchauffement était dûe aux activités anthropiques et à leur impact sur le bilan radiatif net de la planète (*Solomon et al.* [2007]). Cependant, à l'époque de ces études, des incertitudes subsistaient car les modèles de climats ne semblaient pas capables de reproduire précisement la forte variabilité inter-décennale présente dans les observations de température des 700 premiers mètres de l'océan (*Hegerl et al.* [2007]; *Solomon et al.* [2007]). Ceci jetait le doute à la fois sur les modèles de climat et sur les mesures du réchauffement de l'océan. En effet, pour expliquer cette incohérence, la capacité des modèles de climat à reproduire le réchauffement global de l'océan était remise en cause ainsi que la fiabilité des mesures de température de l'océan (*Gregory et al.* [2004]; *AchutaRao et al.* [2006]). Après le 4ème rapport du GIEC, plusieurs auteurs ont étudié les mesures historiques de température de l'océan à la recherche d'éventuels artefacts de mesures. *Gouretski and Koltermann* [2007] ont découvert un biais systématique (dépendant du temps) dans les mesures de température faites par les sondes XBT (voir section 1.3.1). Etant donné le grand nombre de mesures historiques réalisées avec les sondes XBT, ce biais avait un impact significatif sur les courbes de réchauffement global de l'océan. La correction des bases de données globale de température a révélé que ce biais avait pour conséquence un surestimation de la variabilité inter-décennale dans le réchauffement des couches supérieures de l'océan (*Wijffels et al.* [2008]; *Domingues et al.* [2008]; *Ishii and Kimoto* [2009]; *Levitus et al.* [2009]). La comparaison des bases de données corrigées avec un jeu de modèles de climat (de l'exercice CMIP3) soumis à l'ensemble des forçages extérieurs d'origine naturelle et anthropique a montré que désormais, les modèles de climat reproduisaient bien la variabilité inter-décennale et les tendances à long terme des observations du réchauffement océanique (*Domingues et al.* [2008]).

Quand on considère l'ensemble des modèles de climat utilisés pour le 4ème rapport du GIEC (exercice CMIP3), on observe néanmoins que la tendance du réchauffement océanique modélisée (700 premiers mètres) est légèrement plus faible que celle qui est observée. De plus, il est intéressant de noter que les modèles qui ne prennent en compte

que les émissions anthropiques de gaz à effet de serre (i.e sans prendre en compte les éruptions volcaniques et la variabilité solaire) sous estiment la variabilité inter-décennale du réchauffement océanique et surestime sa tendance sur les 50 dernières années. Ceci s'explique par la non-prise en compte des éruptions volcaniques. En effet, l'océan répond à une éruption volcanique par un soudain refroidissement de ses couches supérieures suivi d'une phase de retour à la normale qui peut durer une dizaine à plusieurs dizaines d'années (*Church et al.* [2005]; *Delworth et al.* [2005]; *Domingues et al.* [2008]). Ainsi la série d'éruptions volcaniques qui a eu lieu au cours de la seconde moitié du XX$^{\text{ème}}$ siècle, cumulée sur les 50 ans, a eu pour effet de diminuer la tendance long terme du réchauffement global et d'augmenter la variabilité multi-décennale (*Gregory et al.* [2006]; *Gleckler et al.* [2006]; *AchutaRao et al.* [2007]; *Palmer et al.* [2009]; *Stenchikov et al.* [2009]). *Gleckler et al.* [2012] ont confirmé ces résultats en montrant que parmi toutes les simulations CMIP3 du XX$^{\text{ème}}$, ce sont les simulations qui prennent en compte à la fois les émissions anthropiques de gaz à effet de serre et d'aérosols ainsi que les éruptions volcaniques qui représentaient le mieux le réchauffement global des 700 premiers mètres de l'océan. De plus ces auteurs ont détecté l'impact du forçage anthropique à la fois dans la courbe de réchauffement global des 700 premiers mètres de l'océan mais aussi dans la variabilité du réchauffement entre les différents bassins océaniques. En particulier ils montrent que le réchauffement de l'océan d'origine anthropique devient significatif (à 99% de niveau de confiance) à partir des années 1980 et devient ensuite de plus en plus fort. Ces résultats apparaissent robustes aux incertitudes des observations, des modèles et de la méthode.

Ces différents résultats montrent qu'aujourd'hui il y a un bon accord entre les modèles de climat et les observations en ce qui concerne le réchauffement global des 50 dernières années. Ceci a permis d'établir précisément l'impact des émissions anthropiques ainsi que des éruptions volcaniques sur la variabilité multi-décennale et la tendance du réchauffement océanique. En particulier, l'origine anthropique de l'augmentation du contenu thermique moyen de l'océan, depuis les années 1960, est avéré (*Levitus et al.* [2005, 2009, 2012]; *Hansen et al.* [2011]).

En revanche en ce qui concerne la variabilité régionale du contenu thermique de l'océan, l'origine et les causes sont bien moins claires. Ceci est dû en particulier au très petit nombre d'études qui traitent explicitement ce point dans la littérature. *Gleckler et al.* [2012] précisent à la fin de leur analyse que si l'on ne prend pas en compte le signal global, et que l'on analyse la variabilité régionale du contenu thermique de l'océan à l'echelle des bassins océaniques, seul la moitié des tests de D&A qu'ils ont développés sont positifs laissant la conclusion incertaine. Ceci montre qu'à l'échelle des bassins océaniques la signature du forçage anthropique reste encore difficile à détecter.

4.1.2 La salinité de l'océan

Les variations de salinité de l'océan n'affectent pas les variations du niveau global de la mer, en revanche elles génèrent de la variabilité régionale dans le niveau de la mer (voir section 1.3.1). Dans le 4$^{\text{ème}}$ rapport du GIEC, les observations de la salinité océanique indiquaient une augmentation de la salinité dans les couches supérieures des régions subtropicales et une diminution de la salinité à hautes latitudes au voisinage des régions polaires. La structure spatiale de ces variations de salinité correspond à ce qu'on peut attendre d'une

accélération du cycle hydrologique global. Depuis 2007, ces résultats ont été confirmés avec les données Argo. En effet de nombreuses études révèlent que depuis 2007, les structures spatiales de la salinité rapportée dans le rapport du GIEC se sont intensifiées (*Hosoda et al.* [2009]; *von Schuckmann and Le Traon* [2011]; *Roemmich and Gilson* [2009]; *Durack and Wijffels* [2010]). De plus la différence de salinité entre l'océan Pacifique (faible salinité) et l'océan Atlantique (forte salinité) s'est accrue. A la surface, les structures spatiales se sont intensifiées suggérant aussi l'accélération du cycle hydrologique global (*Hosoda et al.* [2009]; *Roemmich and Gilson* [2009]; *Durack and Wijffels* [2010]; *Durack et al.* [2012]). Les régions de l'océan recevant peu de précipitations ont reçu moins de précipitations depuis 2007. De même, les régions marquées par une forte évaporation ont connu une évaporation accrue depuis 2007. En conséquence, les régions fortement salées de l'océan sont devenues encore plus salées. Le processus inverse s'est passé pour les régions peu salées.

Ces observations globales sont confirmées à l'échelle régionale par plusieurs études avec des mesures plus longues (e.g. *Cravatte et al.* [2009]; *Curry et al.* [2003]). En structure spatio-temporelle, elles correspondent aux variations de salinité simulées par les modèles CMIP3 pour le XX$^{\text{ème}}$ et le XXI$^{\text{ème}}$ siècle (SRES scenarii) (*Durack et al.* [2012]). Cependant, en amplitude, sur la période 1950-2000, les observations montrent une amplification double de celle qui est simulée par les modèles CMIP3 (*Durack et al.* [2012]).

En résumé, de nombreuses études confirment l'observation de changements significatifs dans la salinité océanique (à la surface et dans les couches plus profondes) au cours des dernières décennies à l'échelle globale et régionale. Pourtant on trouve très peu d'études D&A dans la littérature qui ont analysé le lien éventuel entre ces changements de salinité et l'activité anthropique. Concernant la salinité océanique sur les 500 premiers mètres de l'océan, *Stott et al.* [2008] ont montré que dans l'océan Atlantique, l'augmentation de la salinité au Nord (20°N à 50°N) révèle un signal qui pourrait être d'origine anthropique (i.e. correspond à ce que simulent les modèles avec forçage anthropique) cependant ce signal n'est pas significatif comparé à la variabilité interne locale. Concernant la salinité de surface, *Terray et al.* [2012] confirment les résultats de *Stott et al.* [2008] dans le Nord de l'océan Atlantique. En revanche, à plus grande échelle, dans la bande équatoriale (30°S à 50°N) des océans Atlantique et Pacifique, *Terray et al.* [2012] détectent des changements significatifs dans la salinité de surface qui différent de la variabilité interne locale (avec un niveau de confiance de 95%). De plus, ils montrent que ces changements sont dûs au forçage anthropique. Les changements de salinité les plus forts qu'ils ont mis en évidence sont entre les tropiques (entre 30°S et 30°N) et dans l'ouest du Pacifique. Leur étude montre aussi que la différence de salinité de surface entre l'océan Pacifique et l'océan Atlantique s'est accrue entre 1970 et 2002 en partie à cause de l'activité anthropique.

4.1.3 La fonte des glaciers de montagne

Dans le passé, les variations inter-décennales à multi-séculaires de la masse des glaciers de montagne (e.g. *Reichert et al.* [2002]; *Vuille et al.* [2008]; *Roe and O'Neal* [2009]; *Huss et al.* [2010]) et de leur extension (*Chinn et al.* [2005]) ont été dominées par la variabilité interne du système climatique. Aujourd'hui, c'est l'augmentation récente de la température globale qui explique la perte actuelle de masse des glaciers de montagne (*Reichert et al.* [2002]; *Huss and Bauder* [2009]; *Huss et al.* [2010]).

Cependant, il existe très peu d'études D&A qui estiment directement le rôle du forçage anthropique dans la perte de masse actuelle des glaciers. Ceci est dû en particulier aux difficultés engendrées par la différence d'échelle très grande entre d'une part l'aspect global du forçage anthropique et d'autre part la dynamique très locale des glaciers de montagne (*Molg and Kaser* [2011]).

En analysant un site à basse latitude et un site à haute latitude, *Reichert et al.* [2002] ont montré que la variabilité interne du système climatique telle qu'elle est modélisée par le modèle couplé ECHAM4, sur plusieurs millénaires, ne pouvait expliquer le rétrécissement (en longueur) des glaciers observé au cours du XX$^{\text{ème}}$ siècle. A l'échelle du siècle, plusieurs études ont estimé les changements locaux de précipitation et de température de l'air, nécessaires pour expliquer les variations de la longueur ou du bilan de masse des glaciers de montagne (*Oerlemans* [2005]; *Yamaguchi et al.* [2008]; *Huss and Bauder* [2009]; *Huss et al.* [2010]). Ces études montrent que la perte récente (dernières décennies) de masse des glaciers ne peut s'expliquer qu'avec des changements dans les précipitations ou les températures qui excèdent ceux que peut produire la variabilité interne du système climatique.

4.1.4 La perte de masse des calottes polaires

La détection et l'attribution du signal anthropique dans la perte de masse des calottes polaires est difficile car la physique à l'origine de la perte de masse est encore mal comprise (voir section 1.3.2). En conséquence, les mécanismes principalement responsables de cette perte de masse sont mal représentés ou même pas du tout implémentés dans les modèles de climat ce qui empêche toute étude D&A. Pourtant, les observations montrent des changements significatifs dans la perte de masse depuis les années 1990 (voir section 1.3.2).

Pour le Groenland, une part significative ($\sim$50%) de la perte de masse vient d'une augmentation de la fonte en surface or celle-ci a été attribuée par *Hanna et al.* [2008] au réchauffement global. De plus cette augmentation de la fonte de surface est en accord avec les simulations des modèles de climat qui incluent les forçages anthropiques (*Hegerl et al.* [2007]; *Mernild et al.* [2009]). En revanche la perte de masse venant de l'accélération de l'écoulement dynamique de la glace vers l'océan ($\sim$50%) n'a pas encore fait l'objet d'études de D&A ni pour le Groenland, ni pour l'Antarctique où elle constitue la majeure source de perte de glace.

4.2 Cas du niveau de la mer

4.2.1 Le niveau moyen : échelle globale

Jusqu'à aujourd'hui, il n'existe pas, dans la littérature, d'étude D&A proprement dite (faisant intervenir un modèle de climat couplé du type CMIP3) qui traite explicitement du niveau de la mer à l'échelle globale ou régionale .

A l'échelle du globe, on peut cependant faire un lien indirect entre la hausse du niveau de la mer global et le forçage anthropique grâce aux récentes études D&A sur les différentes contributions au niveau de la mer que nous venons de résumer. Celles-ci montrent que le forçage anthropique est impliqué dans une large part des variations des contributions au niveau de la mer sur les dernières décennies. En effet, ce sont les émissions de gaz à effet de serre et d'aérosols d'origine anthropique et volcanique qui expliquent la tendance et la variabilité inter-décennale du réchauffement global des 700 premiers mètres de l'océan depuis 1960. De même, le forçage anthropique explique la fonte anormalement rapide que l'on observe actuellement à la surface des glaciers de montagne et du Groenland. Quand on somme la contribution au niveau de la mer du réchauffement de l'océan (de 0 à 700 m), de la fonte des glaciers de montagne et de la fonte de surface du Groenland, on explique 70% de la hausse du niveau de la mer sur la période 1993-2010 (voir section 1.3) et 65% sur la période 1972-2008 (*Church et al.* [2011]). Les émissions de gaz à effet de serre et d'aérosols d'origine anthropique sont donc impliqués dans 65%, au moins, de l'augmentation du niveau de la mer global observé sur les dernières décennies.

Ce résultat est confirmé par l'étude de *Jevrejeva et al.* [2009] qui utilise un modèle semi-empirique statistique qui lie les différents forçages du climat (comptés en terme de forçage radiatif global) aux variations du niveau de la mer pour estimer la contribution des forçages naturels (variabilité solaire et volcanique) et du forçage anthropique sur la variabilité du niveau de la mer global. Ces auteurs trouvent qu'avant 1800, la variabilité du niveau de la mer global s'explique par les forçages volcanique et solaire. En revanche depuis 1800, ils estiment que seulement 25% de la tendance long terme du niveau de la mer global s'expliquent par la variabilité naturelle tandis que 75% ont pour origine les émissions anthropiques de gaz à effet de serre et d'aérosols.

Ceci répond à la question scientifique n°10 de la section 1.5 en terme de niveau global : l'une des causes de l'augmentation du niveau global de la mer sur les dernières décennies est le réchauffement climatique d'origine anthropique. Ceci vient d'être montré de manière indirecte à travers la détection et l'attribution du signal anthropique dans les contributions au niveau de la mer. Cependant il ne peut être exclu que la variabilité naturelle du système climatique (aux échelles multi-décennales) joue aussi un rôle. Il serait intéressant dans le futur de vérifier que l'on peut détecter et attribuer le signal anthropique directement dans le signal de montée du niveau de la mer global à l'aide de modèles de climat couplés (CMIP5 par exemple) et d'estimer le rôle joué par la variabilité naturelle du système climatique.

4.2.2 La variabilité régionale

A l'échelle régionale, on dispose de moins d'informations concernant l'impact anthropique sur la variabilité du niveau de la mer. Non seulement on ne trouve pas dans la littérature, d'études D&A sur la varibilité régionale du niveau de la mer, mais en plus, les études sur les contributions au niveau de la mer, résumées plus haut, ne traitent en général pas ou très peu de la variabilité régionale. *Gleckler et al.* [2012] expliquent à la fin de leur article que l'attribution de la variabilité régionale du réchauffement de l'océan (à l'échelle des bassins océaniques) n'est pas significative car seuls la moitié des tests D&A qu'ils ont développés sont positifs. Ils soulignent néanmoins que les quelques tests positifs suggèrent qu'un signal anthropique pourrait être détecté et probablement attribué dans

certaines régions. *Terray et al.* [2012] détectent bien un signal anthropique dans la variabilité régionale de la salinité entre 1970 et 2003 mais il s'agit là de la salinité de surface qui a peu d'impact sur le niveau de la mer. En conséquence, nous ne pouvons pas conclure quant à l'impact anthropique sur la variabilité régionale du niveau de la mer, même de manière indirecte.

A défaut de trouver des études D&A, proprement dites, qui s'intéressent à la variabilité régionale du niveau de la mer dans la littérature, on trouve plusieurs études qui ont cherché un lien de cause à effet dans la région indo-pacifique tropicale, entre le réchauffement local, les variations de la circulation atmosphérique et des variations anormales du niveau de la mer.

Dans l'océan Indien tropical

Dans l'océan Indien, *Han et al.* [2010] ont montré que depuis 1960 le niveau de la mer a augmenté partout sauf dans le sud de l'océan Indien tropical. Ils ont reproduit ces observations avec un modèle d'océan forcé par les vents de surface et ont montré que ces variations du niveau de la mer s'expliquaient par les renforcements des cellules de Hadley et de Walker au dessus de l'océan Indien. Les auteurs soulignent qu'une partie de ce renforcement peut être attribuée au réchauffement au dessus de l'océan Indien, lui même lié à l'augmentation des gaz à effet de serre et suggèrent donc une origine anthropique aux tendances du niveau de la mer depuis 1960 dans l'océan Indien. Ceci donne des éléments de réponse à la question scientifique n°10 de la section 1.5 en ce qui concerne le niveau de la mer dans l'océan Indien : la cause première de la structure spatiale du niveau de la mer que l'on observe dans l'océan Indien depuis 1960 semble être liée à l'augmentation des gaz à effet de serre et leur impact sur la circulation atmosphérique actuelle selon *Han et al.* [2010]... De plus, ceci donne aussi des éléments de réponse à la question scientifique n°8 : la variation du niveau de la mer dans l'océan Indien tropical n'apparait pas stable dans le temps, elle semble avoir évolué en temps et en espace au cours des dernières décennies en réponse aux variations basse fréquence locales du vent produites par les changements de circulation atmosphérique.

Dans l'océan Pacifique tropical

Dans l'océan Pacifique tropical, de nombreuses études ont montré que les tendances régionales du niveau de la mer à l'Ouest du Pacifique au cours des dernières décennies étaient liées à un renforcement des vents d'Est (*Carton et al.* [2005]; *Köhl et al.* [2007]; *Lee and McPhaden* [2008]; *Timmermann et al.* [2010]; *Merrifield* [2011]). En particulier *Merrifield* [2011]) a montré à partir de marégraphes situés à l'Ouest du Pacifique, que le niveau de la mer y avait augmenté brutalement dans les années 1990 en réponse à un renforcement des vents d'Est visible dans la réanalyse ORAS3 de l'ECMWF. *Merrifield and Maltrud* [2011] ont confirmé par la suite ce résultat en reproduisant la structure et l'augmentation des tendances du niveau de la mer observés dans la région depuis les années 1990, avec un modèle d'océan forcé par des vent d'Est de force croissante. Comme *Merrifield* [2011] n'avait pas trouvé de corrélation entre le niveau de la mer moyen à l'Ouest du Pacifique (obtenu en moyennant les données marégraphiques) et les modes de variabilité locaux PDO et NGPO (2$^{\text{ème}}$ EOF des hauteurs de mer calculées sur la région 25°-62°N par 180°-110°O, *Di Lorenzo et al.* [2010]) à cause de l'augmentation brutale du niveau de la mer dans les années 1990, il a suggéré que celle-ci ne pouvait résulter de la variabilité

naturelle du sytème climatique. Cette proposition était renforcée par le fait qu'il a trouvé une corrélation entre l'augmentation brutale, dans les années 1990, du niveau de la mer à l'Ouest du Pacifique avec des augmentations similaires de la température de surface et du rayonnement grande longueur d'onde locaux. Dans une étude très récente cependant, *Merrifield and Thompson* [in revision] redéveloppent l'étude de *Merrifield* [2011] en retirant le niveau de la mer global au niveau de la mer de l'Ouest du Pacifique (calculé comme la moyenne des marégraphes de l'Ouest du Pacifique) et en considérant la réanalyse de vent NCEP au lieu de ORAS3 de l'ECMWF qui semble être marqué par des biais anormaux. Ces auteurs trouvent finalement que le niveau de la mer régional dans l'Ouest du Pacifique au cours des dernières décennies est bien corrélé aux fluctuations du mode PDO et aux fluctuations du vent qu'il engendre. En conséquence *Merrifield and Thompson* [in revision] concluent finalement que les tendances régionales actuellement observées dans le Pacifique tropical sont finalement probablement d'origine naturelle et non anthropique.

Feng et al. [2004], en étudiant le niveau de la mer avec le marégraphe de Fremantle (côte Ouest de l'Australie) entre 1900 et 2002, ont eux aussi remarqué un léger faiblissement des vents d'Est sur le Pacifique entre 1950 et 1990 suivi d'une augmentation forte dans les années 1990. Ils ont pu établir ces résultats à l'aide des mesures du niveau de la mer à Fremantle car les variations basses fréquences des vents d'Est au dessus du Pacifique génèrent des ondes très basse fréquence (avec des périodes inter-annuelles à multi-décennales) de variation du niveau de la mer à l'Ouest du Pacifique qui se propagent à travers les détroits indonésiens et sont capturées le long de la côte Ouest Australienne. *Feng et al.* [2010] ont confirmé que les variations du niveau de la mer au marégraphe de Pohnpei situé à l'Ouest du Pacifique étaient cohérentes avec celles de Fremantle aux échelles inter-annuelles à multi-décennales. Dans une étude ultérieure (*Feng et al.* [2011]), ces auteurs ont aussi confirmé que l'augmentation des vents d'Est au dessus du Pacifique dans les années 1990, qu'ils avaient induites du marégraphe de Fremantle, se retrouvaient dans la majorité des produits de réanalyse atmosphérique . En ce sens les observations de *Feng et al.* [2004, 2010, 2011] confirment celles de *Merrifield* [2011]; *Merrifield and Maltrud* [2011] en ce qui concerne les variations du niveau de la mer dans l'Ouest du Pacifique au cours des dernières décennies et leur relation aux variations basse fréquence des vents d'Est. En revanche *Feng et al.* [2004] s'opposent à *Merrifield* [2011] et *Merrifield and Maltrud* [2011] quand à l'origine de ces variations. En effet, *Feng et al.* [2004] trouvent une forte corrélation entre les variations du niveau de la mer à Fremantle et le mode de variabilité PDO sur toute la longueur de l'enregistrement. De plus, à l'aide d'un modèle statistique, ils montrent que la PDO explique 63% de la variabilité du niveau de la mer à Fremantle suggérant que le niveau de la mer à Fremantle tout comme le niveau de la mer dans l'Ouest du Pacifique et les variations de vent d'Est sur le Pacifique observés au cours des dernières décennies résultent essentiellement de la variabilité naturelle du système climatique. In fine, ces conclusions s'accordent avec celles de *Merrifield and Thompson* [in revision].

L'origine principale des variations du niveau de la mer dans le Pacifique au cours des dernières décennies fait donc débat. S'agit-il de la variabilité naturelle du système climatique (hypothèse de *Feng et al.* [2004] et *Merrifield and Thompson* [in revision]) ou observe t'on déjà depuis les années 1990 l'impact du réchauffement global et du forçage anthropique (suggestion de *Merrifield and Maltrud* [2011]) ? Ce point est d'autant plus important que l'Ouest du Pacifique est l'une des régions les plus sensibles du monde à l'augmentation du

niveau de la mer : on y trouve les plus fortes augmentations du niveau de la mer depuis les années 1990 et parmi les îles les plus basses au monde (voir section 3.1).

Pour tirer au clair ce problème et tenter de donner une réponse à la question scientifique n°10 de la section 1.5 pour la région du Pacifique tropical nous avons développé une étude D&A afin de détecter et attribuer le signal du forçage anthropique dans les variations du niveau de la mer local observé depuis les années 1990 (par altimétrie). Cette étude s'intitule "Tropical Pacific spatial trend patterns in observed sea level : internal variability and/or anthropogenic signature ?"

Résumé de l'article : "Tropical Pacific spatial trend patterns in observed sea level : internal variability and/or anthropogenic signature ?" (l'article original est inséré à la fin de cette section 4.2.2).

Dans cette étude nous considérons la variabilité régionale du niveau de la mer telle qu'elle est observée par l'altimétrie dans le Pacifique tropical au cours des 17 dernières années i.e. entre 1993 et 2010. Nous caractérisons cette variabilité régionale par la carte des tendances du niveau de la mer sur le Pacifique tropical au cours de ces 17 ans à laquelle nous retirons la tendance du niveau de la mer global afin de ne garder que le signal de variablité régionale. En effet, l'impact du forçage anthropique sur le niveau global de la mer et sa tendance étant déjà connu par ailleurs (voir section 4.2.2), nous nous sommes intéressés ici uniquement à l'impact anthropique sur variabilité régionale (qui n'a jamais été étudié auparavant).

17 ans de mesures est un enregistrement un peu court pour espérer détecter l'impact de l'augmentation des gaz à effet de serre qui est un processus lent. Pour cette raison, avant de traiter la question de l'impact anthropique, nous cherchons à déterminer si les tendances à 17 ans du niveau de la mer, telles qu'observées par altimétrie, sont représentatives de tendances plus longues ou si elles évoluent avec le temps et l'espace. Pour cela nous utilisons la reconstruction 2D du niveau de la mer développée dans la section 2.2.2. Grâce aux 60 ans couverts par la reconstruction (entre 1950 et 2010), nous calculons 43 cartes de tendances du niveau de la mer dans le Pacifique tropical sur 43 fenêtres successives de 17 ans (en commençant en 1950 et en calculant pour chaque année la carte des tendance sur les 17 années à venir, on obtient 43 cartes). Nous calculons ensuite le premier EOF de ce jeu de 43 cartes de tendances à 17 ans afin de déterminer quelle est la structure spatiale des tendances à 17 ans dominante sur les 60 dernières années (en terme de variance expliquée) et quelle est son évolution temporelle. Il s'avère que c'est la structure spatiale observée au cours des 17 ans d'altimétrie qui est la structure dominante sur les 60 dernières années (37% de la variance expliquée). De plus cette structure a fluctué dans le passé avec une periode autour de 25 ans. Elle a été négative dans les années 1980 puis est redevenue positive dans les années 60.

Ce résultat est totalement nouveau et répond à la question scientifique n°8 de la section 1.5 (qui porte sur l'évolution temporelle de la variabilité régionale des tendances du niveau de la mer) pour l'océan Pacifique tropical. Nous confirmons avec cette observation ce que suggérait l'origine thermostérique de la variabilité régionale du niveau de la mer à savoir que les tendances du niveau de la mer ne sont pas stables dans le temps mais fluctuent en temps et en espace (voir section 2.1.1). Les structures spatiales observées par l'altimétrie dans les tendances du niveau de la mer au cours des 17 dernières années ne sont donc

pas représentatives de structures plus long terme. En revanche, nous mettons en évidence que ces structures ne sont pas aléatoires. Elles sont en fait la manifestation actuelle d'une fluctuation à basses fréquences du niveau de la mer qui suit des basses fréquences du mode de variabilité ENSO (mise en évidence ici avec l'indice niño3.4 reconstruit depuis 1856 à partir des données HadSST de *Kaplan et al.* [1998]).

Ce résultat inattendu est confirmé par les modèles de climat dans les simulations qui ne prennent en compte que la variabilité interne du système climatique (simulations de contrôle) c'est à dire sans les forçages extérieurs que sont la variabilité solaire et volcanique et les émissions anthropiques. En effet, parmi les 8 modèles du projet CMIP3 qui fournissent les variables nécessaires à notre analyse, 6 d'entre eux montrent, dans leur simulation de contrôle, des oscillations basses fréquences (significativement différentes d'un processus aléatoire avec un niveau de confiance de 95%) des tendances régionales à 17 ans du niveau de la mer dans l'océan Pacifique tropical avec une signature spatiale proche de celle qui est observée par l'altimétrie aujourd'hui. De plus 5 d'entre eux montrent que ces oscillations suivent aussi des basses fréquences significatives du mode climatique ENSO. Ceci suggère que les mécanismes physiques en jeu dans ces co-oscillations basses fréquences du niveau de la mer et d'ENSO sont propres au système climatique interne et ne sont pas directement liés à l'existence de forçages extérieurs. Cependant ceci n'exclut pas que les forçages extérieurs jouent un rôle dans la modulation de la fréquence et de l'amplitude de ces oscillations. Parmi les 5 simulations qui confirment les co-oscillations du niveau de la mer avec ENSO, seules 2 montrent des oscillations basses fréquences avec des périodes entre 20 et 30 ans comparable à ce qui est observé dans la reconstruction. Les autres montrent des périodes plus courtes autour de 18-20 ans (sauf pour le modèle UKMO hadcm3). Pourquoi ces périodes sont elles plus courtes ? Est ce parce que les forçages extérieurs n'ont pas été pris en compte ?

Afin de déterminer l'existence éventuelle d'un tel impact des forçages extérieurs (dont les gaz à effet de serre) sur les oscillations des tendances du niveau de la mer à 17 ans dans le Pacifique tropical, nous analysons, pour les mêmes modèles de climat, les simulations du climat du XX$^{\text{ème}}$ siècle (simulations 20c3m) qui comprennent tous les forçages extérieurs. Nous considérons tout d'abord la signature spatiale des tendances à 17 ans de chaque simulation de contrôle calculée plus haut (i.e. 1$^{\text{er}}$ EOF de la série des cartes de tendances à 17 ans qui est similaire pour 5 des 6 simulations de contrôle à celui que l'on observe dans la reconstruction) comme étant la signature du mode naturel de variation des tendances à 17 ans du niveau de la mer. Nous la projetons ensuite sur les simulations du XX$^{\text{ème}}$ siècle correspondants à chaque modèle pour estimer leur évolution temporelle au cours du XX$^{\text{ème}}$ siècle dans un climat comprenant tous les forçages extérieurs. Pour les 5 modèles qui montrent dans leur simulation de contrôle les co-oscillations des tendances à 17 ans du niveau de la mer et d'ENSO, la projection révèle l'existence de co-oscillations similaires sur le XX$^{\text{ème}}$ siècle. De plus, pour chacun des 5 modèles, elle montre que les amplitudes de ces co-oscillations sont légèrement plus fortes et leurs fréquences légèrement plus élevées que dans les simulations de contrôle. Cependant, quand on prend en compte l'intervalle de confiance à 95%, ces différences avec les simulations de contrôle ne sont pas significatives.

Cette étude montre que les forçages exterieurs, parmi lesquels se trouve les émissions anthropiques, n'ont pas jusqu'ici, d'impact significatif sur le comportement des tendances régionales à 17 ans du niveau de la mer dans l'océan Pacifique tropical. En particulier

elle montre que les tendances régionales observées par altimétrie dans le Pacifique tropical aujourd'hui, sont la phase haute d'une oscillation basse fréquence (période entre 20 et 30 ans) liée à ENSO qui est essentiellement la conséquence de la variabilité interne du système climatique. Dans le même temps, cette étude suggère que l'impact potentiel des forçages exterieurs sur cette oscillation pourrait se traduire par une augmentation de son amplitude et de sa fréquence. Cependant, étant donné l'amplitude de la variabilité interne dans la région ceci n'est pas encore détectable. Le rapport signal sur bruit (i.e. forçage anthropique sur variabilité interne du système climatique) est encore trop faible.

En conclusion les résultats de notre étude s'accordent avec les résultats de *Feng et al.* [2004] et *Merrifield and Thompson* [in revision] pour donner la même réponse à la question scientifique n°10 de la section 1.5 : la variabilité régionale du niveau de la mer que l'on observe dans le Pacifique tropical depuis 1993, est d'origine naturelle et plus précisement vient en majorité de la variabilité interne du système climatique. De plus elle est liée à l'évolution basse fréquence d'ENSO.

Clim. Past, 8, 787–802, 2012
www.clim-past.net/8/787/2012/
doi:10.5194/cp-8-787-2012

Climate of the Past

Tropical Pacific spatial trend patterns in observed sea level: internal variability and/or anthropogenic signature?

B. Meyssignac[1,2], D. Salas y Melia[4], M. Becker[1,3,*], W. Llovel[5], and A. Cazenave[1,2]

[1]Université de Toulouse, UPS (OMP-PCA), LEGOS, UMR5566, 14 Av Edouard Belin, 31400 Toulouse, France
[2]CNES, LEGOS, UMR5566, 18 avenue Edouard Belin 31 401 Toulouse, France
[3]CNRS, LEGOS, UMR5566, 14 av Edouard Belin, 31400 Toulouse, France
[4]Météo-France CNRM/GMGEC CNRS/GAME, 31000 Toulouse, France
[5]JPL, California Institute of Technology, Pasadena, California, USA
[*]now at: ESPACE-DEV/UAG, UMR228, Cayenne, French Guiana, France

Correspondence to: B. Meyssignac (benoit.meyssignac@legos.obs-mip.fr)

Received: 12 December 2011 – Published in Clim. Past Discuss.: 13 January 2012
Revised: 28 March 2012 – Accepted: 29 March 2012 – Published: 18 April 2012

Abstract. In this study we focus on the sea level trend pattern observed by satellite altimetry in the tropical Pacific over the 1993–2009 time span (i.e. 17 yr). Our objective is to investigate whether this 17-yr-long trend pattern was different before the altimetry era, what was its spatio-temporal variability and what have been its main drivers. We try to discriminate the respective roles of the internal variability of the climate system and of external forcing factors, in particular anthropogenic emissions (greenhouse gases and aerosols). On the basis of a 2-D past sea level reconstruction over 1950–2009 (based on a combination of observations and ocean modelling) and multi-century control runs (i.e. with constant, preindustrial external forcing) from eight coupled climate models, we have investigated how the observed 17-yr sea level trend pattern evolved during the last decades and centuries, and try to estimate the characteristic time scales of its variability. For that purpose, we have computed sea level trend patterns over successive 17-yr windows (i.e. the length of the altimetry record), both for the 60-yr long reconstructed sea level and the model runs. We find that the 2-D sea level reconstruction shows spatial trend patterns similar to the one observed during the altimetry era. The pattern appears to have fluctuated with time with a characteristic time scale of the order of 25–30 yr. The same behaviour is found in multi-centennial control runs of the coupled climate models. A similar analysis is performed with 20th century coupled climate model runs with complete external forcing (i.e. solar plus volcanic variability and changes in anthropogenic forcing). Results suggest that in the tropical Pacific, sea level trend fluctuations are dominated by the internal variability of the ocean–atmosphere coupled system. While our analysis cannot rule out any influence of anthropogenic forcing, it concludes that the latter effect in that particular region is still hardly detectable.

1 Introduction

Long term sea level rise is a critical issue of the global climate change because of its potential negative impact on many coastal regions of the world (Solomon et al., 2007). For this reason, it has been extensively studied in recent years. Since 1993, sea level is accurately monitored by satellite altimetry (using the Topex/Poseidon, Jason-1, Jason-2, ERS-1/2 and Envisat satellite missions) with high accuracy and global coverage. Recent studies based on these observations showed that sea level is rising at a global mean rate of $3.3\,\mathrm{mm\,yr^{-1}}$ since 1993 (e.g. Ablain et al., 2009; Cazenave and Llovel, 2010; Nerem et al., 2010). They showed as well that sea level does not rise uniformly but displays strong regional variability (see Fig. 1a). To highlight this regional variability, the uniform trend (global mean) of $3.3\,\mathrm{mm\,yr^{-1}}$ has been removed from Fig. 1a. In some regions such as the western Pacific, the North Atlantic around Greenland or the south-eastern Indian ocean, sea level rose up to 4 times faster than the global mean over 1993–2009. Meanwhile,

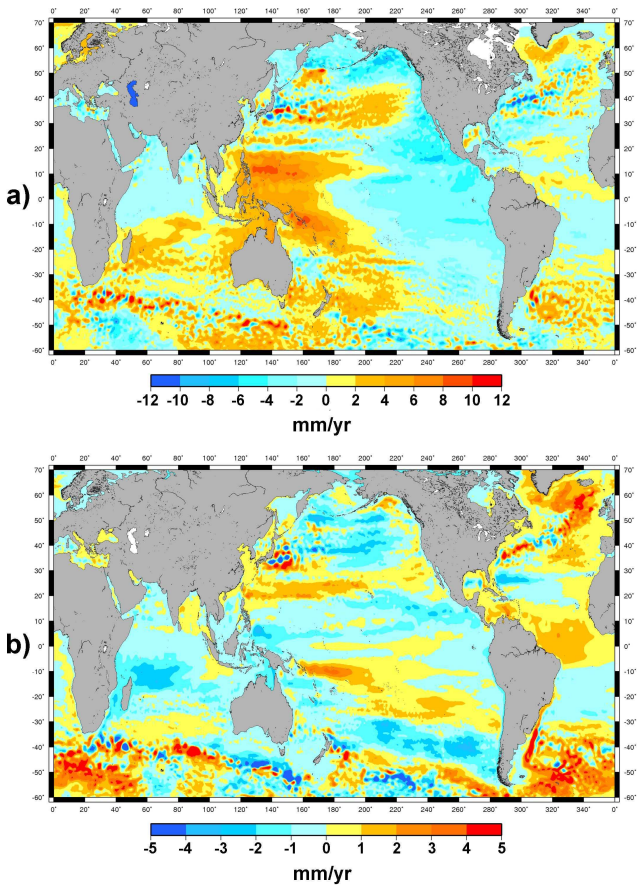

Fig. 1. Satellite altimetry sea level trends over 1993–2009 and reconstructed past sea level trends over 1950–2009. **(a)** Trends computed from the weekly AVISO sea level dataset. Time series have been averaged to annual time series. A global averaged sea level trend of 3.3 mm yr^{-1} has been removed. **(b)** Reconstructed sea level trends over 1950–2009 (the reconstruction total time span); a global averaged sea level trend of 1.76 mm yr^{-1} has been removed. The time series have been averaged to annual time series.

other regions such as the eastern Pacific or the north-western Indian ocean show lower rates of sea level rise. These large deviations from the global mean trend suggest that in different parts of the world, low lying lands are not facing the same risk of sea level rise. Hence, when assessing the potential impacts of sea level rise, it is of primary importance to understand the time variability of observed regional sea level trend patterns and the causes which drive them.

A number of previous studies have shown that sea level trend patterns over the altimetry era mainly result from ocean temperature and salinity changes (e.g. Bindoff et al., 2007). This was evidenced by the comparison between altimetry-based and steric trend patterns deduced from in-situ hydrographic measurements (Ishii and Kimoto, 2009; Levitus, 2005; Levitus et al., 2009; Lombard et al., 2005a, b) and ocean general circulation models (OGCMs) outputs (Wunsch et al., 2007; Kohl and Stammer, 2008; Carton and Giese, 2008; Lombard et al., 2009). Analyses of in situ ocean temperature measurements showed that the thermosteric component is the most important contribution to the observed sea level regional variability. OGCM runs with or without data assimilation have confirmed that point. However salinity changes may also play some role at regional scale, partly compensating temperature effects, as shown by Wunsch et al. (2007) and confirmed by other studies (e.g. Kohl and Stammer, 2008; Lombard et al., 2009).

Other phenomena may also contribute to the regional variability in rates of sea level change. This is the case of gravitational and deformational effects of the solid Earth in response to mass redistributions of the last deglaciation and ongoing land ice melting (Gomez et al., 2010; Milne and Mitrovica, 2008; Milne et al., 2009; Mitrovica et al., 2001, 2009). However, these effects are currently small and have not yet been detected in the altimetry-based sea level patterns.

Observations have shown that thermosteric spatial patterns are not stationary but fluctuate in time and space in response to driving mechanisms such as the ENSO (El Niño-Southern Oscillation), the NAO (North Atlantic Oscillation) and the PDO (Pacific Decadal Oscillation) (Levitus, 2005; Lombard et al., 2005a; Di Lorenzo et al., 2010; Lozier et al., 2010). Thus regional sea level trend patterns observed over the altimetry era were likely different prior to 1993.

The spatial and temporal variability of steric sea level change is tightly linked to complex ocean dynamics. It results from the redistribution of heat and fresh water both horizontally and vertically through sea-air fluxes and changes in the ocean circulation. Several studies have identified surface wind stress as the main driving mechanism of circulation-based heat and salt redistribution over the past few decades (e.g. Kohl and Stammer, 2008), in particular in the Indo-Pacific region (Timmermann et al., 2010; Han et al., 2010). But according to Kohl and Stammer (2008), surface fluxes and particularly buoyancy fluxes may have played an increasing role during the past 2 decades.

This important role of heat and fresh water redistribution in steric sea level trend patterns was previously noticed by Wunsch et al. (2007). These authors argued that given the long memory time of the ocean, observed patterns reflect an integration of the present forcing with internal changes and forcing that occurred in the past. This is another argument suggesting that the sea level trend patterns observed by satellite altimetry over the last 17 yr (the altimetry era) are not steady.

The purpose of the present study is to address two important scientific questions related to the sea level regional variability: (1) if sea level trend patterns are not stationary through time, how have they evolved during the last decades and what are their characteristic time scales? (2) What are the factors that drive them: are they mainly due to internal variability of the climate system or do they already reflect external forcing factors, in particular anthropogenic forcing?

2 Methods

In this study we focus on the sea level spatial trend pattern of the tropical Pacific. To try to answer the above questions concerning this region, we use different observational data sets and climate model outputs. For the sea level observations we use altimetry data since 1993 and a new version of a past sea level reconstruction over 1950–2009 (Meyssignac et al., 2012). For the climate model outputs, we use runs of eight coupled global climate models (CGCM here after) from the Coupled Model Intercomparison Project 3 database (hereafter CMIP3). These datasets are presented hereafter in more details.

Using the altimetry data set, we compute the observed spatial trend pattern over 1993–2009. Using the reconstructed 2-D sea level fields since 1950, we compute sea level trend patterns over successive 17-yr windows (the length of the altimetry data set) for the past 6 decades. The objective is to identify the dominant modes of variability and the characteristic life time of the 17-yr-long spatial trend pattern over the last 60 yr. Then we compute the sea level trend patterns over successive 17-yr windows from the CGCM multi-centennial control run outputs. These runs with constant, preindustrial external forcing give us an estimation of the modelled 17-yr sea level trend pattern produced by the internal variability of the climate system and its evolution with time. We check whether the tropical Pacific sea level trend pattern resembles the observed one or not. A similar analysis is done with the CGCM climate model runs over the 20th century. The latter runs include human-induced changes in atmospheric greenhouse gases and aerosols (as discussed later in this paper, some of these models do not take into account natural forcing such as solar or volcanic variability). Results are compared to those of the control runs. The issue is indeed to detect or not the signature of natural and anthropogenic forcing factors on the sea level trend patterns of the tropical Pacific.

3 Data

3.1 Satellite altimetry sea level data (1993–2009)

We used altimetry-based 2-D sea level fields from AVISO (http://www.aviso.oceanobs.com/en/data/products/sea-surface-height-products/global/index.html). The data consisted of gridded sea level anomalies at weekly intervals on a 1/4° regular grid, from January 1993 to December 2009. We used the DT-MSLA "Ref" series computed at CLS (Collecte Localisation Satellite) by combining several altimeter missions, namely: Topex/Poseidon, Jason 1 and 2, Envisat and ERS 1 and 2. It is a global, homogenous, intercalibrated dataset based on global crossover adjustment (Le Traon and Ogor, 1998) using Topex/Poseidon and then Jason 1 as reference missions. It is corrected for the long wavelength orbit errors (Le Traon et al., 1998), ocean tides, and wet/dry troposphere and ionosphere (see Ablain et al., 2009 for more details). The inverted barometer (IB) correction has also been applied in order to minimize aliasing effects (Volkov et al., 2007) through the MOG2D barotropic model correction that includes the dynamic ocean response to short period ($<$20 day) atmospheric wind and pressure forcing and the static IB correction at periods above 20 day (see Carrere and Lyard, 2003 for details).

3.2 Two-dimensional past sea level reconstruction (1950–2009)

To determine the sea level trend pattern variability over the last decades (i.e. prior to the altimetry era), we updated the previous past sea level reconstruction developed by Llovel et al. (2009) (Meyssignac et al., 2012). Let us briefly summarize Llovel et al. (2009)'s reconstruction. The method, based on the reduced optimal interpolation described by Kaplan et al. (2000), consists of interpolating long tide gauge records with a time varying linear combination of spatial modes of a 2-D sea level field. The method has 2 steps. In the first step, an Empirical Orthogonal Function (EOF) decomposition (Preisendorfer, 1988; Toumazou and Cretaux, 2001) of 2-D sea level fields is performed (based on outputs of the OPA/NEMO ocean circulation model). This decomposition allows separating the spatially well- resolved signal of the model into spatial modes (EOFs) and their related principal components (PCs). The second step consists of computing new PCs over a longer period (1950–2003) covered by the selection of the considered 99 long tide gauge records. This is done through a least-squares optimal procedure that minimizes the differences between the reconstructed field and the tide gauge records at the tide gauge locations. Compared to the previous sea level reconstruction of Church et al. (2004), the originality of Llovel et al. (2009)'s reconstruction is the use of long-term sea level patterns (EOFs) deduced from a 44-yr long run of the OPA/NEMO ocean model, instead of the shorter altimetry record. This, in principle, allows better capturing of the decadal variability of the spatial trend patterns (see Llovel et al., 2009 for more details).

In the present study, we use a new version of the reconstruction based on three modifications. First, we followed Christiansen et al. (2010) and made use of a covariance matrix error and of the so-called EOF0 (i.e. the EOF mode corresponding to the geographically averaged but time-variable sea level, processed separately from the other EOF modes as in Church et al., 2004's reconstruction). This drastically improves the accuracy of the reconstructed trends over the reconstructed period. Second, on the basis of the lastest data available from the Permanent Service For Mean Sea Level (PSMSL: http://www.psmsl.org), we updated the tide gauge records used by Llovel et al. (2009) and reconstructed sea level until December 2009. Thus the new reconstruction provides a monthly time series of global 2-D sea level fields from January 1950 to December 2009. Third, for

the computation of the EOFs patterns, instead of using the OPA/NEMO model, which has a coarse resolution of 2° on average, we preferred to use the ORCA025-B83 run of the DRAKKAR/NEMO model which has a higher resolution of 1/4°. Indeed, Penduff et al. (2010) showed that ocean models with higher resolution bring substantial improvements in the representation of the sea level spatial variability, in particular at interannual time scales. The ORCA025-B83 run is based on the free surface ocean circulation model NEMO version 2.3 (Madec, 2008). This simulation is very close to the simulation ORCA025-G70, analysed and compared to satellite altimetry data by Lombard et al. (2009). It does not assimilate any observational data (e.g. satellite altimetry or in situ data) as in ORCA025-G70. It is forced by the realistic hybrid surface forcing "DRAKKAR forcing set 4.1" described in details by Brodeau et al. (2010). This forcing is based on the CORE dataset assembled by W. Large (Large and Yeager, 2004), the ECMWF (European Center for Medium-Range Weather Forecast) ERA 40 reanalysis (Uppala et al., 2005), and the ECMWF operational analyses for recent years. This new reconstruction has been validated at global scale (Meyssignac et al., 2012) and in the tropical Pacific region (Becker et al., 2012) by comparison with independent tide gauge records not used in the reconstruction process. Figure 1b shows the reconstructed sea level trend patterns over 1950–2009 (uniform trend removed). As expected, regional sea level trend patterns reconstructed over the last 60 yr differ largely from those observed during the last 17 yr (see Fig. 1a for comparison).

3.3 Coupled Climate Model (CGCM) runs

Concerning the CGCM simulations, we analyzed both multi-centennial control runs and runs covering the 20th century starting in the mid 19th century and ending in the 2000s (named picntrl and 20c3m runs respectively in the CMIP3 nomenclature).

The control runs and the 20th century runs differ by the external forcing. For the 20th century runs, external forcing includes changes in greenhouse gases, tropospheric and stratospheric ozone, anthropogenic stratospheric sulfates, black and organic carbon, volcanic aerosols, solar irradiance and the distribution of land cover. In the control runs, all external forcing variables are kept constant at their (preindustrial) 1860 values. These picntrl runs are intended to provide an estimate of the internal variability of the climate system. The 20c3m runs provide an estimate of the 20th century climate. They use observed, time-varying external forcing from around 1860 to 2000.

Among all CGCMs available in CMIP3 we have selected models that provide both sea surface temperature and sea level variables in their control run and 20th century run outputs. Models with less than 300 yr of control run were discarded. This led us to use a subset of 8 models: GFDL cm2.1, CNRM cm3, GISS model er, IAP fgoals g1.0, IPSL cm4, MIROC 3.2 medres, NCAR ccsm3 0, and UKMO hadcm3. The vertical and horizontal resolutions for the atmospheric and oceanic modules of each model are gathered in Table 1 along with the references in which the models are described in details. Note that for each of the selected models, one control run and one 20th century run at least were analyzed. When several 20th century runs were available (see Table 1), they were all analyzed one by one. Note as well that the selected models differ in their 20c3m run external forcing. For example, the IPSL 20c3m run does not include solar and volcanic variability. The IAP 20c3m does not include the volcanic variability. All other models include both solar and volcanic variability (see Table 1). But we decided to keep the IPSL and the IAP models in our selected subset because only few models provide the outputs necessary for this study. The final discussion will show that this does not impact our conclusions.

The sea surface height (SSH) fields given in the model outputs are incomplete and can not be directly compared to the observations in terms of global mean. Indeed the models do not contain the global mean steric sea level signal because they use the Boussinesq assumption that enforces the total ocean volume to remain constant. On the other hand, the models correctly simulate the regional sea level changes because the Boussinesq assumption has no impact on the latter (see Greatbatch, 1994). Hence the SSH output variable is well adapted to the regional analysis performed in this study.

4 Results

All computations were done on the basis of the monthly time series from altimetry, the 2-D past reconstruction and the CGCMs. In this study, we are interested in the regional variations of the sea level trends at inter-annual to multi-decadal time scales. Hence, two processings have been applied to the sea level time series prior to our analysis. (1) The global mean sea level trend was removed from the sea level time series because this study focuses on the regional variability around the global mean (this also removes any internal drift of the CGCM runs at the same time), (2) the time series were averaged on a yearly basis and filtered for the multi-centennial signals to focus on the inter-annual to the multi-decadal time scales. These low frequency signals were filtered out with a high-pass filter with a 80-yr cutoff. The high-pass filter built here is a fast Fourier transform convolution with a Hamming window cutting at $1/80\ \mathrm{yr}^{-1}$ (Brigham, 1974). The choice of the 80-yr filter cutoff enables us to keep signals with periods shorter than 70 yr, in which we are most interested (see further), and to ensure a reliable (somewhat conservative) filtering of the multi-centennial signals.

Table 1. List of coupled Atmosphere-Ocean General Circulation Models considered in this study with key characteristics.

Model	Modelling group	Atmospheric Module		Oceanic Module		Simulation length (yr)	External forcing in the 20c3m runs		
		Vertical resolution	Horizontal resolution	Vertical resolution	Horizontal resolution		Green house gases	Volcanic variability	Solar variability
GFDL cm2.1	NOAA GFDL (USA)	24 levels	Lon: 2.5°, Lat: 2° Delworth et al. (2006)	50 levels Free surface	Lon: 1° Lat: 0.33° (equator) to 1° (outside the tropics) Gnanadesikan et al. (2006)	run picntrl: 500 4 runs 20c3m: 140	Yes	Yes	Yes
CNRM cm3	Météo France/CNRM (France)	45 levels	2.8° on average (T63 triangular truncation) Déqué et al. (1994)	31 levels Rigid lid	Lon: 2° Lat: 0.5° (equator) to 2° (pole) Madec et al. (1998)	run picntrl: 350 1 run 20c3m: 140	Yes	Yes	Yes
GISS model er	NASA/ GISS (USA)	20 levels	Lon:5°, Lat: 4° Schmidt et al. (2006)	13 levels Free surface	Lon:5°, Lat: 4° Russell et al. (1995)	run picntrl: 500 8 runs 20c3m: 124	Yes	Yes	Yes
IAP fgoals g1.0	LASG/ IAP (China)	26 levels	2.8° on average (T42 truncation) Wan et al. (2004)	16 levels Free surface	Lon:1°, Lat: 1° Jin et al. (1999); Liu et al. (2004)	run picntrl : 350 1 run 20c3m: 150	Yes	No	Yes
IPSL cm4	IPSL (France)	19 levels	Lon: 3.75°, Lat: 2.5° Hourdin et al. (2006)	31 levels Free surface	Lon:2°, Lat: 2° Madec et al. (1998)	run picntrl: 500 1 run 20c3m: 141	Yes	No	No
MIROC 3.2 medres	CCSR/ NIES/ FRCGC (Japan)	20 levels	2.8° on average (T42 truncation) K-1 Developers (2004)	43 levels Free surface	Lon: 1.4° Lat: 0.5° (equator) to 1.4° (pole) K-1 Developers (2004)	run picntrl: 500 1 run 20c3m: 151	Yes	Yes	Yes
NCAR ccsm3 0	NCAR (USA)	26 levels	1.4° on average (T85 truncation) Collins et al. (2004)	40 levels Free surface	Lon: 1° Lat: 0.3° (equator) to 1° (pole) Smith and Gent (2002)	run picntrl: 500 2 runs 20c3m: 130	Yes	Yes	Yes
UKMO hadcm3	Met Office (UK)	19 levels	Lon:3.75°, Lat: 2.5° Pope et al. (2000); Gordon et al. (2000)	20 levels Free surface	Lon:1.25°, Lat: 1.25° Johns et al. (2006); Gordon et al. (2000)	run picntrl: 350 1 run 20c3m: 140	Yes	Yes	Yes

4.1 Observed 17-yr trend patterns over the tropical Pacific since 1950

Over the 17 yr of altimetry era, sea level trends show characteristic patterns (see Fig. 1a). The most prominent feature is the strong east-west dipole in the tropical Pacific region, positive in the western part and negative in the eastern part. This pattern has been persistent for several years now. It was already observed over the first 10 yr of the altimetry period (1993–2003) by Cazenave and Nerem (2004) (see their Fig. 7). With the 2-D past sea level reconstruction, we can gain some insights on how the tropical Pacific sea level trend pattern evolved over longer time scales (here, up to 60 yr). We computed spatial trend patterns of the reconstructed sea level over successive 17-yr windows (i.e. the length of the altimetry data set). This gives as an output a set of 43 17-yr-long trend maps (starting in 1950 and shifting by one year the 17-yr time span, this provides 43 trend maps). Figure 2 shows 3 of these reconstructed 17-yr sea level trend patterns over three time spans: 1993–2009, 1976–1992 and 1959–1975. They all exhibit a strong ENSO-like dipole pattern. As expected, we note that the 1993–2009 reconstructed sea level pattern is very close both in shape and amplitude to the observed one. The 1959–1975 trend pattern is somehow different in shape but still exhibits a strong ENSO-like pattern with slightly lower amplitude than over 1993–2009. This indicates that a trend pattern similar to the presently observed one already existed in the late 1960s and the early 1970s. On the other hand, the 1976–1992 pattern is opposite to the 1993–2009 one almost everywhere. This suggests that the tropical Pacific trend pattern seems to have fluctuated with time and was opposite to the present one in the late 1970s and the 1980s.

To investigate this further, we performed an EOF decomposition of the set of 43 reconstructed 17-yr trend maps. On the basis of these EOFs, we computed the first rotated EOF (see von Storch and Zwiers, 1999) to obtain the EOF that maximizes the explained variance among the 43 17-yr-long trend maps. This EOF is presented in Fig. 3. It accounts for 37 % of the total variance. The second rotated EOF explains 25 % of the total variance and the third one 7 %. The leading EOF spatial pattern is very similar to the altimetry spatial pattern (Fig. 1a). This shows that the spatial pattern observed by satellite altimetry during the last 17 yr turns out to be the most frequently observed pattern among all the 17-yr sea level trend maps of the last 60 yr (in terms of explained variance). Its PC indicates that this pattern has fluctuated with time (see Fig. 3). It was opposite to its current value in the 1970s and early 1980s and went back to values similar to what we observe now in the late 1960s (with a lower amplitude), as already suggested by Fig. 2. These fluctuations follow the low frequency variations of the extended NINO3 index (a proxy of El Niño; Kaplan et al., 1998). This index is the average of the sea surface temperatures (SST) over the

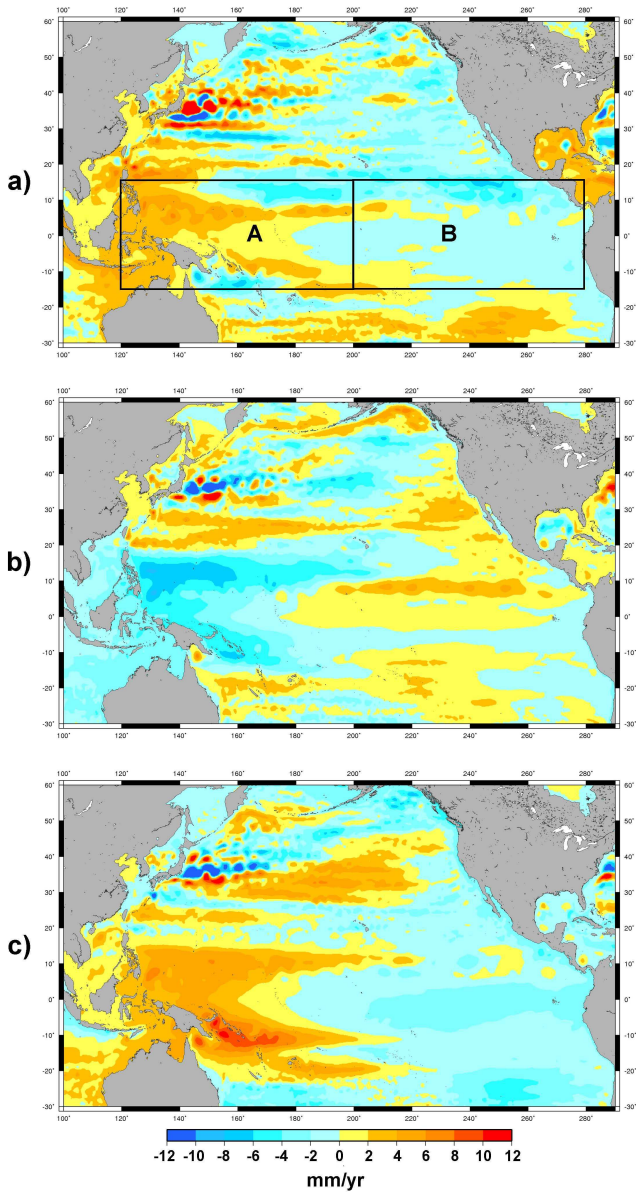

Fig. 2. Reconstructed sea level trends over three different 17-yr windows: **(a)** 1959–1975, **(b)** 1976–1992 and **(c)** 1993–2009. Time series have been averaged to annual time series. The global averaged sea level trend has been removed for each map.

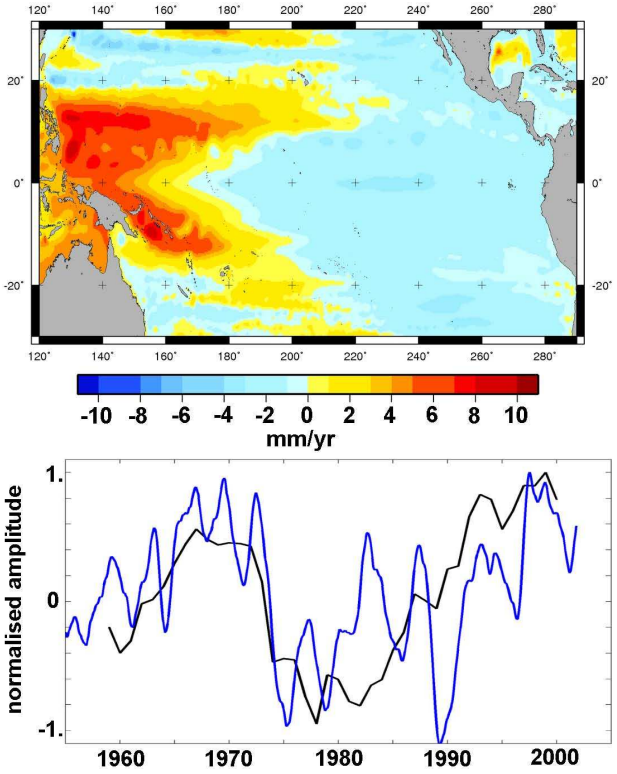

Fig. 3. First rotated EOF of the set of 17-yr trend maps computed with the reconstruction over the tropical Pacific. It explains 37 % of the total variance. The PC is the black curve. The NINO3 index from Kaplan et al. (1998), filtered with a 10-yr running mean and detrended, is superimposed in blue. Their correlation coefficient is 0.63 (SL > 99 %).

NINO3 region (150° W–90° W, 5° S–5° N). Here it has been filtered with a 10-yr running mean (see Fig. 3). The correlation coefficient between the two curves shown in Fig. 3 is 0.63, with a significance level (SL) >99 %. This result suggests that the reconstructed sea level trend pattern fluctuation reflects a natural mode of the climate system: a low frequency modulation of ENSO.

Another way to analyse the reconstructed 17-yr-long sea level trend fluctuations of the tropical Pacific is to look at two regions defined by boxes A and B (see Fig. 2). Box A is located in the western Pacific (15° N–15° S by 120° E–200° E) and box B in the eastern Pacific (15° N–15° S by 200° E–280° E). We computed the mean sea level (global mean sea level trend removed) in each box and compared it to the extended NINO3 index. The resulting curves are presented in Fig. 4a. The mean sea level in box A (western Pacific) covaries (but with opposite sign) with the mean sea level in box B (eastern Pacific). This confirms that the tropical Pacific sea level behaves as an east-west dipole that fluctuates with time. This fluctuation closely follows the ENSO mode of variability represented by the NINO3 index: the correlation between NINO3 index and eastern Pacific mean sea level is 0.73 (SL > 99 %).

We also computed the mean sea level trend in box B over successive 17-yr windows. Its time amplitude is displayed in Fig. 4b along with the NINO3 index time series smoothed with a 10-yr running mean. As suggested by the rotated EOF, this analysis confirms that the 17-yr trends in the tropical Pacific fluctuate with time following some low frequencies of the ENSO mode.

In order to isolate the low frequencies of the extended NINO3 index connected with the 17-yr trends fluctuations, we computed the NINO3 index power spectrum in Fig. 4c.

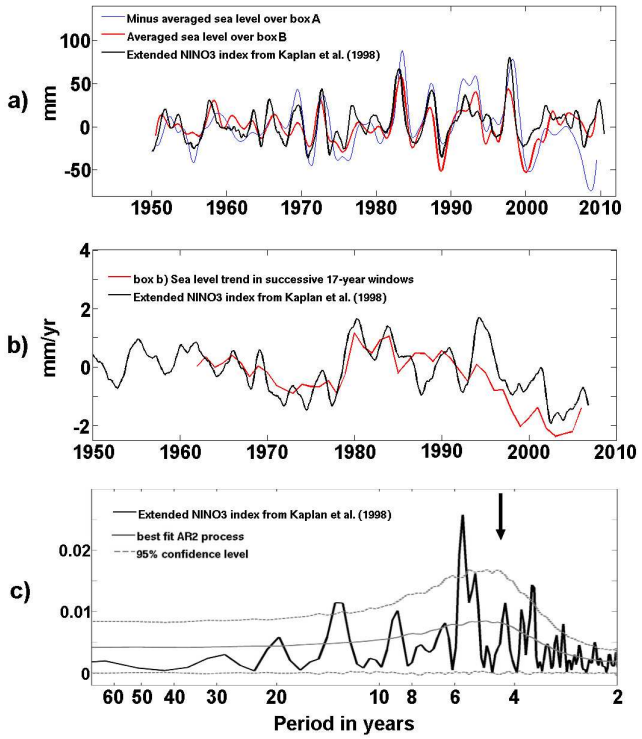

Fig. 4. **(a)**: Minus spatial averaged sea level over box A in blue, spatial averaged sea level over box B in red, and NINO3 index in black. Time series have been smoothed with a 1-yr running mean. The NINO3 index is normalised in amplitude. **(b)**: Spatial average of sea level trends of box B computed over successive 17-yr windows in red. NINO3 index in black, filtered with a 10-yr running mean. Before computation, the spatially averaged sea level trend has been removed from the sea level time series. NINO3 index has been detrended over the period as well and normalised in amplitude. **(c)**: NINO3 index (Kaplan et al., 1998) power spectrum (in black) and the best fit AR2 process in grey as the null hypothesis. The grey dash lines indicate the 95 % confidence level around the null hypothesis

The power spectrum of the best fit random process is also shown. It gives an estimation of what would be the power spectrum of a random process with a variability similar to the NINO3 index one (in terms of mean, variance and power spectrum). We added its 95 % confidence interval in Fig. 4c (it is the area of the power spectrum that is covered by 95 % of the randomly generated series). All frequency bands in which the NINO3 index power rises above the 95 % confidence level reveal the presence of a robust, deterministic ENSO frequency (at the 95 % confidence level), while the signal contained inside the confidence interval can be considered as undistinguishable from random fluctuations (null hypothesis).

The choice of an appropriate random process is a key issue. It has been done here in 2 steps. In the first step we chose the random process among simple random linear processes: the autoregressive models (AR) (this is the classical approach for climate records, see von Storch and Zwiers, 1999). Here we considered an AR process of order 2 because, according to the partial autocorrelation function of the NINO3 index, it appears to be indistinguishable from zero for lag greater than 2 (AR processes of a given order n are known to have a partial autocorrelation function that is indistinguishable from zero for lag greater than n, see von Storch and Zwiers, 1999). Moreover we computed an objective test for AR order (based on the Akaike information criterion, see von Storch and Zwiers, 1999) which indicates that an AR2 should best fit the data as well. In a second step, given the order of the AR process, we computed the parameters that best fit the NINO3 index using a least squares procedure.

Figure 4c confirms that the AR2 process spectrum fits the NINO3 index spectrum well. Thus the extended NINO3 index is well represented by a linearly damped oscillator driven by white noise (AR2 model). It shows a range of preferred time scales centred around 4.3 yr (see the black arrow in Fig. 4c). Some spectral peaks significantly differ from the AR2 model. They can be found in the inter-annual band around the 3.7 yr and 5.8 yr periods and in the inter-decadal band around the 13.2 yr period. But none of these peaks can account for the low frequency modulation of ENSO identified earlier (with periods between 20 yr and 30 yr, see Fig. 4b). The NINO3 index shows actually some power in the 20 yr to 30 yr waveband (see Fig. 4c) but it remains indistinguishable from a random fluctuation either because it is of random origin or because the short length of the NINO3 record does not allow a good estimation of its power spectrum.

The time span covered by the sea level reconstruction is relatively short, covering only 60 yr. Nevertheless, during this time span, the 17-yr long spatial trend pattern observed by satellite altimetry in the tropical Pacific fluctuated with time, revealing periods during which sea level rise accelerated or decelerated. Presently, the sea level trend pattern is similar to what it was in the 1960s. This long-term fluctuation seems to be connected to some multi-decadal frequency of ENSO variability in the 20 yr to 30 yr waveband. But given the short length of the NINO3 index record, these low frequency ENSO fluctuations are not significant at the 95 % confidence level.

4.2 17-yr trend patterns in the tropical Pacific from CGCM runs

4.2.1 PIcntrl runs

The same strategy was applied to analyse the trend patterns of the tropical Pacific from CGCM control runs. We considered 17-yr windows to compute sea level trends from the multi-centennial models outputs. The first rotated EOF and the averaged 17-yr trends over boxes A and B were then derived from the resulting set of 17-yr trend maps following the

method described in Sect. 4.1 for the reconstructed 2-D sea level fields.

In Fig. 5 the spatial patterns of the first rotated EOFs for each CGCM control run are presented, while Fig. 6 shows the power spectra of their respective PCs. Note that, as for the rotated EOF in Fig. 3, the maximum of the PC has been normalised to 1 and the same colour scale has been used.

Looking at Fig. 5, we note that all CGCM control runs show spatial patterns with a magnitude comparable to reconstructed (Fig. 3) and observed fields (Fig. 1a). The magnitudes range from $-12\,\mathrm{mm\,yr^{-1}}$ to $+12\,\mathrm{mm\,yr^{-1}}$. Furthermore, 6 models out of 8 (GFDL, CNRM, GISS, IAP, NCAR and UKMO) show a clear east-west dipole in the tropical Pacific as in the observations. But, in general, patterns differ in shape. In 4 models (GFDL, CNRM, NCAR, and UKMO), patterns are fairly similar to each other and exhibit some common features with the observed ones. They are dominated by a strong positive signal south-east of Papua-New Guinea and a more modest positive anomaly north of Papua-New Guinea that are seen in the observations as well (see Figs. 1a and 3 for comparison). For the NCAR and the UKMO runs, the positive trend anomalies extend slightly too far eastward in the equatorial Pacific. They exhibit as well negative trend anomalies east of the Philippines. The latter are also seen in the observations but are actually centred farther northward (around 20° North).

The power spectra of the first PCs are shown in Fig. 6. Note that the IAP run is an exception: it is the only one showing a significant variance of its PC in the inter-annual waveband. Except for this run, all PCs concentrate their variance into a few peaks in the multi-decadal waveband. This indicates that in the CGCM control runs, the tropical Pacific 17-yr trends appear to fluctuate with time at multi-decadal time scales as in the observations. The GFDL and CNRM runs present a unique peak centred at 28 yr indicating that their spatial trend pattern fluctuate at time scales of 25–33 yr, as in the observations. The GISS, NCAR and UKMO runs show instead three peaks centred at 20 yr, 28 yr and 40 yr (up to 50 yr in the UKMO run).

To investigate this further, we analysed the 17-yr sea level trends averaged over boxes A and B for each model. As for the reconstructed sea level, the two time series exhibit a strong anti-correlation (not shown) indicating that in the control runs as well, 17-yr sea level trends in the tropical Pacific behave as an east-west dipole. Furthermore, the box B signal correlates well with the NINO3 index smoothed with a 10-yr running mean: the correlation coefficients are between 0.58 (for the CNRM cm3 control run) and 0.82 (for the IAP control run) (SL > 99 %).

We computed the power spectra of the NINO3 index and the box B 17-yr sea level trends of each control run (see Fig. 7). The long time period covered by the control runs allows capturing the multi-decadal variability of both signals, unlike with the reconstruction and the satellite altimetry observations.

NINO3 indices of the control runs are shown in Fig. 7 together with their respective autoregressive (AR2) null hypothesis and 95 % confidence interval. The AR2 random processes have been chosen using the same procedure as described in Sect. 4.1. As for the observations, AR2 processes appear to properly fit the NINO3 index spectra. This indicates that for each CGCM control run also, the linear damped oscillator models (AR2) reproduce fairly well the NINO3 index in terms of power spectrum (for the NCAR run, the monotonic spectrum suggests that an AR1 process may have been sufficient). Only the GFDL, GISS and UKMO runs appear to have their range of preferred time scales centred at 4 yr as in the observations (see the black arrow on Fig. 4c) and a fairly good distribution of their variance between inter-annual and multi-decadal time scales. The GISS run shows a too low total variance. The CNRM, IAP, IPSL and NCAR runs have their range of preferred time scales centred around 2–3 yr instead of 4 yr, and show too large variance in the inter-annual timescales compared to the observations. The MIROC run shows too much variance in the multi-decadal time scales. It is interesting to note that most of the CGCM runs (except the IPSL and the IAP ones) show several peaks significant at the 95 % level of confidence in the multi-decadal waveband. But their central periods differ. In particular, the GFDL, CNRM, GISS, MIROC and UKMO runs agree on the presence of a significant peak at periods around 20–30 yr.

Spectra of the 17-yr sea level trends averaged over box B are shown in Fig. 7 along with their null hypothesis. The null hypothesis here is the assertion that the 17-yr box B sea level trends are indistinguishable from the 17-yr trends of the AR2 process that best fit the sea level in box B. This choice was driven by the same reasons as in Sect. 4.1. We also added the 95 % confidence in Fig. 7.

The spectra shown in Fig. 7 are not significant in the inter-annual waveband. At these time scales, the power spectra of the 17-yr trends' time series are actually dominated by the auto-correlation coming from the overlapping of the 17-yr windows. For the multi-decadal waveband, we note that 6 CGCM runs (GFDL, CNRM, IAP, MIROC, NCAR and UKMO) show some significant peaks at the 95 % confidence level. They confirm that 17-yr sea level trends oscillate significantly at multi-decadal time scales in the tropical Pacific. Furthermore, except for the IAP run, each significant peak is associated with a significant peak of its respective NINO3 index spectrum (see Fig. 7), suggesting that for the majority of the control runs, the significant low frequency fluctuation of the 17-yr sea level trends at multi decadal time scales follows an ENSO-related low frequency modulation.

This is confirmed by the squared coherence function of both signals (black curves on Fig. 7). This function, computed using Welch's overlapped averaged periodogram method (Rabiner and Gold, 1975), gives the coherence between two signals (value between 0 and 100 %). Figure 7 shows that for 5 models (GFDL, CNRM, MIROC, NCAR

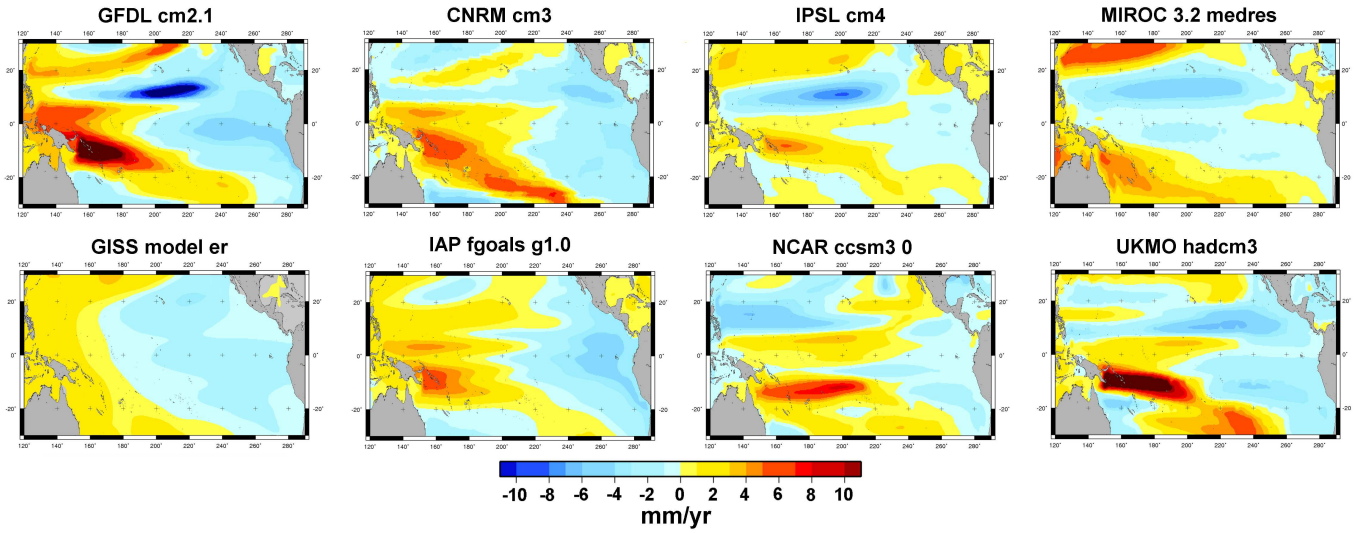

Fig. 5. Spatial patterns of the first rotated EOF of the set of 17-yr trend maps computed with the coupled climate model control runs.

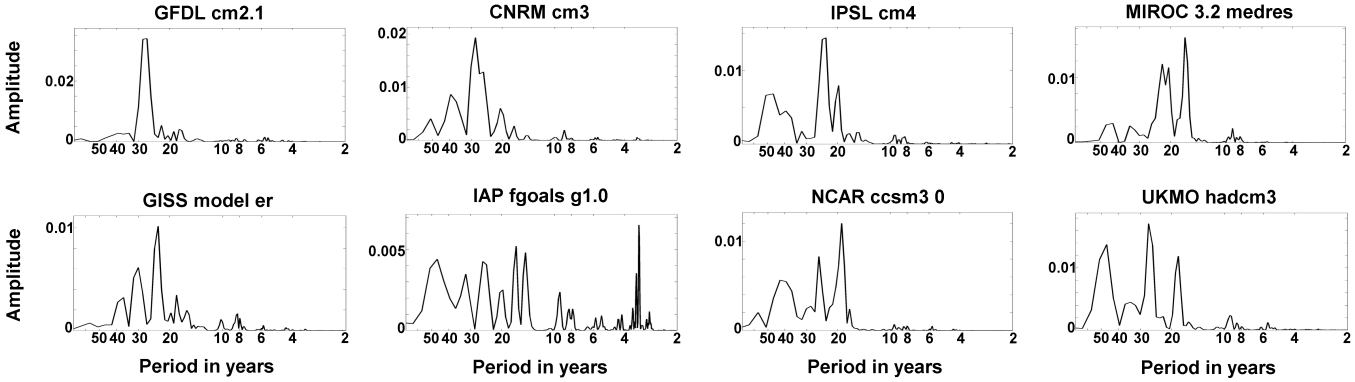

Fig. 6. Power spectra of the first PC of the set of 17-yr trend maps computed with the coupled climate model control runs. The power is plotted against the natural log of frequency so that the era under the curve in a particular frequency band is equal to the variance explained by the signal contained in this band of frequency.

and UKMO), the 17-yr signal in box B is very coherent with the NINO3 index at low frequency. In particular, at each frequency where a significant peak of both the 17-yr sea level trend and its respective NINO3 index can be found (see the grey vertical bars in Fig. 7), the coherence between both signals is very high: more than 70 % for the GFDL, CNRM, MIROC and UKMO models and 60 % for the NCAR model. This confirms a fairly strong relationship between both signals at these low frequencies.

In summary, CGCM control runs show results fairly similar to what was suggested by the reconstructed and the observed ones. Indeed, the tropical Pacific trends computed over successive 17-yr windows also show significant low frequency modulations in 6 out of 8 CGCM control runs. In 5 of them, the fluctuations appear to be tightly linked to significant ENSO low frequency modulation. Furthermore, 4 of these models (GFDL, CNRM, NCAR and UKMO) exhibit almost the same 17-yr spatial trend patterns and they display common features with the reconstruction and the satellite altimetry observations.

There are still some discrepancies between the CGCMs control runs and the reconstruction or the observations. The spatial trend pattern of the first rotated EOF of the GFDL, CNRM, NCAR and UKMO control runs differ from the reconstructed and the observed ones north of 15° N (Fig. 3). The power spectra of the observed NINO3 index and the control runs NINO3 index (compare Figs. 4c and 7) differ as well. The observed NINO3 index does not show any significant multi-decadal variability at time scales superior to 15 yr while the NINO3 indices from control runs do. But discrepancies with the observations are not necessarily significant because the time period covered by the observations is much shorter than for the control runs. In effect, when trend patterns and power spectra are computed from observations they are likely dominated by high frequency or random features that would be smoothed out in the longer control runs. In

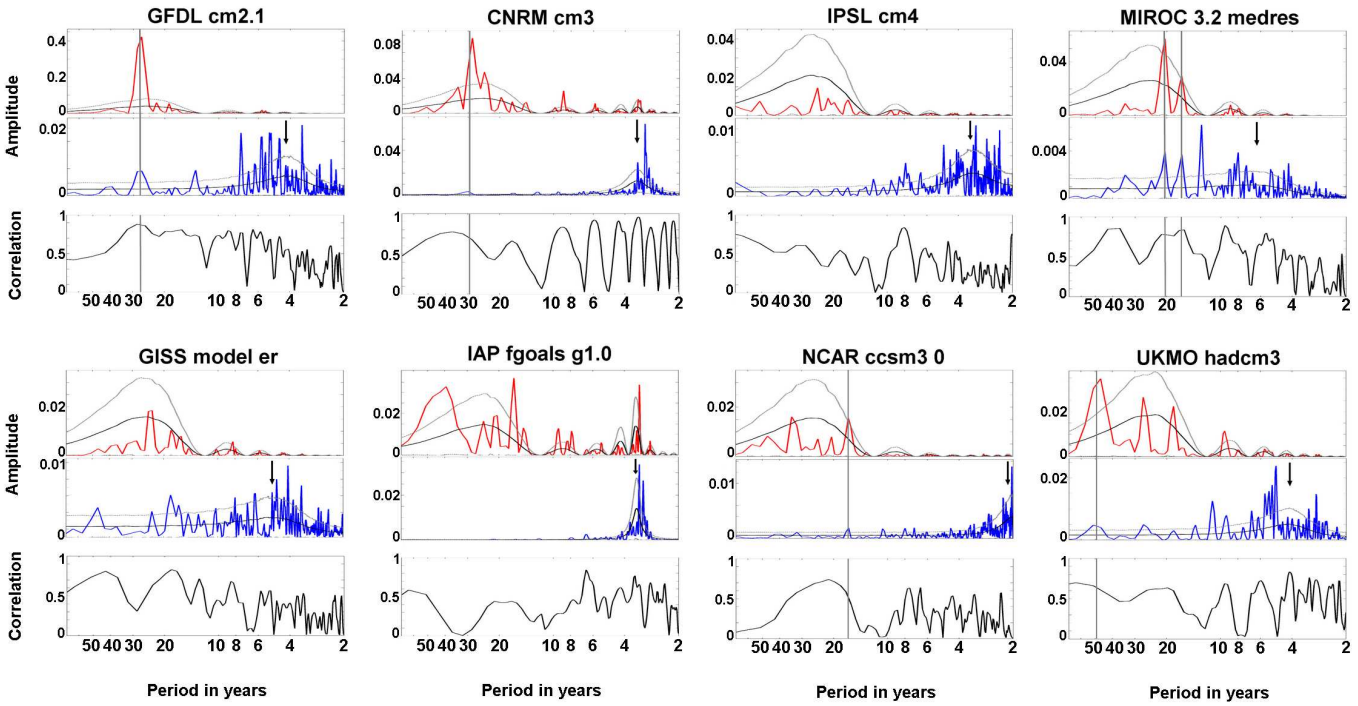

Fig. 7. Power spectra of the box B sea level trends computed over successive 17-yr windows and NINO3 index from the coupled climate model control runs. Top panels: power spectra of box B 17-yr sea level trends (solid red line). They are shown together with the 17-yr trend of the best fit AR2 null hypothesis (solid black line) and the 95 % confidence levels(dashed grey line). Middle panels: power spectra of the NINO3 index (solid blue line), shown together with the best fit AR2 null hypothesis (solid black line) and the 95 % confidence levels(dashed grey line). Bottom Panels: magnitude squared coherence between the box B 17-yr sea level trends and their respective NINO3 index.

long control runs we expect to see lower frequency features that would be missed by the shorter observation datasets. We verified this point in the GFDL control run. We split the 500-yr GFDL control run into 8 independent 60-yr long samples (the time length covered by the reconstruction). For each of these, we computed the first rotated EOF from the 17-yr trend maps as done for the reconstruction in Sect. 4.1. Among the 8 resulting rotated EOFs, 6 were very similar to the rotated EOF computed over the whole control run time span (Fig. 5), while 2 were similar to the observed one (Fig. 3). In Fig. 8 we present one of them: the first rotated EOF computed from the 4th sample (years 220 to 280) of the GFDL control run. It explains 49 % of the total variance. To be fully consistent with the observations, Fig. 8 also shows the power spectrum of the NINO3 index computed over a 155 yr time period, i.e. the time period covered by the NINO3 index (it has been computed over the years 125–280 of the GFDL control run). Comparing Figs. 8 and 3, we note that the model strikingly resembles the observations in the 4th sample case. The spatial pattern of the first rotated EOF is very close to the observed one and the PC follows as well the NINO3 index with a quasi periodicity between 20–30 yr. The NINO3 index is also in better agreement with the data when computed over a 155 yr time period: the multi-decadal peak observed in Fig. 7 around 28-yr appears now under the 95 % confidence level as for the observations (Fig. 4c). This indicates that a 17-yr sea level trend variability similar to the reconstructed one can be found among the 60 yr long samples of a control run.

4.2.2 20c3m runs

In this section we consider the CGCMs 20th century runs (20c3m) to check whether any differences with the control runs can be found or not. Our approach is to consider that the best estimation of the internal modes of variability of the climate system are provided by the control runs and to use them as references against which we test the 20th century runs. The choice of the control runs as reference is motivated by the fact that control runs are multi-centennial runs unperturbed by any changes in the external forcing. Hence, they provide an estimation of the modes of variability of a preindustrial, unperturbed, steady climate. The point is to see whether 20th century runs make any significant differences with respect to a steady state climate in terms of 17-yr sea level trends (the null hypotheses here is the assertion that the 20th century runs are indistinguishable from control runs in terms of 17-yr sea level trend patterns and variability).

As in the previous analysis, we computed for each CGCM 20c3m run sea level trend maps over successive 17-yr windows and we performed two comparisons with the control

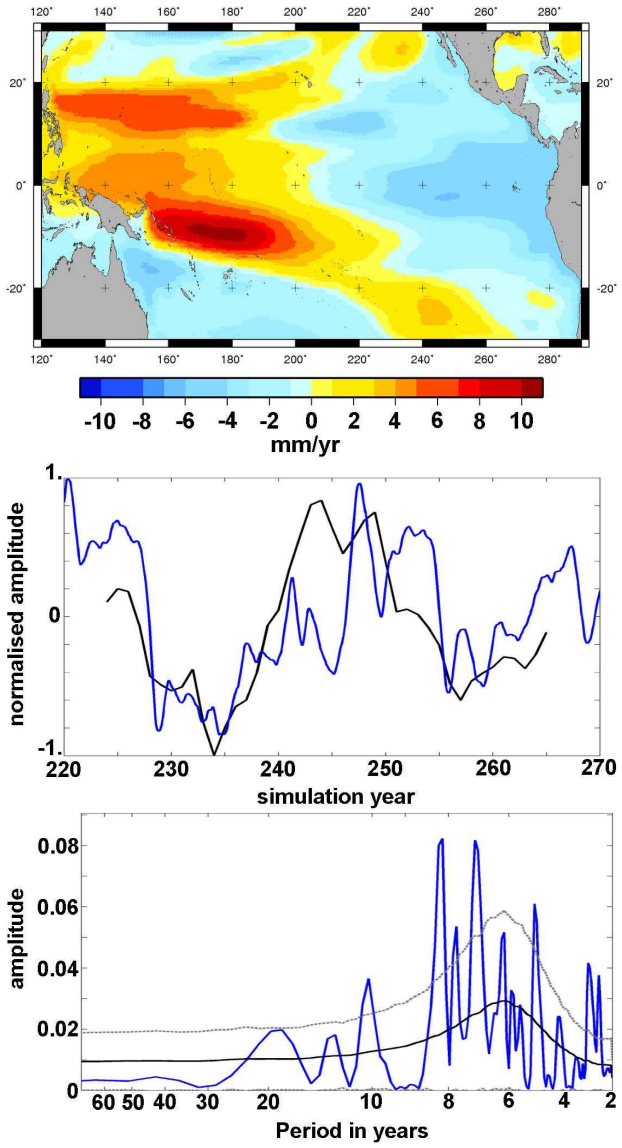

Fig. 8. First rotated EOF of the set of 17-yr trend maps computed with the GFDL control run between years 220 and 280. It explains 43 % of the total variance. Top panel: spatial pattern of the EOF Middle panel: the PC is the black curve. The NINO3 index, filtered with a 10-yr running mean and detrended, is superimposed in blue. Bottom panel: NINO3 index power spectrum (in blue) and the best fit AR2 process in black as the null hypothesis. The grey dashed lines indicate the 95 % confidence level around the null hypothesis.

runs: one with the 17-yr spatial trend patterns and one with the 17-yr averaged trend over box B.

For the first comparison, we considered the 17-yr spatial trend patterns of the rotated EOF of the control runs as the references. Then we projected the set of 17-yr trend maps computed from each 20c3m run outputs on these patterns (each 20c3m run outputs was projected on its respective control run spatial pattern). The resulting PCs show how the reference spatial patterns from the control runs fluctuate through the simulated 20th century climates. Their power spectra are plotted in Fig. 9. When several 20c3m runs were available for a given model, each PC was also plotted on the same graph. We added as well the power spectra of the control run leading PC (previously presented in Fig. 6). For a consistent comparison with the 20c3m power spectra, they were computed over subsets of 140 yr (length of the 20c3m runs) instead of the whole multi-centennial control run. We used a chunk spectral estimator (see von Storch and Zwiers, 1999) to compute them. This method consists in dividing the time series into a number of chunks of equal length and to estimate the spectrum by averaging the spectra obtained over each subset. This allows also estimating the 95 % confidence level. We added them in Fig. 9. But, note that here, only very few independent subsets (2 to 4) of 140 yr could be computed out of the 350 or 500 yr long control runs. So the 95 % confidence level plotted in Fig. 9 can not be considered as fully reliable but only indicative.

It is interesting to note that in Fig. 9, all CGCM 20c3m runs show some low frequency modulation of the spatial pattern as in the reconstruction and the control runs. Among models with complete external forcing (i.e. total anthropogenic forcing plus solar and volcanic variability, see Sect. 3.3 and Table 1), only 1 model (GISS) out of 6 shows significant differences in the leading PC between its control run and its 20c3m run. Three models (GFDL, MIROC and NCAR) show instead differences that are not significant. The 2 models left (CNRM and UKMO) actually show differences that reach the 95 % confidence level. But these 2 models only have 350 yr of control run. This enabled us to compute only 2 chunks to deduce the 95 % confidence level which makes their estimation particularly unreliable. So we assume that, for these 2 models, the differences are not significant. Concerning the IPSL model, which only takes into account the anthropogenic forcing (see Sect. 3.3 and Table 1), significant differences can be seen in the leading PC between the control run and the 20c3m run. But for the IAP model which includes anthropogenic forcing and solar variability (but no volcanic forcing), no significant differences are observed. Finally there are a majority of models (6 out of 8) which do not show significant difference in 17-yr sea level trend patterns between their control run and their 20th century runs. In particular, 5 out of the 6 models which include complete external forcing do not show significant differences.

In the second comparison, we considered the 17-yr sea level trends averaged over box B in the 20c3m runs. Their power spectra are plotted in Fig. 10 along with the power spectra of the 17-yr averaged trends in box B computed from the control runs. The latter power spectra (from the control runs) were already presented in Fig. 7. Here the same power spectra were computed but over subsets of 140 yr (length of the 20c3m runs) instead of the whole multi-centennial control run in order to be consistent with the 20c3m power spectra. We used a chunk spectral estimator to do so. There are too few independent subsets of 140 yr among the

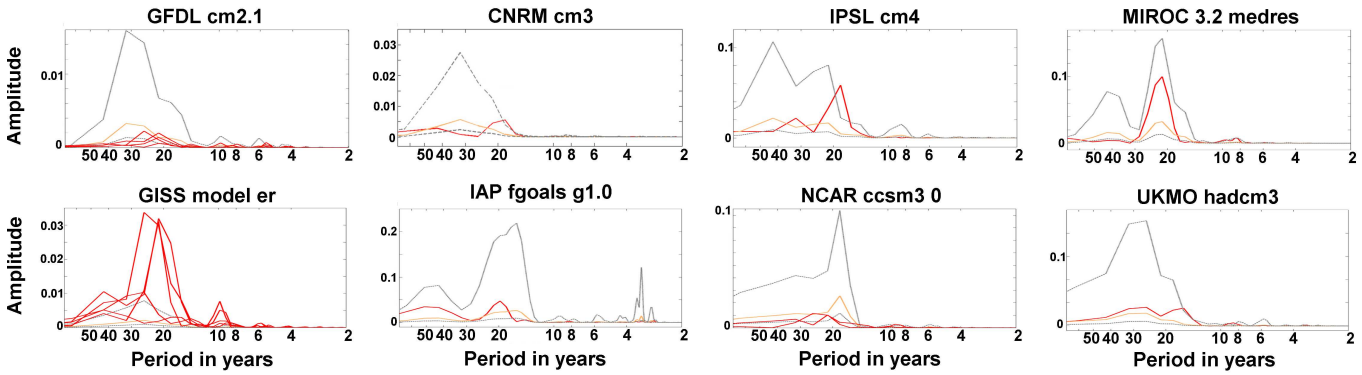

Fig. 9. Power spectra of the first PC of the set of 17-yr trend maps computed with the coupled climate models. The red curves indicate the power spectra of the 20c3m runs while the orange curves indicate the power spectra of their respective control runs. The grey dashed lines indicate the 95 % confidence level computed from the control runs.

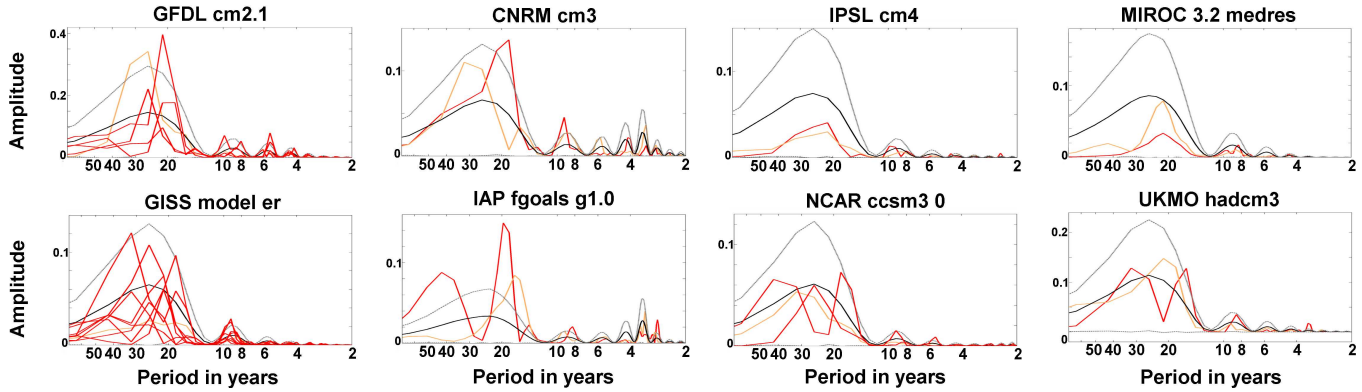

Fig. 10. Power spectra of the box B sea level trend computed over successive 17-yr windows and NINO3 index from the coupled climate models. The red curves indicate the power spectra from the 20c3m runs. The orange curves indicate the power spectra from their respective control runs and the black curves their respective best fit AR2 process. The grey dashed lines indicate the 95 % confidence level computed from the control runs best fit AR2 processes.

multi-centennial control runs to get a reliable estimation of a confidence interval on the control run spectra. So, instead of using the control run spectra as a reference (null hypothesis), we prefered to use their best fit AR2 process computed earlier and shown in Fig. 7. This gives more reliable estimations of the confidence intervals. The AR2 process power spectra and their 95 % confidence level are plotted in Fig. 10. Among models with complete external forcing, 2 models out of 6 (CNRM and UKMO) show a significant difference between the power spectra computed from their control run and their 20c3m run. 3 models (GFDL, GISS and NCAR) show both some 20c3m runs that differ significantly from their control run and some which do not. For each of these 3 models, only one run among all available 20c3m runs shows significant differences (i.e. 1 out of 4 available for the GFDL model, 1 out of 8 for the GISS model and 1 out of 2 for the NCAR model). Finally one model (MIROC) does not show any significant differences between its 20c3m run and its control run.

In this comparison, the IPSL (with anthropogenic forcing only) does not show significant differences between its control run and its 20c3m run, while the IAP model (whose 20c3m run contains greenhouse gas emissions and solar variability) shows some. Finally, among the 19 20c3m runs available from our dataset (see Table 1), 13 of them do not show any significant differences to their respective control runs (this ratio increases to 12 out of 17 when considering only 20c3m runs with complete external forcing). Only 6 20c3m runs show some differences. In total, only 5 20c3m runs show differences if we consider only those with complete external forcing. Nevertheless, it is interesting to note that for each of these 5 runs, the power spectra reveal that the 17-yr trends fluctuations in the 20c3m runs present a peak at higher frequency with more variance than in their respective control run.

5 Summary and discussion

Previous studies have shown that the sea level trend pattern observed in the tropical Pacific through 17-yr long precise altimetry observations (1993–2009) is largely of thermal origin (Ishii and Kimoto, 2009; Levitus, 2005; Levitus et al., 2009; Lombard et al., 2005a, b), the thermosteric sea level trends being themselves driven by surface wind stress (Carton et al., 2005; Kohl and Stammer, 2008; Timmermann et al., 2010). In this region, observed and thermosteric sea level trends are tightly linked to the ENSO mode of variability known to occur on a broad range of time scales, from interannual to multi-decadal (Knutson and Manabe, 1998; Lau and Weng, 1999; Vimont et al., 2002; Vimont, 2005). So the 17-yr trends observed by satellite altimetry in the tropical Pacific are expected to fluctuate on these time scales. Nevertheless, only a few studies have suggested that sea level trends observed prior to the altimetry era changed with time (Wunsch et al., 2007; Khol and Stammer, 2008). Here we show that 17-yr sea level trends are un-steady and fluctuated in the past with a characteristic time scale of around 25 yr (see Sect. 4.1). On the basis of a past sea level reconstruction (1950–2009), we find that the tropical Pacific trend patterns over successive 17-yr windows fluctuate in time and show some periods during which sea level rise accelerates or decelerates (or equivalently, trend patterns display increasing or decreasing intensity). The trend pattern behaves as a fluctuating east-west dipole following a low frequency modulation of ENSO. The relatively short time span of the 60-yr long reconstruction makes it difficult to precisely determine the characteristic time-scales of the pattern fluctuations but some value around 25 yr is suggested by the observations.

The CGCM control runs with constant, preindustrial external forcing, show fairly similar results. Indeed, 4 out of 8 CGCM control runs (GFDL, CNRM, NCAR, and UKMO) show significant 17-yr sea level trend fluctuations tightly linked to significant ENSO low frequency modulations as well. They display the same 17-yr spatial trend pattern which differs slightly from the reconstructed one. We have shown with the GFDL control run that this is probably due to the different time periods covered by the reconstruction and the control runs. So, the internal variability of the climate system, simulated here by the CGCM control runs, seems to be well able to explain most of the sea level trend pattern fluctuations of the tropical Pacific seen in the reconstruction and observed by altimetry. Note nevertheless that the different control runs do not always agree on the characteristic periods of these fluctuations. The GFDL and CNRM control runs exhibit periodicities in the range 25–33 yr close to what is suggested by the reconstruction. But the NCAR and MIROC control runs on the one hand and the UKMO on the other hand show periodicities in the range 18–22 yr and in the range 50–60 yr, respectively.

The CGCM 20th century runs with external forcing (including anthropogenic forcing) show similar sea level trend behaviours for the tropical Pacific as in the control runs. Actually, a majority of the 20c3m runs which include a complete external forcing (12 out of 17) do not show any significant differences to their respective control run, either in terms of temporal or spatial structures. Consequently, because the 20c3m and control runs provide similar results, we conclude that the internal variability of the climate system is still the dominant contributor to the fluctuations of the observed 17-yr spatial trend pattern in the tropical Pacific. In effect, our analysis does not detect any clear signature of external forcing, whether of anthropogenic origin or of natural origin (solar and volcanic variability). In other words, over the short altimetry record (17 yr), the amplitude of the noise represented here by the internal climate variability is so strong in the tropical Pacific that it prevents us from detecting the signal of anthropogenic forcing on the regional variability of the sea level trends in this region. These conclusions are also true when considering windows shorter than 17-yr for both data and model outputs. For example, using 10-yr and 15-yr-long windows led to similar results (with the same dominant low frequency variability of the tropical Pacific trend pattern).

Nevertheless, a minority of 20th century runs (see Sect. 4.2) seem to suggest that the impact of the external forcing could be possibly seen in the characteristic frequency band of the 17-yr trend pattern fluctuations. Several 20th century runs indeed show higher frequency oscillations for the 17-yr trend pattern than their respective control run (as explained earlier). But this remains very unclear. To get a clearer picture, we would need both more 20th century runs (to perform statistics on how many runs support this assertion) and longer runs with external forcing to compute more accurate power spectra. These runs should be available within the CMIP5 project. This will be the subject of future investigations.

Acknowledgements. This study was partially supported by the ANR "CECILE" project. Melanie Becker was funded by the post-doctoral grant of the ANR CECILE project. W. Llovel is supported by a NASA Postdoctorate fellowship. This work was partly supported by CNES.

Edited by: M. Siddall

The publication of this article is financed by CNRS-INSU.

References

Ablain, M., Cazenave, A., Valladeau, G., and Guinehut, S.: A new assessment of the error budget of global mean sea level rate estimated by satellite altimetry over 1993–2008, Ocean Sci., 5,193–201, 2009.

Becker, M., Meyssignac, B., Llovel, W., Cazenave, A., and Delcroix, T.: Sea level variations at Tropical Pacific Islands since 1950, Global Planet. Change, 81–82, 85–98, doi:10.1016/j.gloplacha.2011.09.004, 2012.

Bindoff, N. L., Willebrand, J., Artale, V., Cazenave, A., Gregory, J., Gulev, S., Hanawa, K., Le Quéré, C., Levitus, S., Nojiri, Y., Shum, C. K., Talley, L. D., and Unnikrishnan, A.: Observations: Oceanic Climate Change and Sea Level, in: Climate Change 2007: The Physical Science Basis. Contribution of Working Group I to the Fourth Assessment Report of the Intergovernmental Panel on Climate Change, edited by: Solomon, S., Qin, D., Manning, M., Chen, Z., Marquis, M., Averyt, K. B., Tignor, M., and Miller, H. L., Cambridge University Press, Cambridge, United Kingdom and New York, NY, USA, 2007.

Brigham, E. O.: The Fast Fourier Transform. Prentice-Hall, Englewood Cliffs, 1974.

Brodeau, L., Barnier, B., Treguier, A., Penduff, T., and Gulev, S.: An ERA40-based atmospheric forcing for global ocean circulation models, Ocean Modell., 31, 88–104, 2010.

Carrere, L. and Lyard, F.: Modeling the barotropic response of the global ocean to atmospheric wind and pressure forcing - comparisons with observations, Geophys. Res. Lett., 30, 1275–1279, 2003.

Carton, J. and Giese, B.: A reanalysis of ocean climate using Simple Ocean Data Assimilation (SODA), Mon. Weather Rev., 136, 2999–3017, 2008.

Carton, J., Giese, B., and Grodsky, S.: Sea level rise and the warming of the oceans in the Simple Ocean Data Assimilation (SODA) ocean reanalysis, J. Geophys. Res.-Oceans, 110, C09006, doi:10.1029/2004JC002817, 2005.

Cazenave, A. and Llovel, W.: Contemporary Sea Level Rise, Annual Review of Marine Science, 2, 145–173, 2010.

Cazenave, A. and Nerem, R.: Present-day sea level change: Observations and causes, Rev. Geophys., 42, RG3001, doi:10.1029/2002GL016473, 2004.

Christiansen, B., Schmith, T., and Thejll, P.: A Surrogate Ensemble Study of Sea Level Reconstructions, J. Climate, 23, 4306–4326, 2010.

Church, J. A., White, N. J., Coleman, R., Lambeck, K., and Mitrovica, J. X.: Estimates of the regional distribution of sea level rise over the 1950–2000 period, J. Climate, 17,2609–2625, 2004.

Collins, W. D., Rasch, P. J., Boville, B. A., Hack, J. J., McCaa, J. R., Williamson, D. L., Kiehl, J. T., Briegleb, B., Bitz, C., Lin, S. J., Zhang, M., and Dai, Y.: Description of the NCAR Community Atmosphere Model (CAM3.0), Technical Note TN-464+STR, National Center for Atmospheric Research, Boulder, 2004.

Delworth, T., Broccoli, A., Rosati, A., Stouffer, R., Balaji, V., Beesley, J., Cooke, W., Dixon, K., Dunne, J., Dunne, K., Durachta, J., Findell, K., Ginoux, P., Gnanadesikan, A., Gordon, C., Griffies, S., Gudgel, R., Harrison, M., Held, I., Hemler, R., Horowitz, L., Klein, S., Knutson, T., Kushner, P., Langenhorst, A., Lee, H., Lin, S., Lu, J., Malyshev, S., Milly, P., Ramaswamy, V., Russell, J., Schwarzkopf, M., Shevliakova, E., Sirutis, J., Spelman, M., Stern, W., Winton, M., Wittenberg, A., Wyman, B., Zeng, F., and Zhang, R.: GFDL's CM2 global coupled climate models, Part I: Formulation and simulation characteristics, J. Climate, 19, 643–674, 2006.

Déqué, M., Dreveton, C., Braun, A., and Cariolle, D.: The ARPEGE/IFS atmosphere model – a contribution to the french community climate modeling, Clim. Dynam., 10, 249–266, 1994.

Di Lorenzo, E., Cobb, K. M., Furtado, J. C., Schneider, N., Anderson, B. T., Bracco, A., Alexander, M. A., and Vimont, D. J.: Central Pacific El Niño and decadal climate change in the North Pacific Ocean, Nat. Geosci., 3, 762–765, 2010.

Gnanadesikan, A., Dixon, K., Griffies, S., Balaji, V., Barreiro, M., Beesley, J., Cooke, W., Delworth, T., Gerdes, R., Harrison, M., Held, I., Hurlin, W., Lee, H., Liang, Z., Nong, G., Pacanowski, R., Rosati, A., Russell, J., Samuels, B., Song, Q., Spelman, M., Stouffer, R., Sweeney, C., Vecchi, G., Winton, M., Wittenberg, A., Zeng, F., Zhang, R., and Dunne, J.: GFDL's CM2 global coupled climate models, Part II: The baseline ocean simulation, J. Climate, 19, 675–697, 2006.

Gomez, N., Mitrovica, J., Tamisiea, M., and Clark, P.: A new projection of sea level change in response to collapse of marine sectors of the Antarctic Ice Sheet, Geophys. J. Int., 180, 623–634, 2010.

Gordon, C., Cooper, C., Senior, C. A., Banks, H., Gregory, J. M., Johns, T. C., Mitchell, J. F. B., and Wood, R. A.: The simulation of SST, sea ice extents and ocean heat transports in a version of the Hadley Centre coupled model without flux adjustments, Clim. Dynam., 16, 147–168, 2000.

Greatbatch, R.: A note on the representation of steric sea-level in models that conserve volume rather than mass, J. Geophys. Res.-Oceans, 99, 12767–12771, 1994.

Han, W. Q, Meehl, G. A., Rajagopalan, B., Fasullo, J. T., Hu, A. X., Lin, J. L., Large, W. G., Wang, J. W., Quan, X. W., Trenary, L. L., Wallcraft, A., Shinoda, T., and Yeager, S.: Patterns of Indian Ocean sea-level change in a warming climate, Nat. Geosci., 8, 546–550, 2010.

Hourdin, F., Musat, I., Bony, S., Braconnot, P., Codron, F., Dufresne, J. L., Fairhead, L., Filiberti, M. A., Friedlingstein, P., Grandpeix, J. Y., Krinner, G., Levan, P., Li, Z. X., and Lott, F.: The LMDZ4 general circulation model: Climate performance and sensitivity to parameterized physics with emphasis on tropical convection, Clim. Dynam., 27, 787–813, 2006.

Ishii, M. and Kimoto, M.: Reevaluation of historical ocean heat content variations with time-varying XBT and MBT depth bias corrections, J. Oceanogr., 65, 287–299, 2009.

Jin, X. Z., Zhang, X. H., and Zhou, T. J.: Fundamental framework and experiments of the third generation of the IAP/LASG World Ocean General Circulation, Adv. Atmos. Sci., 16, 197–215, 1999.

Johns, T. C., Durman, C. F., Banks, H. T., Roberts, M. J., McLaren, A. J., Ridley, J. K., Senior, C. A., Williams, K. D., Jones, A., Rickard, G. J., Cusack, S. Ingram, W. J., Crucifix, M. Sexton, D. M. H., Joshi, M. M., Dong, B. W., Spencer, H., Hill, R. S. R., Gregory, J. M., Keen, A. B., Pardaens, A. K., Lowe, J. A., Bodas-Salcedo, A., Stark, S., and Searl, Y.: The new Hadley Centre climate model HadGEM1: Evaluation of coupled simulations, J. Climate, 19, 1327–1353, 2006.

K-1 Model Developers: K-1 Coupled Model (MIROC) Description. K-1 Technical Report 1. Center for Climate System Research, University of Tokyo, 2004.

Kaplan, A., Cane, M., Kushnir, Y., Clement, A., Blumenthal, M., and Rajagopalan, B.: Analyses of global sea surface temperature 1856–1991, J. Geophys. Res.-Oceans, 103, 18567–18589, 1998.

Kaplan, A., Kushnir, Y., and Cane, M. A.: Reduced space optimal interpolation of historical marine sea level pressure: 1854–1992, J. Climate, 13, 2987–3002, 2000.

Knutson, T. and Manabe, S.: Model assessment of decadal variability and trends in the tropical Pacific Ocean, J. Climate, 11, 2273–2296, 1998.

Kohl, A. and Stammer, D.: Decadal sea level changes in the 50-year GECCO ocean synthesis, J. Climate, 21, 1876–1890, 2008.

Large, W. and Yeager, S.: Diurnal to decadal global forcing for ocean and sea-ice models: the datasets and flux climatologies. NCAR technical note: NCAR/TN460+STR, CGD division of the National Center for Atmospheric Research, available on the GFDL CORE web site, available at: http://data1.gfdl.noaa.gov/nomads/forms/mom4/CORE/doc.html, 2004.

Lau, K. and Weng, H.: Interannual, decadal-interdecadal, and global warming signals in sea surface temperature during 1955–97, J. Climate, 12, 1257–1267, 1999.

Le Traon, P. L. and Ogor, F.: ERS-1/2 orbit improvement using TOPEX/POSEIDON: The 2 cm challenge, J. Geophys. Res., 103, 8045–8057, 1998.

Le Traon, P. Y., Nadal, F., and Ducet, N.: An improved mapping method of multisatellite altimeter data, J. Atmos. Ocean. Technol., 15, 522–534, 1998.

Levitus, S.: Warming of the world ocean, 1955–2003, Geophys. Res. Lett., 32, L02604, doi:10.1029/2004GL021592, 2005.

Levitus, S., Antonov, J. I., Boyer, T. P., Locarnini, R. A., Garcia, H. E., and Mishonov, A. V.: Global ocean heat content 1955–2008 in light of recently revealed instrumentation problems, Geophys. Res. Lett., 36, L07608, doi:10.1029/2008GL037155, 2009.

Liu, H. L., Zhang, X. H., Li, W., Yu, Y. Q., and Yu, R. C.: An eddy-permitting oceanic general circulation model and its preliminary evaluations, Adv. Atmos. Sci., 21, 675–690, 2004.

Llovel, W., Cazenave, A., Rogel, P., Lombard, A., and Nguyen, M. B.: Two-dimensional reconstruction of past sea level (1950–2003) from tide gauge data and an Ocean General Circulation Model, Clim. Past, 5, 217–227, doi:10.5194/cp-5-217-2009, 2009.

Lombard, A., Cazenave, A., DoMinh, K., Cabanes, C., and Nerem, R.: Thermosteric sea level rise for the past 50 years; comparison with tide gauges and inference on water mass contribution, Global Planet. Change, 48, 303–312, 2005a.

Lombard, A., Cazenave, A., Le Traon, P., and Ishii, M.: Contribution of thermal expansion to present-day sea-level change revisited, Global Planet. Change, 47, 1–16, 2005b.

Lombard, A., Garric, G., and Penduff, T.: Regional patterns of observed sea level change: insights from a 1/4A degrees global ocean/sea-ice hindcast, Ocean Dynam., 59, 433–449, 2009.

Lozier, M., Roussenov, V., Reed, M., and Williams, R.: Opposing decadal changes for the North Atlantic meridional overturning circulation (3, pp. 728, 2010), Nat. Geosci., 3, 805–805, 2010.

Madec, G.: NEMO ocean engine, Note du Pole de modélisation, Institut Pierre-Simon Laplace (IPSL), France, No. 27, ISSN 1288-1619, 2008.

Madec, G., Delecluse, P., Imbard, M., and Levy, C.: OPA 8.1 general circulation model reference manual, Notes de l'IPSL, University P. et M. Curie, No.11, p. 91, 1998.

Meyssignac, B., Becker, M., Llovel, W., and Cazenave, A.: An assessment of two-dimensional past sea level reconstructions over 1950–2009 based on tide gauge data and different input sea level grids, Surv. Geophys., online first, doi:10.1007/s10712-011-9171-x, 2012.

Milne, G. A. and Mitrovica, J.: Searching for eustasy in deglacial sea-level histories, Quaternary Sci. Rev., 27, 2292–2302, 2008.

Milne, G. A., Gehrels, W. R., Hughes, C. W., and Tamisiea, M. E.: Identifying the causes of sea-level change, Nat. Geosci., 2, 471–478, 2009.

Mitrovica, J., Tamisiea, M., Davis, J., and Milne, G.: Recent mass balance of polar ice sheets inferred from patterns of global sea-level change, Nature, 409, 1026–1029, 2001.

Mitrovica, J., Gomez, N., and Clark, P.: The Sea-Level Fingerprint of West Antarctic Collapse, Science, 323, 753–753, 2009.

Nerem, R. S., Chambers, D. P., Choe, C., and Mitchum, G. T.: Estimating Mean Sea Level Change from the TOPEX and Jason Altimeter Missions, Mar. Geod., 33, 435–446, 2010.

Penduff, T., Juza, M., Brodeau, L., Smith, G., Barnier, B., Molines, J., Treguier, A., and Madec, G.: Impact of global ocean model resolution on sea-level variability with emphasis on interannual time scales, Ocean Sci., 6, 269–284, 2010, http://www.ocean-sci.net/6/269/2010/.

Pope, V. D., Gallani, M. L., Rowntree, P. R., and Stratton, R. A.: The impact of new physical parametrizations in the Hadley Centre climate model: HadAM3, Clim. Dynam., 16, 123–146, 2000.

Preisendorfer, R. W.: Principal Component Analysis in Meteorology and Oceanography, Vol. 17, Developments in Atmospheric Science, Elsevier, Amsterdam, 1988.

Rabiner, L. R. and Gold, B.: Theory and Application of Digital Signal Processing, Prentice-Hall, Englewood Cliffs, 1975.

Russell, G. L., Miller, J. R., and Rind, D.: A coupled atmosphere-ocean model for transient climate change studies, Atmos.-Ocean, 33, 683–730, 1995.

Schmidt, G. A., Ruedy, R., Hansen, J. E., Aleinov, I., Bell, N., Bauer, M., Bauer, S., Cairns, B., Canuto, V., Cheng, Y., Del Genio, A., Faluvegi, G., Friend, A. D., Hall, T. M., Hu, Y. Y., Kelley, M., Kiang, N. Y., Koch, D., Lacis, A. A., Lerner, J., Lo, K. K., Miller, R. L., Nazarenko, L., Oinas, V., Perlwitz, J., Perlwitz, J., Rind, D., Romanou, A., Russell, G. L., Sato, M. Shindell, D. T., Stone, P. H., Sun, S., Tausnev, N., Thresher, D., and Yao, M. S.: Present day atmospheric simulations using GISS ModelE: Comparison to in-situ, satellite and reanalysis data, J. Climate, 19, 153–192, 2006.

Smith, R. D. and Gent, P. R.: Reference Manual for the Parallel Ocean Program (POP), Ocean Component of the Community Climate System Model (CCSM2.0 and 3.0), Technical Report LA-UR-02-2484, Los Alamos National Laboratory, Los Alamos, 2002.

Solomon, S., Qin, D., Manning, M., Chen, Z., Marquis, M., Averyt, K. B., Tignor, M., and Miller, H. L. IPCC: Climate Change 2007: The Physical Science Basis.Contribution of Working Group I to the Fourth Assessment Report of the Intergovernmental Panel on Climate Change, 2007.

Timmermann, A., McGregor, S., and Jin, F.: Wind Effects on Past and Future Regional Sea Level Trends in the Southern Indo-

Pacific, J. Climate, 23, 4429–4437, 2010.

Toumazou, V. and Cretaux, J. F.: Using a Lanczos Eigensolver in the Computation of Empirical Orthogonal Functions, Mon. Weather Rev., 129, 1243–1250, 2001.

Uppala, S., Kallberg, P., Simmons, A., Andrae, U., Bechtold, V., Fiorino, M., Gibson, J., Haseler, J., Hernandez, A., Kelly, G., Li, X., Onogi, K., Saarinen, S., Sokka, N., Allan, R., Andersson, E., Arpe, K., Balmaseda, M., Beljaars, A., Van De Berg, L., Bidlot, J., Bormann, N., Caires, S., Chevallier, F., Dethof, A., Dragosavac, M., Fisher, M., Fuentes, M., Hagemann, S., Holm, E., Hoskins, B., Isaksen, L., Janssen, P., Jenne, R., McNally, A., Mahfouf, J., Morcrette, J., Rayner, N., Saunders, R., Simon, P., Sterl, A., Trenberth, K., Untch, A., Vasiljevic, D., Viterbo, P., and Woollen, J.: The ERA-40 re-analysis, Q. J. Roy. Meteorol. Soc., 131, 2961–3012, 2005.

Vimont, D.: The contribution of the interannual ENSO cycle to the spatial pattern of decadal ENSO-like variability, J. Climate, 18, 2080–2092, 2005.

Vimont, D., Battisti, D., and Hirst, A.: Pacific interannual and interdecadal equatorial variability in a 1000-yr simulation of the CSIRO coupled general circulation model, J. Climate, 15, 160–178, 2002.

Volkov, D., Larnicol, G., and Dorandeu, J.: Improving the quality of satellite altimetry data over continental shelves, J. Geophys. Res.-Oceans, 112, C06020, doi:10.1029/2006JC003765, 2007.

von Storch, H. and Zwiers, F. W.: Statistical Analysis in Climate Research, Cambridge University Press, 1999.

Wan, H., Ji, Z. Z., Zhang, X., Yu, R. C., Yu, Y. Q., and Liu, H. T.: Design of a new dynamical core for global atmospheric models based on some efficient numerical methods, Science in China, Ser. A, 47 Suppl., 4–21, 2004.

Wunsch, C., Ponte, R., and Heimbach, P.: Decadal trends in sea level patterns: 1993–2004, J. Climate, 20, 5889–5911, 2007.

Conclusion et Perspectives

Le 4ème rapport du GIEC (*Solomon et al.* [2007]) identifie la montée du niveau de la mer comme l'une des conséquences majeures du changement climatique. En particulier le groupe de travail n°2 du GIEC, qui a évalué les impacts du réchauffement climatique (*Parry et al.* [2007]), estime que l'élévation du niveau de la mer aura des conséquences néfastes importantes au cours du XXIème siècle sur les plans humains, socio-économiques et environnementaux. Ces conclusions s'appuient sur les simulations des modèles de climat, réalisées dans le cadre du projet CMIP3, pour le 4ème rapport du GIEC, avec différents scenarii d'émissions de gaz à effet de serre. Ces simulations prédisent en 2100 que le niveau de la mer global sera plus élevé de 10 à 60 cm en moyenne avec une valeur médiane de 40 cm. C'est le réchauffement océanique qui domine cette augmentation d'après les modèles, tandis que la fonte des glaciers continentaux est le deuxième contributeur. Ces projections indiquent aussi une variabilité régionale du niveau de la mer plus forte en 2100 qu'aujourd'hui et dominée largement par le signal stérique. Depuis le 4ème rapport du GIEC, l'augmentation du niveau de la mer a été revue à la hausse du fait de la prise en compte de l'accélération de l'écoulement de la glace vers l'océan dans les zones côtières des calottes polaires. Aujourd'hui, dans la littérature récente le niveau de la mer global en 2100 est estimé entre 30 et 80 cm au dessus du niveau actuel. La variabilité régionale a elle aussi été récemment revue à la hausse du fait de la prise en compte de la réponse visco-élastique de la croûte terrestre à la fonte des glaces continentales (*Slangen et al.* [2011, in revision]).

Malgré ces récentes mises à jour, les incertitudes des projections demeurent très grandes ($\pm$25cm pour le niveau global et des différences fortes dans les variabilités régionales entre les différents modèles de climat). Une part de ces incertitudes est liée à la mauvaise estimation de l'activité anthropique future (futures émissions anthropiques de gaz à effet de serre et d'aérosols et occupation future des sols). Mais une autre part d'incertitude substantielle est liée à l'incapacité actuelle des modèles climatiques à modéliser de manière réaliste les différents facteurs responsables de la hausse du niveau des mers (réchauffement des océans, fonte des calottes polaires et échanges d'eau avec les réservoirs continentaux). En ce qui concerne le niveau de la mer global, les incertitudes viennent en majeure partie de la mauvaise connaissance des processus à l'origine de l'accélération de la perte de glace des calottes polaires. En ce qui concerne la variabilité régionale en revanche, l'origine des incertitudes n'est pas claire. Les différents modèles de climat reproduisent une variabilité régionale du niveau de la mer stérique dans le futur et sur les dernières décennies qui est significativement différente d'un modèle à l'autre, surtout aux moyennes et hautes latitudes. A ces latitudes en particulier, le signal des eaux profondes et abyssales est plus fort et les modèles climatiques n'ont en général pas une bonne représentation de ces eaux et de leur signature stérique (dérive des modèles dans les couches profondes). De plus, la con-

tribution provenant de la réponse visco-élastique de la croûte terrestre dépend fortement de l'amplitude de la fonte des glaces et de sa localisation : elle est donc très incertaine, elle aussi. Enfin, en général, les modèles de climat simulent très mal les échanges d'eau entre les réservoirs continentaux et l'océan. En résumé, les projections de la variabilité régionale du niveau de la mer sont particulièrement incertaines car elle pâtissent de la mauvaise connaissance des échelles spatio-temporelles qui la caractérise et des processus qui la gouvernent.

Pourtant au cours de cette thèse nous avons mis en évidence l'importance de la variabilité régionale du niveau de la mer par une meilleure estimation de son signal depuis 1950. Or ces résultats montrent que c'est elle qui domine le signal de montée du niveau de la mer dans la plupart des régions du globe aux échelles inter-annuelles (comme nous avons vu avec l'altimétrie) à multi-décennales (comme nous avons vu avec les reconstruction 2D du niveau de la mer). Ceci montre que si l'on veut pouvoir estimer les impacts liés à la montée du niveau de la mer en 2100, il est crucial de mieux estimer, comprendre et modéliser la variabilité régionale du niveau de la mer. Un autre résultat majeur de cette thèse montre que même si le signal stérique explique plus de 70% de la variabilité régionale du niveau de la mer, le signal de masse dans l'océan ne peut être négligé localement. De manière régionale dans l'espace (à l'échelle des demi-bassins océaniques par exemple) ou de manière ponctuelle dans le temps (au cours des évènements El Niño par exemple) le signal de masse peut dominer le signal stérique et expliquer la variabilité du niveau de la mer. Ce résultat est inattendu et révèle en particulier l'existence de processus de redistribution de masse à la surface de la Terre entre régions éloignées qui sont aujourd'hui encore inexpliqués et mal observés.

Par ailleurs, nous avons analysé dans cette thèse, les facteurs qui sont à l'origine des variations du niveau de la mer. En résumant les études portant sur les contributions au niveau de la mer global, nous avons été en mesure de montrer que les émissions anthropiques de gaz à effet de serre et d'aérosols sont en cause dans au moins 65% de l'augmentation du niveau de la mer global depuis 1972. Nous avons aussi analysé les origines de la variabilité régionale du niveau de la mer. Pour cela nous avons développé la première étude de détection et attribution de la variabilité régionale du niveau de la mer et nous l'avons appliqué au Pacifique tropical. Nous avons montré que la variabilité régionale très forte qui caractérise l'Ouest du Pacifique depuis 17 ans n'est pas permanente. Elle est en fait la manifestation d'une basse fréquence de la variabilité interne du système climatique dont l'amplitude est si forte qu'il est difficile aujourd'hui d'y détecter un impact éventuel de l'activité anthropique. Ainsi ce résultat, confirmé par une étude très récente avec des modèles océaniques, permet de remettre dans un contexte plus large de fluctuation basse fréquence, la hausse extrême du niveau de la mer observée dans l'Ouest du Pacifique par les satellites. Cependant de nombreuses autres régions sensibles aussi à la hausse locale du niveau de la mer restent à analyser.

L'ensemble de ces résultats apparaîtront dans le 5$^{\text{ème}}$ rapport du GIEC qui doit être rendu public en 2013.

Outre les éléments de réponse apportés aux questions scientifiques posées dans la section 1.5, ces résultats ont soulevé de nombreuses questions nouvelles. Parmi celles-ci j'en ai

selectionné 3 qui me paraissent centrales et que je compte étudier tout de suite après cette thèse.

Concernant l'estimation de la variabilité régionale du niveau de la mer :

La reconstruction en 2D du niveau de la mer que nous avons proposée donne des résultats à mi-chemin entre les reconstructions plus anciennes qui ne s'appuyaient que sur une courte période d'altimétrie (8 ans) et les réanalyses d'océan. Ceci pose la question de la validité des reconstructions et des réanalyses en terme de variabilité régionale reconstruite. Pour répondre à ce point il faut (1) continuer de collecter, analyser et corriger les données marégraphiques afin d'avoir des points de comparaisons pour valider les reconstructions ; (2) comparer de manière systématique les modèles d'océan, les réanalyses et les reconstructions, pas seulement en tendances mais aussi en variabilité spatio-temporelle (EOF par exemple) afin de détecter et corriger les défauts de chaque méthode dans l'estimation de la variabilité régionale ; (3) développer une reconstruction moyenne (sur l'exemple des modèles climatiques) qui s'appuie sur un grand nombre de modèles et sur la plus longue période d'altimétrie disponible afin de maximiser le signal physique qui fait consensus parmi les modèles et l'altimétrie et ainsi obtenir la meilleur estimation possible de la variabilité régionale passée (4) continuer de développer des reconstructions locales pour les régions qui ne sont pas ou sont mal couvertes par la reconstruction globale.

Concernant les causes de la variabilité régionale :

Les résultats sur le signal de masse observé par GRACE dans les bassins Pacifique et Atlantique ou observé par la différence "Altimétrie moins Stérique" lors des évènements El Niño, ont mis en évidence l'existence de transferts de masse considérables à la surface de la Terre entre des régions extrêmement éloignées. Malgré leur amplitude ces transferts de masse n'ont pas été identifiés auparavant ni étudiés. Nous proposons de les analyser en utilisant de manière combinée toutes les données géophysiques à notre disposition qui peuvent apporter une mesure ou une contrainte sur ces transferts de masse. Ceci comprend bien sûr les données qui permettent les mesures de variations de masse de l'océan, comme les données altimétriques de Topex/Jason1-2 combinée avec les données hydrographiques des sondes XBT, CTD et des profileurs Argo, ou les données GRACE corrigées du GIA qui donnent aussi les variations de masse des stocks d'eau continentaux et des glaces continentales. Il y a aussi d'autres jeux de données plus globaux qui peuvent apporter des contraintes sur les transferts de masse : ce sont toutes les mesures liées à la matrice d'inertie de la Terre et à ses fluctuations. Parmi ces mesures on trouve la longueur du jour ou la dérive de l'axe des pôles, mesurés depuis longtemps par observation des astres. Il y a aussi les mesures des premières harmoniques du champ de gravité terrestre par les satellites LAGEOS1-2 et Starlette depuis le milieu des années 1970. Enfin nous pouvons aussi utiliser les mesures GPS, les modèles de GIA et les mesures GRACE de la réponse de la croûte terrestre à la fonte actuelle de la glace pour estimer les mouvements de la croûte terrestre et le transfert de masse qu'ils impliquent.

L'ensemble de ces données fournit un réseau d'information sur les transfert de masse dans l'enveloppe fluide de la Terre. Pris individuellement ou en combinant deux à trois jeux de données nous devrions obtenir des informations précises sur les variations de masse des différentes composantes de l'enveloppe fluide : l'océan, les bassins fluviaux, la cryosphère, la croûte etc.. (des études de ce type ont déjà été accomplies dans cette thèse). Pris dans son

ensemble, le réseau complet devrait aussi fournir une synthèse extrêmement intéressante du comportement de l'enveloppe fluide de la Terre aux échelles inter-annuelles à multi-décennales. Dans ce réseau, la plus grande inconnue est sans doute le mouvement de la croûte lié en particulier au GIA. Considéré sous la forme d'un problème inverse, le réseau complet d'information pourrait apporter aussi de nouvelles contraintes pour mieux estimer ce phénomène.

Nous avons commencé à aborder l'analyse globale de ce réseau d'information. Aux échelles inter-annuelles à décennales (de 1993 à 2011), les premiers coefficients des harmoniques sphériques du géoïde la Terre, (C20, C21, S21, C22, S22) mesurés par LAGEOS1-2 présentent des variations significatives quand on les corrige de la dérive liée au GIA. Ces variations sont confirmées par les mesures de la longueur du jour. En faisant un bilan des transferts de masse océanique avec l'altimétrie et les données hydrographiques d'une part et des transferts de masse continentaux avec GRACE et les modèles hydrologiques d'autre part et en projetant ce bilan sur les 3 premières harmoniques sphériques, nous parvenons à expliquer précisement les variations inter-annuelles observées dans les coefficients C20, C21, S21, C22, S22 depuis 1993. Il reste à affiner le bilan, et à tester plusieurs modèles de GIA, mais ces premiers résultats sont extrêmement prometteurs. Ils pourraient ouvrir une nouvelle approche plus globale dans l'analyse des changements climatiques à partir des observations.

Les résultats de cette thèse, une fois rassemblés, ont aussi soulevé un problème concernant la variabilité régionale du niveau de la mer. Jusqu'ici, les différentes analyses de la variabilité régionale du niveau de la mer ont été faites avec les mesures altimétriques, hydrographiques (Argo en particulier) et les mesures de GRACE. Les mesures des satellites altimétriques et de GRACE sont impactées par les effets quasi-statiques liés aux mouvement de la croûte terrestre, comme on l'a vu à la section 1.3.3. Or, lorsque l'on compare ces différents jeux de données (pour l'estimation des variations régionales de la masse de l'océan par exemple), ils ne sont, en général, pas totalement corrigés des effets quasi-statiques. Par exemple, dans la littérature, les mesures altimétriques ne sont jamais corrigées régionalement de l'effet quasi-statique du GIA (i.e. du signal de la Fig. 1.20a) ou de la fonte actuelle des glaces. De même, les données GRACE ne sont jamais corrigées régionalement de l'effet quasi-statique de la fonte actuelle des glaces (la modélisation régionale de cet effet sur les mesures altimétriques ou sur les mesures GRACE n'a, en fait, pas encore été publiée dans la littérature). On s'attend à ce que ces effets soient petits. Cependant, avec le rythme de la fonte actuelle des calottes polaires et des glaciers de montagne, ceci reste à vérifier. Si ces effets sont moins petits qu'attendus, peut être pourront-ils être détectés grâce à la précision de plus en plus grande que l'on obtient dans la mesure du niveau de la mer non-stérique avec Argo ? Peut être expliqueront-ils aussi, les différences que l'on obtient entre les mesures GRACE de la masse de l'océan et les mesures "Altimétrie moins Argo" du niveau de la mer non-stérique. Pour répondre à cette problématique, nous identifions 3 axes de travail : 1) améliorer le rapport signal sur bruit de GRACE sur l'océan, afin d'obtenir un meilleur signal de masse de l'océan car GRACE reste une source importante d'erreurs (voir section 2.1.2) ; 2) estimer, avec nos collègues qui modélisent les réponses visco-élastiques de la croûte terrestre, les impacts régionaux du GIA et de la fonte actuelle des glaces sur tous les instruments de mesure du niveau de la mer (Altimétrie, marégraphes), et de la masse de l'océan (GRACE, LAGEOS1-2, starlette etc) ; 3) établir une référence géodésique pour la comparaison des données entre

l'altimétrie et GRACE : aujourd'hui les 20 ans d'anomalies du niveau de la mer mesurées par altimétrie sont calculées par rapport à un géoïde estimé entre 1993 et 1997 et considéré comme stationnaire, or ce géoïde n'est certainement pas stationnaire du fait de la fonte des glaces actuelle et de plus, il est différent de celui utilisé par GRACE (EIGEN-GRGS.RL02 pour la solution GRACE du GRGS par exemple). Ceci est probablement à recalculer pour établir des comparaisons entre systèmes de mesures par rapport à une même référence.

Concernant l'origine naturelle ou anthropique de la variabilité régionale :

En ce qui concerne le niveau de la mer global, le rôle des émissions anthropiques de gaz à effet de serre sur sa variabilité est déjà avéré à travers son impact sur les contributeurs au niveau de la mer. Il sera cependant intéressant de vérifier que l'on peut détecter et attribuer de manière directe ce rôle. Ceci permettra (1) d'évaluer la capacité des modèles climatiques à reproduire le niveau de la mer du XX$^{\text{ème}}$ siècle et (2) de quantifier précisement le rôle joué par les gaz à effet de serre . Ceci pourrait aussi permettre d'évaluer en retour, le rôle des gaz à effet de serre dans la fonte des calottes polaires par bilan du niveau de la mer.

En ce qui concerne la variabilité régionale du niveau de la mer, de nombreuses questions restent en suspens. Nous avons montré dans le Pacifique tropical que la variabilité régionale des 17 dernières années ne pouvait être attribuée à l'activité anthropique. (1) Mais sur des périodes plus longues de 60 ans, comme dans la reconstruction, ne peut on pas espérer détecter l'impact anthropique ? (2) Peut être peut-on l'identifier dans des régions caractérisées par une variabilité interne du système climatique moins forte comme le Nord de l'Atlantique ou l'océan Arctique. (3) Quelle forme prendrait cet impact ? Nous comptons dans un premier temps identifier la signature des gaz à effet de serre sur la variabilité régionale du niveau de la mer en analysant les simulations CMIP5 (pour le 5$^{\text{ème}}$ rapport du GIEC) qui utilisent un forçage extrême en gaz à effet de serre (scénario d'émission RCP8.5). Par la suite, nous évaluerons si cette signature est présente de manière significative dans la variabilité régionale du niveau de la mer des dernières décennies. Cette étude doit se faire région par région en s'appuyant sur les reconstructions 2D du niveau de la mer les plus fiables. Le fait que certains modèles climatiques aient déjà montré qu'ils reproduisaient dans le Pacifique tropical une part de la variabilité régionale du niveau de la mer observé depuis 1950 est prometteur pour cette étude.

Bibliographie

Ablain, M., A. Cazenave, G. Valladeau, and S. Guinehut, A new assessment of the error budget of global mean sea level rate estimated by satellite altimetry over 1993-2008, *Ocean Science*, *5*(2), 193–201, doi :10.5194/os-5-193-2009, 2009.

AchutaRao, K. M., B. D. Santer, P. J. Gleckler, K. E. Taylor, D. W. Pierce, T. P. Barnett, and T. M. L. Wigley, Variability of ocean heat uptake : Reconciling observations and models, *Journal of Geophysical Research*, *111*, 20 PP., doi :200610.1029/2005JC003136, 2006.

AchutaRao, K. M., M. Ishii, B. D. Santer, P. J. Gleckler, K. E. Taylor, T. P. Barnett, D. W. Pierce, R. J. Stouffer, and T. M. L. Wigley, Simulated and observed variability in ocean temperature and heat content, *Proceedings of the National Academy of Sciences*, *104*(26), 10,768–10,773, doi :10.1073/pnas.0611375104, 2007.

Alley, R. B., S. Anandakrishnan, T. K. Dupont, B. R. Parizek, and D. Pollard, Effect of sedimentation on Ice-Sheet Grounding-Line stability, *Science*, *315*(5820), 1838–1841, doi :10.1126/science.1138396, 2007.

Alley, R. B., M. Fahnestock, and I. Joughin, Understanding glacier flow in changing times, *Science*, *322*(5904), 1061–1062, doi :10.1126/science.1166366, 2008.

Allison, I., R. Alley, H. Fricker, R. Thomas, and R. Warner, Ice sheet mass balance and sea level, *Antarctic Science*, *21*(05), 413–426, doi :10.1017/S0954102009990137, 2009.

Antonioli, F., L. Ferranti, A. Fontana, A. Amorosi, A. Bondesan, C. Braitenberg, A. Dutton, G. Fontolan, S. Furlani, K. Lambeck, G. Mastronuzzi, C. Monaco, G. Spada, and P. Stocchi, Holocene relative sea-level changes and vertical movements along the italian and istrian coastlines, *Quaternary International*, *206*(1-2), 102–133, doi : 10.1016/j.quaint.2008.11.008, 2009.

Antonov, J. I., S. Levitus, and T. P. Boyer, Steric sea level variations during 1957-1994 : Importance of salinity, *Journal of Geophysical Research*, *107*, 8 PP., doi :200210.1029/2001JC000964, 2002.

Antonov, J. I., S. Levitus, and T. P. Boyer, Thermosteric sea level rise, 1955-2003, *Geophysical Research Letters*, *32*, 4 PP., doi :200510.1029/2005GL023112, 2005.

Arendt, A., S. Luthcke, C. Larsen, W. Abdalati, W. Krabill, and M. Beedle, Validation of high-resolution GRACE mascon estimates of glacier mass changes in the st elias mountains, alaska, USA, using aircraft laser altimetry, *Journal of Glaciology*, *54*(188), 778–787, doi :10.3189/002214308787780067, 2008.

Ashok, W. S. K. B. S. A. Rao, Hengyi, and Y. Toshio, El niño modoki and its possible teleconnection, *Journal of Geophysical Research*, *112*, C11,007, doi :10.1029/2006JC003798, 2007.

Aucan, J., and W. Llovel, Deep water trends and variability at the bats site in the subtropical north atlantic and consequences on local closure of the sea level budget, *Deep Sea Research*, in revision.

Balmaseda, M. A., A. Vidard, and D. L. T. Anderson, The ECMWF ocean analysis system : ORA-S3, *Monthly Weather Review*, *136*(8), 3018–3034, doi :10.1175/2008MWR2433.1, WOS :000258450700011, 2008.

Bard, E., R. Fairbanks, B. Hamelin, A. Zindler, and C. Hoang, U-234 anomalies in corals older than 150,000 years, *Geochimica Et Cosmochimica Acta*, *55*(8), 2385–2390, doi : 10.1016/0016-7037(91)90115-L, WOS :A1991GC43900026, 1991.

Bard, E., B. Hamelin, and D. Delanghe-Sabatier, Deglacial meltwater pulse 1B and younger dryas sea levels revisited with boreholes at tahiti, *Science*, *327*(5970), 1235–1237, doi : 10.1126/science.1180557, WOS :000275162100033, 2010.

Beckley, B. D., N. P. Zelensky, S. A. Holmes, F. G. Lemoine, R. D. Ray, G. T. Mitchum, S. D. Desai, and S. T. Brown, Assessment of the jason-2 extension to the TOPEX/Poseidon, jason-1 Sea-Surface height time series for global mean sea level monitoring, *Marine Geodesy*, *33*(sup1), 447–471, doi :10.1080/01490419.2010.491029, 2010.

Behera, S., and T. Yamagata, Imprint of the el niño modoki on decadal sea level changes, *Geophysical Research Letters*, *37*(23), doi :10.1029/2010GL045936, 2010.

Behera, S. K., J. Luo, and T. Yamagata, Unusual IOD event of 2007, *Geophysical Research Letters*, *35*, 5 PP., doi :200810.1029/2008GL034122, 2008.

Bennett, R., and S. Hreinsdottir, Constraints on vertical crustal motion for long baselines in the central mediterranean region using continuous GPS, *Earth and Planetary Science Letters*, *257*(3-4), 419–434, doi :10.1016/j.epsl.2007.03.008, 2007.

Berge-Nguyen, M., A. Cazenave, A. Lombard, W. Llovel, J. Viarre, and J. Cretaux, Reconstruction of past decades sea level using thermosteric sea level, tide gauge, satellite altimetry and ocean reanalysis data, *Global and Planetary Change*, *62*(1-2), 1–13, doi : 10.1016/j.gloplacha.2007.11.007, 2008.

Bernard, B., G. Madec, T. Penduff, J. Molines, A. Treguier, J. Le Sommer, A. Beckmann, A. Biastoch, C. Boning, J. Dengg, C. Derval, E. Durand, S. Gulev, E. Remy, C. Talandier, S. Theetten, M. Maltrud, J. McClean, and B. De Cuevas, Impact of partial steps and momentum advection schemes in a global ocean circulation model at eddy-permitting resolution, *Ocean Dynamics*, *56*(5), 543–567, doi :10.1007/s10236-006-0082-1, 2006.

Berthier, E., C. Vincent, G. Durand, and G. Krinner, Bilan de masse des glaciers et des calottes polaires., in *Le climat à découvert. Outils et méthodes en recherche climatique*, edited by C. Jeandel and R. Mosseri, CNRS Edition, 2011.

Beuvier, J., F. Sevault, M. Herrmann, H. Kontoyiannis, W. Ludwig, M. Rixen, E. Stanev, K. Beranger, and S. Somot, Modeling the mediterranean sea interannual variability during 1961-2000 : Focus on the eastern mediterranean transient, *Journal of Geophysical Research-Oceans*, *115*, doi :10.1029/2009JC005950, 2010.

Bindoff, N., J. Willebrand, V. Artale, C. A, J. Gregory, S. Gulev, K. Hanawa, C. L. Quéré, S. Levitus, Y. Nojiri, C. Shum, L. Talley, and A. Unnikrishnan, Observations : Oceanic climate change and sea level, in *Climate Change 2007 : The Physical Science Basis. Contribution of Working Group I to the Fourth Assessment Report of the Intergovernmental Panel on Climate Change*, edited by S. Solomon, D. Qin, M. Manning, Z. Chen, M. Marquis, K. Averyt, M. Tignor, and H. Miller, Cambridge University Press, Cambridge, United Kingdom and New York, NY, USA, 2007.

Blum, M. D., and H. H. Roberts, Drowning of the mississippi delta due to insufficient sediment supply and global sea-level rise, *Nature Geoscience*, *2*(7), 488–491, doi :10.1038/ngeo553, WOS :000270061600017, 2009.

Boyer, T., J. Antonov, O. Baranova, H. Garcia, D. Johnson, R. Locarnini, A. Mishonov, D. Seidov, I. Smolyar, and M. Zweng, World ocean database 2009, chapter 1 : Introduction, NOAA Atlas NESDIS 66, Ed. S. Levitus, U.S. Gov. Printing Office, Wash., D.C. , 216 pp., DVD, 2009.

Braitenberg, C., P. Mariani, L. Tunini, B. Grillo, and I. Nagy, Vertical crustal motions from differential tide gauge observations and satellite altimetry in southern italy, *Journal of Geodynamics*, *51*(4), 233–244, doi :10.1016/j.jog.2010.09.003, 2011.

Calafat, F., and D. Gomis, Reconstruction of mediterranean sea level fields for the period 1945-2000, *Global and Planetary Change*, *66*(3-4), 225–234, doi :10.1016/j.gloplacha.2008.12.015, 2009.

Calafat, F., M. Marcos, and D. Gomis, Mass contribution to mediterranean sea level variability for the period 1948-2000, *Global and Planetary Change*, *73*(3-4), 193–201, doi :10.1016/j.gloplacha.2010.06.002, 2010.

Carton, J., B. Giese, and S. Grodsky, Sea level rise and the warming of the oceans in the simple ocean data assimilation (SODA) ocean reanalysis, *Journal of Geophysical Research-Oceans*, *110*(C9), doi :10.1029/2004JC002817, 2005.

Carton, J. A., and B. S. Giese, A reanalysis of ocean climate using simple ocean data assimilation (SODA), *Monthly Weather Review*, *136*(8), 2999–3017, doi :10.1175/2007MWR1978.1, 2008.

Cazenave, A., and W. Llovel, Contemporary sea level rise, *Annual Review of Marine Science*, *2*(1), 145–173, doi :10.1146/annurev-marine-120308-081105, 2010.

Cazenave, A., and F. Remy, Sea level and climate : measurements and causes of changes, *Wiley Interdisciplinary Reviews-Climate Change*, *2*(5), 647–662, doi :10.1002/wcc.139, WOS :000295103400001, 2011.

Cazenave, A., and J. Y. Royer, Chapter 11 applications to marine geophysics, in *Satellite Altimetry and Earth Sciences A Handbook of Techniques and Applications*, vol. 69, edited by L. Fu and A. Cazenave, pp. 407–xxxii, Academic Press, 2001.

Cazenave, A., K. Dominh, S. Guinehut, E. Berthier, W. Llovel, G. Ramillien, M. Ablain, and G. Larnicol, Sea level budget over 2003-2008 : A reevaluation from GRACE space gravimetry, satellite altimetry and argo, *Global and Planetary Change*, *65*(1-2), 83–88, doi :10.1016/j.gloplacha.2008.10.004, 2009.

Chambers, D. P., C. A. Mehlhaff, T. J. Urban, D. Fujii, and R. S. Nerem, Low-frequency variations in global mean sea level : 1950-2000, *Journal of Geophysical Research*, *107*(10.1029), 2002.

Chao, B. F., Y. H. Wu, and Y. S. Li, Impact of artificial reservoir water impoundment on global sea level, *Science*, *320*(5873), 212–214, doi :10.1126/science.1154580, 2008.

Chelton, D., Report of the high-resolution ocean topography science working group meeting, college of Oceanic and Atmospheric Sciences Oregon State University, Corvallis, OR (2001, Oct.) Ref. 2001-4, 2001.

Chen, J., B. Tapley, and C. Wilson, Alaskan mountain glacial melting observed by satellite gravimetry, *Earth and Planetary Science Letters*, *248*(1-2), 368–378, doi :10.1016/j.epsl.2006.05.039, 2006.

Chen, J. L., C. R. Wilson, B. D. Tapley, D. D. Blankenship, and E. R. Ivins, Patagonia icefield melting observed by gravity recovery and climate experiment (GRACE), *Geophysical Research Letters*, *34*, 6 PP., doi :200710.1029/2007GL031871, 2007.

Chen, J. L., C. R. Wilson, D. Blankenship, and B. D. Tapley, Accelerated antarctic ice loss from satellite gravity measurements, *Nature Geoscience*, *2*(12), 859–862, doi :10.1038/ngeo694, 2009.

Chinn, T., S. Winkler, M. J. Salinger, and N. Haakensen, Recent glacier advances in Norway and New Zealand : a comparison of their glaciological and meteorological causes, *Geografiska Annaler : Series A, Physical Geography*, *87*(1), 141–157, doi : 10.1111/j.0435-3676.2005.00249.x, 2005.

Church, J., and N. White, A 20th century acceleration in global sea-level rise, *Geophysical Research Letters*, *33*(1), doi :10.1029/2005GL024826, WOS :000234509300010, 2006.

Church, J., N. White, and J. Arblaster, Significant decadal-scale impact of volcanic eruptions on sea level and ocean heat content, *Nature*, *438*(7064), 74–77, doi :10.1038/nature04237, 2005.

Church, J., N. White, and J. Hunter, Sea-level rise at tropical pacific and indian ocean islands, *Global and Planetary Change*, *53*(3), 155–168, doi :10.1016/j.gloplacha.2006.04.001, 2006.

Church, J. A., and N. J. White, Sea-Level rise from the late 19th to the early 21st century, *Surveys in Geophysics*, *32*(4-5), 585–602, doi :10.1007/s10712-011-9119-1, 2011.

Church, J. A., N. J. White, R. Coleman, K. Lambeck, and J. X. Mitrovica, Estimates of the regional distribution of sea level rise over the 1950-2000 period, *Journal of Climate*, *17*(13), 2609–2625, 2004.

Church, J. A., D. Roemmich, C. M. Domingues, J. K. Willis, N. J. White, J. E. Gilson, D. Stammer, A. Köhl, D. P. Chambers, F. W. Landerer, J. Marotzke, J. M. Gregory, T. Suzuki, A. Cazenave, and P. Le Traon, Ocean temperature and salinity contributions to global and regional Sea-Level change, in *Understanding Sea-Level Rise and Variability*, edited by J. A. Church, P. L. Woodworth, T. Aarup, and W. S. Wilson, pp. 143–176, Wiley-Blackwell, 2010.

Church, J. A., N. J. White, L. F. Konikow, C. M. Domingues, J. G. Cogley, E. Rignot, J. M. Gregory, M. R. v. d. Broeke, A. J. Monaghan, and I. Velicogna, Revisiting the earth's sea-level and energy budgets from 1961 to 2008, *Geophysical Research Letters*, *38*, 8 PP., doi :201110.1029/2011GL048794, 2011.

Cogley, J. G., Geodetic and direct mass-balance measurements : comparison and joint analysis, *Annals of Glaciology*, *50*(50), 96–100, doi :10.3189/172756409787769744, 2009.

Cogley, J. G., A more complete version of the world glacier inventory, *Annals of Glaciology*, *50*(53), 32–38, doi :10.3189/172756410790595859, 2010.

Cogné, J., and E. Humler, Temporal variation of oceanic spreading and crustal production rates during the last 180 my, *Earth and Planetary Science Letters*, *227*(3-4), 427–439, doi :10.1016/j.epsl.2004.09.002, 2004.

Cramer, B. S., J. R. Toggweiler, J. D. Wright, M. E. Katz, and K. G. Miller, Ocean overturning since the late cretaceous : Inferences from a new benthic foraminiferal isotope compilation, *Paleoceanography*, *24*, 14 PP., doi :200910.1029/2008PA001683, 2009.

Cravatte, S., T. Delcroix, D. Zhang, M. McPhaden, and J. Leloup, Observed freshening and warming of the western pacific warm pool, *Climate Dynamics*, *33*(4), 565–589, doi : 10.1007/s00382-009-0526-7, 2009.

Curry, R., B. Dickson, and I. Yashayaev, A change in the freshwater balance of the atlantic ocean over the past four decades, *Nature*, *426*(6968), 826–829, doi :10.1038/nature02206, 2003.

Delworth, T. L., V. Ramaswamy, and G. L. Stenchikov, The impact of aerosols on simulated ocean temperature and heat content in the 20th century, *Geophysical Research Letters*, *32*, 4 PP., doi :200510.1029/2005GL024457, 2005.

Deschamps, P., N. Durand, E. Bard, B. Hamelin, G. Camoin, A. L. Thomas, G. M. Henderson, J. Okuno, and Y. Yokoyama, Ice-sheet collapse and sea-level rise at the bolling warming 14,600 years ago, *Nature*, *483*(7391), 559–564, doi :10.1038/nature10902, WOS :000302006100031, 2012.

Di Lorenzo, E., K. M. Cobb, J. C. Furtado, N. Schneider, B. T. Anderson, A. Bracco, M. A. Alexander, and D. J. Vimont, Central pacific el nino and decadal climate change in the north pacific ocean, *Nature Geoscience*, *advance online publication*, doi :10.1038/ ngeo984, 2010.

Domingues, C. M., J. A. Church, N. J. White, P. J. Gleckler, S. E. Wijffels, P. M. Barker, and J. R. Dunn, Improved estimates of upper-ocean warming and multi-decadal sea-level rise, *Nature*, *453*(7198), 1090–U6, doi :10.1038/nature07080, WOS :000256839900054, 2008.

Douglas, B. C., Global sea level rise, *Journal of Geophysical Research*, *96*(C4), PP. 6981–6992, doi :199110.1029/91JC00064, 1991.

Douglas, B. C., Global sea level acceleration, *Journal of Geophysical Research*, *97*(C8), PP. 12,699–12,706, doi :199210.1029/92JC01133, 1992.

Douglas, B. C., M. S. K. Bruce C. Douglas, and S. P. Leatherman, Chapter 3 sea level change in the era of the recording tide gauge, in *Sea Level Rise History and Consequences*, vol. 75, pp. 37–64, Academic Press, 2001.

Durack, P. J., and S. E. Wijffels, Fifty-Year trends in global ocean salinities and their relationship to Broad-Scale warming, *Journal of Climate*, *23*(16), 4342–4362, doi :10.1175/2010JCLI3377.1, 2010.

Durack, P. J., S. E. Wijffels, and R. J. Matear, Ocean salinities reveal strong global water cycle intensification during 1950 to 2000, *Science*, *336*(6080), 455–458, doi :10.1126/science.1212222, 2012.

Durant, A. J., C. Le Quéré, C. Hope, and A. D. Friend, Economic value of improved quantification in global sources and sinks of carbon dioxide, *Philosophical Transactions of the Royal Society A : Mathematical, Physical and Engineering Sciences*, *369*(1943), 1967–1979, doi :10.1098/rsta.2011.0002, 2011.

Dussin, R., A. Treguier, J. Molines, B. Barnier, T. Penduff, L. Brodeau, and G. Madec, Definition of the interannual experiment orca025-b83, 1958-2007., lPO Report 902, 2009.

Dutton, A., E. Bard, F. Antonioli, T. M. Esat, K. Lambeck, and M. T. McCulloch, Phasing and amplitude of sea-level and climate change during the penultimate interglacial, *Nature Geoscience*, *2*(5), 355–359, doi :10.1038/ngeo470, 2009.

Dyurgerov, M., Reanalysis of glacier changes : From the igy to the ipy, 1960-2008., in *Data of Glaciological Studies*, vol. 108, p. 116, Moscow, 2010.

Ekman, M., Climate changes detected through the world's longest sea level series, *Global and Planetary Change*, *21*(4), 215–224, doi :10.1016/S0921-8181(99)00045-4, WOS :000083394600002, 1999.

Fadil, A., L. Sichoix, J. Barriot, P. Ortega, and P. Willis, Evidence for a slow subsidence of the tahiti island from GPS, DORIS, and combined satellite altimetry and tide gauge sea level records, *Comptes Rendus Geoscience*, *343*(5), 331–341, doi :10.1016/j.crte.2011.02.002, 2011.

Feng, M., Y. Li, and G. Meyers, Multidecadal variations of fremantle sea level : Footprint of climate variability in the tropical pacific, *Geophysical Research Letters*, *31*, 4 PP., doi :200410.1029/2004GL019947, 2004.

Feng, M., M. J. McPhaden, and T. Lee, Decadal variability of the pacific subtropical cells and their influence on the southeast indian ocean, *Geophysical Research Letters*, *37*, 6 PP., doi :201010.1029/2010GL042796, 2010.

Feng, M., C. Boning, A. Biastoch, E. Behrens, E. Weller, and Y. Masumoto, The reversal of the multi-decadal trends of the equatorial pacific easterly winds, and the indonesian throughflow and leeuwin current transports, *Geophysical Research Letters*, *38*, 6 PP., doi :201110.1029/2011GL047291, 2011.

Fenoglio-Marc, L., J. Kusche, and M. Becker, Mass variation in the mediterranean sea from GRACE and its validation by altimetry, steric and hydrologic fields, *Geophysical Research Letters*, *33*, 5 PP., doi :200610.1029/2006GL026851, 2006.

Fenoglio-Marc, L., C. Braitenberg, and L. Tunini, Sea level variability and trends in the adriatic sea in 1993-2008 from tide gauges and satellite altimetry, *Physics and Chemistry of the Earth, Parts A/B/C*, *40-41*, 47–58, doi :10.1016/j.pce.2011.05.014, 2012.

Ferry, N., L. Parent, G. Garric, M. Drévillon, C. Desportes, C. Bricaud, and F. Hernandez, Scientific validation report (scvr) for v1 reprocessed analysis and reanalysis, wP04-GLO-MERCATOR Toulouse, France., 2011.

Friedlingstein, P., R. A. Houghton, G. Marland, J. Hackler, T. A. Boden, T. J. Conway, J. G. Canadell, M. R. Raupach, P. Ciais, and C. Le Quere, Update on CO(2) emissions RID e-9419-2010, *Nature Geoscience*, *3*(12), 811–812, doi :10.1038/ngeo1022, WOS :000284755800002, 2010.

Frihy, O., E. Deabes, S. Shereet, and F. Abdalla, Alexandria-Nile delta coast, egypt : update and future projection of relative sea-level rise, *Environmental Earth Sciences*, *61*(2), 253–273, doi :10.1007/s12665-009-0340-x, 2010.

Fu, L., and A. Cazenave, *Satellite Altimetry and Earth Sciences : A Handbook of Techniques and Applications*, Academic Press, 2001.

Gardelle, J., E. Berthier, and Y. Arnaud, Slight mass gain of karakoram glaciers in the early twenty-first century, *Nature Geoscience*, *5*(5), 322–325, doi :10.1038/ngeo1450, 2012.

Gehrels, W. R., J. R. Kirby, A. Prokoph, R. M. Newnham, E. P. Achterberg, H. Evans, S. Black, and D. B. Scott, Onset of recent rapid sea-level rise in the western atlantic ocean, *Quaternary Science Reviews*, *24*(18-19), 2083–2100, doi :10.1016/j.quascirev.2004.11.016, 2005.

Gehrels, W. R., W. A. Marshall, M. J. Gehrels, G. Larsen, J. R. Kirby, J. Eiriksson, J. Heinemeier, and T. Shimmield, Rapid sea-level rise in the north atlantic ocean since the first half of the nineteenth century RID b-4483-2010, *Holocene*, *16*(7), 949–965, doi :10.1177/0959683606hl986rp, WOS :000242939200003, 2006a.

Gehrels, W. R., K. Szkornik, J. Bartholdy, J. R. Kirby, S. L. Bradley, W. A. Marshall, J. Heinemeier, and J. B. Pedersen, Late holocene sea-level changes and isostasy in western denmark, *Quaternary Research*, *66*(2), 288–302, doi :10.1016/j.yqres.2006.05.004, 2006b.

Gille, S. T., Decadal-Scale temperature trends in the southern hemisphere ocean, *Journal of Climate*, *21*(18), 4749–4765, doi :10.1175/2008JCLI2131.1, 2008.

Gleckler, P. J., T. M. L. Wigley, B. D. Santer, J. M. Gregory, K. AchutaRao, and K. E. Taylor, Volcanoes and climate : Krakatoa's signature persists in the ocean, *Nature*, *439*(7077), 675–675, doi :10.1038/439675a, 2006.

Gleckler, P. J., B. D. Santer, C. M. Domingues, D. W. Pierce, T. P. Barnett, J. A. Church, K. E. Taylor, K. M. AchutaRao, T. P. Boyer, M. Ishii, and P. M. Caldwell, Human-induced global ocean warming on multidecadal timescales, *Nature Climate Change*, doi : 10.1038/nclimate1553, 2012.

Gomez, N., J. Mitrovica, M. Tamisiea, and P. Clark, A new projection of sea level change in response to collapse of marine sectors of the antarctic ice sheet, *Geophysical Journal International*, *180*(2), 623–634, doi :10.1111/j.1365-246X.2009.04419.x, 2010.

Gornitz, V., and S. Lebedeff, Global sea-level changes during the past century, *The Society of Economic Paleontologists and Mineralogists*, *Special Pu*, 3–16, 1987.

Gornitz, V., and A. Solow, Observations of long-term tide-gauge records for indications of accelerated sea level rise, in *Greenhouse-gas-induced climatic change : a critical appraisal of simulations and observations*, edited by M. Schlesinger, pp. 347–367, Elsevier Science Ltd, Amsterdam, 1991.

Gouretski, V., and K. P. Koltermann, How much is the ocean really warming ?, *Geophysical Research Letters*, *34*, 5 PP., doi :200710.1029/2006GL027834, 2007.

Gregory, J. M., H. T. Banks, P. A. Stott, J. A. Lowe, and M. D. Palmer, Simulated and observed decadal variability in ocean heat content, *Geophysical Research Letters*, *31*, 4 PP., doi :200410.1029/2004GL020258, 2004.

Gregory, J. M., J. A. Lowe, and S. F. B. Tett, Simulated Global-Mean sea level changes over the last Half-Millennium, *Journal of Climate*, *19*(18), 4576–4591, doi :10.1175/ JCLI3881.1, 2006.

Grinsted, A., J. Moore, and S. Jevrejeva, Reconstructing sea level from paleo and projected temperatures 200 to 2100 ad, *Climate Dynamics*, *34*(4), 461–472, doi : 10.1007/s00382-008-0507-2, 2010.

Gu, G., and R. F. Adler, Precipitation and temperature variations on the interannual time scale : Assessing the impact of ENSO and volcanic eruptions, *Journal of Climate*, *24*(9), 2258–2270, doi :10.1175/2010JCLI3727.1, 2011.

Guinehut, S., P. Le Traon, G. Larnicol, and S. Philipps, Combining argo and remote-sensing data to estimate the ocean three-dimensional temperature fields : a first approach based on simulated observations, *Journal of Marine Systems*, *46*(1-4), 85–98, doi :10.1016/j. jmarsys.2003.11.022, 2004.

Hamlington, B. D., R. R. Leben, R. S. Nerem, W. Han, and K. Y. Kim, Reconstructing sea level using cyclostationary empirical orthogonal functions, *Journal of Geophysical Research-Oceans*, *116*, doi :10.1029/2011JC007529, WOS :000298252700004, 2011.

Han, W., G. A. Meehl, B. Rajagopalan, J. T. Fasullo, A. Hu, J. Lin, W. G. Large, J.-w. Wang, X. Quan, L. L. Trenary, A. Wallcraft, T. Shinoda, and S. Yeager, Patterns of indian ocean sea-level change in a warming climate, *Nature Geoscience*, *3*(8), 546–550, doi :10.1038/ngeo901, 2010.

Hanawa, K., P. Rual, R. Bailey, A. Sy, and M. Szabados, A new depth-time equation for sippican or TSK t-7, t-6 and t-4 expendable bathythermographs (XBT), *Deep Sea Research Part I : Oceanographic Research Papers*, *42*(8), 1423–1451, doi : 10.1016/0967-0637(95)97154-Z, 1995.

Hanebuth, T., K. Stattegger, and A. Bojanowski, Termination of the last glacial maximum sea-level lowstand : The Sunda-Shelf data revisited, *Global and Planetary Change*, *66*(1-2), 76–84, doi :10.1016/j.gloplacha.2008.03.011, 2009.

Hanna, E., P. Huybrechts, K. Steffen, J. Cappelen, R. Huff, C. Shuman, T. Irvine-Fynn, S. Wise, and M. Griffiths, Increased runoff from melt from the greenland ice sheet : A response to global warming, *Journal of Climate*, *21*(2), 331–341, doi : 10.1175/2007JCLI1964.1, 2008.

Hansen, J., M. Sato, P. Kharecha, and K. von Schuckmann, Earth's energy imbalance and implications, *Atmospheric Chemistry and Physics*, *11*(24), 13,421–13,449, doi :10.5194/acp-11-13421-2011, 2011.

Haq, B. U., and A. M. Al-Qahtani, Phanerozoic cycles of sea-level change on the arabian platform, *Geoarabia*, *10*(2), 127–160, WOS :000231694200005, 2005.

Haq, B. U., and S. R. Schutter, A chronology of paleozoic sea-level changes, *Science*, *322*(5898), 64–68, doi :10.1126/science.1161648, WOS :000259680200036, 2008.

Hasselmann, K., Stochastic climate models part I. theory, *Tellus*, *28*(6), 473–485, doi : 10.1111/j.2153-3490.1976.tb00696.x, 2010.

Hegerl, G., F. W. Zwiers, P. Braconnot, N. Gillett, Y. Luo, J. M. Orsini, N. Nichols, J. Penner, and P. Stott, Understanding and attributing climate change, in *Climate Change 2007 : The Physical Science Basis. Contribution of Working Group I to the Fourth Assessment Report of the Intergovernmental Panel on Climate Change*, edited by S. Solomon, D. Qin, M. Manning, Z. Chen, M. Marquis, K. Averyt, M. Tignor, and H. Miller, Cambridge University Press, Cambridge, United Kingdom and New York, NY, USA, 2007.

Herrmann, M., F. Sevault, J. Beuvier, and S. Somot, What induced the exceptional 2005 convection event in the northwestern mediterranean basin ? answers from a modeling study, *Journal of Geophysical Research-Oceans*, *115*, doi :10.1029/2010JC006162, 2010.

Hogg, A. M. C., W. K. Dewar, P. Berloff, S. Kravtsov, and D. K. Hutchinson, The effects of mesoscale Ocean-Atmosphere coupling on the Large-Scale ocean circulation, *Journal of Climate*, *22*(15), 4066–4082, doi :10.1175/2009JCLI2629.1, 2009.

Holgate, S. J., On the decadal rates of sea level change during the twentieth century, *Geophysical Research Letters*, *34*, 4 PP., doi :200710.1029/2006GL028492, 2007.

Holland, D. M., R. H. Thomas, B. d. Young, M. H. Ribergaard, and B. Lyberth, Acceleration of jakobshavn isbrae triggered by warm subsurface ocean waters, *Nature Geoscience*, *1*(10), 659–664, doi :10.1038/ngeo316, 2008.

Horton, R., C. Herweijer, C. Rosenzweig, J. Liu, V. Gornitz, and A. C. Ruane, Sea level rise projections for current generation CGCMs based on the semi-empirical method, *Geophysical Research Letters*, *35*, 5 PP., doi :200810.1029/2007GL032486, 2008.

Hosoda, S., T. Suga, N. Shikama, and K. Mizuno, Global surface layer salinity change detected by argo and its implication for hydrological cycle intensification, *Journal of Oceanography*, *65*(4), 579–586, doi :10.1007/s10872-009-0049-1, 2009.

Houghton, J., G. Jenkins, and J. Ephraums (Eds.), *Report prepared for Intergovernmental Panel on Climate Change by Working Group I*, Cambridge University Press, Cambridge, United Kingdom and New York, NY, USA, 1990.

Houghton, J., Y. Ding, D. Griggs, M. Noguer, P. van der Linden, X. Dai, K. Maskell, and C. Johnson (Eds.), *Contribution of Working Group I to the Third Assessment Report of the Intergovernmental Panel on Climate Change, 2001*, Cambridge University Press, Cambridge, United Kingdom and New York, NY, USA, 2001.

Hunter, J., R. Coleman, and D. Pugh, The sea level at port arthur, tasmania, from 1841 to the present, *Geophysical Research Letters*, *30*, 4 PP., doi :200310.1029/2002GL016813, 2003.

Huntington, T. G., Evidence for intensification of the global water cycle : Review and synthesis, *Journal of Hydrology*, *319*(1-4), 83–95, 2006.

Huss, M., and A. Bauder, 20th-century climate change inferred from four long-term point observations of seasonal mass balance, *Annals of Glaciology*, *50*(50), 207–214, doi :10.3189/172756409787769645, 2009.

Huss, M., R. Hock, A. Bauder, and M. Funk, 100-year mass changes in the swiss alps linked to the atlantic multidecadal oscillation, *Geophysical Research Letters*, *37*, 5 PP., doi :201010.1029/2010GL042616, 2010.

Ingleby, B., and M. Huddleston, Quality control of ocean temperature and salinity profiles : Historical and real-time data, *Journal of Marine Systems*, *65*(1-4), 158–175, doi :10.1016/j.jmarsys.2005.11.019, 2007.

Ishii, M., and M. Kimoto, Reevaluation of historical ocean heat content variations with time-varying XBT and MBT depth bias corrections, *Journal of Oceanography*, *65*(3), 287–299, doi :10.1007/s10872-009-0027-7, 2009.

Ishii, M., M. Kimoto, K. Sakamoto, and S. Iwasaki, Steric sea level changes estimated from historical ocean subsurface temperature and salinity analyses, *Journal of Oceanography*, *62*(2), 155–170, doi :10.1007/s10872-006-0041-y, 2006.

Jacob, T., J. Wahr, W. T. Pfeffer, and S. Swenson, Recent contributions of glaciers and ice caps to sea level rise, *Nature*, *482*(7386), 514–518, doi :10.1038/nature10847, 2012.

Jevrejeva, S., A. Grinsted, J. C. Moore, and S. Holgate, Nonlinear trends and multiyear cycles in sea level records, *Journal of Geophysical Research*, *111*, 11 PP., doi :200610. 1029/2005JC003229, 2006.

Jevrejeva, S., J. C. Moore, A. Grinsted, and P. L. Woodworth, Recent global sea level acceleration started over 200 years ago ?, *Geophysical Research Letters*, *35*, 4 PP., doi : 200810.1029/2008GL033611, 2008.

Jevrejeva, S., A. Grinsted, and J. C. Moore, Anthropogenic forcing dominates sea level rise since 1850, *Geophysical Research Letters*, *36*, 5 PP., doi :200910.1029/2009GL040216, 2009.

Jevrejeva, S., J. C. Moore, and A. Grinsted, How will sea level respond to changes in natural and anthropogenic forcings by 2100 ?, *Geophysical Research Letters*, *37*, doi : 10.1029/2010GL042947, WOS :000276314800003, 2010.

Jevrejeva, S., J. Moore, and A. Grinsted, Sea level projections to AD2500 with a new generation of climate change scenarios, *Global and Planetary Change*, *80-81*(0), 14–20, doi :10.1016/j.gloplacha.2011.09.006, 2012.

Johnson, G. C., Quantifying antarctic bottom water and north atlantic deep water volumes, *Journal of Geophysical Research*, *113*, 13 PP., doi :200810.1029/2007JC004477, 2008.

Josey, S. A., Changes in the heat and freshwater forcing of the eastern mediterranean and their influence on deep water formation, *Journal of Geophysical Research*, *108*(C7), 3237, doi :10.1029/2003JC001778, 2003.

Kaplan, A., M. Cane, Y. Kushnir, A. Clement, M. Blumenthal, and B. Rajagopalan, Analyses of global sea surface temperature 1856-1991, *Journal of Geophysical Research-Oceans*, *103*(C9), 18,567–18,589, 1998.

Kaplan, A., Y. Kushnir, and M. A. Cane, Reduced space optimal interpolation of historical marine sea level pressure : 1854-1992, *Journal of Climate*, *13*(16), 2987–3002, 2000.

Kaser, G., J. G. Cogley, M. B. Dyurgerov, M. F. Meier, and A. Ohmura, Mass balance of glaciers and ice caps : Consensus estimates for 1961-2004, *Geophysical Research Letters*, *33*, 5 PP., doi :200610.1029/2006GL027511, 2006.

Kay, J. E., M. M. Holland, and A. Jahn, Inter-annual to multi-decadal arctic sea ice extent trends in a warming world, *Geophysical Research Letters*, *38*, 6 PP., doi :201110.1029/ 2011GL048008, 2011.

Kemp, A. C., B. P. Horton, J. P. Donnelly, M. E. Mann, M. Vermeer, and S. Rahmstorf, Climate related sea-level variations over the past two millennia RID a-8465-2010, *Proceedings of the National Academy of Sciences of the United States of America*, *108*(27), 11,017–11,022, doi :10.1073/pnas.1015619108, WOS :000292376700025, 2011.

Kominz, M. A., J. V. Browning, K. G. Miller, P. J. Sugarman, S. Mizintseva, and C. R. Scotese, Late cretaceous to miocene sea-level estimates from the new jersey and delaware coastal plain coreholes : an error analysis, *Basin Research*, *20*(2), 211–226, doi :10.1111/ j.1365-2117.2008.00354.x, WOS :000256236100004, 2008.

Konikow, L. F., Contribution of global groundwater depletion since 1900 to sea-level rise, *Geophysical Research Letters*, *38*, 5 PP., doi :201110.1029/2011GL048604, 2011.

Kontogianni, V. A., N. Tsoulos, and S. C. Stiros, Coastal uplift, earthquakes and active faulting of rhodes island (Aegean arc) : modeling based on geodetic inversion, *Marine Geology*, *186*(3-4), 299–317, doi :10.1016/S0025-3227(02)00334-1, 2002.

Kopp, R. E., J. X. Mitrovica, S. M. Griffies, J. Yin, C. C. Hay, and R. J. Stouffer, The impact of greenland melt on local sea levels : a partially coupled analysis of dynamic and static equilibrium effects in idealized water-hosing experiments, *Climatic Change*, *103*(3-4), 619–625, doi :10.1007/s10584-010-9935-1, 2010.

Köhl, A., and D. Stammer, Decadal sea level changes in the 50-Year GECCO ocean synthesis, *Journal of Climate*, *21*(9), 1876–1890, doi :10.1175/2007JCLI2081.1, 2008.

Köhl, A., D. Stammer, and B. Cornuelle, Interannual to decadal changes in the ECCO global synthesis, *Journal of Physical Oceanography*, *37*(2), 313–337, doi :10.1175/JPO3014.1, 2007.

Lambeck, K., T. Esat, and E. Potter, Links between climate and sea levels for the past three million years, *Nature*, *419*(6903), 199–206, doi :10.1038/nature01089, WOS :000177931200049, 2002.

Lambeck, K., M. Anzidei, F. Antonioli, A. Benini, and A. Esposito, Sea level in roman time in the central mediterranean and implications for recent change, *Earth and Planetary Science Letters*, *224*(3-4), 563–575, doi :10.1016/j.espal.2004.05.031, WOS :000223582400024, 2004.

Lambeck, K., C. D. Woodroffe, F. Antonioli, M. Anzidei, W. R. Gehrels, J. Laborel, and A. J. Wright, Paleoenvironmental records, geophysical modeling, and reconstruction of Sea-Level trends and variability on centennial and longer timescales, in *Understanding Sea-Level Rise and Variability*, edited by J. A. Church, P. L. Woodworth, T. Aarup, and W. S. Wilson, pp. 61–121, Wiley-Blackwell, 2010.

Lee, T., and M. J. McPhaden, Decadal phase change in large-scale sea level and winds in the Indo-Pacific region at the end of the 20th century, *Geophysical Research Letters*, *35*, 7 PP., doi :200810.1029/2007GL032419, 2008.

Leorri, E., W. R. Gehrels, B. P. Horton, F. Fatela, and A. Cearreta, Distribution of foraminifera in salt marshes along the atlantic coast of SW europe : Tools to reconstruct past sea-level variations, *Quaternary International*, *221*(1-2), 104–115, doi : 10.1016/j.quaint.2009.10.033, 2010.

Leuliette, E. W., and L. Miller, Closing the sea level rise budget with altimetry, argo, and GRACE, *Geophysical Research Letters*, *36*, 5 PP., doi :200910.1029/2008GL036010, 2009.

Levitus, S., Interannual variability of temperature at a depth of 125 meters in the north atlantic ocean, *Science*, *266*(5182), 96, 1994.

Levitus, S., J. I. Antonov, J. Wang, T. L. Delworth, K. W. Dixon, and A. J. Broccoli, Anthropogenic warming of earth's climate system, *Science*, *292*(5515), 267–270, doi : 10.1126/science.1058154, 2001.

Levitus, S., J. Antonov, and T. Boyer, Warming of the world ocean, 1955-2003, *Geophysical Research Letters*, *32*, 4 PP., doi :200510.1029/2004GL021592, 2005.

Levitus, S., J. I. Antonov, T. P. Boyer, R. A. Locarnini, H. E. Garcia, and A. V. Mishonov, Global ocean heat content 1955-2008 in light of recently revealed instrumentation problems, *Geophysical Research Letters*, *36*, 5 PP., doi :200910.1029/2008GL037155, 2009.

Levitus, S., J. I. Antonov, T. P. Boyer, O. K. Baranova, H. E. Garcia, R. A. Locarnini, A. V. Mishonov, J. R. Reagan, D. Seidov, E. S. Yarosh, and M. M. Zweng, World ocean heat content and thermosteric sea level change (0-2000 m), 1955-2010, *Geophysical Research Letters*, *39*, 5 PP., doi :201210.1029/2012GL051106, 2012.

Llovel, W., A. Cazenave, P. Rogel, A. Lombard, and M. Nguyen, Two-dimensional reconstruction of past sea level (1950-2003) from tide gauge data and an ocean general circulation model, *Climate of the Past*, *5*(2), 217–227, 2009.

Llovel, W., M. Becker, A. Cazenave, J. CrÃ©taux, and G. Ramillien, Global land water storage change from GRACE over 2002-2009 ; inference on sea level, *Comptes Rendus Geoscience*, *342*(3), 179–188, doi :10.1016/j.crte.2009.12.004, 2010a.

Llovel, W., S. Guinehut, and A. Cazenave, Regional and interannual variability in sea level over 2002-2009 based on satellite altimetry, argo float data and GRACE ocean mass, *Ocean Dynamics*, *60*(5), 1193–1204, doi :10.1007/s10236-010-0324-0, 2010b.

Llovel, W., M. Becker, A. Cazenave, S. Jevrejeva, R. Alkama, B. Decharme, H. Douville, M. Ablain, and B. Beckley, Terrestrial waters and sea level variations on interannual time scale, *Global and Planetary Change*, *75*(1-2), 76–82, doi :10.1016/j.gloplacha.2010.10.008, 2011a.

Llovel, W., B. Meyssignac, and A. Cazenave, Steric sea level variations over 2004-2010 as a function of region and depth : Inference on the mass component variability in the north atlantic ocean, *Geophysical Research Letters*, *38*, 6 PP., doi :201110.1029/2011GL047411, 2011b.

Lombard, A., A. Cazenave, K. DoMinh, C. Cabanes, and R. S. Nerem, Thermosteric sea level rise for the past 50 years ; comparison with tide gauges and inference on water mass contribution, *Global and Planetary Change*, *48*(4), 303–312, doi :10.1016/j.gloplacha.2005.02.007, 2005a.

Lombard, A., A. Cazenave, P. Le Traon, and M. Ishii, Contribution of thermal expansion to present-day sea-level change revisited, *Global and Planetary Change*, *47*(1), 1–16, doi :10.1016/j.gloplacha.2004.11.016, 2005b.

Lombard, A., G. Garric, and T. Penduff, Regional patterns of observed sea level change : insights from a 1/4 degrees global ocean/sea-ice hindcast, *Ocean Dynamics*, *59*(3), 433–449, doi :10.1007/s10236-008-0161-6, WOS :000266392100002, 2009.

Lozier, M., V. Roussenov, M. Reed, and R. Williams, Opposing decadal changes for the north atlantic meridional overturning circulation (vol 3, pg 728, 2010), *Nature Geoscience*, *3*(11), 805–805, doi :10.1038/ngeo1010, 2010.

Luthcke, S. B., A. A. Arendt, D. D. Rowlands, J. J. McCarthy, and C. F. Larsen, Recent glacier mass changes in the gulf of alaska region from GRACE mascon solutions, *Journal of Glaciology*, *54*(188), 767–777, doi :10.3189/002214308787779933, 2008.

Lyman, J. M., S. A. Good, V. V. Gouretski, M. Ishii, G. C. Johnson, M. D. Palmer, D. M. Smith, and J. K. Willis, Robust warming of the global upper ocean, *Nature*, *465*(7296), 334–337, doi :10.1038/nature09043, 2010.

Madec, G., Nemo ocean engine, note du pôle de modélisation de l'IPSL n° 27, ISSN :1288-1619., 2008.

Malanotte-Rizzoli, P., B. B. Manca, M. R. d'Alcala, A. Theocharis, S. Brenner, G. Budillon, and E. Ozsoy, The eastern mediterranean in the 80s and in the 90s : the big transition in the intermediate and deep circulations, *Dynamics of Atmospheres and Oceans*, *29*(2-4), 365–395, doi :10.1016/S0377-0265(99)00011-1, 1999.

Marcos, M., and M. Tsimplis, Variations of the seasonal sea level cycle in southern europe, *Journal of Geophysical Research-Oceans*, *112*(C12), doi :10.1029/2006JC004049, 2007.

Marcos, M., and M. Tsimplis, Coastal sea level trends in southern europe, *Geophysical Journal International*, *175*(1), 70–82, doi :10.1111/j.1365-246X.2008.03892.x, 2008.

Mariotti, A., M. V. Struglia, N. Zeng, and K. Lau, The hydrological cycle in the mediterranean region and implications for the water budget of the mediterranean sea, *Journal of Climate*, *15*(13), 1674–1690, doi :10.1175/1520-0442(2002)015⟨1674:THCITM⟩2.0.CO;2, 2002.

Masters, D., R. S. Nerem, C. Choe, E. Leuliette, B. Beckley, N. White, and M. Ablain, Comparison of global mean sea level time series from topex/poseidon, jason-1, and jason-2, *Marine Geodesy*, in press.

McPhee, M. G., A. Proshutinsky, J. H. Morison, M. Steele, and M. B. Alkire, Rapid change in freshwater content of the arctic ocean, *Geophysical Research Letters*, *36*, 6 PP., doi : 200910.1029/2009GL037525, 2009.

Meier, M. F., M. B. Dyurgerov, U. K. Rick, S. O'Neel, W. T. Pfeffer, R. S. Anderson, S. P. Anderson, and A. F. Glazovsky, Glaciers dominate eustatic Sea-Level rise in the 21st century, *Science*, *317*(5841), 1064–1067, doi :10.1126/science.1143906, 2007.

Meltzner, A. J., K. Sieh, M. Abrams, D. C. Agnew, K. W. Hudnut, J. Avouac, and D. H. Natawidjaja, Uplift and subsidence associated with the great Aceh-Andaman earthquake of 2004, *Journal of Geophysical Research*, *111*, 8 PP., doi :200610.1029/2005JB003891, 2006.

Mernild, S. H., G. E. Liston, C. A. Hiemstra, K. Steffen, E. Hanna, and J. H. Christensen, Greenland ice sheet surface mass-balance modelling and freshwater flux for 2007, and in a 1995-2007 perspective, *Hydrological Processes*, *23*(17), 2470–2484, doi :10.1002/hyp.7354, 2009.

Merrifield, M., and P. Thompson, Multidecadal sea level heights and trends in the western tropical pacific, *Journal of Climate*, in revision.

Merrifield, M. A., A shift in western tropical pacific sea level trends during the 1990s, *Journal of Climate*, *24*(15), 4126–4138, doi :10.1175/2011JCLI3932.1, 2011.

Merrifield, M. A., and M. E. Maltrud, Regional sea level trends due to a pacific trade wind intensification, *Geophysical Research Letters*, *38*, 5 PP., doi :201110.1029/2011GL049576, 2011.

Merrifield, M. A., S. T. Merrifield, and G. T. Mitchum, An anomalous recent acceleration of global sea level rise, *Journal of Climate*, *22*(21), 5772–5781, doi :10.1175/2009JCLI2985.1, 2009.

Meyssignac, B., and A. Cazenave, Sea level : A review of present-day and recent-past changes and variability, *Journal of Geodynamics*, *58*(0), 96–109, doi :10.1016/j.jog.2012.03.005, 2012.

Meyssignac, B., F. Calafat, S. Somot, V. Rupolo, P. Stocchi, W. Llovel, and A. Cazenave, Two-dimensional reconstruction of the mediterranean sea level over 1970-2006 from tide gage data and regional ocean circulation model outputs, *Global and Planetary Change*, *77*(1-2), 49–61, doi :10.1016/j.gloplacha.2011.03.002, 2011.

Meyssignac, B., M. Becker, W. Llovel, and A. Cazenave, An assessment of Two-Dimensional past sea level reconstructions over 1950-2009 based on Tide-Gauge data and different input sea level grids, *Surveys in Geophysics*, pp. 1–28, doi :10.1007/s10712-011-9171-x, 2012.

Miller, K. G., M. A. Kominz, J. V. Browning, J. D. Wright, G. S. Mountain, M. E. Katz, P. J. Sugarman, B. S. Cramer, N. Christie-Blick, and S. F. Pekar, The phanerozoic record of global Sea-Level change, *Science*, *310*(5752), 1293–1298, doi :10.1126/science.1116412, 2005.

Miller, K. G., P. J. Sugarman, J. V. Browning, B. P. Horton, A. Stanley, A. Kahn, J. Uptegrove, and M. Aucott, Sea-level rise in new jersey over the past 5000 years : Implications to anthropogenic changes, *Global and Planetary Change*, *66*(1-2), 10–18, doi : 10.1016/j.gloplacha.2008.03.008, 2009.

Miller, K. G., G. S. Mountain, J. D. Wright, and J. V. Browning, A 180-Million-Year record of sea level and ice volume variations from continental margin and Deep-Sea isotopic records, *Oceanography*, *24*(2), 40–53, WOS :000292348000008, 2011.

Milly, P. C. D., A. Cazenave, and C. Gennero, Contribution of climate-driven change in continental water storage to recent sea-level rise, *Proceedings of the National Academy of Sciences*, *100*(23), 13,158–13,161, 2003.

Milly, P. C. D. C., A. Cazenave, J. S. Famiglietti, V. Gornitz, K. Laval, D. P. Lettenmaier, D. L. Sahagian, J. M. Wahr, and C. R. Wilson, Terrestrial Water-Storage contributions to Sea-Level rise and variability, in *Understanding Sea-Level Rise and Variability*, edited by J. A. Church, P. L. Woodworth, T. Aarup, and W. S. Wilson, pp. 226–255, Wiley-Blackwell, 2010.

Milne, G., and J. Mitrovica, Searching for eustasy in deglacial sea-level histories, *Quaternary Science Reviews*, *27*(25-26), 2292–2302, doi :10.1016/j.quascirev.2008.08.018, 2008.

Milne, G. A., W. R. Gehrels, C. W. Hughes, and M. E. Tamisiea, Identifying the causes of sea-level change, *Nature Geoscience*, *2*(7), 471–478, doi :10.1038/ngeo544, 2009.

Mimura, N., L. Nurse, R. McLean, J. Agard, L. Briguglio, P. Lefale, R. Payet, and G. Sem, Small islands, in *Climate Change 2007 : Impacts, Adaptation and Vulnerability. Contribution of Working Group II to the Fourth Assessment Report of the Intergovernmental Panel on Climate Change*, edited by M. Parry, O. Canziani, J. Palutikof, P. van der Linden, and C. Hanson, Cambridge University Press, Cambridge, United Kingdom and New York, NY, USA, 2007.

Mitchum, G. T., R. S. Nerem, M. A. Merrifield, and W. R. Gehrels, Modern sea level change estimates, in *Understanding Sea-Level Rise and Variability*, edited by J. A. Church, P. L. Woodworth, T. Aarup, and W. S. Wilson, pp. 122–142, Wiley-Blackwell, 2010.

Mitrovica, J., M. Tamisiea, J. Davis, and G. Milne, Recent mass balance of polar ice sheets inferred from patterns of global sea-level change, *Nature*, *409*(6823), 1026–1029, 2001.

Mitrovica, J., N. Gomez, and P. Clark, The Sea-Level fingerprint of west antarctic collapse, *Science*, *323*(5915), 753–753, doi :10.1126/science.1166510, 2009.

Molg, T., and G. Kaser, A new approach to resolving climate-cryosphere relations : Downscaling climate dynamics to glacier-scale mass and energy balance without statistical scale linking, *Journal of Geophysical Research*, *116*, 13 PP., doi :201110.1029/2011JD015669, 2011.

Morrow, R., M. L. Ward, A. M. Hogg, and S. Pasquet, Eddy response to southern ocean climate modes, *Journal of Geophysical Research*, *115*, 12 PP., doi :201010.1029/2009JC005894, 2010.

Moss, R. H., J. A. Edmonds, K. A. Hibbard, M. R. Manning, S. K. Rose, D. P. van Vuuren, T. R. Carter, S. Emori, M. Kainuma, T. Kram, G. A. Meehl, J. F. B. Mitchell, N. Nakicenovic, K. Riahi, S. J. Smith, R. J. Stouffer, A. M. Thomson, J. P. Weyant, and T. J. Wilbanks, The next generation of scenarios for climate change research and assessment, *Nature*, *463*(7282), 747–756, doi :10.1038/nature08823, WOS :000274394300028, 2010.

Moucha, R., A. M. Forte, J. X. Mitrovica, D. B. Rowley, S. Quéré, N. A. Simmons, and S. P. Grand, Dynamic topography and long-term sea-level variations : There is no such thing as a stable continental platform, *Earth and Planetary Science Letters*, *271*(1-4), 101–108, doi :10.1016/j.epsl.2008.03.056, 2008.

Munk, W., Ocean freshening, sea level rising, *Science*, *300*(5628), 2041–2043, doi :10.1126/science.1085534, 2003.

Müller, R. D., M. Sdrolias, C. Gaina, B. Steinberger, and C. Heine, Long-Term Sea-Level fluctuations driven by ocean basin dynamics, *Science*, *319*(5868), 1357–1362, doi :10.1126/science.1151540, 2008.

Nerem, R. S., D. P. Chambers, C. Choe, and G. T. Mitchum, Estimating mean sea level change from the TOPEX and jason altimeter missions, *Marine Geodesy*, *33*(sup1), 435–446, doi :10.1080/01490419.2010.491031, 2010.

Ngo-Duc, K. Laval, J. Polcher, A. Lombard, and A. Cazenave, Effects of land water storage on global mean sea level over the past half century, *Geophysical Research Letters*, *32*(9), 9704, doi :10.1029/2005GL022719, 2005.

Nicholls, R., and A. Cazenave, Sea-level rise and its impact on coastal zones (June, pg 1517, 2007), *Science*, *329*(5992), 628–628, 2010.

Nicholls, R., and F. Hoozemans, The mediterranean : vulnerability to coastal implications of climate change, *Ocean & Coastal Management*, *31*(2-3), 105–132, doi : 10.1016/S0964-5691(96)00037-3, 1996.

Nicholls, R., P. Wong, V. Burkett, J. Codignotto, J. Hay, R. McLean, S. Ragoonaden, and C. Woodroffe, Coastal systems and low-lying areas, in *Climate Change 2007 : Impacts, Adaptation and Vulnerability. Contribution of Working Group II to the Fourth Assessment Report of the Intergovernmental Panel on Climate Change*, edited by M. Parry, O. Canziani, J. Palutikof, P. van der Linden, and C. Hanson, Cambridge University Press, Cambridge, United Kingdom and New York, NY, USA, 2007.

Nicholls, R. J., Impacts of and responses to Sea-Level rise, in *Understanding Sea-Level Rise and Variability*, edited by J. A. Church, P. L. Woodworth, T. Aarup, and W. S. Wilson, pp. 17–51, Wiley-Blackwell, 2010.

Nicholls, R. J., S. Hanson, C. Herweijer, N. Patmore, S. Hallegatte, J. Corfee-Morlot, J. Chateau, and R. Muir-Wood, Ranking port cities with high exposure and vulnerability to climate extremes : Exposure estimates, OECD Environment Working Papers, No. 1, OECD Publishing. http ://dx.doi.org/10.1787/011766488208, 2008.

Oerlemans, J., Extracting a climate signal from 169 glacier records, *Science*, *308*(5722), 675–677, doi :10.1126/science.1107046, 2005.

Okumura, Y. M., C. Deser, A. Hu, A. Timmermann, and S. Xie, North pacific climate response to freshwater forcing in the subarctic north atlantic : Oceanic and atmospheric pathways, *Journal of Climate*, *22*(6), 1424–1445, doi :10.1175/2008JCLI2511.1, 2009.

Overland, J. E., K. R. Wood, and M. Wang, Warm arctic-cold continents : climate impacts of the newly open arctic sea, *Polar Research*, *30*(0), doi :10.3402/polar.v30i0.15787, 2011.

Palmer, M. D., S. A. Good, K. Haines, N. A. Rayner, and P. A. Stott, A new perspective on warming of the global oceans, *Geophysical Research Letters*, *36*, 5 PP., doi :200910. 1029/2009GL039491, 2009.

Pardaens, A., J. Gregory, and J. Lowe, A model study of factors influencing projected changes in regional sea level over the twenty-first century, *Climate Dynamics*, *36*(9), 2015–2033, doi :10.1007/s00382-009-0738-x, 2011.

Parry, M., O. Canziani, J. Palutikof, P. van der Linden, and C. Hanson (Eds.), *Contribution of Working Group II to the Fourth Assessment Report of the Intergovernmental Panel on Climate Change, 2007*, Cambridge University Press, Cambridge, United Kingdom and New York, NY, USA, 2007.

Peltier, W., M. S. K. Bruce C. Douglas, and S. P. Leatherman, Chapter 4 global glacial isostatic adjustment and modern instrumental records of relative sea level history, in *Sea Level Rise History and Consequences*, vol. 75, pp. 65–95, Academic Press, 2001.

Peltier, W. R., Global glacial isostasy and the surface of the ice-age earth : The ice-5G (VM2) model and grace, *Annual Review of Earth and Planetary Sciences*, *32*, 111–149, doi :10.1146/annurev.earth.32.082503.144359, WOS :000221752500007, 2004.

Penduff, T., M. Juza, L. Brodeau, G. C. Smith, B. Barnier, J. Molines, A. Treguier, and G. Madec, Impact of global ocean model resolution on sea-level variability with emphasis on interannual time scales, *Ocean Science*, *6*(1), 269–284, doi :10.5194/os-6-269-2010, 2010.

Pfeffer, W. T., J. T. Harper, and S. O'Neel, Kinematic constraints on glacier contributions to 21st-Century Sea-Level rise, *Science*, *321*(5894), 1340–1343, doi :10.1126/science.1159099, 2008.

Piecuch, C. G., and R. M. Ponte, Buoyancy-driven interannual sea level changes in the southeast tropical pacific, *Geophysical Research Letters*, *39*, 5 PP., doi :201210.1029/2012GL051130, 2012.

Pirazzoli, P., Tectonic shorelines, in *Coastal Evolution : Late Quaternary Shoreline Morphodynamics*, edited by R. Carter and C. Woodroffe, pp. 451–476, Cambridge University Press, Cambridge, United Kingdom and New York, NY, USA, 1995.

Pitman, W., and X. Golovchenko, The effect of sea level change on the shelf edge and slope of passive margins, in *The Shelfbreak : Critical Interface and Continental Margins*, edited by D. Stanley and G. Moore, pp. 41–58, Society of Economic Paleontologists and Mineralogists, 1983.

Pokhrel, Y. N., N. Hanasaki, P. J. Yeh, T. J. Yamada, S. Kanae, and T. Oki, Model estimates of sea-level change due to anthropogenic impacts on terrestrial water storage, *Nature Geoscience*, *5*(6), 389–392, doi :10.1038/ngeo1476, 2012.

Polyakov, I. V., J. E. Walsh, and R. Kwok, Recent changes of arctic multiyear sea ice coverage and the likely causes, *Bulletin of the American Meteorological Society*, *93*(2), 145–151, doi :10.1175/BAMS-D-11-00070.1, 2012.

Prandi, P., A. Cazenave, and M. Becker, Is coastal mean sea level rising faster than the global mean ? a comparison between tide gauges and satellite altimetry over 1993-2007, *Geophysical Research Letters*, *36*, 5 PP., doi :200910.1029/2008GL036564, 2009.

Prandi, P., M. Ablain, A. Cazenave, and N. Picot, A new estimation of mean sea level in the arctic ocean from satellite altimetry, *Marine Geodesy*, in press.

Pritchard, H. D., S. R. M. Ligtenberg, H. A. Fricker, D. G. Vaughan, M. R. v. d. Broeke, and L. Padman, Antarctic ice-sheet loss driven by basal melting of ice shelves, *Nature*, *484*(7395), 502–505, doi :10.1038/nature10968, 2012.

Purkey, S. G., and G. C. Johnson, Warming of global abyssal and deep southern ocean waters between the 1990s and 2000s : Contributions to global heat and sea level rise budgets, *Journal of Climate*, *23*(23), 6336–6351, doi :10.1175/2010JCLI3682.1, 2010.

Radic, V., and R. Hock, Regional and global volumes of glaciers derived from statistical upscaling of glacier inventory data, *Journal of Geophysical Research*, *115*, 10 PP., doi : 201010.1029/2009JF001373, 2010.

Rahmstorf, S., M. Perrette, and M. Vermeer, Testing the robustness of semi-empirical sea level projections, *Climate Dynamics*, doi :10.1007/s00382-011-1226-7, 2011.

Ramillien, G., S. Bouhours, A. Lombard, A. Cazenave, F. Flechtner, and R. Schmidt, Land water storage contribution to sea level from GRACE geoid data over 2003-2006, *Global and Planetary Change*, *60*(3-4), 381–392, doi :10.1016/j.gloplacha.2007.04.002, 2008.

Ray, R. D., and B. C. Douglas, Experiments in reconstructing twentieth-century sea levels, *Progress In Oceanography*, *91*(4), 496–515, doi :10.1016/j.pocean.2011.07.021, 2011.

Raymo, M. E., and J. X. Mitrovica, Collapse of polar ice sheets during the stage 11 interglacial, *Nature*, *483*(7390), 453–456, doi :10.1038/nature10891, WOS :000301771200040, 2012.

Reichert, B. K., L. Bengtsson, and J. Oerlemans, Recent glacier retreat exceeds internal variability, *Journal of Climate*, *15*(21), 3069–3081, doi :10.1175/1520-0442(2002)015⟨3069:RGREIV⟩2.0.CO;2, 2002.

Rignot, E., J. L. Bamber, M. R. v. d. Broeke, C. Davis, Y. Li, W. J. v. d. Berg, and E. v. Meijgaard, Recent antarctic ice mass loss from radar-interferometry and regional climate-modelling, *Nature Geoscience*, *1*(2), 106–110, doi :10.1038/ngeo102, 2008a.

Rignot, E., J. E. Box, E. Burgess, and E. Hanna, Mass balance of the greenland ice sheet from 1958 to 2007, *Geophysical Research Letters*, *35*, 5 PP., doi :200810.1029/2008GL035417, 2008b.

Rignot, E., I. Velicogna, M. R. v. d. Broeke, A. Monaghan, and J. Lenaerts, Acceleration of the contribution of the greenland and antarctic ice sheets to sea level rise, *Geophysical Research Letters*, *38*, 5 PP., doi :201110.1029/2011GL046583, 2011.

Rixen, M., J. Beckers, S. Levitus, J. Antonov, T. Boyer, C. Maillard, M. Fichaut, E. Balopoulos, S. Iona, H. Dooley, M. Garcia, B. Manca, A. Giorgetti, G. Manzella, N. Mikhailov, N. Pinardi, and M. Zavatarelli, The western mediterranean deep water : A proxy for climate change, *Geophysical Research Letters*, *32*(12), doi :10.1029/2005GL022702, 2005.

Roe, G. H., and M. A. O'Neal, The response of glaciers to intrinsic climate variability : observations and models of late-Holocene variations in the pacific northwest, *Journal of Glaciology*, *55*(193), 839–854, doi :10.3189/002214309790152438, 2009.

Roemmich, D., and J. Gilson, The 2004-2008 mean and annual cycle of temperature, salinity, and steric height in the global ocean from the argo program, *Progress In Oceanography*, *82*(2), 81–100, doi :10.1016/j.pocean.2009.03.004, 2009.

Roemmich, D., J. Gilson, R. Davis, P. Sutton, S. Wijffels, and S. Riser, Decadal spinup of the south pacific subtropical gyre, *Journal of Physical Oceanography*, *37*(2), 162–173, doi :10.1175/JPO3004.1, 2007.

Roemmich, D., G. C. Johnson, S. Riser, R. Davis, J. Gilson, W. B. Owens, S. L. Garzoli, C. Schmid, and M. Ignaszewski, The argo program observing the global ocean with profiling floats RID a-3556-2010, *Oceanography*, *22*(2), 34–43, WOS :000266964200010, 2009.

Roether, W., B. Klein, B. Manca, A. Theocharis, and S. Kioroglou, Transient eastern mediterranean deep waters in response to the massive dense-water output of the aegean sea in the 1990s, *Progress in Oceanography*, *74*(4), 540–571, doi :10.1016/j.pocean.2007.001, 2007.

Rohling, E. J., R. Marsh, N. C. Wells, M. Siddall, and N. R. Edwards, Similar meltwater contributions to glacial sea level changes from antarctic and northern ice sheets, *Nature*, *430*(7003), 1016–1021, doi :10.1038/nature02859, WOS :000223514900040, 2004.

Rohling, E. J., K. Grant, C. Hemleben, M. Siddall, B. a. A. Hoogakker, M. Bolshaw, and M. Kucera, High rates of sea-level rise during the last interglacial period, *Nature Geoscience*, *1*(1), 38–42, doi :10.1038/ngeo.2007.28, 2007.

Rohling, E. J., K. Grant, M. Bolshaw, A. P. Roberts, M. Siddall, C. Hemleben, and M. Kucera, Antarctic temperature and global sea level closely coupled over the past five glacial cycles, *Nature Geoscience*, *2*(7), 500–504, doi :10.1038/ngeo557, 2009.

Rowley, D. B., Rate of plate creation and destruction : 180 ma to present, *Geological Society of America Bulletin*, *114*(8), 927–933, doi :10.1130/0016-7606(2002)114⟨0927:ROPCAD⟩2.0.CO;2, 2002.

Samuel, S., K. Haines, S. Josey, and P. G. Myers, Response of the mediterranean sea thermohaline circulation to observed changes in the winter wind stress field in the period 1980-1993, *Journal of Geophysical Research*, *104*(C4), PP. 7771–7784, doi :199910.1029/1998JC900130, 1999.

Santamaria-Gomez, A., M. Bouin, X. Collilieux, and G. Woppelmann, Correlated errors in GPS position time series : Implications for velocity estimates, *Journal of Geophysical Research*, *116*, 14 PP., doi :201110.1029/2010JB007701, 2011.

Sasgen, I., M. van den Broeke, J. L. Bamber, E. Rignot, L. S. Sorensen, B. Wouters, Z. Martinec, I. Velicogna, and S. B. Simonsen, Timing and origin of recent regional ice-mass loss in greenland, *Earth and Planetary Science Letters*, *333-334*(0), 293–303, doi :10.1016/j.epsl.2012.03.033, 2012.

Schott, F. A., S. Xie, and J. P. M. Jr, Indian ocean circulation and climate variability, *Reviews of Geophysics*, *47*, 46 PP., doi :200910.1029/2007RG000245, 2009.

Sen Gupta, A., A. Santoso, A. S. Taschetto, C. C. Ummenhofer, J. Trevena, and M. H. England, Projected changes to the southern hemisphere ocean and sea ice in the IPCC AR4 climate models, *Journal of Climate*, *22*(11), 3047–3078, doi :10.1175/2008JCLI2827.1, 2009.

Shaw, B., N. N. Ambraseys, P. C. England, M. A. Floyd, G. J. Gorman, T. F. G. Higham, J. A. Jackson, J. Nocquet, C. C. Pain, and M. D. Piggott, Eastern mediterranean tectonics and tsunami hazard inferred from the AD-365 earthquake, *Nature Geoscience*, *1*(4), 268–276, doi :10.1038/ngeo151, 2008.

Siddall, M., E. J. Rohling, A. Almogi-Labin, C. Hemleben, D. Meischner, I. Schmelzer, and D. A. Smeed, Sea-level fluctuations during the last glacial cycle, *Nature*, *423*(6942), 853–858, doi :10.1038/nature01690, WOS :000183585300041, 2003.

Siddall, M., E. Bard, E. J. Rohling, and C. Hemleben, Sea-Level reversal during termination II, *Geology*, *34*(10), 817–820, doi :10.1130/G22705.1, 2006.

Slangen, A., M. Carson, C. Katsman, R. van deWal, A. Kohl, L. Vermeersen, and D. Stammer, Projecting twenty-first century regional sea-level changes, *Nature*, in revision.

Slangen, A. B. A., C. A. Katsman, R. S. W. Wal, L. L. A. Vermeersen, and R. E. M. Riva, Towards regional projections of twenty-first century sea-level change based on IPCC SRES scenarios, *Climate Dynamics*, *38*(5-6), 1191–1209, doi :10.1007/s00382-011-1057-6, 2011.

Smith, T. M., R. E. Livezey, and S. S. Shen, An improved method for analyzing sparse and irregularly distributed SST data on a regular grid : The tropical pacific ocean, *Journal of Climate*, *11*(7), 1998.

Solomon, S., D. Qin, M. Manning, Z. Chen, M. Marquis, K. Averyt, M. Tignor, and H. Miller (Eds.), *Contribution of Working Group I to the Fourth Assessment Report of the Intergovernmental Panel on Climate Change, 2007*, Cambridge University Press, Cambridge, United Kingdom and New York, NY, USA, 2007.

Stammer, D., Response of the global ocean to greenland and antarctic ice melting, *Journal of Geophysical Research-Oceans*, *113*(C6), doi :10.1029/2006JC004079, 2008.

Stammer, D., N. Agarwal, P. Herrmann, A. Köhl, and C. Mechoso, Response of a coupled Ocean-Atmosphere model to greenland ice melting, *Surveys in Geophysics*, *32*(4), 621–642, doi :10.1007/s10712-011-9142-2, 2011.

Steffen, K., R. H. Thomas, E. Rignot, J. G. Cogley, M. B. Dyurgerov, S. C. B. Raper, P. Huybrechts, and E. Hanna, Cryospheric contributions to Sea-Level rise and variability, in *Understanding Sea-Level Rise and Variability*, edited by J. A. Church, P. L. Woodworth, T. Aarup, and W. S. Wilson, pp. 177–225, Wiley-Blackwell, 2010.

Stenchikov, G., T. L. Delworth, V. Ramaswamy, R. J. Stouffer, A. Wittenberg, and F. Zeng, Volcanic signals in oceans, *Journal of Geophysical Research*, *114*, 13 PP., doi :200910.1029/2008JD011673, 2009.

Stott, P. A., R. T. Sutton, and D. M. Smith, Detection and attribution of atlantic salinity changes, *Geophysical Research Letters*, *35*, 5 PP., doi :200810.1029/2008GL035874, 2008.

Suzuki, T., and M. Ishii, Long-term regional sea level changes due to variations in water mass density during the period 1981-2007, *Geophysical Research Letters*, *38*, 6 PP., doi : 201110.1029/2011GL049326, 2011.

Syvitski, J. P. M., A. J. Kettner, I. Overeem, E. W. H. Hutton, M. T. Hannon, G. R. Brakenridge, J. Day, C. Vorosmarty, Y. Saito, L. Giosan, and R. J. Nicholls, Sinking deltas due to human activities, *Nature Geoscience*, *advance online publication*, doi : 10.1038/ngeo629, 2009.

Tamisiea, M., and J. Mitrovica, The moving boundaries of sea level change : Understanding the origins of geographic variability, *Oceanography*, *24*(2), 24–39, doi :10.5670/oceanog. 2011.25, 2011.

Terray, L., L. Corre, S. Cravatte, T. Delcroix, G. Reverdin, and A. Ribes, Near-Surface salinity as nature's rain gauge to detect human influence on the tropical water cycle, *Journal of Climate*, *25*(3), 958–977, doi :10.1175/JCLI-D-10-05025.1, 2012.

The PROTHEUS Group, V. Artale, S. Calmanti, A. Carillo, A. Dell-Aquila, M. Herrmann, G. Pisacane, P. M. Ruti, G. Sannino, M. V. Struglia, F. Giorgi, X. Bi, J. S. Pal, and S. Rauscher, An atmosphere-ocean regional climate model for the mediterranean area : assessment of a present climate simulation, *Climate Dynamics*, *35*(5), 721–740, doi : 10.1007/s00382-009-0691-8, 2009.

Tillinger, D., and A. Gordon, Transport weighted temperature and internal energy transport of the indonesian throughflow, *Dynamics of Atmospheres and Oceans*, *50*(2), 224–232, doi :10.1016/j.dynatmoce.2010.01.002, 2010.

Timmermann, A., S. McGregor, and F. Jin, Wind effects on past and future regional sea level trends in the southern Indo-Pacific, *Journal of Climate*, *23*(16), 4429–4437, doi : 10.1175/2010JCLI3519.1, 2010.

Tsimplis, M., M. Marcos, J. Colin, S. Somot, A. Pascual, and A. Shaw, Sea level variability in the mediterranean sea during the 1990s on the basis of two 2d and one 3d model, *Journal of Marine Systems*, *78*(1), 109–123, doi :10.1016/j.jmarsys.2009.04.003, 2009.

Vail, P., R. Mitchum, and S. T. III, Seismic stratigraphy and global changes of sea level, part 4 : global cycles of relative changes of sea level, in *Seismic stratigraphy-Applications to Hydrocarbon Exploration*, edited by C. Payton, pp. 83–98, American Association of Petroleum Geologists Memoir, 26, Tulsa, Oklahoma, 1977.

van den Broeke, M., J. Bamber, J. Ettema, E. Rignot, E. Schrama, W. J. van de Berg, E. van Meijgaard, I. Velicogna, and B. Wouters, Partitioning recent greenland mass loss, *Science*, *326*(5955), 984–986, doi :10.1126/science.1178176, WOS :000271712300037, 2009.

van Vuuren, D. P., K. Riahi, R. Moss, J. Edmonds, A. Thomson, N. Nakicenovic, T. Kram, F. Berkhout, R. Swart, A. Janetos, S. K. Rose, and N. Arnell, A proposal for a new scenario framework to support research and assessment in different climate research communities, *Global Environmental Change*, *22*(1), 21–35, doi :10.1016/j.gloenvcha.2011.08.002, 2012.

Velicogna, I., Increasing rates of ice mass loss from the greenland and antarctic ice sheets revealed by GRACE, *Geophysical Research Letters*, *36*, 4 PP., doi :200910.1029/2009GL040222, 2009.

Vera, J., F. Criado-Aldeanueva, J. Garcia-Lafuente, and F. Soto-Navarro, A new insight on the decreasing sea level trend over the ionian basin in the last decades, *Global and Planetary Change*, *68*(3), 232–235, doi :10.1016/j.gloplacha.2009.04.002, 2009.

Vermeer, M., and S. Rahmstorf, Global sea level linked to global temperature RID a-8465-2010, *Proceedings of the National Academy of Sciences of the United States of America*, *106*(51), 21,527–21,532, doi :10.1073/pnas.0907765106, WOS :000272994200014, 2009.

von Schuckmann, K., and P. Le Traon, How well can we derive global ocean indicators from argo data ?, *Ocean Science*, *7*(6), 783–791, doi :10.5194/os-7-783-2011, 2011.

Vuille, M., G. Kaser, and I. Juen, Glacier mass balance variability in the cordillera blanca, peru and its relationship with climate and the large-scale circulation, *Global and Planetary Change*, *62*(1-2), 14–28, doi :10.1016/j.gloplacha.2007.11.003, 2008.

Wada, Y., L. P. H. v. Beek, C. M. v. Kempen, J. W. T. M. Reckman, S. Vasak, and M. F. P. Bierkens, Global depletion of groundwater resources, *Geophysical Research Letters*, *37*, 5 PP., doi :201010.1029/2010GL044571, 2010.

Wada, Y., L. P. H. v. Beek, F. C. S. Weiland, B. F. Chao, Y. Wu, and M. F. P. Bierkens, Past and future contribution of global groundwater depletion to sea-level rise, *Geophysical Research Letters*, *39*, 6 PP., doi :201210.1029/2012GL051230, 2012.

Wadhams, P., and W. Munk, Ocean freshening, sea level rising, sea ice melting, *Geophysical Research Letters*, *31*, 4 PP., doi :200410.1029/2004GL020039, 2004.

Webb, A. P., and P. S. Kench, The dynamic response of reef islands to sea-level rise : Evidence from multi-decadal analysis of island change in the central pacific, *Global and Planetary Change*, *72*(3), 234–246, doi :10.1016/j.gloplacha.2010.05.003, 2010.

Wijffels, S. E., J. Willis, C. M. Domingues, P. Barker, N. J. White, A. Gronell, K. Ridgway, and J. A. Church, Changing expendable bathythermograph fall rates and their impact on estimates of thermosteric sea level rise, *Journal of Climate*, *21*(21), 5657–5672, doi : 10.1175/2008JCLI2290.1, 2008.

Willis, J. K., D. Roemmich, and B. Cornuelle, Interannual variability in upper ocean heat content, temperature, and thermosteric expansion on global scales, *Journal of Geophysical Research*, *109*, 13 PP., doi :200410.1029/2003JC002260, 2004.

Willis, J. K., D. P. Chambers, and R. S. Nerem, Assessing the globally averaged sea level budget on seasonal to interannual timescales, *Journal of Geophysical Research*, *113*, 9 PP., doi :200810.1029/2007JC004517, 2008.

Wolff, J., E. Maier-Reimer, and S. Legutke, The hamburg ocean primitive equation model, deutsches Klimarechenzentrum Technical Report n°13, Hamburg, Germany., 1997.

Woodworth, P., N. White, S. Jevrejeva, S. Holgate, J. Church, and W. Gehrels, Evidence for the accelerations of sea level on multi-decade and century timescales, *International Journal of Climatology*, *29*(6), 777–789, doi :10.1002/joc.1771, 2009.

Woodworth, P. L., High waters at liverpool since 1768 : the UK's longest sea level record, *Geophysical Research Letters*, *26*(11), PP. 1589–1592, doi :199910.1029/1999GL900323, 1999.

Woodworth, P. L., and R. Player, The permanent service for mean sea level : An update to the 21st century, *Journal of Coastal Research*, *19*(2), 287–295, WOS :000182896000006, 2003.

Woodworth, P. L., M. Menendez, and W. R. Gehrels, Evidence for Century-Timescale acceleration in mean sea levels and for recent changes in extreme sea levels, *Surveys in Geophysics*, *32*(4-5), 603–618, doi :10.1007/s10712-011-9112-8, WOS :000295332800018, 2011.

Woppelmann, G., N. Pouvreau, and B. Simon, Brest sea level record : a time series construction back to the early eighteenth century, *Ocean Dynamics*, *56*(5), 487–497, doi : 10.1007/s10236-005-0044-z, 2006.

Woppelmann, G., B. Martin Miguez, M. Bouin, and Z. Altamimi, Geocentric sea-level trend estimates from GPS analyses at relevant tide gauges world-wide, *Global and Planetary Change*, *57*(3-4), 396–406, doi :10.1016/j.gloplacha.2007.02.002, 2007.

Woppelmann, G., N. Pouvreau, A. Coulomb, B. Simon, and P. L. Woodworth, Tide gauge datum continuity at brest since 1711 : France's longest sea-level record, *Geophysical Research Letters*, *35*, 5 PP., doi :200810.1029/2008GL035783, 2008.

Woppelmann, G., C. Letetrel, A. Santamaria, M. Bouin, X. Collilieux, Z. Altamimi, S. Williams, and B. Miguez, Rates of sea-level change over the past century in a geocentric reference frame, *Geophysical Research Letters*, *36*, doi :10.1029/2009GL038720, 2009.

Wunsch, C., R. M. Ponte, and P. Heimbach, Decadal trends in sea level patterns : 1993-2004, *Journal of Climate*, *20*(24), 5889–5911, doi :10.1175/2007JCLI1840.1, WOS :000252000800002, 2007.

Xavier, L., M. Becker, A. Cazenave, L. Longuevergne, W. Llovel, and O. Rotunno Filho, Interannual variability in water storage over 2003-2008 in the amazon basin from GRACE space gravimetry, in situ river level and precipitation data, *Remote sensing of Environement*, 2010.

Yamaguchi, S., R. Naruse, and T. Shiraiwa, Climate reconstruction since the little ice age by modelling koryto glacier, kamchatka peninsula, russia, *Journal of Glaciology*, *54*(184), 125–130, doi :10.3189/002214308784409026, 2008.

Yin, J., S. M. Griffies, and R. J. Stouffer, Spatial variability of sea level rise in Twenty-First century projections, *Journal of Climate*, *23*(17), 4585–4607, doi :10.1175/2010JCLI3533.1, 2010.

Annexe A : Liste des publications

Becker M., **Meyssignac B.**, Xavier L., Cazenave A., Alkama R. and Decharme B, **2011a**. Past terrestrial water storage (1980-2008) in the Amazon Basin reconstructed from GRACE and in situ river gauging data. *Hydrology and Earth System Science*. 15 : 533-546. doi : 10.5194/hess-15-533.

Marcos M., Calafat F. M., Llovel W., Gomis D. and **Meyssignac B.**, **2011**. Regional distribution of steric and mass contributions to sea level changes. *Global and Planetary Change*. 3/4 : 206-218. doi : 10.1016/j.gloplacha.2011.01.007.

Meyssignac B., Calafat F.M., Somot S., Rupolo V., Stocchi P., Llovel W. and Cazenave A., **2011**. Two-dimensional reconstruction of the Mediterranean sea level over 1970-2006 from tide gauge data and regional ocean circulation model outputs. *Global and Planetary change*. 1/2 : 49-61. doi : 10.1016/j.gloplacha.2011.03.002.

Llovel W., **Meyssignac B.** and Cazenave A., **2011**. Steric sea level variations over 2004-2010 as a function of region and depth ; inference on the mass component variability in the North Atlantic Ocean. *Geophysical Research Letter*. 38 : L15608. doi : 10.1029/2011GL047411.

Becker M., **Meyssignac B.**, Llovel W., Cazenave A. and Delcroix T., **2011b**. Sea level variations at Tropical Pacific Islands during 1950-2009. *Global and Planetary Change*. 80/81 : 85-98. doi :10.1016/j.gloplacha.2011.09.004.

Meyssignac B., Becker M., Llovel W. and Cazenave A., **2012a**. An assessment of two-dimensional past sea level reconstructions over 1950-2009 based on tide gauge data and different input sea level grids. *Survey in Geophysics*, online. doi :10.1007/s10712-011-9171-x.

Meyssignac B. and Cazenave A, **2012b**. Sea level : a review of present-day and recent past changes and variability. *Journal of Geodynamics*, online.

doi :10.1016/j.jog.2012.03.005.

Meyssignac B., Salas-Melia D., Becker M., Llovel W. and Cazenave A., **2012c**. Spatial trend patterns in observed sea level : internal variability and/or anthropogenic signature ? *Climate of the Past*, 8 :787-802. doi :10.5194/cp-8-787-2012.

Henry O., Prandi P., Llovel W., Cazenave A., Jevrejeva S., Stammer D.,**Meyssignac B.**, Koldunov N. and Cazenave A. Sea level variations since 1950 along the coasts of the Arctic Ocean. *Journal of Geophysical Research*, in press.

Fenoglio-Marc L., Mariotti A., Sannino G.,**Meyssignac B.**, Carillo A. and Struglia M.V. Decadal variability of net water flux at the Mediterranean sea Gibraltar strait. *Global and Planetary Change*, in revision.

Cazenave A., Henry O., Munier S.,**Meyssignac B.**, Delcroix T., Llovel W., Palanisamy H. and Gordon A.L. Estimating ENSO influence on the global mean sea level during 1993-2010. *Marine Geodesy*, accepted.

Crétaux J.F., Bergé-Nguyen M., **Meyssignac B.**, Calmant S., Romanovski V., Perosanz F., Tashbaeva S., Arsen A., Fund F., Martignago N., bonnefond P., Laurain O. and Maisongrande P. Calibration of Envisat altimeter over the Lake Issykkul. *Advances in Space Research*, in revision.

Llovel W., Fukumori I., **Meyssignac B.**, Depth-dependent temperature change contributions to global mean thermosteric sea level rise from 1960 to 2010. *Geophysical Research Letter*, in revision.

Palanisamy H., Becker M., **Meyssignac B.**, Henry O., Cazenave A., Regional Sea Level Change and Variability in 20 the Caribbean Sea since 1950. *Journal of Geodetic Science*, in revision.

Annexe B : Articles non intégrés dans le corps du texte

Dans cette annexe nous ajoutons 3 articles auxquels nous avons participé et qui sont aujourd'hui en révision. Les études présentées dans ces articles n'étaient pas assez avancées pour être intégrées dans le corps du texte au moment de la rédaction de cette thèse. Pour cette raison nous les rassemblons seulement ici en annexe.

Calibration of Envisat radar altimeter over Lake Issykkul.

Crétaux J-F[1]., Bergé-Nguyen M[1]., Calmant S[2]., Romanovski V.V[3]., Meyssignac B[1]., Perosanz F[4]., Tashbaeva S[3]., Arsen A[1]., Fund F[4]., Martignago N[1]., Bonnefond P[5]., Laurain O[5]., Morrow R.[6], Maisongrande P[1]

Corresponding author: Dr J-F Crétaux, CNES/LEGOS, 14 av Edouard Belin, 31400 Toulouse, France, Tel: 33 5 61 33 29 89, Fax: 33 5 61 25 32 05, jean-francois.Crétaux@legos.obs-mip.fr

(1) CNES/LEGOS, Toulouse, France
(2) IRD/LEGOS, Toulouse, France
(3) IWPH, Bishkek, Kyrgyzstan
(4) CNES/GRGS, Toulouse, France
(5) Géoazur - Observatoire de la Côte d'Azur, Grasse, France
(6) OMP/LEGOS, Toulouse, France

Abstract

This study presents the results of Calibration/Validation (C/V) of Envisat satellite radar altimeter over Lake Issykkul located in Kyrgyzstan, which was chosen as a dedicated radar altimetry C/V site in 2004. The objectives are to estimate the absolute altimeter bias of Envisat and its orbit based on cross-over analysis with TOPEX / Poseidon (T/P), Jason-1 and Jason-2 over the ocean. We have used a new method of GPS data processing in a kinematic mode, developed at the Groupe de Recherche de Geodesie Spatiale (GRGS), which allows us to calculate the position of the GPS antenna without needing a GPS reference station. The C/V is conducted using various equipments: a local GPS network, a moving GPS antenna along the satellites tracks over Lake Issykkul, In Situ level gauges and weather stations. The absolute bias obtained for Envisat from field campaigns conducted in 2009 and 2010 is between 62.1 and 63.4 +/- 3.7 cm, using the *Ice-1* retracking algorithm, and between 46.9 and 51.2 cm with the *ocean* retracking algorithm. These results differ by about 10 cm from previous studies, principally due to improvement of the C/V procedure. Apart from the new algorithm for GPS data processing and the orbit error reduction, more attention has been paid to the GPS antenna height calculation, and we have reduced the errors induced by seiche over Lake Issykkul. This has been assured using cruise data along the Envisat satellite track at the exact date of the pass of the satellite for the two campaigns. The calculation of the Envisat radar altimeter bias with respect to the GPS levelling is essential to allow the continuity of multi-mission data on the same orbit, with the expected launch of SARAL/Altika mission in 2012. Implications for hydrology in particular, will be to produce long term homogeneous and reliable time series of lake levels worldwide.

Keywords: Absolute altimeter calibration; Envisat; GPS; Cross-over analysis; Geophysical corrections; Lake Issykkul

1. Introduction

1.1 C/V of radar altimeters: objectives

Radar altimetry has been used for ocean sea level estimation for a few decades, with high precision (~3 cm; Lambin et al. 2010) since the launch of T/P in 1992. However, linking time series from different missions requires accurate monitoring of the biases and drifts for each parameter contributing to the final estimate of the water surface height. Over the last 15 years, several groups have developed C/V sites to measure the absolute altimeter bias of each satellite. Such calibration activities have been performed in the framework of "post launch" calibration purposes in order to quantify system performances for each mission, and have been repeated at different sites worldwide. Repeat C/V campaigns have been performed at Harvest platform in California (Haines et al. 2003. 2010.); Corsica site -Cape Senetosa and Aspretto- (Bonnefond et al. 2003, 2010, Jan et al. 2004); Gavdos Island (Pavlis et al. 2004, Mertikas et al. 2010); Ibiza (Martinez-Benjamin et al. 2000[1], 2004) in the Mediterranean; and Bass Strait in Australia (Watson et al. 2004, 2011). This different sites have allowed us to detect biases and drifts due to data processing errors.

Calibration of radar altimeters is based on the principle of estimating a Sea Surface Height (SSH) at some comparison point using independent data, including tide gauges, GPS surveys, moorings or gravity/levelling profiles. GPS buoys are often deployed to determine the absolute datum of the SSH gauge (Watson et al. 2004) or the geoid slope (Bonnefond et al. 2003). While many articles have been dedicated to the computation of the absolute bias of T/P, Jason-1 and Jason-2 missions, much less effort has been applied to the Envisat mission. An absolute bias of 47.6 cm for this satellite has been obtained by Faugere et al. (2006), and between 46.9 and 51.2 cm in Crétaux et al. (2009) with the *ocean* retracking algorithm.

[1] Martinez-Bejamin, J., Martinez-Garcia, M., Garate, J., et al. The T/P CATALA altimeter calibration campaign, presented at the Spring AGU meeting, 2000.

1.2 Specificities of C/V over lakes

Although it has been designed for ocean applications, radar altimetry is also widely used in hydrology by several groups in the world for a wide range of applications: survey of lakes, rivers and floodplains (Birkett, 1995, Calmant et al. 2008, Crétaux and Birket 2006, Berry et al. 2007, Birkinshaw et al. 2010, Ricko et al. 2011). However over continental waters, this technique is limited by several factors.

First of all, the onboard retrackers were designed for ocean surfaces, hence the radar echo waveform is not always processed correctly and may provide erroneous range measurements. Moreover, rapidly varying topography or complex terrain may inhibit the retrieval of the correct elevation data. This leads the user community to develop new algorithms (namely "retracking") to better fit these complex waveform echoes. Relative range biases between various retracking have been computed in Crétaux et al. (2009), and Crétaux et al. (2011). Other limitation comes from the corrections of range measurements due to the radar propagation in the atmosphere. Several effects have been highlighted in our previous studies based on Lake Issykkul, but also in Birkett and Beckley, (2010).

Indeed, there is clear evidence that the calibration of satellite altimetry over the ocean does not apply to inland seas (e.g., corrections, retracking, geographical effects). (Shum et al. 2003, Cheng et al. 2010, and Crétaux et al. 2009, 2011) pointed out that the number and variety of C/V sites for altimetry have to be increased in order to have more global distribution and more robust assessment of the altimetry system over different water surface, e.g., inland water bodies. This allows us to verify whether specific hydrological conditions would lead to a different estimation of the absolute bias of the instruments.

Moreover, C/V over lakes surfaces has interesting characteristics with respect to ocean surface. The surface of the reflecting water body is little affected by tide effects, wind waves are reduced, the surface dynamic variability is small and the Sea State Bias (SSB) which is one source of errors in C/V over ocean (Shum et al. 2003, Gaspar et al. 2002) is very negligible over lakes (Shum et al.

2003, Crétaux et al. 2011). Finally, for some big lakes, like Lake Issykkul, it is also possible to perform multi mission C/V on a same site (Crétaux et al. 2009).
The comparison of altimeter biases of T/P, Jason-1, and Jason-2, obtained over lakes and over ocean sites, shows an agreement at better than 2 cm (Cheng et al. 2010, Crétaux et al. 2011) which indicates that lakes can be relevant sites for future multi mission C/V.

1.3 A new estimation of Envisat absolute altimeter bias: for which reason?

Crétaux et al. (2009), have doperformedne a first calculation of theEnvisat altimeter bias over Lake Issykkul. This was based on two field campaigns (in 2004 and 2005). This first study highlighted some errors in the geophysical corrections (ionospheric, tropospheric and SSB). The GPS data were processed using the GINS software for the static GPS stations, and from the Total Trimble Control software for the mobile GPS. The calculation was done using all existing passes of Envisat tracks over Lake Issykkul from cycles 10 to 38 and using the historical In Situ measurement of a tide gauge located on the north coast of the lake (Cholpon Ata).

This initial study was one of the first to calculate the Envisat altimeter bias over a hydrological surface; the main C/V experiments have been focused on T/P, Jason-1 and Jason-2 satellites. The results obtained in Crétaux et al. (2009), for Envisat absolute bias, were affected by several limitations in the calculation. In the following years we have carried out new field campaigns on Lake Issykkul trying to improve the results of the first C/V experiments. This was done in the framework of the C/V of Jason-1 and Jason-2 after the launch of Jason-2 in 2008. Four field campaigns have therefore been conducted, in 2008, 2009 and 2010. The procedure of calculation of altimeter biases has been drastically changed to take into account the limitations that were pointed out in the first article. Firstly we have used In Situ and pressure data from a weather station on the vessel and on the ground to avoid high errors in the Dry Tropospheric Corrections (DTC) that were observed in 2004 and 2005. The error budget has been reduced by 3 to 4, and currently the DTC over the lake is estimated with an accuracy of about 0.5 cm (Crétaux et al. 2011). Another effect of wind on Lake Issykkul is the so-called seiche effect. It corresponds to an oscillation of the lake which may reach several centimeters (Crétaux et al. 2011), and which is not precisely detected by historical tide gauges on Lake Issykkul. If a seiche occurrs at the time when the satellite is measuring the lake level, this could not be taken into account in the estimation of altimeter bias, as we were obliged to use historical In Situ data to correct the altimetry data for lake level changes. In Crétaux et al. (2011), we have decided to navigate along the altimetry track at the exact date when the satellite is passing over the lake. The reason was to cancel potential errors due to seiches and the need to use In Situ water height to correct for altimetry data. We thus consider that the lake surface deduced from GPS measurements was exactly the same as those measured by the altimeter. Another problem was inferred from the SSB. This electromagnetic effect, which is correlated to wave height and wind in the open ocean (Gaspar et al. 2002), is not calibrated correctly for low values of these two parameters. Our field campaigns were made when the weather conditions were very calm, which also eliminated potential errors due to SSB. No SSB correction was applied to the altimeter range, as theorically, for very small wind and waves it has zero value. By chance, during our different field campaigns the weather conditions were favorable. Obviously this led us to consider only one or two altimetry cycles for the absolute bias computation, since we could not cover all satellite tracks in a RDV mode[2] during each campaign and we therefore had to select some track preferentially to others. This led us to publish in Crétaux et al. (2011), new values of the altimeter biases for Jason-1 and Jason-2. Other four reasons have led us to propose this new study on Envisat.

1. We have developed at GRGS a new mode of GPS Precise Point Positioning (PPP) from the GINS software (see section 5, Loyer et al. 2012). The derived accuracy of water level of Lake Issykkul from the GPS survey is expected to be more accurate than that in the first studies (Crétaux et al. 2009, 2011) from the TTC software.

[2] In the following we will call «RDV mode» the time of the pass of the satellite during the cruise

2. In contrast to T/P and Jason satellites, the Envisat mission is much less used in ocean science, particularly for the computation of the Global Sea Level (GSL). One of the main reasons is that the early orbits of Envisat were not precise enough to fulfill the accuracy requirements of GSL estimation. However, improvements have been recently realized in the framework of Envisat reprocessing and the precision now meets the Jason GDR-C standards. In the near future, new sets of orbits in the GDR-D standards will probably allow us to reconcile Jason & Envisat Global Sea Level trends. However, since these new orbits are not available for all users, we have calculated corrections of the vertical coordinates of the Envisat satellite, based on an inverse method applied to the ocean cross over points between the high accurate Jason1, Jason-2 and T/P and Envisat satellites (see section 6). Orbit corrections are a few centimeters, and consequently we have benefited from an improved orbit in the computation of the altimeter bias of this satellite with respect to the previous estimation. This study is also a first attempt to validate the Envisat orbit error estimation method, which could be used in the future for GSL estimation with much higher precision. Orbit correction on the orbit will also have impacts on lake level determination from Envisat, although the need in precision is less important than for GSL. Further validation must be done but the use of Lake Issykkul is a first positive step.

3. In 2012, the CNES and ISRO (Indian Space Research Organization) will launch a new satellite, which will carry an altimeter onboard. This is the SARAL/Altika mission, which will have the specificity of using a Ka band altimeter instead of a Ku band (with a lot of expected improvements for Hydrology that will not be detail here). It will also be placed on the same orbit as Envisat. Since the end of 2010, the Envisat satellite was no longer in an exactly repeating orbit, and the data definitively stopped in May 2012, so we will have a gap of about one year and half until the SARAL/Altika data are available. In order to benefit from long term time series for lakes and rivers water level (starting in 2002 thanks to Envisat), it is therefore necessary to estimate very accurately the absolute bias of each of these satellites with respect to In Situ observations to compute relative bias, as it is usually done with the T/P, Jason series of satellites.

4. The last reason is that with the improved data processing and field experiment's procedures (applied for Jason-1 and Jason-2 in Crétaux et al. (2011) but not for Envisat), we wish to enhance the role of Lake Issykkul as an operational C/V site in a multi mission perspective.

In the following section we will describe Lake Issykkul C/V site and the reason why we think this is well suited for calculating absolute altimeter biases (Section 2). In section 3 we will describe the main characteristics of the field campaigns made over Lake Issykkul and the principle of C/V over this lake. Section 4 is dedicated to altimetry error budget assessment for Lake Issykkul during the field experiment. Section 5 describes the GINS software application to GPS data and specifically the new PPP mode. We will then in section 6 describe the method of improving the Envisat orbit from cross over point analysis between T/P, Jason1, Jason-2 and Envisat over the ocean, and the projection of corrected orbit over Lake Issykkul. Section 7 is dedicated to the main results obtained for Envisat absolute bias from two campaigns, in September 2009 and 2010. We will conclude this manuscript in section 8.

2. Lake Issykkul: a C/V site for altimetry

Lake Issykkul (42°10'–42°40' North, 76–78° East, Republic of Kyrgyzstan) has been selected to determine altimeter biases because it fulfils key criteria for scientific, technical and logistical reasons.

-The first criteria is given by the size of the Lake: ranked 25th by the Global Lake and Wetland Database (total area of ~6000 km^2), its water height can be measured by all past and current altimeters in orbit: T/P, Jason-1/2, Envisat, Geosat, Icesat, and the future mission such as SARAL/Altika, Jason-3, Sentinel-3, Jason-CS, and SWOT. This is an advantage in the perspective of multi-satellite cross calibration, and it gives at one unique site the opportunity to calibrate and validate the range measurements and different associated corrections for each mission.

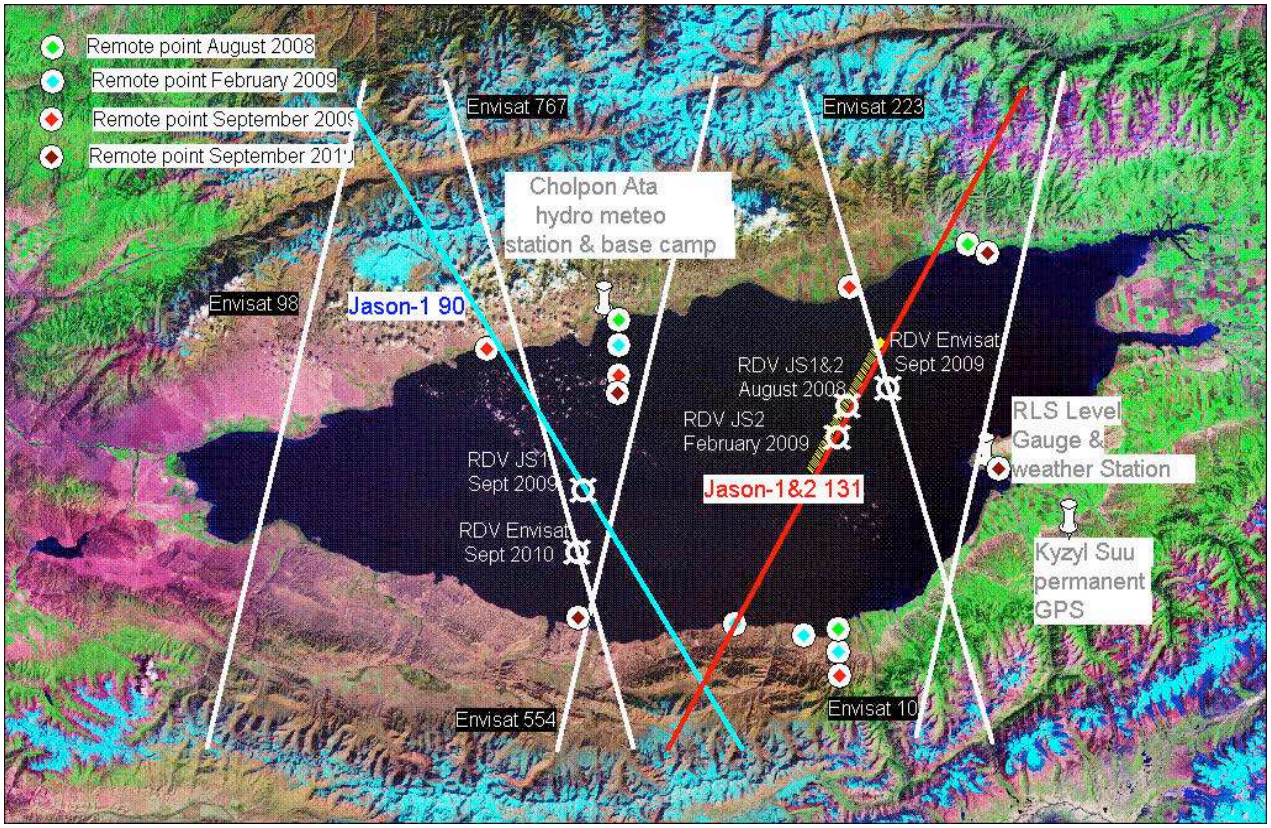

Fig. 6: Lake Issykkul from landsat satellite image. Altimetry tracks, position of the tide gauges,2008 to 2010's cruises and other instrumentation.

-This lake also provides a complementary C/V site, which is now included in the "pool" of C/V sites classically used for the T/P and Jason satellites that are all localized in the ocean. It is therefore in a different geophysical environment, far from all oceans, in a mountainous region (altitude of the lake is ~1600 m a.s.l) allowing us to test the altimeter performances for hydrology. In particular it has allowed us to investigate different geophysical corrections. Previous results published with Lake Issykkul data have already shown that this lake is also pertinent for "classical" estimation of altimeter biases with results that differ from ocean C/V site results (Crétaux et al. 2009). Discrepancies, especially for Jason-1, have been widely discussed in Crétaux et al. (2011), Shum et al. (2003) and Cheng et al. (2010) (composed to similar studies and results over Lake Erie in USA). This has clearly reinforced the need to extend the type and location of C/V sites for satellite radar altimeters.

The second main reason why Lake Issykkul is well suitable for C/V of altimeters lies in the question of the weather and hydrological conditions at this Lake. In contrast to oceans, such a lake is not affected by tides: it has been shown that generally lake tides are in the range of a few millimetres: (Birkett et al. 2010, Crétaux et al. 2011). There is also no need to apply the inverse barometer correction to the data since the size of the lake is too small to be influenced by pressure differential effects (Crétaux et al. 2009) and the most interesting characteristic is that SSB is negligible and thus not even taken into account (Crétaux et al. 2009, 2011). It consequently diminishes the source of error in the estimation of altimeter bias.

A last condition, which is fulfilled with Lake Issykkul, is the availability of In Situ infrastructure and the possibility to carry out GPS measurements on the lake itself along the altimetry track. For the DTC correction for example we use a weather station which provides atmospheric pressure twice a day and which has been proven to be accurate enough to determine an independent DTC correction for the altimetry measurement (Crétaux et al. 2011). We also benefit from a long cooperation between Legos and Institute of Water Problem and Hydropower (IWPH) of Kyrgyzstan who provide ground

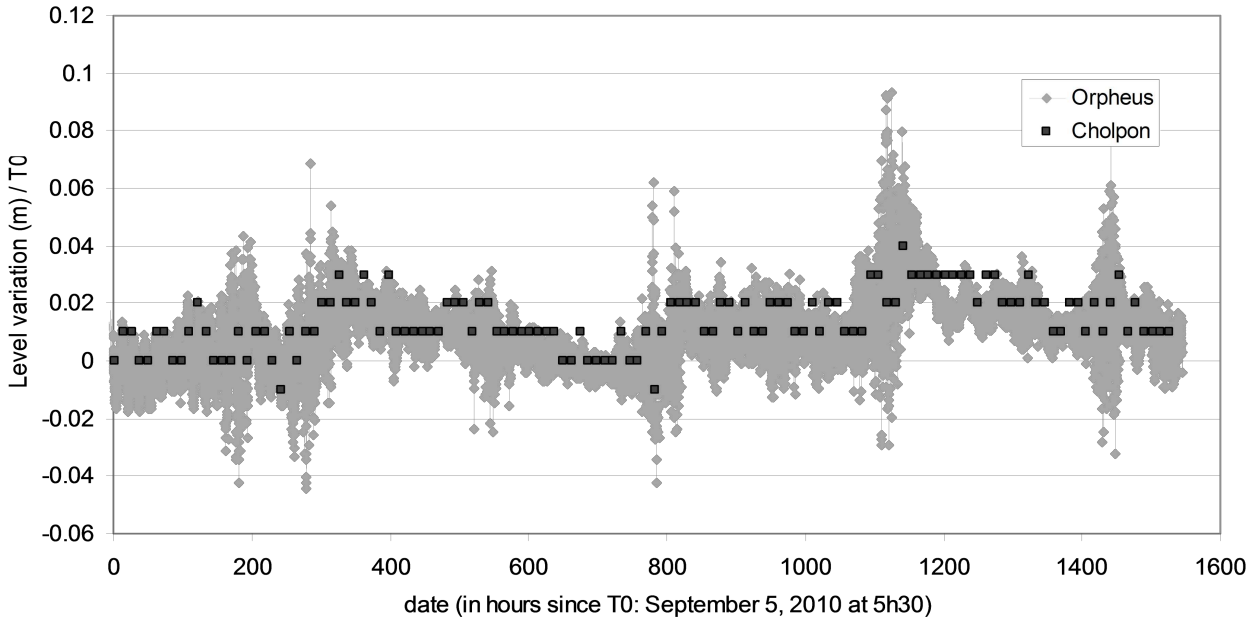

Fig. 1: Variation of water height at the Cholpon Ata site (north shore of the Lake) measured by a bottom pressure gauge (named Orpheus) and by a historical limnigraph.

facilities such as In Situ water level data, as well as two long vessels (namely "Multur" and "Storm" fully equipped for scientific field work) which allow us to navigate for many consecutive days on the Lake. Weather station data and all administrative authorizations to perform our own In Situ measurements and install permanent instruments are also an advantage.

In the perspective of using Lake Issykkul as an operational C/V site for all altimetry missions, we also have installed several instruments around the lake: a permanent GPS receiver (10 km South to the Lake) since July 2008, a weather station and a level gauge on the South East bank of the lake, that provide atmospheric pressure, air temperature and humidity, and water level every 5 minutes since September 2010, and a pressure probe installed in September 2010 in Cholpon Ata close to the historical tide gauge in order to estimate the accuracy of the In Situ water level record (Figure 6). Two level gauges installed in September 2010 on opposite sides of the lake will also help to better characterize the seiche effect on the lake, which was one of the main sources of error in our first study (Crétaux et al. 2009). These new gauges will also allow a more accurate estimate of the altimetry biases over this lake compared to the historical gauge because of a higher time sampling of the measurements.

3. C/V procedure over Lake Issykkul

Regarding the principal objective of the experiment, which is to estimate the altimeter absolute bias, we have developed a strategy of field measurements based on GPS surveys of the lake surface along the altimetry track for each targeted satellite (Envisat in this study). The principle is to install one or two GPS antennas on the top of a Vessel, and to navigate along the track, with one condition, which is to measure the ellipsoidal altitude all along the satellite track at the exact time of the pass of the satellite (what we call RDV mode). This measurement allows us to cancel errors due to the potential seiche effects, which statistically may occur during the experiment. Through this procedure, if a seiche is observed during the experiment (which may reach 10 cm of amplitude (Figure 1) and Crétaux et al. 2011), it is naturally removed in the estimation of the altimeter bias, as both, the GPS and altimeter measure this seiche instantaneously. This procedure has been applied with success in a previous study (Crétaux et al. 2011) for the estimation of Jason1 and Jason-2 absolute and relative biases. The biases obtained for both satellites were very similar to estimations made over Lake Erie by an American team (Ohio State University, Shum et al. 2003) and differs slightly for Jason-1 with estimations made by other authors over the C/V oceanic sites (Bonnefond et

al. 2010, Haines et al. 2010, Mertikas et al. 2010). The observed discrepancies do not exceedi 2 cm and are still subject to discussion (See Cheng et al. 2010 and Crétaux et al. 2011).

In order to determine the altimeter absolute bias we must calculate the ellipsoidal altitude of the lake along the altimeter track by two means: from altimetry data and from the GPS receivers installed on the boat. The absolute bias is simply the averaged difference between both estimations along the track. It is obviously also necessary to quantify the error budget of this calculation which originates from both water altitude estimations. So part of the uncertainty is due to altimetry errors, the other part from the GPS data processing.

Figure 2 illustrates the general principle of C/V over Lake Issykkul. In the two following sections we will describe this error budget, and how we have improved it since the first studies and field campaigns made in 2004 and 2005.

4. Water level of Lake Issykkul from satellite altimetry

The method to extract water height above a lake from radar altimetry is rather similar to that over the ocean. The satellite embarks an altimeter, which transmit a short microwave pulse in the nadir direction, which is reflected back by the lake surface to the satellite. The time taken to reflect a given pulse corresponds to double the distance between the water surface and the satellite (called the Range), divided by the light velocity as a first approximation. Due to the propagation delay of the signal through the atmosphere, the range has to be corrected for three main terms, DTC, the Wet tropospheric Correction (WTC) and the Ionospheric Correction (IC). Other terms have to be taken into account like the SSB, which is electromagnetic bias due to wind and wave effect over the altimetry footprint. Corrections due to Earth, Lake and Pole tide (ET, LT and PT) should also been taken into account. The water height over the ellipsoid of reference is given by the difference between the altitude of the satellite and the corrected range, and is expressed by equation (1). Since the atmospheric pressure variability is very low (Crétaux et al. 2009) the atmospheric barometer pressure effect is ignored in the calculation.

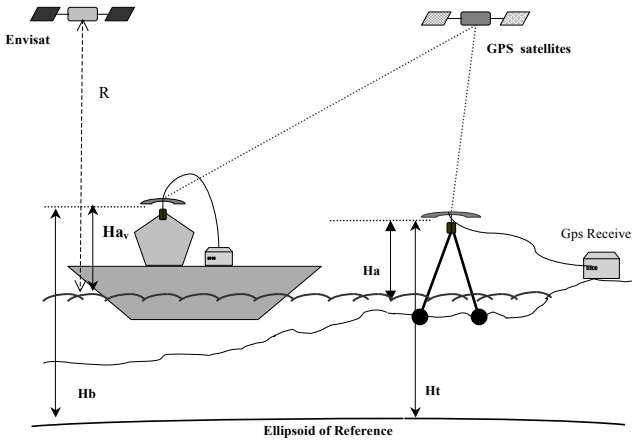

Fig. 2: Principle of C/V over a lake, and the principle of GPS antenna measurements. Ha_y, Ha : Antenna height above the lake (vessel land fixed points respectively). Hb, ht : Vertical position of GPS antennas above the ellipsoid of reference (vessel, and land fixed point). R : Altimeter Range

$$H=Alt-R+[DTC+WTC+IC+SSB+ET+PT+LT] \quad (1)$$

We discuss below the different terms on the right hand side of this equation.

4.1. The altitude of the satellite (Alt) is calculated by the ground segment of each mission, and is usually provided by the so called GDRs[3] (Geophysical Data Records) that are made available to us by ESA and via the data centre developed at Legos and called CTOH (Centre de Topographie des Océans et de l'Hydrosphère). For Envisat, the orbit has been computed from the different positioning systems onboard (Doris and Laser systems), and in the section 6 we will describe the method developed to improve this orbit in the nadir direction. We have used in our study both the GDR-B available at the CTOH, and the GDR-C released version provided by ESA (Envisat-1 products specifications, 2009); this reprocessing improved lots of parameters (environmental corrections, SSB, …) including the orbit that follows the same GDR-C standards as adopted in the framework of Jason-1 and Jason-2 missions (Cerri et al. 2010).

4.2. The ET and PT are given in the GDRs. For the PT, a scaling factor of 0.468 has been applied as recommended in Birkett and Beckley, (2010).

[3] Envisat-1 Products Specifications, Volume 14: Ra-2 Products Specifications, PO-RS-MDA-GS-2009, S4, Rev.: C, 2009.

The ET is estimated from the model developed by Cartwright and Tayler, (1971). The standard deviation of this correction is sub millimetre (Bonnefond et al. 2010). The LT has not been taken into account as no model currently exists for this geophysical effect. For Great Lake of North America, they may reach 8 cm (Birkett and Beckley 2010), but over Lake Issykkul, which is much smaller, a previous study (Crétaux et al. 2011) shows that it does not exceed a magnitude of 0.2-0.3 cm. The Lake tide may also alter the GPS data processing along the satellite tracks as they were not taken into account.

4.3. The SSB is the combination of an electromagnetic bias and instrumental bias, both of them, correlated with the Significant Wave Height (SWH). The usual way to estimate the SSB is empirical for practical reasons, and is based on a polynomial function of SWH and of the wind speed intensity. Basically SSB increases non linearly with high wave height and strong wind. The SSB corrections may reach several centimeters over the ocean and thus must be calculated with precision. Over Lake Issykkul, they are both generally very small (in average the wind speed is 2 cm/s and wave height rarely exceed 50 cm to 1 m which in the model belongs to the domain of negligible SSB). Moreover during our field campaigns the weather was rather calm with very small wave and wind conditions. In Crétaux et al. (2009) we have shown that the empirical estimation of SSB usually considered by the oceanographers and that are given in the GDRs may even be totally unrealistic over lakes. SSB is now considered as one of the major issues in C/V over the ocean (Shum et al. 2003, Haines et al. 2010) and changes in the model used to correct for this effect had some significant impact on the calculation of the absolute altimeter biases of the T/P and Jason satellites by different authors (Haines et al. 2010, Bonnefond et al. 2010). Therefore we have an interesting advantage over Lake Issykkul since we do not have additional source of error resulting from the SSB.

4.4. For the range (R), we have used the 18 Hz data (about 300 m between two individual's measurements). They provide a better fit for the geoid undulations along the satellite track, and will be more convenient for comparisons with the GPS data. Moreover, it has been demonstrated by Frappart et al. (2006), and Crétaux et al. (2009), that for Envisat, the range calculated using the "*Ice-1*" algorithm is more accurate than the two other ones that are "*Ice-2*" and the classical "*Ocean*" algorithms. Indeed, Calmant et al. (2008) stated that a major issue in using radar altimetry over continental water surfaces is related to the retrieval of the range variable among a large variety of waveform shapes. A retracking algorithm extracts the range from the received energy but with the ocean-designed algorithm, a wrong estimation of the range may result from analytical function not suitable for the returned waveform over lakes or rivers. The GDRs available with Envisat offer the choice between four different retrackers, and the "*Ice-1*" has proven to be more robust for non-standard waveforms such as those encountered over lakes and rivers.

In Crétaux et al. (2009) and Crétaux et al. (2011) we have calculated from Lake Issykkul experiment the relative biases of each algorithm and found that "*Ice-1*" minus "*Ice-2*" is in the range 23/24 cm. The same has been computed for "*Ice-1*" minus "*Ocean*". For this study, we have based all of our computations on the "*Ice-1*" model of retracking that are available only with the 18 Hz range data.

4.5. *Ionospheric correction*

As the IC is inversely proportional to the square of the frequency, for the current satellites it is derived from the dual frequency altimeters, in Ku and C bands for T/P, Jason-1 and Jason-2, and in Ku and S band for Envisat. In the CTOH database an IC is also derived from the Global Ionospheric Maps (GIM) inferred from GPS worldwide network. Over the lakes, the dual frequency IC can be erroneous with high spatial variability due to land contamination as shown in Birkett and Beckley (2010). From data 10 km away from the land, we have estimated (Crétaux et al. 2011) that the coherence between the dual frequency correction and the GIM model is about 1.1 cm for Jason-1. With Jason-2 the agreement was still better with an average difference of 0.4 +/- 1.1 cm. With Envisat, unfortunately the IC from the dual frenquency correction is totally erroneous after 2008 due to problems occurred on the S band. We see in Figure 3 that after this date the

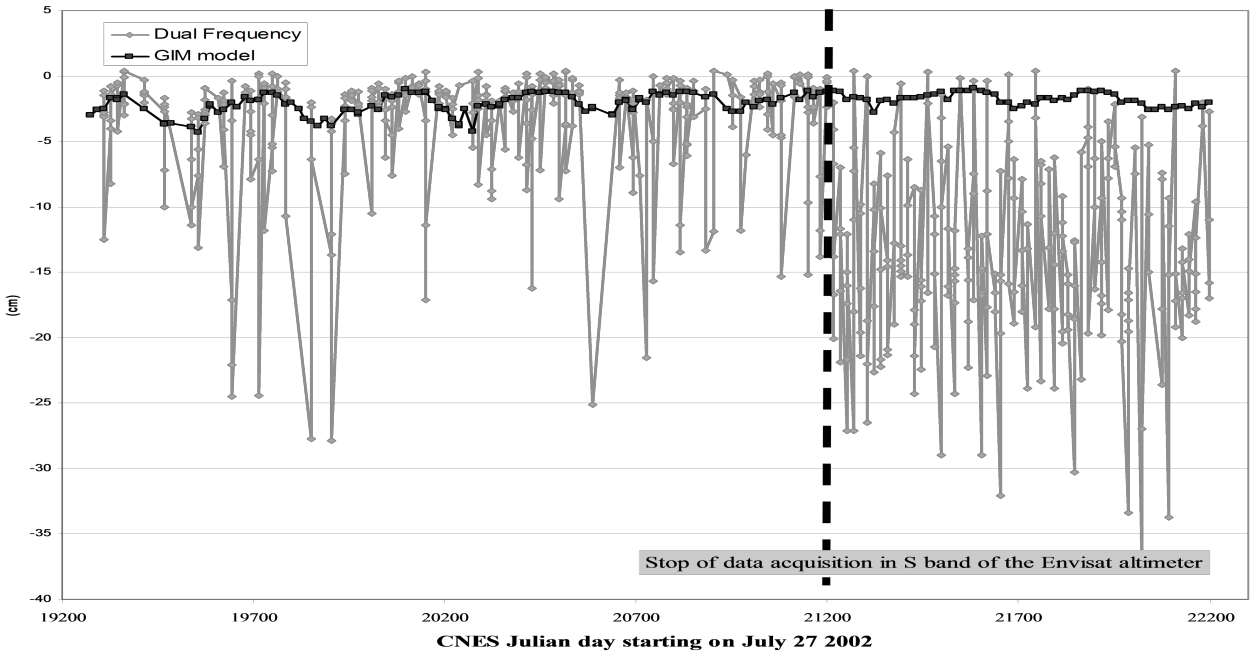

Fig. 3: Comparison of IC from Dual Frequency measurements and GIM model over Lake Issykkul for Envisat.

dual frequency correction is not valid anymore, and we were obliged to choose the GIM model. Without any investigation found in the literature about this model, and following the Birkett and Beckley (2010) assessment, the error associated with the IC, is assumed to be on the order of 2 cm.

4.6. *Dry Tropospheric Correction*

The DTC is proportional to the atmospheric pressure with the following relationship (Saastamoinen 1972):

$$DTC(cm) = -0.2277 \times P_{atm}(mb)[1 + 0.0026 \times \cos(2\phi)] \quad (2)$$

Where P_{atm} is the atmospheric pressure at the level of the lake and ϕ is the latitude of the point of measurement.

Over lakes in altitude and with surrounding mountain like Lake Issykkul we have demonstrated in Crétaux et al. 2009 that the DTC may be significantly wrong due to bad interpolation of the atmospheric pressure from global gridded meteorological data sets. In Particular near the land the effect of the interpolation is the worst. To avoid this problem, for usual lake level calculations from altimetry, one may ignore the erroneous data too close to the shoreline. For the C/V made over Lake Issykkul we have extracted the direct measurement of atmospheric pressure twice a day from a weather station at Cholpon Ata (Figure 1 and 6), and calculated the DTC from Eq. (2). However in order to assess the accuracy of the DTC provided in the GDRs, we have plotted the DTC calculated from In Situ data and those provided by the GDRs for measurements at least 5 km away from the land. As shown in Figure 4, the GDR DTC is well estimated in the center of the lake with a precision better than 1 cm in RMS. For the DTC used in the C/V of Envisat we have chosen the In Situ data for atmospheric pressure. During the field campaigns, a barometer was installed on the Vessel to control the data provided by the station in Cholpon Ata. In Crétaux et al. (2011) we have demonstrated that they were very coherent (better than 0.1 cm). For future improvements, and a better characterization of the spatial distribution of the DTC over Lake Issykkul, we have installed in June 2011 another weather station on the South East coast in close vicinity to an Envisat track.

4.7. *Wet Tropospheric Correction*

Bonnefond et al. (2010) have shown that the WTC is an important source of geographically correlated bias due to land contamination of the onboard radiometer. In our previous studies (Crétaux et al. 2009, Crétaux et al. 2011) it has also been pointed out that the WTC is one significant source of error for the C/V of radar

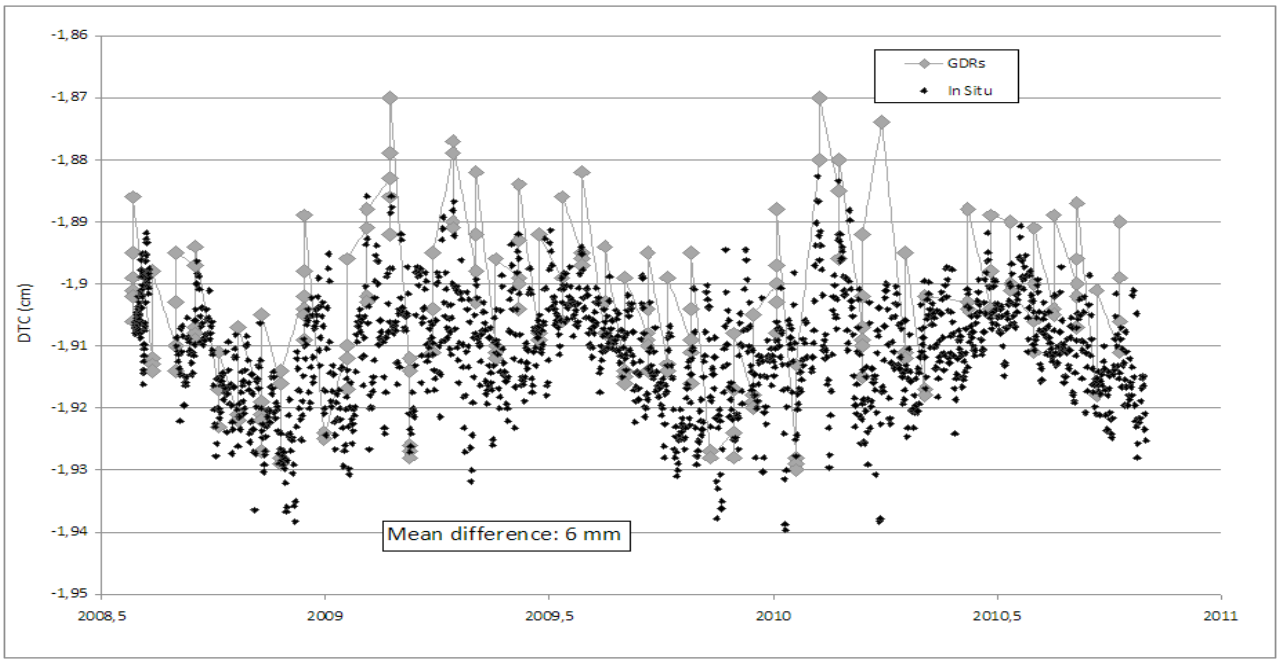

Fig. 4: Comparison of DTC between GDR-B products and In situ data of atmospheric pressure.

altimeters over lakes. It has been largely demonstrated in particular with the T/P, Jason-1 and Jason-2 satellites.

In (Brown, 2010 (MSB)) a model has been developed to improve the WTC estimation in the coastal regions the land. The improvement has been demonstrated in Bonnefond et al. (2010). It has been calculated that the accuracy of this model near the coastline approaches the centimeter level (1.2, 1 and 0.8 cm at 5 and 10 and 15 km from land respectively). For Envisat GDRs, unfortunately the WTC from this model are still not available. However for Jason-2 data, over Lake Issykkul, we have compared the model from CLS, the MSB and the radiometer for the whole cycle of this satellite up to now. We obtained averaged differences at the cm level between the CLS model (-7.2 cm in average over the 3 first year of Jason-2) and the MSB (-6.2 cm), while the radiometer measures some additional bias with respect to the two models (4.8 cm).

For Envisat, we also have analyzed the WTC given by the radiometer. We observed a significant bias of about 7 cm with respect to the model given by CLS In the absence of the MSB for Envisat, we prefer to use the WTC given by the model of CLS.

The WTC can also be derived from GPS data processing. In fact the total Zenital Tropospheric Delay (ZTD), in other words DTC plus WTC, has been estimated during each GPS static session around the lake (see 5.1). We have used the static points that were the closest to the position of the satellite track during the RDV mode, and then have calculated the total tropospheric zenith delay during observational sessions. First, a correction to the DTC (derived from Eq. 2 and In Situ atmospheric pressure measurements) has to be calculated in order to take into account the height of the station above the lake. Then by subtracting this DTC from the estimated ZTD we could get a new estimate of WTC. For cycle 82 (September 2009) during the RDV mode, the WTC deduced from GPS and from the model differs by a value of 5.7 cm, and for the cycle 92 (September 2010) by only 1.3 cm. Although the WTC estimated along the shoreline (by GPS static point) may differ from that over the center of the lake (where the altimetry data were processed for estimation of absolute bias) we have decided to use the WTC derived from GPS data. However, the WTC still remains the principal limitation of our calculation but this is also a source of error for other C/V oceanic sites that are usually located along the coast.

5. GPS data processing

The accuracy of the absolute altimeter bias of Envisat depends significantly on the quality of the GPS data acquisition (field experiments) and processing. The sources of errors are multiple. This has been a significant source of uncertainty in the previous study that we have tried to diminish. It concerns firstly the GPS data processing, and particularly the kinematic GPS positioning (section 5.1), and secondly we have tried to improve the procedure of GPS data acquisition with a specific care on the height antenna estimation (section 5.2)

5.1 Strategy of GPS Precise Point Positioning

Considering the global sources of uncertainties of our experiment we consider that the required accuracy of the GPS solutions should be at the centimetre level in RMS for both the tide gauge static leveling and for the boat kinematic tracking. To reach such an objective, we used the GINS CNES/GRGS software (Marty et al. 2011) in order to process both 2009 and 2010 data campaigns[4]. This scientific tool is currently operated by several groups in the world including the CNES-CLS International GNSS Service (IGS) (Dow et al. 2009) Analysis Center (AC). The latest version computes weekly precise GNSS satellites ephemeris products (Loyer et al. 2012) called "GRG"[5]. Both static and kinematic GPS observation sessions were processed using the PPP technique (Laurichesse et al. 2007) and these GRG GPS satellite and clock solutions. In our case PPP was an interesting alternative to the classical differential approach because for long baseline (superior to 10 km) the classical double difference data processing is degraded as demonstrated by Fund et al. (2012). For C/V over Lake Issykkul, due to land contamination on the altimetry waveform, we indeed have to calculate the altimeter bias away from the shoreline by more than 10-15 km. In addition, PPP could satisfy our accuracy specification (Bertiger et al. 2010) with a fast and straightforward processing. It moreover prevents us from data gaps during the transfer time between one static point to another one around the lake, as this technique allows calculating GPS points without any reference fixed station.

- Processing strategy:

In a pre-processing step, outliers and phase observation cycle slips are detected. Then the ionosphere-free linear combination of pseudo-range and phase observations from the two GPS frequencies is formed. A relative weighting factor of 100 is applied to range and phase observations (respectively 35 cm and 0.35 cm). Finally a cut-off angle of 10 degrees is considered.

- Models:

We followed all of the IERS conventions (Petit[6] et al. 2010) applicable to our cases. Cartesian coordinates were expressed in the ITRF05 (Altamimi et al. 2007) reference frame and then transformed into geographic coordinates using the GRS80 ellipsoid. In addition, as we used GRG IGS orbit and clock products in a PPP mode we have applied the recommendations from Kouba[7], (2009). In particular we were careful in using specific satellite and receiver phase center offsets and variations that were consistent with the GRG products. GPS observations must also be corrected from the propagation of the signal through the troposphere. In fact the ZTDs have been estimated together with the other parameters. We used the Global Pressure and Temperature (GPT) model given by Boehm et al. (2007) as a priori value.Then, in order to take into account the incident angles of each satellite signal, the Global Mapping Function (GMF) (Boehm et al. 2006) has been applied

[4] www.igsac-cnes.cls.fr/documents/gins/GINS_Doc_Algo.html

[5] www.igsacc-cnes.cls.fr

[6] Petit, G., Luzum B., (eds.). IERS Conventions (2010), IERS Technical Note No. 36, 2010

[7] Kouba, J. A Guide To using International GNSS Service (IGS) products, igscb.jpl.nasa.gov/igscb/resource/pubs/UsingIGSProductsVer21.pdf, 2009.

Positioning Mode	*Kinematic*		*Static*	
	PPP	IPPP	PPP	IPPP
Phase ambiguities	« float » real	« fixed » integer	« float » real	« fixed » integer
Receiver coordinates	Every epoch (30s)		1 per day	
Receiver clock	Every epoch (30s)			
Zenithal tropospheric delays	Piece wise linear (2 hours)			

Table 1: Summary of the estimated parameters for static and kinematic sessions

Session	*% fixed ambiguities (GPS receiver 1/2)*
Julian Day 22160 (09/03/2010)	80,8 / 92,6
Julian Day 22161 (09/04/2010)	92,0 / 91,8
Julian Day 22162 (09/05/2010)	94,0 / 95,9
Julian Day 22163 (09/06/2010)	89,7 / 93,1

Table 2: Kinematic sessions: Percentage of fixed ambiguities

- PPP processing :

Both static and kinematic sessions were processed using a PPP method. Table 1 gives the details of the respective parameter estimation strategies.

- Integer PPP processing :

Fixing phase observations ambiguities to their integer value obviously improves GPS solutions. If the double-differentiation of the observations was the only method to recover the integer nature of the ambiguities, recent publications (Laurichesse et al. 2007, Geng et al. 2010) demonstrate that this goal can be reached in a zero-difference approach. In other words PPP with (integer) fixed ambiguities is now possible (Gee et al. 2010). This innovative processing strategy has been implemented into the GINS software (Loyer at al. 2012). However, this approach requires orbit and clock products that conserve the integer nature of the ambiguities as well as the a priori knowledge of specific satellite un-calibrated phase delays which usually are eliminated through double-differentiation (Collins et al. 2010). As the CNES-CLS AC is being providing these products since October 2009, we were able to test this new approach on the 2010 data campaign.

Bertiger et al. (2010) have quantified the impact of fixing ambiguities in terms of both coordinates bias and repeatability. PPP kinematic solutions derived from real « float » phase ambiguities may suffer from various spurious signatures including biases, discontinuities but also slopes and low frequencies signals (Perosanz[8] et al. 2010). The rate of ambiguities fixed during an observation session is also a processing accuracy indicator. Table 2 gives the percentages of fixed ambiguities for the different kinematic sessions of the 2010 campaign. Because most of them are exceeding 90% we believe that the fixed series are more accurate than the float ones.

The Figure 5 represents along one boat route on the last field campaign (September 2010) the difference between the vertical position of the GPS antenna calculated in fix and floating ambiguities. It shows that differences are not negligible. As expected the difference are below one (narrow-line) cycle (10.7 cm). This plot also shows how an estimating float real ambiguity generates not only biases but also slopes and discontinuities as a function of the satellite geometry changes. Fixing ambiguities to their integer values drastically reduces these artefacts and consequently improves the solution (Perosanz et al. personal communication).

5.2. Computation of GPS height antenna on the Vessel above water surface

Along the 6 field campaigns made over Lake Issykkul, the issue of the estimation of the height antenna (HA) of the mobile GPS has been a key point in the C/V data processing. Several difficulties have to be solved and we have paid special attention to this question on this study in order to diminish the total error budget.

-The GPS antenna is generally installed on a place on the Vessel where it is quite impossible to make

[8] Perosanz F., Fund F., Rude V., et al. Spurious signals analysis in high frequency PPP solutions. Poster, IGS Workshop, 28 June - 2 July 2010, Newcastle upon Tyne, England, 2010

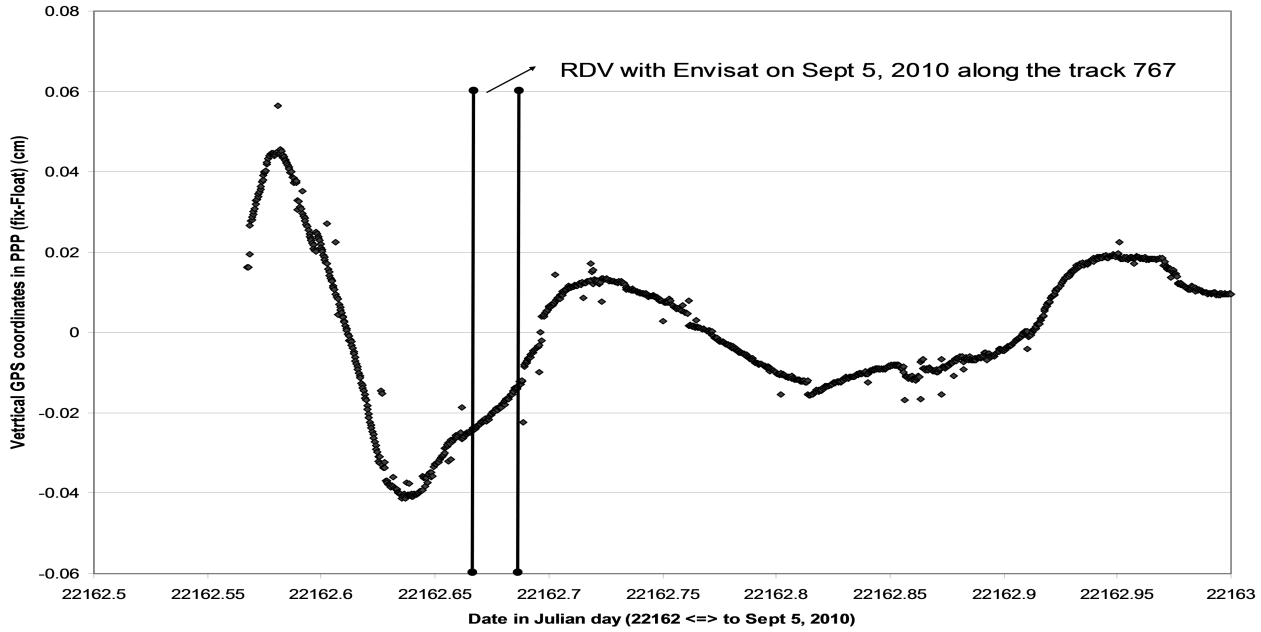

Fig. 5: Difference of vertical coordinates of the GPS antenna onboard the Storm's vessel during the 2010 campaign, calculated from Fix and floating ambiguities in PPP mode.

a direct measurement of the HA. To perform this computation we relied on the GPS static antenna (SA) directly installed over the water surface on the lake's shore (Figure 2). All receivers used for this work were dual-frequency receivers, namely 5700 Trimble receivers and Topcon GB1000. The initial time sampling was 1s, but for GINS data processing we have used 30s. Comparison of water height from 30s and 1s time sampling has been performing over a short distance along the cruise, and the coherence was at the millimetre level.

Each night the vessel stops in the very close vicinity of the fix GPS receiver (less than 100 meters) allowing to subtract from the vertical component of the GPS antenna, the vertical component of the SA which is calculated from the GPS data long session of several hours (ranging from 4 to 12 hours). Moreover the vertical coordinate of the GPS antenna in the terrestrial reference system (ITRF2005) is then converted into vertical height of the water surface below the antenna. During the 5 first campaigns we have performed direct visual measurements of this distance between the base of the antenna and the water surface (see Crétaux et al. 2009, 2011). The precision was altered by small undulations of the water surface, and accordingly we had estimated the RMS errors of this estimation from 0.2-0.3 cm in the best cases to 1-2 cm in the worse. For the last campaign of September 2010 we have used a photo camera to take between 30 and 40 pictures at each station (at the beginning and at the end of each session respectively) in high-speed mode in order to then average the values of HA and eliminate the effects of small waves. The precision we have reached was in all cases between 0.1 and 0.2 cm. From this simple method we have reduced one non-negligible source of error of the C/V of altimeters.

-On the previous studies we have calculated the position of the SAs from the GINS software in static mode. In Crétaux et al. (2011) we have shown that this calculation method suffered from an error of about 2 cm. We then estimated the mobile GPS antenna vertical coordinate (for the GPS installed on the ship) using the Total Trimble Control software. In order to make a consistent and accurate computation of GPS coordinates, especially for the SA, we have made all calculations in PPP mode.

Two other error sources also needed to be corrected.

-During the 3-4 days of navigation on the Lake, the fuel consumption leads to change in the waterline of the Vessel. This may reach a few

Error budget of HA calculation	Crétaux et al., 2009	This study
SA vertical coordinates	GINS in static mode: 2 cm	GINS in PPP mode: 1 cm
HA of SA	Visual with a ruler: 1-2 cm	series of photographies: 1-2 mm
Fuel consomption	One value from at the beginning and at the end of the campaign: 2 cm	daily estimation, 5 mm
Velocity effect	Not considered. Potential error of few cm (nevertheless in the first 2 campaigns, we have followed the satellite track with a slow velocity of the Multur of about 5-6 km/h which has probably attenuated the error made.)	Estimation from different pass with varying velocity: 1cm

Table 3: Summary of error in the calculation of Height antenna at the time of the RDV

centimetres per day. A simple way to correct for this effect is to perform regular (at least every day) height antenna estimations from the comparison between the SA and mobile GPS vertical components after removal of all of the corrections described above. This is done every night during the campaigns. Changes between each estimation epoch are associated with the fuel consumption. It is worth noting that during a campaign on the lake the height antenna is therefore regularly increasing. During the RDV mode, we paid particular attention to this correction, and it reaches about 2 to 4 cm depending on the boat used (the Multur in 2009 and the Storm in 2010). The HA used to calculate the altimeter bias was therefore the mean value of these two HA estimates (before and after the RDV mode).

-The last correction to be applied concerns the changing waterline of the vessel when it moves at different velocities. This effect can reach few centimetres and has been calibrated from dedicated experiments on the lake with each vessel. We simply passed over the same trajectory at different velocities, and the resulting HA changes was easily measured. A similar procedure has been setup by Bouin et al. (2009), where they defined a linear model of ship height variations with respect to speed changes. For the Multur we estimated that for a ship's velocity of 10 km/h the antenna was lowered by 8 cm, while for the Storm at the same velocity the lowering was 17 cm (the differences result from the different size and weight of each vessel, and the location of the GPS antenna with respect to their barycentre). This explains this correction is rather small on the Multur, which is much heavier than the Storm, and where we have installed the GPS near the centre of the boat. Whereas the correction is higher on the Storm, where the two GPS antennas have been installed near the back of the boat. In comparison, in Bouin et al. (2009), the effect was about 19 cm for a velocity change of 10 km/h. This correction has been applied to the previous study using Jason-1 and Jason-2 (Crétaux et al. 2011) but was not considered in the first article (Crétaux et al. 2009). This may partly explain the discrepancies with the results we have obtained here for Envisat.

A final error is inherent to the Lake Issykkul C/V, which, at this stage, cannot be assessed accurately. Over a lake like Issykkul, the slope of the geoid may be very steep over short distance, and the GPS measurements along the satellite track may differ from the average water height within a 3-5 km radius footprint. Depending on the exact position of the GPS point measured at a given time, we therefore might obtain some incoherence between both estimations of steep height. We have tried to reduce this error by taking into account only data far from the lake shoreline. Indeed, the slope of the geoid over Lake Issykkul is much smoother at the centre of the lake than near the land.

In summary the ensemble of these error reduction techniques means that error on the absolute bias due to the GPS point positioning is significantly reduced (from 5.3 to 1.5 cm) with respect to previous studies (see Table 3).

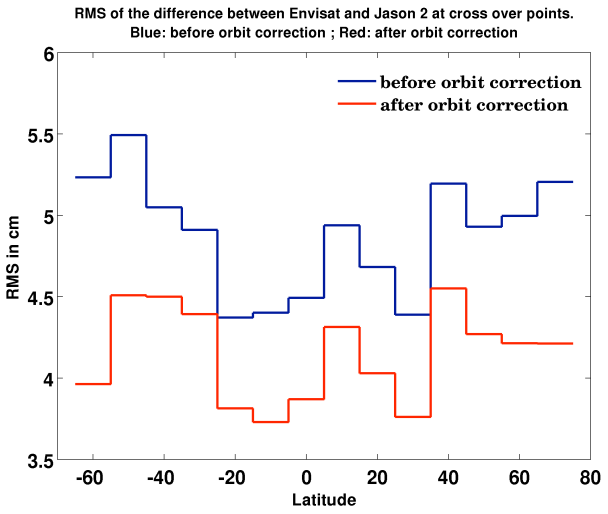

Fig. 7: latitudinal distribution of E-J2 crossover differences before (blue curve) and after (red curve) orbit error adjustment.

6. Method of Envisat orbit improvement from cross over point analysis

Envisat (E) orbit error was reduced using the cross over differences with Jason-2 (J2). We used the method developed by Le Traon et al. (1995a,b) and Carnochan et al. (1995) to improve ERS-1/2 orbits using the cross over differences with T/P (Le Traon et al. 1995a,1998; Carnochan et al. 1995).

This method consists in a global minimisation of the differences in the measured sea surface topography between Envisat and Jason-2 at cross over points. It takes advantage of the very precise orbit of Jason-2 to evaluate and correct the Envisat orbit error at their oceanic cross over points. Smoothing cubic spline functions are then used to interpolate the Envisat orbit error along the Envisat tracks and estimate a continuous Envisat orbit error, which can be applied over coastal or terrestrial surface waters (for a detailed description of the method see Le Traon et al. (1995a)).

The method was applied to the cycles 71 to 93 of Envisat. Over this period (from the 5th of August 2008 to the 19th of October 2010) Envisat was kept on the same 35 day repeat cycle orbit and Jason-2 on the same 9.9156 day repeat cycle orbit. This is unlike Jason-1, whose orbit was changed on mid-February, 2009. For this reason we chose Jason-2 rather than Jason-1 as the reference mission to correct Envisat orbit errors. It enables us to keep a stable common reference over the 24 cycles of Envisat (cycle 71 to 93).

We used the reprocessed Envisat-B (ENVISAT RA-2/MWR Product Handbook, Issue 2.2, 2007) and Jason-2 GDRC data (OSTM/Jason-2 Products Handbook, Issue 1.4, 2009) that are enhanced, validated and distributed by the CTOH at Legos. To get the most homogeneous sea level height measurements between Envisat and Jason-2, we corrected both datasets for ocean tides (and the induced tidal loading) with the FES model (Lyard et al. 2004), for barotropic ocean response to wind and surface pressure forcing using the MOG2D barotropic model (Carrere and Lyard., 2003) and for the SSB with the non-parametric SSB from CLS (Labroue[9] et al. 2006). As the Envisat radiometer band S module is lost since January 2008, there is no measurement of the ionospheric correction by the radiometer available for Envisat. Instead we used the IC from the GIM model (Harris et al. 1999). For homogeneity, the same correction was applied to the Jason-2 dataset. For all other geophysical corrections (ET, PT, orbit WTC and DTC) we applied the corrections recommended in the Envisat Product Handbook (Envisat RA-2/MWR Product Handbook, Issue 2.2, 2007, Issue 2.2, 2007) and the Jason-2 Product handbook (OSTM/Jason-2 Products Handbook, Issue 1.4, 2009).

As in Le Traon et al. (1995a,b) and in Le Traon and Ogor (1998) we only used E-J2 cross-over differences over the deep ocean (deeper than 2000m) where the highest quality data is available. To ensure that E-J2 cross-over differences give an orbit error estimation of Envisat and do not include too much oceanic signal, only E-J2 crossovers with time differences less than four days were considered.

Before this large-scale orbit error adjustment the mean E-J2 cross-over differences for the 23 cycles (cycle 71 to 93) is 0.0520 cm and their standard deviation (rms) is 5.1 cm. After the orbit correction, the mean is 0.0003 cm and their standard deviation is 4.2 cm, which is similar to the standard deviation of the J1-J2 crossover differences over the same period (4.0 cm). Figure 7 shows the latitudinal distribution of E-J2 crossover differences before and after the orbit adjustment during the 23 cycles of Envisat. Before the orbit correction, the crossover differences

[9] Labroue, S., Gaspar, P., Dorandeu, J., et al. Overview of the Improvements Made on the Empirical Determination of the Sea State Bias Correction in 15 years of progress in radar altimetry Symposium, Venice, Italy, 2006

Cycle/Track	10	223	554	767
71	-2.43	-1.95	1.44	-2.04
72	-0.18	-0.57	1.33	1.66
73	4.40	-0.91	-0.28	0.80
74	-3.1	-3.5	-1.23	0.04
75	-0.22	4.75	-1.18	-4.14
76	4.66	NA	NA	NA
77	0.25	-4.99	-2.63	1.41
78	6.79	7.73	3.56	0.24
79	NA	4.36	-0.74	4.78
80	4.77	3.72	5.13	3.07
81	0.85	-1.43	-2.19	-3.73
82	-1.46	-0.39	-0.50	-3.11
83	-6.70	-3.25	0.36	-1.86
84	1.61	-0.96	-2.69	0.08
85	1.41	-1.65	-2.21	-2.72
86	4.15	0.92	-3.01	-1.45
87	0.61	-1.92	-3.51	2.44
88	0.01	NA	NA	0.06
89	4.68	-0.73	-0.59	-4.58
90	-1.39	1.81	-4.64	-4.59
91	1.18	0.002	-3.23	-0.97
92	-3.09	-0.25	-3.34	-2.96
93	1.83	-1.14	-1.59	-1.45

Table 4: Orbital error for each cycle and for each track over Lake Issykkul (in cm)

show large values particularly in the southern ocean and at high latitude in the northern hemisphere. After the orbit correction, crossover differences are smaller for all latitudes. Large values are only observed at latitudes where regions of high oceanic variability can be found (between -30 and -70 degrees south, where there is the Antartic Circumpolar current, Brazil-Malvinas confluence area and the Agulhas current and between 30 and 50 degrees north, near the Gulf stream and the Kurushio currents).

The use of cubic spline functions to interpolate the Envisat orbit error along the Envisat track allows us to estimate a continuous Envisat orbit error at each Envisat position and not only at the crossover points with Jason2. When computed over the 23 cycles of Envisat the orbit error shows some variability largely dominated by the one-cycle-per-revolution and the two-cycles-per-revolution frequencies. Besides these large scale frequencies, some higher frequencies can be observed but of smaller amplitude. Over the 23 cycles, the mean estimated Envisat orbit error is 0.186 cm and its standard deviation is 2.68cm.

Now we can deduce the Envisat orbit error over the Lake Issykul. Given the large scale variations that dominate the orbit error (~44000 km along track for the one-cycle-per-revolution and ~22000 km along track for the two-cycle-per-revolution) we can consider its value over the Lake Issykul to be constant during each flying over of Envisat. For each cycle, Envisat flies over Lake Issykul four times, during the tracks 10, 223, 554 and 767. Table 4 shows for each Envisat cycle and track the estimated orbit error. The mean of Envisat orbit error over the Lake Issykul during the 23 cycles is -0.10 cm and its standard deviation is 2.8 cm.

We could have compared the water height of Lake Issykkul, deduced from the altimeter data with a corrected orbit with In Situ measurements in order to detect improvement from the orbital correction. However since the orbit error correction is only of 2-3 cm level (calculated over over Lake Issykkul for cycles 71 to 93), the In Situ data are not accurate enough due their time sampling, which does not allow us to estimate the seiche effect. Indeed we have demonstrated in Crétaux et al. (2011) that errors in the In Situ measurement can reach up to 10 cm due to this effect (see also Figure 1).

7. Absolute bias of Envisat mission. Results and discussions

The absolute bias of the Envisat altimeter has been estimated from the two RDV in September 2009 (cycle 82, over the track number 223) and in September 2010 (cycle 92, over the track 767). The procedure to calculate water height above the reference ellipsoid (WGS-84) from altimetry is given by Eq. 1 (Section 4). The procedure to calculate water height from the GPS PPP method described in section 5 has been used over the two altimeter tracks for the two RDV. All of the height antenna corrections as described in section 5 have been applied. The absolute altimeter bias is simply the average difference between both series of water height (from altimetry and GPS data), with data selection made at the exact RDV between the vessel and Envisat (we used ship the data over a 5 km distance centered on the RDV to calculate the altimeter bias).

The calculation has been done for different cases. We have tested the three type of orbits (from GDR-B, GDR-C and using cross-over orbit corrections) for the calculation of absolute altimeter bias. The aim is to determine which orbit allows the most coherent bias which is calculated independently with data on cycle 82 and track 223, and cycle 92 and cycle 767.

	GRD-B	GDR-C	Cross-Over analysis
Cycle 82 (cm)	64.8	66.8	65.3
Cycle 92 Float Amb (cm)	61.8	62.6	64.8
Cycle 92 Fix Amb (cm)	59.8	60.6	62.8
Average bias (cm)	62.1 (+/-3.7)	63.4(+/-3.7)	64.3 (+/-3.7)

Table 5: Envisat Altimeter bias (in cm) for cycle 82, Cycle 92 (with fixed and floating GPS ambiguities calculation), and averaged bias. All calculation made with WTC inferred from GPS data at fixed stations.

From Crétaux et al. (2009) we have seen that the *Ice-1* retracker is more precise than the *ocean* retracker for Lake Issykkul. From Crétaux et al. (2009, 2011) we estimated the absolute bias between the two retracker's algorithms (*Ice-1* minus *Ocean*) which *was* equal to 25 and 23.4 cm respectively. This difference is due to the physical quantity retracked by both algorithms. *Ocean* is retracking the two-way travel time on the rising front of the waveform (Legresy et al. 1997). This procedure is supposed to catch the range for the very nadir point and the time tracked by this way is rather independent of the energy arriving late to the onboard reception device. In contrast, the *Ice-1* algorithm performs a mean of the reception times, weighted by the energy amplitude. This algorithm proves very robust for non-standard waveforms such as those frequently encountered over continental waters (Frappart et al. 2006). In this study we have again calculated the absolute bias for the water height of Lake Issykkul inferred from *Ice1* and *Ocean* retrackers. We obtained similar results with the previous studies (23.6 cm) which indicates that this bias is not depending on the satellite mission, and also does not drift in time. Figure 8a and 8b show the water height variations obtained from both Ice1 and *Ocean* retrackers compared to GPS data processing for cycles 82 and 92 respectively. We see from those figures that the retrackers did not significantly influence the noise of the altimeter bias calculation. Here we propose a new estimation of the altimeter bias of Envisat based on the measurements over Lake Issykkul from the *Ice-1* algorithm. All results for the *Ocean* retracker can be simply inferred from these results knowing *Ice-1* / *Ocean* relative bias: 23.6 cm.

a)

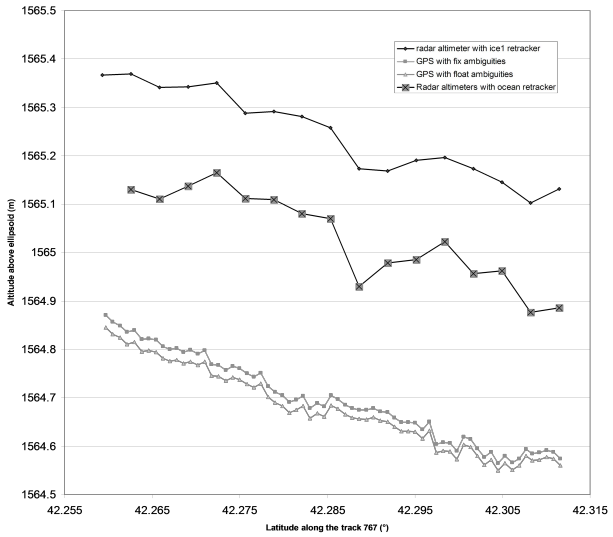

b)

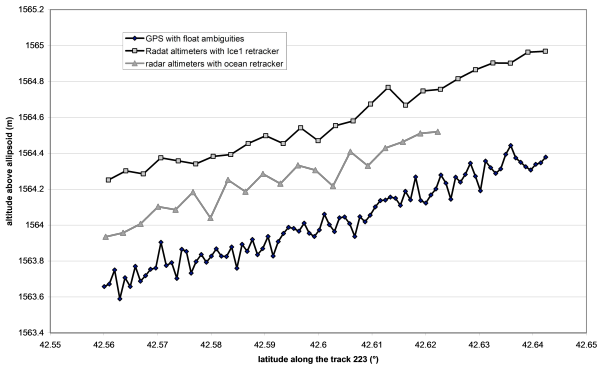

Fig. 8: (a) Water heights above ellipsoid from: Envisat altimeter measurement over the track 767 at the RDV in September 2010, and GPS antenna onboard the Storm boat with fix and floating ambiguities in PPP (b) Water heights above ellipsoid from: Envisat altimeter measurement over the track 223 at RDV in September 2009, and GPS antenna onboard the Multur boat with floating ambiguities in PPP. Calculation has been done with *Ice-1* and *Ocean* retrackers

For the altimetry data processing, we have used the WTC correction deduced from the GPS measurements on the shoreline as described in section 4.7. The differences of WTC estimated from GPS and WTC from the model was 1 cm for cycle 92 and 6 cm for cycle 82. Finally we have calculated the GPS positions of the antenna onboard the vessel in the two mode of calculation, with fix and floating ambiguities. Unfortunately, it has been possible only for the cycle 92.

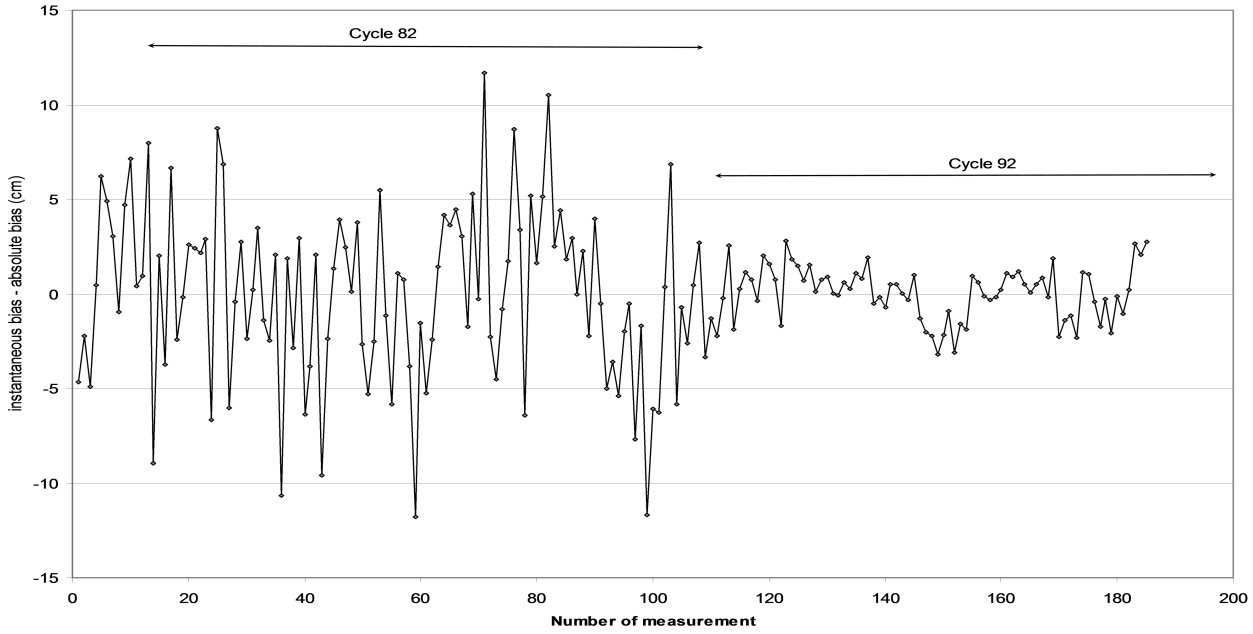

Fig. 9: Differences of instantaneous absolute altimeter biases at each point along the track for the RDV in September 2009 and 2010 with the average absolute biases estimated for each campaign.

Figure 8 shows the water heights of Lake Issykkul along the satellite track and from the GPS antenna on the Vessel, plotted for the RDV with cycle 92, with the two mode of PPP (with fix and floating ambiguities). The bias calculated is given in Table 5

We observe a quite good stability of the GPS solution with respect to the altimetry. This is particularly illustrated by the standard deviation of the altimeter bias (3.7 cm), which is better than in previous studies: 5 cm in Crétaux et al. (2009). We also note that the calculation done in PPP with fix and floating ambiguities show a difference of 2 cm (Table 5 and Figure **5**).

From Figure 9, we also observe that the standard deviation of the bias calculated from cycle 82 and 92 have different qualities. The left part of the figure represents the bias at each measurement point along the track (altimetry minus GPS) with the average bias calculated for cycle 82, while the right part corresponds to cycle 92. For an unknown reason, the dispersion of the biases is much better (1.4 cm to compare to 4.4 cm) with cycle 92 than for cycle 82. For cycle 82, only floating ambiguities have been used, which may be part of the explanation.

Table 5 gives us a first estimation of the quality of the orbit used. Since we have calculated the Envisat altimeter bias for two different cycles over two different tracks, and since we have used vertical positions of Envisat from different products (GDR-B, GDR-C and from our own cross-over orbit corrections) we might from It is given by the differences of the bias observed in each case for cycle 82 and cycle 92. It turns out that GDR-B and GDR-C are close together with a difference of Envisat altimeter bias of about 3 to 4 cm for the case where float ambiguities PPP has been used and 5 to 6 when fix ambiguities has been used for cycle 92. Unfortunately, without the possibility of fixing the ambiguities for cycle 82 we cannot conclude on the question of GPS mode of computation. When we have used the orbit correction from the cross-over analysis (see section 6) the difference of the Envisat altimeter bias between cycle 82 and 92 has been reduced to less than one cm in with the floating ambiguities case and 2.5 cm with fix ambiguities (to be compared to 3 to 6 cm with the GDR-B and GDR-C). It is obviously too premature to conclude on the quality of our cross-over analysis based on two tracks of Envisat, but these results are promising. A better way to confirm the accuracy of these orbital corrections would be to compare water height variations over a wide range of

continental lakes with In Situ data. This is the aim of a further study.

In comparison to the previous study by Crétaux et al. (2009) we can also note that the Envisat altimeter bias has been significantly modified. For the *Ice-1* retracker we had obtained 72.4 +/-4.8 cm, to be compared with 62.1 to 64.3 +-3.7 cm from this study. We assume that the different evolutions of the C/V procedure setup on this study have led to this improvement with a new mode of GPS point positioning, a better estimation of the antenna height, a better estimation of the atmospheric corrections for altimetry, and a calculation of the bias during the RDV only. This has led to a more precise estimation of the bias with a reduced standard deviation.

8. Conclusions and perspectives

Lake Issykkul is a suitable natural target for radar altimetry multi-satellite C/V, for past missions (T/P, GFO, Envisat, Jason-1 and Jason-2) and future (SARAL/Altika, Jason-3, Sentinel-3, Jason-CS and SWOT). C/V sites over lakes present the advantages to firstly all reduce the source of errors in the absolute altimeter bias computation (lower tides, water dynamic topography, Barometric Pressure, SSB), and secondly to make a quality assessment of this technique for the study of continental waters. In particular, it allows us to quantify errors in the corrections due to radar propagation in the atmosphere, and to cross compare the different retracking algorithms of the wave form and to calculate their respective relative biases.
First campaigns over Lake Issykkul were made in 2004 and 2005. Since 2008 four new campaigns were carried out in the framewotk of the Jason-2 project. Results of the two first campaigns were presented in Crétaux et al. (2009) for estimating the absolute altimeter bias of T/P, Jason-1, GFO and Envisat. From two campaigns made in February and September 2009 we have calculated the absolute bias of Jason-1 and Jason-2 (Crétaux et al. 2011). The results of the campaigns carried out in September 2009 and 2010 are presented in this article for a new computation of the Envisat altimeter bias.

The principal reason to calculate an Envisat absolute altimeter bias is to allow for the continuity with further mission on the same orbit, principally SARAL/Altika, which should be launched in 2012. For hydrology in particular it is essential to calculate long term (multi-decadal) water level time series, in order to catch eventual worldwide climate change effects on lakes. Continuity can be obtained if during a certain period of time (few months) the satellites are in the same orbit in a so-called tandem phase, as it has been done for T/P with Jason-1 (9 months in 2002) and then Jason-1 with Jason-2 (8 months in 2008). In the case of the Envisat / SARAL/Altika continuity, unfortunately, it has not been possible, and at least a one and half year will separate the last repeat cycle of Envisat with the first one of SARAL/Altika. The same C/V operation will be performed over Lake Issykkul when this satellite will be launch, therefore allowing the relative bias between both satellites to be calculated.

An improved absolute altimeter bias is also possible using the 7 fields campaigns from 2004 to 2011 where new In Situ instruments have been progressively installed around the lake, making it a good multi satellite C/V. From one campaign to another one, new problems have been identified and solutions have been developed in order to improve the precision and accuracy of the calculation.

Several aspects have been modified, that have been largely described in this article. We might highlight: the GPS data processing, the new antenna height calculations, the improved orbit estimates for Envisat, and the improved geophysical corrections.

This has allowed us to propose a new absolute bias of the Envisat radar altimeter, which is significantly lower than the first estimation proposed in Crétaux et al. (2009) and Faugere et al. (2006). The absolute bias of Envisat radar altimeter made with the *Ice-1* retracker, is between 62.1 and 64.3 +/-3.7 cm, to be compared with previous estimations, all higher than 72 cm with standard deviations of about 5 cm. From results of previous studies, we might also conclude that the absolute bias, when using the *ocean* retracker algorithm, is between 37.1 and 40.9 cm instead of values between 46.9 and 51.2

cm (Cretaux et al. 2009). This large relative bias observed for different algorithms also indicates that it is not appropriate to mix algorithm in a single processing for lakes and rivers monitoring from radar altimetry without, taking into account this local relative bias.

These Envisat results do not have the higher precision needed by the "ocean" community (for which the millimetre level is required) but we think that it may be useful to "inland water" community, for which when the first measurements of SARAL/Altika will be available, the continuity with Envisat will be essential and possible from the results presented in this article.

In this study we also have used new modes of calculation for the GPS vertical position of the ship, which is particularly interesting when it cruises far from the shoreline where we have installed fix GPS stations. Indeed, from the PPP mode of calculation, which is still under investigation in other articles (Fund et al. submitted), the gain with respect to double difference data processing (strongly dependant on the length of the baseline), could be significant. For short baseline <10 km) double difference still provides better results but for our experiments on Lake Issykkul, we principally have used GPS height profile at least 10 km away from the shoreline where our SA were installed. Moreover, it allows to process kinematic GPS data when no fix station is operating.

This will be developed in further studies to establish a mean Lake Issykkul surface from synergy of laser and radar altimetry and GPS vertical profile from all of the campaigns. In 6 different cruises, we have covered the whole lake in different routes, (to join for example one satellite track to another) and the network of GPS point positioning on the lake is now very dense.

The currently available global models are not accurate in remote areas like Lake Issykkul to provide the short wavelength undulations of the local geoid. For example over this lake, the errors of geoid may reach decimetre level. We expect that the establishment of a mean lake surface at high spatial resolution, merging the satellite data and GPS data of each campaign, will allow to provide the "gravity" community, an accurate element to validate different updated models of the gravity field. This will be the object of a further study and will also benefit from improvement in GPS data processing.

From this study, we have also implemented corrections on the orbit of Envisat, based on cross-over analysis with Jason-2 over the ocean. This has led to corrections of up to 10 cm, depending on the cycle of the Envisat orbit. Further analysis (from comparison with In Situ precise data over several lakes in different regions of the Earth) are still needed, but from this study on Lake Issykkul, the coherence of the altimeter biases obtained from 2 different campaigns, in September 2009 and September 2010, has been improved by a factor of at least 2.

One of the remaining high error sources in the C/V still remains in the WTC corrections. We have decided in this study to use WTC deduced from GPS data processing on the fix point on the shoreline, which have presented non negligible differences with the usual model provided in the GDRs. The radiometer instrument is limited in precision in such inland region. However we still suspect that this should be improved in the future. No ideal solution exists yet for this problem. In the future the model of S. Brown will be tested over Lake Issykkul with SARAL/Altika and Jason-2, thanks to deployment of a regional network of fix GPS stations in the next 2-3 years. Actually there is a permanent GPS receiver south of the lake, but still far from the lake (by more than 10 km), and for validating of the model of S. Brown for this lake, permanent GPS stations on the shoreline must be deployed.

List of Acronyms

AC: Analysis Center

CLS: Collecte Localisation Satellite

CNES: Centre National d'Etudes Spatiales

CTOH: Centre de topographie des Océans et de l'Hydrosphère

C/V: Calibration / Validation

ET: Earth Tide

DTC: Dry Tropospheric Correction

GDR: Geophysical Data Records

GIM: Global Ionospheric Maps

GMF: Global Mapping Function

GPT: Global Pressure and Temperature

GRGS: Groupe de Recherche de Geodesie Spatiale

HA: Height Antenna

IC: ionospheric Correction

IGS: International GNSS Service

ISRO: Indian Space Research Organization

ITRF: International Terrestrial Reference Frame

IWPH: Institute of Water Problem and Hydropower

LT: lake Tide

MSB: Model from Shannon Brown (for WTC)

PPP: Precise point positioning

PT: pole Tide

RDV: RenDez Vous

SA: Static antenna

SSB: Sea State Bias

SWH: Significant Wave Height

SWOT: Surface Water and Ocean Topography

T/P: topex / Poseidon

WTC: Wet Tropospheric Correction

ZTD: Zenital Tropospheric Delay

Acknowledgements

This work has been supported by the Centre National d'Etudes Spatiales (CNES) in the frame of the TOSCA program. The altimetry data are downloaded from the CTOH at Legos. We thus gratefully acknowledge the CNES and the CTOH. We dedicate this article to the crews of the Multur and the Storm in Cholpon Ata and the team of Kyrgyz colleagues from Kyzyl Suu who host and maintain our instrumentation. We also dedicate this article to Gulia, with whom we now work for about 7 years in Cholpon Ata, for her hospitality.

References

Altamimi, Z., Collilieux X., Legrand J., et al. ITRF2005: A new release of the International Terrestrial Reference Frame based on time series of station positions and Earth Orientation Parameters, J. Geophys. Res., 112, B09401, doi:10.1029/2007JB004949, 2007.

Berry, P. A. M., Freeman, J.A., Smith, R.G., et al. "Near Real Time Global Lake and River Monitoring using the Envisat RA-2," in Proceedings Envisat Symposium 2007, Montreux, Switzerland, ESA SP-636, 2007.

Bertiger W., Desai S., Haines B., et al. Single receiver phase ambiguity resolution with GPS data, J. Geod., 84, 5, 327-337, DOI: 10.1007/s00190-010-0371-9, 2010.

Birkett, C.M. The contribution of TOPEX/POSEIDON to the global monitoring of climatically sensitive lakes, *J. Geophys. Res. [Oceans]* **100**(C12), 25179–25204, 1995.

Birkett, C.M., Beckley, B. Investigating the performance of the Jason- 2/OSTM Radar Altimeter over Lakes and Reservoirs, Marine Geod., 33 (S1), 204-238, 2010.

Birkinshaw, S.J., O'Donnell, G.M., Moore, P., et al. Using satellite altimetry data to augment flow estimation technique on the Mekong River, Hydrol. Process. 24, 3811-3825, 2010.

Boehm, J., Niell, A., Tregoning, P., et al. The Global Mapping Function (GMF): A new

empirical mapping function based on numerical weather model data, Geophys. Res. Lett., 33, L07304, doi:10.1029/2005GL025546, 2006.

Boehm J., Heinkelmann R . Schuh H. A global model of pressure and temperature for geodetic applications, J. Geod., doi:10.1007/s00190-007-0135-3, 2007.

Bonnefond P., Exertier P., Laurain O., et al. Absolute calibration of Jason-1 and Topex / poseidon Altimeters in Corsica, Mar. Geod., 26 (S3-4), 261-284, 2003.

Bonnefond P., Exertier P., Laurain O., et al. Absolute Calibration of Jason-1 and Jason-2 Altimeters in Corsica during the Formation Flight Phase, Marine Geod., 33 (S1), 80-90, 2010.

Bouin M-N, Ballu, V., Calmant, S., et al. A kinematic GPS methodology for sea surface mapping, Vanuatu, J. Geod., 83, 1203-1217, doi 10.1007/s00190-009-0338-x, 2009.

Brown, S. A Novel Near-Land Radiometer Wet Path-Delay Retrieval Algorithm: Application to the Jason-2/OSTM Advanced Microwave Radiometer, Geoscience and Remote Sensing, IEEE Transactions, 48, 4, 1986-1992, doi: 10.1109/TGRS.2009.2037220, 2010.

Calmant S., Seyler, F., Crétaux, J-F. Monitoring Continental Surface Waters by Satellite Altimetry, Survey in Geophysics, 29 (S4-5), 247-269, 2008.

Carnochan, S., Moore, P. Ehlers, S. ERS-1 radial positioning refinement by dual crossover analysis with TOPEX/POSEIDON. Adv. Space Res. 16, 119-122, 1995.

Carrere L., Lyard F. Modeling the barotropic response of the global ocean to atmospheric wind and pressure forcing - comparisons with observations. Geophysical Res. Lett. 30, 6, 1275, doi:10:1029/2002GL016473, 2003.

Cartwright, D. E. , Tayler, R.J. New computations of the tide-generating potential,Geophys. J. R. Astr. Soc., 23, 45-74, 1971.

Cerri, L. , Berthias, J. P. , Bertiger, W. I. , et al. Precision Orbit Determination Standards for the Jason Series of Altimeter Missions, Marine Geod., 33 (S1), 379-418, doi: 10.1080/01490419.2010.488966, 2010.

Cheng, K-C., Kuo, C-Y., Tseng, H-Z., et al. Lake surface height Calibration of Jason-1 and Jason-2 over the Great Lakes, Marine Geod., 33, (S1), 186-203, 2010.

Collins, P., Bisnath, S., Lahaye, F. et al. Undifferenced GPS Ambiguity Resolution Using the Decoupled Clock Model and Ambiguity Datum Fixing, J. Inst. Navigat., 57, 2, 123-135, 2010.

Crétaux, J-F., Birkett. C. Lake studies from satellite altimetry, C R Geoscience, doi: 10.1016/J.cre.2006.08.002, 2006.

Crétaux, J-F., Calmant, S., Romanovski, V., et al. An absolute calibration site for radar altimeters in the continental domain: Lake Issykkul in Central Asia, J. Geod., 83, 723-735 DOI: 10.1007/s00190-008-0289-7, 2009.

Crétaux, J-F., Calmant, S., Romanovski V., et al. Absolute Calibration of Jason radar altimeters from GPS kinematic campaigns over Lake Issykkul, Marine Geod., 34 (S3-4),291-318, 2011.

Dow, J.M., Neilan, R. E., Rizos, C. The International GNSS Service in a changing landscape of Global Navigation Satellite Systems, J. Geod., 83, 191–198, doi: 10.1007/s00190-008-0300-3, 2009

Faugere, Y., Dorandeu, J., Lefevre, F., et al. Envisat Ocean altimetry Performance Assessment and Cross Calibration, sensors, 6, 100-130, 2006.

Frappart F., Calmant, S., Cauhopé, M., et al. Preliminary results of Envisat RA-2-derived water levels validation over the Amazon basin, Remote sensing of Environment, 100, 252-264, 2006.

Fund F., Perosanz, F., Testut, L., et al. Integer Precise Point Positioning Technique for Sea

Surface Observations Using a GPS Buoy, submitted to Ad. Space Res., 2012.

Gaspar P., Labroue, S., Ogor, F., et al. Improving nonparametric estimates of the sea state bias in radar altimeter measurements of sea level, J. Atmos. & Oceanic Tech. 19, 1690-1707, 2002.

Ge, M., Gendt, G., Rothacher, M., et al. Resolution of GPS carrier-phase ambiguities in precise point positioning (PPP) with daily observations. J. Geod., 82, 389-399, doi: 10.1007/s00190-007-0187-4, 2007

Geng, J., Meng, X., Dodson, A. et al. Integer ambiguity resolution in precise point positioning: method comparison, J. Geod., 84, 569–581, doi 10.1007/s00190-010-0399-x, 2010

Haines, B.J., Dong, D., Born, G.H., et al. The Harvest Experiment : Monitoring Jason-1 and Topex / Poseidon from California Offshore Platform, Mar. Geod., 26 (S3-4), 239-259, 2003.

Haines, B.J., Desai, S.D., Born, G.H. 'The Harvest Experiment: Calibration of the Climate Data Record from TOPEX/Poseidon, Jason-1 and the Ocean Surface Topography Mission', Mar. Geod., 33 (S1), 91-113, 2010.

Harris, B.A., Ho, I.L., Lindqwister, C.M., et al. Automated daily process for global ionospheric total electron content maps and satellite ocean altimeter ionospheric calibration based on Global Positioning System data, Journal of Atmospheric and Solar-Terrestrial Physics, 61, 1205-1218, 1999.

Jan, G., Menard, Y., Faillot, M., et al. Offshore absolute calibration of Space born radar altimeters, Mar. Geod., 27, (S3-4), 615-629,2004.

Lambin, J., Morrow, R., Fu, L.-L., et al. 'The OSTM/Jason-2 Mission', Marine Geod., 33 (S1), 4-25, DOI: 10.1080/01490419.2010.491030, 2010

Laurichesse, D., Mercier, F., Berthias, J-P., et al. Integer Ambiguity Resolution on Undifferenced GPS Phase Measurements and Its Application to PPP and Satellite Precise Orbit Determination. NAVIGATION, 56, 2, 135-149, 2007.

Legresy B., Remy, F. Surface characteristics of the Antartic ice Sheet and altimetric observations, J. of Glaciology, 43, 144, 197-206, 1997.

Le Traon, P.Y. Ogor, F. ERS-1/2 orbit improvement using TOPEX/POSEIDON: the 2cm challenge. J. Geophys. Res., 103, 8045-8057, 1998.

Le Traon, P.Y., Gaspar, P., Bouyssel, F., et al. Use of TOPEX/POSEIDON data to enhance ERS-1 data. J. Atmos. Oceanic technol., 12,161-170, 1995a.

Le Traon, P.Y., Gaspar, P., Ogor, F., et al. Satellites work in tandem to improve accuracy of data. EOS Trans. AGU 76(39)385-389, 1995b.

Loyer, S, Perosanz, F., Mercier, F., et al. Zero-difference GPS ambiguity resolution at CNES-CLS IGS Analysis Center, in press, J. Geod., 2012.

Lyard, F., Lefebre, F, Letellier, T., et al. Modeling the global ocean tides: modern insights from FES2004. Ocean dynamics, 10.1007/s10236-006-0086-x, 2004.

Martinez-Benjamin, J.J., Martinez-Garcia, M., Gonzalez Lopez, S., et al. Ibiza absolute calibration experiment: survey and preliminary results, Mar. Geod., 27 (S3-4), pp 657-681, 2004

Marty JC., Loyer S., Perosanz, F., et al. GINS : the CNES/GRGS GNSS scientific software, 3rd International Colloquium Scientific and Fundamental Aspects of the Galileo Programme, ESA Proceedings WPP326, 31 August - 2 September 2011, Copenhagen, Denmark, 2011

Mertikas, S.P., R.T. Ioannides, R.T., Tziavos, I.N., et al. Statistical Models and Latest Results in the Determination of the Absolute Bias for the Radar Altimeters of Jason Satellites using the Gavdos Facility, Marine Geod., 33 (S1), 114-149, 2010

Pavlis E.C., Stelios, P., Mertikas, P., et al., The Gavdos mean sea level and altimeter calibration facility: Results for Jason-1, , Mar. Geod., 27 (S3-4), 631-655, 2004.

Petit, G., Luzum B., (eds.). IERS Conventions (2010), IERS Technical Note No. 36, 2010

Ricko, M., Carton, J., Birkett, C. Climatic Effects on Lake Basins. Part I: Modeling Tropical Lake Levels, J. Clim., 24, 2983-2999, doi: 10.1175/2010JCLI3602.1, 2011.

Saastamoinen, J. Atmospheric correction for the troposphere and stratosphere in radio ranging of satellites, Geophys. Monogr, 15, American Geophysical Union, Washington DC, 1972.

Shum, C.K., Yi, Y., Cheng, K., et al. Calibration of Jason-1 Altimeter over lake Erie, Mar. Geod., 26 (S3-4), 335-354, 2003.

Watson, C., White, R.N., Coleman, R., et al. R.,Topex / Poseidon and Jason-1: Absolute Calibration in Bass Strait, Australia, Mar. Geod., 27 (S3-4), 107-131, 2004.

Watson, C., White, R.N., Church, J., et al. Absolute Calibration in Bass Strait, Australia : TOPEX, Jason-1 and OSTM/Jason-2, Mar. Geod., 34, 242-260, 2011.

Depth-dependent temperature change contributions to global mean thermosteric sea level rise from 1960 to 2010

W. Llovel[(1)], I. Fukumori[(1)] and B. Meyssignac[(2)]

(1) CALTECH, Jet Propulsion Laboratory, Pasadena, USA
(2) LEGOS/CNES, OMP, Toulouse, France

Abstract
The dependency of global mean thermosteric sea level changes to temperature at different depths is investigated from 1960 to 2010 using two separate gridded temperature data sets and an ocean general circulation model. Good agreements are found among the thermosteric sea level changes inferred by the temperature datasets and the model, especially for the upper oceanic layer (down to 300m depth). The evolution of thermosteric sea level change is further studied and compared with reconstructed estimates of sea level change. Thermosteric changes of the upper layer are especially in good agreement with reconstructed sea level estimates. A 22-year lag is found between thermal anomalies of the upper (0-300m) and lower (300-700m) layers in the historical temperature data sets, which is not resolved by the numerical model. This model-data discrepancy suggests either a deficiency of the numerical model or an artifact of changes in the observing system.

1. Introduction

Sea level rise is one of the most important consequences of global warming. Understanding causes of sea level rise is one of the most important goals of climate research. The last Intergovernmental Panel on Climate Change-4th Assessment Report (IPCC-AR4) notes that global mean sea level rose at a rate of 1.8 +/- 0.5 mm/yr (2-sigma uncertainty) over 1961-2003 of which 0.42 +/- 0.12 mm/yr is ascribed to thermal expansion of the ocean and 0.69 +/- 0.46 mm/yr is attributed to additional freshwater added to the ocean from melting ice sheets and mountain glaciers. From 1993 to 2003, based on satellite altimetry data, sea level rose at a rate of 3.1 +/- 0.7 mm/yr (2-sigma uncertainty) with 1.6 +/- 0.5 mm/yr being attributed to thermal expansion and 1.19 +/- 0.42 mm/yr coming from continental water mass input (Bindoff et al., 2007). Thermal expansion estimates over 1993-2003 are nearly twice of that over the past four decades. Over the entire altimetry period starting in 1993, the rate of global mean sea level rise amounts to 3.3 +/- 0.4 mm/yr (e.g., Ablain et al, 2009; Nerem et al, 2010; considering 1-sigma uncertainty) of which 1 +/- 0.3 mm/yr is attributed to thermal expansion and 1.8 +/- 0.3 mm/yr to additional fresh water input (e.g., Cazenave and Llovel, 2010). These climatic contributions to sea level rise are not steady but fluctuate with time. Since the entire deployment of ~3000 Argo floats in 2004, a slowdown in steric sea level rise has been reported by many investigations (Willis et al., 2008, 2010; Levitus et al., 2009; Cazenave et al., 2009; Leuliette and Miller, 2009; Leuliette and Willis, 2011), although with a significant scatter among these estimates (Llovel et al., 2010), even while sea level has kept rising, however at lower rate than the whole altimetry period since 1993. Over 2004-2010 and using only Argo records, Llovel et al. (2011) investigated the behavior of steric sea level change at global and regional basin scales and temperature contributions to this change from different depths. A large amount of the steric and thermosteric signal is explained by changes in the upper oceanic layer (i.e., down to 300m depth) and a compensation is noticed between warming in the Indian Ocean and cooling of the Atlantic Ocean whereas the Pacific Ocean depicts large interannual variability (linked with El Nino Southern Oscillation -ENSO- events) associated with a small short-term trend.

In the present study, we investigate temperature change as a function of depth and its contribution to thermosteric sea level variations over a longer multi-decadal period (1960-2010) using different datasets (both in situ and numerical model outputs) at global scale. After a brief description of the different datasets used in this paper, we will present our results based on thermosteric mean sea level computed down to 700m depth and then, consider two different layers from the ocean surface to 300m depth and from 300m to 700m depth. For each layer, we compute associated contributions to thermosteric mean sea level changes and compare them with reconstructed mean sea level time series estimates provided by different research groups.

2. Datasets

2.1. Reconstructed Sea level data

Sea level estimates of Church and White (2011) (available at http://www.cmar.csiro.au/sealevel/sl_data_cmar.html website) and Meyssignac et al. (2012) that cover the periods 1880-2009 and 1950-2009, respectively, are employed in this study. Church and White (2011) reconstruct global sea level over 1880-2009 by combining 17-years of satellite altimetry data with available tide gauge stations that vary with time (see Church and White, 2011 for more details). Meyssignac et al. (2012) reconstruct the sea level over the past 60 years using the same reconstruction method as Church and White (2011) but employ only 91 tide gauge records with almost complete data coverage over 1950-2009. Furthermore, the latter reconstruction averages three different reconstructions based on principal modes of

variability inferred from satellite altimetry, a model-data synthesis and results of an ocean model simulation (see Meyssignac et al., 2012, for additional details). In this paper, we employ global mean sea level estimates from both estimates over 1960-2009.

2.2 Thermosteric sea level data

Thermosteric sea level is computed using in situ ocean temperature data from Levitus et al. (2009) and Ishii and Kimoto (2009) (hereinafter referred to as L09 and IK09 respectively). Since 1950, ocean temperature has been principally measured by mechanical bathythermographs (MBT) and after 1960 with expandable bathythermographs (XBT) along ship tracks, complemented by Conductivity- Temperature-Depth (CTD) systems. Then, XBT depth is deduced from a fall-rate equation and time elapsed since the probe entered the sea surface. Even with calibrated fall-rate equations (Hanawa et al. 1995), systematic depth errors are assumed to remain (Gouretski & Koltermann 2007). Both datasets are corrected for these XBT depth biases and are available every 3 months for L09 and monthly for IK09. These 2 datasets provide gridded temperature data over 16-depth levels from the surface to 700-meter depth on a global 1° x 1° grid from 1955 to 2010 (for L09 dataset) and from 1945 to 2010 (for IK09 dataset). We first compute density at each standard level to 700m depth by considering the temperature measurements and associated climatology data (both temperature and salinity climatologies are provided by the World Ocean Database –WOA09- website) using the standard equation of state of the ocean (Gill, 1982; Levitus et al., 2005; Lombard et al., 2005). The density anomalies, inferred by computing the difference between the density estimate (considering temperature data and salinity climatology) and the reference density defined here at fixed temperature and salinity (T=0°C and S=35 psu), are integrated vertically at each grid point and each time step to obtain corresponding thermosteric sea level anomalies.

We start our analysis from 1960 after which the data sets provide a near global coverage. Thermosteric sea level anomalies are computed over the whole depth (0-700m) but also as a function of depth from the surface to 300m depth and from 300m to 700m depth. We do not consider halosteric anomalies because of limited global salinity data coverage before the full Argo profiling float deployment around 2004. Unlike regional anomalies, salinity variations do not contribute to global mean steric sea level change (Wunsch et al., 2007).

2.3 GECCO outputs

We also estimate thermosteric sea level variations using temperature data from a synthesis of observations and an ocean general circulation model by the German partner of the Consortium for Estimating the Circulation and Climate of the Ocean (GECCO; Kohl and Stammer, 2008). The analysis provides temperature estimates on a 1°x1° grid from the surface to 5450m depth on 23 levels. Because GECCO depth levels differ from those of the gridded temperature data sets described above, we compute GECCO thermosteric sea level variations down to ~850m. GECCO estimates are based on in situ data assimilated with the MIT general circulation model forced by surface fluxes of the National Centers for Environmental Prediction (NCEP) reanalysis (Kalnay et al., 1996). We consider GECCO outputs over the whole time span covering 1952-2001 but here, we show results over the period of 1960-2001 that overlaps the other data sets previously described.

3. Results

3.1. Global analysis

Figure 1 shows mean thermosteric sea level anomalies (which are deduced when removing the temporal mean of the considered time series) between +/-65° of latitude based on L09 (blue curve) and IK09 (red curve) temperature data over 1960-2010. Annual and semi-annual signals have been removed by a least-square fit and a 1-year running mean is also applied to these curves. In the remainder of this paper, the

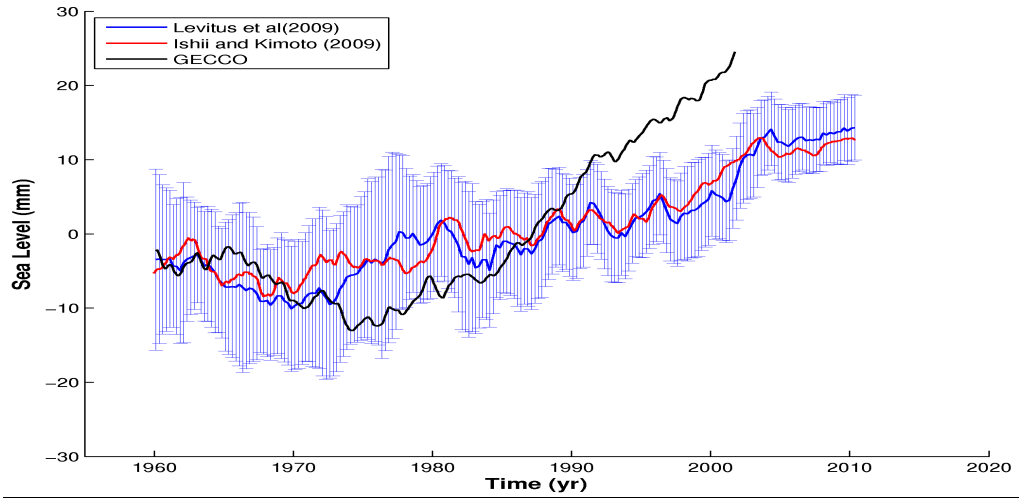

Figure 1: Global mean thermosteric sea level from gridded temperature data of Levitus et al. (2009) -blue curve with 1-sigma uncertainty-, Ishii and Kimoto (2009) -red curve- and from GECCO outputs -black curve-. Annual and semi-annual signal have been removed. A 1-year running mean has been applied.

same temporal filtering is applied to all the time series shown.

Uncertainties associated with the thermosteric sea level anomalies are estimated for L09 based on differences between observed temperature profiles and the gridded temperature data set. These differences represent estimates of gridded temperature errors due to interpolation and smoothing associated with forming the gridded estimate (some description of these fields can be found at ftp://ftp.nodc.noaa.gov/pub/WOA09/DOC/woa09documentation.pdf , Locarnini et al., 2009). These temperature errors are given on a global 1° x 1° grid and at each standard depth over 1955-2010. Thereby, we estimate the thermosteric sea level errors by computing density errors for each considered depth layers and grid points. Then, we propagate density errors when computing thermosteric sea level. So, we obtain error estimates at each grid point and each time steps. In our analysis, we assume that errors are Gaussian and spatially correlated within a 440 km radius of influence (the same radius is used during the interpolation method). The plotted error bars of time series in this paper represent 1-sigma uncertainty (~68% confidence interval).

The global mean thermosteric sea level time-series show a flattening for the most recent years that have been reported by several studies (Willis et al., 2008; Leuliette and Miller, 2009; Cazenave et al., 2009; Cazenave and Llovel, 2010; Llovel et al., 2010, Leuliette and Willis, 2011). Figure 1 shows good agreement in terms of trend between L09 and IK09 thermosteric sea level over 1960-2010. We also note good agreement in terms of interannual variability between these two previous curves especially after 1980. Furthermore, the red curve (based on IK09 temperature data) is almost always within 1-sigma uncertainty of the blue curve (based on L09 temperature data).

Figure1 also displays an estimate using GECCO-based temperature data (black curve) over 1960-2001. Before ~1990, GECCO-based thermosteric sea level is almost always within the 1-sigma uncertainty of the blue curve based on the L09 dataset. However, after ~1990, we note a large discrepancy between GECCO-based and observed thermosteric mean sea level anomalies, the first one being outside 1-sigma uncertainty of the blue curve. Furthermore, it is also worth noting that the GECCO-based thermosteric global mean sea level estimate does not reproduce the interannual variability observed in those inferred by L09 and IK09 temperature data.

	1960-2010	1993-2010	1960-2001	1993-2001
L09	0.42+/-0.1	0.92+/-0.27	0.29+/-0.13	0.54+/- 0.81
IK09	0.38+/-0.01	0.74+/-0.02	0.30+/-0.01	1.+/-0.06
GECCO	NA	NA	0.67+/-0.02	1.48+/-0.02

Table 1: Global mean thermosteric sea level trends computed over corresponded periods. Note that quoted error bars represent only linear least square fit for IK09 and GECCO. All quoted errors represent 1-sigma uncertainty (~68% confidence interval).

Table 1 summarizes the global mean thermosteric sea level trends computed over different time periods. Global mean thermosteric sea level trends, computed between +/-65° latitude, amount to 0.42+/-0.1 mm/yr and 0.38+/-0.01 mm/yr over 1960-2010 and to 0.29+/-0.13 mm/yr and 0.30+/-0.01 mm/yr over 1960-2001 based respectively on L09 and IK09 temperature data (note that the trend errors of L09 are more realistic than the other estimates which merely correspond to uncertainties of the least-square fit). These estimations agree quite well considering their uncertainties for both time periods. Over 1960-2001, GECCO-based thermosteric mean sea level amounts to 0.67+/-0.02 mm/yr. This value is much higher than observed thermosteric mean sea level trend considering their uncertainties. Therefore, GECCO does not reproduce the long-term trend inferred by observations.

For the last 2 decades, 1993-2010, global mean thermosteric sea level trends are larger than those during 1960-2010 and amount to 0.92+/-0.27 mm/yr and 0.74+/-0.02 mm/yr based on L09 and IK09 datasets, respectively. Over 1993-2001 for which GECCO also provides estimates for, the GECCO-based thermosteric sea level trend is 1.48+/- 0.02 mm/yr whereas the observed thermosteric sea level trends are 0.54+/-0.81 and 1.00 +/-0.06 from L09 and IK09 temperature data, respectively. The GECCO-based sea level trends are again much higher than observations.

To illustrate variations in the rate of global mean sea level rise, Figure 2 shows the thermosteric sea level rates as a function of time computed over successive 16-year periods for L09 (the blue curve), IK09 (the red curve) and GECCO outputs (the black curve). The observed thermosteric sea level rates computed using L09 and IK09 datasets are within 1-sigma uncertainty of each other and agree quite well. Although variations before 1960 are somewhat uncertain principally due to data distribution, the observed thermosteric sea level rates display a slight acceleration with time over the entire considered period. Nevertheless, this result should be interpreted with caution because of large associated uncertainties. In comparison, the GECCO-based thermosteric sea level rates have large discrepancies with observed thermosteric sea level rates that are larger than the error estimates.

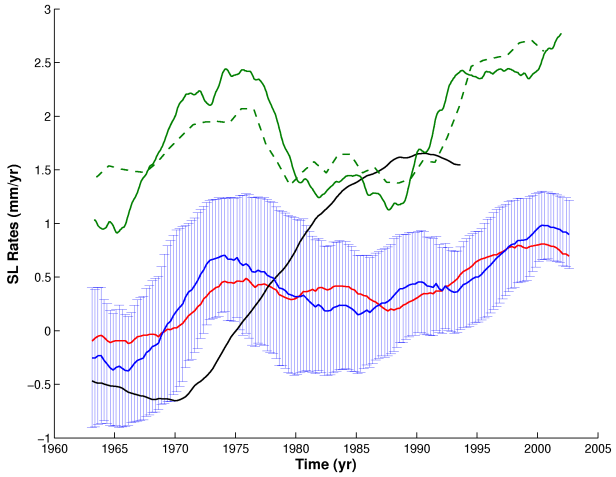

Figure 2: Linear trends in thermosteric sea level over successive 16 year periods for the global mean thermosteric sea level for Levitus et al. (2009) –blue curve with 1-sigma uncertainty-, Ishii and Kimoto (2009) –red curve- and GECCO outputs –black curve-. The green curves represent the reconstructed global mean sea level inferred by Church and White (2011) -solid green line- and Meyssignac et al. (2012) –dashed green line-.

Rates of global mean sea level change based on sea level reconstructions by Church and White (2011) and Meyssignac et al. (2012),

shown as solid and dashed green curves in Figure 2, respectively, display large decadal to multi-decadal variability as noted by Church and White (2011). These two reconstructed sea level curves agree quite well with each other even though amplitudes show some differences especially before 1980. The comparison of the rates of sea level rise between reconstructed sea level and thermosteric sea level shows an intriguing coherence in multi-decadal variability. The rate of sea level rise increased from the 1960s to 1975 as well as from 1990 to present but decreased in between. However, the rate in general and the amplitude of the multi-decadal variability are larger in the reconstructed sea level estimates than in the thermosteric sea level analyses. However, global mean thermosteric sea level rates are smaller than reconstructed sea level rates. Furthermore, thermosteric sea level rates do not entirely explain the reconstructed mean sea level rates over 1960-2010.

3.2 depth analysis

Temperature anomalies from different depths are further investigated to examine differences in their contribution to global mean thermosteric sea level changes. For this purpose, we consider 2 oceanic layers spanning 0-300m and 300-700m depths, respectively, from 1960 to 2010.

Figures 3a and b show the global mean thermosteric sea level contributions for temperature anomalies in the upper (0-300m, figure 3a) and lower (300-700m, figure 3b) layers based on L09 (blue curves with 1-sigma uncertainty) and IK09 (red curves) temperature data as well as those for the GECCO estimates (black curves).

As with net thermosteric sea level (Figure 1), estimates based on L09 and IK09 are consistent with each other for both layers (Figure 3). The upper oceanic layer (figure 3a) depicts a similar variation to the larger water column considered previously in Figure 1 (i.e., 0-700m depth). The upper layer contribution to thermosteric mean sea level increase starts in 1970 for both blue and red

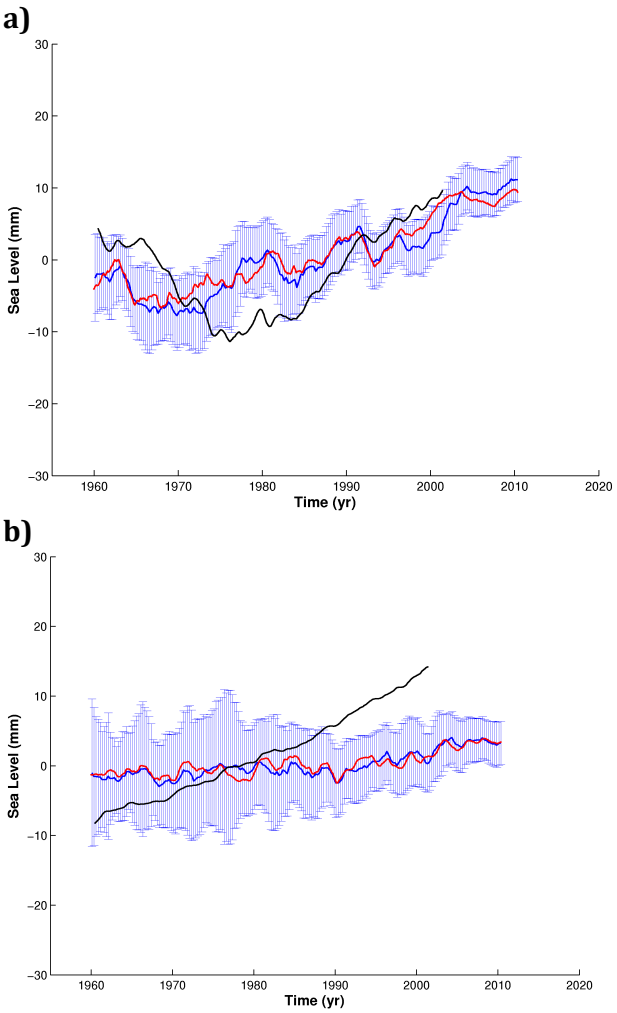

Fig. 3: Global mean thermosteric sea level from in situ data of Levitus et al. (2009) -blue curve with 1-sigma uncertainty-, Ishii and Kimoto (2009) -red curve- and from GECCO outputs -black curve- for a) 0-300m depth and b) 300-700m depth. Annual and semi-annual signal have been removed. A 1-year running mean has been applied.

curves. The L09 temperature data that have a more reliable error estimates have a statistically significant trend of 0.40 +/- 0.06 mm/yr over 1970-2010 (1-sigma uncertainty and the trend over 1960-1969 is not statistically significant). The upper layer thermosteric sea level contributions display a slowdown in the rate of increase for the most recent years as was also seen when considering the water column down to 700m depth.

The GECCO-based estimate of the upper layer contribution to thermosteric mean sea level, in contrast to the estimate for 0-700m, is

nearly always within the 1-sigma uncertainty of the corresponding L09 estimate and displays a similar decadal variation as the observations over 1960 to 2010. However, we note that the GECCO-based upper-layer estimate does not accurately resolve the shorter-period interannual variabilities found in the observations.

The lower layer's contributions to global mean thermosteric sea level change (i.e., 300-700m, figure 3b) display some but statistically insignificant interannual variability from 1960 to 1989 with negligible trend (0.05+/-0.07 mm/yr; 1-sigma uncertainty). However, the lower layer's contribution starts rising after 1990 with a statistically significant trend of 0.26+/-0.08 mm/yr over 1990 to 2010 (1-sigma uncertainty). This rise in the lower layer's contribution to increasing thermosteric sea level appears to lag that of the upper layer. By computing running correlation coefficient between the two layer contributions, we find a significant lag amounting to 22+/- 1.15 yr (2-sigma uncertainty).
Figure 3b also shows the corresponding lower-layer contributions based on the GECCO estimate over 1960-2001. Although the GECCO estimate is statistically in agreement with the observations over much of this period owing to the relatively large formal uncertainties, the two become significantly different after 1990 beyond the estimated errors. Differences in this lower layer appear to be the main cause for the discrepancy noted earlier for the net thermosteric sea level anomalies computed down to 700m (Figure 1). Unlike the observations, the GECCO-based thermosteric mean sea level displays a positive long-term trend over the entire period and lacks much of the interannual variability found in the observed estimates.

Figures 4a,b display global mean thermosteric sea level rates for the 2 oceanic layers (i.e., 0-300m and 300-700m respectively) based on L09 (blue curves with 1-sigma uncertainty)

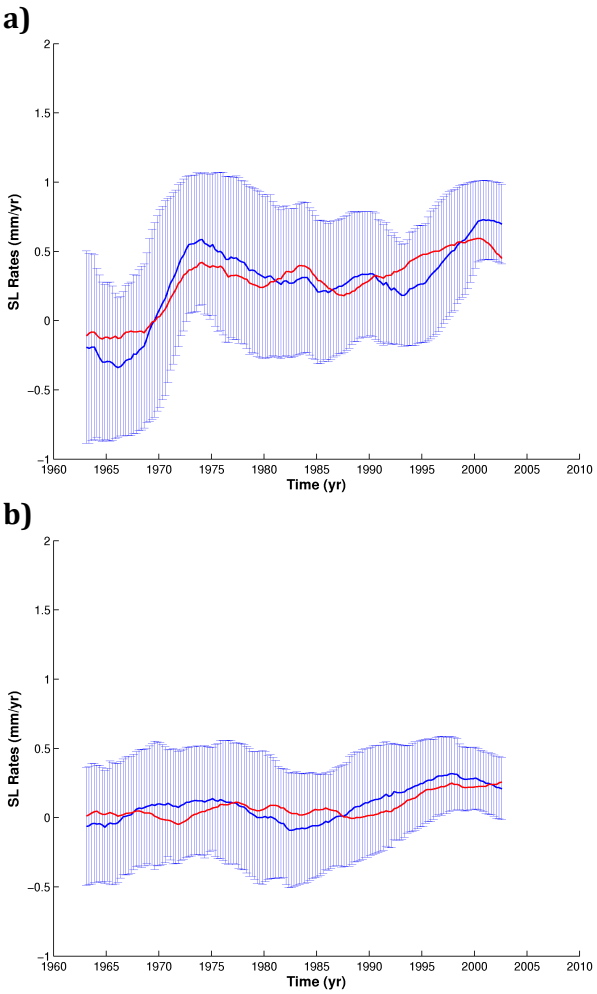

Fig. 4: Linear trends in thermosteric sea level over successive 16 year periods for the global mean thermosteric sea level for Levitus et al. (2009) – blue curves with 1-sigma uncertainty-, Ishii and Kimoto (2009) – the red curve- and GECCO outputs –the black curve- for a) for the 0-300m depth layer b) 300-700m depth layer.

and IK09 (red curves) datasets over 1960-2010 computed as in Figure 2. For the upper layer (0-300m depth, figure4a), both estimates display a slight positive slope and large decadal to multi-decadal variability, which are statistically significant around 1975 and 2000s, depicting successive acceleration/deceleration phases. It is worth noting that this upper layer level explains a large part of the total water column down to 700m depth. For the lower layer (i.e., 300-700m), figure 4b shows slight thermosteric sea level rate variations for both observed datasets.

4. Discussion and conclusion

The present study describes an analysis of global mean thermosteric sea level variability form 1960 to 2010 based on two separate gridded temperature data sets; Levitus et al. (2009) (L09) and Ishii and Kimoto (2009) (IK09). Integrating temperature anomalies from 700m depth to the surface, the global mean thermosteric sea level anomalies of the two data sets are consistent with each other in terms of trend and interannual variability. An increased rate of thermosteric sea level rise starting around 1970 is found in both data sets. For the most recent years, the global mean thermosteric sea level estimates reveal a reduced rate of increase that has also been noticed by other recent studies. Thermosteric sea level estimates from a model-data synthesis (Kohl and Stammer, 2008; GECCO) is further compared with those from the observations to assess the consistency and fidelity of the two and to ascertain their possible deficiencies. We highlight some discrepancies between GECCO-based and observed thermosteric mean sea level down to 700m depth. In fact, for the total water column, GECCO-based estimate shows discrepancy with observed thermosteric mean sea level inferred by L09 after ~1990. Furthermore, interannual variability identified by the observations is not resolved by GECCO. There is good agreement in trend between L09 and IK09 data sets but GECCO estimates are larger and disagree with observations.

Analyzing temperature anomaly contributions to global mean thermosteric sea level as a function of depth, the GECCO-synthesis is found to be consistent with observed variations for the upper ocean (i.e., 0-300m) but the two significantly differ from each other at deeper levels (i.e., 300-700m). The discrepancy between the model-data synthesis and observations noted above for the 0-700m thermosteric sea level change is, thus, due to differences at depth. It is also worth noting that the 0-300m depth layer explains a large part of the observed global mean thermosteric sea level computed down to 700m depth over 1960-2010. As for the total water column, GECCO does not resolve the interannual variability identified in the observations. More detailed investigations are needed to discern the cause of the discrepancies between GECCO-based and observed thermosteric mean sea levels.

We also note the relatively large formal uncertainties associated with the lower layer estimates (i.e., 300-700m depth) in comparison to the observed variabilities and to corresponding error estimates of the upper layer, especially before 1990, owing to probably limited number of available observations.

The present study identifies a significant 22-year lag in ocean warming contributing to the global mean thermosteric sea level increase between the upper (i.e., 0-300m) and lower (i.e., 300-700m) oceanic layers. Significant net warming starts in 1970 in the upper layer but does not begin until 1990 for the lower layer. However, the GECCO model does not reproduce such lag. Johnson and Wijffels (2011) summarize the number of historically available observations per year and as a function of instrument type. In particular, XBT measurements appear in the archive from 1966 starting with shallow XBTs (recording until 460m) and then later deep XBTs (recording until 760m). The number of deep XBTs increases significantly just before 1990. That the apparent lag in warming between the upper and lower layers might is an artifact of in situ data coverage cannot entirely be ruled out.

Variations in the observed rates of global mean thermosteric sea level change are found to be coherent with that of reconstructed sea level time-series inferred by Church and White (2011) and Meyssignac et al. (2012). In particular, large decadal to multi decadal variability in global mean sea level change can be explained by temperature changes of the analyzed water column (i.e., 0-700m depth layer) with a large part owing to its upper layer (i.e., 0-300m). In comparison,

temperature changes in the lower layer (i.e., 300-700m depth) are relatively small and do not contribute as much changes in mean thermosteric sea level rates. However, temperature changes do not entirely explain the estimated rates of global mean sea level change over the past decades (1960-2010). In particular, the rate of global mean sea level rise has increased faster since 1990 than inferred from temperature change alone. This discrepancy suggests that another climate component could be involved in the sea level rate fluctuations. Recently it has been reported that ice mass loss from ice sheets (Greenland and West Antarctic ice sheet, Rignot et al., 2011) and mountain glaciers and ice caps (Cogley, 2009) increased in the early 90's. These climate components must also be considered in the future to investigate mean sea level rate variations in more detail and to understand the mechanisms involved in these fluctuations.

Acknowledgements
William Llovel is supported by a NASA postdoctoral fellowship.

References

Ablain, M., A. Cazenave, G. Valladeau, and S. Guinehut (2009), A new assessment of the error budget of global mean sea level rate estimated by satellite altimetry over 1993–2008, Ocean Sci., 5, 193–201, doi:10.5194/os-5-193-2009.

Bindoff, N., et al. (2007), Observations: Oceanic climate and sea level, in Climate Change 2007: The Physical Science Basis. Contribution of Working Group I to the Fourth Assessment Report of the Intergovernmental Panel on Climate Change, edited by S. Solomon et al., pp. 385–432, Cambridge Univ. Press, Cambridge, U. K.

Cazenave A. and W. Llovel (2010). Contemporary sea level rise, *Annual Review in Marine Science,* 2, 145-173.

Cazenave, A., K. Dominh, S. Guinehut, E. Berthier, W. Llovel, G. Ramillien, M. Ablain, and G. Larnicol (2009), Sea level budget over 2003–2008: A reevaluation from GRACE space gravimetry, satellite altimetry and Argo, Global Planet. Change, 65, 83–88, doi:10.1016/j.gloplacha.2008.10.004.

Church J.A. and N.J. White (2011), Sea-Level Rise from the Late 19th to the early 21st Century, Surv Geophys, pp1-18. doi:10.1007/s10712-011-9119-1

Cogley JC. 2009. Geodetic and direct mass balance measurements: Comparison and joint analysis. Ann. Glaciol. 50:96–100

Gill A.E., Atmosphere–ocean dynamics, Academic Press, San Diego (1982) 662 pp.

Gouretski V, Koltermann KP. 2007. How much is the ocean really warming? Geophys. Res. Lett. 34:L011610, doi: 10.1029/GL027834

Hanawa K, Rual P, Bailey R, Sy A, Szabados M. 1995. A new depth-time equation for Sippican or TSK T-7, T-6 and T-4 expandable bathythermographs (XBT). Deep Sea Res. Part I 42:1423–51

Ishii, M., and M. Kimoto (2009), Reevaluation of historical ocean heat content variations with time-varying XBT and MBT bias, J. Oceanogr., 65, 287–299. DOI: 10.1007/s10872-009-0027-7

Johnson, G.C., and S.E. Wijffels. 2011. Ocean density change contributions to sea level rise. Oceanography 24(2):112–121, doi:10.5670/oceanog.2011.31.

Kalnay, E., and Coauthors, 1996: The NCEP/NCAR 40-Year Reanalysis Project. Bull. Amer. Meteor. Soc., 77, 437–471.

Köhl A. and D. Stammer, Decadal sea level changes in the 50-year GECCO ocean synthesis. *J. Climate*, 21 (2008), pp. 1866–1890. DOI: 10.1175/2007JCLI2081.1

Leuliette, E., and L. Miller (2009), Closing the sea level rise budget with altimetry, Argo and GRACE, Geophys. Res. Lett., 36, L04608, doi:10.1029/2008GL036010.

Leuliette, E.W., and J.K. Willis (2011), Balancing the sea level budget. Oceanography 24(2):122–129, doi:10.5670/oceanog.2011.32.

Levitus, S., J. I. Antonov, T. P. Boyer, R. A. Locarnini, H. E. Garcia, and A. V. Mishonov (2009), Global ocean heat content 1955–2008 in light of recently revealed instrumentation problems, *Geophys. Res. Lett.*, 36, L07608, doi:10.1029/2008GL037155.

Levitus, S., J. I. Antonov, T. P. Boyer, H. E. Garcia, and R. A. Locarnini (2005), Linear trends of zonally averaged thermosteric, halosteric, and total steric sea level for individual ocean basins and the world ocean, (1955–1959)–(1994–1998), Geophys. Res. Lett., 32, L16601, doi:10.1029/2005GL023761.

A. Lombard, A. Cazenave, P.Y. Le Traon, M. Ishii, Contribution of thermal expansion to present-day sea level rise revisited, Global Planet. Change 47 (2005) 1–16.

Llovel, W., S. Guinehut, and A. Cazenave (2010), Regional and interannual variability in sea level over 2002–2009 based on satellite altimetry, Argo float data and GRACE ocean mass, Ocean Dyn., 60, 1193–1204, doi:10.1007/s10236-010-0324-0.

Llovel,W., B. Meyssignac, and A. Cazenave (2011), Steric sea level variations over 2004–2010 as a function of region and depth: Inference on the mass component variability in the North Atlantic Ocean, Geophys. Res. Lett., 38, L15608, doi:10.1029/2011GL047411.

Locarnini, R. A., A. V. Mishonov, J. I. Antonov, T. P. Boyer, H. E. Garcia, O. K. Baranova, M. M. Zweng, and D. R. Johnson, 2010. World Ocean Atlas 2009, Volume 1: Temperature. S. Levitus, Ed. NOAA Atlas NESDIS 68, U.S. Government Printing Office, Washington, D.C., 184 pp.

Nerem, R.S., Chambers, D.P., Choe, C., Mitchum, G.T., 2010. Estimating mean sea level change from the TOPEX and Jason altimetermissions. Mar. Geodesy 33 (1), 435–446.

Meyssignac B., M. Becker, W. Llovel and A. Cazenave (2012) An Assessment of Two-Dimensional Past Sea Level Reconstructions Over 1950–2009 Based on Tide-Gauge Data and Different Input Sea Level Grids, Survey in Geophysics, in press. doi:10.1007/s10712-011-9171-x

Willis, J. K., D. T. Chambers, and R. S. Nerem (2008), Assessing the globally averaged sea level budget on seasonal to interannual time scales, J. Geophys. Res., 113, C06015, doi:10.1029/2007JC004517.

Willis, J. K., D. P. Chambers, C. Y. Kuo, and C. K. Shum (2010), Global Sea Level Rise recent progress and challenges for the decade to come, Oceanography, 23, 26–35, doi:10.5670/oceanog.2010.03.

Wunsch C, Ponte RM, Heimbach P. 2007. Decadal trends in sea level patterns: 1993–2004. J. Clim. 20:5889-911, doi:10.1175/2007JCLI1840.

Journal of Geodetic Science

• 2(2) • 2012 • 125-133 DOI: 10.2478/v10156-011-0029-4 •

Regional sea level change and variability in the Caribbean sea since 1950

Research Article

H. Palanisamy[1*], M. Becker[2], B. Meyssignac[1], O. Henry[1], A. Cazenave[1]

1 *LEGOS/OMP, Toulouse, France*
2 *UMR 228 ESPACE-DEV/UAG, Cayenne, French Guiana*

Abstract:
We investigate the regional variability in sea level in the Caribbean Sea region over the past 60 years (1950-2009) using an Empirical Orthogonal Function (EOF)-based 2-dimensional past sea level reconstruction (a mean of 3 reconstructions based on few long tide gauge records and different sea level grids from satellite altimetry and ocean circulation models) and satellite altimetry data for the last two decades. We find that over the past 60 years, the mean rate of sea level rise in the region was similar to the global mean rise (∼1.8 mm/yr). The interannual mean sea level of the placeCaribbean region appears highly correlated with El Nino-Southern Oscillation (ENSO) indices. Interpolation of the sea level reconstruction grid at different sites, in particular at the Caribbean Islands where tide gauge records are either very short or inexistent, shows that locally, the sea level trend is on the order of 2 mm/yr, i.e. only slightly larger than the mean trend over the region. Besides, correlation with ENSO is in general good, especially since the mid-1980s. We also find a significant correlation between the interannual variability in sea level and hurricane activity, especially over the past decade during which hurricane intensity and sea level interannual variability have both increased.

Keywords:
Caribbean Sea • sea level variability • 2-D past sea level reconstruction • satellite altimetry • tide gauge • ENSO • hurricane

Received 23-03-2012 ; accepted 06-04-2012

1. Introduction

Sea level is a very sensitive indicator of climate change and variability as it integrates the responses of all components of the climate system to natural and human-induced forcing. Sea level also reflects the natural variability of the climate system. During the 20th century, the global mean sea level (GMSL) has risen at an average rate of ∼1.8 mm/yr (e.g., Church and White, 2011). Since the early 1990s, sea level is routinely measured by high-precision satellite altimetry which indicates a GMSL rise of 3.2 mm/yr since over 1993-2011. Sea level budget studies conducted over the altimetry era (since 1993) have shown the GMSL rise results from ocean thermal expansion (contributing by ∼30%) and land ice loss from glaciers and the Greenland and Antarctica ice sheets (contributing in total to ∼55%-60%) (e.g., Church et al., 2011, Cazenave and Llovel, 2010, Cazenave and Remy, 2011).

Satellite altimetry has revealed high regional variability in the rates of sea level rise, with faster rates (up to 3 times than the global mean) in the western Pacific, North Atlantic and southern oceans. The main cause of regional variability over the altimetry era is non uniform ocean heat content as well as salinity variations (e.g., Lombard et al., 2005, 2009). 2-dimensional past sea level reconstructions developed to study the regional variability in sea level prior to the altimetry era (e.g., Church et al., 2004, Llovel et al., 2009, Ray and Douglas, 2011, Meyssignac et al., 2012a) have shown that the spatial trend patterns are not stationary but fluctuate in time and space in responses to the natural modes of the ocean-atmosphere coupled system like El Nino-Southern Oscillation (ENSO), Pacific Decadal Oscillation (PDO), North Atlantic Oscillation (NAO) (e.g., Meyssignac et al, 2012a, b). This indicates that, at regional scale,

*E-mail: hindu@legos.obs-mip.fr, 18, Av. E. Belin, 31400 Toulouse, France, tel. +33 5 61 33 29 72

there is a low-frequency (multidecadal) component of the regional variability that superimposes to the GMSL rise. This component may either amplify or reduce the GMSL rise. When investigating the effective rate of sea level change in selected regions, it is of primary importance to account for this regional component in addition to the global mean rise. In a previous study focusing on the western tropical Pacific islands, (Becker et al., 2012) found that at Funafuti, an island in the Tropical Pacific belonging to the nation of Tuvalu, because of the low-frequency regional variability component, the total (absolute) sea level rise is almost three times the global mean rate of sea level rise over the past half century (i.e., ∼5 mm/yr versus 1.8 mm/yr over 1950-2010). This shows the importance of estimating the rate of sea level rise not only globally but also in terms of regional variability in order to understand the level of impacts that the sea level rise can have on the local population.

In the present study, we focus on the Caribbean Sea, a region surrounded by highly populated countries and islands, and develop an approach similar to that of (Becker et al., 2012) to determine the total sea level change (i.e., GMSL plus regional variability) in this area since 1950.

The Caribbean Sea, located between 9°N and 22°N latitude and between 60°W and 89°W longitude is bound by South America to the South, Central America to the West. The Antilles, a chain of islands, separate the Caribbean Sea from the Atlantic Ocean to the North and East and from the Gulf of Mexico to the South West. The Caribbean region, situated largely on the Caribbean plate comprises more than 7000 islands, islets, reefs and cays. Most of the Caribbean islands lie close to the boundaries of the Caribbean plate and hence are geologically active with earthquakes from time to time and a number of volcanic activities. The Caribbean islands are considered to be one of the vulnerable islands under future sea level rise (Nicholls and Cazenave, 2010) with more than 50% of the population living within 1.5 km of the shore (Mimura et al., 2007).

To estimate the low-frequency regional sea level variability in the Caribbean, we make use of an Empirical Orthogonal Function (EOF)-based (Preisendorfer, 1988) 2-dimensional past sea level reconstruction (Meyssignac et al., 2012a). This is a mean of 3 reconstructions that combines nearly one hundred long tide gauge records (1950-2009) with different sea level grids of shorter duration. The Caribbean does not possess many good quality tide gauge records and even the few available (about 10) do not cover the whole 60 years period. Of the available records, only Magueyes has been used in the global sea level reconstruction. Thus the reconstruction is an important tool to study the regional sea level variability. To understand what drives the Caribbean Sea regional variability, we estimate the effects of ocean temperature and salinity on the observed sea level variations and also compare the sea level with different climatic indices, in particular ENSO indices. We also investigate a potential link between sea level variability and hurricane activity in the Caribbean region.

2. Data

2.1. Satellite Altimetry

We use the DT-MSLA "Ref" series of satellite altimetry data provided by Collecte Localisation Satellite (http://www.aviso.oceanobs.com/en/data/products/sea-surface-height-products/global/msla/index.html). The data set is based on the combination of several altimetry missions namely Topex/Poseidon (T/P), Jason-1 and 2, Envisat and ERS 1 and 2. It is a global homogenous inter-calibrated dataset based on a global crossover adjustment that considers T/P and then Jason-1/2 as reference missions. Usual geophysical corrections are applied: solid Earth, ocean and pole tides, wet and dry troposphere, ionosphere (see Ablain et al., 2009 for details) and inverted barometric correction (Carrere and Lyard, 2003). The altimetry data set is used over the time span from January 1993 until December 2009. It is available as 0.25° x 0.25°Mercator projection grids at weekly intervals.

2.2. Tide gauges

Revised Local Reference monthly mean sea level data of the Permanent Service for the Mean Sea Level (PSMSL; Woodworth and Player, 2003; http://www.psmsl.org/) are used in this study. As mentioned above, the tide gauge coverage in the Caribbean Sea region is rather poor. Only 7 tide gauges have >30 years of data between 1950 and 2009. In this study, we have made use of 10 tide gauge records: 7 having > 30 years of data and 3 having data only between 15 to 20 years but of good quality. Linear interpolation was performed to introduce missing data in the gaps whenever the gaps are ≤ 4 consecutive years (otherwise the record is not considered). Gaps and discontinuities occur in the tide gauge records due to natural factors like earthquakes or changes in instrumentation or even due to anthropogenic factors. Fig. 1 (as star symbols) shows the location of the tide gauges and their characteristics are given in Table 1 (in Fig. 1 -as blue dots- and Table 1 are also listed a few additional tide gauges with shorter records, records with time gaps exceeding 4 consecutive years or incorrect tide gauge data. In view of the poor quality of the tide gauge records, only the past sea level reconstruction (see Section 2.3), and observed altimetry data have been considered in these locations in order to study the past and recent sea level variability.

The tide gauge time series have been corrected for the inverted barometric response of sea level to atmospheric pressure forcing using the surface pressure grids from the National Centre for Environmental Prediction (NCEP, Kalnay et al., 1996). Glacial Isostatic Adjustment (GIA) is very small in the placeCaribbean region and henceforth the tide gauge records have not been corrected for GIA. In order to concentrate only on the interannual variability, the seasonal cycles have been filtered through a least-squares fit of 12-month and 6-month period sinusoids.

Table 1. Tide gauge locations, MRESL and altimetry trends at the tide gauge locations, correlation coefficients between the detrended tide gauge and detrended MRESL and between detrended tide gauge and detrended altimetry. Also shown is the correlation existing between detrended MRESL and detrended altimetry-based sea level over 1993-2009.

Tide Gauge Stations	Tide Gauge							MRESL 1950-2009			Observed Altimetry 1993-2009	
	Start	*End*	*Span (yr)*	*Trend (mm/yr)*	*Error*	*Corr.Coeff with MRESL*	*Corr.Coeff with Obs.alti*	*Trend (mm/yr)*	*Error*	*Corr.Coeff with Obs.alti*	*Trend (mm/yr)*	*Error*
Cabo San Antonio	1971	2009	39	3,5	0,7	0,6	0,5	2,1	0,1	0,7	0,8	1,5
Gibara	1974	2009	36	1,5	0,5	0,7	1,0	2,3	0,1	0,7	0,5	1,5
Port Royal	1954	1969	16	1,1	2,1	0,7	-	2,0	0,1	0,7	1,5	1,6
Magueyes	1955	2010	56	1,4	0,2	0,8	1,0	1,7	0,1	0,8	2	1,1
San Juan	1962	2010	49	1,6	0,3	0,7	1,0	1,7	0,1	0,8	1,7	1,2
Lima Tree Bay	1977	2010	34	1,0	0,5	0,6	1,0	1,6	0,1	0,8	2,4	1,3
Cartagena	1950	1992	43	5,6	0,2	0,3	-	2,0	0,1	0,5	2,5	0,7
Cristobal	1950	1980	31	2,5	0,4	0,2	-	2,0	0,1	0,5	1,9	0,6
Puerto Limon	1950	1968	19	2,2	0,6	0,5	-	2,0	0,1	0,7	2	0,8
Puerto Cortes	1950	1968	19	9,3	0,9	0,5	-	2,0	0,1	0,5	0,9	0,9
North Sound	1976	1996	21	-	-	-	-	2,3	0,1	0,7	0,9	1,7
Port Au Prince	1950	1961	12	-	-	-	-	1,9	0,1	0,6	0,2	1,0
Port of Spain	1983	1992	10	-	-	-	-	1,9	0,1	0,9	3,1	0,7
Marigot	-	-	-	-	-	-	-	1,6	0,1	0,8	2,4	1,2
Gustavia	-	-	-	-	-	-	-	1,6	0,1	0,8	2,4	1,1
Pointe-a-Pitre	1991	2010	20	-	-	-	-	1,7	0,1	0,6	1,9	0,8
Fort de France	-	-	-	-	-	-	-	2,0	0,1	0,3	1,5	0,8

2.3. Sea level reconstruction

Satellite altimetry since 1993 shows that sea level rise is not uniform and that it follows a characteristic spatial pattern. However this mostly reflects the interannual-decadal variability and the low frequency trends cannot be captured because the altimetry record is still short. Numerical ocean models and ocean reanalyses tools can produce the regional sea level trends on a longer time span (e.g., Carton and Giese., 2008; Kohl and Stammer, 2008; Penduff et al., 2010). To retrieve past regional variability in sea level prior to the altimetry era, other approaches can be made use. These approaches called reconstruction techniques combine long tide gauge records of limited spatial coverage with shorter, global gridded sea level data, either from satellite altimetry or from numerical ocean models (Church et al., 2004, Hamlington et al., 2011; Llovel et al., 2009; Meyssignac et al., 2012a; Ray and Douglas, 2011). Most of these studies interpolate in an optimal way (see Kaplan et al., 2000 for more details) the long tide gauge records with the principal EOF modes of ocean variability deduced from the altimetry-based gridded sea level data or ocean model outputs. Results do depend on underlying assumptions, i.e., that the principal modes of variability of the ocean are well captured by the relatively short altimetry record or from imperfect ocean models, and thus are representative over the longer time span of the reconstructed period (generally since the early 1950s). Here we use a mean of 3 different global reconstructions developed by Meyssignac et al. (2012a) over 1950-2009. These reconstructions are derived from 2-D sea level grids from the ocean circulation model DRAKKAR (Penduff et al., 2010), the SODA reanalysis (Carton et al., 2008) and from satellite altimetry (data from AVISO). For more details, (refer to Meyssignac et al., 2012a)

In the following, we call the mean reconstruction as MRESL.

2.4. Steric sea level (effects of ocean temperature and salinity changes)

Changes in the climate system's energy budget are predominantly revealed in ocean temperatures (Levitus et al., 2005, Bindoff et al., 2007) and the associated thermal expansion contribution to sea-level rise (Bindoff et al., 2007). Anomalies in temperature and salinity in the ocean water column change density, which further gives rise to sea level variations. In this study, we have used the annual-mean steric sea level anomalies for the period 1950-2009 computed from the global gridded temperature (T) and salinity (S) data set of Ishii and Kimoto, 2009 (version 6.12). Steric sea level anomalies were computed over the range of 0-700 m depth. The annual and semi-annual signals were removed and the annual average was performed.

3. Spatial Trend Patterns in the placeCaribbean Sea

3.1. Trend patterns from satellite altimetry and the mean sea level reconstruction over 1993-2009

Over the period from 1993 to 2009, the altimetry-based mean sea level trend averaged over the Caribbean Sea region – see Fig. 1a for the area contours– amounts to 1.7 $\pm$ 0.6 mm/yr. The spatial trend patterns over 1993-2009 in the region are shown in Fig. 1a. Strong positive trends are observed along the coast of the South American continent with trend maxima in the range of 4-5 mm/yr around 10°N and 60°W to 70°W, an area containing the Lesser Antilles islands of La Tortuga, Curaçao and Aruba. High trends are also observed around 10°N and 80°W to 83°W. Smaller trends of about 2 mm/yr are observed around the Greater Antilles islands of Jamaica, Cayman and around the islands of the Lesser Antilles in the eastern Caribbean.

For comparison, Fig. 1b shows the spatial trend patterns in the Caribbean Sea during 1993 to 2009 as derived from the mean re-

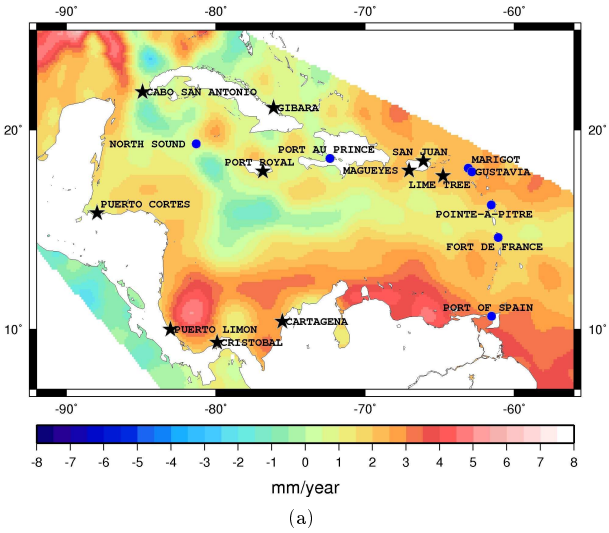

(a)

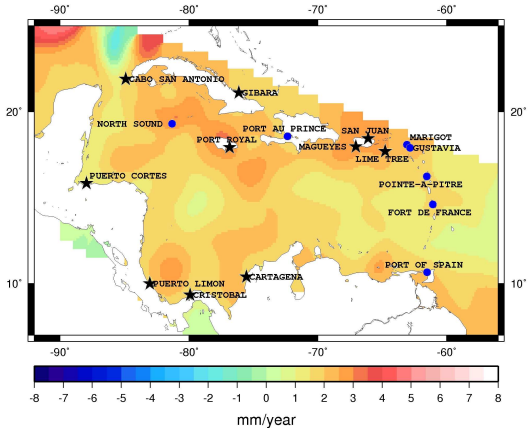

(b)

Figure 1. (a) Map of altimetry based sea level trends from 1993 to 2009 with the tide gauge locations superimposed. (b) Map of sea level trends from Mean Reconstruction from 1993 to 2009. Stars correspond to the 10 tide gauges used in the study while the blue dots correspond to other locations with only MRESL and altimetry data.

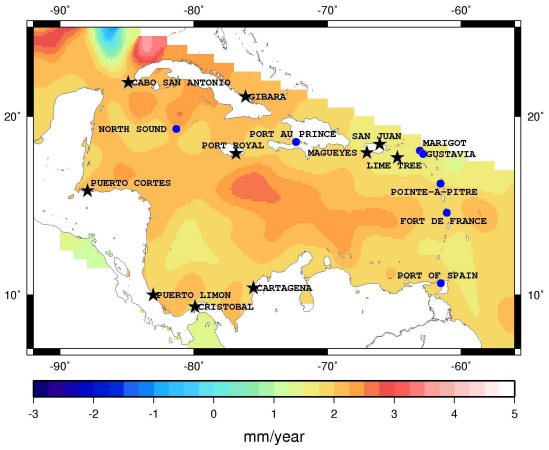

Figure 2. Map of sea level trends from the mean reconstruction over 1950-2009.

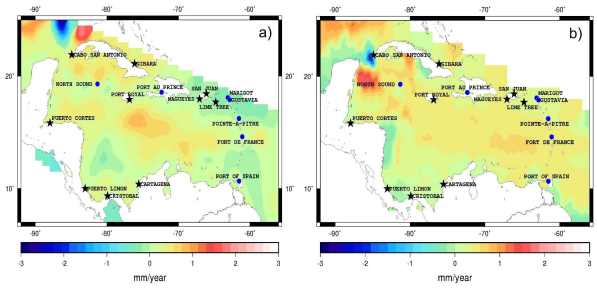

Figure 3. (a) Map of MRESL trend over 1950-2009 with the global mean trend (∼1.8 mm/yr) removed. (b) Map of steric sea level trend over 1950-2009 with the global mean trend of 0.3 mm/yr removed.

construction sea level (MRESL). We can observe that the spatial trend patterns between the satellite altimetry and MRESL are well correlated spatially but the altimetry-based trend amplitudes are larger, especially along the coasts of South America.

Fig. 2 shows the spatial sea level trend pattern from 1950 to 2009 over the Caribbean Sea based on the MRESL. As expected the spatial patterns are different from those on the shorter period (altimetry era) (see the difference in colour scale). Over 1950-2009, the mean sea level trend over the region amounts to 1.8 ± 0.1 mm/yr, a value very similar to the global mean sea level rate ($\approx 1.8 \pm 0.5$ mm/yr) for the past 60 years as obtained from Church and White (2011) and Meyssignac et al. (2012a). In Fig. 2, we also note a local maximum reaching 3 mm/yr in the central Caribbean Sea.

3.2. Steric effects on the placeCaribbean sea level

Fig 3a and Fig 3b show the spatial trend pattern of the MRESL and steric sea level (sum of thermal expansion and salinity effects) over the Caribbean Sea between 1950 and 2009 after having removed the global mean trend of each data set (i.e., 1.8 mm/yr and 0.3 mm/yr for MRESL and steric sea level respectively). Both figures show similar positive trend above 1 mm/yr in the centre of the Caribbean Sea with the trend more concentrated below the Jamaican island in the case of MRESL, whereas the concentration is more towards the Lesser Antilles in the case of the steric sea level. Positive trend patterns to the south of the Cuban island are also clearly visible in both the MRESL and steric sea level. We observe a strong dipole-like positive-negative trend pattern in the steric sea level at the mouth of the Caribbean Sea opening to the placeGulf of Mexico. Similar pattern, however not inside the placeCaribbean region is also observed in the MRESL above the island of Cuba.

Fig. 4 shows the interannual sea level variability over the Caribbean Sea obtained by geographically averaging the MRESL over the Caribbean from 1950 to 2009. The mean trend of 1.8 mm/yr has

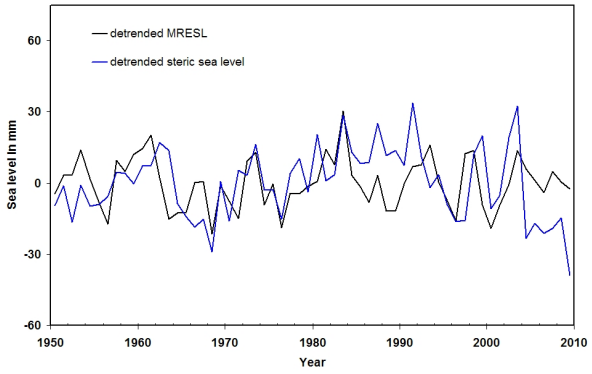

Figure 4. Comparison between detrended MRESL (in mm) and detrended steric sea level (in mm) over the placeCaribbean region from 1950 to 2009.

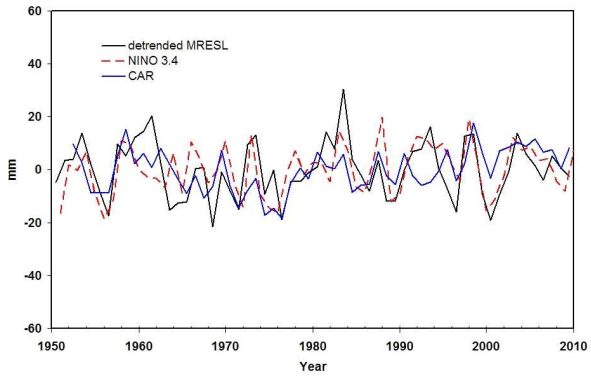

Figure 5. Comparison between detrended MRESL in mm, NINO 3.4 and CAR from 1950 to 2009.

been removed. The detrended steric sea level has been superimposed to the detrended MRESL curve. We observe that the maxima and minima of the steric sea level and MRESL curves are well correlated, suggesting that the same processes drive the interannual variability of the sea level and its steric component.

3.3. Interannual sea level variability and climate indices

In this section, we investigate what are the main climate modes that drive the interannual to multidecadal variability in sea level in the Caribbean region.

Fig. 5 shows the comparison between detrended MRESL and climate index NINO3.4. NINO3.4 index is one of the several ENSO proxies. It is based on sea surface temperature (SST) anomalies averaged in the region bound by 5°N to 5°S and from 170°W to 120°W. It is to be noted that there is a time lag of 6 months between NINO3.4 and MRESL (NINO3.4 leads MRESL) and this lag has been corrected. Though there is no significant correlation between NINO3.4 and MRESL over the entire time period, the correlation is equal to 0.6 between 1985 and 2009. Fig. 5 also shows the climate index CAR superimposed to the detrended MRESL. CAR-Caribbean SST index is the time series of SST anomalies averaged over the Caribbean (Penland and Matrosova, 1998). Overall we note a correlation of 0.5 between CAR and MRESL over the whole time span. Neglecting the temporary anti-correlation in the early 1990s, the correlation increases to 0.7 between 1985 and 2009. The reasonably good correlations existing between MRESL, NINO3.4 and CAR indices indicate that the interannual sea level variability in the Caribbean is influenced by and responds to ENSO events.

In order to capture the characteristics of the Caribbean Sea level variability, an EOF decomposition of the MRESL was performed over the Caribbean for the 1950-2009 time span. Fig. 6a, b show the 1st and 2nd modes of MRESL EOF decomposition respectively. The EOF mode 1 with 88% of the total variance captures the trend over the Caribbean. Indeed, the spatial map on Fig. 6a corresponds well

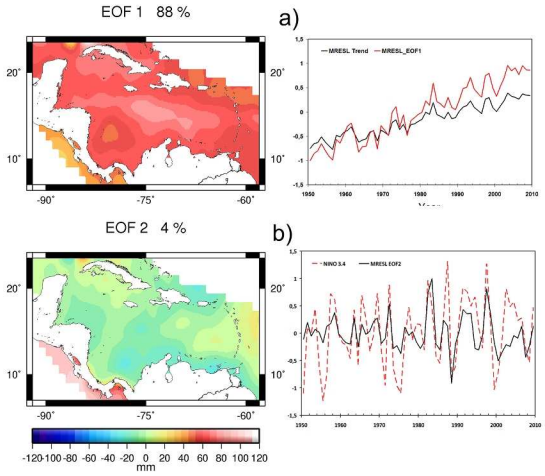

Figure 6. (a) EOF 1st mode of decomposition of the MRESL over 1950-2009 with the mean trend superimposed to the temporal curve of EOF1. (b) EOF 2nd mode of decomposition of the MRESL over 1950-2009 with NINO3.4 climate index superimposed to the temporal curve.

to the trend map on Fig. 1b. Fig. 6a also shows the geographically averaged trend over the Caribbean superimposed to the temporal curve corresponding to the EOF mode 1. Both the temporal curves are highly correlated (correlation equal to 1). The temporal curve corresponding to the 2nd EOF mode with 4% of total variance has a correlation of 0.6 with NINO 3.4 climate index as shown in Fig. 6b.

4. Sea level variability from tide gauge, MRESL and observed altimetry at various locations in the placeCaribbean region.

Sea level variability at different locations in the Caribbean was analysed by making use of tide gauge data, MRESL and observed altimetry at the tide gauge sites. Though there are many tide gauges available in the Caribbean, only ten sites could be used in the

study. In effect, the selection of the tide gauges from the available records was performed based on the time period of availability of the data, time gap between the discontinuities and the quality of their data. The chosen records were then compared with the MRESL and in certain cases, with observed altimetry data depending on the availability of the tide gauge data during the altimetry era. Table 1 summarizes tide gauge as well as reconstructed and altimetry trends, correlation coefficients between detrended tide gauge, reconstructed and altimetry time series.

In Fig. 7 is shown the comparison of the detrended tide gauge series (in red) with the detrended MRESL (in black) and altimetry series (in blue) interpolated at the corresponding tide gauge locations. Except for two tide gauges (Cartagena and Cristobal), the rest of the (detrended) tide gauges records have correlations ($\geq$ 0.5) with detrended MRESL. Magueyes, located in Puerto Rico is the only tide gauge site that has been used in the 2-D global sea level reconstruction of Meyssignac et al. (2012a). So, when possible, comparison between other tide gauges and the reconstruction is a validation of the reconstruction, allowing us to assess its quality (at least in terms of interannual variability).

Between 1950 and 2009, the individual mean sea level trend from MRESL at several tide gauge sites is in the range of 1.9 to 2.3 mm/yr. In few cases (Magueyes, San Juan, Lime Tree Bay, Marigot, Gustavia and Pointe-a-Pitre), it is even lesser than the global mean trend (1.8 mm/yr).

4.1. North, South and the Eastern Caribbean

As we have seen in Fig. 7 and Table 1, there is overall good correlation between available tide gauge records and reconstructed sea level on interannual time scale. Thus, the tide gauge records could be replaced by the MRESL in the Caribbean in order to provide information on the sea level variability at islands and coastal zones that do not have long term tide gauge records. Fig. 8 shows the detrended mean reconstructed sea level (in black) over the last 60 years in three different zones: 1) the Southern Caribbean comprising the Central and South American countries of Costa Rica, Guatemala, Honduras, Panama, Colombia and Venezuela; 2) the Northern Caribbean containing the island nations of Cayman Islands, Cuba, Dominican Republic, Haiti, Jamaica, Puerto Rico, U.S Virgin islands and 3) Eastern Caribbean with islands of Guadeloupe, Martinique, Saint Barthélemy and St.Martin. The altimetry based detrended sea level (in blue) between 1993 and 2009 is also superimposed to the detrended MRESL. The difference between Fig. 7 and Fig. 8 is that in Fig. 7, only locations with the availability of tide gauges (star symbols in trend maps) are considered whereas in Fig. 8 few other stations (blue dots in trend maps) where only the MRESL and altimetry are available are also included in order to study the 3 above mentioned zones. In Fig. 8, we can observe that on a longer time scale, the interannual sea level variability in the North Caribbean is higher than in the Southern Caribbean while the Eastern Caribbean shows greater interannual variability during the recent decades. Both the Northern and Eastern Caribbean

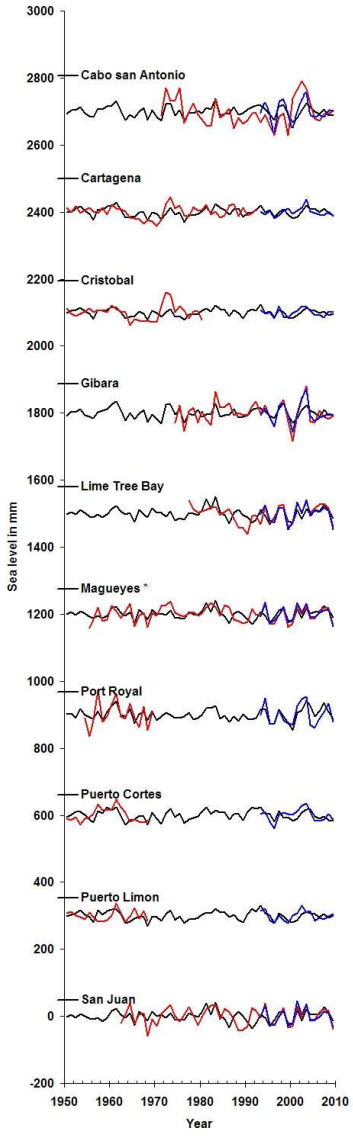

Figure 7. Detrended MRESL and altimetry sea level curves in mm, interpolated at the tide gauge locations since 1950. MRESL in black, tide gauge in red and observed altimetry in blue. The star symbol indicates the station used in 2-D past sea level reconstruction.

show prominent peak during 1982, roughly coinciding with the El Niño event in 1982.

4.2. Sea level variability and hurricanes

Klotzbach (2011) showed that the interannual variability of hurricanes in the Caribbean region is driven by ENSO and that more activity occurs with La Nina conditions than with El Nino conditions. The last two decades (in particular since 1999) have recorded more La Niña events (in particular in 1999/2000, 2007/2008 and

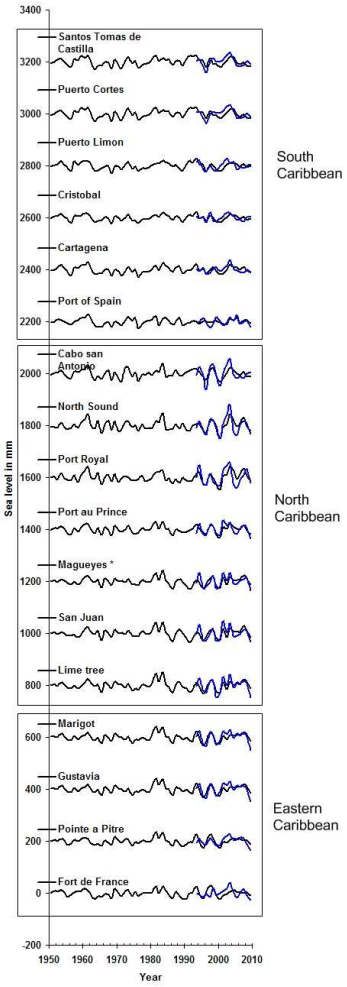

Figure 8. Detrended MRESL (in black) and altimetry sea level (in blue) curves in mm since 1950 at the tide gauge locations arranged based on their location: Southern Caribbean, Northern Caribbean and Eastern Caribbean.

2010/2011) than before. Furthermore, Goldenberg et al. (2001) showed that the years 1995 to 2000 have seen a 2.5 fold increase in major hurricane activity and a fivefold increase in hurricane activity affecting the Caribbean due to simultaneous increases in North Atlantic sea surface temperatures and decreases in vertical wind shear. These authors also showed that this phenomenon is likely to persist for an additional 10 to 40 years. In section 3.2 we have seen that the NINO3.4, a proxy of El Nino and La Nina events and CAR, an index based on the Caribbean SST correlate well with MRESL over the Caribbean since 1985. This period also corresponds to the increased frequency of La Niña events and hurricane activity.

Pielke et al. (2003) showed that between 1944 and 1999, the Northern Caribbean hurricanes (hurricanes hitting Bahamas, British Virgin Islands, Cayman Islands, Cuba, Dominican Republic, Haiti, Jamaica, Puerto Rico etc.) show high interannual variability as well as large multi decadal changes with a long term average of 1.0 hurricane strike per year. The Eastern Caribbean experiences hurricanes at a lower rate than the Northern Caribbean with 0.4 hurricane strike per year, whereas the hurricanes hitting the Central and South American part of the Caribbean show small decadal changes with only 0.2 strike per year. The pattern is very similar to the interannual variability in sea level observed in the Northern and Southern Caribbean as discussed in section 4.1, i.e. Northern Caribbean showing higher interannual sea level variability than the Southern. This seems to suggest that both the sea level interannual variability and hurricane activity in the placeCaribbean are related. Further investigation is needed to understand the link between the sea level variability and hurricane activity in that region.

5. Conclusion

In this study, we have analysed the sea level variability in the Caribbean since 1950 by making use of the mean of a mean 2-D past sea level reconstruction, observed satellite altimetry and tide gauge records wherever available. We observe that the spatial trend pattern in sea level during 1950 -2009 is quite different from that during the altimetry era (since 1993). Moreover the mean sea level trend in the Caribbean is very similar to the global mean sea level rise rate thereby indicating that the Caribbean is not facing a sea level rise larger than the global mean rise (unlike at some islands of the western tropical Pacific, as shown by Becker et al., 2012). Our results also show that the increase in the number of hurricanes during the recent decades have caused so far more damages to the coastal areas than the sea level rise itself. However, projected sea level rise in the future decades in response to global warming will represent an additional threat in this region.

Acknowledgements

Hindumathi Palanisamy is supported by the 'CECILE' project of the Agence Nationale de la Recherche (ANR) while Olivier Henry is supported by the European project MONARCH.

References

Ablain M., Cazenave A., Guinehut S. and Valladeau G., 2009, A new assessment of global mean sea level from altimeters highlights a reduction of global slope from 2005 to 2008 in agreement with in-situ measurements Ocean Sciences, 5, 193-201.

Becker M., Meyssignac B., Llovel W., Cazenave A. and Delcroix T., 2012, Sea level variations at Tropical Pacific Islands during 1950-2009, Glob. Planet. Chan., 80/81, 85-98.

Bindoff N.L., Willebrand J., Artale V., Cazenave A., Gregory J., Gulev S., Hanawa K., Le Quéré C., Levitus S., Nojiri Y., Shum C.K., Talley L.D. and Unnikrishnan A., 2007, Observations:

Oceanic Climate Change and Sea Level. In: Climate Change 2007: The Physical Science Basis. Contribution of Working Group I to the Fourth Assessment Report of the intergovernmental Panel on Climate Change [Solomon, S., D. Qin, M. Manning, Z. Chen, M. Marquis, K.B. Averyt, M. Tignor and H.L. Miller (eds.)]. Cambridge University Press, Cambridge, United Kingdom and New York, NY, USA.

Carrere L. and Lyard F., 2003, Modeling the barotropic response of the global ocean to atmospheric wind and pressure forcing -comparisons with observations, Geophys. Res. Lett., 30, 6, 1275, DOI:10.1029/2002GL016473.

Carton J.A. and Giese B.S., 2008, A reanalysis of ocean climate using Simple Ocean Data Assimilation (SODA), Mon. Weath. Rev., 136, 2999–3017.

Cazenave A. and Llovel W., 2010, Contemporary sea level rise, Ann. Rev. Marine Sci., 2, 145-173.

Cazenave A. and Remy F., 2011, Sea level and climate: measurements and causes of changes, Interdisciplinary Reviews: Climate Change, 2, 5, 647–662, DOI:10.1002/wcc.139.

Church J.A., White N.J., Konikow L.F., Domingues C.M., Cogley J.C., Rignot E., Gregory J. M., van den Broeke M. R., Monaghan A. J., and Velicogna I., 2011, Revisiting the Earth's sea-level and energy budgets from 1961 to 2008, Geophys. Res. Lett., 38, L18601, DOI: 10.1029/2011GL048794.

Church J.A., White N.J., Coleman R., Lambeck K. and Mitrovica J.X., 2004, Estimates of the regional distribution of sea level rise over the 1950–2000 period, J Climat., 17, 2609–2625.

Church J.A. and White N.J., 2011, Changes in the rate of sea level rise from the late 19th to the early 21st century, Surv. Geophys., 1–18, DOI:10.1007/s10712-011-9119-1.

Goldenberg S.B., Landsea C. W., Mestas-Nunez A.M., and Gray W.M., 2001, The recent increase in Atlantic hurricane activity: Causes and implications, Science, 293, 474–79

Hamlington B.D., Leben R., Nerem S., Han W. and Kim K.Y., 2011, Reconstructing sea level using cyclostationary empirical orthogonal functions, J Geophys. Res., 116, C12, DOI: 10.1029/2011JC007529.

Ishii M. and Kimoto M., 2009, Reevaluation of historical ocean heat content variations with varying XBT and MBT depth bias corrections, J Oceanog., 65, 287-299.

Kalnay E.C., Kanamitsu M., Kistler R., Collins W., Deaven D., Gandin L., Iredell M., Saha S., White G., Woollen J., Zhu Y., Leetmaa A., Reynolds B., Chelliah M., Ebisuzaki W., Higgins W., Janowiak J., Mo K. C., Ropelewski C., Wang J., Jenne R. and Dennis J., 1996, The NCEP/NCAR 40-year reanalysis project. Bull. American Meteo. Soci., 77, 437–472.

Kaplan A., Kushnir Y. and Cane M.A., 2000, Reduced space optimal interpolation of historical marine sea level pressure: 1854–1992, J Climat., 13, 2987–3002.

Klotzback P.J., 2011, The influence of El Nino-southern oscillation and the atlantic multidecadal oscillation on Caribean tropical cyclone activity, J Climat., 721-731.

Kohl A. and Stammer D., 2008, Decadal sea level changes in the 50-year GECCO ocean synthesis. J Climat., 21, 1876–90.

Levitus S., Antonov J. and Boyer T., 2005, Warming of the world ocean, 1955–2003, Geophys. Res. Lett., 32, L02604, DOI:10.1029/2004GL021592.

Llovel W., Cazenave A., Rogel P. and Berge-Nguyen M., 2009, 2-D reconstruction of past sea level (1950-2003) using tide gauge records and spatial patterns from a general ocean circulation model, Climat. Past, 5, 1-11.

Lombard A., Cazenave A., DoMinh K., Cabanes C., Nerem R., 2005, Thermosteric sea level rise for the past 50 years; comparison with tide gauges and inference on water mass contribution. Global and Planetary Change, 48, 303-312.

Lombard A., Cazenave A., Le Traon P.Y. and Ishii M., 2005, Contribution of thermal expansion to present-day sea level rise revisited, Glob. Planet. Chan., 47, 1-16.

Lombard A., Garric G., Penduff T. and Molines J.M., 2009, Regional variability of sea level change using a global ocean model at 1/4_ resolution, Ocean Dyn., DOI: 10.1007/s10236-009-0161-6.

Meyssignac B., Llovel W., Becker M. and Cazenave A., 2012, An assessment of two-dimensional past sea level reconstructions over 1950 - 2009 based on tide gauge data and different input sea level grids, Surv. Geophys., in press, DOI:10.1007/s10712-011-9171-x.

Meyssignac B., Salas y Melia D., Becker M., Llovel W., and Cazenave A., 2012, Tropical Pacific spatial trend patterns in observed sea level: internal variability and/or anthropogenic signature?, Climat. Past, in press, DOI: 10.5194/cpd-8-349-2012.

Mimura N., Nurse L., McLean R.F., Agard J., Briguglio L,

Lefale P., et al., 2007, Small islands. Climate Change, 2007: Impacts, Adaptation and Vulnerability. Contribution of Working Group II to the Fourth Assessment Report of the Intergovernmental Panel on Climate Change, M.L. Parry, O.F. Canziani, J.P. Palutikof, P.J. van der Linden and C.E. Hanson, Eds., Cambridge University Press, Cambridge, UK, 687-716.

Nicholls R. and Cazenave A., 2010, Sea level change and the impacts in coastal zones, Science, 328, 1517-1520.

Peltier W.R., 2010, Global glacial isostasy and the surface of the ice-age Earth: The ICE-5G (VM2) model and GRACE, Ann. Rev. Earth Planet. Sci., 32, 111-149.

Penduff T., Juza M., Brodeau L., Smith G., Barnier B., Molines J., Treguier A.-M., and Madec G., 2010, Impact of global ocean model resolution on sea-level variability with emphasis on interannual time scales, Ocean Sci., 6, 269-284.

Penland C. and Matrosova L., 1998, Prediction of tropical Atlantic sea surface temperatures using linear inverse modeling, J Climat., 483-496.

Pielke A.J., Rubiera J., Landsea C., Fernandez M.L. and Klein R., 2003, Hurricane Vulnerability in Latin America and the Caribbean: Normalized Damage and Loss Potentials. Nat. Haz. Rev., 4, 3, DOI: 10.1061/(ASCE)1527- 6988(2003)4:3(101).

Preisendorfer R.W., 1988, Principal component Analysis in Meteorology and oceanography, Develop. Atmos. Sci., 17, Elsevier, 425pp.

Ray R. and Douglas B., 2011, Experiments in reconstructing twentieth-century sea levels. Prog. Oceanog., 91, 4, 496-515.

Woodworth P.L. and Player R., 2003, The permanent service for mean sea level: an update to the 21st century, J Coas. Res., 19, 287-295.